









UNIVERSITÀ DEGLI STUDI DI PADOVA



Università degli Studi di Padova

Department of Mathematics "Tullio Levi-Civita"
Doctoral Program in Mathematical Sciences
Computational Mathematics Curriculum
Cycle XXXVII

Numerical Methods for the Simulation of Wave Propagation Phenomena in Linear Viscoelastic Kelvin-Voigt Materials

Coordinator
Prof. Giovanni Colombo

Supervisor
Prof. Antonia Larese

Candidate
Nicolò Crescenzio

La borsa di dottorato è stata cofinanziata con risorse del programma PON REACT-EU

(The doctoral scholarship was co-financed with resources from the PON REACT-EU programme)

Abstract

Numerical simulation of wave propagation phenomena is a relevant subject in many different fields of science and engineering, such as, among others, geophysics, ocean acoustics, materials science and biomedical engineering. In particular, we develop a mathematical and numerical strategy to accurately simulate acoustic waves, as this could be a critical element in defining effective Early Warning Systems aiming at reducing the possibility of harm or loss due to extreme natural disasters. An effective modelling of wave propagation phenomena in real media requires to take into account several non-trivial but fundamental physical aspects, such as energy dissipation due to viscous effects and heterogeneous spatial distribution of material properties, which pose additional challenges from both a mathematical modelling and numerical point of view. In this thesis we consider a linear viscoelastic material behaviour described by means of the well-known Kelvin-Voigt rheology. Material heterogeneity has been taken into account by dividing the domain into multiple layers, each of them being associated with a distinct material and therefore characterised by a particular set of coefficients that define its physical properties. The system of Partial Differential Equations obtained combining the Cauchy momentum equations with the Kelvin-Voigt constitutive model has been reduced from second order to first order in time by doubling the solution variables, that are the displacement and velocity fields. Then, existence, uniqueness and regularity results for the solution of the resulting initial-boundary value problem have been obtained by relying on the standard theory of linear evolution equations in Hilbert spaces. The weak formulation of the problem has been discretised in space by means of both the linear Lagrangian Finite Element Method and the Spectral/Spectral Element Method. The latter approach is based on the partition of the domain into a set of material subdomains and the approximation of the unknown displacement and velocity fields by means of linear combinations of either Legendre or Chebyshev polynomials defined within each material subdomain. Two different strategies have been considered for enforcing the continuity of the solution across the material interfaces. The first approach consists of using boundary-adapted polynomials defined in such a way they match at the interfaces, whereas the second strategy relies on a Mortar-like approach, thus requiring L^2 weak continuity of the basis functions at the material interfaces. The discretisation in space of the weak formulation yields a system of Ordinary Differential Equations that are solved either by means of standard numerical time-stepping schemes or by exact integration via eigenvalue decomposition. The spatial convergence of the implemented numerical schemes has been investigated by solving several problems with manufactured solution. Finally, numerical simulations of wave propagation phenomena in homogeneous and heterogeneous materials due to the action of a point source are also carried out to validate the proposed numerical strategy.

Sommario

La simulazione numerica di fenomeni riguardanti la propagazione delle onde è un argomento rilevante in molti campi scientifici e ingegneristici, come la geofisica, la scienza dei materiali e la bioingegneria. In particolare, in questa tesi viene sviluppato un modello matematico e numerico in grado di effettuare simulazioni accurate di onde acustiche nel sottosuolo, poichè questo può rivelarsi uno strumento di importanza significativa nella realizzazione di sistemi di monitoraggio (i cosiddetti Early Warning Systems) che hanno lo scopo di ridurre il rischio di danni o vittime causate da eventi naturali quali frane e colate detritiche. Una modellazione accurata dei fenomeni di propagazione ondosa nel sottosuolo richiede di tenere in considerazione anche alcuni aspetti fisici non banali ma fondamentali come la dissipazione dell'energia dovuta agli effetti viscosi e la non omogeneità del materiale. Questi aspetti causano ulteriori difficoltà sia da un punto di vista matematico che numerico. In questa tesi vengono considerati materiali con un comportamento lineare viscoelastico descritto tramite la legge costitutiva di Kelvin-Voigt. L'eterogeneità del materiale è stata presa in considerazione dividendo il dominio in piu sottodomini, ciascuno associato a un materiale diverso e caratterizzato da uno specifico insieme di parametri che definiscono le sue properietà fisiche. Il sistema di equazioni differenziali alle derivate parziali, ottenuto combinando le equazioni di conservazione della quantità di moto di Cauchy con la legge costitutiva di Kelvin-Voigt, è stato ridotto da sistema del secondo ordine nel tempo a sistema del primo ordine aggiungendo una ulteriore incognita (la velocità) a quella di partenza (lo spostamento). Risultati riguardanti l'esistenza, l'unicità e la regolarità della soluzione sono stati ottenuti applicando risultati già noti nel campo delle equazioni differenziali alle derivate parziali. La formulazione debole del problema è stata discretizzata nello spazio usando sia il metodo degli elementi finiti sia il metodo spettrale/degli elementi spettrali. Riguardo quest'ultimo approccio, il dominio è stato discretizzato in un insieme di elementi, ciascuno associato ad un materiale diverso, e i campi di spostamento e velocità sono stati approssimati tramite una combinazione lineare di polinomi di Chebyshev o di Legendre definiti su ogni elemento. Sono state considerate due strategie per garantire la continuità della soluzione all'interfaccia tra elementi adiacenti. La prima consiste nell'utilizzare una particolare combinazione lineare di polinomi (boundary-adapted) che coincidono all'interfaccia, mentre il secondo approccio è simile a quello comunemente impigato nel metodo mortar e consiste nell'imporre la continuità delle funzioni di base in modo debole in L^2. La discretizzazione nello spazio della formulazione debole produce un sistema di equazioni differenziali ordinarie che è stato risolto sia tramite schemi numerici che tramite integrazione esatta. La convergenza nello spazio dei metodi numerici che sono stati implementati è stata investigata risolvendo alcuni problemi la cui soluzione esatta è nota. Infine, l'approccio numerico proposto in questa tesi è stato validato anche attraverso la simulazione di fenomeni riguardanti la propagazione di onde generate dell'azione di una forza localizzata in materiali omogenei e eterogenei.

Contents

Notation 1

1 Introduction 3
- 1.1 Landslides Classification . . . 4
- 1.2 Numerical Models for Flow-like Landslides . . . 5
  - 1.2.1 Depth-Average Models . . . 6
  - 1.2.2 Flexible Barriers and Three-dimensional Models . . . 7
- 1.3 Early Warning Systems . . . 8
  - 1.3.1 Acoustic Emissions . . . 9
- 1.4 Linear Viscoelastic Materials . . . 10
  - 1.4.1 Numerical Methods for Wave Propagation in Viscoelastic Materials . . . 12
- 1.5 Scientific Objectives of the Thesis . . . 14
  - 1.5.1 Contribution of the Thesis . . . 15
  - 1.5.2 Structure of the Thesis . . . 15

I Background and Preliminary Results 17

2 Linear Viscoelasticity and Wave Propagation 19
- 2.1 Linear Viscoelasticity . . . 19
  - 2.1.1 Integral Form of Viscoelastic Constitutive Equations . . . 20
  - 2.1.2 Differential Operator Form of Viscoelastic Constitutive Equations . . . 23
  - 2.1.3 Viscoelastic Fluids and Solids . . . 24
  - 2.1.4 Dynamic Loading and Complex Modulus . . . 27
  - 2.1.5 One-dimensional Mechanical Models . . . 29
- 2.2 Wave Propagation . . . 34
  - 2.2.1 Governing Equations . . . 34
  - 2.2.2 Lamb's Problem . . . 39

3 Partial Differential Equations in Hilbert Spaces 45
- 3.1 Preliminary Definitions . . . 45
- 3.2 Preliminary Results on Elliptic Problems . . . 46
  - 3.2.1 An Elliptic Second Order Example . . . 46
  - 3.2.2 Approximation of Elliptic Problems . . . 48
  - 3.2.3 Linear Elasticity . . . 51
- 3.3 Explicit First Order Evolution Equations . . . 57
- 3.4 Implicit First Order Evolution Equations . . . 60
  - 3.4.1 Introduction . . . 60
  - 3.4.2 Semi-Discrete Faedo-Galerkin Approximation . . . 61
  - 3.4.3 Error Estimate . . . 62
- 3.5 Abstract Second Order Evolution Equations . . . 64

4 Orthogonal Polynomials **65**
4.1 Sturm-Liouville Problem . . . 66
4.2 Jacobi Polynomials . . . 66
4.3 Legendre Polynomials . . . 67
4.3.1 Boundary Adapted Legendre Polynomials . . . 68
4.4 Chebyshev Polynomials . . . 71
4.4.1 Boundary Adapted Chebyshev Polynomials . . . 72
4.5 Multidimensional Basis Functions: Tensor-Product Expansion . . . 76
4.6 Polynomial Approximation Theory . . . 77

II Initial-Boundary Value Problem and Numerical Solution **81**

5 The Kelvin-Voigt Model **83**
5.1 The Initial-Boundary Value Problem . . . 83
5.2 Weak Formulation . . . 84
5.2.1 Dirichlet Boundary Lifting . . . 85
5.2.2 From Second-Order to First-Order in Time . . . 86
5.3 Numerical Discretisation . . . 89
5.3.1 Galerkin Space Discretisation . . . 89
5.3.2 Convergence Semi-Discrete Solution . . . 92
5.3.3 Solution in Time . . . 95

6 Numerical Results and Discussion **97**
6.1 One-dimensional Problem . . . 97
6.1.1 Problem Formulation . . . 97
6.1.2 Basis Functions Definition . . . 102
6.1.3 Convergence of the Semi-Discrete Solution . . . 107
6.1.4 Numerical Simulations . . . 108
6.2 Two-dimensional Cartesian Coordinates . . . 113
6.2.1 Problem Formulation . . . 115
6.2.2 Basis Functions Definition . . . 116
6.2.3 Numerical Simulations . . . 126
6.3 Axisymmetric Cylindrical Coordinates . . . 134
6.3.1 Problem Formulation . . . 134
6.3.2 Basis Functions Definition . . . 135
6.3.3 Numerical Simulations . . . 140
6.4 Full 3D Cylindrical Coordinates . . . 145
6.4.1 Geometrical Setting . . . 146
6.4.2 Basis Functions Definition . . . 146
6.4.3 Imposition of Continuity Conditions at Material Interfaces . . . 150
6.4.4 Computation of Matrices . . . 153

7 Conclusions **159**

References **161**

Notation

Let V and W be the linear spaces over $\mathbb{K}$. We denote by $L(V,W)$ the set of linear functions from V to W and by $\mathcal{L}(V,W)$ the set of *continuous* linear functions from V to W. This clearly is a subset of $L(V,W)$. Then, we denote by V' the algebraic dual of V, i.e., the linear space of all conjugate linear functionals from $V \to \mathbb{K}$. Given $F \in V'$ and $v \in V$, the functional is usually denoted by $F(v) = \langle F, v\rangle$, where $< \cdot, \cdot >$ is called duality pairing. Sometimes we also write $\langle F, u\rangle_{V'\times V}$ to highlight the space in which F is defined.

L^p spaces. Let $\Omega \subset \mathbb{R}^d$. We denote by $L^p(\Omega)$ the space of measurable functions $v\colon \Omega \to \mathbb{R}^d$ such that $\|v\|_{L^p} < \infty$, where

$$\begin{aligned} \|v\|_{L^p} &:= \left(\int_\Omega |v(x)|^p \, dx\right)^{1/p}, && 1 \le p < \infty, \\ \|v\|_{L^\infty} &:= \inf\left\{C \,:\, |v(x)| \le C \text{ a.e. on } \Omega\right\}, && p = \infty. \end{aligned}$$

In the case of vector-valued functions $\boldsymbol{v}\colon \Omega \to \mathbb{R}^d$, i.e., $\boldsymbol{v} = (v_1, \dots, v_d)$ with $v_i\colon \Omega \to \mathbb{R}$ for all $i = 1, \dots, d$, we say that $\boldsymbol{v} \in [L^p(\Omega)]^d$ (or simply $\boldsymbol{v} \in L^p(\Omega)^d$) if $v_i \in L^p(\Omega)$ for all $i = 1, \dots, d$. The space $[L^p(\Omega)]^d$ is endowed with the norm

$$\|\boldsymbol{v}\|_{L^p} := \left(\sum_{i=1}^d \|v_i\|_{L^p}^p\right)^{1/p}.$$

Similarly, given a tensor-valued function $\boldsymbol{v} = (v_{11}, \dots, v_{ij}, \dots, v_{dd})$, where $v_{ij}\colon \Omega \to \mathbb{R}$ for all $i, j = 1, \dots, d$, we say that $\boldsymbol{v} \in [L^p(\Omega)]^{d\times d}$ if $v_i \in L^p(\Omega)$ for all $i, j = 1, \dots, d$ and we define the norm of $\boldsymbol{v} \in [L^p(\Omega)]^{d\times d}$ as

$$\|\boldsymbol{v}\|_{L^p} := \left(\sum_{i,j=1}^d \|v_{ij}\|_{L^p}^p\right)^{1/p}.$$

Sobolev Spaces. Let $\Omega \subset \mathbb{R}^d$ be open. For $k \in \mathbb{N}_0$, $1 \le p \le \infty$, we denote by $W^{k,p}(\Omega)$ the Sobolev space

$$W^{k,p}(\Omega) = \left\{u \in L^p(\Omega) \,:\, u \text{ has weak derivative } \partial^\alpha u \in L^p(\Omega)\, \forall \alpha \in \mathbb{N}_0^d \,:\, |\alpha| \le k\right\}$$

equipped with the norm

$$\begin{aligned} \|u\|_{W^{k,p}} &:= \left(\textstyle\sum_{|\alpha|\le k} \|\partial^\alpha u\|_{L^p}^p\right)^{1/p}, && 1 \le p < \infty, \\ \|u\|_{W^{k,\infty}} &:= \max\nolimits_{|\alpha|\le k} \|\partial^\alpha u\|_{L^\infty}, && p = \infty. \end{aligned}$$

Moreover, we denote by $|\cdot|_{W^{k,p}}$ the semi-norm of $W^{k,p}(\Omega)$, i.e.,

$$\begin{aligned} |u|_{W^{k,p}} &:= \left(\textstyle\sum_{|\alpha|= k} \|\partial^\alpha u\|_{L^p}^p\right)^{1/p}, && 1 \le p < \infty, \\ |u|_{W^{k,\infty}} &:= \max\nolimits_{|\alpha|= k} \|\partial^\alpha u\|_{L^\infty}, && p = \infty. \end{aligned}$$

We denote by $W_0^{k,p}(\Omega)$ the closure of $C_c^\infty(\Omega)$ in $W^{k,p}(\Omega)$. For $p = 2$, we also use the notation $H^k(\Omega) := W^{k,2}(\Omega)$ and $H_0^k(\Omega) := W_0^{k,2}(\Omega)$. We extend the definition of the space $H^1(\Omega)$ to vector-valued functions as follows:

$$[H^1(\Omega)]^d := \left\{\boldsymbol{v}\colon \Omega \to \mathbb{R}^d \,:\, v_i \in H^1(\Omega)\ \forall i = 1, \dots, d\right\},$$

endowed with the norm

$$\|\boldsymbol{v}\|_{H^1} = \left(\sum_{i=1}^d \|v_i\|_{H^1}^2\right)^{1/2}.$$

Finally, for tensor-valued functions $\boldsymbol{v}\colon \Omega \to \mathbb{R}^{d\times d}$, we define the space

$$[H^1(\Omega)]^{d\times d} := \left\{\boldsymbol{v}\colon \Omega \to \mathbb{R}^{d\times d} \,:\, v_{ij} \in H^1(\Omega)\ \forall i,j = 1,\dots,d\right\}$$

equipped with the norm

$$\|\boldsymbol{v}\|_{H^1} = \left(\sum_{i,j=1}^d \|v_{ij}\|_{H^1}^2\right)^{1/2}.$$

Spaces of time-dependent functions Let X be a Banach space endowed with the norm $\|\cdot\|_X$. We now denote $X-$valued L^p spaces by $L^p([0,T],X)$, which consists of all strongly measurable functions $v\colon [0,T]\to X$ such that

$$\|v\|_{L^p([0,T],X)} := \left(\int_0^T \|v(t)\|_X^p\, dt\right)^{1/p} < \infty, \qquad 1 \le p < \infty,$$
$$\|v\|_{L^\infty([0,T],X)} := \operatorname{ess\,sup}_{0\le t\le T} \|v(t)\|_X < \infty, \qquad p = \infty.$$

The space $C([0,T],X)$ consists of all continuous $v\colon [0,T]\to X$ such that

$$\|v\|_{C([0,T],X)} := \max_{0\le t\le T} \|v(t)\|_X < \infty.$$

The space $W^{1,p}([0,T],X)$ is defined as

$$W^{k,p}([0,T],X) := \left\{u \in L^p([0,T],X) \,:\, u \text{ has weak derivative } \partial_t^\alpha u \in L^p([0,T],X)\ \forall \alpha \in \mathbb{N}_0^d \,:\, |\alpha| \le k\right\}.$$

On $W^{1,p}([0,T],X)$ we define the norm

$$\|u\|_{W^{k,p}([0,T],X)} := \left(\int_0^T \sum_{|\alpha|\le k} \|\partial_t^\alpha u(t)\|_X^p\, dt\right)^{1/p}, \qquad 1 \le p < \infty,$$
$$\|v\|_{W^{k,\infty}([0,T],X)} := \operatorname{ess\,sup}_{0\le t\le T} \left(\sum_{|\alpha|\le k} \|\partial_t^\alpha u(t)\|_X\right).$$

For $p = 2$, we also write $H^m([0,T],X) := W^{m,2}([0,T],X)$.

Finally, a comment about the notation used to identify the derivative of a scalar function with respect to the time or space variable. Given a scalar function $u = u(x,t)$, where x is the space variable and t is the time variable, its derivative in time will be denoted either by $\partial u/\partial t$ or by $\dot{u}(x,t)$, whereas for its space derivative we will use either $\partial u/\partial x$ or $u'(x,t)$.

Chapter 1

Introduction

This doctoral thesis has been co-financed with resources from the *PON REACT-EU programme* (M.D. n. 1061/2021, Action IV.5 *"PhD programmes on Green related topics"*, scholarship code DOT1319984-1). The objective of the project was the development and validation of numerical tools capable of playing an important role in the minimization of the damage induced by floods and landslides on civil infrastructures. In the last decades, we have observed a significant growth in the intensity of extreme natural hazards that are affecting more and more frequently our lives. The latest report from the Centre for Research on the Epidemiology of Disasters (CRED) [1] highlights the significant socio-economic impact of these events: in 2023, the Emergency Events Database (EM-DAT) recorded a total of 399 disasters related to natural hazards, a number exceeding the 20-year average of 369 events; these calamities resulted in 86473 fatalities and affected 93.1 million people, with estimated economic losses amounting to US$202.7 billion. The report also shows that, in the last 20 years, floods and landslides have been responsible for almost 10% of all fatalities from natural hazards worldwide. Unfortunately, real numbers are even larger than reported: indeed, the socio-economic impact of landslides is often underestimated because this type of event, in many countries, is taken as a consequence of other triggering natural events, such as extreme precipitation, floods or earthquakes [2]. This underestimation also contributes to reducing the awareness and concern of both authorities and general public about landslide risk [3]. Moreover, as a consequence of climate change, existing scenarios predictions are indicating that the risk associated to landslides will keep growing in the near future. Owing to the increasing frequency and intensity of extreme weather events, existing civil structures, such as bridges, levees, dams, check dams and flood control structures are often exposed to solicitations that may significantly exceed those assumed in their original design. As a consequence, existing structures suffer serious demage, with a high possibility of leading to a complete loss of effectiveness and integrity. The scientific community has a duty to react and exploit the potential of cutting-edge research and technology to protect our structures, and therefore our lives, in case of exceptional weather-related natural disasters. In what follows, we focus on landslides, a term that is typically used to denote a wide range of mass movement phenomena, and we provide an overview of the most renowed classification schemes available in the literature (§1.1). Then, starting from Section 1.2, we restrict our attention to landslides of the flow type and discuss mathematical and numerical models that have proven to be reliable and powerful tools for simulating this type of mass movement. More specifically, we will see that Depth-Averaged Methods are used for the assessment of landslides mobility and the forecast of runout distance (§1.2.1), whereas three-dimensional methods are effective in improving the design and efficiency of risk mitigation structures, such as rigid and flexible barriers (§1.2.2). We provide only a brief overview of these two class of methods, as they do not represent the focus of this thesis. In Section 1.3 we describe Early Warning Syetems, i.e., the set of capacities needed to generate and disseminate timely warning information to people threatened by natural hazards, with the aim of reducing the possibility of harm or loss. In particular, Early Warning Systems based on the monitoring of acoustic emissions, i.e., transient, high-frequency, ground-generated stress waves, represent a recent and promising approach for the early detection of flow-like landslides (§1.3.1). Owing to several factors, including geometric spreading, material heretogeneity and inelastic behaviour, acoustic waves propagating on the ground suffer significant attenuation even at short distance from the source. Since wave attenuation represents

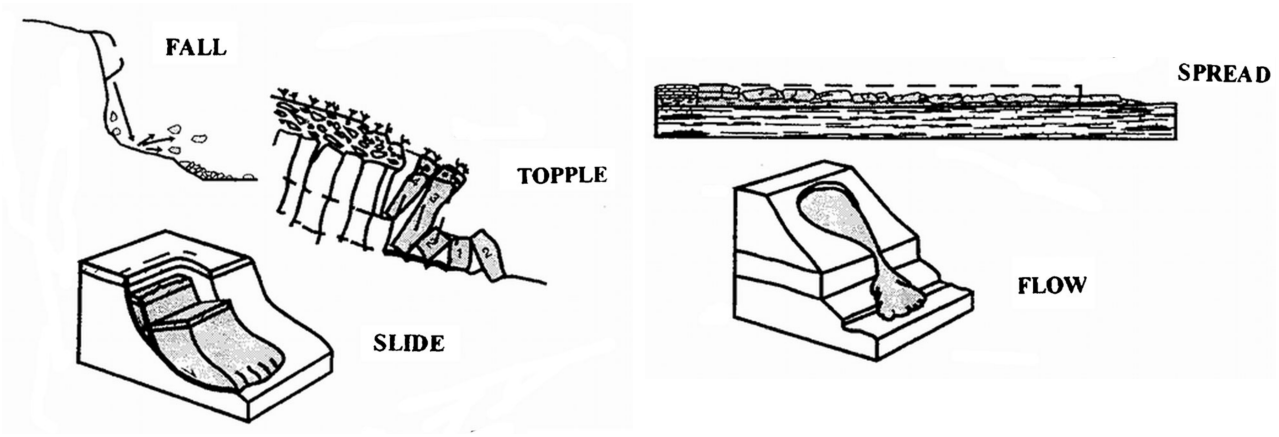


Figure 1.1: Type of landslide movements according to Varnes classifications [4, 5] (source [9]).

one of the major technical challenges hindering application of such Early Warning System, in this thesis we study how waves propagate in natural materials characterised by heterogeneous viscoelastic behaviour and develop numerical methods for the simulation of this phenomenon. In this regard, Section 1.4 provides a concise introduction to the theory of linear viscoelasticity, with a particular emphasis on the Kelvin-Voigt constitutive model, which is the model considered in this thesis. Then, in Section 1.4.1 we discuss the most popular numerical methods available in the scientific literature and used to simulate the propagation of waves in elastic and viscoelastic materials. Finally, in Section 1.5 we describe the scientific objectives of this thesis and in Section 1.5.2 we briefly summarize the content of each chapter.

1.1 Landslides Classification

The generic term *landslide* is typically used to denote a variety of different phenomena involving mass movement. Several classification schemes have been proposed and are available in the scientific literature since the second half of 20th century [4–9]. Varnes [4] provided a review of the whole range of earth movements that may be regarded as landslides and classified them according to the *types of movement* and *types of material* involved. In particular, the author used the term landslide to denote the *"downward and outward movement of slope-forming materials"*. The types of movement are divided into three main groups: *falls*, *slides* and *flows* (see Figure 1.1). A fourth group, called *complex slides*, is used to denote a combination of the other three types of movements. Materials are classified, for falls and slides, into bedrock and soils, while in the case of flows the unconsolidated material may consist of rock fragments, sand, silt, mixed rock/soil or plastic clay. Varnes [5] extended his own classification, proposed 20 years before, by including two other types of movement: *topples* and *spreads* (see Figure 1.1). Within this classification only two groups of materials are considered for all the types of movement: *bedrock* and *engineering soil*. Bedrock denotes hard or firm rock that was intact and in its natural place before the initiation of movement. Engineering soil includes any loose, unconsolidated or poorly cemented aggregate of solid particles, generally of natural mineral, rock or inorganic composition and either transported or residual, together with any interstitial gas or liquid. Soil is further divided into *debris* and *earth*. Debris refers to a soil that contains a significant proportion of coarse material, i.e., a material in which 20-80% of the fragments are larger than 2 mm in size and the remaining fragments are smaller than 2 mm. Earth denotes material in which about 80% or more of the fragments are smaller than 2 mm and includes a range of materials from nonplastic sand to highly plastic clay. The group of material used to describe a mass movement should refer to the material involved before the mass was displaced. For instance, the term "rock fall" means that the displacing mass was a rock mass at the initiation of the movement, although it may later have become debris. If the landslide is complex and the type of movement changes as it progresses, the material should be described at the beginning of each successive movement. For example, a rock-fall that was followed by the flow of the displaced material can be described as a "rock fall-debris

flow". Cruden and Varnes [6] used the term landslide to denote *"the movement of a mass of rock, debris or earth down a slope"*. They highlighted that the phenomena referred to as landslides are not limited either to the land or to sliding, as it is sometimes erroneously thought, but rather the word as it is used has a much more extensive meaning than its component parts suggest. Moreover, Cruden and Varnes proposed some modifications to the classification proposed by Varnes, in particular regarding the adopted naming convention. They suggested that, even though any mass movement could in principle be classified and described by using two nouns, the first describing the material and the second describing the type of movement (e.g., rock fall, debris flow), the name of a landslide can become more elaborate as more information about the movement becomes available. Therefore, they proposed to add a sequence of descriptors in front of the two-noun classification with the aim of providing a complete identification of the mass movement phenomenon. The recommended sequence of descriptors characterises first the *activity* and then the *movements* of the displacing mass. More specifically, the broad aspects defining the landslide activity are the *state*, which describes what is known about the timing of movements (active, reactivated, suspended and inactive), the *distribution*, which describes where the landslide is moving (advancing, retrogressive, widening, enlarging, confined, diminishing and moving) and the *style*, which indicates the manner in which different movements contribute to the landslide (complex, composite, multiple, successive, single). The description of the movements of the mass includes information about the *rate of movement* (extremely rapid, very rapid, rapid, moderate, slow, very slow and extremely slow), the *water content* (dry, moist, wet and very wet), the *material* (rock, earth and debris) and the *type of movement* (fall, topple, slide, spread and flow). Second or subsequent movements in complex or composite landslides can be described by repeating, as many times as necessary, the descriptors. Descriptors that are the same as those for the first movement, may then be dropped from the name. The classification of landslides proposed by Varnes [4, 5] and then extendend by Cruden and Varnes [6] had a great success in North America, where it has been widely adopted. On the other hand, in the United Kingdom, the established classification was the one proposed by Hutchinson [7], which focuses on failure and propagation mechanisms and uses the following characteristics of the landslide: material, morphology, water content, rate, and kinematics. An attempt to correlate Varnes and Hutchinson classifications for flow-like landslides was proposed by Hungr et al. [8], who tried to give more precise definition of some terms, thus making their usage less ambiguous, and to relate the North American terms to established terminology present in the United Kingdom, therefore providing way to translate terms between the two most widely used systems. Moreover, Hungr et al. [8] simplified the classification, showing that landslides phenomena can be usefully divided into a small number of classes, which preserve established concepts and, at the same time, highlight the most important attributes of landslides phenomena. This is achieved more easily using a typological, purpose-oriented classification, rather that a multi-dimensional taxonomy framework as the one introduced by Cruden and Varnes in [6]. Within this classification, the type of flow-like landslide is identified based on the material type, water content, presence of excess pore-pressure or liquefaction at the landslide source, presence of a defined recurrent path (channel) and deposition area (fan), velocity and peak discharge of the event. In the remaining part of this chapter we will discuss flow-like landslides and simply use the word *landslide* when not referring to a particular type.

1.2 Numerical Models for Flow-like Landslides

Coupled with laboratory experiments, field observations and historical records, the development and the numerical implementation of landslide models have became an essential part of risk analysis. Indeed, theoretical models and computer siulations have proven to be reliable and powerful tools in understanding the behaviour of gravity-driven geophysical mass movements on general complex three-dimensional terrain and in predicting key parameters, such as path movement, flow depth and velocity, runout distances and impact pressures, that are used for improving both the *risk assessment procedures* (hazard mappings) and the *design of mitigation structures*.

1.2.1 Depth-Average Models

As a matter of fact, the assessment of landslides mobility through reliable forecasts of potential runout distance (or accumulation zone) is an important step in estimating the extension of the hazardous areas caused by the debris flow and, as a consequence, in avoiding to make decisions that are exceedingly conservative or not conservative enough regarding the safety of an area. The models that are mainly used to describe the whole propagation path, from onset to runout, of a geophysical mass movement on a complex three-dimensional terrain are the so-called *depth-averaged models*. Within these models, the mass and momentum conservation equations are averaged throughout the depth of the moving mass, thus yielding governing equations in which the horizontal component of the velocity is constant along the direction orthogonal to the base surface where the material is moving. Savage and Hutter [10] have been the first to apply the theory of depth-averaging to the problem of debris flow modelling. In their seminal work, they analysed a very simple scenario in which a finite mass of granular material initially released from rest is moving down a rough inclined plane. The model proposed by Savage and Hutter [10] has been validated by comparing the results from the laboratory experiments reported in [11] with the numerical outcomes obtained by solving the continuous depth-averaged model using a Lagrangian Finite Difference scheme. The good agreement between the laboratory findings and the numerical predictions in terms of the propagation of the front and rear margins of the granular mass as well as the evolution of the shape of the depth profile has suggested that depth-averaged models could represent an effective tool in simulating the whole dynamics of real landslides and debris flows. As a consequence, the original formulation proposed in [10] has been generalized several times over the years with the aim of describing the dynamics of granular materials flowing over complex three-dimensional topographies [12–21]. Furthermore, having the possibility to rely on depth-averaged models, thus avoiding the full three-dimensional description of the flow dynamics, represents a notable advantage because of the reduced computational costs that are involved. In light of the numerous attractive features of these models, several numerical techniques have been proposed over the last three decades for the computation of approximate solutions of the depth-averaged equations of motion. For example, Hungr [22, 23] developed a model based on Lagrangian Finite Difference, Chen and Lee [24–26] used the Galerkin Finite Element Method, McDougall and Hungr [27] employed the Smoothed Particle Hydrodynamics (SPH) [28, 29], whereas Mangeney-Castelnau et al. [30], Pirulli [31–33] and the WSL Institute for Snow and Avalanche Research SLF [34–37] proposed numerical algorithms based on of the Finite Volume method. Most of the mentioned numerical models were validated by trying to replicate small-scale laboratory experiments involving several materials and problem configurations [19, 11] and all of them were used to back-analyse known real events by comparing numerical findings with field observations in terms of total displacement, distribution of deposit in the run-out area and movement velocity [22, 33, 38–41], showing how effective these models are and helping to improve the understanding of the complex dynamics of landslides and debris flows. The wide range of depth-averaged numerical models proposed to simulate the dynamics of complex geophysical mass movements with flow-like behaviour do not only differ by the numerical method used to discretise the equations of motion but also by the type of rheology employed to describe the material behaviour. In depth-averaged models, the complex rheology of the granular material is incorporated in a term describing the frictional stress that develops at the interface between the flowing material and the rough surface (bed or base). In the original model developed by Savage and Hutter, the base surface satisfies a Coulomb dry-friction law which defines the magnitude of the basal shear stress as the product between the normal basal pressure and a friction coefficient that is assumed to be constant. On the other hand, a Coulomb law employing a non-constant friction coefficient depending on both the Froude number and the thickness of the granular avalanche has been implemented in the numerical models proposed in [30, 42–45]. This type of friction law was first proposed by Pouliquen [46], who conducted a series of laboratory experiments whose results have shown that the assumption of constant basal friction angle fails for granular flows over rough bedrock in a range of inclination angles; in this range, the frictional force was able to balance the gravity force, indicating a shear rate dependence. Mangeney-Castelnau et al. [30] performed a series of simulations with the aim of comparing the behaviour of the Coulomb friction law when based on a constant or variable basal friction angle. The numerical outcomes have shown that the shape of the deposit strongly depends on the used friction law, thereby suggesting that

frictional effects may play a significant role in debris avalanche mechanics. Another rheology that is widely used is the Voellmy-Salm friction law [47–49], which was initially introduced for snow avalanches and subsequently employed also in the simulation of debris flow and landslides. This friction law splits the total basal stress into a velocity independent dry-Coulomb term and a velocity dependent *viscous* or *turbulent* friction term proportional to the square of the velocity; the former term dominates when the flow is close to stopping, the latter when the flow is running quickly. The validity of this friction law was also corroborated by the results of some laboratory experiments reported in [50]. A modified version of this rheology has been implemeneted in the numerical model developed by the WSL [34–37]. It includes a yield stress (cohesion) which takes into account the fact that many materials, like mud and snow, do not exhibit a simple linear relation between the shear stress and the normal stress.

1.2.2 Flexible Barriers and Three-dimensional Models

As we have already pointed out, the numerical modelling of debris flow dynamics is not only applied in risk assessment procedures that aims at estimating the location and extension of hazardous areas through the simulation of the motion of geophysical mass movements from initiation to runout, but it can also play a significant role in the design of efficients protection structures, such as rigid and flexible barriers. In particular, in the last decades, flexible net barriers have proven to be a really effective mitigation measure against debris flows events and a lot of research institutes as well as companies have been working on the development of their design and the improvement of their ability to withstand high intensity debris flow events. However, before being used for debris flows mitigation, flexible nets and cable barriers were being employed, already more than sixty years ago, as protective structures against alpine natural hazards. Indeed, according to [51], these structures were initially designed for torrent control and for protection against snow avalanches. Then, in the late 1950s, net barriers started to be used for rockfall protection after observing that nets installed for protection against snow avalanches were frequently exposed to rockfalls during the snow-free season and were able to withstand them successfully. Similarly, the idea of using flexible ring net barriers for protection against debris flows originated in the late 1990s by observing that some barriers originally built to mitigate rockfalls were also able to contain several rainfall-induced debris flows [51, 52]. This is possible because the ring net retains the coarse blocks and stones of the solid-fluid mixture and allows the dissolved mud to pass through with the liquid phase. The solid material is thereby stopped behind the net. Moreover, the remarkable advantage of this kind of protection structures during the retention process lies in the flexibility and the large deformation capacity of the net barrier itself. Indeed, peak forces, which would be produced in the case of an impact with a rigid structure, can be reduced by the deformation of the ring net and of other energy dissipating devices [53]. With flexible net barriers, the maximum load occurs when the barrier has reached its maximum deformation, while with rigid barriers, i.e., barriers that cannot deform on impact, the increase in load to maximum value takes place very rapidly since they lack the energy dissipation process provided by the deformation of individual components. Another advantage of ring-net barriers in comparison to traditional concrete rigid structures is that they form a light and flexible system that can easily be installed in hardly accessible regions. Following these observations, a lot of small-scale laboratory and real-scale flume tests have been conducted with the aim of evaluating the performance of ring net barriers to protect against debris flows [51, 54–59]. These experiments are certainly importants as, together with data obtained from the continuous monitoring of some sites where natural events are frequently observed, they provide a lot of information about the interaction between the impacting debris flow and the flexible barrier. Unfortunately, they are also really expensive and difficult to set-up. As a consequence, it is essential to also rely on numerical models that are able to accurately simulate this phenomenon and that can be used with the aim improving the understanding and the design of flexible barriers for debris flow mitigation. The depth-averaged models discussed before are unable to provide a reliable and accurate description of the impact mechanism of a mass of granular material on a (flexible) barrier. This is clearly a consequence of the nature of these models, which assume the horizontal velocity field to be constant throughout the depth of the moving mass. On the orther hand, numerical models based on the solution of the full *three-dimensional* governing equations are able to capture the complex evolution of the flow as well as the correct interaction with the soil or the structure in terms of both force and displacement.

Unfortunately, the solution of the three-dimensional equations also implies a higher complexity and computer power demand compared to depth-averaged models, thus limiting their usage to problems, like the one we are discussing, that require more accurate solutions. Owing to the complexity of the problem, several different approaches based on a wide range of numerical methods have been proposed and are available in the literature. Some of them are based on the classical Finite Element Method (FEM), which nowadays is the most known and widely used numerical method for performing simulations of solid mechanics and fluid dynamics problems in engineering. The good reputation of FEM is a consequence of the fact that it is a method with a long tradition and with a solid and well-established theory that has been developed over the years by many researchers all over the world. However, the classical FEM is not particularly suited for solving problems involving severe deformations such as the ones that we encounter when analysing the motion of a flowing granular material and its impact against a (flexible) barrier. In fact, these large deformations may result in an excessive mesh distortion and element entanglement which lead to numerical difficulties and thus loss of accuracy of the numerical solution. A possible solution to this issue has been proposed in [60–66], where the debris flow mass is treated as a continuum body discretised by Finite Elements and an Arbitrary Lagrangian-Eulerian (ALE, see [67]) formulation to handle the large deformations occurring during the flow process. However, the accurate simulation of the dynamics of flowing granular masses impacting on (flexible) structures nowadays mostly relies on the usage of particle-based methods, which have been proved to be particularly suited to address huge displacements and deformations. Among the methods belonging to this family, we mention the Discrete Element Method (DEM) [68–71], the Lattice Boltzmann Method (LBM) [71–73], the Smoothed Particle Hydrodynamics (SPH) [28, 29, 69, 74, 75], the Particle Finite Element Method (PFEM) [76–79] and the Material Point Method (MPM) [80–83]. In particular, the Material Point Method, represents one of the most popular methods for the simulation of landslides, debris flows and snow avalanches. This method, originally proposed by Sulsky et al. [84], combines the advantages of both mesh-free and mesh-based methods. Indeed, the physical domain is discretized by means of a set of Lagrangian moving particles, called material points, which carry the history-dependent variables. At each time step, the data stored on the material points is projected onto the nodes of a background grid, which is used to discretise and solve the governing equations by means of the Finite Element Method. Then, the updated nodal values are projected back to the material points and their position is updated. Finally, the background grid is reset. Therefore, the Material Point Method can be interpreted as a modified updated-Lagrangian Finite Element technique with moving integration points, i.e., the material points, while the background grid is fixed, thereby overcoming the mesh entanglement problem characterising the standard Lagrangian FEM approach. Furthermore, MPM also avoids other expensive procedures, such as neighbour search or re-meshing, yet preserving all the advantages of a FEM-based method. In general, particle-based methods are only employed to simulate the dynamics of debris flows, whereas all the structural components of the flexible barrier are usually modelled by means of Finite Elements. As a consequence, the interaction between the flexible barrier and the impacting debris flow is described by complex coupled approaches which require the implementation of suitable coupling boundary condition for the exchange of data (usually forces and displacements) at the interface between the two systems [85–88].

1.3 Early Warning Systems

Risk associated to gravitational mass movements can be mitigated not only by means of protection structures aiming at decreasing the vulnerability of elements at risk, but also by adopting the so-called *Early Warning Systems (EWSs)*. The United Nations International Strategy for Disaster Reduct (UNISDR) [89] defines Early warning systems as the set of capacities needed to generate and disseminate timely and meaningful warning information to enable individuals, communities and organizations threatened by a hazard to prepare and to act appropriately and in sufficient time to reduce the possibility of harm or loss. According to UNISDR, EWSs must comprise four elements:

i) *risk knowledge*, i.e., the undertaking of risk assessment through systematic collection and analysis of data;

ii) *monitoring and warning service*, i.e., the development systems capable of continuously monitoring hazard parameters and providing timely and accurate estimates of potential risks to communities, economies, and the environment;

iii) *dissemination and communication*, i.e., the transfer to people at risk of warnings containing useful and clear information through multiple communication channels;

iv) *response capability*, which ecompasses important factors such as coordination, good governance, formulation of effective action plans and promotion of public awareness and education.

Therefore, a reliable early warning system can be described as the interaction between both technical and social aspects, such as public statements, public response and education. A weakness or failure in any part of an EWS could result in the failure of the whole system. For example, accurate warnings will have no impact if the population is not prepared or if the alerts are received but not disseminated by the agencies receiving the messages. According to [90, 91], EWSs can be classified into alarm, warning and forecasting systems. *Alarm systems* detect specific parameters related to ongoing hazard events to automatically initiate an alarm (in the form of, e.g., red flashing lights accompanied by sirens) when the values of these parameters are above a predefined threshold. The accuracy of the prediction is high, but the lead time is short. *Warning systems* aim to detect significant changes in the environment, such as crack opening, presence of debris material and potential triggering events, before the actual disaster occurs and thus allow experts to analyse the situation and to implement appropriate intervention measures. The information provided by the data is lower in this early stage, but the lead time is extended. *Forecasting systems* predict the level of danger of a rapid mass movement process at regular intervals. In contrast with warning systems, the interpretation of data is not based on a threshold but is conducted on regular basis (e.g., daily) by experts who analyse sensor data and consult models to forecast the regional danger levels, which are then communicated in a bullettin. Regardless of the classification, experience has shown that an EWS must fullfill some criteria [92]: it must be easy to implement, comprhensible and manageable for people in charge of issuing warnings, redundant (i.e., the EWS must not depend on single sensors and transmission lines but must be based on a range of different installations), precise, independent in terms of electricity and data transfer (as it has work in remote regions), robust (i.e., able to resist the expected range of environmental conditions) and affordable in terms of price. During the last decades, early warning systems for weather-induced landslides have been increasingly adopted in different areas for the world, mainly because of the continuous development of new technologies for landslide monitoring and because of the lower economic costs and environmental impacts of these systems compared to structural risk mitigation measures [93]. In this framework, EWSs can be designed and employed at two different scales [94]: systems addressing a single landslides at slope scale are named as *local*, whereas systems operating over wide areas (e.g., a basin, a municipality, a region or a nation) and dealing with multiple landslides are referred to as *territorial*. The purpose of local systems is the temporary evacuation of people from areas where, at specific times, the risk level to which they are exposed is too high. They typically implement a network of instruments to monitor the variables most relevant for the type of landslide under surveillance, considering its nature and triggering factors. On the other hand, the purpose of territorial systems is to provide generalized warnings to authorities and the population when the probability of occurrence of multiple landslides over wide areas increases. Local systems are typically implemented as either alarm or warning systems, whereas territorial systems are generally used as either warning or forecasting systems. The range of environment parameters that are investigated and the range of techonologies used in current EWSs to collect data and monitor these parameters are very broad. In the case of weather-induced mass movements, two parameters are usually considered: *rainfall*, which is responsible for the triggering of these natural events and is especially employed in territorial systems, and *acoustic emissions*. This thesis will study and develop mathematical and numerical methods for analysing the latters, which will therefore be presented in more details in the next section.

1.3.1 Acoustic Emissions

A more recent and novel approach for predicting the onset of slides and for early detection of debris flow events is based on the usage of ground-generated *acoustic emissions* (AE). Acoustic emissions are

transient, high-frequency, stress waves generated by a rapid release of stored energy and propagating through the ground. Sources of acoustic emissions includes many small-scale mechanical failure events, such as the destruction of mechanical bonding agents (biological fibers, cemented grain contacts, plant roots, ice crystals), frictional sliding and rolling between soil grains and between soil particles and structural elements, redistribution of internal stresses or crack formation. Signals are generated at a high frequency because of the small size/scale of precursor failure events: tests with natural soils revealed characteristic frequency ranges between 1 and 100 kHz for acoustic emissions associated with failure [95]. Recent studies and advances in instrumentation have resulted in successful applications of acoustic emissions to detect and monitor soil slope instability [96–99]. In particular, since AE are actual precursors of slope failure events, significant acoustic activity can be detected even before the occurrence of measurable internal or surface displacements. Moreover, AE allows to detect debris flows in their initial stage by recording the ground vibration produced by the moving mass of water and debris. Acoustic emissions travelling through the medium are captured by instruments consisting of a waveguide that propagate the signal from its source in the soil to sensors that transform the pressure wave into an electrical signal. Signal processing then gives information about the mechanisms of deformation. A change in the signal properties towards more frequent events with high amplitudes indicates an acceleration in the movement of a slope, thus indicating that a full landslide failure is going to occur. The instrument can be set up to transmit data regularly to geotechnical experts for interpretation, or simply to alert the user when a pre-determined level of activity has been exceeded, thus highlighting the need for onsite investigation. The use of waveguides is necessary because of the significant attenuation that high-frequency waves suffer even at short distance from the source. Indeed, the attenuation of stress waves propagating through the natural media represents one of the major technical challenges hindering application of such early warning system. The strong wave attenuation may introduce ambiguity in the interpretation of the magnitude (severity) or may lead to loss of detection for events away from the sensor. Hence, there is the possibility that a microcrack event is measured as a large event if occurring close to the sensor and as a small event if far from the sensor (or may not be detected at all). Therefore, in addition to using instruments based on waveguides, practical usability is achieved by installing a dense network of sensors that enables localization of sources and thus the determination of initial energy released with each event [100]. Several factors are responsible for the attenuation of the acoustic waves propagating in natural media, including *geometric spreading*, which refers to the attenuation of the wave due to geometrical reduction in elastic energy density with distance from the source, material *heterogeneity*, which is responsible for signal scattering, and *inelastic material behaviour*, which refers to the fact that, in the majority of the cases, natural the materials through which waves propagate are not characterized by purely elastic mechanical behaviour but they also manifest viscous properties. For this reason, these materials are called viscoelastic materials. Viscoelastic attenuation and scattering effects are frequency dependent, being especially relevant for high frequency modes. It is therefore important to understand how waves propagates in viscoelastic materials and how waveguides can be used to propagate an high frequency signal from the source to the sensor. Then, in this thesis we will discuss the propagation of waves on linear viscoelastic heterogeneous materials, focusing on the numerical simulation these kind of phenomena; in particular, we will consider viscoelastic materials of *Kelvin-Voigt* type.

1.4 Linear Viscoelastic Materials

In the last decades, the modelling of wave propagation phenomena in both elastic and viscoelastic materials has been the focus of a growing interest across different areas of the scientific community, such as mathematics, geoscience and engineering. In particular, three-dimensional numerical simulations represent nowadays a really powerful and essential tool to study several problems arising at different scales and involving the propagation of waves. As suggested by the name, viscoelastic materials manifest by both elastic and viscous behaviour, the latter being responsible of a loss of mechanical energy when waves propagate through this type of materials. In general, such energy dissipation is reflected by the attenuation of the wave amplitude and in velocity dispersion. Therefore, it is of utmost importance to consider rhological models that are able to account for both dissipation and dispersion

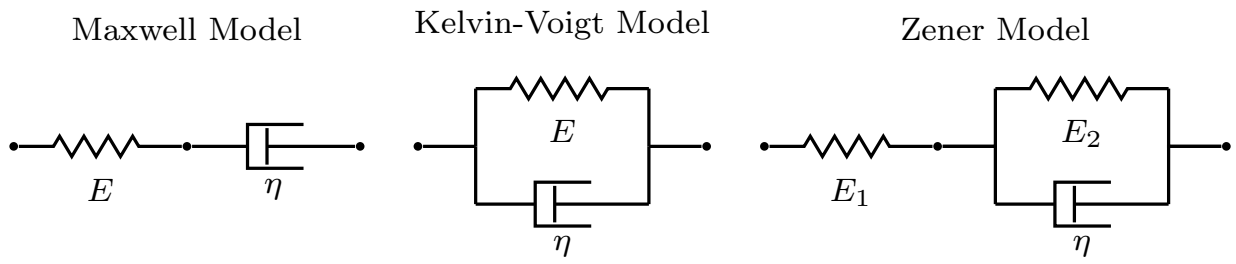


Figure 1.2: One-dimensional viscoelastic models represented in terms of mechanical systems. These systems are obtained by combining springs and dashpots in series and in parallel as in electrical circuits.

effects observed during wave propagation. In the framework of linear viscoelasticity [101–105], some of the most famous models describing the viscoelastic material behaviour are Maxwell, Kelvin-Voigt, Zener (or Standard-Linear-Solid) and Burgers models. In the one-dimensional case, these models can be described in terms of mechanical systems by combining weightless elastic springs and viscous dashpots in series and/or in parallel as in electrical circuits (see Figure 1.2). The springs are responsible for the elastic behaviour of the materials and are modelled by Hooke's law $\boldsymbol{\sigma}_{\text{el}} = E\boldsymbol{\varepsilon}$, which relates the elastic stress $\boldsymbol{\sigma}_{\text{el}}$ to the strain $\boldsymbol{\varepsilon}$ through the Young modulus E, whereas the dashpots are responsible for the viscous behaviour and are governed by Newton's Law $\boldsymbol{\sigma}_{\text{vi}} = \eta\dot{\boldsymbol{\varepsilon}}$, which relates the viscous stress $\boldsymbol{\sigma}_{\text{vi}}$ to the strain rate $\dot{\boldsymbol{\varepsilon}}$ through the dynamic viscosity η. The different number and arrangement of mechanical elements used to define the system results in constitutive relations that are capable of describing the viscoelastic behaviour of different materials. In this work we consider the Kelvin-Voigt model, which is obtained by connecting a spring and a dashpot in parallel. These are subjected to the same strain and to a total stress which is given by the sum of two contribution, i.e., $\boldsymbol{\sigma} = \boldsymbol{\sigma}_{\text{el}} + \boldsymbol{\sigma}_{\text{vi}}$, the elastic one ($\boldsymbol{\sigma}_{\text{el}}$) due to the spring and the viscous one ($\boldsymbol{\sigma}_{\text{vi}}$) due to the dashpot. The two and three-dimensional extension of this model has been proposed and solved numerically for the first time by Carcione et al. [106], who defined the stress tensor as the sum of an linear elastic stress tensor and a viscous stress tensor. This is the constitutive model that will be combined with the Cauchy equations of motion in the present work. Despite its simple definition, the Kelvin-Voigt model has been widely adopted and studied over the years, with many reasearchers also considering non-linear generalization of the model. For example, in [107] the strain and the symmetric part of the velocity gradient are expressed using non-linear functions of the stress and the possibility of using implicit constitutive relations between the stress and the strain for both the elastic and viscous components of the material is also considered. Another non-linear generalization is proposed in [108], where the Cauchy stress depends non-linearly on the linearized strain while the viscous part of the Cauchy stress is expressed through a nonlinear function of the symmetric part of the velocity gradient. The Kelvin-Voigt model, as well as the other simple mechanical models mentioned above, have been also generalized by introducing operators of fractional calculus into the stress-strain constitutive relationship [109, 110]. More specifically, the usage of fractional calculus within the theory of linear viscoelasticity leads to generalized classical mechanical models in which the basic Newton viscous element (i.e., the dashpot) is replaced by the more general Scott-Blair element [111, 112], sometimes also referred to as pot, which is characterized by a stress that is proportional to the fractional derivative of the strain. Scott-Blair [111, 112] has been the first to propose a framework based on fractional order temporal derivatives to simultaneously model the observations made by Nutting [113], who reported that the stress relaxation phenomenon could be modelled by fractional powers of time, and by Gemant [114], who analysed frequency dependence. Another contribution based on fractional calculus is given by Slonimsky [115], who provided an example of the dynamic behaviour of a linear polymer by defining a viscoelastic strain behaviour that is intermediate between the strain of a Hookean elastic body and a Kelvin-Voigt viscoelastic body. More recently, Wang [116, 117] proposed a modified version of Slonimsky model by including a combining factor that ensures as limiting behaviours the purely elastic and the Kelvin-Voigt viscoelastic ones.

1.4.1 Numerical Methods for Wave Propagation in Viscoelastic Materials

Numerical simulations of viscoelastic wave propagation have been conducted over the years using a wide range of numerical methods, including finite differences, pseudospectral methods, finite elements and spectral elements methods. An overview of all these methods within the framework of wave propagation for computational seismology is given in [118]. Historically, the first numerical method to be employed for the solution of the acustic, elastic and viscoelastic wave equation has been the finite difference (FD) method [119, 120]. Owing to its computational efficiency, small memory requirement, and easy implementation, the finite difference method became extremely popular and a widely adopted tool for the computation of synthetic seismograms. The first application of the finite difference method to elastic wave propagation is due to Aterman and Karal [121], who provided numerical solutions to the problem of a layered half-space with a buried point source emitting a compressional pulse (a version of the so-called Lamb's Problem [122]). Because of the axial symmetry of the problem, the displacement equation of motions were solved in cylindrical coordinates. Then, Boore [123] used the FD method to simulate Love waves and to solve various wave-propagation problems possessing analytical solutions. Few years later, Alford [124] examined the accuracy of finite difference methods for the treatment of geometries containing sharp corners by comparing the solution of the acoustic wave equation obtained by finite difference methods to that obtained by classical analytical methods. Similar investigations in the case of elastic waves were carried out by Kelly et al. [125], who also discussed several numerical aspects such as grid dispersion, artificial reflections from the edge of the model, and choice of spatial and temporal sampling increments. In the same year, Madariaga [126, 127] proposed a FD scheme based on staggered grids and on a velocity-stress formulation to study crack propagation. This approach have been later extended to simulate SH (Shear Horizontal) [128] and P-SV (Pressure-Shear Vertical) [129] wave propagation in generally heterogeneous media, gaining considerable popularity in the FD community. A drawback of the finite difference method is that it often comes with significant numerical dispersion and anisotropy, which cause the wave phase speed to become a function of the discretization interval, especially when modeling surface waves [130]. To mitigate this issue and improve the accuracy of the solution, high-order schemes have been then introduced for the scalar wave equation [131] and for the computation of waves in an elastic (and possibly heterogeneous) 2D material [132, 133]. A detailed overview of the dispersion and stability properties of a 3D fourth-order FD scheme based on the velocity-stress formulation is given in [134]. Other major challenges for FD methods are related to the treatment of complicated domains and material interfaces and to the implementation of free-surface or absorbing boundary conditions. Several suitable techniques have been developed in order to account for a general non-flat and highly irregular surface topography in [133, 135–138] and to deal with material discontinuities not aligned with the coordinate axes [139–143]. More recently, the FD method has been also employed for the simulation of waves propagating in viscoelastic materials [138, 137, 141, 144]. In the case of Kelvin-Voigt rheology, Sadovskii et al. [145] proposed a numerical algorithm based of Ivanov's [146] method of constructing finite difference schemes with predetermined artificial energy dissipation. In [147], an explicit and recursive second-order finite difference scheme is employed to simulate SH waves, while in [148] the generalized finite difference method is used for the simulation of the propagation of P-SV and SH waves on complex geometries. Wang et al. [149] used 16th-order staggered finite difference scheme to solve the viscoelastic wave equations written in a velocity-stress formulation and based on both Kelvin-Voigt and Zener constitutive relations with Nearly Perfectly Matched Layer absorbing boundary conditions. Another numerical methods that has been extensively used since the early eighties for the simulation of acoustic, elastic and viscoelastic wave propagation phenomena is the pseudospectral (or collocation) method. This method belongs to the class of spectral methods, which also includes the Tau method and the spectral-Galerkin method [150–155]. Spectral methods are all based on the idea of approximating the solution of a partial differential equation by using a truncated series of global basis functions, which are usually trigonometric functions or orthogonal polynomials of Jacobi type, allowing to obtain exponential convergence in the case of particularly smooth solutions. Initially, pseudospectral schemes were based on the approximation of the solution through a truncated Fourier series, the coefficients of the series expansion being computed by requiring that the strong formulation of the PDE is exactly satisfied at the so-called collocation points, in this case defined by equidistant sampling points, where spatial derivatives are calculated by means of

the Fast Fourier Transform (FFT). Fourier-based pseudospectral method has been firstly applied to hyperbolic equations in [156, 157]. Subsequently, it has been used to simulate seismic acoustic wave propagation in [158, 159] and has been later extended to the elastic case [160, 161], becoming the first numerical method after finite differences to be massively employed in the context of computational seismology. The pseudospectral method gained a lot of popularity as a consequence of the fact that, compared to finite difference schemes, it requires fewer grid points per wavelength (thus implying memory efficiency) and it produces a high order solution with less numerical dispersion and no numerical anisotropy. Moreover, in pseudospectral methods staggered grids are not used, meaning that all the fields are defined at the same grid locations. The usage of Fourier functions for the series expansion of the numerical solution implies periodicity at the boundaries of the physical domain. However, most of the real-world applications require the implementation of more general boundary conditions like, e.g., free-surface or non-reflecting boundary conditions. This issue has been overcome by replacing Fourier basis with other basis functions having similar interpolation behaviour, but with non-periodic properties, such as the Chebyshev polynomials [162–167]. Even in this case, the spatial derivatives are computed at the collocation points, the Gauss-Chebyshev-Lobatto points, by means of the Fast Fourier Transform (FFT). However, the Gauss-Chebyshev-Lobatto collocation points are not equispaced and densify towards the boundaries of the domain. As a consequence, the grid distance near the boundary is responsible for the global simulation time step, and very small time steps are required when using explicit time schemes [168]. A possible strategy to avoid this issue has been proposed by Carcione and Wang [165] and consists of stretching the grids near the boundaries by a coordinate transformation. A coordinate transformation based on grid stretching has also been proposed to accurately model curved internal interfaces and surface topography in the case of acoustic and elastic wave-propagation problems [169, 170]. Another issue related to the pseudospectral method is that it cannot be efficiently implemented on parallel computers with distributed memory architectures. Indeed, the derivative operations of pseudospectral methods are of a global nature, which means that every point on a spatial grid contributes to the computation of the derivative. Therefore, the method requires global communication and, since communication is usually the bottleneck, efficient and scalable parallelization of pseudospectral methods is a very difficult task. The pseudospectral method has also been used to simulate waves propagating in a Kelvin-Voigt viscoelastic material. Carcione et al. [106] employed a velocity-stress formulation and used the Fourier and Chebyshev methods to compute the spatial derivatives along the horizontal and vertical directions, respectively. The same approach has been proposed in [171] for simulating synthetic seismograms generated by multipole borehole sources in an axisymmetric medium. Then, Wang et al. [149] used a Fourier pseudospectral method in combination with Nearly Perfectly Matched Layer absorbing boundary conditions and compared the numerical results with the ones obtained using a high order FD scheme. Both the Finite Difference method and the pseudospectral method employs the strong formulation of the Partial Differential Equation and are implemented in terms of the physical space values of the unknown function on a grid of points. On the other hand, the spectral-Galerkin method relies on the weak formulation of the boundary value problem, wherein the basis functions (usually trigonometric functions or orthogonal polynomials) are of modal type. The use of modal basis functions implies that, unlike the pseudospectral method, the coefficients that allows to write the approximate solution as a linear combination of basis functions do not represent the values of the solution at specific points of the computational domain. However, there is also a version of the pure spectral-Galerkin method, also known as Galerkin with Numerical Integration (G-NI), which aims at preserving the advantages of collocation methods by representing the approximate solution in the physical space through its values at a selected set of nodes using nodal basis functions. In the G-NI method, these nodes usually are the Gauss-Legendre-Lobatto (GLL) nodes and the basis functions are Lagrange polynomials defined at these points. Then, the integrals appearing in the weak formulation of the problem are efficiently approximated by means of quadrature formulas. In particular, the usage of the same set of GLL nodes for both the definition of the Lagrangian basis functions and for the computation of the intgrals leads to a diagonal mass matrix. This clearly represents an advantage when dealing with time-dependent problems implementing an explicit time scheme, as the inversion of the mass matrix can be avoided, thus making the algorithm computationally more efficient. A drawback of the spectral-Galerkin method is that it is difficult to apply

to problems defined on complex geometries. On the other hand, the classical Finite Element Method is well suited to deal with this kind of problems as it relies on a discretisation of the computational domain with, e.g., triangles or quadrilaterals in 2D and tetrahedra or hexahedra in 3D. However, the usage low-order basis functions, which is common in classical FEM, results in significant numerical dispersion [130]. The Spectral Element Method (SEM) overcomes these issues by combining the high accuracy of spectral methods with the ability of the classical Finite Element Method to handle complex geometries and sharp material interfaces. The Spectral Element Method has been firstly proposed in the context of Computational Fluid Dynamics by Patera [172, 173] and subsequently applied to solve the acoustic wave equation [174] and the elastodynamics equations in [175–179]. A version of the Spectral Element Method that uses numerical integration (SEM-NI) has been proposed as well and, as for the G-NI, has the advantage of being charactersized by a diagonal mass matrix. For all the aforementioned reasons, the SEM-NI probably represents nowadays the most successful and adopted tool in computational seismology, in particular when dealing with large scale applications [180, 181].

1.5 Scientific Objectives of the Thesis

In this thesis we investigate the propagation of waves on linear viscoelastic materials of Kelvin-Voigt type. The system of Partial Differential Equations governing the propagation of waves has been obtained by combining the Cauchy momentum conservation equations with the Kelvin-Voigt constitutive law proposed in [106]. The equations of motion have been reduced from second order to first order in time by doubling the solution variables, that are the displacement and velocity fields. Then, existence, uniqueness and regularity results for such a problem have been obtained by relying on the standard theory of linear evolution equations in Hilbert spaces [182]. The weak formulation has been discretised in space by employing both the Linear Lagrangian Finite Element Method and a spectral approach. In particular, the spectral approach that we propose in the present work shares certain similarities with both the global spectral-Galerkin method and the Spectral Element Method. Indeed, when simulating waves propagating in homogeneous materials, we employ a spectral-Galerkin method wherein the numerical solution to be sought is expressed through the expansion of global basis functions defined in the whole domain. On the other hand, in the case of layered heterogeneous material, we assume that the domain can be partitioned into a set of several elements (or subdomains), each one associated to a different material, and we define a different set of basis functions for each of them. However, in contrast with the typical approach employed in the Spectral Element Method, which relies on nodal Lagrangian basis functions defined at the GLL points, we consider a *modal* set of basis functions, which are suitable linear combinations of either Legendre or Chebyshev polynomials. In the heterogeneous case, two different strategies have been considered for enforcing the continuity of the solution across the material interfaces, thus deriving globally continuous basis functions over the whole domain. The first approach consists of using boundary-adapted polynomials defined in such a way they match at the interfaces, thereby providing a straightforward definition of globally continuous basis. The second strategy enforces weak L^2 continuity of the local basis at the material interfaces, thus using an approach that is analogous to the one adopted in the Mortar Element Method (MEM) [183]. It is worth emphasizing that, within this second approach, different resolutions (i.e, polynomial degrees) can be considered on subdomain (material) interfaces. Compared to other spectral (element) methods relying on approximated numerical integration for the computation of the integrals appearing into the weak formulation of the initial-boundary value problem (in particular those related to the components of the mass matrix), in the proposed numerical algorithm we employ quadrature formulas only when closed form expressions are not available and, in any case, we do not perform any kind of approximation, thus always computing the integrals exactly (up to machine precision). Finally, notice that, unlike the other approaches based on the pseudospectral method and previously used to simulate waves propagating in Kelvin-Voigt materials, the spectral method that we consider here does not need to define any grid of points. The system of Ordinary Differential Equations arising from the Galerkin discretisation in space of the weak formulation has been solved either by means of standard numerical time-stepping integration schemes or by exact integration via eigenvalue decomposition. The exact integration clearly has the remarkable advantage of being able to compute the full solution at any time without introducing

any additional approximation error when solving the system of ODEs. However, this strategy is limited to forcing vectors that can be written as the product between a function depending on space and a function depending on time and it also requires to compute the spectral decomposition of a matrix that might be particularly large and dense, thus imposing a significant computational burden. The numerical methods discussed in this work have been used to simulate the propagation of waves in possibly heterogeneous viscoelastic Kelvin-Voigt materials characterized by a layered geometry. We address four settings, which differ by either the ambient dimension in which they are posed ($\mathbb{R}^d$, $d = 1, 2, 3$) or the type of system coordinates that is used (Cartesian/cylindrical). In particular, we consider the one-dimensional problem, the two-dimensional problem with Cartesian coordinates and both the axisymmetric and three-dimensional problem with cylindrical coordinates. The implemented numerical algorithms have been validated by solving some problems with manufactured solution and the convergence has been investigated by experimentally obtaining the same convergence rate suggested by the theory. Numerical simulations of other test cases involving the propagation of waves generated by the action of a point load have also been reported.

1.5.1 Contribution of the Thesis

Summarizing, the main contributions given by this thesis are the following.

- Theoretical analyisis of the second order linear evolution equations governing the propagation of waves on linear viscoelastic Kelvin-Voigt materials. Existence and uniqueness of the solution is proved by means of standard results about the theory of Partial Differential Equations in Hilbert Spaces.

- Computation of the numerical solution of the initial-boundary value problem defined in $\Omega \subset \mathbb{R}^d$, where $d = 1, 2$, by discretising the weak formulation in space by means of the Linear Lagrangian Finite Element Method. Both homogeneous and layered heterogeneous materials are considered.

- Computation of the numerical solution of the initial-boundary value problem defined in $\Omega \subset \mathbb{R}^d$, where $d = 1, 2, 3$, by means of a spectral-Galerkin approach. This numerical method is used to solve problems defined using Cartesian coordinates (in $\mathbb{R}^2$) and cylindrical coordinates (in $\mathbb{R}^2$), with and without the assumption of axial symmetry of the solution. Both homogeneous and layered heterogeneous materials are considered. In the former case, global basis functions are employed, whereas in the latter the proposed spectral approach considers a partition of the domain in material subdomains, i.e., each element is associated to a different material. Within each element, modal basis functions not requiring a grid of points are defined.

- Definition of globally continuous basis functions by means of an alternative approach which enforces weak L^2 continuity of the local basis functions at the material interfaces.

1.5.2 Structure of the Thesis

The thesis is divided into two parts. Part I contains some preliminary results needed to understand Part II and has the following structure.

- Chapter 2 contains a brief introduction to the theory of linear viscoelasticity and to the propagation of waves on both elastic and viscoelastic materials. More precisely, we start by presenting the integral and differential form of the constitutive laws for linear and isotropic viscoelastic materials and then we discuss the difference between viscoelastic fluids and solids by introducing the concepts of creep and relaxation. Dynamic loading and complex modulus are also presented. We show that, in the one-dimensional setting, constitutive equations for linear viscoelastic materials are equivalent to mechanical models consisting of weightless springs and dashpots connected in series and parallel as in electrical circuits. Moreover, we present the main properties of some of the most famous models, namely the Maxwell model, the Kelvin-Voigt model and the Zener model. The last part of this chapter is devoted to the introduction of the equations governing the propagation of waves on both elastic and viscoelastic materials, with a particular focus on

the Kelvin-Voigt constitutive model and to the presentation of Lamb's problem, which is used in Chapter 6 to test the implementation of the proposed numerical approach.

- Chapter 3 contains some useful results on the solution of Partial Differential Equations on Hilbert spaces. We first introduce some preliminary definitions and results on elliptic problems and subsequently we present first and second order linear evolution equations. The theory introduced in this Chapter is applied in Chapter 5 to prove the existence and uniqueness of the solution of the second order linear evolution equation governing the propagation of waves on linear viscoelastic materials of Kelvin-Voigt type.

- Chapter 4 contains the main results on Legendre and Chebyshev polynomials that are used in Chapter 6 for the implementation of the Spectral/Spectral Element Method. In particular, boundary-adapted polynomials based on linear combinations of these two families of one-dimensional orthogonal polynomials are introduced and the computation of matrices involving their product (or the product of their derivatives) is addressed. Then, two-dimensional boundary-adapted polynomial basis functions obtained by tensor-product of two one-dimensional bases are discussed. Finally, some results on polynomial approximation theory used to derive error estimates are also presented.

Part II contains the main results of this thesis and it has the following structure

- In Chapter 5 we introduce and analyse the initial-boundary value (IBV) problem describing the propagation of waves on linear viscoelastic materials of Kelvin-Voigt type. In particular, we show how to deal with non-homogeneous time dependent Dirichlet boundary conditions and we discuss how to reduce the problem from second-order to first-order in time by introducing the velocity as additional unknown. Then, we derive the weak formulation of the system of Partial Differential Equations and show how to prove existence and uniqueness of the solution by relying on the standard theory of linear evolution equations on Hilbert spaces presented in Chapter 3. Subsequently, we introduce the Galerkin discretisation in space of the weak formulation and start to derive some prelimary results about the covergence of the numerical solution. Finally, we address the solution of the resulting system of Ordinary Differential Equations by considering two strategies, one based on exact integration via eigenvalue decomposition and the other based on time-stepping schemes.

- In Chapter 6 we compute the numerical solution of the problem introduced in Chapter 5, provide implementation details and present some numerical results. In particular, we address four different problems, which differ by either the ambient dimension in which they are defined ($\mathbb{R}^d$, $d = 1, 2, 3$) or the type of system coordinates that is used (Cartesian/cylindrical). We start with the one and two-dimensional settings, the latter described by means of Cartesian coordinates; in both cases we apply both the Spectral/Spectral Element Method and the Finite Element Method. Then, we consider the axisymmetric and full three-dimensional settings, both defined by means of cylindrical coordinates; in this case the numerical solution is computed by applying the Spectral/Spectral Element Method.

Finally, in Chapter 7 some conclusions are drawn.

Part I

Background and Preliminary Results

Chapter 2

Linear Viscoelasticity and Wave Propagation

This Chapter is divided into two sections: Section 2.1 introduces the theory of linear viscoelasticity, while Section 2.2 discusses the propagation of waves on both elastic and viscoelastic materials. More precisely, in Section 2.1, we start by presenting the integral (§2.1.1) and differential (§2.1.2) form of constitutive laws for linear and isotropic viscoelastic materials and then we discuss the difference between viscoelastic fluids and solids (§2.1.3) by introducing the concepts of creep and relaxation. Dynamic loading and complex modulus are also presented in Section 2.1.4. In Section 2.1.5, we show that, in the one-dimensional setting, constitutive equations for linear viscoelastic materials are equivalent to mechanical models consisting of weightless springs and dashpots connected in series and parallel as in electrical circuits and we describe the main properties of some of the most famous models (Maxwell, Kelvin-Voigt, Zener). In Section 2.2, we begin by presenting the Partial Differential Equations governing wave propagation phenomena in both the one-dimensional and multi-dimensional settings (§2.2.1). These equations are applied to both elastic and linear viscoelastic materials, with a particular focus on Kelvin-Voigt materials. Indeed, we recall that the analysis and the numerical solution of the Partial Differential Equations governing the propagation of waves in viscoelastic Kelvin-Voigt materials will be the subject of Part II of this thesis. Furthermore, in Section 2.2.1, we also introduce the notions of phase velocity, attenuation factor and dissipation factor and, in the multi-dimensional framework, we discuss the difference between pressure and shear waves. In Section 2.2.2 we present the so-called Lamb's problem, which is one of the benchmark problems that will be considered in Chapter 6.

2.1 Linear Viscoelasticity

Many materials, such as plastics, wood, natural and synthetic fibers, concrete and metals at high temperatures, exhibit a mechanical behaviour that is intermediate between the elastic and the viscous one. Consequently, these materials cannot be adequately described using the well-known classical theories of *elasticity* and *viscosity*. It is therefore necessary to develop a more general theory that is capable of modelling the behaviour of these materials, also known as *viscoelastic materials*, which possess both an elastic and a viscous component and that are characterised by a time-dependent stress-strain constitutive relation. The intermediate behaviour of viscoelastic materials is exemplified by their capability of storing and dissipating mechanical energy. Therefore, hysteresis is observed in the stress-strain curve, with the area of the loop being equal to the energy lost (dissipated) during the loading-unloading cycle. This behaviour cannot clearly be described by either any elasticity or viscosity theory as it combines features of each. Indeed, purely elastic materials are able to store mechanical energy without dissipating it, whereas Newtonian viscous fluids in a nonhydrostatic stress state are able to dissipate energy without storing it. Material properties can also be characterized experimentally through simple laboratory tests. In particular, when dealing with viscoelastic materials, mechanical characterization is obtained by observing the time dependency of the material response when a stress or strain is suddenly applied and held constant thereafter. For example, when a constant load is

applied, it has been observed that elastic materials respond instantaneously with a state of deformation that remains constant, whereas Newtonian viscous fluids respond with a steady flow process. Then, viscoelastic materials exhibit an instantaneous deformation followed by a flow process which may or may not be limited in magnitude as time grows. A material manifesting this behaviour is said to display both instantaneous elasticity and creep effects. These two possible behaviours of the deformation of a viscoelastic material over time allow to distinguish between viscoelastic solids and fluids. More specifically, if the deformation is limited in time, the viscoelastic material is referred to as a *viscoelastic solid*. Conversely, if the deformation increases indefinitely, the viscoelastic material is considererd a *viscoelastic fluid*. Furthermore, upon unloading, viscoelastic materials display an instantaneous elastic partial recovery followed by an anelastic recovery at decreasing rate that may or may not be complete depending again on whether the viscoelastic materials is a solid or a fluid, respectively. On the other hand, when a deformation is suddenly applied and held constant, viscoelastic materials exhibit the so-called *relaxation of stress*, i.e., the stress is observed to decrease over time until it goes to zero (viscoelastic fluids) or it reaches a limit value (viscoelastic solids). Another important property of viscoelastic materials is that they are not simply characterized by a time-dependent behaviour, but they also possess a memory effect. This means that, in the case the stress is speciefied, the material deformation response is determined by the complete history of stress and not only by the current state. However, the strength of the dependence on the past is greater for more recent events and decreases as they become more remote in time (fading memory). Similarly, it has been observed that, if one considers the deformation as being specified, the current stress depends upon the entire past history of deformation. The theory of viscoelasticity has been developed starting from the nineteenth century with the contribution of many eminent scientists, including Maxwell [184], who derived a mechanical contitutive model for viscoelasticity (later named after him) while he was working on the theory of gases and used this model for calculating the viscosity of a gas. Some years later, Kelvin and Voigt [185] independently derived another mechanical model for linear viscoelasticity. Subsequently, Boltzmann [186] proposed the general hereditary integral form of the linear viscoelastic constitutive relations for isotropic bodies, while Volterra [187–189] developed the general anisotropic form and further extended the theory to the modern formulation of non-linear viscoelasticity. The reasearch in the field of viscoelasticity has further increased in the twentieth century, when synthetic polymers have started to be engineered and used at large scale in a variety of applications. The viscoelasticity theory that is discussed here is mainly based on the comprehensive surveys [101–105] and it holds only for infinitesimal displacements and deformations. In this framework, the constitutive equation to be sought is the one relating the Cauchy stress tensor $\boldsymbol{\sigma}$ and the strain tensor $\boldsymbol{\varepsilon}$. In particular, this relationship is assumed to be linear, i.e., the stress is given as a linear functional of the strain. For this reason, the theory that is presentd here is also referred to as *linear viscoelasticity theory*. In this context, the linearity property of the theory is also called *Boltzmann Superposition Principle*, and it states that the sum of the stress responses resulting from different strain inputs acting separately is equal to the stress response resulting from the combined strain inputs. We also require the constitutive relation to be local, which means that the stress at a certain position depends only on the strain at that position, thus excluding "action at a distance" forces. Moreover, for the sake of simplicity, we only consider spatially homogeneous materials, thereby completely neglecting the dependence of $\boldsymbol{\sigma}_{ij}$ and $\boldsymbol{\varepsilon}_{ij}$ upon x, and we restrict our study to non-aging materials, i.e., materials whose mechanical properties do not change over time. The linear viscoelasticity theory that we discuss is therefore a simplified model based on specific assumptions and, as such, it cannot be always employed. Consequently, in situations where the linear constitutive equations yield only a poor approximation of the actual behaviour of the material, a nonlinear viscoelastic theory needs to be taken into account. Furthermore, we shall also neglect the thermal effects, but it is worth empasizing that they might also be necessary depending on the problem we are dealing with. For the presentation of a far more complex and general theory of viscoelasticity, which considers both the nonlinear and thermal contributions, we refer to, e.g., [103, 190–195].

2.1.1 Integral Form of Viscoelastic Constitutive Equations

Given the assumptions stated in the introduction, the theory of linear viscoelasticity is based on the *Principle of Causality*, which affirms that the current value of the components of the stess tensor

depends not only upon the present value of the components of the strain tensor, but also on their complete past history. More formally, assuming that the components of the strain tensor are continuous, the Principle of Causality is expressed using the Stieltjes convolution, that is

$$\boldsymbol{\sigma}_{ij}(t) = \int_0^{\infty} \boldsymbol{\varepsilon}_{kl}(t-s)\, dG_{ijkl}(s), \tag{2.1}$$

where the integrating function $G_{ijkl}(t)$ is a fourth-order tensor such that $G_{ijkl}(t) = 0$ for $-\infty < t < 0$ and with each component being of bounded variation in every closed subinterval of $-\infty < t < \infty$. The functions $G_{ijkl}(t)$ describes the mechanical properties of the material and are termed *relaxation functions*. Integrals over the history of strain, as the one in equation (2.1), are sometimes referred to as hereditary integrals and materials whose contitutive relations contain such integrals are described as having memory. It is worth highlighting that the constitutive equation (2.1) is independent of any shifts in the time scale. In other words, this means that the mechanical properties of the material do not vary with time, at least over the timescale of interest. This behaviour is also known as *time translational invariance*. Moreover, it is also easy to see that the symmetry of the stress and strain tensors yields the following relations:

$$G_{ijkl}(t) = G_{jikl}(t) = G_{ijlk}(t).$$

Now, assuming thet $\boldsymbol{\varepsilon}_{ij}(t) = 0$ for $t < 0$ and that G_{ijkl} and its first time derivative are continuous in the interval $0 \leq t < \infty$, it can be shown that equation (2.1) can be written in the following equivalent form:

$$\boldsymbol{\sigma}_{ij}(t) = G_{ijkl}(0)\boldsymbol{\varepsilon}_{kl}(t) + \int_0^t \boldsymbol{\varepsilon}_{kl}(t-s)\frac{dG_{ijkl}(s)}{ds}\, ds. \tag{2.2}$$

If the hereditary integral is not present in equation (2.2), it is easy to see that the constitutive relation reduces to the well known Hooke's Law defining elastic materials. Another equivalent form of the stress-strain ralation can be obtained from (2.2) by performing the change of variable $\tau = t - s$ and using integration by parts to obtain

$$\boldsymbol{\sigma}_{ij}(t) = \int_0^t G_{ijkl}(t-\tau)\frac{d\boldsymbol{\varepsilon}_{kl}(\tau)}{d\tau}\, d\tau. \tag{2.3}$$

Until this point, the components of the strain tensor $\boldsymbol{\varepsilon}_{kl}(t)$ have been assumed to be continuous functions of time. However, in the general case in which the strain histories are discontinuous in $t = 0$, [103] have shown that equation (2.3) can be generalized to

$$\boldsymbol{\sigma}_{ij}(t) = G_{ijkl}(t)\boldsymbol{\varepsilon}_{kl}(0) + \int_0^t G_{ijkl}(t-\tau)\frac{d\boldsymbol{\varepsilon}_{kl}(\tau)}{d\tau}\, d\tau. \tag{2.4}$$

These stress-strain relations can also be considered to be the formulation of Boltzmann's superposition principle such that the current stress is determined by the superposition of the reposnses to the complete spectrum of increments of strain. An alternative form of the stress-strain relationship can be obtained by reversing the role of the stress and the strain, namely, the current strain is now determined by the current value and past history of stress:

$$\boldsymbol{\varepsilon}_{ij}(t) = \int_{-\infty}^t J_{ijkl}(t-\tau)\frac{d\boldsymbol{\sigma}_{kl}(t)}{d\tau}\, d\tau,$$

where

$$J_{ijkl}(t) = J_{jikl}(t) = J_{ijlk}(t),$$

$J_{ijkl}(t) = 0$ for $-\infty < t < 0$ and $J_{ijkl}(t)$ and its first derivative are continuous on $0 \leq t < \infty$. The functions $J_{ijkl}(t)$ are termed *creep functions* and represent the mechanical properties of the materials. Two other expressions of the strain components involving the creep functions are

$$\boldsymbol{\varepsilon}_{ij}(t) = J_{ijkl}(t)\boldsymbol{\sigma}_{kl}(0) + \int_0^t J_{ijkl}(t-\tau)\frac{d\boldsymbol{\sigma}_{kl}(t)}{d\tau}\, d\tau \tag{2.5}$$

and

$$\boldsymbol{\varepsilon}_{ij}(t) = J_{ijkl}(0)\boldsymbol{\sigma}_{kl}(t) + \int_0^t \boldsymbol{\sigma}_{kl}(t-\tau)\frac{dJ_{ijkl}(\tau)}{d\tau}\,d\tau.$$

Further identities and properties of the Stieltjes convolution in the context of the theory of linear viscoelasticity can be found in, e.g., [103].

Isotropic Viscoelastic Materials

In this section, the isotropic forms of the stress-strain relationships are derived. In order to obtain these relationships, let us recall that, if a medium is mechanically isotropic, the number of independent components required to define the relaxation function $G_{ijkl}(t)$ and the creep function $J_{ijkl}(t)$ reduces to two. Therefore, the general isotropic representation of the fourth-order relaxation tensor function is given by

$$G_{ijkl}(t) = \frac{1}{3}\left[G_2(t) - G_1(t)\right]\delta_{ij}\delta_{kl} + \frac{1}{2}G_1(t)\left(\delta_{ik}\delta_{jl} + \delta_{il}\delta_{jk}\right), \tag{2.6}$$

where $G_1(t)$ and $G_2(t)$ are independent relaxation functions. Now, denoting by s_{ij} and e_{ij} the deviatoric components of the stress and strain tensors, equation (2.3) can be reduced, using (2.6), to

$$s_{ij} = \int_{-\infty}^t G_1(t-\tau)\frac{de_{ij}(\tau)}{d\tau}\,d\tau \qquad \boldsymbol{\sigma}_{kk} = \int_{-\infty}^t G_2(t-\tau)\frac{d\boldsymbol{\varepsilon}_{kk}(\tau)}{d\tau}\,d\tau,$$

where

$$\begin{aligned} s_{ij} &= \boldsymbol{\sigma}_{ij} - \frac{1}{3}\delta_{ij}\boldsymbol{\sigma}_{kk}, & s_{ii} &= 0, \\ e_{ij} &= \boldsymbol{\varepsilon}_{ij} - \frac{1}{3}\delta_{ij}\boldsymbol{\varepsilon}_{kk}, & e_{ii} &= 0. \end{aligned}$$

Similarly, the creep integral form of the stress-strain relationship has the following isotropic form:

$$e_{ij} = \int_{-\infty}^t J_1(t-\tau)\frac{ds_{ij}(\tau)}{d\tau}\,d\tau, \qquad \boldsymbol{\varepsilon}_{kk} = \int_{-\infty}^t J_2(t-\tau)\frac{d\boldsymbol{\sigma}_{kk}(\tau)}{d\tau}\,d\tau$$

where $J_1(t)$ and $J_2(t)$ are two independent isotropic creep functions. From the relations derived above, it follows that $G_1(t)$ and $J_1(t)$ are the relaxation and creep functions appropriate to describe states of shear, whereas $G_2(t)$ and $J_2(t)$ describe states of dilatation. Obviously, the relaxation and creep functions G_α and J_α must be somehow related. In particular, the relationships between these functions can be found by means of the Laplace transform and they are given by

$$\hat{J}_\alpha = \left(s^2\hat{G}_\alpha\right)^{-1}, \quad \alpha = 1, 2,$$

where s is the Laplace parameter and $\hat{J}_\alpha$ and $\hat{G}_\alpha$ are the Laplace transoforms of the creep and relaxation functions, respectively. Moreover, using the properties of the Laplace transform, it can be shown that, in general,

$$\lim_{t\to 0} J_\alpha(t) = \lim_{t\to 0} G_\alpha(t)^{-1} \qquad \lim_{t\to\infty} J_\alpha(t) = \lim_{t\to\infty} G_\alpha(t)^{-1}.$$

In order to be consisent with the notation usually employed in the theory of linear elasticity, the isotropic relaxation functions in simple shear and dilatation are frequently denoted as $\mu(t)$ and $K(t)$, where

$$\mu(t) = G_1(t)/2, \qquad K(t) = G_2(t)/3.$$

Furthermore, a relaxation function $\lambda(t)$ analogous to the first Lamè constant in elasticity can also be defined as follows

$$\lambda(t) := \frac{1}{3}\left[G_2(t) - G_1(t)\right] = K(t) - \frac{2}{3}\mu(t).$$

Then, the viscoelastic stress-strain relation in terms of the Lamè relaxation functions $\lambda(t)$ and $\mu(t)$ is given by

$$\boldsymbol{\sigma}_{ij}(t) = \delta_{ij}\int_{-\infty}^t \lambda(t-\tau)\frac{d\boldsymbol{\varepsilon}_{kk}(\tau)}{d\tau}\,d\tau + 2\int_{-\infty}^t \mu(t-\tau)\frac{d\boldsymbol{\varepsilon}_{ij}(\tau)}{d\tau}\,d\tau.$$

As in the linear elastic case, it is possible to use $\lambda(t)$ and $\mu(t)$ to define relaxation functions that are appropriate to describe other states of uniform stress. More specifically, these other relaxation functions can be defined using the analogous elasticity relationships, expressed in terms of the Lamè constants, by simply replacing the elastic parameters λ and μ with the s multiplied Laplace tranforms of the viscoelastic functions $\lambda(t)$ and $\mu(t)$. For example, the relaxation function which characterizes a state of uniaxial extension is defined, through is Laplace transform, as

$$\hat{E}(s) = \frac{\hat{\mu}(s)(3\hat{\lambda}(s) + 2\hat{\mu}(s))}{\hat{\lambda}(s) + \hat{\mu}(s)}.$$

Similarly, the Laplace transform of the viscoelastic Poisson's ratio is defined as

$$\hat{\nu}(s) = \frac{\hat{\lambda}(s)}{2s(\hat{\lambda}(s) + \hat{\mu}(s))}.$$

Fading Memory

It is worth empasizing that, so far, we have not used any physical intuition or model representation in our discussion. Indeed, the stress-strain relations have been derived using nothing more than the memory hypothesis, some smoothness assumptions and mathematical tools. We are now interested in examining the consequences due to the introduction of a possible physical hypothesis. In particular, the physical hypothesis we consider concerns the choice of the specific type of memory behaviour knonw as *fading memory* [102]. The fading memory hypothesis states that current value of the stress depends more strongly upon the recent history than upon the distant history of the strain. More specifically, the dependence of the current value of the stress upon the values of the strain at previous times is determined through a "weighting function" which must assign a continuously decreasing dependence upon past events which are more distant from the current time. This hypothesis is reasonable in the sense that it would clearly be physically unrealistic to expect materials to have a growing memory for the more distant events. From the constitutive equations (2.1) or (2.2), it can be seen that the slopes of the relaxation functions are the weighting functions characterizing the extent to which the current value of each component of stress is influenced by the values of the strain at past times. Therefore, the fading memory type behaviour is satisfied if the magnitude of the slope of each component of the relaxation function tensor is a continuously decreasing function of time, namely if

$$\left|\frac{dG_{ijkl}(t)}{dt}\right|_{t=t_1} \leq \left|\frac{dG_{ijkl}(t)}{dt}\right|_{t=t_2} \qquad \text{for } t_1 > t_2 > 0.$$

Similarly, the fading memory hypothesis is also satisfied if the components of the creep function tensort satisfy the following condition

$$\left|\frac{dJ_{ijkl}(t)}{dt}\right|_{t=t_1} \leq \left|\frac{dJ_{ijkl}(t)}{dt}\right|_{t=t_2} \qquad \text{for } t_1 > t_2 > 0.$$

2.1.2 Differential Operator Form of Constitutive Equations

The constitutive relation between the components of the stress tensor and the components of the strain tensor can also be expressed using the following differential operator form:

$$p_0\boldsymbol{\sigma}_{ij}(t) + p_1\frac{d\boldsymbol{\sigma}_{ij}(t)}{dt} + p_2\frac{d^2\boldsymbol{\sigma}_{ij}(t)}{dt^2} + \cdots = q_0\boldsymbol{\varepsilon}_{ij}(t) + q_1\frac{d\boldsymbol{\varepsilon}_{ij}(t)}{dt} + q_2\frac{d^2\boldsymbol{\varepsilon}_{ij}(t)}{dt^2} + \ldots.$$

This relation can be written, in a more compact way, as

$$P(D)\boldsymbol{\sigma}_{ij}(t) = Q(D)\boldsymbol{\varepsilon}_{ij}(t) \tag{2.7}$$

where

$$P(D) = \textstyle\sum_{k=0}^{N} p_k D^k, \qquad Q(D) = \sum_{k=0}^{N} q_k D^k,$$

and D designating the operator d/dt. The connection between the integral form of the linear viscoelastic constitutive equation presented in Section 2.1.1 and the operator form given by equation (2.7) can be found by means of the Laplace Transform. In particular, the Laplace Transform of equation (2.7) is given by:

$$P(s)\hat{\boldsymbol{\sigma}}_{ij}(s) - \frac{1}{s}\sum_{k=1}^{N} p_k \sum_{r=1}^{k} s^r \boldsymbol{\sigma}_{ij}^{(k-r)}(0) = Q(s)\hat{\boldsymbol{\varepsilon}}_{ij}(s) - \frac{1}{s}\sum_{k=1}^{N} q_k \sum_{r=1}^{k} s^r \boldsymbol{\varepsilon}_{ij}^{(k-r)}(0) \tag{2.8}$$

where

$$P(s) = \textstyle\sum_{k=0}^{N} p_k (s)^k, \qquad Q(s) = \sum_{k=0}^{N} q_k (s)^k$$

and $\boldsymbol{\sigma}_{ij}^{(k-r)}(0)$ designates the $k-r$ order derivative of $\boldsymbol{\sigma}_{ij}(t)$ evaluated at $t = 0$, with similar relationships for the strain components $\boldsymbol{\varepsilon}_{ij}(t)$. On the other hand, the Laplace Transform of equation (2.3) is given by

$$\hat{\boldsymbol{\sigma}}_{ij}(s) = s\hat{G}_{ijkl}\hat{\boldsymbol{\varepsilon}}_{kl}(s). \tag{2.9}$$

Then, equations (2.8) and (2.9) are equivalent if

$$s\hat{G}_{ijkl} = \frac{Q(s)}{P(s)} \tag{2.10}$$

and

$$\sum_{r=k}^{N} p_r \boldsymbol{\sigma}_{ij}^{(r-k)}(0) = \sum_{r=k}^{N} q_r \boldsymbol{\varepsilon}_{ij}^{(r-k)}(0), \qquad k = 1, 2, \ldots, N. \tag{2.11}$$

Equation (2.10) provides the conditions under which the integral and the operator forms of the stress-strain constitutive equations are equivalent, while equation (2.11) imposes a constrain on the initial conditions which cannot be completely independent.

2.1.3 Viscoelastic Fluids and Solids

So far, our discussion has been confined to the realm of linear viscoelastic materials, without specifying whether they are solids or fluids. This is because viscoelastic materials can manifest in both solid and fluid forms. Thus, the aim of this section is to discuss the distinction between isotropic viscoelastic solids and isotropic viscoelastic fluids. Following [102], a material can be defined as a *viscoelastic fluid* if, when subject to a simple shear state of stress, it will respond with a steady state of flow, after transient effects have died out, and, when subject to a simple shear state of deformation, will produce a shear stress that will eventually decay to zero. On the other hand, an isotropic *viscoelastic solid* is a material that, when subject to a simple shear state of deformation, will have a corresponding component of stress which remains non-zero as long as the state of deformation is mantained. In order to provide a mechanical characterization of the viscoelastic materials and to better understand how the rough definitions given above are related to the tensor functions G and J, we now describe the behaviour of the viscoelastic fluids and solids when performing two simple laboratory tests, that are *relaxation* and *creep*. For the sake of simiplicity, we will restric our analysis to the one-dimensional case. A particular one-dimensional problem is the one in which every component of the stress and strain tensors is zero except for instance the xy components $\boldsymbol{\sigma}_{12}$ and $\boldsymbol{\varepsilon}_{12}$. This can be obtained, for example, when a stress $\boldsymbol{\sigma}_{12}$ is imposed on a medium in which the displacement takes place only in the y direction and depends on x alone. For this reason, in the following discussion we will simplify the notation by dropping the subscripts, thus referring to the shear relaxation and creep functions G_1 and J_1 just as G and J, respectively. Finally, we remark that, even though we are considering only G_1 and J_1, similar results will be understood to apply for the volumetric relaxation and creep functions G_2 and J_2 [102].

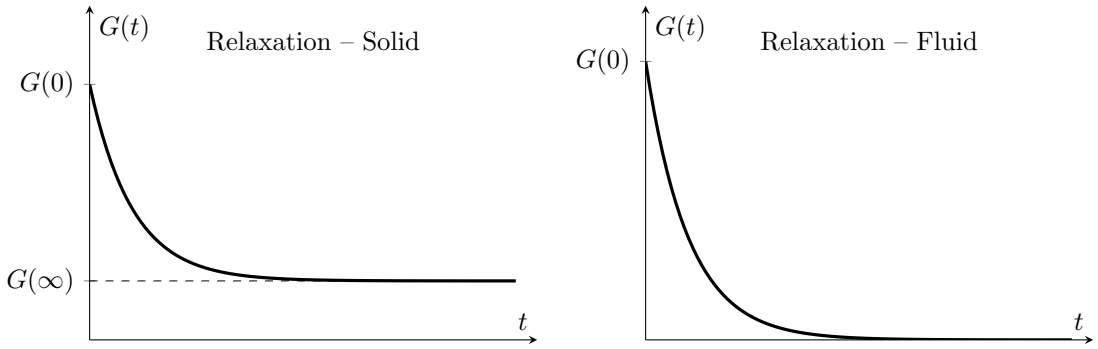


Figure 2.1: Qualitative behaviour of the relaxation function $G(t)$ for viscoelastic solid materials (left panel) and viscoelastic fluid materials (right panel). In both cases the function shows a decreasing behaviour over time, approaching a final value that is non-zero for solids and zero for fluids.

Relaxation of Stress

Let us consider a sudden constant shear strain $\boldsymbol{\varepsilon}$ applied starting from time $t = 0$ to an undeformed body, i.e., $\boldsymbol{\varepsilon}(t) = \boldsymbol{\varepsilon}_0 H(t)$. From equation (2.4) it is clear that the resulting stress is given by:

$$\boldsymbol{\sigma}(t) = G(t)\boldsymbol{\varepsilon}_0.$$

Experimental observations have shown that the initial stress is high and then it relaxes over time to some final value. Specifically, the initial value is due the elastic reponse of the material, whereas the relaxation is due to the viscous effects. From a physical viewpoint, the high initial resistance to deformation is due to frictional forces opposing the reorganization of molecules required by the change of shape. These internal forces are gradually overcome leading to what is called *relaxation* of stress. The final value of the stress is determined by $G(\infty) := \lim_{t\to\infty} G(t)$, which represents a generalization of the elastic modulus. From the definitions of viscoelastic solid and fluid given at the beginning of this section, it follows that the necessary and sufficient condition for an isotropic viscoelastic material to be a solid is that

$$G(\infty) \to \text{ positive constant},$$

while for a viscoelastic material to be fluid it is necessary that

$$G(\infty) \to 0. \tag{2.12}$$

The qualitative behaviour of the relaxation function for both viscoelastic solids and fluids is shown in Figure 2.1. However, condition (2.12) is only necessary but not sufficient for a viscoelastic material to be a fluid, whereas sufficiency requires that the material allow flow in a steady state condition. As a consequence, for a sufficiently large time, a viscoelastic fluid, that is subjected only to steady rates of deformation, behaves as a Newtonian viscous fluid. Then, it can be shown that the material is characterised by a coefficient of viscosity η, also called *zero shear rate viscosity*, defined in terms of the relaxation function as follows:

$$\eta = \frac{1}{2}\int_0^\infty G(s)\, ds. \tag{2.13}$$

It must be emphasized that these considerations hold only for large values of time and that viscoelastic fluids will behave quite differently than viscous fluids over short time periods.

Creep

Let us now consider the behaviour of a material subject to a constant shear stress $\boldsymbol{\sigma}$ starting from time $t = 0$, i.e., $\boldsymbol{\sigma}(t) = H(t)\boldsymbol{\sigma}_0$. Using equation (2.5), the strain-stress relation is given by

$$\boldsymbol{\varepsilon}(t) = J(t)\boldsymbol{\sigma}_0,$$

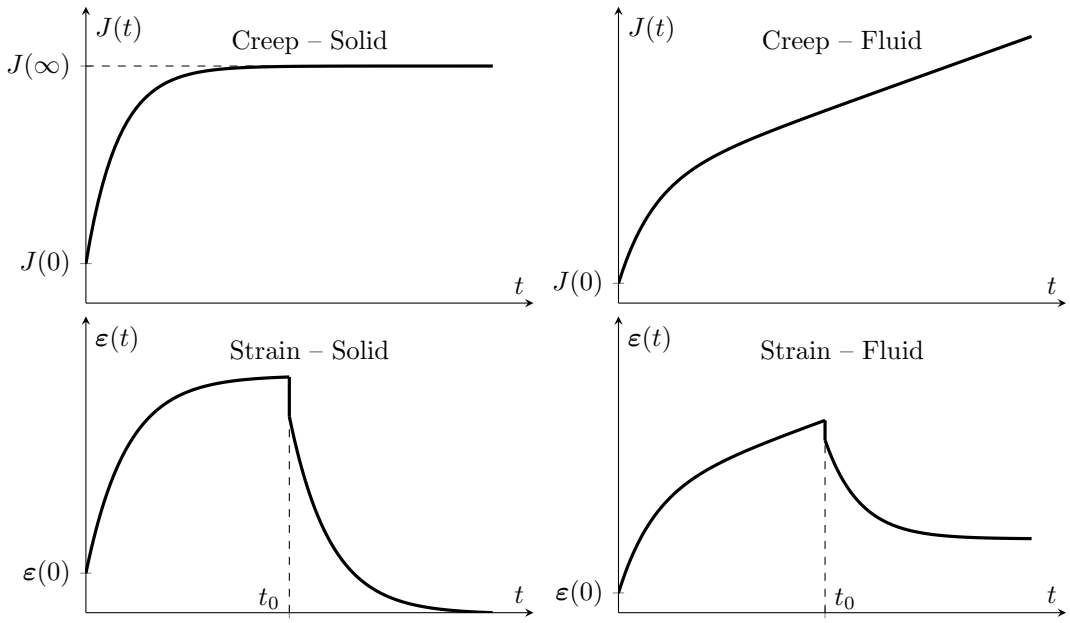


Figure 2.2: Top row shows the qualitative behaviour of the creep function. In viscoelastic solid materials (left) the creep function increases over time and then reaches a finite value, whereas in viscoelastic fluid materials (right) it increases indefinitely. Bottom row shows the strain response to a constant stress applied for time values in the interval $[0, t_0]$: solid materials recover completely (left), while fluids are characterized by a permanent deformation (right).

which shows that the resultant strain is not instantaneous but develops over time. It has been observed experimentally that a suddenly imposed stress causes a certain instantaneous strain, which is due to the elastic response of the material and is given by $J(0)\boldsymbol{\sigma}$ in the equation above. Subsequently, the strain increases over time to some final value (for a solid) or indefinitely (for a liquid). This material behaviour is named *creep*. Having defined

$$J(\infty) := \lim_{t\to\infty} J(t), \qquad \dot{J}(\infty) := \lim_{t\to\infty} \dot{J}(t)$$

we see that, for a solid material, saying that creep ceases is equivalent to $J(\infty)$ being finite (see Figure 2.2, top left panel) and in this case $J(\infty)$ may be regarded as a natural generalization of the inverse of the elastic modulus (i.e., the compliance). Moreover, for viscoelastic solid materials $\dot{J}(\infty)$ is zero. On the other hand, for viscoelastic fluids creep continues indefinitely and $\dot{J}(\infty)$ is a non-zero constant (see Figure 2.2, top right panel).

Now consider a material that is subject to a constant shear stress $\boldsymbol{\sigma}_0$ only for a limited amount of time, say for $t \in [0, t_0]$, after which it is released. In this case, experiments have shown that, after $t = t_0$, the strain immediately decreases (elastic recovery) and it then continuous to gradually decrease over time (anelastic recovery) until a residual strain is reached. Specifically, the strain, at large values of time, can be approximated as follows

$$\boldsymbol{\varepsilon}(t) \approx \dot{J}(t) t_0 \boldsymbol{\sigma}_0.$$

This relation clearly shows that if $\dot{J}(t)$ tends to zero, then $\boldsymbol{\varepsilon}(t)$ vanishes. This is the expected behaviour of a viscoelastic solid materials that has the capability to recover completely from applied stresses, like an elastic body does, but with a time delay due to internal losses (see Figure 2.2, bottom left panel). On the other hand, if $\dot{J}(t)$ is finite, then the permanent deformation occurs as a result of the application and removal of stress and this justifies the term viscoelastic fluid (see Figure 2.2, bottom right panel). However, even these materials partially exhibit recovery, since the creep function has the form

$$J(t) = \tilde{J}(t) + \frac{t}{2\eta}$$

where $\tilde{J}(t)$ approaches a finite positive asymptote for large values of time and η is the zero shear rate viscosity defined in (2.13).

2.1.4 Dynamic Loading and Complex Modulus

In addition to the creep and stress relaxation tests, a dynamic test might be useful when studying the behaviour of viscoelastic materials. The dynamic load testing consists in prescribing a cyclic history of strain given by

$$\boldsymbol{\varepsilon}(t) = \boldsymbol{\varepsilon}_0 \cos(\omega t), \tag{2.14}$$

where $\boldsymbol{\varepsilon}_0$ is the amplitude and ω is the frequency of oscillation. The stress response as a function of time t depends on the characteristics of the material. Specifically, for an elastic solid material, the stress is proportional to the strain through the Young modulus E, i.e., $\boldsymbol{\sigma}(t) = E\boldsymbol{\varepsilon}(t)$. Therefore, when the strain is defined as in equation (2.14), the stress response of an elastic material it is given by

$$\boldsymbol{\sigma}(t) = E\boldsymbol{\varepsilon}_0 \cos(\omega t),$$

which implies that the stress response caused by the strain is immediate. In this case, we also say that the stress is in phase with the strain. For a viscous material, the stress is proportional to the strain rate through the dynamic viscosity η, i.e., $\boldsymbol{\sigma}(t) = \eta\dot{\boldsymbol{\varepsilon}}(t)$. Thus, for a strain history defined as in (2.14), the stress response has the form:

$$\boldsymbol{\sigma}(t) = -\eta\boldsymbol{\varepsilon}_0\omega \sin(\omega t) = \eta\boldsymbol{\varepsilon}_0\omega \cos\left(\omega t + \frac{\pi}{2}\right),$$

which shows that the stress is out of phase with the strain and that, in particular, the strain is behind the stress by a 90 degree phase lag. In a linear viscoelastic material, laboratory experiments have shown that the stress as a function of time appears complicated in the very first few cycles but it eventually reaches a steady-state condition in which the resulting stress is also sinusoidal, having the same angular frequency ω but retarded in phase by an angle δ. Moreover, the same result has been observed even when the controlled variable was the stress and not the strain. So, we write the stress response function as:

$$\boldsymbol{\sigma}(t) = \boldsymbol{\sigma}_0 \cos(\omega t + \delta), \tag{2.15}$$

where $\delta \in [0, \pi/2]$ and $\boldsymbol{\sigma}_0 = \boldsymbol{\sigma}_0(\omega)$. Writing equation (2.15) in the equivalent form

$$\boldsymbol{\sigma}(t) = \boldsymbol{\sigma}_0 \cos\delta \cos(\omega t) - \boldsymbol{\sigma}_0 \sin\delta \sin(\omega t),$$

it is clear that the stress response is the sum of an in-phase and an out-of-pase response. It is often more useful to consider a strain history specified by the following complex function of time

$$\boldsymbol{\varepsilon}(t) = \boldsymbol{\varepsilon}_0 \exp(i\omega t) \tag{2.16}$$

and a complex response stress function having the form

$$\boldsymbol{\sigma}(t) = \boldsymbol{\sigma}_0 \exp(i\omega t + i\delta).$$

This equation can also be written as

$$\boldsymbol{\sigma}(t) = M(\omega)\boldsymbol{\varepsilon}_0 \exp(i\omega t),$$

where $M(\omega)$ is the so-called *complex modulus* and it is a complex function of the frequency defined by

$$M(\omega) = \frac{\boldsymbol{\sigma}_0}{\boldsymbol{\varepsilon}_0} \exp(i\delta) = \frac{\boldsymbol{\sigma}_0}{\boldsymbol{\varepsilon}_0} \cos\delta + i\frac{\boldsymbol{\sigma}_0}{\boldsymbol{\varepsilon}_0} \sin\delta.$$

Decomposing $M(\omega)$ into its real and imaginary part, we have

$$M(\omega) = M'(\omega) + iM''(\omega),$$

where

$$M'(\omega) = \frac{\boldsymbol{\sigma}_0}{\boldsymbol{\varepsilon}_0}\cos\delta, \qquad M''(\omega) = \frac{\boldsymbol{\sigma}_0}{\boldsymbol{\varepsilon}_0}\sin\delta.$$

The functions $M'(\omega)$ and $M''(\omega)$ are often referred to as the *storage* and *loss* moduli, respectively. The names are motivated by the fact that the storage modulus is associated with energy storage and release during periodic deformation, whereas the loss modulus is associated with the dissipation of energy and its transformation into heat. Finally, the phase angle δ, also called *loss angle*, is defined as

$$\delta(\omega) = \tan^{-1}\frac{M''(\omega)}{M'(\omega)}.$$

In the remaining part of this section we derive the relation between the complex modulus $M(\omega)$ and the relaxation function $G(t)$. Now let us decompose the relaxation function $G(t)$ into two components $\mathring{G}$ and $\tilde{G}(t)$ such that

$$G(t) = \mathring{G} + \tilde{G}(t) \tag{2.17}$$

and $\tilde{G}(t) \to 0$ when $t \to \infty$. Substituting equations (2.16) and (2.17) into the stress-strain constitutive relation (2.3) and performing a suitable change of variables, we obtain

$$\begin{aligned}
\boldsymbol{\sigma}(t) &= \int_{-\infty}^{t} G(t-\tau)\frac{d\boldsymbol{\varepsilon}}{d\tau}\,d\tau = \int_{-\infty}^{t}\left(\mathring{G} + \tilde{G}(t-\tau)\right)\frac{d\boldsymbol{\varepsilon}}{d\tau}\,d\tau \\
&= \mathring{G}\boldsymbol{\varepsilon}(t) + i\omega\int_{-\infty}^{t}\tilde{G}(t-\tau)\boldsymbol{\varepsilon}(\tau)\,d\tau \quad \text{(change of variable } t-\tau=\eta\text{)} \\
&= \mathring{G}\boldsymbol{\varepsilon}(t) + i\omega\left(\int_0^{\infty}\tilde{G}(\eta)\exp(-i\omega\eta)\,d\eta\right)\boldsymbol{\varepsilon}(t) \\
&= \left[\mathring{G} + \omega\int_0^{\infty}\sin\omega\eta\,\tilde{G}(\eta)\,d\eta + i\omega\int_0^{\infty}\cos\omega\eta\,\tilde{G}(\eta)\,d\eta\right]\boldsymbol{\varepsilon}_0\exp(i\omega t).
\end{aligned} \tag{2.18}$$

The expression inside the square brackets is the complex modulus $M(\omega)$. Then, M' and M'' have the form

$$M'(\omega) = \mathring{G} + \omega\int_0^{\infty}\tilde{G}(\eta)\sin\omega\eta\,d\eta, \qquad M''(\omega) = \omega\int_0^{\infty}\tilde{G}(\eta)\cos\omega\eta\,d\eta, \tag{2.19}$$

or equivalently, using integration by parts,

$$M'(\omega) = \mathring{G} + \tilde{G}(0) + \int_0^{\infty}\frac{d\tilde{G}(\eta)}{d\eta}\cos\omega\eta\,d\eta \qquad M''(\omega) = -\int_0^{\infty}\frac{d\tilde{G}(\eta)}{d\eta}\sin\omega\eta\,d\eta,$$

The integrals in equation (2.19) are the one-sided Fourier sine and cosine transforms and they can be inverted to give $\tilde{G}(t)$ in terms of $M'(\omega)$ or $M''(\omega)$ as follows:

$$\tilde{G}(t) = \frac{2}{\pi}\int_0^{\infty}\frac{M'(\omega)-\mathring{G}}{\omega}\sin\omega t\,d\omega \qquad \tilde{G}(t) = \frac{2}{\pi}\int_0^{\infty}\frac{M''(\omega)}{\omega}\cos\omega t\,d\omega.$$

Moreover, it can be shown that the complex modulus can also be derived by computing the Fourier transform of the general relaxation integral form of the stress-strain relation (2.2), which can be recasted in the following form:

$$\hat{\boldsymbol{\sigma}}(\omega) = M(\omega)\hat{\boldsymbol{\varepsilon}}(\omega).$$

This expression shows that, in the frequency domain, the stress-strain relation has the same form of the elastic stress strain relation, the only difference being that the modulus is complex and frequency-dependent. Finally, it is worth noting that, at zero frequency, the storage and loss moduli satisfy

$$M'(0) = \mathring{G} = \lim_{t\to\infty} G(t), \qquad M''(0) = 0,$$

which means that the material behaves either as an elastic solid or as a visous fluid. On the other hand, at infinite frequencies the storage and loss moduli satisfy

$$M'(\infty) = \mathring{G} + \tilde{G}(0) = \lim_{t\to 0} G(t), \qquad M''(\infty) = 0,$$

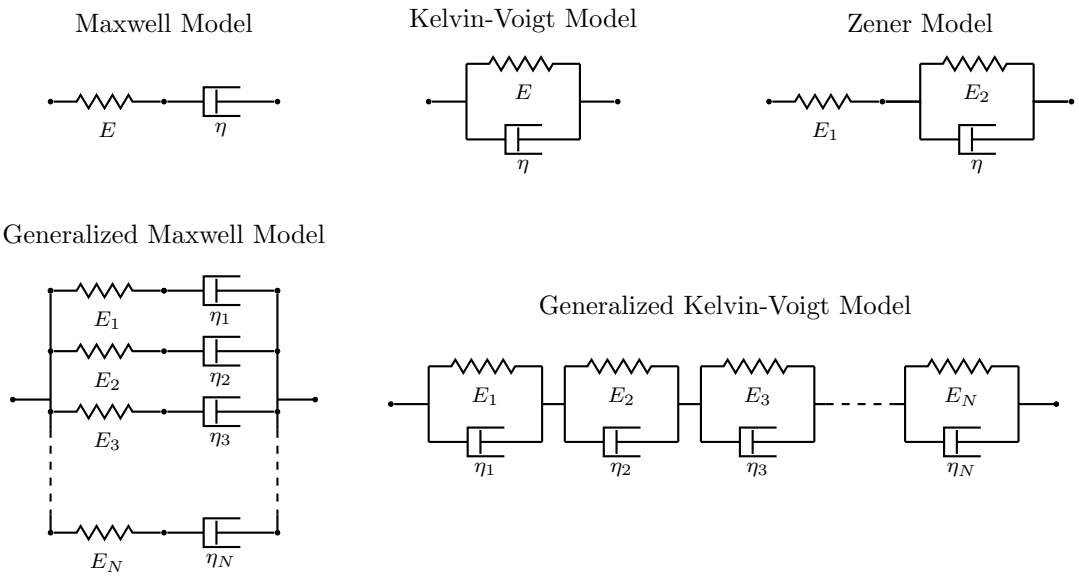


Figure 2.3: Examples of well-known mechanical models obtained by arranging weightless elastic springs and viscous dashpots in series and in parallel, in analogy with electrical circuits. These models define one-dimensional linear viscoelastic constitutive laws.

implying that the material behaves as an elastic solid. In other words, viscoelastic solids undergoing very fast or very slow processes, respond like elastic materials, whereas a viscoelastic fluid behaves as an elastic material for very fast processes and as a viscous material for very slow processes. Even though in this section we focused only on the relaxation function and the complex modulus, it is worth highlighting that similar expressions involving the creep function and the complex compliance can be derived as well (see, e.g., [190]).

2.1.5 One-dimensional Mechanical Models

In the one-dimensional setting, linear viscoelastic constitutive equations can be defined in terms of mechanical models consisting of two basic elements, weightless springs and dashpots, that are connected in series and parallel as in electrical circuits. The *spring*, whose stress-strain relation is given by $\boldsymbol{\sigma} = E\boldsymbol{\varepsilon}$, describes the elastic property of the masterial, as it is able to undergo an instantaneous elastic strain when loaded, to mantain that strain as long as the load is applied and then to undergo an instantaneous de-straining when the load is removed. The *dashpot* is a positon-cylinder mechanism filled with a viscous liquid and characterized by a stress-strain relation having the form $\boldsymbol{\sigma} = \eta\dot{\boldsymbol{\varepsilon}}$, where η is the dynamic viscosity of the fluid in the cylinder. A strain in the dashpot is achieved by dragging the piston through the fluid. When suddenly applying a constant load, the strain is seen to increase linearly as long as the stress is applied. There is no instantaneous movement of the dashpot at the onset of load, as it takes time for the strain to build up. Then, when the load is removed, there is no stress to move the piston back throug the fluid and therefore any strain built up is permanent. On the other hand, when a constant strain $\boldsymbol{\varepsilon}_0$ is imposed on the dashpot, the stress is given by $\boldsymbol{\sigma} = \eta\boldsymbol{\varepsilon}_0\delta(t)$. However, since an infinite stress is impossible in reality, it is therefore impossible to impose an instantaneous finite deformation on the dashpot. The Maxwell, Kelvin-Voigt and Zener models (see Figure 2.3) are the simplest and most known mechanical models capable of describing the mechanical properties of viscoelastic fluids and solids and they will be analysed in the remaining part of this section. Moreover, we will also provide a brief overview of more complex models.

The Maxwell Model

The Maxwell model consists of a spring and a dashpot connected in series (see Figure 2.3, top left panel). In this two-element model, both the string and the dashpot are subjects to the same stress $\boldsymbol{\sigma}$

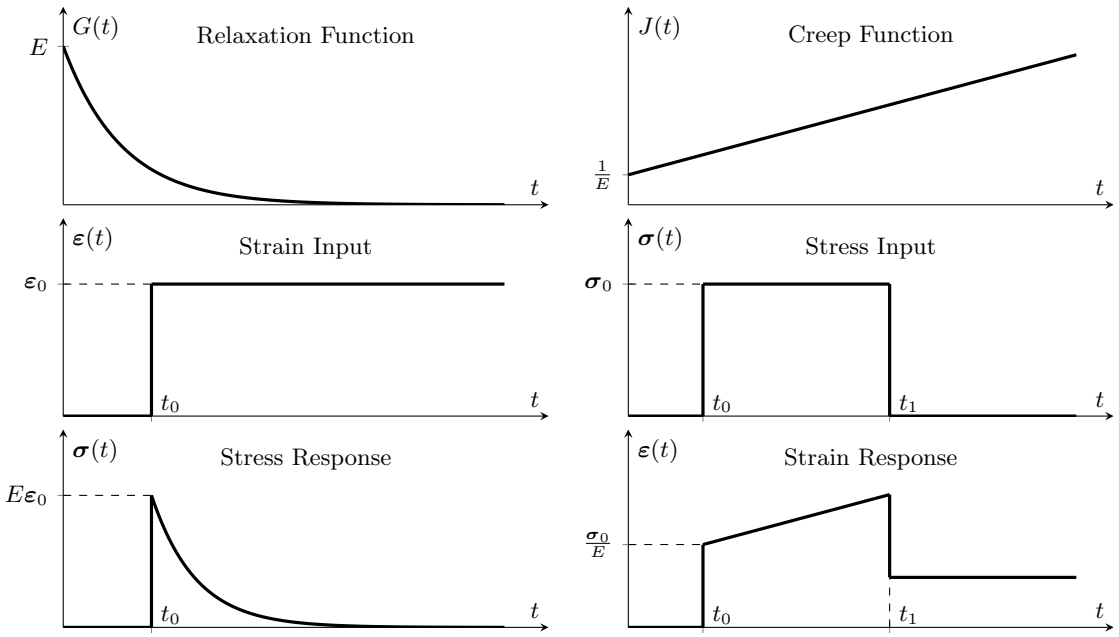


Figure 2.4: Maxwell model for viscoelastic fluid materials. Left column shows the behaviour of the relaxation function (top row), the constant strain applied starting from time $t = t_0$ in a relaxation experiment (middle row) and the stress response to the applied constant strain (bottom row). Right column shows the creep function (top row), the constant stress applied in a creep experiment starting from time $t = t_0$ and mantained until $t = t_1$ (middle row) and the strain response to the constant applied stress (bottom row).

but have independent strains that we denote with $\boldsymbol{\varepsilon}_1$ for the spring and with $\boldsymbol{\varepsilon}_2$ for the dashpot. Now, recalling that the stress-strain relation for the spring is

$$\boldsymbol{\sigma} = E\boldsymbol{\varepsilon}_1$$

and that the stress-strain relation in the dashpot has the form

$$\boldsymbol{\sigma} = \eta\dot{\boldsymbol{\varepsilon}}_2,$$

we obatin that the differential operator form of the stress-strain relation of the Maxwell element is

$$\frac{1}{\eta}\boldsymbol{\sigma} + \frac{1}{M}\frac{d\boldsymbol{\sigma}}{dt} = \frac{d\boldsymbol{\varepsilon}}{dt}.$$

Then, the relaxation function is given by

$$G(t) = E\exp\left(-\frac{t}{\tau}\right)H(t),$$

while the creep function has the form

$$J(t) = \frac{1}{E}\left(1 + \frac{t}{\tau}\right)H(t),$$

where $\tau = \eta/E$ is the relaxation time and $H(t)$ is the Heaviside step function. The relaxation and creep functions are shown in Figure 2.4, top row. The relaxation and creep functions are not representative of the creep behaviour of real solids and they rather resemble the relaxation and creep functions of a viscous fluid.

In the relaxation experiment, both the spring and the dashpot experience the same force, and since it is impossible to have an instantaneous deformation in the dashpot, the extension is initially in the

spring. Then, the dashpot extends and the spring contracts to keep the total elongation constant. At the end, the force in the spring relaxes completely, and the relaxation function does not present asymptotical residual stress as in the case of real solids (see Figure 2.4, bottom left). In the creep experiment, once the model is loaded with a constant stress, the strain increases instantaneously due to the elastic response of the spring. Subsequently, the strain continues to increase at constant rate over time due to the Newtonian viscous fluid term associated with the dashpot. Then, when the stress is removed from the model at time $t = t_1$, there is an instantaneous elastic recoverable portion of the strain corresponding to the instantaneous deformation of the spring, while a permanent strain due to the dashpot does not disappear (see Figure 2.4, bottom right).

The Maxwell model can be generalized by arranging in a parallel fashion N Maxwell elements (see Figure 2.3, bottom left panel), where the i-th element, $i = 1, \dots, N$, is characterised by a spring having elastic modulus E_i and a dashpot having viscosity η_i. In this model, the relaxation function is simply given by the sum of the relaxation functions associated to each single Maxwell element:

$$G(t) = \sum_{i=1}^{N} E_i \exp\left(-t/\tau_i\right) H(t),$$

where $\tau_i = \eta_i / E_i$, $i = 1, \dots, N$, is the relaxation time of each Maxwell element.

The Kelvin-Voigt Model

This model, developed independentely by Kelvin and Voigt, consists of a spring and a dashpot connected in parallel (see Figure 2.3, top middle panel). In this model the total stress $\boldsymbol{\sigma}$ is composed of an elastic stress

$$\boldsymbol{\sigma}_1 = E\boldsymbol{\varepsilon}$$

and a viscous stress

$$\boldsymbol{\sigma}_2 = \eta\dot{\boldsymbol{\varepsilon}}.$$

In this case, the differential operator form of the stress-strain relation becomes:

$$\boldsymbol{\sigma} = \boldsymbol{\sigma}_1 + \boldsymbol{\sigma}_2 = E\boldsymbol{\varepsilon} + \eta\frac{d\boldsymbol{\varepsilon}}{dt}.$$

and it can be shown that the relaxation function is given by

$$G(t) = EH(t) + \eta\delta(t)$$

whereas the creep function has the form

$$J(t) = \frac{1}{E}\left(1 - \exp\left(-\frac{t}{\tau}\right)\right) H(t),$$

where $\tau = \eta/E$ is the retardation time. The relaxation and creep functions are represented in Figure 2.5, top row, and they clearly suggest that the Kelvin-Voigt model is more appropriate to represent viscoelastic solid materials. In particular, the relaxation function does not show any time dependence, as in the case of pure elastic solids. Moreover, the presence of the delta function implies that, in practice, it is impossible to impose an instantaneous strain on the medium, as it would require an infinite stress to be applied (see also Figure 2.5, bottom left). In other words this means that there is no instantaneous response to a suddenly applied finite stress. In the creep experiment, the spring would want to stretch, but it is held back by the dashpot, which cannot react instantaneously and then takes all the stress. For this reason, the creep function does not present an instantaneous strain. Subsequently, the dashpot extends and begins to transfer the stress to the spring which starts to strain at decreasing rate. At infinite time, the entire stress is on the spring and the strain approaches an asymptotical value. This behaviour is also called *delayed elasticity*. When the Kelvin-Voigt model is unloaded, the spring will want to contract but again the dashpot hold it back. However, the spring eventually gradually relaxes to its undeformed state and full recovery occurs (see Figure 2.5, bottom right).

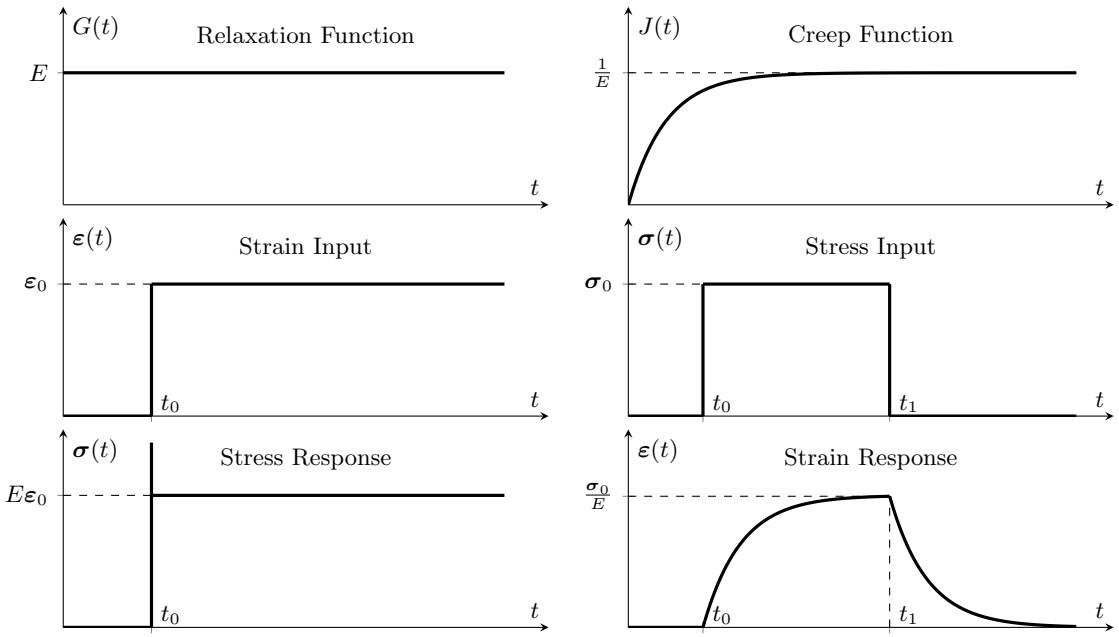


Figure 2.5: Kelvin-Voigt model for viscoelastic solid materials. Left column shows the behaviour of the relaxation function (top row), the constant strain applied starting from time $t = t_0$ in a relaxation experiment (middle row) and the stress response to the applied constant strain (bottom row). Right column shows the creep function (top row), the constant stress applied in a creep experiment starting from time $t = t_0$ and mantained until $t = t_1$ (middle row) and the strain response to the constant applied stress (bottom row).

Similarly to what we have done with the Maxwell model, we can generalize the Kelvin-Voigt model by connecting N Kelvin-Voigt elements in series (see Figure 2.3, bottom right panel). The creep function of the generalized model is given by the sum of the creep functions associated to each Kelvin-Voigt model:

$$J(t) = \sum_{i=1}^{N} E_i^{-1} \left(1 - \exp\left(-t/\tau_i\right)\right) H(t),$$

where $\tau_i = \eta_i / E_i$, $i = 1, \ldots, N$, is the retardation time of each Kelvin-Voigt element.

The Zener Model

The Zener model, also known as standard-linear-solid model, consists in a series combination of a spring and a Kelvin-Voigt model (see Figure 2.3, top right panel). The stress-strain relations for the single elements are

$$\boldsymbol{\sigma} = E_1 \boldsymbol{\varepsilon}_1, \qquad \boldsymbol{\sigma}_1 = \eta \dot{\boldsymbol{\varepsilon}}_2, \qquad \boldsymbol{\sigma}_2 = E_2 \boldsymbol{\varepsilon}_2.$$

Having defined the total strain $\boldsymbol{\varepsilon} = \boldsymbol{\varepsilon}_1 + \boldsymbol{\varepsilon}_2$ and the total stress $\boldsymbol{\sigma} = \boldsymbol{\sigma}_1 + \boldsymbol{\sigma}_2$, the differential operator form of the stress-strain relations of the Zener model has the form:

$$\boldsymbol{\sigma} + \tau_{\boldsymbol{\sigma}} \frac{d\boldsymbol{\sigma}}{dt} = E \left(\boldsymbol{\varepsilon} + \tau_{\boldsymbol{\varepsilon}} \frac{d\boldsymbol{\varepsilon}}{dt} \right),$$

where

$$E_R = \frac{E_1 E_2}{E_1 + E_2}$$

is the relaxed modulus and

$$\tau_{\boldsymbol{\sigma}} = \frac{\eta}{E_1 + E_2}, \qquad \tau_{\boldsymbol{\varepsilon}} = \frac{\eta}{E_2} \geq \tau_{\boldsymbol{\sigma}}$$

are the relaxation times. The relaxation and creep functions are given, respectively, by

$$G(t) = E_R \left[1 - \left(1 - \frac{\tau_{\boldsymbol{\varepsilon}}}{\tau_{\boldsymbol{\sigma}}} \right) \exp\left(-\frac{t}{\tau_{\boldsymbol{\sigma}}} \right) \right] H(t)$$

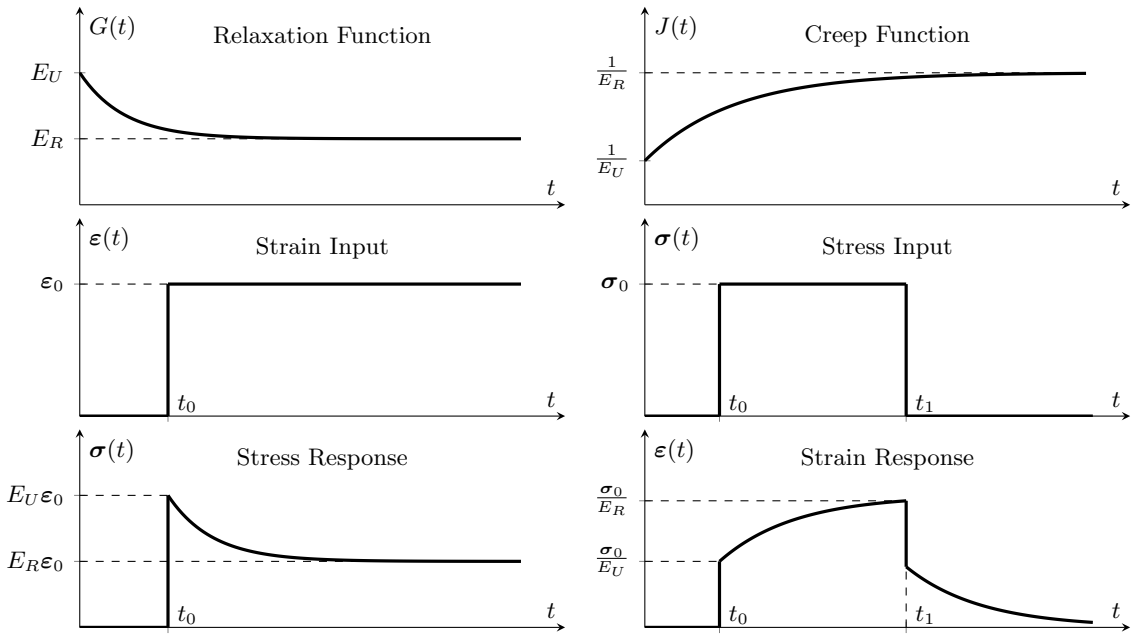


Figure 2.6: Zener model for viscoelastic materials. Left column shows the behaviour of the relaxation function (top row), the constant strain applied starting from time $t = t_0$ in a relaxation experiment (middle row) and the stress response to the applied constant strain (bottom row). Right column shows the creep function (top row), the constant stress applied in a creep experiment starting from time $t = t_0$ and mantained until $t = t_1$ (middle row) and the strain response to the constant applied stress (bottom row).

and

$$J(t) = \frac{1}{E_R}\left[1 - \left(1 - \frac{\tau_{\boldsymbol{\sigma}}}{\tau_{\boldsymbol{\varepsilon}}}\right)\exp\left(-\frac{t}{\tau_{\boldsymbol{\varepsilon}}}\right)\right] H(t)$$

The relaxation and creep functions are shown in Figure 2.6 (top row). In the creep experiment, there is an instantaneous strain of value $\boldsymbol{\sigma}_0/E_U$, where $E_U = E_1$ is the unrelaxed modulus, and an asymptotic strain of magnitude $\boldsymbol{\sigma}_0/E_R$ that are determined only by the springs constants. More specifically, we observe that, after the first instantaneous strain, the force in the dashpot is gradually relaxed by deformation therein, resulting in a gradual increase in the observed overall deformation, and eventually an asymptotic value is reached. When the model is unloaded at time $t = t_1$, we observe a discontinuity in the strain history that is due to the instantaneous elastic recovery. Subsequently, the strain continues to gradually decrease over time, undergoing anelastic recovery until it reaches zero strain and full recovery is achieved (see Figure 2.6, bottom right). In the relaxation experiment, the stress history exhibits an instantaneous unrelaxed state of magnitude $E_U\boldsymbol{\varepsilon}_0$, while at the end of the process the system has relaxed completely to the value $E_R\boldsymbol{\varepsilon}_0$ (see Figure 2.6, bottom left).

Other Models

The three mechanical models presented so far are the simplest and most popular models used to describe the mechanical behaviour of viscoelastic materials. Clearly, a larger number and a different arrangement of springs and dashpots will yield different and possibly more complex models capable of accurately characterize viscoelastic fluids and solids. Among these, we mention the *generalized Zener model*, which was introduced to obtain a nearly constant quality factor over the seismic frequency range of interest, and that consists of L Zener elements connected in parallel. Another well-known model is the *Burgers model*, which is formed with a series connection of a Zener element and a dashpot or, equivalently, with a series connnection of a Kelvin-Voigt and a Maxwell element, is used to accurately describe both the transient and steady state creep process. It is worth highlighting that springs and dashpots are not really necessary to define a linear viscoelastic constitutive model, what is needed

is a differential equation of the form given by (2.7). This means that an arbitrarily complex linear viscoelastic model can also be created by simply chosing values for the coefficients in the differential form of the viscoelastic constitutive equations, without referring to any particular spring – dashpot arrangement. However, the use of springs and dashpots is helpful, in particular for simple models, as it provides a physical intuition about the way a material might respond. It is clear that, in general, the more elements one has, the more accurate a model will be in describing the response of real materials. However, it must be emphasized that more complex models require more material parameters to be evaluated by laboratory experiments and this could prove to be a difficult task.

2.2 Wave Propagation

2.2.1 Governing Equations

The propagation of waves in both elastic and viscoelastic materials is governed by the so-called Cauchy equilibrium equations:

$$\rho \ddot{\boldsymbol{u}} = \operatorname{div} \boldsymbol{\sigma}(\boldsymbol{u}) + \boldsymbol{f}, \tag{2.20}$$

where ρ is the density of the material, $\boldsymbol{u}$ is the displacement field, $\ddot{\boldsymbol{u}}$ is the second derivative in time of the displacement (i.e., the acceleration), $\boldsymbol{\sigma}$ is the stress tensor and $\boldsymbol{f}$ is an external force acting on the body. This vector Partial Differential Equation describes the conservation of linear momentum in any continuum, either fluid or solid. The displacement equations of motion associated to a particular material are then obtained by specifing the constitutive law that relates the stress $\boldsymbol{\sigma}$ to the displacement field $\boldsymbol{u}$. We now briefly discuss the main aspects of wave propagation in a homogeneous and isotropic elastic or viscoelastic material: in particular, we start again by considering the one-dimensional case, since it is easier to introduce, and subsequently move to the more general multi-dimensional case.

One-dimensional Wave Propagation

In the one-dimensional case, Cauchy equations rewrite as follows:

$$\rho \ddot{u} = \sigma'(u) + f, \tag{2.21}$$

where σ' denotes the first derivative with respect to the space variable x of the stress σ, i.e., $\partial\sigma/\partial x$. As we have already seen in Section 2.1.5, for a linear elastic material the stress-displacement relation is defined by Hooke's law, meaning that stress is proportional to the strain ε through the Young's Modulus E, i.e., $\sigma = E\varepsilon$. Substituting the constitutive model into equation (2.21), we obtain

$$\rho \ddot{u} = E u'' + f,$$

which is a non-homogeneous wave equation with speed of propagation equal to $c = \sqrt{E/\rho}$. For the dicusssion of wave propagation in a one-dimensional viscoelastic material, we will assume the external forcing function to be zero and we will consider a displacement wave having the following expression:

$$u(t, x) = u_0 \exp\left(i\omega t - ikx\right), \tag{2.22}$$

where $k \in \mathbb{C}$ is the complex wavenumber and $\omega \in \mathbb{R}$ is the angular frequency. Substituting expression (2.22) into Cauchy equation (2.21), using the stress-strain consitutive relation (2.3) and employing the procedure previously applied in (2.18) for deriving the expression of the complex modulus $M(\omega)$, it can be shown that the following dispersion relation holds:

$$M(\omega)k^2 = \rho\omega^2.$$

This relation provides the following expression of the complex velocity

$$v_c(\omega) = \frac{\omega}{k} = \sqrt{\frac{M(\omega)}{\rho}}.$$

Now, writing the complex wavenumber as $k = \kappa - i\alpha$, where $\kappa, \alpha \in \mathbb{R}_+$, we can rewrite the expression for the plane displacement wave as follows

$$u(t, x) = u_0 \exp(-\alpha x) \exp(i\omega t - i\kappa x).$$

This shows that α is responsible for the change in amplitude of the wave as it propagates in a viscoelastic material. For this reason α is also called *attenuation factor* and it can be computed as follows:

$$\alpha(\omega) = -\omega \operatorname{Im}\left(\frac{1}{v_c}\right). \tag{2.23}$$

Moreover, the real wavenumber κ allows to define the *phase velocity* as

$$v_p(\omega) = \frac{\omega}{\kappa} = \left[\operatorname{Re}\left(\frac{1}{v_c}\right)\right]^{-1}. \tag{2.24}$$

Finally, another parameter that allows to quantify dissipation is the *quality factor* Q, as its inverse, Q^{-1}, is the *dissipation factor*. The quality factor is defined as twice the time-averaged strain-energy density divided by the time-averaged dissipated-energy density and it can be computed as

$$Q = \frac{\operatorname{Re}(v_c^2)}{\operatorname{Im}(v_c^2)}. \tag{2.25}$$

Kelvin-Voigt Material We now consider the specific case of a one-dimensional Kelvin-Voigt viscoelastic material and derive the expressions of some of the quantities defined above. It can be shown that the complex modulus $M(\omega)$ is given by

$$M(\omega) = E + i\omega\eta,$$

where it is easy to see that the real and imaginary part are only related to the elastic and viscous parameters, respectively. Then, using equation (2.24), we obatin the following expression of the phase velocity

$$v_p(\omega) = \sqrt{\frac{E}{\rho}} \frac{\sqrt{1 + (\omega\eta/E)^2}}{\sqrt{\frac{1}{2}\left(\sqrt{1 + (\omega\eta/E)^2} + 1\right)}}.$$

This shows that $v_p \to \sqrt{E/\rho}$ for $\omega \to 0$ and that $v_p \to \infty$ for $\omega \to \infty$, which means that the elastic (lossless) velocity is obtained at the low-frequency limit whereas high frequencies propagate with infinite velocity. The qualitative behaviour of the phase velocity for a Kelvin-Voigt material is shown in the left panel of Figure 2.7. The attenuation factor in a Kelvin-Voigt material can be computed using equation (2.23) and it is given by

$$\alpha(\omega) = \omega \frac{\sqrt{\frac{1}{2}\left(\sqrt{(E/\rho)^2 + (\omega\eta/\rho)^2} - E/\rho\right)}}{\sqrt{(E/\rho)^2 + (\omega\eta/\rho)^2}},$$

which shows that the higher the angular frequency of the propagating wave, the greater the attenuation of its amplitude in space (see Figure 2.7, right panel). Finally, using equation (2.25), it is possible to see that the quality factor is given by

$$Q(\omega) = \frac{E}{\omega\eta}.$$

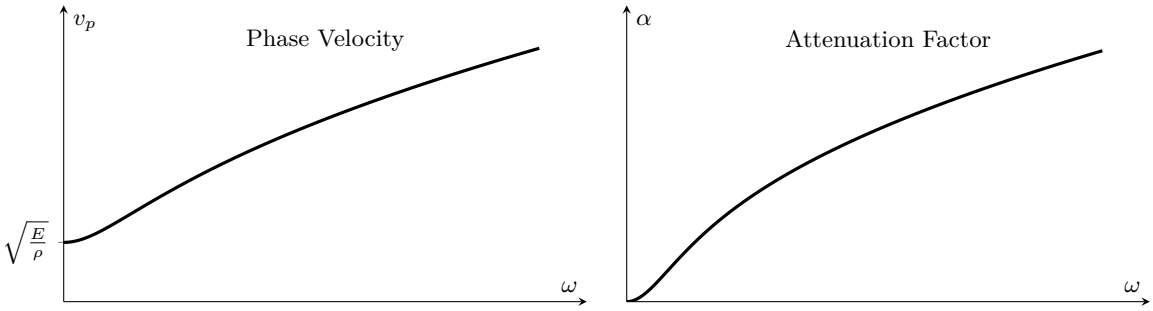


Figure 2.7: Qualitative behaviour of the phase velocity v_p (left panel) and the attenuation factor α (right panel) in a one-dimensional Kelvin-Voigt viscoelastic material.

Multi-dimensional Wave Propagation

In the multi-dimensional setting, the deformation is described by means of the strain tensor

$$\boldsymbol{\varepsilon}(\boldsymbol{u}) = \frac{\nabla \boldsymbol{u} + \nabla \boldsymbol{u}^\top}{2}.$$

In the following it will be useful to distinguish two contributions when referring to deformations, namely *dilatation* and *rotation*. In particular, the dilatation, hereafter denoted by φ, represents the relative change in volume and it is defined as the divergence of the displacement field, i.e., $\varphi := \nabla \cdot \boldsymbol{u}$. On the other hand, the rotation refers to the change in shape and we can associate it to the displacement field by means of the curl operator by defining the rotation vector $\boldsymbol{\psi} := \nabla \times \boldsymbol{u}$. As in the one-dimensional case, the relation between the stress $\boldsymbol{\sigma}$ and the strain $\boldsymbol{\varepsilon}$ in a linear elastic body is given by Hooke's law, which states that the stress is proportional to the strain, i.e.,

$$\boldsymbol{\sigma} = \mathbb{C} : \boldsymbol{\varepsilon},$$

where $\mathbb{C}$ is a fourth-order tensor. In the case of linear elastic isotropic materials, the components of the fourth-order tensor $\mathbb{C}$ can be expressed by using two coefficients, i.e., λ and μ, called Lamè elastic parameters,

$$\mathbb{C}_{ijkl} = \lambda \delta_{ij}\delta_{kl} + \mu(\delta_{ik}\delta_{jl} + \delta_{il}\delta_{jk}).$$

Therefore, the stress tensor can be written as

$$\boldsymbol{\sigma}(\boldsymbol{u}) = \lambda \operatorname{Tr}(\boldsymbol{\varepsilon}(\boldsymbol{u})) + 2\mu\boldsymbol{\varepsilon}(\boldsymbol{u}), \tag{2.26}$$

or, equivalently, using the index notation,

$$\boldsymbol{\sigma}_{ij}(\boldsymbol{u}) = \lambda \boldsymbol{\varepsilon}_{kk}\delta_{ij} + 2\mu\boldsymbol{\varepsilon}_{ij} = \lambda \partial_k \boldsymbol{u}_k \delta_{ij} + \mu(\partial_i \boldsymbol{u}_j + \partial_j \boldsymbol{u}_i).$$

Substituting (2.26) into (2.20) we obtain the following displacement equations of motion:

$$\rho \ddot{\boldsymbol{u}} = (\lambda + \mu)\nabla(\nabla \cdot \boldsymbol{u}) + \mu \Delta \boldsymbol{u} + \boldsymbol{f}, \tag{2.27}$$

which can also be written in index notation as

$$\rho \ddot{\boldsymbol{u}}_i = (\lambda + \mu)\, \partial_i \partial_j \boldsymbol{u}_j + \mu\, \partial_j \partial_j \boldsymbol{u}_i + \boldsymbol{f}_i.$$

Using the identity $\Delta \boldsymbol{u} = \nabla(\nabla \cdot \boldsymbol{u}) - \nabla \times \nabla \times \boldsymbol{u}$, the displacement equations (2.27) becomes

$$\rho \ddot{\boldsymbol{u}} = (\lambda + 2\mu)\nabla(\nabla \cdot \boldsymbol{u}) - \mu \nabla \times (\nabla \times \boldsymbol{u}) + \boldsymbol{f}. \tag{2.28}$$

This last form of the displacement equations of motion describes the propagation of the deformations in terms of both the dilatation $\varphi = \nabla \cdot \boldsymbol{u}$ (which accounts for the change in volume) and the rotation

vector $\boldsymbol{\psi} = \nabla \times \boldsymbol{u}$ (which accounts for the change in shape) in an isotropic homogeneous elastic continuum. Assuming the external forces to be zero, we can rewrite the equation as:

$$\rho\ddot{\boldsymbol{u}} = (\lambda + 2\mu)\nabla\varphi - \mu\nabla \times \boldsymbol{\psi}.$$

Now assuming the dilatation φ equal to zero, we obtain a wave equation for the displacement $\boldsymbol{u}$ governing equivoluminal waves in which the deformation consists of shear and rotation only (no change in volume),

$$\ddot{\boldsymbol{u}} = C_S^2\Delta\boldsymbol{u}, \quad C_S = \sqrt{\frac{\mu}{\rho}}.$$

On the other hand, if we set the rotation vector $\boldsymbol{\psi}$ equal to zero, we obtain a wave equation for $\boldsymbol{u}$ governing the dilatational waves, in which deformation consists of dilatation, or volume change, only (no rotation),

$$\ddot{\boldsymbol{u}} = C_P^2\,\Delta\boldsymbol{u}, \quad C_P = \sqrt{\frac{\lambda + 2\mu}{\rho}}.$$

The displacement equations of motion also contain wave equations for the dilatation and the rotation vector. Indeed, taking the divergence of equation (2.28) and assuming that ρ, λ and μ are constants, we obtain

$$\nabla \cdot (\rho\ddot{\boldsymbol{u}}) = (\lambda + 2\mu)\nabla \cdot \nabla\varphi - \mu\nabla \cdot \nabla \times \boldsymbol{\psi}.$$

Then, recalling that $\nabla \cdot \nabla \times \boldsymbol{\psi} = 0$, for all $\boldsymbol{\psi}$, we have

$$\ddot{\varphi} = C_P^2\,\Delta\varphi. \tag{2.29}$$

On the other hand, taking the curl of equation (2.28) yields

$$\nabla \times (\rho\ddot{\boldsymbol{u}}) = (\lambda + 2\mu)\nabla \times \nabla\boldsymbol{u} - \mu\nabla \times \nabla \times \boldsymbol{\psi}$$

and since $\nabla \times \nabla\varphi = \mathbf{0}$ for all φ we obtain

$$\rho\ddot{\boldsymbol{u}} = -\mu\nabla \times (\nabla \times \boldsymbol{\psi}).$$

Finally, using again the vector identity $\Delta\boldsymbol{\psi} = \cancel{\nabla(\nabla \cdot \boldsymbol{\psi})} - \nabla \times \nabla \times \boldsymbol{\psi} = -\nabla \times \nabla \times \boldsymbol{\psi}$, we get

$$\ddot{\boldsymbol{\psi}} = C_S^2\Delta\boldsymbol{\psi}. \tag{2.30}$$

Because φ represents changes in volume without changes in shape, solutions of equation (2.29) correspond to compressional and dilational motion, or longitudinal waves. As waves propagate, the elastic material expands and contracts in the direction of propagation keeping the same form. This waves are also called pressure waves or P-waves. On the other hand, solutions of equation (2.30) represent shear waves, or simply S-waves. In these waves the deformation consists of shear and rotation only, with the dilatation or volume change being equal to zero, since the divergence of the rotation vector is null. For this reason they are also called equivoluminal waves. Moreover, the particle motion of the S-wave is perpendicular (transverse) to the direction of propagation. There are two variants of S-wave: if the particle motion of the S-wave is up and down in the vertical plane, then it is named as SV-wave, whereas if the S-wave oscillates in the horizontal plane, then it is referred to as SH-wave. Since the speed of P-waves is always greater than the speed of S-waves, P- and S-waves are sometimes referred to as primary and secondary waves, respectively. The difference between P- and S-waves is also shown in Figure 2.8. It is clear that a disturbance is in general composed of both the fundamental types of displacement waves, i.e., the dilatational and equivoluminal waves. We now show that the displacement field solution of the elastodynamic equations can be actually written as the sum of two contributions, one related to P-waves and the other related to S-waves. Assuming that the external forces are equal to zero, it can be shown that, if the displacement field $\boldsymbol{u}$ is solution of the elastodynamic displacement equations, there exists a scalar potential function Φ and a vector potential function $\boldsymbol{\Psi}$ such that $\boldsymbol{u}$ is given by

$$\boldsymbol{u} = \nabla\Phi + \nabla \times \boldsymbol{\Psi}, \qquad \nabla \cdot \boldsymbol{\Psi} = 0. \tag{2.31}$$

and Φ and $\boldsymbol{\Psi}$ satisfy the following wave equations:

$$\ddot{\Phi} = C_P^2 \, \Delta\Phi \qquad \ddot{\boldsymbol{\Psi}} = C_S^2 \, \Delta\boldsymbol{\Psi}. \tag{2.32}$$

where the terms C_P and C_S are the compressional or longitudinal wavespead and the shear or transverse wavespead, respectively. From (2.32) it results that the scalar potential Φ describes a wave of compressional motion, thus being associated to P-waves, while the vector potential $\boldsymbol{\Psi}$ describes a wave of shear motion, thereby being related to S-waves. This was also clear by observing that the first term in the decomposition (2.31) is free of rotation since the curl of the gradient is zero, whereas the second term describes a motion without change of volume since the divergence of the curl is zero. The decomposition of the displacement field given in (2.31), is also known as *Helmholtz decomposition* or Helmholtz resolution of a vector. When the disturbances propagating in the interior region of an elastic body are due to external forces acting on the body itserìlf, it can be shown that the same result holds, i.e., the displacement $\boldsymbol{u}$ solution of the elastodynamic equations with $\boldsymbol{f} \neq \boldsymbol{0}$ can be written using Helmholtz decomposition (2.31) provided that the two potentials satisfy the following non-homogeneous wave equations

$$\ddot{\Phi} = C_P^2 \, \Delta\Phi + f_\Phi \qquad \ddot{\boldsymbol{\Psi}} = C_S^2 \, \Delta\boldsymbol{\Psi} + \boldsymbol{f}_{\boldsymbol{\Psi}},$$

where

$$\boldsymbol{f} = \nabla f_\Phi + \nabla \times \boldsymbol{f}_{\boldsymbol{\Psi}}.$$

Nearly Incompressible Materials A continuum body is said to be incompressible if any motion it undergoes is isochoric, i.e. characterised by a constant volume. In mathematical terms, this means that the displacement field is divergence-free, i.e. $\operatorname{div} \boldsymbol{u} = 0$. As the name suggests, *nearly incompressible materials* are characterised by very small compressibility effects; in other words, dilatational changes require significantly more external work than volume-preserving deformations. For nearly-incompressible materials the Lamè coefficient λ approaches ∞ or, equivalently, the Poisson coefficient ν tends to $1/2$. Unfortunately, the (nearly) divergence-free constraint on the displacement field introduces additional challenges in the numerical solution of the governing equations. Therefore, it is of utmost importance to develop robust numerical methods that remain uniformly convergent for all the values of the Lamè parameters. This will be addressed in Section 3.2.3.

Kelvin-Voigt Material The discussion of wave propagation in a multidimensional viscoelastic material can be carried out in a similar way to the one-dimensional case. In particular, the multi-dimensional version of the viscoelastic stress-strain relation of Kelvin-Voigt type has been studied for the first time by Carcione et al. in [106]. Similarly to the one-dimensional setting, the stress tensor is a function of the displacement field $\boldsymbol{u}$ and of the velocity field $\dot{\boldsymbol{u}}$ and can be written as the sum of an elastic and a viscous component:

$$\boldsymbol{\sigma}(\boldsymbol{u}, \dot{\boldsymbol{u}}) = \boldsymbol{\sigma}_{\text{el}}(\boldsymbol{u}) + \boldsymbol{\sigma}_{\text{vi}}(\dot{\boldsymbol{u}}), \tag{2.33}$$

where the elastic stress tensor $\boldsymbol{\sigma}_{\text{el}}$ and the viscous stress tensor $\boldsymbol{\sigma}_{\text{vi}}$ are defined as follows:

$$\boldsymbol{\sigma}_{\text{el}}(\boldsymbol{u}) = \lambda_{\text{el}} \operatorname{tr}(\boldsymbol{\varepsilon}(\boldsymbol{u}))\mathbb{I} + 2\mu\boldsymbol{\varepsilon}(\boldsymbol{u}), \qquad \boldsymbol{\sigma}_{\text{vi}}(\dot{\boldsymbol{u}}) = \lambda_{\text{vi}} \operatorname{tr}(\boldsymbol{\varepsilon}(\dot{\boldsymbol{u}}))\mathbb{I} + 2\eta\boldsymbol{\varepsilon}(\dot{\boldsymbol{u}}), \tag{2.34}$$

where $\lambda_{\text{vi}} \colon \Omega \to \mathbb{R}_+$ and $\eta \colon \Omega \to \mathbb{R}_+$ are the first and second Lamé viscous coefficients, respectively. Combining Cauchy equations (2.20) with the Kelvin-Voigt constitutive relation (2.33) and using the definitions of the elastic and viscous stress tensors given in (2.34), we can deduce the following explicit form for the displacement equations of motion governing the propagation of waves in a Kelvin-Voigt viscoelastic material:

$$\rho\ddot{\boldsymbol{u}} = \operatorname{div}\left(\lambda_{\text{el}} \operatorname{tr}(\boldsymbol{\varepsilon}(\boldsymbol{u}))\mathbb{I} + 2\mu\boldsymbol{\varepsilon}(\boldsymbol{u})\right) + \operatorname{div}\left(\lambda_{\text{vi}} \operatorname{tr}(\boldsymbol{\varepsilon}(\dot{\boldsymbol{u}}))\mathbb{I} + 2\eta\boldsymbol{\varepsilon}(\dot{\boldsymbol{u}})\right) + \boldsymbol{f}.$$

The initial boundary value problem obtained by combining this vector Partial Differential Equation with suitable initial and boundary conditions will be discussed in Part II of this thesis, where existence and uniqueness of the solution will be proved by relying on the theory of linear evolution equations on

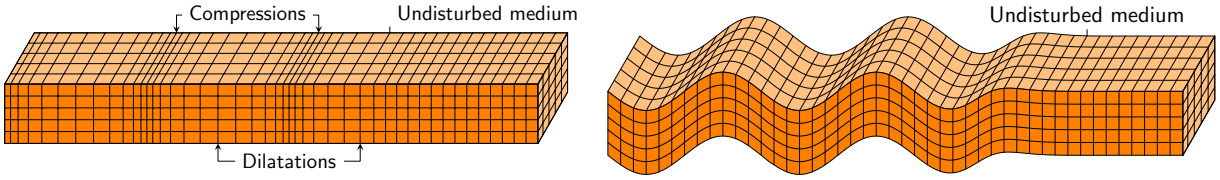


Figure 2.8: Deformations associated to a P-wave (left) and S-wave (right) traveling horizontally. S-wave propagation is pure shear with no volume change, whereas P-waves involve a volume change in the material (source [196]).

Hilbert Spaces and the numerical solution will be computed by means of the Galerkin Finite Element and Spectral methods. For a viscoelastic material of Kelvin-Voigt type, the P- and S-wave complex velocities are given by [101, 106]

$$v_p = \sqrt{\frac{(\lambda_{\text{el}} + 2\mu) + i\omega(\lambda_{\text{vi}} + 2\eta)}{\rho}} \qquad v_s = \sqrt{\frac{\mu + i\omega\eta}{\rho}}.$$

Moreover, the P- and S-wave quality factors are defined as

$$Q_p = \frac{\lambda_{\text{el}} + 2\mu}{\omega(\lambda_{\text{vi}} + 2\eta)}, \qquad Q_s = \frac{\mu}{\omega\eta}. \tag{2.35}$$

2.2.2 Lamb's Problem

The expression *"Lamb's problem"* is usually used in the literature to denote a class of problems dealing with waves that are propagating due to the action of a time-dependent concentrated force suddenly applied to an homogeneous and isotropic elastic half-space. This classical problem dates back to the early twentieth century, when Horace Lamb investigated the propagation of a pulse in an elastic half space [122]. In particular, Lamb started focusing on a two-dimensional problem, namely the motion of an half-space due to a line load acting at the boundary in the vertical direction (i.e., in the direction perpendicular to the boundary plane). Subsequently, he also studied similar problems in which the force is applied on the boundary in the horizontal (i.e., tangential) direction or it is acting at a finite depth within the half-space (buried load). Lamb's intention was to consider the effect of an inpulsive force, thus computing transient solutions of the problem. However, he first started to compute solutions corresponding to the effect produced by a time-harmonic function that were then used to obtain the transient solution by means of Fourier synthesis. Lamb showed that the surface motions are characterized by three distinct epochs agreeing with the arrival of longitudinal, transverse, and surface (or Rayleigh) wavefronts. Then, he studied the axisymmetric three-dimensional version of his problem, in which an elastic half-space is subjected by a vertical point force, acting either as a surface traction or a buried source. Even in this case, surface waves were shown to exist as cylindrical wavefronts traveling away from the point of application of the force. The computation of the boundary solution for the asymmetric three-dimensional case of Lamb's Problem (i.e., the case due to a horizontal force) and the computation of the transient solution for interior points of the half-space were not addressed by Lamb. Since Lamb's initial contributions, there has been a significant interest in this problem that has lead many researchers to study its various aspects and several special cases for decades, resulting in both numerical and closed-form solutions. A schematic overview of some of the most important contributions to this problem, which will be briefly discussed in the remainder of this section, is presented in Table 2.1. In 1955 Pekeris computed transient surface solutions of the Lamb's Problem considering both the case in which the point load is vertically applied to the surface [197] and the case in which the load is applied at a finite depth in the half-space [198, 199]. In the former problem, he was able to obtain closed-form solutions, whereas in the latter, he was able to derive solutions in integral form. In either case, the time-dependence of the load was defined by the Heaviside unit step function. Pekeris' transient surface solutions have shown that the Rayleigh surface wavefront arrives after the longitudinal and transverse wavefronts and it has an amplitude which is

Author	Load Orientation		Load Placement		Solution type		Solution Form		Restriction ν
	Vertical	Horizontal	Surface	Buried	Boundary	Interior	Integral	Closed	
Pekeris [197]	✓		✓		✓			✓	✓
Pekeris [198]	✓			✓	✓		✓		✓
Chao [200]		✓	✓		✓			✓	✓
Mooney [201]	✓		✓		✓		✓		
Eason [202]	✓		✓			✓	✓		
Johnson [203]	✓	✓	✓	✓	✓	✓	✓		
Richards [204]	✓	✓	✓		✓			✓	
Kausel [205]	✓	✓	✓		✓			✓	

Table 2.1: Summary of some papers providing significant contributions to the solution of Lamb's Problem.

infinite if the load is exerted on the surface and finite if the load is applied at an interior point. In 1960, Chao [200] extended the transient surface closed-form solutions of the Lamb's Problem by considering an horizontal point load acting on the free-surface of the half-space. All the results presented so far were based on the assumption that the half-space is composed of a Poisson material, meaning that the Lamè elastic constants of the material are equal ($\lambda = \mu$) and therefore the Poisson's ratio ν is equal to 0.25. This restriction was removed for the first time by Mooney [201], who generalized Pekeris' work by computing integral form solutions of the problem with a vertical point load acting on the surface of the half-space having arbitrary Poisson's ratio. By means of convolution, Mooney also investigated the effect of changing the time dependence of the point source, thereby extending the result to arbitrary source waveforms. In 1966, Eason [202] was the first to investigate the axysimmetric transient interior solutions of the Lamb's Problem. In addition to a vertical surface point load, Eason also studied the case in which axysimmetric patch loads were applied on the surface of the half-space. The solution presented by Eason were given in integral-form and were not restricted to Poisson's materials. The numerical evaluation of the integral transient solutions derived by Eason showed that the amplitude of the Rayleigh travelling surface wavefront diminishes rapidly to finite values as the depth of point within the half-space increases. In 1974, Johnson [203] presented a comprehensive set of transient solutions expressed in integral form and valid for both interior and boundary points. These solutions were derived for both the cases of vertical and horizontal point loads acting either within the half-space or in its free surface. Johnson's work is regarded as the complete and concluding account to the transient solutions of the Lamb's Problem, as far as the final solution is given in integral form. In 1979, Richards [204] presented closed-form transient boundary solutions for the Lamb's Problem that are not restricted to Poisson's materials and valid for a point load acting on the free surface of the half-space in an arbitrary direction. These expressions, lately derived also by Kausel [205], completed the contributions given by Pekeris [197] and Chao [200], which were restricted to Poisson's materials.

Plane Strain Lamb's Problem

Let us consider a uniform (with respect to y) normal line load that is suddenly applied to the surface of an elastic half space, $z \geq 0$, at time $t = 0\,\mathrm{s}$. The uniformity of the loading in the y direction makes this a plane strain problem (i.e., $u_y = 0$ and $\partial/\partial y = 0$). When the applied load has the form $F(x, z, t) = (0, \delta(x)\delta(z)\delta(t))$, $\delta(\cdot)$ being the Dirac delta function, the displacements along the x and z direction for points lying on the surface $z = 0\,\mathrm{m}$ are defined as follows [206]:

$$u_x(\tau, x, z = 0) = \frac{2k^3 C_s}{\pi\mu x}\left\{\frac{\tau STU}{R_1}\left[H(\tau - 1) - H(\tau - k)\right] - \frac{\pi(2 - k_R^2)^3}{8G}\delta(\tau - \zeta_R)\right\}, \tag{2.36a}$$

$$u_z(\tau, x, z = 0) = \frac{k^3 C_s}{\pi\mu x}\left\{\frac{S^2 T}{R_1}\left[H(\tau - 1) - H(\tau - k)\right] - \frac{T}{R_2}H(\tau - k)\right\}, \tag{2.36b}$$

where

$$\tau = C_p t/x, \qquad k = C_p/C_s, \qquad k_R = C_R/C_s, \qquad \zeta_R = k/k_R = C_p/C_R,$$
$$S = k^2 - 2\tau^2, \qquad T = \sqrt{\tau^2 - 1}, \qquad U = \sqrt{k^2 - \tau^2}, \qquad V = \sqrt{\tau^2 - k^2},$$
$$G = 8(k^2-1) - 4k^2k_R^4 + k^2k_R^6, \qquad R_1 = S^4 + 16\tau^4T^2U^2, \qquad R_2 = S^2 - 4\tau^2TV.$$

Notice that τ is a non-dimensional time defined in such a way $\tau = 1$ denotes the time of arrival of P-waves on the point having coordinate x. As a consequence, $\tau = k$ and $\tau = \zeta_R$ denote the time of arrival of S-waves and Rayleigh waves, respectively. The time behaviour of the displacements u_x and u_z at $x = 0.1\,\mathrm{m}$ are shown in Figure 2.9 for a material characterized by a density $\rho = 1\,\mathrm{kg\,m^{-3}}$ and by elasticity parameters $\lambda = 0.27\,\mathrm{Pa}$ and $\mu = 0.033\,\mathrm{Pa}$. In the general case, when the time dependence of the uniform normal line load is defined through a function $f(t)$ that is different from the Delta function considered before, the horizontal and vertical displacement responses can be obtained by means of the convolution between the function $f(t)$ and the functions u_x and u_z defined in (2.36). In particular, if we consider the so-called Ricker Wavelet

$$f(t) = A(1 - 2(\pi f_0(t-t_0))^2)\exp\left(-(\pi f_0(t-t_0))^2\right), \tag{2.37}$$

with parameters $A = 1\,\mathrm{m}$, $f_0 = 2\,\mathrm{Hz}$ and $t_0 = 1\,\mathrm{s}$, we obtain that the displacement field in $x = 0.1\,\mathrm{m}$ and $z = 0\,\mathrm{m}$ is as shown in the top row of Figure 2.10. Similarly, the convolution between the displacement u_x (resp. u_z) and the derivative of the function $f(t)$ provides the horizontal (resp. vertical) component of the velocity shown in the bottom row of Figure 2.10.

Axisymmetric Lamb's Problem

Let us now consider a point load (and not a line load as in the previous case) acting on the free surface $z = 0$ of an homogeneous and isotropic elastic half-space $z \le 0$. Moreover, assume that the direction of the point load is given by the positive direction $z-$axis and consider the time dependence of the point load to be defined by the Heaviside unit step function $H(t)$. Owing to the symmetry of the problem, we shall consider a cylindrical coordinate system r, θ, z. The radial and vertical displacements u_r and u_z at a point on the free surface having coordinate r are given by [205]:

$$u_z(\tau, r) = \frac{1-\nu}{2\pi\mu r}\begin{cases} \dfrac{1}{2}\left(1 - \displaystyle\sum_{i=1}^{3}\frac{A_j}{\sqrt{\tau^2-\kappa_j^2}}\right), & a < \tau < 1, \\ 1 - \dfrac{A_1}{\sqrt{\tau^2-\gamma^2}}, & 1 \le \tau < \gamma, \\ 1, & \tau \ge \gamma, \end{cases} \tag{2.38a}$$

$$u_r(\tau, r) = \frac{\tau}{8\pi\mu r}\begin{cases} \dfrac{1}{\pi(1-a^2)^{3/2}}\left(2K(n) - \sum_{i=1}^{3} B_j \Pi(n^2 m_j, n)\right), & a < \tau < 1, \\ \dfrac{n^{-1}}{\pi(1-a^2)^{3/2}}\left(2K(n^{-1}) - \sum_{i=1}^{3} B_j \Pi(m_j, n^{-1})\right), & 1 \le \tau < \gamma, \\ \dfrac{n^{-1}}{\pi(1-a^2)^{3/2}}\left(2K(n^{-1}) - \sum_{i=1}^{3} B_j \Pi(m_j, n^{-1})\right) + \dfrac{2}{\sqrt{\tau^2-\gamma^2}}D, & \tau \ge \gamma. \end{cases} \tag{2.38b}$$

As in the plane strain problem, the displacemenet field is given in terms of the non-dimensional time $\tau = tC_S/r$. However, in this case τ is defined in such a way it marks the time of arrival of the S-wave (and not the P-wave as before). Moreover, $a = C_S/C_P$ denotes the time of arrival of the pressure P-wave and $\gamma = C_R/C_S$ denotes the time of arrival of the Rayleigh surface wave. Then, κ_1^2, κ_2^2 and κ_3^2 are the three roots of the bi-cubic Rayleigh function

$$16(1-a^2)\kappa^6 - 8(3-2a^2)\kappa^4 + 8\kappa^2 - 1 = 0.$$

In particular, κ_1 is the real, true Rayleigh root and $\kappa_1 \equiv \gamma$, while the remaining two are the non-physical roots. At low Poisson's ratio κ_2 and κ_3 are real-valued, but they turn complex when Poisson's

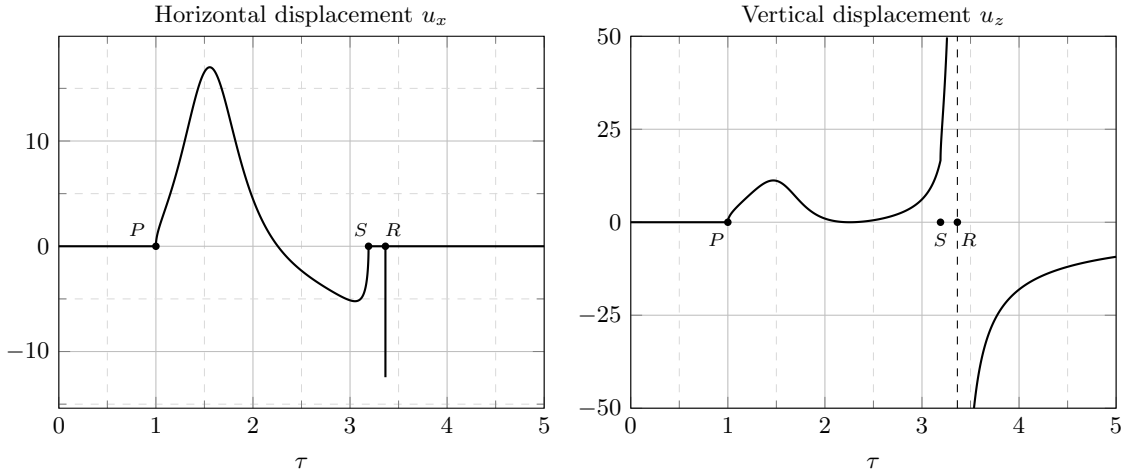


Figure 2.9: Response to a line load suddenly applied along the $y-$axis and normal to the surface $z = 0\,\text{m}$. Both the horizontal and vertical displacement are given as functions of the non-dimensional time τ. The letters P, S and R denote the time of arrival of $P-$waves, $S-$waves and Rayleigh waves. In the horizontal component of the displacement, the vertical segment at $\tau = \zeta_R$ is used to denote the contribution given by the Dirac delta function in (2.36a) and, in particular, the length of the segment is equal to the coefficient of the delta.

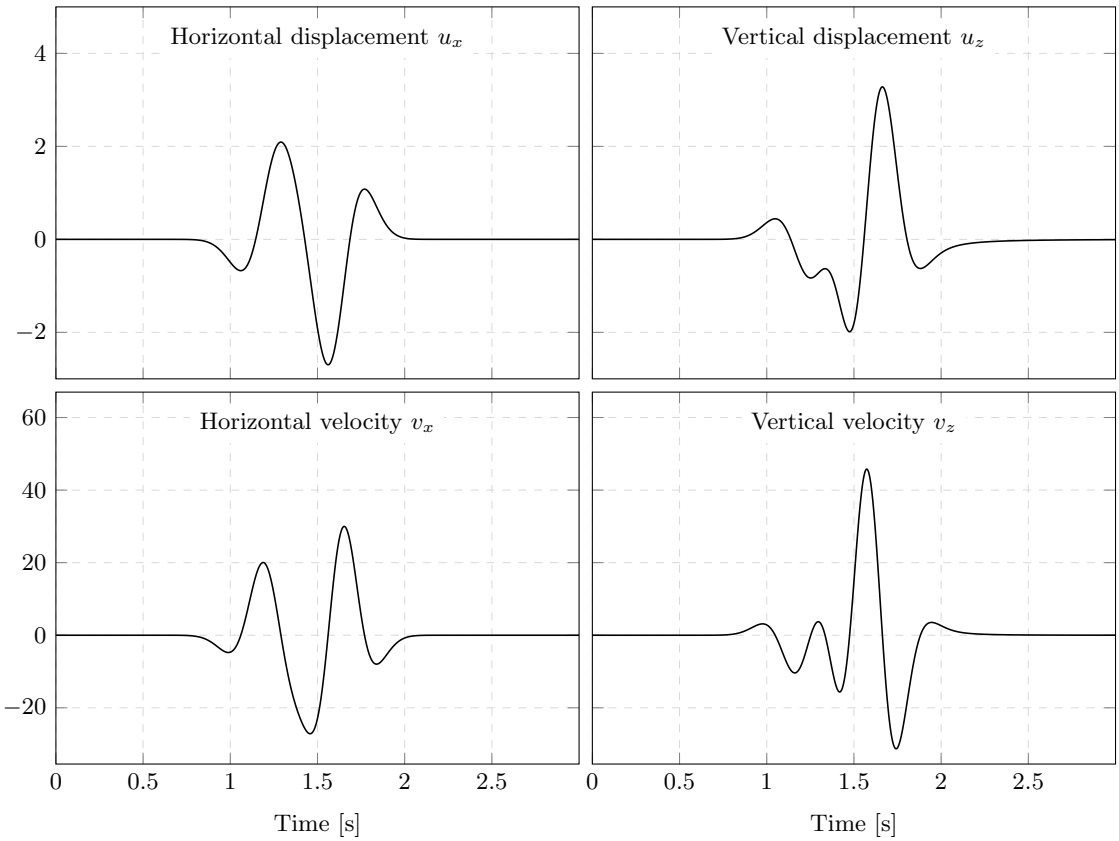


Figure 2.10: Response to a line load applied to the $y-$axis and normal to the surface $z = 0\,\text{m}$. The time dependence of the applied load is given by the Ricker wavelet defined in (2.37). The left and right columns show, respectively, the horizontal and vertical components of the displacement (top row) and the velocity (bottom row) field.

ratio exceeds the threshold $\nu > 0.2631$. Then, the coefficients A_j, B_j, C_j and D_j, $j = 1, 2, 3$, are defined as follows:

$$A_j = \frac{\left(\kappa_j^2 - \frac{1}{2}\right)^2 \sqrt{a^2 - \kappa_j^2}}{D_j}, \qquad B_j = \frac{(1 - 2\kappa_j^2)(1 - \kappa_j^2)}{D_j}, \qquad C_j = \frac{(1 - \kappa_j^2)\sqrt{a^2 - \kappa_j^2}}{D_j},$$

$$D_j = (\kappa_j^2 - \kappa_i^2)(\kappa_j^2 - \kappa_k^2), \qquad i \neq j \neq k.$$

Finally, the coefficients n, m_j and D are defined as

$$n^2 = \frac{\tau^2 - a^2}{1 - a^2} \qquad m_j = \frac{1 - a^2}{a^2 - \kappa_j^2}, \qquad D = \frac{(2\gamma^2 - 1)^3}{8(1 - a^2)\gamma^6 - 4\gamma^2 + 1}.$$

while $K(n)$ and $\Pi(m, n)$ are the complete elliptic functions of the first and third kind, respectively, i.e.,

$$K(n) = \int_0^{\pi/2} \frac{d\theta}{\sqrt{1 - n^2 \sin^2 \theta}}, \qquad \Pi(m, n) = \int_0^{\pi/2} \frac{d\theta}{(1 + m \sin^2 \theta)\sqrt{1 - n^2 \sin^2 \theta}}.$$

The (non-dimensional) time behaviour of the surface displacements u_r and u_z due to the application of a pressure pulse varying in time as the Heaviside unit function $H(t)$ are shown in Figure 2.11. The elastic material is characterized by density $\rho = 1\,\mathrm{kg\,m^{-3}}$ and by Lamè parameters $\lambda = 0.27\,\mathrm{Pa}$ and $\mu = 0.033\,\mathrm{Pa}$. Before the arrival of the pressure wave, the medium is completely at rest while at the arrival of the P-wave both the radial and vertical velocities experience a sudden jump. Then, the arrival of the shear wave is marked only by a discontinuity in slope of the displacement, while at the time of the arrival of the Rayleigh surface wave the displacement becomes infinite. Subsequently, the vertical displacement immediately assumes its steady-state value whereas the radial displacement monotonically approaches its steady state value at infinite time. When the point load varies with time like the Ricker Wavelet defined in (2.37), the radial and vertical displacement responses can be obtained by means of the convolution between the derivative of the wavelet and the functions u_r and u_z defined in (2.38). Moreover, the convolution between the displacement u_r (resp. u_z) and the second derivative of the Ricker Wavelet provides the radial (resp. vertical) component of the velocity. The displacement and velocity fields in $r = 0.1\,\mathrm{m}$ and $z = 0\,\mathrm{m}$ and due to the effect of the point load are shown in Figure 2.12.

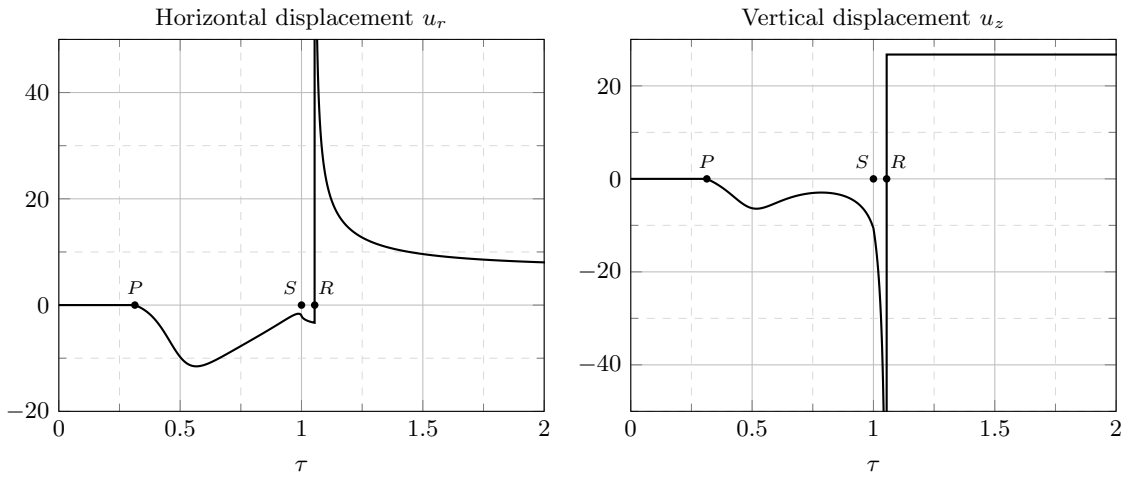


Figure 2.11: Response to a point load varying with time like the Heaviside unit function $H(t)$ and applied at the free surface $z = 0$ of an elastic half space $z \leq 0$ in the direction defined by the positive $z-$axis. Both the horizontal and vertical displacement are given as functions of the non-dimensional time τ. The letters P, S and R denote the time of arrival of $P-$waves, $S-$waves and Rayleigh waves.

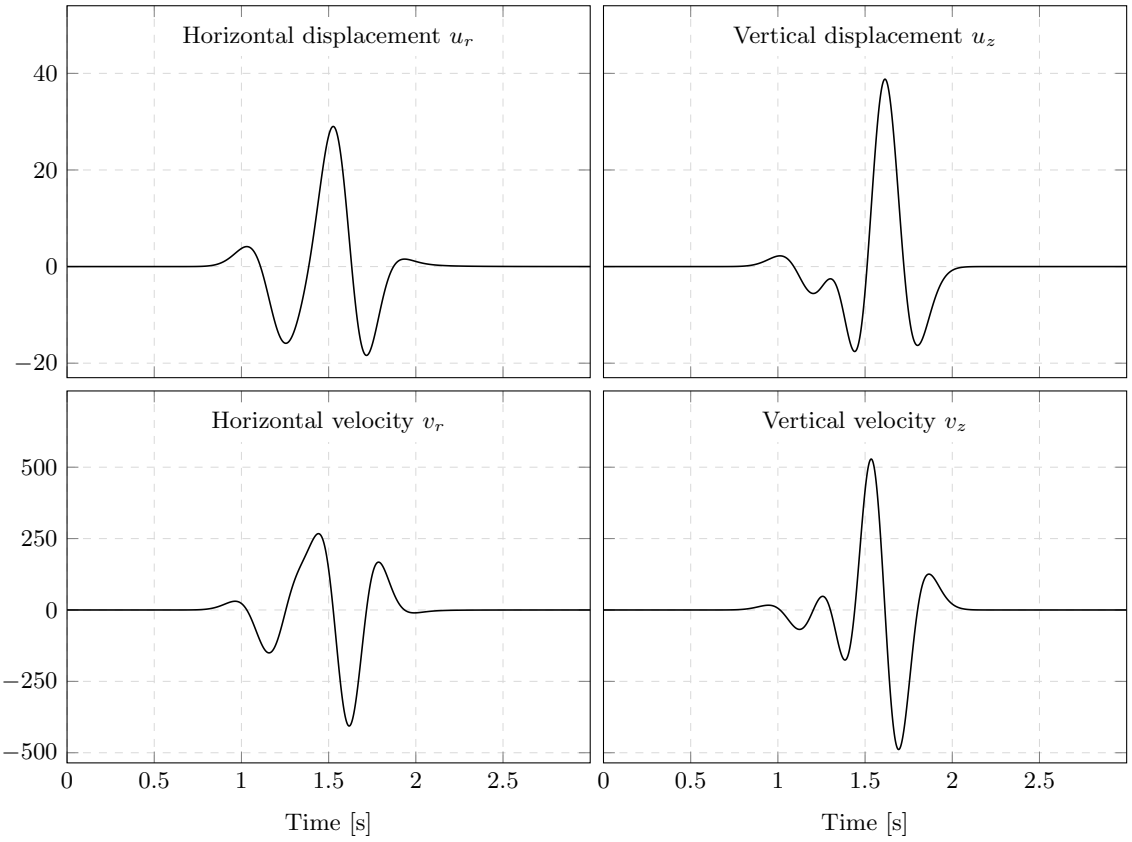


Figure 2.12: Response to a point load applied at the free surface $z = 0$ of an elastic half space $z \leq 0$ in the direction defined by the positive $z-$axis. The time dependence of the applied load is given by the Ricker wavelet defined in (2.37). The left and right columns show, respectively, the horizontal and vertical components of the displacement (top row) and the velocity (bottom row) field.

Chapter 3

PDEs in Hilbert Spaces

As we have seen in Section 2.2.1, the propagation of waves in Kelvin-Voigt linear viscoelastic materials is governed by the following vector Partial Differential Equation:

$$\rho\ddot{\boldsymbol{u}} - \operatorname{div}\boldsymbol{\sigma}_{\text{vi}}(\dot{\boldsymbol{u}}) - \operatorname{div}\boldsymbol{\sigma}_{\text{el}}(\boldsymbol{u}) = \boldsymbol{f}. \tag{3.1}$$

In order to prove the existence and uniqueness of the solution of the boundary value problem obtained by combining equation (3.1) with suitable boundary and initial conditions, we discuss the more general case given by the following abstract second-order linear evolution equation

$$\mathcal{C}\ddot{u}(t) + \mathcal{B}\dot{u}(t) + \mathcal{A}u(t) = f(t), \tag{3.2}$$

where $\mathcal{A}$, $\mathcal{B}$ and $\mathcal{C}$ are linear and continuous operators between Hilbert spaces. However, before addressing second-order linear evolution equations, some knowledge about elliptic problems and first-order evolution equations is required. The aim of this Chapter is to introduce all the necessary results. In Section 3.1 provides some preliminary definitions that are essential for understanding the remaining part of the Chapter. In Section 3.2 we briefly introduce the theory of linear elliptic boundary value problems. In particular, we discuss the classical elliptic second order problem (§3.2.1) and the linear elastic problem (§3.2.3). The latter is particularly important for the purposes of this thesis because, as discussed in detail in Chapter 2 and as can be also seen in equation (3.1), the Kelvin-Voigt constitutive relation defines the stress tensor as the sum of a linear elastic contribution and a linear viscous contribution. In this regard, the results about the coercivity and continuity of the bilinear form associated to the linear elastic differential operator (Propositions 3.2 and 3.3, respectively) will be employed in Chapter 5. In Section 3.2.2 we derive some error estimates for the approximation of the solution of elliptic partial differential equations and we introduce the main properties regarding the classical Finite Element approximation. In Section 3.3 we introduce the theory of linear contraction semigroups and discuss its application to solve initial-boundary value problems for *first-order explicit linear evolution equations*, i.e., Partial Differential Equations in which the first derivative in time of the solution is present and is explicitely given. Then, in Sections 3.4 and 3.5 we extend the results to cover *implicit first-order evolution equations* (i.e., evolution equations in which the time derivative is not given explicitely) and *second-order evolution equations* (i.e., evolution equations in the form given by equation (3.2), where the second derivative in time of the solution is present), respectively. Once again, we emphasize that second-order linear evolution equations represent our case of interest, since the vector Partial Differential Equation governing the propagation of waves in Kelvin-Voigt materials is exactly of this type. Almost all the results presented in this Chapter are taken from the book *"Hilbert Space Methods for Partial Differential Equations"* by Showalter [182], with the exception of the main properties characterising the classical Finite Element approximation, which are presented in Section 3.2.2 and are taken from [207].

3.1 Preliminary Definitions

Definition 3.1 (Sesquilinear form)**.** Let V be a linear space over the field $\mathbb{K}$. A sesquilinear form on V is a $\mathbb{K}-$valued function $a(\cdot,\cdot)$ on the product $V \times V$ such that $x \mapsto a(x,y)$ is linear for every $y \in V$ and $y \mapsto a(x,y)$ is conjugate linear for every $x \in V$.

Definition 3.2 (Continuity)**.** The sesquilinear form $a(\cdot,\cdot)$ defined on the Hilbert space V is said to be continuous if there exists a constant $M > 0$ such that

$$|a(u,v)| \leq M\|u\|_V\|v\|_V, \quad u,v \in V.$$

Definition 3.3 (V-coercivity)**.** The sesquilinear form $a(\cdot,\cdot)$ on the Hilbert space V is said to be $V-$coercive if there is a $c > 0$ such that

$$|a(v,v)| \geq c\|v\|_V^2, \quad \forall v \in V.$$

Definition 3.4 (V-ellipticity)**.** The sesquilinear form $a(\cdot,\cdot)$ on the Hilbert space V is said to be $V-$elliptic if there is a $c > 0$ such that

$$\Re\, a(v,v) \geq c\|v\|_V^2, \qquad \forall v \in V.$$

Definition 3.5 (Monotone Operator)**.** The linear operator $\mathcal{L}\colon V \to V'$ is said to be monotone (or non-negative) if

$$\Re(\mathcal{L}x(x)) \geq 0, \qquad x \in V.$$

We call $\mathcal{L}$ strictly monotone (or positive) if

$$\Re(\mathcal{L}x(x)) > 0, \qquad x \in V,\ x \neq 0.$$

Definition 3.6 (Accretive Operator)**.** Let H be a Hilbert space, $D(A)$ a subspace of H and $A \in \mathcal{L}(D(A), H)$. We say that the operator A is accretive if

$$\Re\,(Ax,x)_H \geq 0, \quad x \in D(A).$$

Definition 3.7 (Gårding Inequality)**.** Let H be an Hilbert space and V a subspace of X for which the injection is continuous, i.e., $V \hookrightarrow X$. The sesquilinear form $a(\cdot,\cdot)\colon V \times V \to \mathbb{K}$ is said to satisfy the Gårding inequality if there exist constants $\alpha, \beta > 0$ such that

$$\Re\, a(u,u) \geq \alpha\|u\|_V^2 - \beta\|u\|_X^2, \quad \forall u \in V.$$

3.2 Preliminary Results on Elliptic Problems

3.2.1 An Elliptic Second Order Example

Let Ω be an open set in $\mathbb{R}^n$ and suppose we are given a collection of functions a_{ij}, $1 \leq i,j \leq n$, b_j, $1 \leq j \leq n$ and c in $L^\infty(\Omega)$. Let $H = L^2(\Omega)$ and $V \subset H$. Consider the linear operator $L \in \mathcal{L}(V, V')$ defined by

$$Lu = -\sum_{i,j=1}^{n} \partial_i(a_{ij}(x)\partial_j u(x)) + \sum_{i=1}^{n} \partial_i(b_j(x)u(x)) + c(x)u(x)$$

and define the sesquilinear form $a(\cdot,\cdot)\colon V \times V \to \mathbb{R}$ associated to the operator L as follows

$$a(u,v) = \int_\Omega \left\{ \sum_{i,j=1}^{n} a_{ij}(x)\partial_i u(x)\partial_j \bar{v}(x) + \sum_{j=1}^{n} b_j(x)\partial_j u(x)\bar{v}(x) + c(x)u(x)\bar{v}(x) \right\} dx. \tag{3.3}$$

Definition 3.8. The sesquilinear form (3.3) is called strongly elliptic if there is a constant $c_0 > 0$ such that

$$\Re\left(\sum_{i,j=0}^{n} a_{ij}(x)\xi_i\bar{\xi}_j \right) \geq c_0 \sum_{j=1}^{n} |\xi_j|^2,$$

for a.e. $x \in \Omega$ and every $\xi = (\xi_1, \ldots, \xi_n) \in \mathbb{R}^n$.

Remark 3.1. Ellipticity means that for each point $x \in \Omega$, the symmetric $n \times n$ matrix $A(x) = (a_{ij}(x))_{i,j=1,\ldots,n}$ is positive definite, with smallest eigenvalue greater than or equal to c_0.

Theorem 3.1 (see [182, Theorem III.5.1]). *Let the sesquilinear form $a(\cdot,\cdot)$ in equation (3.3) be defined on $V \equiv H_0^1(\Omega)$ and be strongly elliptic. Then, it satisfies Gårding inequality, i.e.,*

$$\Re\, a(u,u) \geq \alpha \|u\|_{H^1(\Omega)} - \beta \|u\|^2_{L^2(\Omega)}, \quad \forall u \in H_0^1(\Omega). \tag{3.4}$$

Proof (adapted from [182, Theorem III.5.1]). Let $K_1 = \max\{\|b_j\|_{L^\infty(\Omega)} : 1 \leq j \leq n\}$. Then, for $1 \leq j \leq n$ and each $\varepsilon > 0$ we have

$$\begin{aligned} |(b_j \partial_j u, u)_{L^2(\Omega)}| &\leq K_1 \|\partial_j u\|_{L^2(\Omega)} \|u\|_{L^2(\Omega)} \\ &\leq (K_1/2) \left(\varepsilon \|\partial_j u\|^2_{L^2(\Omega)} + (1/\varepsilon)\|u\|^2_{L^2(\Omega)} \right). \end{aligned}$$

Now let $K_0 = \operatorname{ess\,inf}\{\Re\, c(x) : x \in \Omega\}$. Recalling that the sesquilinear form (3.3) is strongly elliptic, we obtain, for all $u \in H_0^1(\Omega)$,

$$\begin{aligned} \Re\, a(u,u) &\geq c_0 \|\nabla u\|^2_{L^2(\Omega)} + K_0 \|u\|^2_{L^2(\Omega)} - (\varepsilon K_1/2)\|\nabla u\|^2_{L^2(\Omega)} - (nK_1/2\varepsilon)\|u\|^2_{L^2(\Omega)} \\ &\geq (c_0 - \varepsilon K_1/2)\|\nabla u\|^2_{L^2(\Omega)} + (K_0 - nK_1/2\varepsilon)\|u\|^2_{L^2(\Omega)}. \end{aligned}$$

Choosing $\varepsilon > 0$ so that $K_1 \varepsilon = c_0$ and defining $\beta = -(K_0 - nK_1^2/2c_0)$, we get

$$\Re\, a(u,u) \geq (c_0/2)\|\nabla u\|^2_{L^2(\Omega)} - \beta \|u\|^2_{L^2(\Omega)}. \tag{3.5}$$

Owing to Poincarè inequality, we finally obtain equation (3.4). □

Theorem 3.2 (see [182, Theorem III.5.1]). *Let the sesquilinear form $a(\cdot,\cdot)$ in equation (3.3) be defined on $V \equiv H^1(\Omega)$ and be strongly elliptic. Then, there exists a $\lambda_0 \in \mathbb{R}$ such that for every $\lambda > \lambda_0$, the form*

$$a_\lambda(u,v) := a(u,v) + \lambda \int_\Omega u(x)\overline{v}(x)\, dx \tag{3.6}$$

is $H^1(\Omega)-$coercive.

Proof (adapted from [182, Theorem III.5.1]). The proof of Theorem 3.1 has shown that, for all $v \in H^1(\Omega)$, inequality (3.5) holds:

$$\Re\, a(u,u) \geq \alpha \|\nabla u\|^2_{L^2(\Omega)} - \lambda_0 \|u\|^2_{L^2(\Omega)}.$$

Therefore, taking $\lambda > \lambda_0$, we have

$$\begin{aligned} |a_\lambda(u,u)| \geq \Re\, a_\lambda(u,u) &= \Re\, a(u,u) + \lambda \|u\|^2_{L^2(\Omega)} \\ &\geq (c_0/2)\|\nabla u\|^2_{L^2(\Omega)} + (\lambda - \lambda_0)\|u\|^2_{L^2(\Omega)} \\ &\geq \min(c_0/2, \lambda - \lambda_0)\|u\|^2_{H^1(\Omega)}, \end{aligned}$$

which shows that the form defined in equation (3.6) is $H^1(\Omega)$-coercive. □

Definition 3.9 ($k-$regularity). Let V be a closed subspace of $H^1(\Omega)$ with $H_0^1(\Omega) \leq V$, and let $a(\cdot,\cdot)$ be a continuous sesquilinear form on V. Then, $a(\cdot,\cdot)$ is called $k-$regular on V if for every $F \in H^s(\Omega)$ with $0 \leq s \leq k$ and every solution $u \in V$ of

$$a(u,v) = (F,v)_{L^2(\Omega)}, \quad v \in V$$

we have $u \in H^{2+s}(\Omega)$.

Theorem 3.3 (Lax-Milgram, see [208, Section 2.7]). *Given an Hilbert space V, a continuous and coercive bilinear form $a\colon V \times V \to \mathbb{R}$ and a continuous linear functional $F \in V'$, there exists an unique solution $u \in V$ such that*

$$a(u,v) = F(v) \qquad \forall v \in V.$$

3.2.2 Approximation of Elliptic Problems

Let V be a Hilbert space, $a(\cdot,\cdot)\colon V\times V\to\mathbb{K}$ a continuous and sesquilinear form and $f\in V'$. Consider the following abstract boundary value problem:

$$\text{find } u\in V \;:\; a(u,v)=f(v),\quad v\in V. \tag{3.7}$$

Let S be a subspace of V. Then, we consider the related problem

$$\text{find } u_s\in S \;:\; a(u_s,v)=f(v),\quad v\in S. \tag{3.8}$$

The next result show that the error $u-u_s$ is small if S approximates V sufficiently well.

Theorem 3.4 (see [182, Theorem VII.5.1]). *Let $a(\cdot,\cdot)\colon V\times V\to\mathbb{K}$ be a $V-$coercive sesquilinear form and $f\in V'$. Let S be a closed subspace of V. Then problem (3.7) has a unique solution u and problem (3.8) has a unique solution u_s. Furthermore we have the estimate*

$$\|u-u_s\|_V\le\frac{\gamma}{\alpha}\inf\{\|u-v\|_V\;:\;v\in S\}, \tag{3.9}$$

where γ and α are the continuity and coercivity constants of $a(\cdot,\cdot)$, respectively.

Proof (adapted from [182, Theorem VII.5.1]). The existence and uniqueness of the solutions u and u_s of problems (3.7) and (3.8) follow immediately from Lax-Milgram Theorem 3.3. We now have to verify the bound (3.9). Subtracting (3.8) from (3.7), we obtain

$$a(u-u_s,v)=0,\qquad v\in S. \tag{3.10}$$

Therefore, for any $w\in S$ we have

$$a(u-u_s,u-u_s)=a(u-u_s,u-w)+\cancel{a(u-u_s,w-u_s)},$$

where the last term vanishes because $w-u_s\equiv v\in S$. Moreover, since $a(\cdot,\cdot)$ is continuous and coercive, we obtain

$$\alpha\|u-u_s\|_V^2\le a(u-u_s,u-u_s)=a(u-u_s,u-w)\le\gamma\|u-u_s\|_V\|u-w\|_V,\quad\forall w\in S,$$

which implies (3.9). □

Theorem 3.5 (see [182, Theorem VII.5.2]). *Let $a(\cdot,\cdot)$ be a continuous, sesquilinear and coercive form on the Hilber space V and let H be a Hilber space identified with its dual and in which V is dense and continuously embedded. Thus, $V\hookrightarrow H\hookrightarrow V'$. Let $A^*\colon D^*\to H$ be the operator on H which is determined by the adjoint sesquilinear form, i.e.,*

$$\overline{a(v,w)}=(A^*w,v)_H,\qquad w\in D^*,\ v\in V.$$

Let S be a closed subspace of V and $e^*(S)$ a corresponding constant for which we have

$$\inf\{\|w-v\|_V\;:\;v\in S\}\le e^*(S)\|A^*w\|_H,\qquad w\in D^*. \tag{3.11}$$

Then, the solution of problem (3.7), i.e.,

$$\textit{find } u\in V \;:\; a(u,v)=f(v),\quad v\in V,$$

and the solution of problem (3.8), i.e.,

$$\textit{find } u_s\in S \;:\; a(u_s,v)=f(v),\quad v\in S,$$

satisfy the estimate

$$\|u-u_s\|_H\le(\gamma^2/\alpha)\inf\{\|u-v\|_V\;:\;v\in S\}e^*(S). \tag{3.12}$$

Proof (adapted from [182, Theorem VII.5.2]). We assume $u \neq u_s$ and define

$$g = \frac{u - u_s}{\|u - u_s\|_H}.$$

Then, we choose $w \in D^*$ so that $A^*w = g$, that is,

$$a(v, w) = (v, g)_H, \quad v \in V.$$

This implies that

$$\|u - u_s\|_H = (u - u_s, g)_H = a(u - u_s, w).$$

Using the Galerkin orthogonality (3.10), the continuity of $a(\cdot, \cdot)$ and (3.11), we obtain, for any $v \in S$,

$$\begin{aligned} \|u - u_s\|_H &= a(u - u_s, w) \\ (3.10) &= a(u - u_s, w - v) \\ \text{continuity} &\leq \gamma \|u - u_s\|_V \|w - v\|_V \\ (3.11) &\leq \gamma \|u - u_s\|_V e^*(S) \|A^*w\|_H \\ (3.9) &\leq (\gamma^2/\alpha) \|u - v\|_V e^*(S) \|A^*w\|_H. \end{aligned}$$

Since $\|A^*w\|_H = \|g\|_H = 1$, we obtain (3.12). □

Corollary 3.1 (see [182, Corollary VII.5.3]). *Let $A\colon D \to H$ be the operator on H determined by the sesquilinear form $a(\cdot, \cdot)$ defined on the Hilbert space V assumed to be dense and continuously embedded in H, i.e.,*

$$a(w, v) = (Aw, v)_H, \qquad w \in D, v \in V.$$

Let $e(S)$ be a constant for which

$$\inf\{\|w - v\|_V \ : \ v \in S\} \leq e(S) \|Aw\|_H, \quad w \in D. \tag{3.13}$$

Then, the solution of problem (3.7), i.e.,

$$\textit{find } u \in V \ : \ a(u, v) = f(v), \quad v \in V,$$

and the solution of problem (3.8), i.e.,

$$\textit{find } u_s \in S \ : \ a(u_s, v) = f(v), \quad v \in S,$$

satisfy the estimate

$$\|u - u_s\|_H \leq (\gamma^2/\alpha) e^*(S) e(S) \|Au\|_H. \tag{3.14}$$

Proof. Using (3.13) in (3.12) we obtain (3.14). □

Finite Element Approximation Error Estimates

Finite Element Triangulation. Let $\Omega \subset \mathbb{R}^d$, $d = 2, 3$, be a polygonal domain, i.e., Ω is an open and bounded subset such that $\overline{\Omega}$ is the union of a finite number of polyhedra. $\mathcal{T}_h$ is called a *triangulation* of $\overline{\Omega}$ if

$$\overline{\Omega} = \bigcup_{K \in \mathcal{T}_h} K,$$

where

- each K is a polyhedron with $\mathring{K} \neq \emptyset$;
- $\mathring{K}_1 \cap \mathring{K}_2 = \emptyset$ for each distinct $K_1, K_2 \in \mathcal{T}_h$;
- if $F = K_1 \cap K_2 \neq \emptyset$ (K_1 and K_2 distinct elements of $\mathcal{T}_h$) then F is a common face, side or vertex of K_1 and K_2;

- $\mathrm{diam}(K) \leq h$ for each $K \in \mathcal{T}_h$.

Hereafter, we confine ourselves to the case in which K is a triangle, when $d = 2$, or a tetrahedron, when $d = 3$. For the sake of simplicity, we shall also assume that each element K of the triangulation $\mathcal{T}_h$ can be obtained as $K = T_K(\hat{K})$, where $\hat{K}$ is the unit $d-$simplex and T_K is a suitable invertible affine map.

Definition 3.10. A family of triangulations $\mathcal{T}_h$, $h > 0$, is called regular if there exists a constant $\sigma \geq 1$ such that

$$\max_{K \in \mathcal{T}_h} \frac{h_K}{\rho_K} \leq \sigma \qquad \forall h > 0,$$

where

$$h_K := \mathrm{diam}(K), \qquad \rho_K := \sup\{\mathrm{diam}(S) \,|\, S \text{ is a ball contained in } K\}.$$

Piecewise-Polynomial Subspaces. We now define the finite dimensional spaces S_h that are most commonly used in the context of Finite Elements. We start by defining S_h as the space containing all the functions that are piecewise-polynomials and that represents a suitable approximation of the infinite dimensional space V. Let us now denote by $\mathbb{P}_k$, $k \geq 0$, the space of polynomials of degree less than or equal to k in the variables $x_1, \ldots, x_d$. Then, we define the space of *finite elements* S_h of degree k as

$$S_h = S_h^k := \{v_h \in C^0(\overline{\Omega}) \mid v_h|_K \in \mathbb{P}_k \ \forall K \in \mathcal{T}_h\}, \quad k \geq 1. \tag{3.15}$$

Proposition 3.1 (see [207, Proposition 3.2.1])**.** *A function $v\colon \Omega \to \mathbb{R}$ belongs to $H^1(\Omega)$ if and only if*

- *$v|_K \in H^1(\mathring{K})$ for each $K \in \mathcal{T}_h$;*
- *for each common face $F = K_1 \cap K_2$, $K_1, K_2 \in \mathcal{T}_h$, the trace on F of $v|_{K_1}$ and $v|_{K_2}$ is the same*

Owing to this result, $S_h^k \subset H^1(\Omega)$ for all $k \geq 1$.

Interpolation Operator. We define the interpolation operator π_h^k as the operator from the space of continuous functions and valued in the Finite Element space S_h^k, i.e.,

$$\pi_h^k\colon C^0(\overline{\Omega}) \to S_h^k, \qquad v \mapsto \pi_h^k(v) := \textstyle\sum_{i=1}^{N_h} v(a_i)\varphi_i,$$

where a_i are the coordinates of the nodes of the mesh on $\overline{\Omega}$ and φ_i are the corresponding Lagrangian shape functions. The interpolant $\pi_h^k(v)$ is the unique function in S_h^k which takes the same values of the given function $v \in C^0(\Omega)$ at the nodes a_i. We now provide estimates for the interpolation errors $v - \pi_h^k(v)$.

Theorem 3.6 (see [209, Theorem 4.5])**.** *Let $\mathcal{T}_h$ be a regular family of triangulations and assume that $l = \min(k, s-1) \geq 1$ and $m = 0, 1$. Then, there exists a constant C, independent of h, such that*

$$|v - \pi_h^k(v)|_{H^m} \leq C h^{l+1-m} |v|_{H^{l+1}}, \quad \forall v \in H^s(\Omega). \tag{3.16}$$

Projection Operators. The interpolation operator provides optimal estimates in the Sobolev norms whenever the function to be interpolated enjoys the minimal requirement to be continuous. For the Finite Element analysis it is useful to introduce other operators, namely the $L^2(\Omega)$ and the $H^1(\Omega)-$orthogonal projection operators, which make sense on functions that need not to be continuous. So, let H be an Hilbert space and S a closed subspace of H. We define in H the orthogonal projection operator over S, say P_S, in the following way:

$$P_S(v) \in S \ : \ (P_S(v), \varphi)_H = (v, \varphi)_H, \quad \forall \varphi \in S.$$

Clearly, the orthogonal projection operator P_S is characterised by the property

$$\|v - P_S(v)\|_H = \min_{\varphi \in S} \|v - \varphi\|_H. \tag{3.17}$$

In particular, we consider the following projection operators

$$P_h^k \colon L^2(\Omega) \to S_h^k, \qquad P_{1,h}^k \colon H^1(\Omega) \to S_h^k.$$

If $\mathcal{T}_h$ is a regular family of triangulations, from (3.17) and (3.16) we obtain the following estimates

$$\begin{aligned} \|v - P_h^k(v)\|_{L^2} &\le C h^{l+1} |v|_{H^{l+1}}, \qquad 0 \le l \le k, \\ \|v - P_{1,h}^k(v)\|_{H^1} &\le C h^{l} |v|_{H^{l+1}}, \qquad 0 \le l \le k, \end{aligned} \tag{3.18}$$

for all $v \in H^{l+1}(\Omega)$.

Combining the results presented so far, we obtain the following theorem.

Theorem 3.7 (see [182, Theorem VII.5.4]). *Let V be a closed subspace of $H^1(\Omega)$ with $H_0^1(\Omega) \subset V$ and let $a(\cdot,\cdot)\colon V \times V \to \mathbb{K}$ be continuous, sesquilinear, $V-$coercive and $k-$regular on V, for some $k \ge 0$. Let $F \in H^k(\Omega)$ and define $f \in V'$ by $f(v) = (F, v)_H$, $v \in V$, where $H \equiv L^2(\Omega)$. Let $\{\mathcal{T}_h\}_{h\ge 0}$ be a family of regular triangulations of the domain Ω. Let $u \in V$ be the exact solution of problem (3.7) and, for each $h \ge 0$, let u_h be the Finite Element solution of problem (3.8) with $S = S_h^r$. Then, for some constant C_1 we have*

$$\|u - u_h\|_{H^1} \le C_1 h^s \|u\|_{H^{s+1}}, \quad s = \min\{r, k+1\}, \tag{3.19}$$

If in addition the sesquilinear form adjoint to $a(\cdot,\cdot)$ is $0-$regular, then, for some constant C_2 we have

$$\|u - u_h\|_{L^2} \le C_2 h^{s+1} \|u\|_{H^{s+1}}, \quad s = \min\{r, k+1\}. \tag{3.20}$$

Proof (adapted from [182, Theorem VII.5.4]). Since $F \in H^k(\Omega)$ and $a(\cdot,\cdot)$ is $k-$regular it follows that $u \in H^{k+2}(\Omega)$ (see Definition 3.9). Hence, from Theorem 3.4 we have

$$\|u - u_h\|_{H^1} \le \frac{\gamma}{\alpha} \inf\{\|u - v\|_{H^1} \,:\, v \in S_h^r\},$$

whereas from equation (3.17) and from inequality (3.18) we have, for all $1 \le s \le \min\{r, k+1\}$,

$$\inf\{\|w - v\|_{H^1} \,:\, v \in S_h^r\} \le M h^s \|w\|_{H^{s+1}}$$

Combining these two results we obtain the error estimate (3.19). If in addition the sesquilinear form adjoint to $a(\cdot,\cdot)$ is $0-$regular, then in Theorem 3.5 we have $D^* \subset H^2(\Omega)$ and

$$\|w\|_{H^2(\Omega)} \le C \|A^* w\|_{L^2(\Omega)}.$$

Hence, equation (3.17) and inequality (3.18) with $l = 1$ yield

$$\inf\{\|w - v\|_{H^1} \,:\, v \in S_h\} \le Ch \|w\|_{H^2} \le Ch \|A^* w\|_{L^2},$$

which is equal to inequality (3.11) with $e^*(S) = C\,h$. Therefore, from inequality (3.12) and inequality (3.18) we obtain the error estimate (3.20). □

3.2.3 Linear Elasticity

Let $\Omega \subset \mathbb{R}^d$, $d = 2, 3$. In the theory of linear elasticity, the Cauchy stress tensor is a tensor-valued function $\boldsymbol{\sigma}\colon \Omega \to \mathbb{R}^{d\times d}$ defined by:

$$\boldsymbol{\sigma}(\boldsymbol{u}) = \lambda \operatorname{Tr}(\boldsymbol{\varepsilon}(\boldsymbol{u}))\mathbb{I} + 2\mu\boldsymbol{\varepsilon}(\boldsymbol{u}),$$

where $\lambda, \mu \in \mathbb{R}$ are called Lamè parameters and satisfy the conditions $\mu > 0$ and $2\mu + d\lambda > 0$, $\boldsymbol{u}\colon \Omega \to \mathbb{R}^d$ is the displacement field and $\boldsymbol{\varepsilon}(\boldsymbol{u}) = 1/2(\nabla \boldsymbol{u} + \nabla \boldsymbol{u}^\top)$ is the strain tensor. Having denoted

by Γ_D and Γ_D are two open subsets of $\partial\Omega$ such that $\partial\Omega = \bar{\Gamma}_D \cup \bar{\Gamma}_N$ and $\Gamma_D \cap \Gamma_N = \emptyset$, we then consider the following elliptic boundary value problem:

$$
\begin{aligned}
-\operatorname{div}\boldsymbol{\sigma}(\boldsymbol{u}) &= \boldsymbol{f}, && \text{in } \Omega, && \text{(3.21a)}\\
\boldsymbol{\sigma}(\boldsymbol{u}) &= \lambda \operatorname{Tr}(\boldsymbol{\varepsilon}(\boldsymbol{u}))\mathbb{I} + 2\mu\boldsymbol{\varepsilon}(\boldsymbol{u}), && \text{in } \Omega, && \text{(3.21b)}\\
\boldsymbol{u} &= \boldsymbol{u}_D, && \text{on } \Gamma_D, && \text{(3.21c)}\\
\boldsymbol{\sigma}(\boldsymbol{u})\boldsymbol{n} &= \boldsymbol{t}, && \text{on } \Gamma_N. && \text{(3.21d)}
\end{aligned}
$$

Equation (3.21a) governs the conservation of linear momentum (Cauchy equations) in Ω, $\boldsymbol{f}\colon \Omega \to \mathbb{R}^d$ is an external forcing term acting on the body, equation (3.21b) provides the stress-displacement relation for linear elastic materials (constitutive law), and equations (3.21c) and (3.21d) prescribe Dirichlet (displacement) and Neumann (traction) boundary conditions, respectively. Combining equation (3.21a) with the stress-displacement relation (3.21b), multiplying by a test function $\boldsymbol{v} \in H^1_D(\Omega)^d$, where

$$
H^1_D(\Omega)^d := \left\{ v \in H^1(\Omega)^d \,:\, \boldsymbol{v}|_{\Gamma_D} = \boldsymbol{0} \right\}, \tag{3.22}
$$

and integrating by parts, we obtain the following weak formulation of the boundary value problem (3.21): find $\boldsymbol{u} \in H^1(\Omega)^d$ such that $\boldsymbol{u}|_{\Gamma_D} = \boldsymbol{u}_D$ and

$$
\int_\Omega 2\mu\boldsymbol{\varepsilon}(\boldsymbol{u}) : \boldsymbol{\varepsilon}(\boldsymbol{v})\, d\boldsymbol{x} + \int_\Omega \lambda \operatorname{div}\boldsymbol{u} \operatorname{div}\boldsymbol{v}\, d\boldsymbol{x} = \int_\Omega \boldsymbol{f}\cdot\boldsymbol{v}\, d\boldsymbol{x} + \int_{\Gamma_N} \boldsymbol{t}\cdot\boldsymbol{v}\, d\boldsymbol{s} \qquad \forall \boldsymbol{v} \in H^1_D(\Omega)^d.
$$

Now let $\boldsymbol{f} \in L^2(\Omega)^d$, $\boldsymbol{u}_D = \boldsymbol{w}_1|_{\Gamma_D}$, where $\boldsymbol{w}_1 \in H^2(\Omega)^d$, and $\boldsymbol{t} = \boldsymbol{w}_2|_{\Gamma_N}$, where $\boldsymbol{w}_2 \in H^1(\Omega)^d$. Moreover, assume that either $\partial\Omega$ is smooth and $\bar{\Gamma}_D \cap \bar{\Gamma}_N = \emptyset$, or Ω is a convex polygon and either Γ_D or Γ_N is empty. Then, the solution of the weak formulation belongs to $H^2(\Omega)^d$, satisfies the boundary value problem and the following elliptic regularity estimate [208]

$$
\|\boldsymbol{u}\|_{H^2} + \lambda \|\operatorname{div}\boldsymbol{u}\|_{H^1} \le C\Big(\|\boldsymbol{f}\|_{L^2} + \|\boldsymbol{w}_1\|_{H^2} + \|\boldsymbol{w}_2\|_{H^1} \Big), \tag{3.23}
$$

where C is a positive constant independent of the Lamè perameters.

Theorem 3.8 (Korn's second inequality, see [208, Theorem 11.2.22] or [210, Theorem 3.3])**.** *Let $\Omega \subset \mathbb{R}^d$, $d = 2, 3$, be an open bounded set with piecewise smooth boundary. In addition, suppose $\Gamma_D \subset \partial\Omega$ has positive $(d-1)$-dimensional measure. Moreover, let the space $H^1_D(\Omega)^d$ be defined by (3.22). Then, there exists a positive constant $c = c(\Omega, \Gamma_D)$ such that*

$$
\|\boldsymbol{\varepsilon}(\boldsymbol{v})\|_{L^2} \ge c\, \|\boldsymbol{v}\|_{H^1}, \qquad \forall \boldsymbol{v} \in H^1_D(\Omega)^d. \tag{3.24}
$$

Let us define the following bilinear form:

$$
a\colon V \times V \to \mathbb{R}, \qquad a(\boldsymbol{u}, \boldsymbol{v}) := \int_\Omega \boldsymbol{\sigma}(\boldsymbol{u}) : \boldsymbol{\varepsilon}(\boldsymbol{v})\, d\boldsymbol{x} = \int_\Omega 2\mu\boldsymbol{\varepsilon}(\boldsymbol{u}) : \boldsymbol{\varepsilon}(\boldsymbol{v})\, d\boldsymbol{x} + \int_\Omega \lambda \operatorname{div}\boldsymbol{u} \operatorname{div}\boldsymbol{v}\, d\boldsymbol{x}. \tag{3.25}
$$

The following results hold.

Proposition 3.2. *The bilinear form (3.25) defined on $V \equiv H^1_D(\Omega)^d$ is $V-$coercive.*

Proof (adapted from [211, Theorem 5.3.1]). Every symmetric matrix A can be decomposed in the form

$$
A = A^d + A^h, \quad \text{where} \quad \begin{aligned} A^t &= A - (1/d)\operatorname{tr} A\mathbb{I}_d \\ A^h &= (1/d)\operatorname{tr} A\mathbb{I}_d \end{aligned}
$$

in such a way that

$$
A^t : A^h = \textstyle\sum_{i,j=1}^d A^h_{ij} A^t_{ij} = 0, \qquad A : A = |A|^2 = |A^t|^2 + |A^h|^2.
$$

Then, it is easy to see that:

$$
|A^h|^2 = \textstyle\sum_{i=1}^d 1/d^2 (\operatorname{tr} A)^2 = 1/d (\operatorname{tr} A)^2,
$$

from which we obtain that

$$2\mu|A|^2 + \lambda(\operatorname{tr} A)^2 = 2\mu|A^t|^2 + (2\mu + d\lambda)|A^h|^2 \geq \nu|A|^2,$$

where $\nu := \min(2\mu, 2\mu + d\lambda)$. Finally, having set $A := \boldsymbol{\varepsilon}(\boldsymbol{u})$, we obtain

$$a(\boldsymbol{u}, \boldsymbol{u}) = \int_\Omega \left(2\mu|\boldsymbol{\varepsilon}(\boldsymbol{u})|^2 + \lambda|\operatorname{div}\boldsymbol{u}|^2\right) d\boldsymbol{x} \geq \nu \int_\Omega |\boldsymbol{\varepsilon}(\boldsymbol{u})|^2 \, d\boldsymbol{x} = \nu\|\boldsymbol{\varepsilon}(\boldsymbol{u})\|^2_{L^2}. \tag{3.26}$$

Note that $\mu > 0$ and $2\mu + d\lambda > 0$ are natural physical constraints in the theory of continuum mechanics and thermodynamics. Finally, combining equation (3.26) and Korn's inequality (3.24), it follows that

$$a(\boldsymbol{u}, \boldsymbol{u}) \geq \nu\|\boldsymbol{\varepsilon}(\boldsymbol{u})\|^2_{L^2} \geq C\|\boldsymbol{u}\|_{H^1} \qquad \forall \boldsymbol{u} \in V. \qquad \square$$

Proposition 3.3. *The bilinear form (3.25) defined on $V \equiv H^1(\Omega)^d$ is continuous.*

Proof. To prove the continuity of $a(\cdot, \cdot)$ we first apply the Cauchy-Schwarz inequality

$$a(\boldsymbol{u}, \boldsymbol{v}) \leq 2\mu\|\boldsymbol{\varepsilon}(\boldsymbol{u})\|_{L^2}\|\boldsymbol{\varepsilon}(\boldsymbol{v})\|_{L^2} + \lambda\|\operatorname{div}\boldsymbol{u}\|_{L^2}\|\operatorname{div}\boldsymbol{v}\|_{L^2}, \quad \forall \boldsymbol{u}, \boldsymbol{v} \in V.$$

Then, we need to show that there exists a positive constant C, such that $\|\operatorname{div}\boldsymbol{v}\|_{L^2} \leq C\|\nabla\boldsymbol{u}\|_{L^2}$. Let us consider, for the sake of simplicity, a matrix $A = (a_{ij}) \in \mathrm{Mat}_d$ and let us recall the definition of Frobenius norm of a matrix:

$$\|A\|_F := \sqrt{\textstyle\sum_{i=1}^d \sum_{j=1}^d |a_{ij}|^2}.$$

The following result holds:

$$\begin{aligned}|\mathrm{tr}(A)| = \left|\textstyle\sum_{i=1}^d a_{ii}\right| \overset{*}{\leq} \textstyle\sum_{i=1}^d |a_{ii}| = \sum_{i=1}^d |a_{ii}| \cdot 1 \overset{**}{\leq} \sqrt{\textstyle\sum_{i=1}^d |a_{ii}|^2}\sqrt{\textstyle\sum_{i=1}^d 1^2} = \\ = \sqrt{d}\sqrt{\textstyle\sum_{i=1}^d |a_{ii}|^2} \leq \sqrt{d}\sqrt{\textstyle\sum_{i,j=1}^d |a_{ij}|^2} = \|A\|_F,\end{aligned}$$

where we have applied the triangle inequality $(*)$ and Cauchy-Schwarz inequality $(**)$. Therefore, taking $A = \nabla\boldsymbol{u}$, we get $\|\operatorname{div}\boldsymbol{v}\|^2_{L^2} \leq d\|\nabla\boldsymbol{u}\|^2_{L^2}$. Furthermore, we now show that $\|\boldsymbol{\varepsilon}(\boldsymbol{u})\|_{L^2} \leq \|\nabla\boldsymbol{u}\|_{L^2}$. Indeed, let us consider again a matrix $A \in \mathrm{Mat}_d$ and its symmetric part $A^{sym} \in \mathrm{Sym}_d$: if we rewrite the Frobenius norms of A and A^{sym} as

$$\begin{aligned}\|A\|^2_F &= \textstyle\sum_{i,j=1}^d a_{ij}^2 = \sum_{i=1}^d a_{ii}^2 + \sum_{i\neq j} a_{ij}^2 \\ \|A^{sym}\|^2_F &= \textstyle\sum_{i,j=1}^d \frac{1}{4}(a_{ij} + a_{ji})^2 = \sum_{i=1}^d a_{ii}^2 + \sum_{j>i} \frac{1}{2}(a_{ij} + a_{ji})^2 = \\ &= \textstyle\sum_{i=1}^d a_{ii}^2 + \sum_{i\neq j} \frac{1}{2} a_{ij}^2 + \sum_{j>i} a_{ij}a_{ji},\end{aligned}$$

it is straightforward to see that the following result holds

$$\begin{aligned}\|A\|^2_F - \|A^{sym}\|^2_F &= \left(\textstyle\sum_{i=1}^d a_{ii}^2 + \sum_{i\neq j} a_{ij}^2\right) - \left(\sum_{i=1}^d a_{ii}^2 + \sum_{i\neq j} \frac{1}{2} a_{ij}^2 + \sum_{j>i} a_{ij}a_{ji}\right) \\ &= \cancel{\textstyle\sum_{i=1}^d a_{ii}^2} + \textstyle\sum_{i\neq j} a_{ij}^2 - \cancel{\sum_{i=1}^d a_{ii}^2} - \sum_{i\neq j} \frac{1}{2} a_{ij}^2 - \sum_{j>i} a_{ij}a_{ji} \\ &= \textstyle\sum_{i\neq j} \frac{1}{2} a_{ij}^2 - \sum_{j>i} a_{ij}a_{ji} \\ &= \textstyle\sum_{j>i} \frac{1}{2}(a_{ij} - a_{ji})^2 \geq 0,\end{aligned}$$

which implies that, having set $A = \nabla\boldsymbol{u}$, $A^{sym} = (\nabla\boldsymbol{u})^{sym} = \boldsymbol{\varepsilon}(\boldsymbol{u})$, inequality $\|\boldsymbol{\varepsilon}(\boldsymbol{u})\|_{L^2} \leq \|\nabla\boldsymbol{u}\|_{L^2}$ holds. Combining these results we obtain, for all $\boldsymbol{u}, \boldsymbol{v} \in V$,

$$\begin{aligned}a(\boldsymbol{u}, \boldsymbol{v}) &\leq 2\mu\|\boldsymbol{\varepsilon}(\boldsymbol{u})\|_{L^2}\|\boldsymbol{\varepsilon}(\boldsymbol{v})\|_{L^2} + \lambda\|\operatorname{div}\boldsymbol{u}\|_{L^2}\|\operatorname{div}\boldsymbol{v}\|_{L^2} \\ &\leq 2\mu\|\nabla\boldsymbol{u}\|_{L^2}\|\nabla\boldsymbol{v}\|_{L^2} + \lambda d\|\nabla\boldsymbol{u}\|_{L^2}\|\nabla\boldsymbol{v}\|_{L^2} \\ &\leq C\|\boldsymbol{u}\|_{H^1}\|\boldsymbol{v}\|_{H^1},\end{aligned} \tag{3.27}$$

where $C := \max(2\mu, \lambda d)$. $\square$

Nearly Incompressible and Incompressible Materials

The mathematical formulation of various problems involves the dependency on a parameter arising out of physical considerations. For example, plate and shell models involve the thickness d of the plate or shell, the analysis of elastic materials in general involves the Poisson ratio ν and heat transfer involves the ratio of conductivities in different directions. A numerical scheme for the approximation of a parameter-dependent problem is said to exhibit *locking* if the accuracy of the approximations deteriorates as the parameter tends to a limiting value [212]. Locking usually manifests itself both as an increase in the error for a given discretization level and as a reduction in the optimal asymptotic rate of convergence. A numerical scheme for a problem of this type is said to be *robust* if it is essentially uniformly convergent for all values of the parameter. The numerical solution of linear elastic problems involving *nearly incompressible materials*, such as rubber, is known to exhibit locking. Indeed, these materials are characterised by Lamè coefficient λ that tends to ∞ or, equivalently, by a Poisson coefficient ν being very close to $1/2$. In this particular case, one can see from the regualrity estimate (3.23) that the displacement field is nearly divergence-free, namely $\nabla \cdot \boldsymbol{u} \to 0$. Clearly, in the limit case $\nu = 1/2$, the displacement field fully satisfies the divergence-free condition $\nabla \cdot \boldsymbol{u} = 0$ and the material is said to be (fully) incompressible. It is well known that the accuracy of low-order H^1-conforming finite elements approximations deteriorate when dealing with nearly-incompressible materials. In particular, it has been shown that linear H^1-conforming approximation of nearly incompressible materials on triangular meshes may not behave properly for meshes that are not fine enough, since this Finite Elements space is unable to accurately represent divergence-free displacement fields other than the constant ones [213]. In other words, the incompressibility constraint causes a loss of uniformity with respect to λ in the convergence regime of a low-order H^1-conforming Galerkin method. To better understand why H^1-conforming finite elements may fail to converge, we have to inspect how the error estimate depends on the Lamè parameters μ and λ [213]. To simplify the discussion we assume that these parameters are constant and since we are concerned with the case $\lambda \gg \mu$ we assume that λ is non-negative. From the proof of Proposition 3.2, we know that the bilinear form (3.25) is coercive with coercivity constant proportional to μ, i.e.,

$$a(\boldsymbol{v}, \boldsymbol{v}) \geq \mu |\boldsymbol{v}|^2_{H^1}, \qquad \forall \boldsymbol{v} \in H^1_0(\Omega)^d.$$

Moreover, we recall that inequality (3.27) implies the following boundedness property

$$a(\boldsymbol{u}, \boldsymbol{v}) \leq 2\mu |\boldsymbol{u}|_{H^1} |\boldsymbol{v}|_{H^1} + \lambda d |\boldsymbol{u}|_{H^1} |\boldsymbol{v}|_{H^1}, \qquad \forall \boldsymbol{u}, \boldsymbol{v} \in H^1_0(\Omega)^d.$$

Then, following the proof of Cèa lemma (see Theorem 3.4), we infer that

$$|\boldsymbol{u} - \boldsymbol{u}_h|_{H^1} \leq C \inf_{\boldsymbol{v}_h \in V_h} \left(|\boldsymbol{u} - \boldsymbol{v}_h|_{H^1} + \frac{\lambda}{\mu} |\boldsymbol{u} - \boldsymbol{v}_h|_{H^1} \right), \tag{3.28}$$

where the constant C is uniform with respect to the Lamè parameters λ and μ and $V_h \subset H^1_0(\Omega)^d$ denotes the finite element space of vector-valued functions whose components are continuous over Ω and linear over each triangle K of a triangulation $\mathcal{T}_h(\Omega)$, i.e., $V_h := [S^1_h]^d$, where S^1_h is the space defined by equation (3.15). The first term on the right hand side of the error estimate (3.28) decays as the best approximation error of $\boldsymbol{u}$ in V_h. This is also the case for the second term but the multiplicative factor $\lambda/\mu \gg 1$ causes this term to be very large. In other words, the second term tends to zero as $h \to 0$, but this asymptotic range is only visible on meshes that are refined enough to beat the large constant λ/μ. This means that locking will eventually disappear when the level of discretization is increased enough. Unfortunately, it is worth emphasizing that an infeasible level of discretization may be required before convergence can be observed. Robustness for $\lambda \gg \mu$ is achieved, on the other hand, by designing numerical schemes in which this factor is independent of λ and μ. The corresponding error estimate, which is therefore uniform in λ and μ, is referred to as *locking-free* and leads to acceptable error levels using a practical range of discretization, no matter how close the parameter is to its limiting value.

Locking-free numerical methods Several methods have been devised and proposed with the aim of overcoming the locking effects and thus being able to deal with nearly-incompressible and incompressible materials. These include high-order methods, mixed methods, reduced (or inexact) integration techniques, non-conforming methods and discontinuous Galerkin methods. Regarding high-order

methods, it has been shown that the conforming finite element method converges suboptimally when using triangular elements with basis functions having degree $k \in \{2, 3\}$ and delivers locking-free optimal order convergence for $k \geq 4$ [214–216]. On the other hand, on quadrilateral meshes Babuška and Suri have shown that locking cannot be avoided for all $k \geq 1$ [217]. The second appraoch that we discuss consists in employing the so-called mixed formulation of the governing equations. In particular, the development of mixed methods starts by introducing the auxiliary variable $p = -\lambda \operatorname{div} \boldsymbol{u}$, which plays the role of the pressure in the incompressible limit. Then, the linear elastic stress tensor can be written as follows

$$\boldsymbol{\sigma} = -p\mathbb{I} + 2\mu\boldsymbol{\varepsilon}(\boldsymbol{u}), \qquad p = -\lambda \operatorname{div} \boldsymbol{u},$$

and the displacement equations of motion become

$$-2\mu \operatorname{div} \boldsymbol{\varepsilon}(\boldsymbol{u}) + \nabla p = \boldsymbol{f}, \tag{3.29a}$$
$$\operatorname{div} \boldsymbol{u} + \lambda^{-1} p = 0. \tag{3.29b}$$

In the fully-incompressible (limit) case, i.e., when $\operatorname{div} \boldsymbol{u} = 0$, we have $2 \operatorname{div} \boldsymbol{\varepsilon}(\boldsymbol{u}) = \Delta \boldsymbol{u} + \cancel{\nabla(\operatorname{div} \boldsymbol{u})} = \Delta \boldsymbol{u}$ and the governing equations simplify as follows

$$-\mu \Delta \boldsymbol{u} + \nabla p = \boldsymbol{f},$$
$$\operatorname{div} \boldsymbol{u} = 0.$$

In the fluid dynamics framework, these partial differential equations are also known as Stokes equations and they govern the motion of an incompressible Newtonian fluid. In this context, the $\boldsymbol{u}$ denotes the velocity field and μ is the dynamic viscosity. The weak formulation of the boundary-value problem obtained by combining the governing equations (3.29) with zero Dirichlet boundary conditions reads as follows: find $(\boldsymbol{u}, p) \in V \times Q$, where $V \equiv H_0^1(\Omega)$ and $Q \equiv L^2(\Omega)$, such that

$$\int_\Omega 2\mu\boldsymbol{\varepsilon}(\boldsymbol{u}) : \boldsymbol{\varepsilon}(\boldsymbol{v})\, d\boldsymbol{x} - \int_\Omega p \operatorname{div} \boldsymbol{v}\, d\boldsymbol{x} = \int_\Omega \boldsymbol{f} \cdot \boldsymbol{v}\, d\boldsymbol{x}, \qquad \forall \boldsymbol{v} \in V, \tag{3.30a}$$
$$-\int_\Omega \operatorname{div} \boldsymbol{u}\, q\, d\boldsymbol{x} - \int_\Omega \lambda^{-1} p\, q\, d\boldsymbol{x} = 0, \qquad \forall q \in Q. \tag{3.30b}$$

These equations are the optimality conditions for the saddle point problem [218]

$$\inf_{\boldsymbol{v} \in V} \sup_{q \in Q} \mu \int_\Omega \|\boldsymbol{\varepsilon}(\boldsymbol{v})\|^2\, d\boldsymbol{x} - \frac{1}{2\lambda} \int_\Omega |q|^2\, d\boldsymbol{x} + \int_\Omega q \operatorname{div} \boldsymbol{v}\, d\boldsymbol{x} - \int_\Omega \boldsymbol{f} \cdot \boldsymbol{v}\, d\boldsymbol{x}.$$

After having introduced the bilinear forms

$$a \colon V \times V \to \mathbb{R} \qquad \boldsymbol{u} \times \boldsymbol{v} \mapsto a(\boldsymbol{u}, \boldsymbol{v}) := \int_\Omega 2\mu\boldsymbol{\varepsilon}(\boldsymbol{u}) : \boldsymbol{\varepsilon}(\boldsymbol{v})\, d\boldsymbol{x},$$
$$b \colon Q \times V \to \mathbb{R} \qquad q \times \boldsymbol{v} \mapsto b(q, \boldsymbol{v}) := -\int_\Omega q \operatorname{div} \boldsymbol{v}\, d\boldsymbol{x},$$
$$c \colon Q \times Q \to \mathbb{R} \qquad q \times p \mapsto c(q, p) := \int_\Omega \lambda^{-1} q\, p\, d\boldsymbol{x},$$

and the linear functional

$$F \colon V \to \mathbb{R} \qquad \boldsymbol{v} \mapsto F(\boldsymbol{v}) := \int_\Omega \boldsymbol{f} \cdot \boldsymbol{v}\, d\boldsymbol{x},$$

the weak formulation (3.30) can be rewritten as

$$a(\boldsymbol{u}, \boldsymbol{v}) + b(p, \boldsymbol{v}) = F(\boldsymbol{v}), \qquad \forall \boldsymbol{v} \in V,$$
$$b(q, \boldsymbol{u}) - c(q, p) = 0, \qquad \forall q \in Q.$$

The idea is then to introduce a *mixed finite element* approximation for the displacement-pressure pair $(\boldsymbol{u}, p)$. However, this approach requires some care in choosing the finite element spaces used to approximate the displacement and the pressure, as the Babuška-Brezzi (or inf-sup) condition must be

satisfied [219–221]. Another simple and successful method developed to overcome locking effects is the so-called *reduced integration* technique. More precisely, the idea is to use the one-field formulation and to apply reduced (i.e., inexact) numerical quadrature when evaluating the term associated with compressibility effects, i.e., $\lambda \int_\Omega \operatorname{div} \boldsymbol{v} \operatorname{div} \boldsymbol{u}\, d\boldsymbol{x}$, in the bilinear form $a(\cdot,\cdot)$ introduced in (3.25). This approach is only a partial remedy since it cannot provide better results measured in terms of energy, but it makes possible to obtain good approximations to the individual components of the displacement. In many cases there is a close connection between reduced (inexact) integration and the mixed formulation discussed before. For more details, we refer the reader to, e.g., [221]. Non-conforming finite element methods have also proved to be robust and locking-free. For example, the piecewise linear non-conforming displacement finite element method proposed in [222] defines the following finite dimensional space where the numerical solution has to be sought:

$$V_h := \big\{ \boldsymbol{v} \ : \ \boldsymbol{v} \in L^2(\Omega)^2,\ \boldsymbol{v}|_T \in \mathbb{P}_1(T)^2 \text{ for all } T \in \mathcal{T}_h(\Omega),\ \boldsymbol{v} \text{ is continuous at the midpoints of the interelement boundaries and vanishes at the midpoints of edges along } \partial\Omega \big\}.$$

The key to the success of this approach lies in its extra freedom, which allows good approximation of functions with divergence-zero constraints. In the case of a convex polygonal domain, optimal error estimates in the energy and L^2 norms have been obtained and it has been shown that they do not deteriorate for nearly incompressible material. Another linear non-conforming finite element method for nearly-incompressible and fully-incompressible materials has been introduced in [223]. It consists of conforming piecewise linear elements that are continuous over Ω for one of the displacement components and linear non-conforming elements that are continuous at the midpoints of interelement boundaries for the other component. In other words, the numerical solution has to be sought in the finite dimensional space $V_h := V_{1,h} \times V_{1,h}$, where

$$V_{1,h} := \big\{ v \ : \ v \text{ is linear in every triangle of } \mathcal{T}_h(\Omega),\ \text{continuous at midpoints of interelement boundaries, and vanishes at the midpoints of the edges lying on } \partial\Omega \big\}$$

$$V_{2,h} := \big\{ v \ : \ v \text{ is continuous in } \Omega,\ \text{linear in every triangle of } \mathcal{T}_h(\Omega) \text{ and vanishes on } \partial\Omega \big\}$$

Even this definition of the space V_h has been shown to give optimal convergent approximations for all variables and without dependence on the Poisson ratio. As already mentioned, another approach for overcoming locking issues consists in discretising the governing equations by means of a *discontinuous Galerkin method*. In particular, in [224] a discontinuous and piecewise polynomial Galerkin method [225–228] is proposed for simulating both nearly-incompressible and fully incompressible linear elastic materials on triangular meshes. This approach allows for independent approximations on different elements and enforces only weakly continuity of the solution across interelement boundaries, as well as the boundary conditions. The extra flexibility obtained by using discontinuous approximations together with properly chosen stabilization terms results in a locking-free method with optimal error estimates that are uniform with respect to Poisson's ratio. The one-field formulation is used to simulate nearly-incompressible materials, whereas the mixed formulation is used for dealing with fully incompressible materials. The drawback of this approach lies in the increased number of degrees of freedom if compared with a continuous method of the same order of convergence. However, it enables the use of different polynomial degrees of approximation on adjacent elements, as well as hanging nodes and even nonmatching meshes. Subsequently, the discontinuous Galerkin finite element method was also applied to solve linear elasticity problems (with mixed boundary conditions) in convex and non-convex polygons [229]. Moreover, the authors have proved that, even if the exact solutions of the elasticity problems are not in H^2, the $h-$version of the discontinuous Galerkin FEM is locking-free. An adaptive version of the discontinuous Galerkin finite element method for linear elasticity problems was presented in [230]. Furthermore, an a posteriori error estimate was derived and its robustness with respect to nearly incompressible materials was established. Finally, in [231] the authors derived a posteriori error bounds of the energy norm for the $hp-$adaptive discontinuous Galerkin approximations of the mixed form of the two-dimensional linear elasticity equations. The numerical results have shown that both the $hp-$adaptive DG method and the a posteriori error estimator are locking-free. Another method based on the discontinuous Galerkin formulation but employing a different approximation space is the

so-called Locking-Free Enriched Galerkin (LF-EG) presented in [232]. More precisely, the approximation space is a continuous piecewise linear vector-valued function space enriched by some discontinuous piecewise linear vector-valued functions whose gradient is a constant multiple of the identity tensor in each element. In other words, having the denoted by $\mathcal{M}_h$ the standard finite element space of $d-$vectors whose components are continuous piecewise linear polynomials, i.e.,

$$\mathcal{M}_h := \{\psi \in H^1(\Omega)^d \mid \psi|_T \in \mathbb{P}_1(T)^d \ \forall T \in \mathcal{T}_h\}$$

and by $\mathcal{D}_h$ the space of discontinuous vector-valued functions that are piecewise linear in each element, i.e.,

$$\mathcal{D}_h := \{\psi \in L^2(\Omega)^d \mid \psi|_T = c_T(\boldsymbol{x} - \boldsymbol{x}_T),\ c_T \in \mathbb{R},\ \forall T \in \mathcal{T}_h\},$$

where $\boldsymbol{x}_T$ is the position vector of the center of $T \in \mathcal{T}$, the LF-EG finite element space V_h introduced in [232] is defined as a direct sum of the two spaces defined above:

$$V_h := \mathcal{M}_h \oplus \mathcal{D}_h.$$

This new enriched function space requires only one additional local degree of freedom in each element compared to the linear continuous Galerkin space and also requires significantly fewer degrees of freedom than the linear DG space. The new space now has non-trivial divergence free functions, thus being locking-free. Moreover, an optimal-order a priori error estimate in the energy norm is derived under the assumption of H^2 regularity of the true solution and it was shown to be independent of λ, thus showing that the method is robust even for large values of λ. Finally, we mention the arbitrary order locking-free numerical scheme based on the weak Galerkin (WG) finite element methods that has been proposed in [233] for solving linear elasticity problems on general polygonal/polyhedral partitions. The weak Galerkin [234, 235] method is a generic finite element technique for partial differential equations where differential operators are approximated or reconstructed by solving inexpensive local problems on each element. Such local problems are often derived from weak formulations of the corresponding differential operators through integration by parts. In the linear elasticity setting, it has been shown that the WG numerical approximations are naturally robust in terms of the Lamè constant λ. Indeed, locking-free error estimates of optimal order have been derived in a discrete H^1-norm and the usual L^2-norm for the approximate displacement when the exact solution is smooth.

3.3 Explicit First Order Evolution Equations

Let H be a Hilbert space, $D(A) \subset H$ and $A \in L(D(A), H)$. We consider the evolution equation

$$\dot{u}(t) + Au(t) = 0. \tag{3.32}$$

The Cauchy problem is to find a function $u \in C([0,\infty], H) \cap C^1((0,\infty), H)$ such that, for $t > 0$, $u(t) \in D(A)$, equation (3.32) holds and $u(0) = u_0$, where the initial value $u_0 \in H$ is prescribed.

Theorem 3.9 (see [182, Chapter IV.2]). *If the operator $A \in L(D(A), H)$ is accretive and u is the solution of the Cauchy problem (3.32) with initial condition $u(0) = u_0$, then $\|u(t)\|_H \le \|u_0\|_H$, $t > 0$.*

Proof. For $t > 0$, we have

$$\partial_t \left(\|u(t)\|_H^2\right) = 2\Re\left(\dot{u}(t), u(t)\right)_H \overset{(3.32)}{=} -2\Re\left(Au(t), u(t)\right)_H \le 0,$$

where the inequality follows from the definition of accretive operator (see Definition 3.6). So, by integration, it follows that $\|u(t)\|_H \le \|u(0)\|_H$. □

Assume that for every $u_0 \in D(A)$ there exists a unique solution of the Cauchy problem. Define $S(t)u_0 = u(t)$ for $t \ge 0$, $u_0 \in D(A)$, where $u(\cdot)$ denotes the solution of equation (3.32) with $u(0) = u_0$. If $u_0, v_0 \in D(A)$ and if $a, b \in \mathbb{R}$, then the function $t \mapsto aS(t)u_0 + bS(t)v_0$ is a solution of equation (3.32), since A is linear, and the uniqueness of the solution implies

$$S(t)(au_0 + bv_0) = aS(t)u_0 + bS(t)v_0.$$

Therefore, $S(t) \in L(D(A))$ for all $t \geq 0$. If $u_0 \in D(A)$ and $\tau \geq 0$, then the function $t \mapsto S(t+\tau)u_0$ satisfies equation (3.32) and takes the initial value $S(\tau)u_0$. Then, the uniqueness of the solution implies that

$$S(t+\tau)u_0 = S(t)S(\tau)u_0, \quad u_0 \in D(A).$$

Clearly, $S(0) = I$. If A is accretive, owing to Theorem 3.9 we have

$$\|S(t)u_0\|_H \leq \|u_0\|_H, \quad u_0 \in D(A),\ t \geq 0,$$

so each $S(t)$ is a contraction in the $H-$norm and hence has a unique extension to the closure of $D(A)$. When $D(A)$ is dense, we thereby obtain a contraction semigroup on H.

Definition 3.11 (Contraction Semigroup)**.** A contraction semigroup on the Hilbert space H is a set $\{S(t)\}_{t\geq 0}$ of linear operators on H which are contractions and satisfy

- semigroup identity: $S(0) = I$, $S(t+\tau) = S(t)\,S(\tau)$, $t, \tau \geq 0$,
- semigroup strong continuity: $S(\cdot)x \in C([0,\infty), H)$, $x \in H$.

Definition 3.12 (Generator of Contraction Semigroup)**.** The generator of the contraction semigroup $\{S(t)\}_{t\geq 0}$ is the operator with domain

$$D(B) = \left\{ x \in H \ : \ \lim_{h\to 0^+} h^{-1}(S(h) - I)x = D^+(S(0)x) \text{ exists in } H \right\}$$

and value

$$Bx = \lim_{h\to 0^+} h^{-1}(S(h) - I)x = D^+(S(0)x).$$

Theorem 3.10. *Let $A \in L(D(A), H)$ be accretive with $D(A)$ dense in H. Suppose that for every $u_0 \in D(A)$ there is a unique solution $u \in C^1([0,\infty), H)$ of equation (3.32) with $u(0) = u_0$. Then, the family of operators $\{S(t)\}_{t\geq 0}$ defined as above is a contraction semigroup on H whose generator is an extension of $-A$.*

Lemma 3.1 (see [182, Section IV.3])**.** *Let $B\colon D(B) \to H$ be the generator of a contraction semigroup $\{S(t) : t \geq 0\}$. Then, the following properties hold.*

- *For each $x \in D(B)$, $S(\cdot)x \in C^1(\mathbb{R}_0^+, H)$, $S(t)x \in D(B)$, and*

$$S(t)x - x = \int_0^t BS(s)x\,ds = \int_0^t S(s)Bx\,dx, \qquad t \geq 0.$$

- *B is closed.*
- *$D(B)$ is dense in H; for each $t \geq 0$ and $x \in H$, $\int_0^t S(s)x\,ds \in D(B)$ and*

$$S(t)x - x = B\int_0^t S(s)x\,ds.$$

The next results provide a characterization of those operators that generate contraction semigroups.

Theorem 3.11 (see [182, Theorem IV.3.1])**.** *Necessary and sufficient conditions for the operator $B\colon D(B) \to H$ to be the generator of a contraction semigroup on H are that $D(B)$ is dense in H and $\lambda - B\colon D(B) \to H$ is a bijection with $\|\lambda(\lambda - B)^{-1}\|_{\mathcal{L}(H)} \leq 1$ for all $\lambda > 0$.*

Theorem 3.12 (see [182, Corollary IV.3.2])**.** *If $-A$ is the generator of a contraction semigroup, then for each $u_0 \in D(A)$ there is a unique solution $u \in C^1([0,\infty), H)$ of equation (3.32) with $u(0) = u_0$.*

Theorem 3.13 (see [182, Theorem IV.3.3])**.** *If $-A$ is the generator of a contraction semigroup, then for each $u_0 \in D(A)$ and each $f \in C^1([0,\infty), H)$ there is a unique $u \in C^1([0,\infty), H)$ such that $u(0) = u_0$, $u(t) \in D(A)$ for $t \geq 0$, and*

$$\dot{u}(t) + Au(t) = f(t), \quad t \geq 0.$$

The next theorem characterizes the generators of contraction semigroups among the negatives of accretive operators. This result is important in the context of boundary value problems, since the conditions of this characterization will be more easily verified than that of Theorem 3.11.

Theorem 3.14 (see [182, Theorem IV.3.3]). *The linear operator $-A\colon D(A) \to H$ is the generator of a contraction semigroup on H if and only if $D(A)$ is dense in H, A is accretive and $\lambda + A$ is surjective for some $\lambda > 0$.*

Hereafter we consider the Cauchy problem for the evolution equation (3.32) in the special case in which A is a model of an elliptic bounday value problem. Then, equation (3.32) is a corresponding abstract parabolic equation.

Theorem 3.15 (see [182, Theorem IV.6.1]). *Let V and H be Hilbert spaces for which the identity $V \hookrightarrow H$ is continuous. Let $a\colon V \times V \to \mathbb{C}$ be continuous, sesquilinear and $V-$elliptic. In particular*

$$\begin{aligned} |a(u,v)| &\le K\|u\|_V\|v\|_V, && u, v \in V, \\ \Re\, a(u,u) &\ge c\|u\|_V^2, && u \in V, \end{aligned}$$

where $0 < c \le K$. Define

$$D(A) = \{u \in V \,:\, |a(u,v)| \le K_u\|v\|_H,\ v \in V\},$$

where K_u depends on u and let $A \in L(D(A), H)$ be given by

$$a(u,v) = (Au, v)_H, \quad u \in D(A),\ v \in V.$$

Then $D(A)$ is dense in H and there is a θ_0, $0 < \theta_0 < \pi/4$, such that for each $\lambda \in S(\pi/2 + \theta_0) \equiv \{z \in \mathbb{C} \,:\, |\arg(z)| < \pi/2 + \theta_0\}$ we have $(\lambda + A)^{-1} \in \mathcal{L}(H)$. For each θ, $0 < \theta < \theta_0$, there is an M_θ such that

$$\|\lambda(\lambda + A)^{-1}\|_{\mathcal{L}(H)} \le M_\theta, \qquad \lambda \in S(\theta + \pi/2).$$

Theorem 3.16 (see [182, Theorem IV.6.2]). *Let $A \in L(D(A), H)$ be the operator of Theorem 3.15. Then, there is a family of operators $\{T(t) \,:\, t \in S(\theta_0)\}$ satisfying:*

1. *$T(t+\tau) = T(t) \cdot T(\tau)$, $t, \tau \in S(\theta_0)$, and for $x, y \in H$, the function $t \mapsto (T(t)x, y)_H$ is analytic on $S(\theta_0)$;*
2. *for $t \in S(\theta_0)$, $T(t) \in L(H, D(A))$ and*

$$-\frac{dT(t)}{dt} = A \cdot T(t) \in \mathcal{L}(H);$$

3. *if $0 < \varepsilon < \theta_0$, then for some constant $C(\varepsilon)$,*

$$\|T(t)\| \le C(\varepsilon)\|tAT(t)\| \le C(\varepsilon), \qquad t \in S(\theta_0 - \varepsilon), \tag{3.33}$$

and for $x \in H$, $T(t) \to x$ as $t \to 0$, $t \in S(\theta_0 - \varepsilon)$.

Definition 3.13 (Analytic Semigroup). A family of operators $\{T(t) \,:\, t \in S(\theta_0)\}$ which satisfies the properties of Theorem 3.16 and $T(0) = I$, is called an analytic semigroup.

Theorem 3.17 (see [182, Theorem IV.6.3]). *Let $A \in L(D(A), H)$ be the operator of Theorem 3.15, $\{T(t) \,:\, t \in S(\theta_0)\}$ be given by*

$$T(t) = \frac{1}{2\pi i}\int_C e^{\lambda t}(\lambda + A)^{-1}\, d\lambda, \qquad t \in S(2\theta - \theta_0),$$

and $T(0) = I$. Then, the collection of operators $\{T(t)\}_{t \ge 0}$ is the contraction semigroup generated by $-A$.

Theorem 3.18 (see [182, Corollary IV.6.4]). *If A is the operator of Theorem 3.15, then for every $u_0 \in H$ there is a unique solution $u \in C([0,\infty), H) \cap C^\infty((0,\infty), H)$ of equation (3.32) with $u(0) = u_0$. For each $t > 0$, $u(t) \in D(A^p)$ for every $p \geq 1$.*

Remark 3.2. It is worth emphasizing that there are important differences between Theorem 3.12 and Theorem 3.18. In particular, Theorem 3.18 solves the Cauchy problem for initial data in H, while Theorem 3.12 is appropriate only for initial data in $D(A)$. Furthermore, the infinite differentiability of the solution from Theorem 3.18 and the consequential inclusion in the domain of every power of A at each $t > 0$ are properties not generally true in the situation of Theorem 3.12.

Theorem 3.19 (see [182, Theorem IV.6.5]). *If A is the operator of Theorem 3.15, then for each $u_0 \in H$ and each Hölder continuous $f\colon [0,\infty) \to \infty$:*

$$\|f(t) - f(\tau)\| \leq K(t-\tau)^\alpha, \qquad 0 \leq \tau \leq t,$$

where K and α are constant, $0 < \alpha \leq 1$, there is a unique $u \in C([0,\infty), H) \cap C^1((0,\infty), H)$ such that $u(0) = u_0$, $u(t) \in D(A)$ for $t > 0$, and

$$\dot{u}(t) + Au(t) = f(t), \quad t > 0.$$

3.4 Implicit First Order Evolution Equations

3.4.1 Introduction

Let V_m be a Hilbert space with scalar product $(\cdot,\cdot)_m$ and denote the corresponding Riesz map from V_m onto the dual V_m' by $\mathcal{M}$. That is,

$$\mathcal{M}x(y) = (x,y)_m, \quad x, y, \in V_m$$

Let D be a subspace of V_m and $L\colon D \to V_m'$ a linear map. If $u_0 \in V_m$ and $f \in C((0,\infty), V_m')$ are given, we consider the problem of finding $u \in C([0,\infty), V_m) \cap C^1((0,\infty), V_m)$ such that

$$\mathcal{M}\dot{u}(t) + Lu(t) = f(t), \qquad t > 0, \tag{3.34}$$

and $u(0) = u_0$. This is a generalization of the evolution equation (3.32).

Theorem 3.20 (see [182, Chapter V.2]). *If the operator $L\colon D \to V_m'$ is monotone, then there is at most one solution of the Cauchy problem (3.34).*

Proof. Suppose that $u_1(t)$ and $u_2(t)$ are both solutions of problem (3.34) with initial condition u_0. Then, define $w(t) := u_1(t) - u_2(t)$. By linearity, it is easy to see that $w(t)$ is a solution of the evolution equation

$$\mathcal{M}\dot{w}(t) + Lw(t) = 0, \quad t > 0,$$

with initial condition $w(0) = 0$. For such a solution we have

$$\partial_t \left(w(t), w(t)\right)_m = 2\Re\left(\dot{w}(t), w(t)\right)_m = 2\Re\,\mathcal{M}\dot{w}(t)(w(t)) = -2\,\Re Lw(t)(w(t)) \leq 0,$$

which implies that $\|w(t)\|_m \leq 0$, that is, $u_1(t) \equiv u_2(t)$. □

To obtain an explicit evolution equation in V_m which is equivalent to equation (3.34), we apply the inverse of the isomprphism $\mathcal{M}$ to (3.34) obtaining

$$\dot{u}(t) + \mathcal{M}^{-1} \circ Lu(t) = \mathcal{M}^{-1} f(t), \quad t > 0.$$

We define the operator $A := \mathcal{M}^{-1} \circ L$ with domain $D(A) = D$. Then, since $\mathcal{M}$ is the Riesz map determined by the scalar product $(\cdot,\cdot)_m$, we have

$$(Ax, y)_m = \mathcal{M}(Ax)(y) = Lx(y), \qquad x \in D,\, y \in V_m,$$

which shows that L is monotone if and only if A is accretive. Then, by Theorem 3.14 it follows that $-A$ generates a contraction semigroup on V_m if and only if L is monotone and $I + A$ is surjective. Since $\mathcal{M}(I + A) = \mathcal{M} + L$, from Theorem 3.13 we obtain the following result.

Theorem 3.21 (see [182, Theorem V.2.1]). *Let $\mathcal{M}$ be the Riesz map of the Hilbert space V_m with scalar product $(\cdot,\cdot)_m$ and let L be linear from the subspace D of V_m into V_m'. Assume that L is monotone and $\mathcal{M}+L\colon D\to V_m'$ is surjective. Then, for every $f\in C^1([0,\infty),V_m')$ and every $u_0\in D$ there is a unique solution $u(t)$ of equation (3.34) with $u(0)=u_0$.*

Let us now suppose that L is obtained from a continuous sesquilinear form. In particular, let V be a Hilbert space dense and continuously embedded in V_m; hence we can identify $V_m'\subset V'$. Let $\ell(\cdot,\cdot)\colon V\times V\to\mathbb{R}$ be continuous and sesquilinear and define the corresponding linear map $\mathcal{L}\colon V\to V'$ by

$$\mathcal{L}x(y)=\ell(x,y),\quad x,y\in V.$$

Define $D\equiv\{x\in V\ :\ \mathcal{L}x\in V_m'\}$ and $L=\mathcal{L}|_D$. Then, we have

$$\ell(x,y)=(Ax,y)_m,\quad x\in D,\ y\in V,$$

which shows that A is the operator determined by the triple $\{\ell(\cdot,\cdot),V,V_m\}$ as in Theorem 3.15. Therefore, from Theorems 3.17 and 3.19 we obtain the following result.

Theorem 3.22 (see [182, Theorem V.2.2]). *Let $\mathcal{M}$ be the Riesz map of the Hilbert space V_m with scalar product $(\cdot,\cdot)_m$. Let $\ell(\cdot,\cdot)$ be a continuous, sesquilinear and elliptic form on the Hilbert space V, which is assumed dense and continuously embedded in V_m, and denote the corresponding isomprphism of V onto V' by $\mathcal{L}$. Then, for every Hölder continuous $f\colon[0,\infty)\to V_m'$ and $u_0\in V_m$, there is a unique $u\in C([0,\infty),V_m)\cap C^1((0,\infty),V_m)$ such that $u(0)=u_0$, $\mathcal{L}u(t)\in V_m'$ for $t>0$, and*

$$\mathcal{M}\dot u(t)+\mathcal{L}u(t)=f(t),\qquad t>0,\tag{3.35}$$

Remark 3.3. Theorem 3.22 still holds if we remove the hypothesis that $\mathcal{L}$ is $V-$elliptic by $\lambda\mathcal{M}+\mathcal{L}$ is $V-$elliptic for some $\lambda\in\mathbb{R}$. Indeed, if we introduce the change of variable $u_\lambda:=e^{-\lambda t}u$, where u is the solution of the original evolution equation (3.35), the new unknown u_λ satisfies the following new problem:

$$\mathcal{M}\dot u_\lambda(t)+(\mathcal{L}+\lambda\mathcal{M})u_\lambda(t)=e^{-\lambda t}f(t).$$

Therefore, if we replace f with $e^{-\lambda t}f$ and require that $\mathcal{L}+\lambda\mathcal{M}$ is $V-$elliptic for some $\lambda\in\mathbb{R}$, then Theorem 3.22 still holds.

3.4.2 Semi-Discrete Faedo-Galerkin Approximation

The solution $u(t)$ of problem (3.35) satisfies the weak formulation

$$(\dot u(t),v)_m+\ell(u(t),v)=f(t)(v),\qquad v\in V,\ t>0\tag{3.36}$$

and since V is dense in V_m, this is actually equivalent to (3.35). Let now S be a subspace of V and consider the related problem of determining $u_s\in C([0,\infty),S)\cap C^1((0,\infty),S)$ that satisfies

$$(\dot u_s(t),v)_m+\ell(u_s(t),v)=f(t)(v),\qquad v\in S,\ t>0\tag{3.37}$$

and an initial condition to be specified. We then consider the Faedo-Galerkin approximation in which S is a finite-dimensional subspace of V, with $\dim(S)=m$, and let $\{v_1,v_2,\dots,v_m\}$ be a basis for S. Then, the solution of equation (3.37) has the form $u_s(t)=\sum_{i=1}^m x_i(t)v_i$, where $x(t)=(x_1(t),x_2(t),\dots,x_m(t))$ is in $C([0,\infty),\mathbb{R}^m)\cap C^1((0,\infty),\mathbb{R}^m)$, and equation (3.37) is equivalent to the system of Ordinary Differential Equations

$$\sum_{j=1}^m(v_j,v_i)_m\dot x_j(t)+\sum_{j=1}^m\ell(v_j,v_i)x_j(t)=f(t)(v_i),\qquad 1\le i\le m.$$

It is worth noting that the coefficient matrix of $\dot x(t)$ is symmetric and positive definite, hence, non-singular. Then, the linear system has a unique solution $x(t)$ with initial condition $x(0)$ determined by $u_s(0)=\sum_{i=1}^m x_i(0)v_i$.

3.4.3 Error Estimate

We consider for each time $t > 0$ the $\mathcal{L}-$projection of $u(t)$ onto S defined by

$$u_\ell(t) \in S \ : \ \ell(u_\ell(t), v) = \ell(u(t), v), \quad v \in S. \tag{3.38}$$

We now provide estimates on the error $u(t) - u_s(t)$ between the exact solution and the Faedo-Galerkin approximate solution under the assumptions of Theorem 3.22.

Theorem 3.23 (see [182, Theorem VII.6.1]). *Let the real Hilbert spaces V and V_m, operators $\mathcal{M}$ and $\mathcal{L}$, and data u_0 and f be given as in Theorem 3.22, and let S be a closed subspace of V. Then, there exists a unique solution u of equation (3.35) with $u_s(0) = u_0$ and there exists a unique solution u_s of equation (3.37) for any prescribed initial value $u_s(0) \in S$. Assume $u \in C([0,\infty), V)$ and choose $u_s(0) = u_\ell(0)$, i.e., the $\mathcal{L}-$projection of $u(0)$. Then, we have the error estimate*

$$\|u(t) - u_s(t)\|_m \le \|u(t) - u_\ell(t)\|_m + \int_0^t \|\dot{u}(s) - \dot{u}_\ell(s)\|_m \, ds, \qquad t \ge 0. \tag{3.39}$$

Proof (adapted from [182, Theorem VII.6.1]). ⌋ The existence and uniqueness results are immediate consequences of Theorem 3.22. Moreover, $u(0) = u_0$ necessarily belongs to V, so problem (3.38) defines $u_\ell(0) = u_s(0)$. Then, for any $v \in S$, subtracting equation (3.37) from equation (3.36) we obtain

$$(\dot{u}(t) - \dot{u}_s(t), v)_m + \ell\,(u(t) - u_s(t), v) = 0$$

Then, writing the error $u(t) - u_s(t)$ as

$$u(t) - u_s(t) = (u(t) - u_\ell(t)) + (u_\ell(t) - u_s(t))$$

we obtain

$$(\dot{u}(t) - \dot{u}_\ell(t), v)_m = (\dot{u}_s(t) - \dot{u}_\ell(t), v)_m + \cancel{\ell\,(u_\ell(t) - u(t), v)} + \ell\,(u_s(t) - u_\ell(t), v)$$

where the second term on the right hand side vanishes due to problem (3.38). Now, setting $v = u_s(t) - u_\ell(t)$ yields

$$(\dot{u}(t) - \dot{u}_\ell(t), u_s(t) - u_\ell(t))_m = (\dot{u}_s(t) - \dot{u}_\ell(t), u_s(t) - u_\ell(t))_m + \ell\,(u_s(t) - u_\ell(t), u_s(t) - u_\ell(t))$$

and since $\mathcal{L}$ is monotone, we obtain

$$(\dot{u}(t) - \dot{u}_\ell(t), u_s(t) - u_\ell(t))_m \ge (\dot{u}_s(t) - \dot{u}_\ell(t), u_s(t) - u_\ell(t))_m .$$

Moreover, using Cauchy-Schwarz inequality we have

$$\partial_t \|u_s(t) - u_\ell(t)\|_m^2 \le 2\|\dot{u}(t) - \dot{u}_\ell(t)\|_m \|u_s(t) - u_\ell(t)\|_m.$$

The function $t \mapsto \|u_s(t) - u_\ell(t)\|_m$ is absolutely continuous, hence differentiable almost everywhere, and satisfies

$$\partial_t \|u_s(t) - u_\ell(t)\|_m^2 = 2\|u_s(t) - u_\ell(t)\|_m \partial_t \|u_s(t) - u_\ell(t)\|_m.$$

Now let $Z = \{t > 0 \ : \ \|u_s(t) - u_\ell(t)\|_m = 0\}$. Clearly, for any $t \notin Z$ we have from above

$$\partial_t \|u_s(t) - u_\ell(t)\|_m \le \|\dot{u}(t) - \dot{u}_\ell(t)\|_m. \tag{3.40}$$

At an accumulation point of Z, the estimate holds, since the left side is zero at such a point. Since Z has at most a countable number of isolated points, this shows that the estimate holds at almost every $t > 0$. Integration of (3.40) yields

$$\|u_s(t) - u_\ell(t)\|_m \le \int_0^t \|\dot{u}(s) - \dot{u}_\ell(s)\|_m \, ds$$

Finally, by triangle inequality, we obtain

$$\begin{aligned} \|u(t) - u_s(t)\|_m &\le \|u(t) - u_\ell(t)\|_m + \|u_\ell(t) - u_s(t)\|_m \\ &\le \|u(t) - u_\ell(t)\|_m + \int_0^t \|\dot{u}(s) - \dot{u}_\ell(s)\|_m \, ds. \end{aligned}$$

□

The estimate (3.39) shows that the error in the Faedo-Galerkin approximation procedure is determined by the error in the $\mathcal{L}-$projection (3.38). When $u \in C^1((0,\infty), V)$ we differentiate equation (3.38) with respect to t and deduce that $\dot{u}_\ell(t) \in S$ in the $\mathcal{L}-$projection of $\dot{u}(t)$.

We shall illustrate the use of the error estimate (3.39) by applying it to a second order parabolic equation whose solution is numerically approximated by means of linear finite elements.

Example 3.1. Let $\{\mathcal{T}_h\}_{h\geq 0}$ be a family of regular triangulations of the domain Ω and let S_h^1 be the space of linear finite elements defined in equation (3.15) such that S_h^1 is a subspace of the closed subspace V of $H^1(\Omega)$. Set $H = L^2(\Omega) = H'$, so $\mathcal{M}$ is the identity, let $f \equiv 0$ and let $\ell(\cdot,\cdot) = a(\cdot,\cdot)$, where the continuous bilinear form $a(\cdot,\cdot)$ is assumed to be $V-$elliptic and $0-$regular. Moreover, assume that the form adjoint to $a(\cdot,\cdot)$ is also $0-$regular. If $u \in v$ is solution of problem

$$\mathcal{M}\dot{u}(t) + \mathcal{L}u(t) = f(t), \quad t > 0,$$

and $u_h \in S_h^1$ is solution of the problem

$$(\dot{u}_h(t), v)_{L^2} + \ell(u_h(t), v) = f(t)(v), \quad v \in S_h^1,\ t > 0,$$

then the differentiability of these functions in $t > 0$ is given by Theorem 3.18. Since the finite element solution is computed using linear finite elements and both the bilinear form $a(\cdot,\cdot)$ and the form adjoint to $a(\cdot,\cdot)$ are $0-$regular, from Corollary 3.1 and Theorem 3.7 we obtain the following error estimates

$$\|u(t) - u_\ell(t)\|_{L^2} \leq ch^2\|Au(t)\|_{L^2}, \tag{3.41a}$$
$$\|\dot{u}(t) - \dot{u}_\ell(t)\|_{L^2} \leq ch^2\|A\dot{u}(t)\|_{L^2}, \qquad t > 0, \tag{3.41b}$$

where A is the operator associated to the bilinear form $a(\cdot,\cdot)$. Since $f = 0$, we have $\dot{u}(t) = -Au(t)$, which implies that inequality (3.41b) can also be written as

$$\|\dot{u}(t) - \dot{u}_\ell(t)\|_{L^2} \leq ch^2\|A^2u(t)\|_{L^2}, \qquad t > 0.$$

From Theorem 3.9 we know that, if A is accretive, then $\|u(t)\|_H$, where $u(t)$ is solution of $\dot{u}(t)+Au(t) = 0$, is non-increasing. Since from Theorem 3.18 $u(t) \in D(A^p)$ for every $p \geq 1$ and for each $t > 0$, it can be shown that $\|Au(t)\|_H$ and $\|A^2u(t)\|_H$ are non-increasing for $t > 0$. Indeed:

$$\partial_t\left(\|Au(t)\|_{L^2}^2\right) = 2\Re\left(A\dot{u}(t), Au(t)\right)_{L^2} = -2\Re\left(A(Au(t)), Au(t)\right)_{L^2} = -2\Re\left(Az(t), z(t)\right)_{L^2} \leq 0, \quad z(t) := Au(t),$$
$$\partial_t\left(\|A^2u(t)\|_{L^2}^2\right) = 2\Re\left(A^2\dot{u}(t), A^2u(t)\right)_{L^2} = -2\Re\left(A^2(Au(t)), A^2u(t)\right)_{L^2} = -2\Re\left(Az(t), z(t)\right)_{L^2} \leq 0, \quad z(t) := A^2(t),$$

and assuming $u_0 \in D(A^2)$, we have

$$\|Au(t)\|_{L^2} \leq \|Au_0\|_{L^2}, \qquad \|A^2u(t)\|_{L^2} \leq \|A^2u_0\|_{L^2}.$$

Therefore, the error estimates (3.41) become

$$\|u(t) - u_\ell(t)\|_{L^2} \leq ch^2\|Au(t)\|_{L^2} \leq ch^2\|Au_0\|_{L^2},$$
$$\|\dot{u}(t) - \dot{u}_\ell(t)\|_{L^2} \leq ch^2\|A\dot{u}(t)\|_{L^2} \leq ch^2\|A^2u_0\|_{L^2}, \qquad t > 0,$$

Combining this result with inequality (3.39) we obtain

$$\|u(t) - u_h(t)\|_{L^2} \leq ch^2\left(\|Au_0\|_{L^2} + t\|A^2u_0\|_{L^2}\right).$$

The assumption $u_0 \in D(A^2)$ can be relaxed using the estimate (3.33) from Theorem 3.16, which yields

$$t\|A^2u(t)\|_{L^2} = t\|AAu(t)\|_{L^2} = t\|AAT(t)u_0\|_{L^2} = t\|AT(t)Au_0\|_{L^2} \leq t\|AT(t)\|\|Au_0\|_{L^2} \leq c(\varepsilon)\|Au_0\|_{L^2}$$

with $0 < \varepsilon < \theta_0$ and $t \in S(\theta_0 - \varepsilon)$. Then, the error estimate associated to the initial problem, becomes

$$\|u(t) - u_h(t)\|_{L^2} \leq ch^2\|Au_0\|_{L^2}.$$

3.5 Abstract Second Order Evolution Equations

Let V and W be Hilbert spaces with V a dense subspace of W for which the injection is continuous. Thus, we identify $W' \leq V'$ by duality. Let $\mathcal{A}$ and $\mathcal{C}$ be the Riesz maps of the spaces V and W, respectively, and let $\mathcal{B} \in \mathcal{L}(V, V')$. If $u_0 \in V$, $u_1 \in W$ and $f \in C((0,\infty), W')$ are given, we consider the problem of finding $u \in C([0,\infty), V) \cap C^1((0,\infty), V) \cap C^1([0,\infty), W) \cap C^2((0,\infty), W)$ such that $u(0) = u_0$, $u'(0) = u_1$, and

$$\mathcal{C}\ddot{u}(t) + \mathcal{B}\dot{u}(t) + \mathcal{A}u(t) = f(t) \tag{3.42}$$

for all $t > 0$. Note that for any such solution of equation (3.42) we have $\dot{u}(t) \in V$ and $\mathcal{B}\dot{u}(t) + \mathcal{A}u(t) \in W'$ for all $t > 0$. We solve equation (3.42) by reducing it to a first order equation on a product space and then applying the results presented for first order evolution equations. Then, the idea is to write equation (3.42) in the form

$$\begin{pmatrix} \mathcal{C} & 0 \\ 0 & \mathcal{A} \end{pmatrix} \begin{pmatrix} \ddot{u} \\ \dot{u} \end{pmatrix} + \begin{pmatrix} \mathcal{B} & \mathcal{A} \\ -\mathcal{A} & 0 \end{pmatrix} \begin{pmatrix} \dot{u} \\ u \end{pmatrix} = \begin{pmatrix} f(t) \\ 0 \end{pmatrix}.$$

Let us denote by $V_m = W \times V$ the product Hilbert space with scalar product given by

$$([x_1, x_2], [y_1, y_2])_{V_m} = (x_1, y_1)_W + (x_2, y_2)_V, \qquad [x_1, x_2], [y_1, y_2] \in V_m = W \times V.$$

Then we have $V_m' = W' \times V'$ and we define $\mathcal{M} \in \mathcal{L}(V_m, V_m')$ by

$$\mathcal{M}([x_1, x_2]) = [\mathcal{C}x_1, \mathcal{A}x_2], \qquad [x_1, x_2] \in V_m.$$

Since $\mathcal{A}$ and $\mathcal{C}$ are the Riesz maps of V and W, respectively, we obtain

$$\begin{aligned} \mathcal{M}([x_1, x_2], [y_1, y_2]) &= \mathcal{A}x_1(y_1) + \mathcal{C}x_2(y_2) \\ &= (x_1, y_1)_V + (x_2, y_2)_W \\ &= ([x_1, x_2], [y_1, y_2])_{V_m}, \qquad [x_1, x_2], [y_1, y_2] \in V_m, \end{aligned}$$

which means that $\mathcal{M}$ is the Riesz map of V_m onto V_m'. Then define the space $V_\ell = V \times V$ and $\mathcal{L} \in \mathcal{L}(V_\ell, V_\ell')$ by

$$\mathcal{L}([x_1, x_2]) = [\mathcal{B}x_1 + \mathcal{A}x_2, -\mathcal{A}x_1], \qquad [x_1, x_2] \in V_\ell = V \times V.$$

If $u(t)$ is a solution of equation (3.42), then the function defined by $w(t) = [\dot{u}(t), u(t)]$, $t \geq 0$, satisfies the following: $w \in C([0,\infty), V_m) \cap C^1((0,\infty), V_m)$, $w(0) = [u_1, u_0] \in V_m$ with $\mathcal{A}u_0 + \mathcal{B}u_1 \in W'$ and

$$\mathcal{M}\dot{w}(t) + \mathcal{L}w(t) = [f(t), 0], \qquad t > 0.$$

This is precisely the framework described in the previous section. Therefore, we only need to find the conditions on the data in equation (3.42) so that the previous theorems can be applied. This leads to the following result.

Theorem 3.24 (See Theorem VI.2.2 in [182]). *Let $\mathcal{A}$ and $\mathcal{C}$ be the Riesz maps of the Hilbert spaces V and W, respectively, where V is dense and continuously embedded in W. Let $\mathcal{B} \in \mathcal{L}(V, V')$ and assume $\mathcal{B} + \lambda\mathcal{C}$ is $V-$elliptic for some $\lambda > 0$. Then, for every Hölder continuous $f\colon [0,\infty) \to W'$, $u_0 \in V$ and $u_1 \in W$, there is a unique solution $u(t)$ of equation (3.42) on $t > 0$ with $u(0) = u_0$ and $\dot{u}(0) = u_1$.*

Chapter 4

Orthogonal Polynomials

This Chapter provides a brief introduction to the theory of orthogonal polynomials, focusing in particular on Legendre and Chebyshev polynomials. Basis functions based on linear combination of these families of orthogonal polynomials will be used within the Galerkin Spectral (Element) Method applied in Chapter 6 to compute the numerical solution of the boundary value problem describing the propagation of waves in Kelvin-Voigt viscoelastic materials. Within the theory of Spectral Methods for Partial Differential Equations, the numerical solution is expanded in terms of a finite sequence of orthogonal functions. If the solution is periodic, it is expanded by means of Fourier series. In particular, when the function is also infinitely smooth and all its derivatives are periodic, it is observed that all the coefficients of the Fourier series following those necessary to represent the structure of the function decay faster than algebraically. The rapid decay of this coefficients implies that the Fourier series truncated after few terms represents a very good approximation of the function. This characteristic is usually referred to as *spectral accuracy*. Spectral accuracy is also attainable for smooth nonperiodic functions provided that the expansion functions are properly chosen. In particular, the eigenfunctions of the singular Sturm-Liouville eigenvalue problem, that we present in Section 4.1, guarantee spectral accuracy when used to to expand any infinitely smooth function. The only polynomials arising as eigenfunctions of the singular Sturm-Liouville problem are the so-called Jacobi polynomials, which are introduced in Section 4.2. The Legendre and Chebyshev polynomials are special cases of the Jacobi polynomials; their main features are described in Sections 4.3 and 4.4, respectively. Typically, one does not directly employ these polynomials within Spectral Galerkin methods for Partial Differential Equations, but rather considers the so-called boundary-adapted polynomials, which allow for a more easily imposition of Dirichlet boundary conditions. In this regard, we show how to define boundary-adapted polynomials by means of suitable linear combinations of Legendre and Chebyshev polynomials of the First Kind in Sections 4.3.1 and 4.4.1, respectively. These polynomial basis functions will be used in Chapter 6 for the computation of the numerical solution of the boundary value problem (presented in Chapter 5) describing the propagation of waves in Kelvin-Voigt viscoelastic materials. Moreover, in Sections 4.3.1 and 4.4.1 we also detail the construction of the components of some matrices usually arising in the (space) discretisation of the weak formulation of boundary-value problems and obtained by evaluating integrals involving the product of (boundary-adapted) polynomials basis function or their derivatives. In Section 4.5 we show how to build multidimensional basis functions defined on the Cartesian product of intervals by taking the tensor product of one-dimensional basis functions. Furthermore, we will see that the usage of boundary-adapted basis in each direction produce a boundary-adapted basis in $\Omega \subset \mathbb{R}^d$. The results presented in Sections from 4.1 to 4.5 are mainly based on [153, Chapter 2], except for the part discussing the computation of the matrices involving the integrals of boundary-adapted Chebyshev polynomials (§4.4.1), which has been developed by the author of this thesis. Finally, in Section 4.6 we summarize the most fundamental results about the theory of polynomial approximation, i.e., we present some error estimates for the approximation of functions by means of orthogonal polynomials. The results introduced in this Section are based on [153, Chapter 5] and are used in Chapter 6 to derive error estimates for the Spectral Method applied to the boundary value problem describing waves propagation phenomena in Kelvin-Voigt materials.

4.1 Sturm-Liouville Problem

The *Sturm-Liouville problem* is an eigenvalue problem of the form

$$-\frac{d}{dx}\left(p\frac{du}{dx}\right)+qu=\lambda wu \quad \text{in the interval } (-1,+1), \tag{4.1}$$

where the p, q and w are given, real-valued functions such that

- p is continuously differentiable, strictly positive in $(-1,+1)$ and continuous at $x=\pm 1$;
- q is continuous, nonnegative and bounded in $(-1,+1)$;
- the weight function w is continuous, nonnegative and integrable over the interval $(-1,+1)$.

The importance of Sturm-Liouville problems for spectral methods lies in the fact that the spectral approximation of the solution of a differential equation is usually regarded as a finite expansion of eigenfunctions of the so-called *singular* Sturm-Liouville problems, i.e., those Sturm-Liouville problems for which p vanishes in at least one point of the boundary. Indeed, eigenfunctions of singular Sturm-Liouville problems ensure spectral accuracy when used to expand any infinitely smooth function, meaning that the coefficients according to this basis decay faster than algebraically in the inverse of the eigenvalue. This behaviour is therefore similar to the one provided by trigonometric functions, but without requiring any restriction on the boundary behaviour. Among the singular Sturm-Liouville problems, particularly important are the ones whose eigenfunctions are algebraic polynomials because of the efficiency with which they can be evaluated and differentiated numerically. In particular, it can be proven that the only polynomials that are eigenfunctions of a singular Sturm-Liouville problem are the so-called *Jacobi polynomials*.

4.2 Jacobi Polynomials

The class of Jacobi polynomials comprises all the polynomials that are solutions of the *singular Sturm-Liouville* problem defined on the interval $(-1,+1)$. The Jacobi polynomials $P_k^{(\alpha,\beta)}(x)$ of indices $\alpha,\beta>-1$ and degree k are the solutions of the eigenvalue problem (4.1) with

$$p(x)=(1-x)^{1-\alpha}(1+x)^{1+\beta},\quad q(x)=0,\quad w(x)=(1-x)^{\alpha}(1+x)^{\beta}$$

and the corresponding eigenvalues are given by $\lambda_k=k(k+\alpha+\beta+1)$. Jacobi polynomials can be expressed as

$$P_k^{(\alpha,\beta)}(x)=\frac{1}{2^k}\sum_{l=0}^{k}\binom{k+\alpha}{l}\binom{k+\beta}{k-l}(x-1)^l(x+1)^{k-l}$$

or, equivalently, using *Rodriguez formula* as

$$P_k^{(\alpha,\beta)}(x)=\frac{(-1)^k}{2^k k!}(1-x)^{-\alpha}(1+x)^{-\beta}\frac{d^k}{dx^k}((1-x)^{\alpha+k}(1+x)^{\beta+k}).$$

The following orthogonality relation holds:

$$\int_{-1}^{+1}P_m^{(\alpha,\beta)}(x)P_n^{(\alpha,\beta)}(x)(1-x)^{\alpha}(1+x)^{\beta}\,dx=\frac{2^{\alpha+\beta+1}}{2n+\alpha+\beta+1}\frac{\Gamma(n+\alpha+1)\Gamma(n+\beta+1)}{n!\,\Gamma(n+\alpha+\beta+1)}\delta_{nm}.$$

Jacobi polynomials satisfy the following recursion relation

$$P_0^{(\alpha,\beta)}(x)=1,\quad P_1^{(\alpha,\beta)}(x)=\frac{1}{2}[(\alpha-\beta)+(\alpha+\beta+2)x],$$
$$a_{1,k}P_{k+1}^{(\alpha,\beta)}(x)=a_{2,k}P_k^{(\alpha,\beta)}(x)-a_{3,k}P_{k-1}^{(\alpha,\beta)}(x),$$

where

$$a_{1,k} = 2(k+1)(k+\alpha+\beta+1)(2k+\alpha+\beta),$$
$$a_{2,k} = (2k+\alpha+\beta+1)(\alpha^2-\beta^2) + x\Gamma(2k+\alpha+\beta+3)/\Gamma(2k+\alpha+\beta),$$
$$a_{3,k} = 2(k+\alpha)(k+\beta)(2k+\alpha+\beta+2).$$

Jacobi polynomials and their derivatives are related through the following formula

$$\frac{d^m}{dx^m}P_k^{(\alpha,\beta)}(x) = 2^{-m}\frac{\Gamma(k+m+\alpha+\beta+1)}{\Gamma(k+\alpha+\beta+1)}P_{k-m}^{(\alpha+m,\beta+m)}(x).$$

Jacobi polynomials for which $\alpha = \beta$ are called *ultraspherical polynomials* and are simply denoted by $P_k^{(\alpha)}(x)$. Two important special cases of Jacobi polynomials are the *Legendre* polynomials $L_k(x)$, defined by

$$L_k(x) := P_k^{(0)}(x)$$

and *Chebyshev* polynomials of the first kind $T_k(x)$, which are defined by

$$T_k(x) := \frac{2^{2k}(k!)^2}{(2k)!}P_k^{(-1/2)}(x).$$

4.3 Legendre Polynomials

The Legendre polynomials $L_k(x)$, $k = 0, 1, \ldots$, are obtained from the Jacobi polynomials by setting $\alpha = \beta = 0$, i.e., they are the eigenfunctions of the singular Sturm-Liouville problem with

$$p(x) = 1 - x^2, \quad q(x) = 0, \quad w(x) = 1,$$

that is

$$((1-x^2)L_k'(x))' + \lambda_k L_k(x) = 0, \qquad \lambda_k = k(k+1).$$

The Legendre polynomial $L_k(x)$, normalized so that $L_k(1) = 1$, has the expansion

$$L_k(x) = \frac{1}{2^k}\sum_{l=0}^{[k/2]}(-1)^l\binom{k}{l}\binom{2k-2l}{k}x^{k-2l}, \tag{4.2}$$

where $[k/2]$ denotes the integer part of $k/2$. Using Rodriguez's formula $L_k(x)$ can also be expressed as

$$L_k(x) = \frac{1}{2^k k!}\frac{d^k}{dx^k}\left[(x^2-1)^n\right].$$

The Legendre polynomial $L_k(x)$ is even if k is even and odd if k is odd. Moreover they satisfy the following three-term recurrence relation

$$L_0(x) = 1, \quad L_1(x) = x, \quad L_{k+1}(x) = \frac{2k+1}{k+1}xL_k(x) - \frac{k}{k+1}L_{k-1}(x)$$

and the orthogonality condition

$$\int_{-1}^{+1} L_m(x)L_n(x)\,dx = \left(n+\frac{1}{2}\right)^{-1}\delta_{mn}. \tag{4.3}$$

The following uniform bounds hold:

$$|L_k(x)| \le 1, \quad |L_k'(x)| \le \frac{k(k+1)}{2}, \quad -1 \le x \le +1$$

and the values at the endpoints are

$$L_k(\pm 1) = (\pm 1)^k, \quad L_k'(\pm 1) = (\pm 1)^{k+1}\frac{k(k+1)}{2}.$$

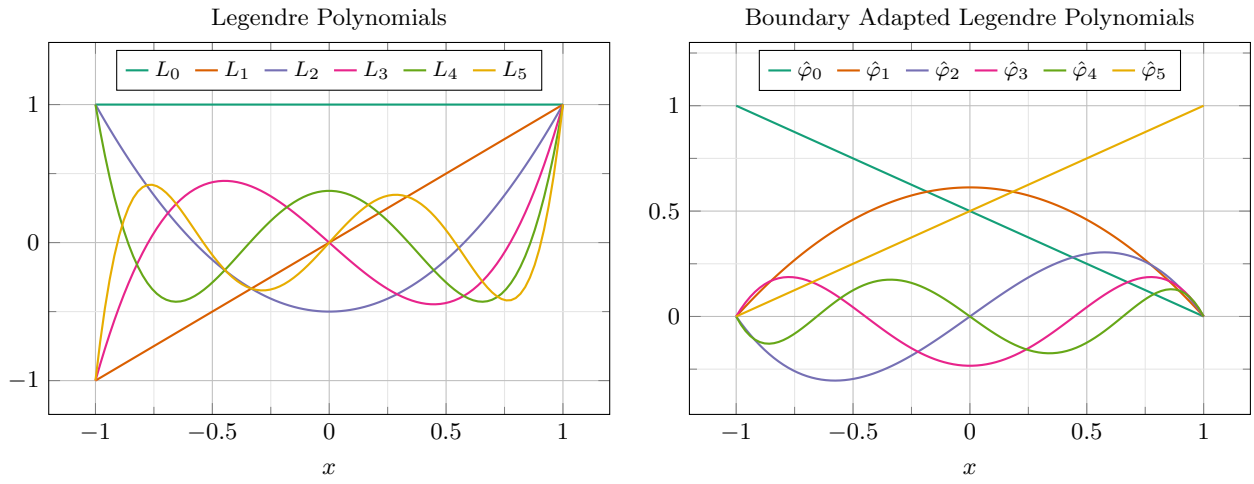


Figure 4.1: Legendre polynomials (left panel) and boundary-adapted Legendre polynomials for $N = 5$.

The expansion of any function $u \in L^2(-1,+1)$ in terms of the Legendre polynomials L_k is given by

$$u(x) = \sum_{k=0}^{\infty} \hat{u}_k L_k(x), \qquad \hat{u}_k = \left(k + \frac{1}{2}\right) \int_{-1}^{+1} u(x) L_k(x)\, dx. \tag{4.4}$$

The first derivative of a function, written in terms of the Legendre expansion of the function itself, is given by

$$u'(x) = \sum_{k=0}^{\infty} \hat{u}_k^{(1)} L_k(x), \tag{4.5}$$

where

$$\hat{u}_k^{(1)} = (2k+1) \sum_{\substack{p=k+1 \\ p+k \text{ odd}}}^{\infty} \hat{u}_p, \qquad k \geq 0.$$

If the function u is a polynomial of degree at most N, i.e., $u \in \mathbb{P}_N(-1,+1)$, then the summations in equations (4.4) and (4.5) clearly involve only the first N and $N-1$ Legendre polynomials, respectively. Then, the coefficients $\hat{u}_k^{(1)}$, $k = 0, 1, \ldots, N-1$, can be computed through the following backward recursive relation

$$\begin{aligned} \hat{u}_{N-1}^{(1)} &= (2N-1)\hat{u}_N, \\ \hat{u}_{k-1}^{(1)} &= (2k-1)\left(\hat{u}_k + \frac{\hat{u}_{k+1}^{(1)}}{2k+3}\right) \qquad k = N-1, N-2, \ldots, 1. \end{aligned}$$

From these relations it follows that the derivative of a Legendre polynomial $L_n(x)$, written in terms of the Legendre polynomials $L_k(x)$, $k = 0, 1, \ldots . n-1$, can be expressed as

$$L_n'(x) = \sum_{\substack{k=0 \\ k+n \text{ odd}}}^{n-1} (2k+1) L_k(x).$$

Legendre polynomials $L_k(x)$, with $k = 0, 1, \ldots, 5$, are shown in Figure 4.1 (left panel).

4.3.1 Boundary Adapted Legendre Polynomials

A *boundary-adapted basis* of $\mathbb{P}_N(-1,+1)$ is a polynomial basis composed of two *vertex functions*, i.e., functions that are nonzero at precisely one endpoint of the interval, and $N-1$ *bubble functions* vanishing at both the endpoints. As we will see in Chapter 6, boundary-adapted basis functions are particularly important in the context of Galerkin spectral methods for two reasons. First, they allow

for an easy enforcement of Dirichlet boundary conditions, as the bubble functions individually satisfy zero Dirichlet boundary conditions, whereas the two vertex functions are used to accommodate the prescribed Dirichlet boundary values, whenever they are nonzero. Second, boundary-adapted bases allow a straightforward definition of global continuous piecewise polynomial functions made by *glueing* local boundary-adapted polynomial functions defined on contiguous domains. A modal boundary-adapted polynomial basis of $\mathbb{P}_N(-1,+1)$ based on Legendre polynomials $L_k(x)$, $k=0,\ldots,N$ can be defined as follows:

$$\begin{aligned}
\text{right vertex function:} \quad & \hat{\varphi}_0(x) = \frac{1}{2}\left(L_0(x) - L_1(x)\right) = \frac{1-x}{2}, \\
\text{bubble basis functions:} \quad & \hat{\varphi}_k(x) = \sqrt{\frac{2k+1}{2}} \int_x^1 L_k(s)\, ds, \qquad 1 \le k \le N-1, \\
\text{left vertex function:} \quad & \hat{\varphi}_N(x) = \frac{1}{2}\left(L_0(x) + L_1(x)\right) = \frac{1+x}{2}.
\end{aligned}$$

Other equivalent expressions for $\hat{\varphi}_k(x)$, $k=1,\ldots,N-1$, are

$$\hat{\varphi}_k(x) = \frac{1}{\sqrt{2(2k+1)}}\left(L_{k-1}(x) - L_{k+1}(x)\right)$$

and

$$\hat{\varphi}_k(x) = \frac{\sqrt{2(2k+1)}}{k+1}\left(\frac{1-x}{2}\right)\left(\frac{1+x}{2}\right)P_{k-1}^{(1,1)}(x),$$

where we recall that $P_k^{(1,1)}$ is the $k-$th Jacobi polynomial, orthogonal with respect to the weight $w(x) = 1-x^2$. Boundary-adapted Legendre polynomials $\hat{\varphi}_k(x)$, with $k=0,1,\ldots,5$, are shown in Figure 4.1 (right panel).

Since the boundary value problems we want to solve numerically are tipically defined on the general interval $I=(x_L,x_R)$ and not on the reference interval $\hat{I}=(-1,+1)$ where the (boundary-adapted) Legendre polynomials are defined, it is necessary to modify the domain where the basis functions $\hat{\varphi}_i$, $i=0,\ldots,N$ are defined. So, we hereafter assume that I is the image of the reference interval $\hat{I}$ under a smooth and invertible mapping F, i.e., $I=F(\hat{I})$. Moreover, we denote by $\hat{x}$ the coordinate in $\hat{I}$ and by $x=F(\hat{x})$ its image in I. We further assume that the transformation is nondegenerate, which means that $F'(\hat{x}) \neq 0$ for all $\hat{x} \in \hat{I}$. In particular, we consider the affine transformation

$$F(\hat{x}) = \frac{x_R - x_L}{2}\hat{x} + \frac{x_R + x_L}{2}. \tag{4.6}$$

Then, we define basis functions $\varphi_i(x)$, $i=0,\ldots,N$, in I by mapping $\hat{\varphi}_i(x)$ from $\hat{I}$ to I, i.e.,

$$\varphi_i(x) := \hat{\varphi}_i(F^{-1}(x)), \qquad i=0,\ldots,N.$$

We now detail the construction of the individual components of some matrices usually arising in the (space) discretisation of the weak formulation of boundary-value problems. The computation of the components of these matrices consists in the evaluation of integrals involving the product of polynomials basis functions φ_i or their derivatives. In particular, we consider the following integrals:

$$K_{ij}^{(0)} := \int_I \varphi_j(x)\varphi_i(x)\, dx, \quad K_{ij}^{(1)} := \int_I \frac{d\varphi_j}{dx}(x)\varphi_i(x)\, dx, \quad K_{ij}^{(2)} := \int_I \frac{d\varphi_j}{dx}(x)\frac{d\varphi_i}{dx}(x)\, dx, \quad i,j=0,1,\ldots,N.$$

In the following we will refer to $K_{ij}^{(0)}$ as the *zeroth-order contributions*, to $K_{ij}^{(1)}$ as the *first-order contributions* and to $K_{ij}^{(2)}$ as the *second-order contributions*, since these integrals are tipically associated with terms involving, respectively, zero, one and two derivatives of the unknown function in the original differential equation.

Zeroth-order contributions The mass matrix, which has components defined as

$$K_{ij}^{(0)} = \int_I \varphi_j(x)\varphi_i(x)\,dx = \int_{\hat{I}} \hat{\varphi}_j(\hat{x})\hat{\varphi}_i(\hat{x})F'(\hat{x})\,d\hat{x} = \frac{x_R - x_L}{2}\int_{\hat{I}} \hat{\varphi}_j(\hat{x})\hat{\varphi}_i(\hat{x})\,d\hat{x} = \frac{x_R - x_L}{2}\hat{K}_{ij}^{(0)} \quad (4.7)$$

has a pentadiagonal structure for the internal (bubble) basis functions. The nonzero entries of the matrix $\hat{K}^{(0)}$, in its upper triangular part, are given by

$$\hat{K}_{00}^{(0)} = \hat{K}_{NN}^{(0)} = \frac{2}{3}, \qquad \hat{K}_{0N}^{(0)} = \frac{1}{3},$$
$$\hat{K}_{01}^{(0)} = \hat{K}_{1N}^{(0)} = \frac{1}{\sqrt{6}}, \qquad \hat{K}_{02}^{(0)} = -\hat{K}_{2N}^{(0)} = -\frac{1}{3\sqrt{10}}$$

and, for $1 \le i \le j \le N-1$,

$$\hat{K}_{ij}^{(0)} = \begin{cases} \dfrac{2}{(2i-1)(2i+3)}, & j = i, \\ -\dfrac{1}{(2i+3)\sqrt{(2i+1)(2i+5)}}, & j = i+2. \end{cases}$$

First-order contributions Since

$$\frac{d\varphi_j}{dx} = \frac{d\hat{\varphi}_j}{d\hat{x}}\frac{d\hat{x}}{dx} = F'(\hat{x})^{-1}\frac{d\hat{\varphi}_j}{d\hat{x}},$$

we have

$$K_{ij}^{(1)} = \int_I \frac{d\varphi_j}{dx}(x)\varphi_i(x)\,dx = \int_{\hat{I}} \frac{d\hat{\varphi}_j}{d\hat{x}}(\hat{x})\hat{\varphi}_i(\hat{x})\,d\hat{x},$$

which has a tridiagonal internal structure and nonzero entries given by

$$K_{00}^{(1)} = -K_{NN}^{(1)} = -\frac{1}{2}, \qquad K_{0N}^{(1)} = -K_{0N}^{(1)} = \frac{1}{2},$$
$$K_{01}^{(1)} = -K_{10}^{(1)} = \frac{1}{\sqrt{6}}, \qquad K_{N1}^{(1)} = -K_{1N}^{(1)} = -\frac{1}{\sqrt{6}}$$

and, for $1 \le i \le j \le N-1$,

$$K_{i,i+1}^{(1)} = -K_{i+1,i}^{(1)} = \frac{1}{\sqrt{4(i+1)^2 - 1}}.$$

Second-order contributions The stiffness matrix, which has components defined as

$$K_{ij}^{(2)} = \int_I \frac{d\varphi_j}{dx}(x)\frac{d\varphi_i}{dx}(x)\,dx = \int_{\hat{I}} \frac{d\hat{\varphi}_j}{d\hat{x}}(\hat{x})\frac{d\hat{\varphi}_i}{d\hat{x}}(\hat{x})F'(\hat{x})^{-1}\,d\hat{x} = \frac{2}{x_R - x_L}\int_{\hat{I}} \frac{d\hat{\varphi}_j}{d\hat{x}}(\hat{x})\frac{d\hat{\varphi}_i}{d\hat{x}}(\hat{x})\,d\hat{x} = \frac{2}{x_R - x_L}\hat{K}_{ij}^{(2)},$$

is diagonal for the internal basis functions. More specifically, the nonzero entries of matrix $\hat{K}^{(2)}$ are

$$\hat{K}_{0N}^{(2)} = \hat{K}_{N0}^{(2)} = -\frac{1}{2}, \qquad \hat{K}_{ii}^{(2)} = \begin{cases} \dfrac{1}{2}, & i = 0 \text{ or } i = N, \\ 1, & 1 \le i \le N-1. \end{cases}$$

It is worth highlighting that the orthogonality relation (4.3) satisfied by the Legendre polynomials implies that the mass matrix associated with the modal Legendre basis of $\mathbb{P}_N(-1,+1)$ is diagonal. On the other hand, the boundary-adapted Legendre basis provides a diagonal stiffness matrix (for the bubble basis functions).

4.4 Chebyshev Polynomials

The Chebyshev polynomials of the first kind $T_k(x)$, $k = 0, 1, \ldots$, are proportional to the ultraspherical Jacobi polynomials obtained by setting $\alpha = \beta = -1/2$:

$$T_k(x) = \frac{2^{2k}(k!)^2}{(2k)!} P_k^{-1/2}(x).$$

Thus, the Chebyshev polynomials are the eigenfunctions of the Sturm-Liouville problem with

$$p(x) = (1-x^2)^{1/2}, \quad q(x) = 0, \quad w(x) = (1-x^2)^{-1/2},$$

which is

$$\left(\sqrt{1-x^2}T_k'(x)\right)' + \frac{\lambda_k}{\sqrt{1-x^2}} T_k(x) = 0, \qquad \lambda_k = k^2.$$

For any k, $T_k(x)$ is even if k is even and odd if k is odd. If $T_k(x)$ is normalized so that $T_k(1) = 1$, then the Chebyshev polynomials can be expressed as

$$T_k(x) = \cos(k \arccos x).$$

Moreover, they can be expanded in power series as

$$T_k(x) = \frac{k}{2} \sum_{l=0}^{[k/2]} (-1)^k \frac{(k-l-1)!}{l!(k-2l)!} (2x)^{k-2l},$$

where, again, $[k/2]$ denotes the integer part of $k/2$. The Chebyshev polynomials of the first kind satisfy the following three-term recurrence relation

$$T_0(x) = 1, \quad T_1(x) = x, \quad T_{k+1}(x) = 2xT_k(x) - T_{k-1}(x) \tag{4.8}$$

and the orthogonality condition

$$\int_{-1}^{+1} \frac{T_m(x)T_n(x)}{\sqrt{1-x^2}}\, dx = \frac{c_n \pi}{2} \delta_{mn}, \qquad c_n = \begin{cases} 2, & n = 0, \\ 1, & n \geq 1. \end{cases} \tag{4.9}$$

The integrals of Chebyshev polynomials are given by:

$$\int_{-1}^{+1} T_i(x)\, dx = \begin{cases} \dfrac{(-1)^n + 1}{1-n^2}, & \text{if } n \neq 1, \\ 0, & \text{if } n = 1. \end{cases} \tag{4.10}$$

The following uniform bounds hold:

$$|T_k(x)| \leq 1. \qquad |T_k'(x)| \leq k^2, \qquad -1 \leq x \leq +1$$

and the values at the endpoints are

$$T_k(\pm 1) = (\pm 1)^k, \qquad T_k'(\pm 1) = (\pm 1)^{k+1} k^2.$$

Another useful property of Chebyshev polynomials of the first kind is given by:

$$2T_m(x)T_n(x) = T_{m+n}(x) + T_{|m-n|}(x), \quad m, n \geq 0. \tag{4.11}$$

The expansion of a function $u \in L_w^2(-1, +1)$ in terms of the Chebyshev polynomials $T_k(x)$ is given by

$$u(x) = \sum_{k=0}^{\infty} \hat{u}_k T_k(x), \qquad \hat{u}_k = \frac{2}{\pi c_k} \int_{-1}^{+1} u(x) T_k(x) w(x)\, dx. \tag{4.12}$$

The first derivative of a function u expressed in terms of Chebyshev polynomials of the first kind, is given by

$$u'(x) = \sum_{k=0}^{\infty} \hat{u}_k^{(1)} T_k(x) \tag{4.13}$$

where

$$\hat{u}_k^{(1)} = \frac{2}{c_k} + \sum_{\substack{p=k+1 \\ p+k \text{ odd}}}^{\infty} p\hat{u}_p, \qquad k \geq 0.$$

If the function u is a polynomial of degree at most N, i.e., $u \in \mathbb{P}_N(-1,+1)$, then the summations in equations (4.12) and (4.13) clearly involve only the first N and $N-1$ Chebyshev polynomials, respectively. Then, the coefficients $\hat{u}_k^{(1)}$, $k = 0, 1, \ldots, N-1$, can be computed through the following backward recursive relation

$$\begin{aligned} \hat{u}_{N-1}^{(1)} &= 2N\hat{u}_N, \\ \hat{u}_{k-1}^{(1)} &= \frac{2k\hat{u}_k + \hat{u}_{k+1}^{(1)}}{c_{k-1}} \qquad k = N-1, N-2, \ldots, 1. \end{aligned}$$

From these relations we obtain that the derivative of a Chebyshev polynomial $T_n(x)$, written in terms of the Chebyshev polynomials $T_k(x)$, $k = 0, 1, \ldots . n-1$, can be expressed as

$$T_n'(x) = 2n \sum_{\substack{k=0 \\ k+n \text{ odd}}}^{n-1} \frac{1}{c_k} T_k(x). \tag{4.14}$$

where the coefficients c_k are defined as in equation (4.9). Chebyshev polynomials $T_k(x)$, with $k = 0, 1, \ldots, 5$, are shown in Figure 4.2 (left panel).

There is another family of Chebyshev polynomials, called Chebyshev polynomials of the second kind, whose elements are denoted by $U_n(x)$ and are defined as follows:

$$U_n(\cos\theta)\sin\theta = \sin((n+1)\theta).$$

These polynomials are defined by the following recurrence relation:

$$U_0(x) = 1, \qquad U_1(x) = 2x, \qquad U_{n+1}(x) = 2x\,U_n(x) - U_{n-1}(x).$$

Chebyshev polynomials of the second kind can be expressed in terms of the Chebyshev polynomials of the first kind using the following formula:

$$U_n(x) = \begin{cases} 2\sum_{\text{odd } j}^{n} T_j(x), & \text{for odd } n, \\ 2\sum_{\text{even } j}^{n} T_j(x) + 1, & \text{for even } n. \end{cases}$$

Another expression relating Chebyshev polynomials of the first and second kind that will be useful in the next subsection is the following:

$$T_{n+1}(x) = xT_n(x) - (1-x^2)U_{n-1}(x). \tag{4.15}$$

4.4.1 Boundary Adapted Chebyshev Polynomials

A modal boundary-adapted polynomial basis for $\mathbb{P}_N(-1,+1)$ based on Chebyshev polynomials of the first kind $T_k(x)$, $k = 0, \ldots, N$, can be defined in a similar way to the one based on Legendre polynomials and discussed in Section 4.3.1. Indeed, we have:

$$\text{left vertex function: } \hat{\varphi}_0(x) = \frac{1}{2}\left(T_0(x) - T_1(x)\right) = \frac{1-x}{2},$$

$$\text{bubble basis functions: } \hat{\varphi}_k(x) = T_{k-1}(x) - T_{k+1}(x), \qquad 1 \leq k \leq N-1, \tag{4.16}$$

$$\text{right vertex function: } \hat{\varphi}_1(x) = \frac{1}{2}\left(T_0(x) + T_1(x)\right) = \frac{1+x}{2}. \tag{4.17}$$

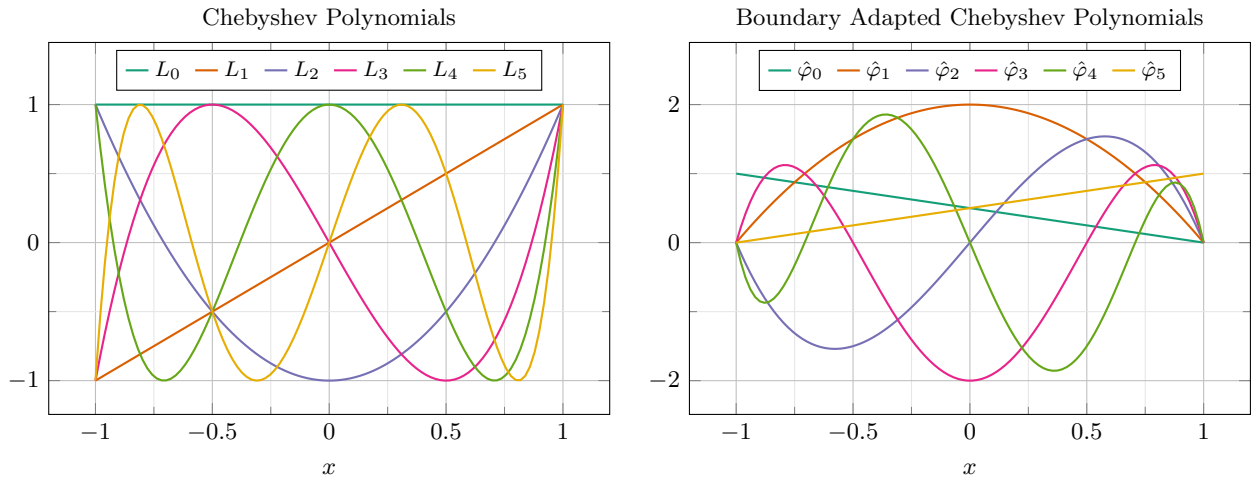


Figure 4.2: Chebyshev polynomials (left panel) and boundary-adapted Chebyshev polynomials for $N = 5$.

Boundary-adapted Chebyshev polynomials $\hat{\varphi}_k(x)$, with $k = 0, 1, \ldots, 5$, are shown in Figure 4.2 (right panel).

Similarly to what we have already done in Section 4.3.1, we define basis functions $\varphi_i(x)$, $i = 0, \ldots, N$, on the interval $I = (x_L, x_R)$ by mapping the boundary-adapted basis functions $\hat{\varphi}_i(x)$ from the reference interval $\hat{I} = (-1, +1)$ to I using the affine mapping given in equation (4.6), i.e., $\varphi_i(x) := \hat{\varphi}_i(F^{-1}(x))$, with $i = 0, \ldots, N$.

The computation of integrals involving the product of basis functions $\varphi_i(x)$ or their derivatives starts by computing the two following integrals:

$$(\mathrm{P}_t)_i = \int_I \tilde{T}_i(x)\,dx, \qquad (\mathrm{P}_{tx})_i = \int_I \tilde{T}_i(x)x\,dx, \qquad i = 0, 1, \ldots, N, \tag{4.18}$$

where $\tilde{T}_i(x)$ denotes the Chebyshev polynomial of the first kind of degree i defined on the interval I, i.e., $\tilde{T}_i(x) := T_i(F^{-1}(x))$. We start with integral $(\mathrm{P}_t)_i$ in equation (4.18), which can be computed as follows:

$$(\mathrm{P}_t)_i = \int_I \tilde{T}_i(x)\,dx = \int_{\hat{I}} T_i(\hat{x})F'(\hat{x})\,d\hat{x} = \frac{x_R - x_L}{2}\int_{\hat{I}} T_i(\hat{x})\,d\hat{x} \overset{(4.10)}{=} \begin{cases} \dfrac{x_R - x_L}{2}\dfrac{(-1)^n + 1}{1 - n^2}, & \text{if } n \neq 1, \\ 0, & \text{if } n = 1. \end{cases}$$

Then, using property (4.11) we can also compute the integral of the product of Chebyshev polynomials mapped on I as follows:

$$\begin{aligned} (\mathrm{P}_{tt})_{ij} &= \int_I \tilde{T}_j(x)\tilde{T}_i(x)\,dx = \int_{\hat{I}} T_j(\hat{x})T_i(\hat{x})F'(\hat{x})\,d\hat{x} \\ &= \frac{1}{2}\int_{\hat{I}} T_{i+j}(\hat{x})F'(\hat{x})\,d\hat{x} + \frac{1}{2}\int_{\hat{I}} T_{|i-j|}(\hat{x})F'(\hat{x})\,d\hat{x} \\ &= \frac{1}{2}\int_I \tilde{T}_{i+j}(x)\,dx + \frac{1}{2}\int_I \tilde{T}_{|i-j|}(x)\,dx = \frac{1}{2}\left[(\mathrm{P}_t)_{i+j} + (\mathrm{P}_t)_{|i-j|}\right]. \end{aligned} \tag{4.19}$$

Let us now denote by B the matrix defining the change of basis from $\tilde{T}_i(x)$ to $\varphi_i(x)$, i.e.,

$$\mathrm{B} = \begin{bmatrix} +\frac{1}{2} & +1 & 0 & \dots & \dots & \dots & +\frac{1}{2} \\ -\frac{1}{2} & 0 & +1 & \dots & \dots & \dots & +\frac{1}{2} \\ 0 & -1 & 0 & \dots & \dots & \dots & 0 \\ 0 & 0 & -1 & \dots & \dots & \dots & \dots \\ \dots & \dots & \dots & \dots & \dots & \dots & \dots \\ 0 & 0 & 0 & \dots & \dots & +1 & 0 \\ 0 & 0 & 0 & \dots & \dots & 0 & 0 \\ 0 & 0 & 0 & \dots & \dots & -1 & 0 \end{bmatrix}$$

and by D the matrix that allows to write the derivative of (mapped) Chebyshev polynomials $\tilde{T}_i'(x)$ using a linear combination of (mapped) Chebyshev polynomials themselves $\tilde{T}_i(x)$, i.e.,

$$\mathrm{D} = \frac{2}{x_R - x_L} \begin{bmatrix} 0 & 1 & 0 & 3 & 0 & 5 & \dots \\ 0 & 0 & 4 & 0 & 8 & 0 & \dots \\ 0 & 0 & 0 & 6 & 0 & 10 & \dots \\ 0 & 0 & 0 & 0 & 8 & 0 & \dots \\ 0 & 0 & 0 & 0 & 0 & 10 & \dots \\ 0 & 0 & 0 & 0 & 0 & 0 & \dots \\ \dots & \dots & \dots & \dots & \dots & \dots & \dots \end{bmatrix}.$$

Matrix D is obtained by writing in matrix notation the relation (4.14) and multiplying it by $F'(x)^{-1}$. Then, combining matrices P_{tt}, B and D, we can easily compute the following integrals:

$$\begin{aligned} \int_I \varphi_i(x)\varphi_j(x)\,dx &= \left(\mathrm{B}^\top \mathrm{P}_{tt}\,\mathrm{B}\right)_{ij}, \\ \int_I \varphi_i'(x)\varphi_j(x)\,dx &= \left(\mathrm{B}^\top \mathrm{D}^\top \mathrm{P}_{tt}\,\mathrm{B}\right)_{ij}, \\ \int_I \varphi_i'(x)\varphi_j'(x)\,dx &= \left(\mathrm{B}^\top \mathrm{D}^\top \mathrm{P}_{tt}\,\mathrm{D}\,\mathrm{B}\right)_{ij}. \end{aligned}$$

We now show how to compute integral $(\mathrm{P}_{tx})_i$ in equation (4.18):

$$\begin{aligned} (\mathrm{P}_{tx})_i &= \int_I \tilde{T}_i(x) x\,dx = \int_{\hat{I}} T_i(\hat{x}) \left(\frac{x_R - x_L}{2}\hat{x} + \frac{x_R + x_L}{2}\right) F'(\hat{x})\,d\hat{x} \\ &= \frac{x_R - x_L}{2} \int_{\hat{I}} T_i(\hat{x})\hat{x}F'(\hat{x})\,d\hat{x} + \frac{x_R + x_L}{2} \int_{\hat{I}} T_i(\hat{x})F'(\hat{x})\,d\hat{x} \\ &= \frac{x_R - x_L}{2} \int_{\hat{I}} T_i(\hat{x})T_1(\hat{x})F'(\hat{x})\,d\hat{x} + \frac{x_R + x_L}{2} \int_{\hat{I}} T_i(\hat{x})F'(\hat{x})\,d\hat{x} \\ &= \frac{1}{2}\frac{x_R - x_L}{2} \int_{\hat{I}} T_{i+1}(\hat{x})F'(\hat{x})\,d\hat{x} + \frac{1}{2}\frac{x_R - x_L}{2} \int_{\hat{I}} T_{|i-1|}(\hat{x})F'(\hat{x})\,d\hat{x} + \frac{x_R + x_L}{2} \int_{\hat{I}} T_i(\hat{x})F'(\hat{x})\,d\hat{x} \\ &= \frac{1}{2}\frac{x_R - x_L}{2} \int_I \tilde{T}_{i+1}(x)\,dx + \frac{1}{2}\frac{x_R - x_L}{2} \int_I \tilde{T}_{|i-1|}(x)\,dx + \frac{x_R + x_L}{2} \int_I \tilde{T}_i(x)\,dx \\ &= \frac{1}{2}\frac{x_R - x_L}{2}(\mathrm{P}_t)_{i+1} + \frac{1}{2}\frac{x_R - x_L}{2}(\mathrm{P}_t)_{|i-1|} + \frac{x_R + x_L}{2}(\mathrm{P}_t)_i, \end{aligned}$$

where the three integrals can all be computed using equation (4.10). Then, using property (4.11) we can compute the following integrals:

$$(\mathrm{P}_{ttx})_{ij} = \int_I \tilde{T}_j(x)\tilde{T}_i(x)x\,dx = \frac{1}{2}\int_I \tilde{T}_{i+j}(x)x\,dx + \frac{1}{2}\int_I \tilde{T}_{|i-j|}(x)x\,dx = \frac{1}{2}\left[(\mathrm{P}_{ttx})_{i+j} + (\mathrm{P}_{ttx})_{|i-j|}\right].$$

Finally, combining matrices P_{ttx}, B and D, we can compute the following intgrals:

$$\int_I \varphi_i(x)\varphi_j(x)x\,dx = \left(\mathrm{B}^\top \mathrm{P}_{ttx}\,\mathrm{B}\right)_{ij},$$
$$\int_I \varphi_i'(x)\varphi_j(x)x\,dx = \left(\mathrm{B}^\top \mathrm{D}^\top \mathrm{P}_{ttx}\,\mathrm{B}\right)_{ij},$$
$$\int_I \varphi_i'(x)\varphi_j'(x)x\,dx = \left(\mathrm{B}^\top \mathrm{D}^\top \mathrm{P}_{ttx}\,\mathrm{D}\,\mathrm{B}\right)_{ij}.$$

The last integral we want to compute is:

$$\int_I \frac{\varphi_i(x)\varphi_j(x)}{x}\,dx.$$

Hereafter we shall assume that the left endpoint of the interval $I = (x_L, x_R)$ is non-negative, i.e., $x_L \geq 0$, since this integral typically appears when dealing with cylindrical coordinates and in that context the variable x plays the role of the non-negative radius r. Rewriting the integral with respect to the reference interval $\hat{I}$, we obtain:

$$\int_I \frac{\varphi_i(x)\varphi_j(x)}{x}\,dx = \int_{\hat{I}} \frac{\hat{\varphi}_i(\hat{x})\hat{\varphi}_j(\hat{x})}{\frac{x_R-x_L}{2}\hat{x}+\frac{x_R+x_L}{2}} F'(\hat{x})\,d\hat{x} = \int_{\hat{I}} \frac{\hat{\varphi}_i(\hat{x})\hat{\varphi}_j(\hat{x})}{\frac{x_R-x_L}{2}\hat{x}+\frac{x_R+x_L}{2}} \frac{x_R-x_L}{2}\,d\hat{x} = \int_{\hat{I}} \frac{\hat{\varphi}_i(\hat{x})\hat{\varphi}_j(\hat{x})}{\hat{x}+\frac{x_R+x_L}{x_R-x_L}}\,d\hat{x}.$$

Now notice that, if $x_L > 0$, the integral becomes:

$$\int_{\hat{I}} \frac{\hat{\varphi}_i(\hat{x})\hat{\varphi}_j(\hat{x})}{\hat{x}+c}\,d\hat{x},$$

where $c := (x_R+x_L)/(x_R-x_L)$ is a constant greater than 1. Integrals of this form have been computed numerically up to machine precision using suitable quadrature rules. More precisely, we have used the theory developed in [236] to compute the Gauss quadrature nodes and weights associated to the weight function $w(x) = (x+c)^{-1}$. On the other hand, if $x_L = 0$, the integral becomes:

$$\int_{\hat{I}} \frac{\hat{\varphi}_i(\hat{x})\hat{\varphi}_j(\hat{x})}{\hat{x}+1}\,d\hat{x}. \tag{4.20}$$

Integrals of this form can be computed exactly using the properties and recurrence relations of Chebyshev polynomials, thus obviating the need to rely an appropriate quadrature formulas. Let us assume that $\hat{\varphi}_i(\hat{x})$ is a bubble basis function, i.e., $i = 1, \ldots, N-1$, and that j is any index between 0 and N. Then, using the definition of Chebyshev bubble basis function (4.16), the three-terms recurrence relation of Chebyshev polynomials of the first kind (4.8) and expression (4.15) relating polynomials of first and second kind, we obtain:

$$\begin{aligned}
\hat{\varphi}_i(\hat{x}) &= T_{i-1}(\hat{x}) - T_{i+1}(\hat{x}) \\
(4.16) &= (2\hat{x}\,T_i(\hat{x}) - T_{i+1}(\hat{x})) - T_{i+1}(\hat{x}) \\
(4.8) &= 2(\hat{x}\,T_i(\hat{x}) - T_{i+1}(\hat{x})) \\
(4.15) &= 2(1-x^2)U_{i-1}(\hat{x}).
\end{aligned}$$

Substituting this result into integral (4.20), we obtain

$$\int_{\hat{I}} \frac{\hat{\varphi}_i(\hat{x})\hat{\varphi}_j(\hat{x})}{\hat{x}+1}\,d\hat{x} = \int_{\hat{I}} \frac{2(1-\hat{x}^2)U_{i-1}(\hat{x})\hat{\varphi}_j(\hat{x})}{\hat{x}+1}\,d\hat{x} = 2\int_{\hat{I}} (1-\hat{x})U_{i-1}(\hat{x})\hat{\varphi}_j(\hat{x})\,d\hat{x}.$$

Finally, having denoted by U the matrix defining the change of basis from the Chebyshev polynomials of the first kind $T_i(\hat{x})$ to the Chebyshev Polynomials of the second kind $U_i(\hat{x})$, the integeral can be computed as follows

$$\int_{\hat{I}} \frac{\hat{\varphi}_i(\hat{x})\hat{\varphi}_j(\hat{x})}{\hat{x}+1}\,d\hat{x} = 2\int_{\hat{I}} (1-\hat{x})U_{i-1}(\hat{x})\hat{\varphi}_j(\hat{x})\,d\hat{x} = 2(\mathrm{U}^\top(\mathrm{P}_{tt} - \mathrm{P}_{ttx})\mathrm{B})_{ij},$$

with $i = 1, \dots, N-1$ and $j = 0, \dots, N$. Since integral (4.20) is symmetric with respect i and j, the same result clearly holds for $j = 1, \dots, N-1$ and $i = 0, \dots, N$. Then, we still have four integrals to compute, namely the integerals involving only the product of vertex basis functions:

$$\int_{\hat{I}} \frac{\hat{\varphi}_0(\hat{x})\hat{\varphi}_0(\hat{x})}{\hat{x}+1}\, d\hat{x}, \qquad \int_{\hat{I}} \frac{\hat{\varphi}_0(\hat{x})\hat{\varphi}_N(\hat{x})}{\hat{x}+1}\, d\hat{x}, \qquad \int_{\hat{I}} \frac{\hat{\varphi}_N(\hat{x})\hat{\varphi}_0(\hat{x})}{\hat{x}+1}\, d\hat{x}, \qquad \int_{\hat{I}} \frac{\hat{\varphi}_N(\hat{x})\hat{\varphi}_N(\hat{x})}{\hat{x}+1}\, d\hat{x}. \tag{4.21}$$

The first integeral cannot be computed as is does not converge due to the singularity at $\hat{x} = -1$, whereas the other integrals can be computed by using the definition of Chebyshev right vertex basis function (4.17) which yields for the second (and third) integral in (4.21) the following result:

$$\int_{\hat{I}} \frac{\hat{\varphi}_0(\hat{x})\hat{\varphi}_N(\hat{x})}{\hat{x}+1}\, d\hat{x} = \int_{\hat{I}} \frac{\hat{\varphi}_0(\hat{x})}{\hat{x}+1}\frac{\hat{x}+1}{2}\, d\hat{x} = \frac{1}{2}\int_{\hat{I}} \hat{\varphi}_0(\hat{x})\, d\hat{x} = \frac{1}{2}\int_{\hat{I}} \frac{T_0(\hat{x})}{2}\, d\hat{x} - \frac{1}{2}\cancel{\int_{\hat{I}} \frac{T_1(\hat{x})}{2}\, d\hat{x}} = \frac{1}{2}.$$

Similarly, for the last integral in (4.21), we have

$$\int_{\hat{I}} \frac{\hat{\varphi}_N(\hat{x})\hat{\varphi}_N(\hat{x})}{\hat{x}+1}\, d\hat{x} = \int_{\hat{I}} \frac{\hat{\varphi}_N(\hat{x})}{\hat{x}+1}\frac{\hat{x}+1}{2}\, d\hat{x} = \frac{1}{2}\int_{\hat{I}} \hat{\varphi}_N(\hat{x})\, d\hat{x} = \frac{1}{2}\int_{\hat{I}} \frac{T_0(\hat{x})}{2}\, d\hat{x} + \frac{1}{2}\cancel{\int_{\hat{I}} \frac{T_1(\hat{x})}{2}\, d\hat{x}} = \frac{1}{2}.$$

4.5 Multidimensional Basis Functions: Tensor-Product Expansion

We now construct multidimensional basis functions by exploiting the one-dimensional features discussed in the previous sections. The most natural way to proceed is to take the tensor products of the one-dimensional expansions. Then, the resulting functions will be defined on the Cartesian product of intervals. More precisely, given d families $\{\varphi^{(l)}_{k_l}\}_{k_l}$, $l = 1, \dots, d$, of one dimensional basis functions defined on the intervals (a_l, b_l), then the family $\{\varphi_{\mathbf{k}}(\boldsymbol{x})\}_{\mathbf{k}}$ defined as

$$\varphi_{\mathbf{k}}(\boldsymbol{x}) = \prod_{l=1}^{d} \varphi^{(l)}_{k_l}(x_l), \qquad \mathbf{k} = (k_1, \dots, k_d), \qquad \boldsymbol{x} = (x_1, \dots, x_d),$$

is a multidimensional basis on the domain $\Omega = \prod_{l=1}^{d}(a_l, b_l)$. In particular, if the families of one-dimensional basis functions $\{\varphi^{(l)}_{k_l}\}_{k_l}$ are orthogonal polynomials (e.g. Legendre or Chebyshev polynomials), then the orthogonality of each one-dimensional family with respect to a weight function $w_l(x_l)$ implies the orthogonality of the tensor-product family with respect to the weight $w(\boldsymbol{x}) = \prod_{l=1}^{d} w_l(x_l)$. Sometimes it is more convenient to use a single-index notation to identity the multidimensional tensor product basis functions. More precisely, assuming that each entry k_l of the multi-index $\mathbf{k} = (k_1, k_2, \dots, k_d)$ varies in the range $0, 1, \dots, N$, we will write $\varphi_k(\boldsymbol{x})$ instead of $\varphi_{\mathbf{k}}(\boldsymbol{x})$ (i.e., we will not use the boldface type for the index), where the k is defined according to the lexicographic ordering, that is $k = k_1 + k_2(N+1) + \cdots + k_d(N+1)^{d-1}$.

Multidimensional Boundary Adapted Basis Functions Boundary-adapted bases in each spatial direction tensorize to produce a boundary-adapted basis in $\Omega \subset \mathbb{R}^d$. This multidimensional boundary-adapted basis is formed by bubble basis functions vanishing on $\partial\Omega$ and by vertex functions not vanishing at precisely one vertex, edge functions not vanishing at precisely one edge, face functions not vanishing at precisely one face, and so on. For example, in the two-dimensional case, the tensor product $\varphi_{\mathbf{k}}(\boldsymbol{x}) = \varphi^{(1)}_{k_1}(x_1)\varphi^{(2)}_{k_2}(x_2)$ of two boundary-adapted (Legendre or Chebyshev) modal basis functions $\varphi^{(1)}$ and $\varphi^{(2)}$, defined on the intervals (a_1, b_1) and (a_2, b_2), respectively, and with indices k_1 and k_2 varying in the range $0, \dots, N$, contains

- $(N-1)^2$ bubble functions for $1 \le k_1, k_2 \le N-1$,
- 4 vertex functions for $k_1, k_2 \in \{0, N\}$,
- $4(N-1)$ edge functions for $k_1 \in \{0, N\}$, $1 \le k_2 \le N-1$ and $k_2 \in \{0, N\}$, $1 \le k_1 \le N-1$.

Computation of Matrices The computation of matrices whose entries are defined as the integral of the product of multidimensional tensor basis functions (or their first order derivatives) relies on the results presented in the previous sections of this Chapter. More precisely, these matrices can be computed through the tensor product of the matrices involving the integrals of the product of the one-dimensional polynomial basis functions defining the tensorized basis. For example, let $\{\varphi_k(\boldsymbol{x})\}$ be a tensor-product basis defined on $\Omega = (a_1, b_1) \times (a_2, b_2)$ and built by tensorizing two univariate boundary-adapted modal polynomial basis of Legendre of Chebyshev type. Then, for any $i, j = 0, 1, \ldots, (N+1)^2 - 1$, the components of the mass matrix are given by:

$$\begin{aligned} K^{(0)}_{i,j} = \int_\Omega \varphi_i(\boldsymbol{x})\varphi_j(\boldsymbol{x})\, d\boldsymbol{x} &= \int_{a_1}^{b_1}\int_{a_2}^{b_2} \varphi^{(1)}_{k_1(i)}(x_1)\varphi^{(2)}_{k_2(i)}(x_2)\varphi^{(1)}_{k_1(j)}(x_1)\varphi^{(2)}_{k_2(j)}(x_2)\, dx_1 dx_2 \\ &= \left(\int_{a_1}^{b_1} \varphi^{(1)}_{k_1(i)}(x_1)\varphi^{(1)}_{k_1(j)}(x_1)\, dx_1\right)\left(\int_{a_2}^{b_2} \varphi^{(2)}_{k_2(i)}(x_2)\varphi^{(2)}_{k_2(j)}(x_2)\, dx_2\right) \\ &= K^{(0;x_1)}_{k_1(i),k_1(j)}\, K^{(0;x_2)}_{k_2(i),k_2(j)}, \end{aligned}$$

where we have used the notation $k_1(i)$ and $k_2(i)$ (resp. $k_1(j)$ and $k_2(j)$) to identify the entries k_1 and k_2 of the multi-index $\mathbf{k} = (k_1, k_2)$ associated to the single-index i (resp. j). The matrices $K^{(0;x_1)}$ and $K^{(0;,x_2)}$ of order $N+1$ are the mass matrices associated to the set of one-dimensional basis functions $\{\varphi^{(1)}(x_1)\}$ and $\{\varphi^{(2)}(x_2)\}$. So, if $\varphi^{(k)}(x_k)$, $k = 1, 2$, is a boundary-adapted modal basis defined using Legendre polynomials, then the matrix $K^{(0;x_k)}$ is computed as shown in equation (4.7), whereas if the basis is defined using Chebyshev polynomials of the First Kind, matrix $K^{(0;x_k)}$ is computed as explained in equation (4.19).

Basis Functions on General Domains When the domain of interest $\Omega \subset \mathbb{R}^d$ is not defined as the tensor product of one-dimensional intervals, one usually resorts on a map that transforms the domain of interest into an hypercube. A standard mapping technique that is widely used in two-dimensional fluid dynamical problems is based on conformal transformations. An extensive discussion about this kind of mappings can be found in, e.g., [237–241]. We now report the procedure for mapping a square $\hat{\Omega}$ into a quadrilateral Ω with curved boundaries. Let the four sides of the quadrilateral be denoted by Γ_i, with $i = 1, 2, 3, 4$, and those of the square by $\hat{\Gamma}$. We assume that the arcs Γ_1 and Γ_3 are oriented from left to right and the arcs Γ_2 and Γ_4 from bottom to top. One uses parametrizations π_i from the interval $[0, 1]$ to Γ_i to construct the mapping F from $\hat{\Omega}$ to Ω such that $F(\hat{\Gamma}_i) = \Gamma_i$ for all i. The linear blending mapping introduced by Gordon and Hall [242, 243] defines the mapping F in terms of π_i as follows

$$\begin{aligned} F(\xi,\eta) = &\frac{1-\eta}{2}\pi_3(\xi) + \frac{1+\eta}{2}\pi_1(\xi) \\ &+ \frac{1-\xi}{2}\left[\pi_2(\eta) - \frac{1+\eta}{2}\pi_2(1) - \frac{1-\eta}{2}\pi_2(-1)\right] \\ &+ \frac{1+\xi}{2}\left[\pi_4(\eta) - \frac{1+\eta}{2}\pi_4(1) - \frac{1-\eta}{2}\pi_4(-1)\right]. \end{aligned}$$

When the domain of interest Ω is a subdomain in a multidomain method, the curves Γ_i are usually chosen so that they are exactly parametrizable by polynomials of the same order as the discretization within Ω. This approach is common in Finite Element Methods [244] and was used first in Spectral Element Methods by Korczak and Patera [245].

4.6 Polynomial Approximation Theory

In this section we present several results concerning 1D polynomial approximation in L^p-spaces or in Sobolev spaces, in which the integration is performed with respect to the Legendre weight, i.e., $w(x) \equiv 1$.

We start by recalling the inverse inequality concerning summability, which states that, for any real p and q with $1 \le p \le q \le \infty$, there exists a positive constant C independent of N such that

$$\|\phi\|_{L^q(-1,+1)} \le CN^{2(1/p-1/q)}\|\phi\|_{L^p(-1,+1)}, \quad \text{for all } \phi \in \mathbb{P}_N. \tag{4.22}$$

On the other hand, the inverse inequality concerning differentiation states that, for any p with $2 \le p \le \infty$, and for all integers $r \ge 1$, there exists a positive constant C independent of N such that

$$\|\phi^{(r)}\|_{L^p(-1,+1)} \le CN^{2r}\|\phi\|_{L^p(-1,+1)}, \quad \text{for all } \phi \in \mathbb{P}_N. \tag{4.23}$$

The exponent of N in both equations (4.22) and (4.23) is the smallest possible. Inverse inequalities with smaller powers of N can be obtained at the expenses of inserting a weaker weight in the left-hand side norm or a stronger weight in the right-hand side norm.

We will measure several approximation errors for the Legendre weight in terms of Sobolev norms. The most commonly used Sobolev norm of order $m \ge 0$ is given by

$$\|u\|_{H^m(-1,+1)} = \left(\sum_{k=0}^{m} \|u^{(k)}\|^2_{L^2(-1,+1)}\right)^{1/2}. \tag{4.24}$$

In bounding from above the approximation error, only some of the L^2-norms appearing on the right-hand side of equation (4.24) enter into play. Therefore, it is convenient to introduce the seminorm

$$|u|_{H^{m;N}(-1,+1)} := \left(\sum_{k=\min(m,N+1)}^{m} \|u^{(k)}\|^2_{L^2(-1,+1)}\right)^{1/2}.$$

It is easy to see that, whenever $N \ge m-1$, one has

$$|u|_{H^{m;N}(-1,+1)} = \|u^{(m)}\|_{L^2(-1,+1)} = |u|_{H^m(-1,+1)}.$$

For an integer $N > 0$ the *truncated series* of $u \in L^2(-1,+1)$ is the polynomial

$$P_N u(x) = \sum_{k=0}^{N} \hat{u}_k L_k(x),$$

where the coefficients $\hat{u}_k$ are defined as

$$\hat{u}_k = \frac{(u, L_k)_{L^2(-1,+1)}}{\|L_k\|^2_{L^2(-1,+1)}} = \left(k + \frac{1}{2}\right)\int_{-1}^{+1} u(x)L_k(x)\,dx$$

Since $(L_i(x), L_j(x))_{L^2(-1,+1)} = \delta_{ij}$, $P_N u$ is the orthogonal projection of u upon $\mathbb{P}_N$ in the L^2-inner product, i.e.,

$$(P_N u, v)_{L^2(-1,+1)} = (u, v)_{L^2(-1,+1)} \quad \text{for all } v \in \mathbb{P}_N.$$

The truncation error $u - P_N u$ can be estimated as follows: for all $u \in H^m(-1,+1)$, $m \ge 0$, one has

$$\|u - P_N u\|_{L^2(-1,+1)} \le CN^{-m}|u|_{H^{m;N}(-1,+1)}, \tag{4.25}$$

where C depends on m. Since $|u|_{H^{m;N}(-1,+1)} \le \|u\|_{H^m(-1,+1)}$, from estimate (4.25) we also have

$$\|u - P_N u\|_{L^2(-1,+1)} \le CN^{-m}\|u\|_{H^m(-1,+1)}. \tag{4.26}$$

Remark 4.1. The presence of the seminorm, rather than the norm, on the right-hand side of estimate (4.25) not only implies that estimate (4.25) is sharper than estimate (4.26), but also expresses the fact that the projection operator P_N is exact for all the polynomials in $\mathbb{P}_N$. Indeed, taking $m = N+1$, we observe that $\|u^{(N+1)}\|_{L^2(-1,+1)}$ is equivalent to $u^{(N+1)}$ vanishing for a.e. $x \in (-1,+1)$, which in turn is equivalent to u being a polynomial of degree $\le N$. Thus, from estimate (4.25) we obtain $P_N u - u = 0$, i.e., $P_N u = u$.

The truncated Legendre series $P_N u$ is the polynomial of best approximation of u in the L^2-norm. However, one may also consider the problem of the best approximation polynomial of u with respect to a general norm. Then, for any normed linear space X and any $u \in X$, there exists a polynomial $\phi^* \in \mathbb{P}_N$ such that

$$\|u - \phi^*\|_X = \inf_{\phi \in \mathbb{P}_N} \|u - \phi\|_X,$$

where ϕ^* is said to be the best approximation polynomial of u in the norm of X. In the case $X \equiv L^p(-1,+1)$, with $2 \leq p \leq \infty$, ϕ^* is unique and the best approximation error decays as

$$\inf_{\phi \in \mathbb{P}_N} \|u - \phi\|_{L^p(-1,+1)} \leq CN^{-m} \left(\sum_{k=\min(m,N+1)}^{m} \|u^{(k)}\|^p_{L^p(-1,+1)} \right)^{1/p}.$$

Clearly, this estimate holds for all the functions $u \in W^{m,p}(-1,+1)$, i.e., for all the functions whose (distributional) derivatives of order up to m belongs to $L^p(-1,+1)$.

Estimate (4.25) can be extended to higher order Sobolev norms as

$$\|u - P_N u\|_{H^l(-1,+1)} \leq CN^{2l-1/2-m} |u|_{H^{m;N}(-1,+1)}, \tag{4.27}$$

for $u \in H^m(-1,+1)$ with $m \geq 1$ and for any l such that $1 \leq l \leq m$.

Remark 4.2. It is worth noting that, in the important case $l = m = 1$, inequality (4.27) does not imply convergence of the derivative of the truncated series. Indeed, it is possible to construct a function u such that the truncated Legendre series converges in $L^2(-1,+1)$ but not in $H^1(-1,+1)$.

The rate of decay of inequality (4.27) is not optimal, in the sense that the best approximation error has a faster rate of convergence in the same norms. We will confine our discussion to the $H^1(-1,+1)$ norm. Since $H^1(-1,+1)$ is an Hilbert space, the best polynomial approximation for u is the orthogonal projection of u upon $\mathbb{P}_N$ in the scalar product that induces the norm of $H^1(-1,+1)$, that is,

$$(u,v)_{H^1(-1,+1)} := \int_{-1}^{+1} \left(u'v' + uv \right) dx \quad \text{for all } u, v \in H^1(-1,+1).$$

Then, the polynomial $P_N^1 u \in \mathbb{P}_N$ such that

$$(P_N^1 u, \phi)_{H^1(-1,+1)} = (u,\phi)_{H^1(-1,+1)}, \quad \text{for all } \phi \in \mathbb{P}_N$$

satisfies the identity

$$\|u - P_N^1 u\|_{H^1(-1,+1)} = \inf_{\phi \in \mathbb{P}_N} \|u - \phi\|_{H^1(-1,+1)}. \tag{4.28}$$

The approximation error (4.28) satisfies, for all $u \in H^m(-1,+1)$, with $m \geq 1$, the estimate

$$\|u - P_N^1 u\|_{H^1(-1,+1)} \leq CN^{1-m} |u|_{H^{m;N}(-1,+1)}. \tag{4.29}$$

This error bound extends to higher order Sobolev norms as follows: let $P_N^l u$ be the orthogonal projection of u onto $\mathbb{P}_N$, under the inner product of $H^l(-1,+1)$. Then

$$\|u - P_N^l u\|_{H^k(-1,+1)} \leq CN^{k-m} |u|_{H^{m;N}(-1,+1)}$$

for $m \geq 0$, $0 \leq k \leq l$, provided $u \in H^m(-1,+1)$. On the other hand, the error $u - P_N^1 u$ in the L^2-norm satisfies

$$\|u - P_N^1 u\|_{L^2(-1,+1)} \leq CN^{-m} |u|_{H^{m;N}(-1,+1)}.$$

The exponent of N is the same here as it is for the best approximation error in the L^2-norm.

In the context of spectral approximations of boundary-value problems, it may be more appropriate to consider the projection onto the space of polynomials satisfying the boundary data. Let us consider, for instance, homogeneous Dirichlet boundary conditions at both the endpoints of the interval

$(-1,+1)$. The functions of $H^1(-1,+1)$ that satisfy such conditions form a subspace that is denoted by $H_0^1(-1,+1)$, i.e.,

$$H_0^1(-1,+1) := \{v \in H^1(-1,+1) \ : \ v(-1) = v(+1) = 0\}.$$

Similarly, the polynomials of degree N that vanish at the endpoints form a subspace P_N^0 of $\mathbb{P}_N$, i.e.,

$$\mathbb{P}_N^0 := \{v \in \mathbb{P}_N \mid v(-1) = v(+1) = 0\}.$$

In this case we consider the inner product

$$(v,u)_{H_0^1(-1,+1)} := \int_{-1}^{+1} v'(x)u'(x)\,dx \quad \text{for all } v,u \in H_0^1(-1,+1)$$

that induces a norm on $H_0^1(-1,+1)$ which is equivalent, due to Poincarè inequality, to the H^1-norm. The H_0^1-projection of a function $u \in H_0^1(-1,+1)$ upon $\mathbb{P}_N^0$ is the polynomial $P_N^{1,0}u \in \mathbb{P}_N^0$ such that

$$(P_N^{1,0}u, \phi) = (u,\phi), \quad \text{for all } \phi \in \mathbb{P}_N^0.$$

We have the error estimate

$$\|u - P_N^{1,0}\|_{H^k(-1,+1)} \leq CN^{k-m}|u|_{H^{m;N}(-1,+1)} \tag{4.30}$$

for all $u \in H^m(-1,+1)$ vanishing at the boundary, with $m \geq 1$ and $k = 0,1$. More generally, for any function $u \in H^1(-1,+1)$ we can introduce the affine polynomial

$$r(x) = u(-1)\frac{1-x}{2} + u(+1)\frac{1+x}{2}, \quad x \in (-1,+1)$$

and then construct

$$P_N^{1,b}u = r + P_N^{1,0}(u-r).$$

Note that $P_N^{1,b}u(\pm 1) = u(\pm 1)$, i.e., $P_N^{1,b}u$ matches the boundary values of u. The difference $u - P_N^{1,b}u$ can be estimated exactly as in estimate (4.30), provided $u \in H^m(-1,+1)$ for some $m \geq 1$.

Part II

Initial-Boundary Value Problem and Numerical Solution

Chapter 5

The Kelvin-Voigt Model

In this Chapter we apply the results introduced in Chapter 3 to the initial-boundary value problem describing the propagation of waves on Kelvin-Voigt materials. Moreover, we start to apply a general Galerkin approach for the computation of the numerical solution of the problem. This abstract numerical framework will be the starting point in Chapter 6, where the Galerkin Spectral Method and Finite Element Method will be employed to compute an approximate solution of the problem under investigation. The current Chapter has the following structure. In Section 5.1 we introduce the boundary value problem obtained by combining the Partial Differential Equations governing the propagation of waves in linear viscoelastic materials of Kelvin-Voigt type (see Section 2.2.1) with suitable initial and boundary conditions. In Section 5.2 we develop the weak formulation of the initial-boundary value problem. In particular, in Section 5.2.1 we show how to handle time-dependent Dirichlet boundary conditions by means of a lifting operator. This operator allows to introduce a new initial-boundary value problem with zero Dirichlet boundary conditions and an additional forcing term that takes into account those that were imposed in the original problem. In Section 5.2.2 we show how to reduce the problem from second-order to first-order in time by applying the theory introduced in Section 3.5 and based on [182]. Moreover, we prove the existence and uniqueness of the solution by relying on the results presented in Section 3.4. In Section 5.3 we describe a possible general approach for the computation of the numerical solution of the weak formulation derived in Section 5.2.2. More precisely, in Section 5.3.1 we develop the Galerkin discretisation in space (or semi-discretisation) of the weak formulation, which yields a system of first-order Ordinary Differential Equations. Then, in Section 5.3.2 we start to derive some preliminary estimates about the error between the exact and the numerical solution. These results provide the basis for the derivation of error estimates about the approximation of the solution of the initial-boundary value problem by means of the Spectral Method and Finite Element Method that will be addressed in Chapter 6. Finally, in Section 5.3.3 we consider two alternative strategies for the solution of the system of Ordinary Differential Equations arising from the Galerkin discretisation in space.

5.1 The Initial-Boundary Value Problem

As we have seen in Section 2.2.1, the propagation of waves in a viscoelastic material can be described by combining the Cauchy equations of momentum conservation with the constitutive model (stress-strain relations) of the material. So, let us consider a finite temporal interval $(0, T]$, with $T > 0$, and a domain $\Omega \subset \mathbb{R}^d$, where $d = 2, 3$. The momentum conservation equations, or Cauchy equations, are given by

$$\rho \ddot{\boldsymbol{u}} = \operatorname{div} \boldsymbol{\sigma} + \boldsymbol{f}_{ext}, \tag{5.1}$$

where $\rho \colon \Omega \to \mathbb{R}_+$ is the density, $\boldsymbol{u} \colon [0, T] \times \mathbb{R}^d \to \mathbb{R}^d$ is the displacement, $\ddot{\boldsymbol{u}}$ is the second derivative with respect to time of the displacement (i.e., the acceleration), $\boldsymbol{\sigma} \colon [0, T] \times \Omega \to \mathbb{R}^{d \times d}$ is the stress tensor and $\boldsymbol{f}_{ext} \colon [0, T] \times \mathbb{R}^d \to \mathbb{R}^d$ is a given external load (representing, e.g., a seismic source). The Kelvin-Voigt viscoelastic constitutive relation [106] defines the stress tensor as a function of the displacement $\boldsymbol{u}$ and

the velocity $\dot{\boldsymbol{u}}$ and can be written as the sum of an elastic and a viscous component:

$$\boldsymbol{\sigma}(\boldsymbol{u}, \dot{\boldsymbol{u}}) = \boldsymbol{\sigma}_{\text{el}}(\boldsymbol{u}) + \boldsymbol{\sigma}_{\text{vi}}(\dot{\boldsymbol{u}}). \tag{5.2}$$

The elastic stress tensor is assumed to be defined by Hooke's Law for linear elastic isotropic materials:

$$\boldsymbol{\sigma}_{\text{el}}(\boldsymbol{u}) = \lambda_{\text{el}} \operatorname{tr}(\boldsymbol{\varepsilon}(\boldsymbol{u}))\mathbb{I} + 2\mu\boldsymbol{\varepsilon}(\boldsymbol{u}), \tag{5.3}$$

where $\boldsymbol{\varepsilon}(\boldsymbol{u}) = (\nabla \boldsymbol{u} + \nabla \boldsymbol{u}^{\mathsf{T}})/2$ is the strain tensor, $\mathbb{I}$ is the $d \times d$ identity tensor, $\lambda_{\text{el}} \colon \Omega \to \mathbb{R}_+$ and $\mu \colon \Omega \to \mathbb{R}_+$ are the first and second Lamé elastic coefficients, respectively, and $\operatorname{tr}(\boldsymbol{\varepsilon})$ denotes the trace of tensor $\boldsymbol{\varepsilon}$. Similarly, the linear viscous stress tensor is given by

$$\boldsymbol{\sigma}_{\text{vi}}(\dot{\boldsymbol{u}}) = \lambda_{\text{vi}} \operatorname{tr}(\boldsymbol{\varepsilon}(\dot{\boldsymbol{u}}))\mathbb{I} + 2\eta\boldsymbol{\varepsilon}(\dot{\boldsymbol{u}}), \tag{5.4}$$

where $\lambda_{\text{vi}} \colon \Omega \to \mathbb{R}_+$ and $\eta \colon \Omega \to \mathbb{R}_+$ are the first and second Lamé viscous coefficients, respectively. Combining equations (5.1), (5.2), (5.3) and (5.4), we can deduce the following explicit form for the displacement equations of motion in a Kelvin-Voigt viscoelastic material:

$$\rho\ddot{\boldsymbol{u}} = \operatorname{div}\left(\lambda_{\text{el}} \operatorname{tr}(\boldsymbol{\varepsilon}(\boldsymbol{u}))\mathbb{I} + 2\mu\boldsymbol{\varepsilon}(\boldsymbol{u})\right) + \operatorname{div}\left(\lambda_{\text{vi}} \operatorname{tr}(\boldsymbol{\varepsilon}(\dot{\boldsymbol{u}}))\mathbb{I} + 2\eta\boldsymbol{\varepsilon}(\dot{\boldsymbol{u}})\right) + \boldsymbol{f}_{ext}. \tag{5.5}$$

The momentum conservation equations must be complemented with boundary and initial conditions. So, let us assume that the boundary of Ω is such that $\partial\Omega \equiv \Gamma := \Gamma_D \cup \Gamma_N$, with $\Gamma_N \cap \Gamma_D = \emptyset$ and $\text{meas}(\Gamma_D) > 0$, and denote with $\boldsymbol{n}$ the outward unit normal to Γ. Then, we consider time-dependent Neumann boundary conditions imposed on the Neumann boundary Γ_N and time-dependent Dirichlet boundary conditions imposed on the Dirichlet boundary Γ_D. Moreover, we consider initial values $\boldsymbol{u}_0$ and $\boldsymbol{v}_0$ for the displacement and velocity fields, respectively. Summarizing, the Initial-Boundary Value Problem to be solved can be written as:

$$\rho\ddot{\boldsymbol{u}} = \operatorname{div}(\boldsymbol{\sigma}_{\text{el}}(\boldsymbol{u}) + \boldsymbol{\sigma}_{\text{vi}}(\dot{\boldsymbol{u}})) + \boldsymbol{f}_{ext}(\boldsymbol{x}, t) \qquad \text{in } (0,T] \times \Omega \text{ (Cauchy Eqs + KV model)}, \tag{5.6a}$$

$$[(\boldsymbol{\sigma}_{\text{el}}(\boldsymbol{u}) + \boldsymbol{\sigma}_{\text{vi}}(\dot{\boldsymbol{u}}))\boldsymbol{n}](\boldsymbol{x}, t) = \boldsymbol{t}(\boldsymbol{x}, t), \qquad \text{in } (0,T] \times \Gamma_N \text{ (Neumann BCs)}, \tag{5.6b}$$

$$\boldsymbol{u}(\boldsymbol{x}, t) = \boldsymbol{u}_D(\boldsymbol{x}, t), \quad \dot{\boldsymbol{u}}(\boldsymbol{x}, t) = \dot{\boldsymbol{u}}_D(\boldsymbol{x}, t), \qquad \text{in } (0,T] \times \Gamma_D \text{ (Dirichlet BCs)}, \tag{5.6c}$$

$$\boldsymbol{u}(\boldsymbol{x}, 0) = \boldsymbol{u}_0(\boldsymbol{x}), \quad \dot{\boldsymbol{u}}(\boldsymbol{x}, 0) = \boldsymbol{v}_0(\boldsymbol{x}), \qquad \text{in } \Omega \text{ (initial conditions)}. \tag{5.6d}$$

We now present some assumptions about the data that allow us to derive some results concerning the existence of the solution and its regularity. Hereafter, we will assume these conditions to hold, unless otherwise stated.

Assumption 5.1. The following conditions hold.

- The physical parameters ρ, λ_{el}, μ, λ_{vi} and η are uniformly Lipschitz continuous.
- The forcing term $\boldsymbol{f}_{ext}$ belongs to $C^{\alpha}([0,T], L^2(\Omega)^d)$.
- The Dirichlet boundary value $\boldsymbol{u}_D$ belongs to $C^{2+\alpha}([0,T], H^{1/2}(\Gamma_D)^d)$.
- The initial values $\boldsymbol{u}_0$ and $\boldsymbol{v}_0$ belong to $H^1(\Omega)$ and $L^2(\Omega)$, respectively.

5.2 Weak Formulation

The presence of the non-homogeneous *time-dependent* Dirichlet boundary conditions in system (5.6) implies that, if we directly attack the problem in such a formulation, we would need to search for the solution of the system in a family of *time-dependent affine subspaces* of a suitable Hilbert space, e.g., $[H^1(\Omega)]^d$. In order to overcome this difficulty, we consider the following approach. First, we suitably construct an operator $\mathcal{L}_D$ such that the pair $(\mathcal{L}_D\dot{\boldsymbol{u}}_D, \mathcal{L}_D\boldsymbol{u}_D)$ meets the boundary conditions at any time $t \geq 0$, and enjoys some regularity properties both in space and time. Second, by linearity, we look for a solution of the *weak formulation* of the equation derived for $\tilde{\boldsymbol{u}} := \boldsymbol{u} - \mathcal{L}_D\boldsymbol{u}_D$. Within this setting, it is possible to provide existence, uniqueness, and regularity results for such a problem, relying on the standard theory of linear evolution equations in Hilbert spaces (see Chapter 3 and [182]).

5.2.1 Dirichlet Boundary Lifting

Clearly, the function $\mathcal{L}_D\boldsymbol{u}_D(t)$ must satisfy Dirichlet boundary conditions on Γ_D but can be chosen with more freedom in the interior of Ω. More formally, there exists a linear bounded operator, termed *lifting operator* $\mathcal{L}_D$,

$$\mathcal{L}_D : H^{1/2}(\Gamma_D)^d \to H^2(\Omega)^d, \tag{5.7}$$

such that, denoting by T_D the trace operator

$$T_D \colon H^1(\Omega)^d \to H^{1/2}(\Gamma_D)^d,$$

for any curve $\boldsymbol{u}_D \in C^{2+\alpha}([0,T], H^{1/2}(\Gamma_D)^d)$ we have

$$T_D\mathcal{L}_D\boldsymbol{u}_D(t) = \boldsymbol{u}_D(t) \quad \text{ on } \Gamma_D, \text{ for any } t \geq 0.$$

Moreover, as a consequence of the linearity and continuity of the operators $\mathcal{L}_D$ and T_D, we have

$$\begin{aligned} &T_D\frac{d}{dt}(\mathcal{L}_D\boldsymbol{u}_D) = \frac{d}{dt}(T_D\mathcal{L}_D\boldsymbol{u}_D) = \dot{\boldsymbol{u}}_D, \\ &(\mathcal{L}_D\boldsymbol{u}_D)^{\cdot\cdot} = \mathcal{L}_D\ddot{\boldsymbol{u}}_D. \end{aligned}$$

Furthermore, we also denote by $\boldsymbol{t}_D$ the flux at Γ_D due to the pair $(\mathcal{L}_D\dot{\boldsymbol{u}}_D, \mathcal{L}_D\boldsymbol{u}_D)$, i.e.,

$$\boldsymbol{t}_D := [\boldsymbol{\sigma}_{\text{el}}(\mathcal{L}_D\boldsymbol{u}_D) + \boldsymbol{\sigma}_{\text{vi}}(\mathcal{L}_D\dot{\boldsymbol{u}}_D)]\boldsymbol{n} \quad \text{ on } \Gamma_N.$$

We can now reformulate the system with respect to the new unknown $\tilde{\boldsymbol{u}} := \boldsymbol{u} - \mathcal{L}_D\boldsymbol{u}_D$:

$$\begin{cases} \rho\ddot{\tilde{\boldsymbol{u}}} - \operatorname{div}(\boldsymbol{\sigma}_{\text{el}}(\tilde{\boldsymbol{u}}) + \boldsymbol{\sigma}_{\text{vi}}(\dot{\tilde{\boldsymbol{u}}})) = \operatorname{div}(\boldsymbol{\sigma}_{\text{el}}(\mathcal{L}_D\boldsymbol{u}_D) + \boldsymbol{\sigma}_{\text{vi}}(\mathcal{L}_D\dot{\boldsymbol{u}}_D)) - \rho\mathcal{L}_D\ddot{\boldsymbol{u}}_D + \boldsymbol{f}_{ext}, & \text{in } (0,T]\times\Omega, \\ [(\boldsymbol{\sigma}_{\text{el}}(\tilde{\boldsymbol{u}}) + \boldsymbol{\sigma}_{\text{vi}}(\dot{\tilde{\boldsymbol{u}}}))\boldsymbol{n}](\boldsymbol{x},t) = \tilde{\boldsymbol{t}}(\boldsymbol{x},t), & \text{in } (0,T]\times\Gamma_N, \\ \tilde{\boldsymbol{u}}(\boldsymbol{x},t) = \boldsymbol{0}, \quad \dot{\tilde{\boldsymbol{u}}}(\boldsymbol{x},t) = \boldsymbol{0}, & \text{in } (0,T]\times\Gamma_D, \\ \tilde{\boldsymbol{u}}(\boldsymbol{x},0) = \tilde{\boldsymbol{v}}_0(\boldsymbol{x}), \quad \dot{\tilde{\boldsymbol{u}}}(\boldsymbol{x},0) = \tilde{\boldsymbol{u}}_0(\boldsymbol{x}), & \text{in } \Omega, \end{cases} \tag{5.8}$$

where the new Neumann data $\tilde{\boldsymbol{t}}$ and initial conditions $\tilde{\boldsymbol{u}}_0$ and $\tilde{\boldsymbol{v}}_0$ are defined as follows:

$$\tilde{\boldsymbol{t}}(\boldsymbol{x},t) := \boldsymbol{t}(\boldsymbol{x},t) - \boldsymbol{t}_D(\boldsymbol{x},t), \qquad \tilde{\boldsymbol{v}}_0(\boldsymbol{x}) := \boldsymbol{v}_0(\boldsymbol{x}) - \mathcal{L}_D\dot{\boldsymbol{u}}_D(0), \qquad \tilde{\boldsymbol{u}}_0(\boldsymbol{x}) := \boldsymbol{u}_0(\boldsymbol{x}) - \mathcal{L}_D\boldsymbol{u}_D(0).$$

Moreover, the right hand side of the first equation provides the following new forcing term

$$\tilde{\boldsymbol{f}} := \boldsymbol{f}_{ext} + \operatorname{div}(\boldsymbol{\sigma}_{\text{el}}(\mathcal{L}_D\boldsymbol{u}_D) + \boldsymbol{\sigma}_{\text{vi}}(\mathcal{L}_D\dot{\boldsymbol{u}}_D)) - \rho\mathcal{L}_D\ddot{\boldsymbol{u}}_D. \tag{5.9}$$

Remark 5.1. If $\boldsymbol{f}\colon [0,T] \to L^2(\Omega)^d$ is Holder continuous, then, owing to the definition (5.7), we have $\tilde{\boldsymbol{f}} \in C^\alpha([0,T], L^2(\Omega)^d)$.

Clearly, if $\tilde{\boldsymbol{u}}$ solves system (5.8), then $\boldsymbol{u} := \tilde{\boldsymbol{u}} + \mathcal{L}_D\boldsymbol{u}_D$ solves our original problem, i.e., the system of equations (5.6). Hereafter we drop the tilda from system (5.8) to simplify the notation. Without loss of generality we shall also assume zero Neumann boundary conditions on Γ_N. Therefore, we will consider the following system:

$$\begin{cases} \rho\ddot{\boldsymbol{u}} - \operatorname{div}(\boldsymbol{\sigma}_{\text{el}}(\boldsymbol{u}) + \boldsymbol{\sigma}_{\text{vi}}(\dot{\boldsymbol{u}})) = \boldsymbol{f}, & \text{in } (0,T]\times\Omega, \\ [(\boldsymbol{\sigma}_{\text{el}}(\boldsymbol{u}) + \boldsymbol{\sigma}_{\text{vi}}(\dot{\boldsymbol{u}}))\boldsymbol{n}](\boldsymbol{x},t) = \boldsymbol{0}, & \text{in } (0,T]\times\Gamma_N, \\ \boldsymbol{u}(\boldsymbol{x},t) = \boldsymbol{0}, \quad \dot{\boldsymbol{u}}(\boldsymbol{x},t) = \boldsymbol{0}, & \text{in } (0,T]\times\Gamma_D, \\ \boldsymbol{u}(\boldsymbol{x},0) = \boldsymbol{v}_0(\boldsymbol{x}), \quad \dot{\boldsymbol{u}}(\boldsymbol{x},0) = \boldsymbol{u}_0(\boldsymbol{x}), & \text{in } \Omega. \end{cases} \tag{5.10}$$

5.2.2 From Second-Order to First-Order in Time

As it is customary in the treatment of second order linear evolution equations such as system (5.8), we can reduce our problem to a system of first order linear evolution equations by doubling the variables. The most intuitive way to proceed is to introduce a new unknown $\boldsymbol{v}$, to set $\boldsymbol{v} = \dot{\boldsymbol{u}}$ and to rewrite system (5.10) as follows

$$\begin{cases} \rho\dot{\boldsymbol{v}} - \operatorname{div}(\boldsymbol{\sigma}_{\mathrm{el}}(\boldsymbol{u}) + \boldsymbol{\sigma}_{\mathrm{vi}}(\boldsymbol{v})) = \boldsymbol{f}, & \text{in } (0,T]\times\Omega, \\ \dot{\boldsymbol{u}} = \boldsymbol{v}, & \text{in } (0,T]\times\Omega, \\ [(\boldsymbol{\sigma}_{\mathrm{el}}(\boldsymbol{u}) + \boldsymbol{\sigma}_{\mathrm{vi}}(\boldsymbol{v}))\boldsymbol{n}](\boldsymbol{x},t) = \boldsymbol{0}, & \text{in } (0,T]\times\Gamma_N, \\ \boldsymbol{u}(\boldsymbol{x},t) = \boldsymbol{0}, \quad \boldsymbol{v}(\boldsymbol{x},t) = \boldsymbol{0}, & \text{in } (0,T]\times\Gamma_D, \\ \boldsymbol{u}(\boldsymbol{x},0) = \boldsymbol{u}_0(\boldsymbol{x}), \quad \boldsymbol{v}(\boldsymbol{x},0) = \boldsymbol{v}_0(\boldsymbol{x}), & \text{in } \Omega. \end{cases} \tag{5.11}$$

Thus, we test against basis functions $(\boldsymbol{\phi}^v, \boldsymbol{\phi}^u)$ and, after integration by parts, we obtain the weak formulation associated to system (5.11), which consists of finding, for any $t \geq 0$, the pair $(\boldsymbol{v}(t), \boldsymbol{u}(t))$ solution of

$$\begin{aligned} &\int_\Omega (\dot{\boldsymbol{v}}(t)\cdot\boldsymbol{\phi}^v + (\boldsymbol{\sigma}_{\mathrm{el}}(\boldsymbol{u}(t)) + \boldsymbol{\sigma}_{\mathrm{vi}}(\dot{\boldsymbol{u}}(t))) : \boldsymbol{\varepsilon}(\boldsymbol{\phi}^v))\, d\boldsymbol{x} = \int_\Omega \boldsymbol{f}(t)\cdot\boldsymbol{\phi}^v\, d\boldsymbol{x} \\ &\int_\Omega \dot{\boldsymbol{u}}(t)\cdot\boldsymbol{\phi}^u\, d\boldsymbol{x} = \int_\Omega \boldsymbol{v}(t)\cdot\boldsymbol{\phi}^u\, d\boldsymbol{x} = \boldsymbol{0}, \end{aligned}$$

for any $(\boldsymbol{\phi}^v, \boldsymbol{\phi}^u)$. However, this procedure does not exploit the mathematical structure of the problem and as a consequence it does not reveal the real "dissipative" nature of the mathematical model. A more fruitful approach for reducing second order evolution equations to a system of first order evolution equations consists of imposing the equality $\boldsymbol{v} = \dot{\boldsymbol{u}}$ in a weaker sense. This procedure is widely discussed in Section 3.5 and in our problem it consists of considering the following system:

$$\begin{cases} \rho\dot{\boldsymbol{v}} - \operatorname{div}(\boldsymbol{\sigma}_{\mathrm{el}}(\boldsymbol{u}) + \boldsymbol{\sigma}_{\mathrm{vi}}(\boldsymbol{v})) = \boldsymbol{f}, & \text{in } (0,T]\times\Omega, \\ -\operatorname{div}(\boldsymbol{\sigma}_{\mathrm{el}}(\dot{\boldsymbol{u}})) = -\operatorname{div}(\boldsymbol{\sigma}_{\mathrm{el}}(\boldsymbol{v})), & \text{in } (0,T]\times\Omega, \\ [(\boldsymbol{\sigma}_{\mathrm{el}}(\boldsymbol{u}) + \boldsymbol{\sigma}_{\mathrm{vi}}(\boldsymbol{v}))\boldsymbol{n}](\boldsymbol{x},t) = \boldsymbol{0}, & \text{in } (0,T]\times\Gamma_N, \\ \boldsymbol{u}(\boldsymbol{x},t) = \boldsymbol{0}, \quad \boldsymbol{v}(\boldsymbol{x},t) = \boldsymbol{0}, & \text{in } (0,T]\times\Gamma_D, \\ \boldsymbol{u}(\boldsymbol{x},0) = \boldsymbol{u}_0(\boldsymbol{x}), \quad \boldsymbol{v}(\boldsymbol{x},0) = \boldsymbol{v}_0(\boldsymbol{x}), & \text{in } \Omega. \end{cases} \tag{5.12}$$

Let us now define the following spaces:

$$V \equiv H^1_D(\Omega)^d := \{\boldsymbol{v} \in H^1(\Omega)^d \,:\, \boldsymbol{v}|_{\Gamma_D} = \boldsymbol{0}\}, \qquad W \equiv L^2(\Omega)^d, \qquad V_m := W \times V, \qquad V_\ell := V \times V \tag{5.13}$$

endowed with the norms

$$\begin{aligned} \|\boldsymbol{\phi}\|_V &:= \|\boldsymbol{\phi}\|_{H^1(\Omega)} \quad \forall \boldsymbol{\phi} \in V, & \|\boldsymbol{\phi}\|_W &:= \|\boldsymbol{\phi}\|_{L^2(\Omega)}, \quad \forall \boldsymbol{\phi} \in W, \\ \|\boldsymbol{\Psi}\|_{V_m} &:= (\|\boldsymbol{\psi}_1\|_W^2 + \|\boldsymbol{\psi}_2\|_V^2)^{1/2}, & &\forall \boldsymbol{\Psi} = (\boldsymbol{\psi}_1, \boldsymbol{\psi}_2) \in V_m, \\ \|\boldsymbol{\Phi}\|_{V_\ell} &:= (\|\boldsymbol{\phi}_1\|_V^2 + \|\boldsymbol{\phi}_2\|_V^2)^{1/2}, & &\forall \boldsymbol{\Phi} = (\boldsymbol{\phi}_1, \boldsymbol{\phi}_2) \in V_\ell. \end{aligned} \tag{5.14}$$

The weak formulation of system (5.12) is obtained by testing the first two equations against $(\boldsymbol{\phi}^v, \boldsymbol{\phi}^u) \in V_\ell$ and integrating by parts the terms containing the divergence. Then, the weak formulation consists in finding, for any $t \geq 0$, the pair $(\boldsymbol{v}(t), \boldsymbol{u}(t)) \in V_\ell$ such that

$$\int_\Omega \dot{\boldsymbol{v}}(t)\cdot\boldsymbol{\phi}^v\, d\boldsymbol{x} + \int_\Omega (\boldsymbol{\sigma}_{\mathrm{vi}}(\boldsymbol{v}(t)) + \boldsymbol{\sigma}_{\mathrm{el}}(\boldsymbol{u}(t))) \,:\, \boldsymbol{\varepsilon}(\boldsymbol{\phi}^v)\, d\boldsymbol{x} = \int_\Omega \boldsymbol{f}(t)\cdot\boldsymbol{\phi}^v\, d\boldsymbol{x}, \qquad \forall \boldsymbol{\phi}^v \in V, \tag{5.15a}$$

$$\int_\Omega \boldsymbol{\sigma}_{\mathrm{el}}(\dot{\boldsymbol{u}}(t)) \,:\, \boldsymbol{\varepsilon}(\boldsymbol{\phi}^u)\, d\boldsymbol{x} - \int_\Omega \boldsymbol{\sigma}_{\mathrm{el}}(\boldsymbol{v}(t)) \,:\, \boldsymbol{\varepsilon}(\boldsymbol{\phi}^u)\, d\boldsymbol{x} = 0, \qquad \forall \boldsymbol{\phi}^u \in V. \tag{5.15b}$$

Having defined the following bilinear forms:

$$c\colon W \times W \to \mathbb{R} \qquad \boldsymbol{\psi} \times \boldsymbol{\phi} \mapsto c(\boldsymbol{\psi}, \boldsymbol{\phi}) := \int_\Omega \rho\, \boldsymbol{\psi} \cdot \boldsymbol{\phi}\, d\boldsymbol{x}, \tag{5.16a}$$

$$b\colon V \times V \to \mathbb{R} \qquad \boldsymbol{\psi} \times \boldsymbol{\phi} \mapsto b(\boldsymbol{\psi}, \boldsymbol{\phi}) := \int_\Omega \boldsymbol{\sigma}_{\mathrm{vi}}(\boldsymbol{\psi}) \,:\, \boldsymbol{\varepsilon}(\boldsymbol{\phi})\, d\boldsymbol{x}, \tag{5.16b}$$

$$a\colon V \times V \to \mathbb{R} \qquad \boldsymbol{\psi} \times \boldsymbol{\phi} \mapsto a(\boldsymbol{\psi}, \boldsymbol{\phi}) := \int_\Omega \boldsymbol{\sigma}_{\mathrm{el}}(\boldsymbol{\psi}) \,:\, \boldsymbol{\varepsilon}(\boldsymbol{\phi})\, d\boldsymbol{x}, \tag{5.16c}$$

and, for any $t \geq 0$, the linear functional

$$\mathrm{f}(t)\colon W \to \mathbb{R} \qquad \boldsymbol{\phi} \mapsto \mathrm{f}(t)(\boldsymbol{\phi}) := \int_\Omega \boldsymbol{f}(t) \cdot \boldsymbol{\phi}\, d\boldsymbol{x}, \tag{5.17}$$

we can rewrite the weak formulation (5.15) as: find, for any $t \geq 0$, $(\boldsymbol{v}(t), \boldsymbol{u}(t)) \in V_\ell$ such that

$$\begin{aligned} &c(\dot{\boldsymbol{v}}(t), \boldsymbol{\phi}^v) + b(\boldsymbol{v}(t), \boldsymbol{\phi}^v) + a(\boldsymbol{u}(t), \boldsymbol{\phi}^v) = \mathrm{f}(t)(\boldsymbol{\phi}^v), && \forall \boldsymbol{\phi}^v \in V, \\ &a(\dot{\boldsymbol{u}}(t), \boldsymbol{\phi}^u) - a(\boldsymbol{v}(t), \boldsymbol{\phi}^u) = 0, && \forall \boldsymbol{\phi}^u \in V. \end{aligned}$$

This system can also be written as a single equation as: find, for any $t \geq 0$, $\boldsymbol{U}(t) = (\boldsymbol{v}(t), \boldsymbol{u}(t)) \in V_\ell$ such that

$$m(\dot{\boldsymbol{U}}(t), \boldsymbol{\Phi}) + \ell(\boldsymbol{U}(t), \boldsymbol{\Phi}) = F(t)(\boldsymbol{\Phi}), \qquad \forall \boldsymbol{\Phi} := (\boldsymbol{\phi}^v, \boldsymbol{\phi}^u) \in V_\ell. \tag{5.18}$$

where

$$m\colon V_m \times V_m \to \mathbb{R} \qquad \boldsymbol{\Psi} \times \boldsymbol{\Phi} \mapsto m(\boldsymbol{\Psi}, \boldsymbol{\Phi}) := c(\boldsymbol{\psi}^v, \boldsymbol{\phi}^v) + a(\boldsymbol{\phi}^u, \boldsymbol{\phi}^u), \tag{5.19a}$$

$$\ell\colon V_\ell \times V_\ell \to \mathbb{R} \qquad \boldsymbol{\Psi} \times \boldsymbol{\Phi} \mapsto \ell(\boldsymbol{\Psi}, \boldsymbol{\Phi}) := b(\boldsymbol{\psi}^v, \boldsymbol{\phi}^v) + a(\boldsymbol{\psi}^u, \boldsymbol{\phi}^v) - a(\boldsymbol{\psi}^v, \boldsymbol{\phi}^u), \tag{5.19b}$$

$$F(t)\colon V_m \to \mathbb{R} \qquad \boldsymbol{\Phi} \mapsto F(t)(\boldsymbol{\Phi}) := \mathrm{f}(t)(\boldsymbol{\phi}^v), \quad t \geq 0. \tag{5.19c}$$

Notice that, for all $\boldsymbol{\Psi}, \boldsymbol{\Phi} \in V_m$,

$$(\boldsymbol{\Psi}, \boldsymbol{\Phi})_{V_m} := m(\boldsymbol{\Psi}, \boldsymbol{\Phi}) = c(\boldsymbol{\psi}^v, \boldsymbol{\phi}^v) + a(\boldsymbol{\psi}^u, \boldsymbol{\phi}^u) \tag{5.20}$$

is a scalar product on V_m. Indeed, $m(\cdot, \cdot)$ is bilinear and symmetric and it is possible to show that it is also positive-definite, i.e., $m(\boldsymbol{\Phi}, \boldsymbol{\Phi}) > 0$ for all $\boldsymbol{\Phi} \in V_m$ such that $\boldsymbol{\Phi} \neq \boldsymbol{0}$. The positive-definiteness property of $m(\cdot, \cdot)$ follows immediately from the fact that both the bilinear forms $c(\cdot, \cdot)$ and $a(\cdot, \cdot)$ are positive definite, the former because ρ is a function in $\mathbb{R}_+$ and the latter because of Korn's inequality and Proposition 3.2, i.e.,

$$c(\boldsymbol{\phi}, \boldsymbol{\phi}) = \int_\Omega \rho\, \boldsymbol{\phi} \cdot \boldsymbol{\phi}\, d\boldsymbol{x} \geq \min_{\boldsymbol{x} \in \Omega} \rho \int_\Omega \boldsymbol{\phi} \cdot \boldsymbol{\phi}\, d\boldsymbol{x} = \min_{\boldsymbol{x} \in \Omega} \rho\, \|\boldsymbol{\phi}\|^2_{L^2(\Omega)} > 0, \qquad \forall \boldsymbol{\phi} \in W,\ \boldsymbol{\phi} \neq \boldsymbol{0}, \tag{5.21}$$

$$a(\boldsymbol{\phi}, \boldsymbol{\phi}) = \int_\Omega \boldsymbol{\sigma}_{\mathrm{el}}(\boldsymbol{\phi}) \,:\, \boldsymbol{\varepsilon}(\boldsymbol{\phi})\, d\boldsymbol{x} \geq C \|\boldsymbol{\phi}\|^2_{H^1(\Omega)} > 0, \qquad \forall \boldsymbol{\phi} \in V,\ \boldsymbol{\phi} \neq \boldsymbol{0}. \tag{5.22}$$

The scalar product (5.20) induces the norm

$$\|\boldsymbol{\Phi}\|_m := \sqrt{(\boldsymbol{\Phi}, \boldsymbol{\Phi})_{V_m}}, \tag{5.23}$$

which is equivalent to the norm defined in (5.14), i.e., there exist two real constants $C_1 > 0$ and $C_2 > 0$ such that $C_1 \|\boldsymbol{\Phi}\|_{V_m} \leq \|\boldsymbol{\Phi}\|_m \leq C_2 \|\boldsymbol{\Phi}\|_{V_m}$ for all $\boldsymbol{\phi} \in V_m$. This can be proven by showing that there exists positive constants $C_{1,V}, C_{1,W}, C_{2,V}$ and $C_{2,W}$ such that the following inequalities hold:

$$C_{1,W} \|\boldsymbol{\phi}\|^2_{L^2} \leq c(\boldsymbol{\phi}, \boldsymbol{\phi}) \leq C_{2,W} \|\boldsymbol{\phi}\|^2_{L^2} \tag{5.24a}$$

$$C_{1,V} \|\boldsymbol{\phi}\|^2_{H^1} \leq a(\boldsymbol{\phi}, \boldsymbol{\phi}) \leq C_{2,V} \|\boldsymbol{\phi}\|^2_{H^1}. \tag{5.24b}$$

The lower bound on inequality (5.24a) follows from inequality (5.21) while the upper bound is given by

$$c(\boldsymbol{\phi},\boldsymbol{\phi}) = \int_\Omega \rho\,\boldsymbol{\phi}\cdot\boldsymbol{\phi}\,d\boldsymbol{x} \le \|\rho\|_\infty \int_\Omega \boldsymbol{\phi}\cdot\boldsymbol{\phi}\,d\boldsymbol{x} = \|\rho\|_\infty \|\boldsymbol{\phi}\|_{L^2}^2, \qquad \forall \boldsymbol{\phi}\in W.$$

Similarly, the lower bound on inequality (5.24b) follows from inequality (5.22) while the upper bound is given by Proposition 3.3. Finally, we want to rewrite problem (5.18) in operator form. Thus, we introduce the Riesz map $\mathcal{M}\colon V_m \to V_m'$ defined by

$$\langle \mathcal{M}\boldsymbol{\Psi}, \boldsymbol{\Phi}\rangle_{V_m'\times V_m} := (\boldsymbol{\Psi},\boldsymbol{\Phi})_{V_m}$$

and we also define the operator $\mathcal{L}\in\mathcal{L}(V_\ell, V_\ell')$ associated to the bilinear form $\ell(\cdot,\cdot)$ as

$$\langle \mathcal{L}\boldsymbol{\Psi},\boldsymbol{\Phi}\rangle := \ell(\boldsymbol{\Psi},\boldsymbol{\Phi}).$$

Therefore, in operator form, problem (5.18) rewrites as follows

$$\mathcal{M}\dot{\boldsymbol{U}}(t) + \mathcal{L}\boldsymbol{U}(t) = F(t), \quad t\ge 0, \tag{5.25}$$

with $\boldsymbol{U}(0) = (\boldsymbol{v}_0,\boldsymbol{u}_0)$. The idea now is to rely on the standard theory of implicit first order linear evolution equations presented in Section 3.4, and in particular on Theorem 3.22, to prove the existence and the uniqueness of the solution and to provide regularity results. However, Theorem 3.22 requires the bilinear form $\ell(\cdot,\cdot)$ to be $V_\ell-$coercive, which is not the case in our problem. Indeed, for all $\boldsymbol{U}=(\boldsymbol{v},\boldsymbol{u})\in V_\ell$, we have

$$\ell(\boldsymbol{U},\boldsymbol{U}) = b(\boldsymbol{v},\boldsymbol{v}) + \cancel{a(\boldsymbol{u},\boldsymbol{v}) - a(\boldsymbol{v},\boldsymbol{u})} = b(\boldsymbol{v},\boldsymbol{v}) = \int_\Omega \boldsymbol{\sigma}_{\mathrm{vi}}(\boldsymbol{v}) : \boldsymbol{v}\,d\boldsymbol{x} \ge C\|\boldsymbol{v}\|_V^2, \tag{5.26}$$

where we have used Korn's inequality (see Proposition 3.2) and the fact that the bilinear form $a(\cdot,\cdot)$ is symmetric. Clearly the $V-$norm of $\boldsymbol{u}$ is missing in equation (5.26) and therefore the bilinear form is not $V_\ell-$coercive. We then proceed as explained in Remark 3.3 by defining a bilinear form based on the operator $\mathcal{L}_\lambda := \lambda\mathcal{M}+\mathcal{L}$ and showing that it is coercive for some $\lambda\in\mathbb{R}$. So, we define the bilinear form $\ell_\lambda(\cdot,\cdot)$ as

$$\ell_\lambda\colon V_\ell\times V_\ell\to\mathbb{R} \qquad \boldsymbol{\Psi}\times\boldsymbol{\Phi}\mapsto \ell_\lambda(\boldsymbol{\Psi},\boldsymbol{\Phi}) := \ell(\boldsymbol{\Psi},\boldsymbol{\Phi}) + \lambda\, m(\boldsymbol{\Psi},\boldsymbol{\Phi}), \qquad \lambda\in\mathbb{R}. \tag{5.27}$$

Then, we have the following results.

Proposition 5.1. *The bilinear form $\ell_\lambda(\cdot,\cdot)$ defined in equation (5.27) is $V_\ell-$coercive for all $\lambda>0$.*

Proof. Owing to the symmetry of the bilinear form $a(\cdot,\cdot)$, for all $\boldsymbol{U}=(\boldsymbol{v},\boldsymbol{u})\in V_\ell$, we have

$$\begin{aligned}\ell_\lambda(\boldsymbol{U},\boldsymbol{U}) &= \ell(\boldsymbol{U},\boldsymbol{U}) + \lambda\, m(\boldsymbol{U},\boldsymbol{U})\\ &= b(\boldsymbol{v},\boldsymbol{v}) + \cancel{a(\boldsymbol{u},\boldsymbol{v}) - a(\boldsymbol{v},\boldsymbol{u})} + \lambda\, c(\boldsymbol{v},\boldsymbol{v}) + \lambda\, a(\boldsymbol{u},\boldsymbol{u})\\ &= b(\boldsymbol{v},\boldsymbol{v}) + \lambda\, a(\boldsymbol{u},\boldsymbol{u}) + \lambda\, c(\boldsymbol{v},\boldsymbol{v}).\end{aligned}$$

Moreover, since $\lambda c(\boldsymbol{v},\boldsymbol{v})\ge 0$ for all $\boldsymbol{v}\in V$, we obtain

$$\ell_\lambda(\boldsymbol{U},\boldsymbol{U}) = b(\boldsymbol{v},\boldsymbol{v}) + \lambda\, a(\boldsymbol{u},\boldsymbol{u}) + \lambda\, c(\boldsymbol{v},\boldsymbol{v}) \ge b(\boldsymbol{v},\boldsymbol{v}) + \lambda\, a(\boldsymbol{u},\boldsymbol{u}).$$

Finally, from the $V-$coercivity of the bilinear forms $a(\cdot,\cdot)$ and $b(\cdot,\cdot)$ (see Proposition 3.2), it follows that

$$\begin{aligned}\ell_\lambda(\boldsymbol{U},\boldsymbol{U}) &\ge b(\boldsymbol{v},\boldsymbol{v}) + \lambda\, a(\boldsymbol{u},\boldsymbol{u})\\ &\ge \min(C_v,\lambda C_u)\left(\|\boldsymbol{v}\|_V^2 + \|\boldsymbol{u}\|_V^2\right)\\ &= \alpha\|\boldsymbol{U}\|_{V_\ell}^2,\end{aligned}$$

where $\alpha := \min(C_v,\lambda C_u)$. □

Proposition 5.2. *The bilinear form $\ell_\lambda(\cdot,\cdot)$ defined in equation (5.27) is continuous on V_ℓ.*

Proof. For $\boldsymbol{U}=(\boldsymbol{v},\boldsymbol{u}),\boldsymbol{W}=(\boldsymbol{w},\boldsymbol{z})\in V_\ell$, we have, using the triangle inequality,

$$\begin{aligned}|\ell_\lambda(\boldsymbol{U},\boldsymbol{W})| &= |b(\boldsymbol{v},\boldsymbol{w})+a(\boldsymbol{u},\boldsymbol{w})-a(\boldsymbol{v},\boldsymbol{z})+\lambda\, c(\boldsymbol{v},\boldsymbol{w})+\lambda\, a(\boldsymbol{u},\boldsymbol{z})|\\ &\le |b(\boldsymbol{v},\boldsymbol{w})|+|a(\boldsymbol{u},\boldsymbol{w})|+|a(\boldsymbol{v},\boldsymbol{z})|+\lambda\,|c(\boldsymbol{v},\boldsymbol{w})|+\lambda\,|a(\boldsymbol{u},\boldsymbol{z})|.\end{aligned}$$

The bilinear form $c(\cdot,\cdot)$ is clearly continuous, whereas the continuity of the bilinear forms $a(\cdot,\cdot)$ and $b(\cdot,\cdot)$ follows from Proposition 3.3. Then, we obtain:

$$\begin{aligned}|\ell_\lambda(\boldsymbol{U},\boldsymbol{W})| &\le |b(\boldsymbol{v},\boldsymbol{w})|+|a(\boldsymbol{u},\boldsymbol{w})|+|a(\boldsymbol{v},\boldsymbol{z})|+\lambda\,|c(\boldsymbol{v},\boldsymbol{w})|+\lambda\,|a(\boldsymbol{u},\boldsymbol{z})|\\ &\le C_1\|\boldsymbol{v}\|_V\|\boldsymbol{w}\|_V+C_2\|\boldsymbol{u}\|_V\|\boldsymbol{w}\|_V+C_2\|\boldsymbol{v}\|_V\|\boldsymbol{z}\|_V+\lambda\,C_3\|\boldsymbol{v}\|_V\|\boldsymbol{w}\|_V+\lambda\,C_2\|\boldsymbol{u}\|_V\|\boldsymbol{z}\|_V\\ &\le C\left(\|\boldsymbol{v}\|_V\|\boldsymbol{w}\|_V+\|\boldsymbol{u}\|_V\|\boldsymbol{w}\|_V+\|\boldsymbol{v}\|_V\|\boldsymbol{z}\|_V+\|\boldsymbol{u}\|_V\|\boldsymbol{z}\|_V\right)\\ &\le \gamma\sqrt{\|\boldsymbol{v}\|_V^2\|\boldsymbol{w}\|_V^2+\|\boldsymbol{u}\|_V^2\|\boldsymbol{w}\|_V^2+\|\boldsymbol{v}\|_V^2\|\boldsymbol{z}\|_V^2+\|\boldsymbol{u}\|_V^2\|\boldsymbol{z}\|_V^2}\\ &= \gamma\sqrt{\left(\|\boldsymbol{u}\|_V^2+\|\boldsymbol{v}\|_V^2\right)}\sqrt{\left(\|\boldsymbol{w}\|_V^2+\|\boldsymbol{z}\|_V^2\right)}\\ &= \gamma\|\boldsymbol{U}\|_{V_\ell}\|\boldsymbol{W}\|_{V_\ell},\end{aligned}$$

where $C:=\max(C_1,C_2,\lambda C_2,\lambda C_3)$ and $\gamma:=\sqrt{2}C$. □

Summarizing, we have the following Theorem.

Theorem 5.1. *Let the spaces V_m and V_ℓ be defined as in relations (5.13). Then, for every Hölder continuous function $F\colon[0,\infty)\to V_m'$ and $(\boldsymbol{v}_0,\boldsymbol{u}_0)\in V_m$, there is a unique $\boldsymbol{U}\in C([0,\infty),V_m)\cap C^1((0,\infty),V_m)$ such that $\boldsymbol{U}(0)=(\boldsymbol{v}_0,\boldsymbol{u}_0)$, $\mathcal{L}\boldsymbol{U}(t)\in V_m'$ for $t>0$, and $\boldsymbol{U}(t)$ is solution of problem (5.25).*

Proof. We proceed as in Remark 3.3 by introducing the change of variable $\boldsymbol{U}_\lambda(t):=e^{-\lambda t}\boldsymbol{U}(t)$, where $\lambda\in\mathbb{R}_+$ and $\boldsymbol{U}$ is the solution of the original evolution equation (5.25). Then, the new unknown $\boldsymbol{U}_\lambda(t)$ satisfies:

$$\mathcal{M}\dot{\boldsymbol{U}}_\lambda(t)+(\mathcal{L}+\lambda\mathcal{M})\boldsymbol{U}_\lambda(t)=e^{-\lambda t}F(t).$$

We define the new operator $\mathcal{L}_\lambda:=\mathcal{L}+\lambda\mathcal{M}$ and denote by $\ell_\lambda(\cdot,\cdot)$ the bilinear form defined on $V_\ell\times V_\ell$ and associated to $\mathcal{L}_\lambda$. Then, owing to Propositions 5.1 and 5.2 it follows that $\ell_\lambda(\cdot,\cdot)$ is $V_\ell-$coercive and continuous, respectively. Then, the result follows from Theorem 3.22. □

5.3 Numerical Discretisation

The aim of this section is to describe a possible general approach for the numerical solution of the above system of partial differential equations (5.10). In particular, we rely on the Galerkin discretisation in space (also known as semi-discretisation) of the weak formulation derived in equation (5.15). The resulting system of Ordinary Differential Equations (ODEs) will be solved by considering two alternative strategies, the first one consisting of exact integration via eigenvalues decomposition and the second one based on time-stepping schemes.

5.3.1 Galerkin Space Discretisation

Basis Functions

The numerical scheme starts by defining the finite dimensional subspace V_{N_0} of $V\equiv H_D^1(\Omega)^d$ where we look for both the functions $\boldsymbol{v}_N(t)$ and $\boldsymbol{u}_N(t)$, for any $t\ge 0$. These functions are an approximation in space of $\boldsymbol{v}(t)$ and $\boldsymbol{u}(t)$, with the pair $(\boldsymbol{v}(t),\boldsymbol{u}(t))$ being the exact solution, at time t, of the weak formulation (5.15). Similarly, we define the finite dimensional subspace $V_N\ge V_{N_0}$ of $H^1(\Omega)^d$. Then, we define four sets of basis functions $\mathcal{B}_{N_0}^v$, $\mathcal{B}_{N_0}^u$, $\mathcal{B}_N^v$ and $\mathcal{B}_N^u$ such that

$$\begin{aligned}&\mathcal{B}_N^v:=\{\hat{\boldsymbol{\phi}}_1^v,\dots,\hat{\boldsymbol{\phi}}_N^v\},\quad \mathcal{B}_N^u:=\{\hat{\boldsymbol{\phi}}_1^u,\dots,\hat{\boldsymbol{\phi}}_N^u\},\quad V_N=\mathrm{span}(\mathcal{B}_N^v)=\mathrm{span}(\mathcal{B}_N^u),\quad \dim(V_N)=N,\\ &\mathcal{B}_{N_0}^v:=\{\boldsymbol{\phi}_1^v,\dots,\boldsymbol{\phi}_{N_0}^v\},\quad \mathcal{B}_{N_0}^u:=\{\boldsymbol{\phi}_1^u,\dots,\boldsymbol{\phi}_{N_0}^u\},\quad V_{N_0}=\mathrm{span}(\mathcal{B}_{N_0}^v)=\mathrm{span}(\mathcal{B}_{N_0}^u),\quad \dim(V_{N_0})=N_0<N.\end{aligned}$$

It is also useful to define the following product spaces

$$\mathcal{V}_{N_0} := V_{N_0} \times V_{N_0} \qquad \text{with} \qquad \dim(\mathcal{V}_{N_0}) = 2N_0,$$
$$\mathcal{V}_N := V_N \times V_N \qquad \text{with} \qquad \dim(\mathcal{V}_N) = 2N$$

and their corresponding vector basis functions, $\boldsymbol{\Phi}_i$ and $\hat{\boldsymbol{\Phi}}_i$:

$$\boldsymbol{\Phi}_i := \begin{cases} (\boldsymbol{\phi}_i^v, \mathbf{0}), & i = 1, \dots, N_0, \\ (\mathbf{0}, \boldsymbol{\phi}_{i-N_0}^u), & i = N_0+1, \dots, 2N_0, \end{cases} \qquad \hat{\boldsymbol{\Phi}}_i := \begin{cases} (\hat{\boldsymbol{\phi}}_i^v, \mathbf{0}), & i = 1, \dots, N, \\ (\mathbf{0}, \hat{\boldsymbol{\phi}}_{i-N}^u), & i = N+1, \dots, 2N. \end{cases}$$

We choose our basis functions by picking *continuous* and *piecewise smooth* functions. We will provide more details about the type of basis functions in the next sections. Then, we can write:

$$\boldsymbol{v}_N = \textstyle\sum_{j=1}^{N_0} \eta_j \boldsymbol{\phi}_j^v, \quad \dot{\boldsymbol{v}}_N = \sum_{j=1}^{N_0} \dot{\eta}_j \boldsymbol{\phi}_j^v, \quad \nabla \boldsymbol{v}_N = \sum_{j=1}^{N_0} \eta_j \nabla \boldsymbol{\phi}_j^v, \quad \nabla \dot{\boldsymbol{v}}_N = \sum_{j=1}^{N_0} \dot{\eta}_j \nabla \boldsymbol{\phi}_j^v, \tag{5.28a}$$
$$\boldsymbol{u}_N = \textstyle\sum_{j=1}^{N_0} \theta_j \boldsymbol{\phi}_j^u, \quad \dot{\boldsymbol{u}}_N = \sum_{j=1}^{N_0} \dot{\theta}_j \boldsymbol{\phi}_j^u, \quad \nabla \boldsymbol{u}_N = \sum_{j=1}^{N_0} \theta_j \nabla \boldsymbol{\phi}_j^u, \quad \nabla \dot{\boldsymbol{u}}_N = \sum_{j=1}^{N_0} \dot{\theta}_j \nabla \boldsymbol{\phi}_j^u. \tag{5.28b}$$

where $\boldsymbol{\eta}$ and $\boldsymbol{\theta}$ are time-dependent coefficients. As we will see, these coefficients are the unknowns of our problem in the semi-discrete formulation. Clearly, the spatial gradient of the expansion applies to the basis functions $\boldsymbol{\Phi}$ whereas the time derivative applies to the coefficients $(\boldsymbol{\eta}^\mathsf{T}, \boldsymbol{\theta}^\mathsf{T})^\mathsf{T}$. Moreover, because of linearity, we can also write the elastic and viscous stress tensors in the same way:

$$\boldsymbol{\sigma}_{\text{vi}}(\boldsymbol{v}_N) = \textstyle\sum_{j=1}^{N_0} \eta_j \boldsymbol{\sigma}_{\text{vi}}(\boldsymbol{\phi}_j^v), \qquad \boldsymbol{\sigma}_{\text{el}}(\boldsymbol{u}_N) = \sum_{j=1}^{N_0} \theta_j \boldsymbol{\sigma}_{\text{el}}(\boldsymbol{\phi}_j^u). \tag{5.29}$$

Finally, we consider the expansion of the lifting of the time-dependent Dirichlet data (and its time derivatives) with respect both the basis functions $\boldsymbol{\phi}^v$ and $\boldsymbol{\phi}^u$, i.e., we write

$$\mathcal{L}_D \boldsymbol{u}_D = \textstyle\sum_{j=1}^{N} \eta_{j,D} \hat{\boldsymbol{\phi}}_j^v = \sum_{j=1}^{N} \theta_{j,D} \hat{\boldsymbol{\phi}}_j^u, \tag{5.30a}$$
$$\mathcal{L}_D \dot{\boldsymbol{u}}_D = \textstyle\sum_{j=1}^{N} \dot{\eta}_{j,D} \hat{\boldsymbol{\phi}}_j^v = \sum_{j=1}^{N} \dot{\theta}_{j,D} \hat{\boldsymbol{\phi}}_j^u, \tag{5.30b}$$
$$\mathcal{L}_D \ddot{\boldsymbol{u}}_D = \textstyle\sum_{j=1}^{N} \ddot{\eta}_{j,D} \hat{\boldsymbol{\phi}}_j^v = \sum_{j=1}^{N} \ddot{\theta}_{j,D} \hat{\boldsymbol{\phi}}_j^u, \tag{5.30c}$$

where the coefficients $\boldsymbol{\eta}_D$ and $\boldsymbol{\theta}_D$ are known.

Galerkin Weak Formulation

The Galerkin semi-discretisation of the weak formulation (5.15) is obtained by taking test function $\boldsymbol{\phi}^v \in \mathcal{B}_{N_0}^v$ and $\boldsymbol{\phi}^u \in \mathcal{B}_{N_0}^u$. Then, the problem consists in finding, for any $t \geq 0$, the pair $(\boldsymbol{v}_N(t), \boldsymbol{u}_N(t)) \in \mathcal{V}_{N_0}$ such that:

$$\int_\Omega \dot{\boldsymbol{v}}_N(t) \cdot \boldsymbol{\phi}_i^v \, d\boldsymbol{x} + \int_\Omega (\boldsymbol{\sigma}_{\text{vi}}(\boldsymbol{v}_N(t)) + \boldsymbol{\sigma}_{\text{el}}(\boldsymbol{u}_N(t))) : \boldsymbol{\varepsilon}(\boldsymbol{\phi}_i^v) \, d\boldsymbol{x} = \int_\Omega \boldsymbol{f}(t) \cdot \boldsymbol{\phi}_i^v \, d\boldsymbol{x}, \qquad i = 1, \dots, N_0, \tag{5.31a}$$
$$\int_\Omega \boldsymbol{\sigma}_{\text{el}}(\dot{\boldsymbol{u}}_N(t)) : \boldsymbol{\varepsilon}(\boldsymbol{\phi}_i^u) \, d\boldsymbol{x} - \int_\Omega \boldsymbol{\sigma}_{\text{el}}(\boldsymbol{v}_N(t)) : \boldsymbol{\varepsilon}(\boldsymbol{\phi}_i^u) \, d\boldsymbol{x} = 0, \qquad i = 1, \dots, N_0. \tag{5.31b}$$

Substituting the expressions defined in (5.28) and (5.29) into system (5.31) we obtain, for $i = 1, \dots, N_0$,

$$\sum_{j=1}^{N_0} \dot{\eta}_j(t) \int_\Omega \boldsymbol{\phi}_j^v \cdot \boldsymbol{\phi}_i^v \, d\boldsymbol{x} + \sum_{j=1}^{N_0} \eta_j(t) \int_\Omega \boldsymbol{\sigma}_{\text{vi}}(\boldsymbol{\phi}_j^v) : \boldsymbol{\varepsilon}(\boldsymbol{\phi}_i^v) \, d\boldsymbol{x} + \sum_{j=1}^{N_0} \theta_j(t) \int_\Omega \boldsymbol{\sigma}_{\text{el}}(\boldsymbol{\phi}_j^u) : \boldsymbol{\varepsilon}(\boldsymbol{\phi}_i^v) \, d\boldsymbol{x} = \int_\Omega \boldsymbol{f}(t) \cdot \boldsymbol{\phi}_i^v \, d\boldsymbol{x},$$
$$\sum_{j=1}^{N_0} \dot{\theta}_j(t) \int_\Omega \boldsymbol{\sigma}_{\text{el}}(\boldsymbol{\phi}_j^u) : \boldsymbol{\varepsilon}(\boldsymbol{\phi}_i^u) \, d\boldsymbol{x} - \sum_{j=1}^{N_0} \eta_j(t) \int_\Omega \boldsymbol{\sigma}_{\text{el}}(\boldsymbol{\phi}_j^v) : \boldsymbol{\varepsilon}(\boldsymbol{\phi}_i^u) \, d\boldsymbol{x} = 0.$$

Moreover, using the bilinear forms and the linear functional introduced in relations (5.16) and (5.17), we can also write the Galerkin semi-discrete weak formulation as

$$\sum_{j=1}^{N_0} \dot{\eta}_j(t) c(\boldsymbol{\phi}_j^v, \boldsymbol{\phi}_i^v) + \sum_{j=1}^{N_0} \eta_j(t) b(\boldsymbol{\phi}_j^v, \boldsymbol{\phi}_i^v) + \sum_{j=1}^{N_0} \theta_j(t) a(\boldsymbol{\phi}_j^u, \boldsymbol{\phi}_i^v) = f(t)(\boldsymbol{\phi}_i^v), \qquad i = 1, \dots, N_0,$$
$$\sum_{j=1}^{N_0} \theta_j(t) a(\boldsymbol{\phi}_j^u, \boldsymbol{\phi}_i^u) - \sum_{j=1}^{N_0} \eta_j(t) a(\boldsymbol{\phi}_j^v, \boldsymbol{\phi}_i^u) = 0, \qquad i = 1, \dots, N_0.$$

As in the continuous case, the semi-discrete problem above can be rewritten using a more compact notation, so that the problem consists in finding, for any $t \geq 0$, $\boldsymbol{U}_N(t) = (\boldsymbol{v}_N(t), \boldsymbol{u}_N(t)) \in \mathcal{V}_{N_0}$ such that

$$m(\dot{\boldsymbol{U}}_N(t), \boldsymbol{\Phi}_i) + \ell(\boldsymbol{U}_N(t), \boldsymbol{\Phi}_i) = F(t)(\boldsymbol{\Phi}_i), \qquad \boldsymbol{\Phi}_i \in \mathcal{V}_{N_0},\ i = 1, \dots, 2N_0.$$

Then, we have obtained a system of first order Ordinary Differential Equations for the coefficients $\boldsymbol{\eta}$ and $\boldsymbol{\theta}$ and it can be written, in compact form, as:

$$\begin{aligned} &\mathbf{M}\dot{\boldsymbol{\xi}} + \mathbf{H}\boldsymbol{\xi} = \boldsymbol{F} \\ &\boldsymbol{\xi}(0) = \boldsymbol{\xi}_0, \end{aligned} \tag{5.32}$$

where $\boldsymbol{\xi} = (\boldsymbol{\eta}^{\mathsf{T}}, \boldsymbol{\theta}^{\mathsf{T}})^{\mathsf{T}}$ and $\boldsymbol{\xi}_0$ is the given initial condition.

Mass and Stiffness Matrices

The matrices $\mathbf{M}$ and $\mathbf{H}$ appearing in the system of ODEs (5.32) are given by

$$\mathbf{M} = \begin{pmatrix} \mathbf{M}^v & \mathbf{0} \\ \mathbf{0} & \mathbf{M}^u \end{pmatrix} \qquad \mathbf{H} = \begin{pmatrix} \mathbf{H}_{11} & \mathbf{H}_{12} \\ \mathbf{H}_{21} & \mathbf{0} \end{pmatrix} \tag{5.33}$$

and their blocks have dimension $N_0 \times N_0$ with components (i, j) defined, for any $i, j = 1, \dots, N_0$, by

$$(\mathbf{M}^v)_{i,j} = c(\boldsymbol{\phi}_i^v, \boldsymbol{\phi}_j^v) = \int_\Omega \rho\, \boldsymbol{\phi}_j^v \cdot \boldsymbol{\phi}_i^v \, d\boldsymbol{x}, \qquad (\mathbf{M}^u)_{i,j} = a(\boldsymbol{\phi}_j^u, \boldsymbol{\phi}_i^u) = \int_\Omega \boldsymbol{\sigma}_{\text{el}}(\boldsymbol{\phi}_j^u) : \boldsymbol{\varepsilon}(\boldsymbol{\phi}_i^u) \, d\boldsymbol{x} \tag{5.34}$$

and

$$(\mathbf{H}_{11})_{i,j} = b(\boldsymbol{\phi}_j^v, \boldsymbol{\phi}_i^v) = \int_\Omega \boldsymbol{\sigma}_{\text{vi}}(\boldsymbol{\phi}_j^v) : \boldsymbol{\varepsilon}(\boldsymbol{\phi}_i^v) \, d\boldsymbol{x}, \tag{5.35a}$$

$$(\mathbf{H}_{12})_{i,j} = a(\boldsymbol{\phi}_j^u, \boldsymbol{\phi}_i^v) = \int_\Omega \boldsymbol{\sigma}_{\text{el}}(\boldsymbol{\phi}_j^u) : \boldsymbol{\varepsilon}(\boldsymbol{\phi}_i^v) \, d\boldsymbol{x}, \tag{5.35b}$$

$$(\mathbf{H}_{21})_{i,j} = a(\boldsymbol{\phi}_j^v, \boldsymbol{\phi}_i^u) = -\int_\Omega \boldsymbol{\sigma}_{\text{el}}(\boldsymbol{\phi}_j^v) : \boldsymbol{\varepsilon}(\boldsymbol{\phi}_i^u) \, d\boldsymbol{x}. \tag{5.35c}$$

Forcing Vector

Then, the forcing vector $\boldsymbol{F}$ appearing in system (5.32) is defined by setting

$$\boldsymbol{F}_i := \begin{cases} \int_\Omega \boldsymbol{f}(t) \cdot \boldsymbol{\phi}_i^v \, d\boldsymbol{x} & i = 1, 2, \dots, N_0, \\ 0 & i = N_0 + 1, \dots, 2N_0, \end{cases}$$

It is worth recalling that, in general, the forcing vector $\boldsymbol{F}$ can be expressed as the sum of three contributions, i.e.,

$$\boldsymbol{F} = \boldsymbol{F}^{ext} + \boldsymbol{F}^{neu} + \boldsymbol{F}^{dir},$$

where $\boldsymbol{F}^{ext}$ is due to the external volume forcing function acting on the body, $\boldsymbol{F}^{neu}$ is the contribution associated to the time-dependent Neumann boundary condition imposed on Γ_N and $\boldsymbol{F}^{dir}$ is the contribution arising from the boundary lifting of the time-dependent Dirichlet boundary conditions appearing in the original problem (5.6) and imposed on Γ_D. From definition (5.9) and integration by parts it follows that $\boldsymbol{F}^{dir}$ can be written as

$$\boldsymbol{F}_i^{dir} := \begin{cases} \int_\Omega -(\boldsymbol{\sigma}_{\text{el}}(\mathcal{L}_D \boldsymbol{u}_D(t)) + \boldsymbol{\sigma}_{\text{vi}}(\mathcal{L}_D \dot{\boldsymbol{u}}_D(t))) : \boldsymbol{\varepsilon}(\boldsymbol{\phi}_i^v) - \rho \mathcal{L}_D \ddot{\boldsymbol{u}}_D(t) \cdot \boldsymbol{\phi}_i^v \, d\boldsymbol{x} & i = 1, 2, \dots, N_0, \\ 0 & i = N_0 + 1, \dots, 2N_0. \end{cases}$$

Using the expressions defined in equation (5.30) the vector $\boldsymbol{F}^{dir}$ can be computed as

$$\boldsymbol{F}^{dir} = -\begin{pmatrix} \mathbf{B}_{11} & \mathbf{B}_{12} \\ \mathbf{0} & \mathbf{0} \end{pmatrix} \begin{pmatrix} \dot{\boldsymbol{\eta}}_D \\ \boldsymbol{\theta}_D \end{pmatrix} - \begin{pmatrix} \mathbf{N}_{11} \ddot{\boldsymbol{\eta}}_D \\ \mathbf{0} \end{pmatrix}, \tag{5.36}$$

where the vector of coefficients $\dot{\boldsymbol{\eta}}_D$, $\ddot{\boldsymbol{\eta}}_D$ and $\boldsymbol{\theta}_D$ are known and for any $i = 1, \dots, N_0$ and $j = 1, \dots, N$, the components of the block matrices $\mathbf{B}_{11}$, $\mathbf{B}_{12}$ and $\mathbf{N}_{11}$ are defined as

$$(\mathbf{B}_{11})_{i,j} = b(\hat{\boldsymbol{\phi}}_j^v, \boldsymbol{\phi}_i^v) = \int_\Omega \boldsymbol{\sigma}_{\text{vi}}(\hat{\boldsymbol{\phi}}_j^v) : \boldsymbol{\varepsilon}(\boldsymbol{\phi}_i^v)\, d\boldsymbol{x},$$
$$(\mathbf{B}_{12})_{i,j} = a(\hat{\boldsymbol{\phi}}_j^u, \boldsymbol{\phi}_i^v) = \int_\Omega \boldsymbol{\sigma}_{\text{el}}(\hat{\boldsymbol{\phi}}_j^u) : \boldsymbol{\varepsilon}(\boldsymbol{\phi}_i^v)\, d\boldsymbol{x},$$
$$(\mathbf{N}_{11})_{i,j} = c(\hat{\boldsymbol{\phi}}_j^v, \boldsymbol{\phi}_i^v) = \int_\Omega \hat{\boldsymbol{\phi}}_j^v \cdot \boldsymbol{\phi}_i^v\, d\boldsymbol{x}\,.$$

Dirichlet Boundary Conditions

The homogeneous Dirichlet boundary conditions

$$\boldsymbol{u}(\boldsymbol{x}, t) = 0 \quad \text{and} \quad \boldsymbol{v}(\boldsymbol{x}, t) = 0 \quad \text{in} \quad (0, T] \times \Gamma_D$$

appearing in the system of Partial Differential Equations (5.12) are clearly enforced in strong form in our numerical scheme, i.e., we impose such conditions directly on the basis functions $\boldsymbol{\phi}^v \in V_{N_0}$ and $\boldsymbol{\phi}^u \in V_{N_0}$.

Initial Condition

The initial data

$$\boldsymbol{u}(x, 0) = \boldsymbol{u}_0(x) \quad \text{and} \quad \boldsymbol{v}(x, 0) = \boldsymbol{v}_0(x) \quad \text{in} \quad \Omega,$$

are imposed in weak form, that is

$$\left(\begin{pmatrix} \boldsymbol{v}_N|_{t=0} \\ \boldsymbol{u}_N|_{t=0} \end{pmatrix}, \boldsymbol{\Phi} \right)_{V_m} = \left(\begin{pmatrix} \boldsymbol{v}_0 \\ \boldsymbol{u}_0 \end{pmatrix}, \boldsymbol{\Phi} \right)_{V_m}, \qquad \forall \boldsymbol{\Phi} \in \mathcal{V}_{N_0}.$$

This is equivalent to set

$$\boldsymbol{\xi}(0) = \begin{pmatrix} \boldsymbol{\eta}(0) \\ \boldsymbol{\theta}(0) \end{pmatrix} = \mathbf{M}^{-1} \boldsymbol{m} =: \boldsymbol{\xi}_0,$$

where

$$\boldsymbol{m}_i := \begin{cases} \displaystyle\int_\Omega \boldsymbol{\phi}_j^v \cdot \boldsymbol{v}_0\, d\boldsymbol{x}, & i = j = 1, 2, \dots, N_0, \\ \displaystyle\int_\Omega \boldsymbol{\sigma}_{\text{el}}(\boldsymbol{\phi}_j^u) : \boldsymbol{\varepsilon}(\boldsymbol{u}_0)\, d\boldsymbol{x}, & i = N_0 + 1, 2, \dots, 2N_0,\ j = i - N_0. \end{cases}$$

5.3.2 Convergence Semi-Discrete Solution

In this section we develop estimates on the error $\boldsymbol{U}(t) - \boldsymbol{U}_N(t)$ in the situation of Theorem 5.1. In particular, we will show that the norm of this error is bounded by the norm of the error arising from the Galerkin procedure applied to the elliptic problem determined by the operator $\mathcal{L}_\lambda$. Therefore, we start by presenting a Theorem, already discussed in Section 3.2.2 and here adapted to the notation of the current Section, that provides an estimate about the error resulting from the Galerkin approximation of the solution of the elliptic problem determined by the bilinear form $\ell_\lambda(\cdot, \cdot)$ associated to $\mathcal{L}_\lambda$.

Theorem 5.2 (adapted from [182, Theorem VII.5.1])**.** *Let V_ℓ be the space defined in equation (5.13), $\ell_\lambda(\cdot, \cdot)$ the bilinear form defined by (5.27), with $\lambda \in \mathbb{R}_+$, and $F \in V_\ell'$. Moreover, let S be a closed subspace of V_ℓ. Then, there exists an unique solution to the problem*

$$\textit{find } \boldsymbol{U}_\lambda \in V_\ell \ : \ \ell_\lambda(\boldsymbol{U}_\lambda, \boldsymbol{\Phi}) = F(\boldsymbol{\Phi}), \quad \forall \boldsymbol{\Phi} \in V_\ell,$$

and an unique solution to the problem

$$\textit{find } \boldsymbol{U}_{\lambda,s} \in S \ : \ \ell_\lambda(\boldsymbol{U}_{\lambda,s}, \boldsymbol{\Phi}) = F(\boldsymbol{\Phi}), \quad \forall \boldsymbol{\Phi} \in S.$$

Furthermore, the following estimate holds:

$$\|\boldsymbol{U}_\lambda - \boldsymbol{U}_{\lambda,s}\|_{V_\ell} \leq \frac{\gamma}{\alpha} \inf\{\|\boldsymbol{U}_\lambda - \boldsymbol{\Phi}\|_{V_\ell} \ : \ \boldsymbol{\Phi} \in S\}, \tag{5.37}$$

where γ and α are the continuity and coercivity constants of $\ell_\lambda(\cdot,\cdot)$, respectively.

The estimates (5.37) shows that the error $\boldsymbol{U}_\lambda(t) - \boldsymbol{U}_{\lambda,s}(t)$ is small if S approximate V_ℓ sufficiently well. This estimate is a bound on the error in the norm of the Hilbert space V_ℓ and in applications to elliptic boundary value problems it is also referred to as *energy estimate*. The next result gives an estimate of the error arising from the application of the Galerkin procedure to the first-order evolution equation whose elliptic operator is given by $\mathcal{L}_\lambda$.

Theorem 5.3. *Let the real Hilbert spaces V_ℓ and V_m be defined as in equation (5.13) and let S be a finite-dimensional subspace of V_ℓ. Let the bilinear forms $m(\cdot,\cdot)$, $\ell(\cdot,\cdot)$ and $\ell_\lambda(\cdot,\cdot)$, with $\lambda \in \mathbb{R}_+$, be defined by equations (5.19a), (5.19b) and (5.27), respectively, and data F be given as in Theorem 5.1. Moreover, assume $\boldsymbol{U}_0 \in V_\ell$. Then, there exists a unique solution $\boldsymbol{U}_\lambda(t)$, in the sense of Theorem 5.1, to the problem*

$$m(\dot{\boldsymbol{U}}_\lambda(t), \boldsymbol{\Phi}) + \ell_\lambda(\boldsymbol{U}_\lambda(t), \boldsymbol{\Phi}) = F_\lambda(t)(\boldsymbol{\Phi}), \quad \forall \boldsymbol{\Phi} \in V_\ell, \tag{5.38}$$

with $\boldsymbol{U}_\lambda(0) = \boldsymbol{U}_0$ and $F_\lambda(t) := e^{-\lambda t} F(t)$ and there exists a unique solution $\boldsymbol{U}_{\lambda,N}(t) \in S$, in the sense of Theorem 5.1, to the semi-discrete problem

$$m(\dot{\boldsymbol{U}}_{\lambda,N}(t), \boldsymbol{\Phi}) + \ell_\lambda(\boldsymbol{U}_{\lambda,N}(t), \boldsymbol{\Phi}) = F_\lambda(t)(\boldsymbol{\Phi}), \quad \forall \boldsymbol{\Phi} \in S, \tag{5.39}$$

for any prescribed initial value $\boldsymbol{U}_{\lambda,N}(0) \in S$. Then, for any $t \geq 0$, the following error estimate holds:

$$\|\boldsymbol{U}_\lambda(t) - \boldsymbol{U}_{\lambda,N}(t)\|_{V_m} \leq \|\boldsymbol{U}_\lambda(t) - \boldsymbol{U}_{\lambda,\ell}(t)\|_{V_m} + \|\boldsymbol{U}_{\lambda,\ell}(0) - \boldsymbol{U}_{\lambda,N}(0)\|_{V_m} + \int_0^t \|\dot{\boldsymbol{U}}_\lambda(s) - \dot{\boldsymbol{U}}_{\lambda,\ell}(s)\|_{V_m}\, ds, \tag{5.40}$$

where, for any $t \geq 0$, $\boldsymbol{U}_{\lambda,\ell}(t)$ is the $\mathcal{L}_\lambda-$projection of $\boldsymbol{U}_\lambda(t)$ onto S defined by

$$\boldsymbol{U}_{\lambda,\ell}(t) \in S \ : \quad \ell_\lambda(\boldsymbol{U}_{\lambda,\ell}(t), \boldsymbol{\Phi}) = \ell_\lambda(\boldsymbol{U}_\lambda(t), \boldsymbol{\Phi}), \quad \forall \boldsymbol{\Phi} \in S. \tag{5.41}$$

Proof (adapted from [182, Theorem VII.6.1]). The existence and uniqueness results are immediate consequence of Theorem 3.22. Then, we only have to prove inequality (5.40). For any $\boldsymbol{\Phi} \in S$, subtracting problem (5.39) from problem (5.38) we obtain

$$m(\dot{\boldsymbol{U}}_\lambda(t) - \dot{\boldsymbol{U}}_{\lambda,N}(t), \boldsymbol{\Phi}) + \ell_\lambda(\boldsymbol{U}_\lambda(t) - \boldsymbol{U}_{\lambda,N}(t), \boldsymbol{\Phi}) = \boldsymbol{0}. \tag{5.42}$$

Then, writing the error $\boldsymbol{U}_\lambda(t) - \boldsymbol{U}_{\lambda,N}(t)$ as

$$\boldsymbol{U}_\lambda(t) - \boldsymbol{U}_{\lambda,N}(t) = \boldsymbol{\theta}(t) + \boldsymbol{\rho}(t), \tag{5.43}$$

where

$$\boldsymbol{\theta}(t) := \boldsymbol{U}_\lambda(t) - \boldsymbol{U}_{\lambda,\ell}(t), \quad \text{and} \quad \boldsymbol{\rho}(t) := \boldsymbol{U}_{\lambda,\ell}(t) - \boldsymbol{U}_{\lambda,N}(t), \tag{5.44}$$

we obtain, from equation (5.42),

$$m(\dot{\boldsymbol{\theta}}(t) + \dot{\boldsymbol{\rho}}(t), \boldsymbol{\Phi}) + \ell_\lambda(\boldsymbol{\theta}(t) + \boldsymbol{\rho}(t), \boldsymbol{\Phi}) = \boldsymbol{0},$$

which is equivalent to

$$(\dot{\boldsymbol{\theta}}(t), \boldsymbol{\Phi})_{V_m} = -(\dot{\boldsymbol{\rho}}(t), \boldsymbol{\Phi})_{V_m} - \cancel{\ell_\lambda(\boldsymbol{\theta}(t), \boldsymbol{\Phi})} - \ell_\lambda(\boldsymbol{\rho}(t), \boldsymbol{\Phi}),$$

where the second term on the right hand side vanishes due to definition (5.41). Setting $\boldsymbol{\Phi} := -\boldsymbol{\rho}(t)$ yields

$$-(\dot{\boldsymbol{\theta}}(t), \boldsymbol{\rho}(t))_{V_m} = (\dot{\boldsymbol{\rho}}(t), \boldsymbol{\rho}(t))_{V_m} + \ell(\boldsymbol{\rho}(t), \boldsymbol{\rho}(t))$$

and since the bilinear form $\ell_\lambda(\cdot,\cdot)$ is coercive (see Proposition 5.1), we obtain

$$-(\dot{\boldsymbol{\theta}}(t), \boldsymbol{\rho}(t))_{V_m} = (\dot{\boldsymbol{\rho}}(t), \boldsymbol{\rho}(t))_{V_m} + \ell_\lambda(\boldsymbol{\rho}(t), \boldsymbol{\rho}(t)) \geq (\dot{\boldsymbol{\rho}}(t), \boldsymbol{\rho}(t))_{V_m} + \alpha\|\boldsymbol{\rho}(t)\|^2_{V_\ell} \geq (\dot{\boldsymbol{\rho}}(t), \boldsymbol{\rho}(t))_{V_m}. \tag{5.45}$$

Moreover, using Cauchy-Schwarz inequality on the left hand side of relation (5.45), we have

$$\|\dot{\boldsymbol{\theta}}(t)\|_{V_m}\|\boldsymbol{\rho}(t)\|_{V_m} \geq -(\dot{\boldsymbol{\theta}}(t),\boldsymbol{\rho}(t))_{V_m} \geq (\dot{\boldsymbol{\rho}}(t),\boldsymbol{\rho}(t))_{V_m}, \tag{5.46}$$

whereas the left hand side of the inequality can be rewriten as

$$(\dot{\boldsymbol{\rho}}(t),\boldsymbol{\rho})_{V_m} = 1/2\,\partial_t\|\boldsymbol{\rho}(t)\|^2_{V_m} = \|\boldsymbol{\rho}(t)\|_{V_m}\,\partial\|\boldsymbol{\rho}(t)\|_{V_m}. \tag{5.47}$$

Combining relations (5.46) and (5.47), we obtain the following inequality:

$$\|\boldsymbol{\rho}(t)\|_{V_m}\,\partial_t\|\boldsymbol{\rho}(t)\|_{V_m} \leq \|\dot{\boldsymbol{\theta}}(t)\|_{V_m}\|\boldsymbol{\rho}(t)\|_{V_m}. \tag{5.48}$$

Now let $Z = \{t > 0 \ : \ \|\boldsymbol{\rho}(t)\|_{V_m} = 0\}$. Clearly, for any $t \notin Z$ we have from inequality (5.48)

$$\partial_t\|\boldsymbol{\rho}(t)\|_{V_m} \leq \|\dot{\boldsymbol{\theta}}(t)\|_{V_m}. \tag{5.49}$$

On the other hand, for $t \in Z$, the estimate still holds, since the left side is zero at such a point. Then, integration of inequality (5.49) yields

$$\|\boldsymbol{\rho}(t)\|_{V_m} \leq \|\boldsymbol{\rho}(0)\|_{V_m} + \int_0^t \|\dot{\boldsymbol{\theta}}(s)\|_{V_m}\,ds. \tag{5.50}$$

Applying the triangle inequality to (5.43) and using inequality (5.50), we obtain

$$\|\boldsymbol{U}_\lambda(t) - \boldsymbol{U}_{\lambda,N}(t)\|_{V_m} \leq \|\boldsymbol{\theta}(t)\|_{V_m} + \|\boldsymbol{\rho}(t)\|_{V_m} \leq \|\boldsymbol{\theta}(t)\|_{V_m} + \|\boldsymbol{\rho}(0)\|_{V_m} + \int_0^t \|\dot{\boldsymbol{\theta}}(s)\|_{V_m}\,ds.$$

Finally, using the definitions of $\boldsymbol{\theta}(t)$ and $\boldsymbol{\rho}(t)$ introduced in definitions (5.44), the above inequality becomes

$$\|\boldsymbol{U}_\lambda(t)-\boldsymbol{U}_{\lambda,N}(t)\|_{V_m} \leq \|\boldsymbol{U}_\lambda(t)-\boldsymbol{U}_{\lambda,\ell}(t)\|_{V_m}+\|\boldsymbol{U}_{\lambda,\ell}(0)-\boldsymbol{U}_{\lambda,N}(0)\|_{V_m}+\int_0^t \|\dot{\boldsymbol{U}}_\lambda(s)-\dot{\boldsymbol{U}}_{\lambda,\ell}(s)\|_{V_m}\,ds. \ \square$$

Remark 5.2. Assuming $\boldsymbol{U} \in C([0,\infty), V_\ell)$, $\boldsymbol{U}(0) = \boldsymbol{U}_0$ necessarily belongs to V_ℓ, so equation (5.41) defines $\boldsymbol{U}_{\lambda,\ell}(0)$. Then, choosing $\boldsymbol{U}_{\lambda,N}(0) = \boldsymbol{U}_{\lambda,\ell}(0)$, the error estimate (5.40) simplifies as follows

$$\|\boldsymbol{U}_\lambda(t) - \boldsymbol{U}_{\lambda,N}(t)\|_{V_m} \leq \|\boldsymbol{U}_\lambda(t) - \boldsymbol{U}_{\lambda,\ell}(t)\|_{V_m} + \int_0^t \|\dot{\boldsymbol{U}}_\lambda(s) - \dot{\boldsymbol{U}}_{\lambda,\ell}(s)\|_{V_m}\,ds.$$

Remark 5.3. We can obtain a slightly different bound by taking advantage of the term $\alpha\|\boldsymbol{\rho}(t)\|^2_{V_\ell}$ in inequality (5.45). Indeed, keeping this term and using the fact that $\|\boldsymbol{w}\|_{V_m} \leq \|\boldsymbol{w}\|_{V_\ell}$ for all $\boldsymbol{w} \in V_\ell$, the inequality (5.49) becomes

$$\partial_t\|\boldsymbol{\rho}(t)\|_{V_m} + \alpha\|\boldsymbol{\rho}(t)\|_{V_m} \leq \|\dot{\boldsymbol{\theta}}(t)\|_{V_m}$$

or, equivalently,

$$\partial_t(\exp(\alpha t)\|\boldsymbol{\rho}(t)\|_{V_m}) \leq \exp(\alpha t)\|\dot{\boldsymbol{\theta}}(t)\|_{V_m}.$$

Integration over the interval $(0,t)$ yields

$$\|\boldsymbol{\rho}(t)\|_{V_m} \leq \|\boldsymbol{\rho}(0)\|_{V_m}\exp(-\alpha t) + \int_0^t \exp(-\alpha(t-s))\|\dot{\boldsymbol{\theta}}(s)\|_{V_m}\,ds,$$

which leads to the following inequality for the error $\boldsymbol{U}_{\lambda,N}(t) - \boldsymbol{U}_\lambda$:

$$\begin{aligned}\|\boldsymbol{U}_\lambda(t) - \boldsymbol{U}_{\lambda,N}(t)\|_{V_m} \leq \|\boldsymbol{U}_\lambda(t) - \boldsymbol{U}_{\lambda,\ell}(t)\|_{V_m} + \|\boldsymbol{U}_{\lambda,\ell}(0) - \boldsymbol{U}_{\lambda,N}(0)\|_{V_m}\exp(-\alpha t)\\ + \int_0^t \exp(-\alpha(t-s))\|\dot{\boldsymbol{U}}_\lambda(s) - \dot{\boldsymbol{U}}_{\lambda,\ell}(s)\|_{V_m}\,ds.\end{aligned}$$

Using again the fact that, for all $\boldsymbol{\Phi} \in V_m$, $\|\boldsymbol{\Phi}\|_{V_m} \leq C\|\boldsymbol{\Phi}\|_{V_\ell}$, the V_m-norms on the right hand side of the error estimate (5.40) can be replaced with the $V_\ell-$norm, thus providing the following result:

$$\|\boldsymbol{U}_\lambda(t) - \boldsymbol{U}_{\lambda,N}(t)\|_{V_m} \lesssim \|\boldsymbol{U}_\lambda(t) - \boldsymbol{U}_{\lambda,\ell}(t)\|_{V_\ell} + \|\boldsymbol{U}_{\lambda,\ell}(0) - \boldsymbol{U}_{\lambda,N}(0)\|_{V_\ell} + \int_0^t \|\dot{\boldsymbol{U}}_\lambda(s) - \dot{\boldsymbol{U}}_{\lambda,\ell}(s)\|_{V_\ell}\, ds. \quad (5.51)$$

This error estimate shows that, for any $t \geq 0$, the error in the approximation procedure is determined by the error of the $\mathcal{L}_\lambda-$projection in the $V_\ell-$norm. Then, Theorem 5.2, with $\boldsymbol{U}_{\lambda,s} \equiv U_{\lambda,N}(t)$, yields

$$\|\boldsymbol{U}_\lambda(t) - \boldsymbol{U}_{\lambda,N}(t)\|_{V_\ell} \leq \frac{\gamma}{\alpha} \inf\{\|\boldsymbol{U}_\lambda(t) - \boldsymbol{\Phi}\|_{V_\ell} \ : \ \boldsymbol{\Phi} \in \mathcal{V}_{N_0}\}. \quad (5.52)$$

Moreover, when $\boldsymbol{U}_\lambda(t) \in C^1((0,\infty), V_\ell)$, we can differentiate equation (5.41) with respect to the time variable t and deduce that $\dot{\boldsymbol{U}}_{\lambda,\ell}(t) \in \mathcal{V}_{N_0}$ is the $\mathcal{L}_\lambda-$projection of $\dot{\boldsymbol{U}}_\lambda(t)$, from which it follows that

$$\|\dot{\boldsymbol{U}}_\lambda(t) - \dot{\boldsymbol{U}}_{\lambda,N}(t)\|_{V_\ell} \leq \frac{\gamma}{\alpha} \inf\{\|\dot{\boldsymbol{U}}_\lambda(t) - \boldsymbol{\Phi}\|_{V_\ell} \ : \ \boldsymbol{\Phi} \in \mathcal{V}_{N_0}\}. \quad (5.53)$$

Corollary 5.1. *For any $t \geq 0$, under the assumptions of Theorem 5.3 and Remark 5.2, the following estimate holds:*

$$\|\boldsymbol{U}(t) - \boldsymbol{U}_N(t)\|_{V_m} \lesssim \inf\{\|\boldsymbol{U}(t) - \boldsymbol{\Phi}\|_{V_\ell} \ : \ \boldsymbol{\Phi} \in \mathcal{V}_{N_0}\} + e^{\lambda t} \int_0^t \inf\{\|\partial_s(e^{-\lambda s}\boldsymbol{U}(s)) - \boldsymbol{\Phi}\|_{V_\ell} \ : \ \boldsymbol{\Phi} \in \mathcal{V}_{N_0}\}\, ds.$$

Proof. The inequality immediately follows by substituting $\boldsymbol{U}_\lambda(t) = e^{-\lambda t}\boldsymbol{U}(t)$ and $\boldsymbol{U}_{\lambda,N}(t) = e^{-\lambda t}\boldsymbol{U}_N(t)$ into inequality (5.51), using Remark 5.2 and estimates (5.52) and (5.53). □

This error estimate will be used in the next Chapter to derive appropriate convergence rates for the proposed numerical methods used to approximate the Galerkin weak formulation in space.

5.3.3 Solution in Time

We consider two different strategies for the solution of the system of Ordinary Differential Equations. The first one consists in computing the exact solution. The symmetric and positive definite matrix $\mathbf{M}$ is spectrally factorized into $\mathbf{M} = \mathbf{U}\boldsymbol{\Sigma}\mathbf{U}^\mathsf{T}$ where $\mathbf{U}$ contains the eigevectors as columns and $\boldsymbol{\Sigma}$ is the diagonal matrix containing the related (positive) eigenvalues. Therefore, system (5.32) can be written as:

$$\mathbf{U}\boldsymbol{\Sigma}^{1/2}\boldsymbol{\Sigma}^{1/2}\mathbf{U}^\mathsf{T}\dot{\boldsymbol{\xi}} = \mathbf{H}\mathbf{U}\boldsymbol{\Sigma}^{-1/2}\boldsymbol{\Sigma}^{1/2}\mathbf{U}^\mathsf{T}\boldsymbol{\xi}\ .$$

Now, letting $\boldsymbol{\zeta} = \boldsymbol{\Sigma}^{1/2}\mathbf{U}^\mathsf{T}\boldsymbol{\xi}$, $\tilde{\mathbf{H}} = \boldsymbol{\Sigma}^{-1/2}\mathbf{U}^\mathsf{T}\mathbf{H}\mathbf{U}\boldsymbol{\Sigma}^{-1/2}$ and $\tilde{\boldsymbol{F}} := \boldsymbol{\Sigma}^{-1/2}\mathbf{U}^\mathsf{T}\mathbf{F}$, we obtain

$$\begin{aligned} &\dot{\boldsymbol{\zeta}} + \tilde{\mathbf{H}}\boldsymbol{\zeta} = \tilde{\mathbf{F}}, \\ &\boldsymbol{\zeta}(0) = \boldsymbol{\zeta}_0\ , \end{aligned} \quad (5.54)$$

whose exact solution is given by

$$\boldsymbol{\zeta}(t) = \exp(-t\tilde{\mathbf{H}})\boldsymbol{\zeta}_0 + \int_0^t \exp(-(t-s)\tilde{\mathbf{H}})\tilde{\mathbf{F}}(s)\, ds,$$

where $\boldsymbol{\zeta}_0 = \boldsymbol{\Sigma}^{1/2}\mathbf{U}^\mathsf{T}\boldsymbol{\xi}_0$ is the given initial condition written with respect to the new basis. Then, the matrix exponential is computed via eigenvalue decomposition $\tilde{\mathbf{H}} = \mathbf{V}\boldsymbol{\Lambda}\mathbf{V}^\top$, where each column $\boldsymbol{\nu}_i$ of $\mathbf{V} = \{\boldsymbol{\nu}_1, \ldots, \boldsymbol{\nu}_{2N_0}\}$ is an eigenvector of $\tilde{\mathbf{H}}$ and $\boldsymbol{\Lambda}$ is the diagonal matrix storing the related eigenvalues $\lambda_1, \ldots, \lambda_{2N_0}$. The solution of problem (5.54) can be written as a linear combination of the eigenvectors of $\tilde{\mathbf{H}}$, that is

$$\boldsymbol{\zeta}(t) = \gamma_1(t)\boldsymbol{\nu}_1 + \gamma_2(t)\boldsymbol{\nu}_2 + \cdots + \gamma_{2N_0}(t)\boldsymbol{\nu}_{2N_0}. \quad (5.55)$$

Also $\tilde{\mathbf{F}}(t)$ can be expanded in terms of the eigenvectors of $\tilde{\mathbf{H}}$:

$$\tilde{\mathbf{F}}(t) = \delta_1(t)\boldsymbol{\nu}_1 + \delta_2(t)\boldsymbol{\nu}_2 + \cdots + \delta_{2N_0}(t)\boldsymbol{\nu}_{2N_0}, \quad (5.56)$$

where $\boldsymbol{\delta}(t) = (\delta_1(t), \delta_2(t), \dots, \delta_{2N_0}(t))$ is computed at a given time t by solving the linear system $\mathbf{V}\boldsymbol{\delta}(t) = \tilde{\mathbf{F}}(t)$. Substituting the relations (5.55) and (5.56) into the system of equations (5.54) we obtain:

$$\begin{aligned}
\boldsymbol{\nu}_1\dot{\gamma}_1 + \boldsymbol{\nu}_2\dot{\gamma}_2 + \cdots + \boldsymbol{\nu}_{2N_0}\dot{\gamma}_{2N_0} &= \tilde{\mathbf{H}}\left(\boldsymbol{\nu}_1\gamma_1 + \boldsymbol{\nu}_2\gamma_2 + \cdots + \boldsymbol{\nu}_{2N_0}\gamma_{2N_0}\right) + \left(\boldsymbol{\nu}_1\delta_1 + \boldsymbol{\nu}_2\delta_2 + \cdots + \boldsymbol{\nu}_{2N_0}\delta_{2N_0}\right) \\
&= \tilde{\mathbf{H}}\boldsymbol{\nu}_1\gamma_1 + \tilde{\mathbf{H}}\boldsymbol{\nu}_2\gamma_2 + \cdots + \tilde{\mathbf{H}}\boldsymbol{\nu}_{2N_0}\gamma_{2N_0} + \boldsymbol{\nu}_1\delta_1 + \boldsymbol{\nu}_2\delta_2 + \cdots + \boldsymbol{\nu}_{2N_0}\delta_{2N_0} \\
&= \lambda_1\boldsymbol{\nu}_1\gamma_1 + \lambda_2\boldsymbol{\nu}_2\gamma_2 + \cdots + \lambda_{2N_0}\boldsymbol{\nu}_{2N_0}\gamma_{2N_0} + \boldsymbol{\nu}_1\delta_1 + \boldsymbol{\nu}_2\delta_2 + \cdots + \boldsymbol{\nu}_{2N_0}\delta_{2N_0} \\
&= \boldsymbol{\nu}_1\left(\lambda_1\gamma_1 + \delta_1\right) + \boldsymbol{\nu}_2\left(\lambda_2\gamma_2 + \delta_2\right) + \cdots + \boldsymbol{\nu}_{2N_0}\left(\lambda_{2N_0}\gamma_{2N_0} + \delta_{2N_0}\right),
\end{aligned}$$

from which we get, for all $k = 1, \dots, 2N_0$:

$$\dot{\gamma}_k = \lambda_k\gamma_k + \delta_k.$$

These equations are linearly independent linear Ordinary Differential Equations of the first order, whose time integration is given by:

$$\gamma_k(t) = a_k e^{\lambda_k t} + e^{\lambda_k t}\int_0^t e^{-\lambda_k s}\delta_k(s)\,ds, \tag{5.57}$$

where $a_1, a_2, \dots, a_{2N_0}$ are the coefficients that allow to write the initial condition $\boldsymbol{\zeta}_0$ as linear combination of the eigenvectors $\boldsymbol{\nu}_1, \boldsymbol{\nu}_2, \dots, \boldsymbol{\nu}_{2N_0}$, i.e.:

$$\boldsymbol{\zeta}_0 = a_1\boldsymbol{\nu}_1 + a_2\boldsymbol{\nu}_2 + \cdots + a_{2N_0}\boldsymbol{\nu}_{2N_0}.$$

The computation of equation (5.57) requires only the computation of one-dimensional integrals and it can be performed using appropriate quadrature rules. Once $\gamma_1(t), \gamma_2(t), \dots, \gamma_{2N_0}(t)$ have been computed, we obtain $\boldsymbol{\zeta}(t)$ using Equation (5.55). This procedure turns out to be particularly convenient when the forcing vector $\tilde{\mathbf{F}}(t)$ can be written as the Hadamard product between a constant vector $\tilde{\mathbf{F}}_x$ defining the dependence on space of the forcing term and a vector $\tilde{\mathbf{F}}_t(t)$ whose components depend on time, i.e., $(\tilde{\mathbf{F}}(t))_i := (\tilde{\mathbf{F}}_t(t))_i(\tilde{\mathbf{F}}_x)_i$. Indeed, in this case $(\boldsymbol{\delta}(t))_i := (\tilde{\mathbf{F}}(t))_i(\boldsymbol{\delta}_x)_i$, where the vector $\boldsymbol{\delta}_x$ is obtained by solving the linear system $\mathbf{V}\boldsymbol{\delta}_x = \tilde{\mathbf{F}}_x$. It is worth highlighting that in this case we need to solve just one linear system and not one for each time t, thereby remarkably reducing the computational effort. Moreover, we will often consider a forcing term whose time-dependence is defined by damped Fourier functions having the form $e^{\varepsilon t}e^{i(2\pi k t+\phi)}$, where $\varepsilon < 0$, k is the frequency and ϕ is the phase. In this particular case we can evaluate the integral in equation (5.57) exactly as follows:

$$\int_0^t e^{\lambda(t-s)}e^{2\pi i k s}e^{i\phi}e^{\varepsilon s}\,ds = e^{\lambda t}e^{i\phi}\int_0^t e^{(-\lambda+2\pi i k+\varepsilon)s}\,ds = e^{\lambda t}e^{i\phi}\left[\frac{e^{(-\lambda+2\pi i k s+\varepsilon)s}}{-\lambda+2\pi i k+\varepsilon}\right]_0^t = e^{i\phi}\left[\frac{e^{(2\pi i k+\varepsilon)t}-e^{\lambda t}}{2\pi i k-\lambda+\varepsilon}\right]$$

Summarising, this approach has the remarkable advantage of providing an exact integration in time given that the forcing vector $\tilde{\mathbf{F}}(t)$ can be written as the element-wise product between a function depending on space and a function depending on time and given that we know how to compute the integrals in equation (5.57). However, this approach also requires to compute the spectral decomposition of both matrices $\mathbf{M}$ and $\tilde{\mathbf{H}}$, which might be computationally expensive if the matrices are particularly large. The second strategy consists on using time stepping schemes for the computation of an approximate solution of the system of ODEs. In particular, we employed Backward Euler and Crank-Nicolson time integration scheme. These schemes are defined as follows.

Backward Euler

$$\left(\frac{\mathbf{M}}{\Delta t} + \mathbf{H}\right)\boldsymbol{\xi}_{n+1} = \frac{\mathbf{M}}{\Delta t}\boldsymbol{\xi}_n + \mathbf{F}(t_{n+1}).$$

Crank-Nicolson

$$\left(\frac{\mathbf{M}}{\Delta t} + \frac{\mathbf{H}}{2}\right)\boldsymbol{\xi}_{n+1} = \left(\frac{\mathbf{M}}{\Delta t} - \frac{\mathbf{H}}{2}\right)\boldsymbol{\xi}_n + \frac{1}{2}\left(\mathbf{F}(t_{n+1}) + \mathbf{F}(t_n)\right).$$

Chapter 6

Numerical Results and Discussion

In this Chapter we discuss the numerical solution of the initial-boundary value problem presented in Chapter 5 and consider different ambient dimensions and systems of coordinates. More precisely, in Section 6.1 we address the solution of the one-dimensional problem, in Section 6.2 we solve the two-dimensional problem using Cartesian coordinates, in Section 6.3 we consider the numerical solution of the three-dimensional problem with cylindrical coordinates and under the assumption of axial symmetry and, finally, in Section 6.4 we solve the fully three-dimensional problem by using an approach that considers vector field components defined along the directions of a Cartesian coordinate system and cylindrical coordinates for the independent variables.

6.1 One-dimensional Problem

In this section we discuss the numerical solution of the one-dimensional version of the initial-boundary value problem presented in 5.1. Section 6.1.1 is a summary of what we have already presented in Chapter 5 and it aims at adapting the notation to the one-dimensional framework, which is slightly different from the multi-dimensional setting treated in the subsequent sections (§6.2, §6.3 and §6.4). Therefore, it contains a brief introduction to the boundary value problem, the derivation of the weak formulation and the Galerkin discretisation in space. In Section 6.1.2 we show how to construct sets of basis functions used to solve the Galerkin semi-discrete problem by means of the Spectral Element Method and of the Finite Element Method. In particular, we consider boundary-adapted basis functions based on linear combinations of orthogonal polynomials for the Spectral Element Method and linear Lagrangian basis functions for the Finite Element Method. In Section 6.1.3 we continue the convergence analysis started in Section 5.3.2 and derive convergence rates with respect to the V_m-norm for both the Spectral and Finite Element methods. Finally, in Section 6.1.4 we present some results that have been obtained by applying the discussed numerical approaches: we first validate the derived convergence rates by solving some problems with manufactured solution and then we investigate the propagation of 1D waves in both homogeneous and heterogeneous materials.

6.1.1 Problem Formulation

Initial Boundary-Value Problem

Let us recall that the propagation of elastic and viscoelastic waves in a one-dimensional material is described by means of the following Cauchy momentum equation

$$\rho\frac{\partial^2 u}{\partial t^2} = \frac{\partial \sigma}{\partial x} + f_{ext}, \qquad x \in \Omega := (a,b), \quad t \in [0,T). \tag{6.1}$$

where $u\colon \bar{\Omega} \times [0,T) \to \mathbb{R}$ is the displacement and $\sigma\colon \bar{\Omega} \times [0,T) \to \mathbb{R}$ is the stress. In the viscoelastic Kelvin-Voigt model, the stress σ is defined as

$$\sigma = \sigma(u, \dot{u}) = \sigma_{\text{el}}(u) + \sigma_{\text{vi}}(\dot{u}), \tag{6.2}$$

where

$$\sigma_{\text{el}}(u) = \lambda_{\text{el}} \frac{\partial u}{\partial x}, \qquad \sigma_{\text{vi}}(\dot{u}) = \lambda_{\text{vi}} \frac{\partial}{\partial x} \frac{\partial u}{\partial t}.$$

The functions $\lambda_{\text{el}} \colon \Omega \to \mathbb{R}_+$ and $\lambda_{\text{vi}} \colon \Omega \to \mathbb{R}_+$ are the Young modulus and the dynamic viscosity, respectively, and, together with the density $\rho \colon \Omega \to \mathbb{R}_+$, they are hereafter assumed to be piecewise constant positive functions. Therefore, the domain Ω where the problem has to be solved can be seen as the union of a certain number of homogeneous materials. The Partial Differential Equation obtained by combining the Cauchy equation (6.1) and the Kelvin-Voigt model (6.2) is complemented with initial conditions for both the displacement and the velocity and boundary conditions at the domain endpoints a and b. In particular, we will assume time-dependent Dirichlet boundary condition imposed on $x = a$ and time-dependent Neumann boundary condition imposed on $x = b$. Therefore, the initial boundary-value problem rewrites as follows:

$$\begin{aligned}
&\text{Cauchy eq + Kelvin-Voigt:} && \rho \frac{\partial^2 u}{\partial t^2} = \frac{\partial}{\partial x}\left(\lambda_{\text{el}} \frac{\partial u}{\partial x} + \lambda_{\text{vi}} \frac{\partial}{\partial x}\frac{\partial u}{\partial t}\right) + f_{ext}, && (x,t) \in \Omega \times (0,T), && \text{(6.3a)}\\
&\text{Initial condition:} && u(x,0) = u_0(x),\ \dot{u}(x,0) = v_0(x), && x \in \Omega, && \text{(6.3b)}\\
&\text{Dirichlet bc:} && u(a,t) = u_D(t),\ \dot{u}(a,t) = \dot{u}_D(t), && t \in (0,T), && \text{(6.3c)}\\
&\text{Neumann bc:} && \sigma(b,t) = s(t), && t \in (0,T). && \text{(6.3d)}
\end{aligned}$$

Weak Formulation

As we have explained in Section 5.2, where we have derived the weak formulation for the multidimensional problem, we handle the time-dependent Dirichlet boundary conditions imposed on Γ_D (in this case the endpoint $x = a$) by introducing a *lifting operator* $\mathcal{L}$ that, roughly speaking, extends the Dirichlet boundary data to a function defined in the whole domain $\bar{\Omega}$. Then, the new unknowns of the problem become the functions $\tilde{u} := u - \mathcal{L}u_D$ and $\tilde{v} := v - \mathcal{L}\dot{u}_D$, where the variable v (i.e., the velocity) has been introduced with the aim of reducing the problem from second order to first order in time (we refer again to Section 5.2 for a detailed discussion). Finally, dropping the tildas to simplify the notation and defining the spaces

$$V \equiv H^1_D(\Omega) := \{v \in H^1(\Omega) \ : \ v(a) = 0\}, \qquad W \equiv L^2(\Omega), \qquad V_m := W \times V, \qquad V_\ell := V \times V,$$

the weak formulation of problem (6.3) consists in finding, for any $t \geq 0$, the pair $(v(t), u(t)) \in V_\ell$ such that

$$\begin{aligned}
&\int_\Omega \rho\, \dot{v}(t)\, \phi^v \, dx = -\int_\Omega \sigma(t)\, \frac{d\phi^v}{dx}\, dx + s(t)\phi^v(b) + \int_\Omega f(t)\, \phi^v \, dx && \forall \phi^v \in V,\\
&\int_\Omega \lambda_{\text{el}}\, \frac{d\dot{u}(t)}{dx}\, \frac{d\phi^v}{dx}\, dx = \int_\Omega \lambda_{\text{el}}\, \frac{dv(t)}{dx}\, \frac{d\phi^v}{dx}\, dx && \forall \phi^v \in V,
\end{aligned} \qquad (6.4)$$

where f is a forcing term that takes into account both the contribution due to the original forcing f_{ext} in (6.1) and the contribution due to the lifting of the time-dependent Dirichlet boundary conditions, i.e.,

$$f(x,t) := f_{ext}(x,t) - \int_\Omega \left(\sigma(\mathcal{L}u_D, \mathcal{L}\dot{u}_D)\, \frac{d\phi^v}{dx} + \rho\, \mathcal{L}\ddot{u}_D\, \phi^v\right) dx.$$

Having defined the bilinear forms

$$c \colon W \times W \to \mathbb{R} \qquad \psi \times \phi \mapsto c(\psi,\phi) := \int_\Omega \rho\, \psi\, \phi \, dx, \qquad (6.5a)$$

$$b \colon V \times V \to \mathbb{R} \qquad \psi \times \phi \mapsto b(\psi,\phi) := \int_\Omega \sigma_{\text{vi}}(\psi)\, \frac{d\phi}{dx}\, dx = \int \lambda_{\text{vi}}\, \frac{d\psi}{dx}\, \frac{d\phi}{dx}\, dx, \qquad (6.5b)$$

$$a \colon V \times V \to \mathbb{R} \qquad \psi \times \phi \mapsto a(\psi,\phi) := \int_\Omega \sigma_{\text{el}}(\psi)\, \frac{d\phi}{dx}\, dx = \int \lambda_{\text{el}}\, \frac{d\psi}{dx}\, \frac{d\phi}{dx}\, dx, \qquad (6.5c)$$

and, for any $t \geq 0$, the linear functional

$$\mathrm{f}(t) \colon W \to \mathbb{R} \qquad \phi \mapsto \mathrm{f}(t)(\phi) := s(t)\phi(b) + \int_\Omega f(t)\, \phi \, dx, \qquad (6.6)$$

we can rewrite the weak formulation (6.4) as the problem of finding, for any $t \geq 0$, $(v(t), u(t)) \in V_\ell$ such that

$$\begin{aligned} &c(\dot{v}(t), \phi^v) + b(v(t), \phi^v) + a(u(t), \phi^v) = \mathrm{f}(t)(\phi^v), \qquad \forall \phi^v \in V, \\ &a(\dot{u}(t), \phi^u) - a(v(t), \phi^u) = 0, \qquad \forall \phi^u \in V. \end{aligned}$$

This system can also be written as a single equation as: find, for any $t \geq 0$, $U(t) = (v(t), u(t)) \in V_\ell$ such that

$$m(\dot{U}(t), \Phi) + \ell(U(t), \Phi) = F(t)(\Phi), \qquad \forall \Phi := (\phi^v, \phi^u) \in V_\ell, \tag{6.7}$$

where

$$\begin{aligned} m &\colon V_m \times V_m \to \mathbb{R} \qquad \Psi \times \Phi \mapsto m(\Psi, \Phi) := c(\psi^v, \phi^v) + a(\phi^u, \phi^u), \\ \ell &\colon V_\ell \times V_\ell \to \mathbb{R} \qquad \Psi \times \Phi \mapsto \ell(\Psi, \Phi) := b(\psi^v, \phi^v) + a(\psi^u, \phi^v) - a(\psi^v, \phi^u), \\ F(t) &\colon V_m \to \mathbb{R} \qquad \Phi \mapsto F(t)(\Phi) := \mathrm{f}(t)(\phi^v), \quad t \geq 0. \end{aligned}$$

Galerkin Space Discretisation

The Galerkin discretisation in space starts by defining a finite dimensional subspace V_N of $H^1(\Omega)$, having dimension N, and a finite dimensional subspace $V_{N_0} \leq V_N$ of $H^1_D(\Omega)$ having dimension $N_0 < N$. In particular, V_{N_0} is the space containing all the functions that are in V_N and vanishing at the left endpoint of the domain where Dirichlet boundary condition is imposed, i.e.,

$$V_{N_0} = \{v \in V_N \ : \ v(a) = 0\}, \qquad \dim V_{N_0} = N_0 < N = \dim V_N < \infty.$$

Let us now denote by $\mathcal{B}_N$ and $\mathcal{B}_{N_0}$ two sets of linearly independent basis functions generating the finite dimensional subspaces V_N and V_{N_0}, respectively, i.e.,

$$\begin{aligned} \mathcal{B}_N &:= \{\hat{\phi}_i \ : \ i = 1, \dots, N\}, \qquad V_N := \mathrm{span}\{\hat{\phi}_i \ : \ \hat{\phi}_i \in \mathcal{B}_N\}, \qquad \dim(V_N) = N, \\ \mathcal{B}_{N_0} &:= \{\phi_i \ : \ i = 1, \dots, N_0\}, \qquad V_{N_0} := \mathrm{span}\{\phi_i \ : \ \phi_i \in \mathcal{B}_{N_0}\}, \qquad \dim(V_{N_0}) = N_0 < N. \end{aligned}$$

Moreover, we define the following finite-dimensional product spaces

$$\begin{aligned} \mathcal{V}_{N_0} &:= V_{N_0} \times V_{N_0}, \qquad \text{with} \qquad \dim(\mathcal{V}_{N_0}) = 2N_0, \\ \mathcal{V}_N &:= V_N \times V_N, \qquad \text{with} \qquad \dim(\mathcal{V}_N) = 2N. \end{aligned}$$

Having denoted by $u_N(t) \in V_{N_0}$ and by $v_N(t) \in V_{N_0}$ a suitable approximation in space of the displacement $u(t)$ and the velocity $v(t)$ solution of the weak formulation (6.4) at time t, we can expand them and their space and time derivatives using the basis functions in $\mathcal{B}_{N_0}$ as follows

$$\begin{aligned} v_N(x,t) &= \textstyle\sum_{i=1}^{N_0} \eta_i(t)\, \phi_i(x), \qquad \dot{v}_N(x,t) = \sum_{i=1}^{N_0} \dot{\eta}_i(t)\, \phi_i(x), \qquad v'_N(x,t) = \sum_{i=1}^{N_0} \eta_i(t)\, \phi'_i(x), \\ u_N(x,t) &= \textstyle\sum_{i=1}^{N_0} \theta_i(t)\, \phi_i(x), \qquad \dot{u}_N(x,t) = \sum_{i=1}^{N_0} \dot{\theta}_i(t)\, \phi_i(x), \qquad u'_N(x,t) = \sum_{i=1}^{N_0} \theta_i(t)\, \phi'_i(x), \end{aligned} \tag{6.8}$$

where the time-dependent vectors of coefficients $\boldsymbol{\eta} = (\eta_1(t), \dots, \eta_{N_0}(t))^\mathsf{T}$ and $\boldsymbol{\theta} = (\theta_1(t), \dots, \theta_{N_0}(t))^\mathsf{T}$ are the unknowns of the problem. Similarly, we can write the stress $\sigma_N(v_N, u_N)(t) \in V_{N_0}$ using the basis $\mathcal{B}_{N_0}$:

$$\sigma_N(x,t) = \lambda_{\mathrm{vi}} v'_N(x,t) + \lambda_{\mathrm{el}} u'_N(x,t) = \lambda_{\mathrm{vi}} \textstyle\sum_{i=1}^{N_0} \eta_i(t)\, \phi'_i(x) + \lambda_{\mathrm{el}} \sum_{i=1}^{N_0} \theta_i(t)\, \phi'_i(x). \tag{6.9}$$

Moreover, using the basis functions in $\mathcal{B}_N$, the lifting function can be written as

$$\mathcal{L}u_D = \textstyle\sum_{i=1}^{N} \theta_{i,D}(t)\, \hat{\phi}_i(x), \qquad \mathcal{L}\dot{u}_D = \sum_{i=1}^{N} \dot{\theta}_{i,D}(t)\, \hat{\phi}_i(x), \quad \mathcal{L}\ddot{u}_D = \sum_{i=1}^{N} \ddot{\theta}_{i,D}(t)\, \hat{\phi}_i(x), \tag{6.10}$$

where the vector of time-dependent coefficients $\boldsymbol{\theta}_D = (\theta_{D,1}(t), \dots, \theta_{D,N}(t))^\mathsf{T}$ and its time derivatives $\dot{\boldsymbol{\theta}}_D$ and $\ddot{\boldsymbol{\theta}}_D$ are known. Replacing both the test functions $\phi^v, \phi^u \in V$ with $\phi_i \in \mathcal{B}_{N_0}$, $i = 1, \dots, N_0$, the

Galerkin semi-discretisation of problem (6.4) consists of finding, for any $t \geq 0$, the pair $(v_N(t), u_N(t)) \in \mathcal{V}_{N_0}$ such that:

$$\begin{aligned} &\int_\Omega \rho\, \dot{v}_N(t)\, \phi_i\, dx = -\int_\Omega \sigma_N(t)\, \frac{d\phi_i}{dx}\, dx + s(t)\phi_i(b) + \int_\Omega f(t)\, \phi_i\, dx && i = 1, \ldots, N_0, \\ &\int_\Omega \lambda_{\text{el}}\, \frac{d\dot{u}_N(t)}{dx}\, \frac{d\phi_i}{dx}\, dx = \int_\Omega \lambda_{\text{el}}\, \frac{dv_N(t)}{dx}\, \frac{d\phi_i}{dx}\, dx && i = 1, \ldots, N_0. \end{aligned} \tag{6.11}$$

Using the expressions defined in equations (6.8) and (6.9), the Galerkin semi-discrete weak formulation (6.11) becomes:

$$\begin{aligned} &\sum_{j=1}^{N_0} \dot{\eta}_j(t) \int_\Omega \rho\, \phi_j\, \phi_i\, dx = -\sum_{i=1}^{N_0} \eta_j(t) \int_\Omega \lambda_{\text{vi}}\, \frac{d\phi_j}{dx}\, \frac{d\phi_i}{dx}\, dx - \sum_{i=1}^{N_0} \theta_j(t) \int_\Omega \lambda_{\text{el}}\, \frac{d\phi_j}{dx}\, \frac{d\phi_i}{dx}\, dx + s(t)\phi_i(b) + \int_\Omega f(t)\, \phi_i\, dx, \\ &\sum_{j=1}^{N_0} \dot{\theta}_j(t) \int_\Omega \lambda_{\text{el}}\, \frac{d\phi_j}{dx}\, \frac{d\phi_i}{dx}\, dx = \sum_{j=1}^{N_0} \eta_j(t) \int_\Omega \lambda_{\text{el}}\, \frac{d\phi_j}{dx}\, \frac{d\phi_i}{dx}\, dx, \end{aligned}$$

where $i = 1, \ldots, N_0$. Moreover, the bilinear forms and the linear functional introduced in relations (6.5) and (6.6), respectively, yields the following compact form of the Galerkin weak formulation:

$$\begin{aligned} &\sum_{j=1}^{N_0} \dot{\eta}_j(t)\, c(\phi_j, \phi_i) + \sum_{j=1}^{N_0} \eta_j(t)\, b(\phi_j, \phi_i) + \sum_{j=1}^{N_0} \theta_j(t)\, a(\phi_j, \phi_i) = \mathrm{f}(t)(\phi_i), && i = 1, \ldots, N_0, \\ &\sum_{j=1}^{N_0} \dot{\theta}_j(t)\, a(\phi_j, \phi_i) - \sum_{j=1}^{N_0} \eta_j(t)\, a(\phi_j, \phi_i) = 0, && i = 1, \ldots, N_0. \end{aligned}$$

As usual, the semi-discrete problem above can be rewritten using a more compact notation as: find, for any $t \geq 0$, $U_N(t) = (v_N(t), u_N(t)) \in \mathcal{V}_{N_0}$ such that

$$m(\dot{U}_N(t), \Phi_i) + \ell(U_N(t), \Phi_i) = F(t)(\Phi_i), \qquad \Phi_i \in \mathcal{V}_{N_0},\ i = 1, \ldots, 2N_0. \tag{6.12}$$

This system of Ordinary Differential Equations can be written in matrix form as in system (5.32), i.e.,

$$\begin{aligned} &\mathbf{M}\dot{\boldsymbol{\xi}} + \mathbf{H}\boldsymbol{\xi} = \boldsymbol{F} \\ &\boldsymbol{\xi}(0) = \boldsymbol{\xi}_0, \end{aligned}$$

where $\boldsymbol{\xi} = (\boldsymbol{\eta}^\mathsf{T}, \boldsymbol{\theta}^\mathsf{T})^\mathsf{T}$ and $\boldsymbol{\xi}_0$ is the given initial condition. The matrices $\mathbf{M}$ and $\mathbf{H}$, have the same block structure already shown in system (5.33), namely,

$$\mathbf{M} = \begin{pmatrix} \mathbf{M}^v & \mathbf{0} \\ \mathbf{0} & \mathbf{M}^u \end{pmatrix} \qquad \mathbf{H} = \begin{pmatrix} \mathbf{H}_{11} & \mathbf{H}_{12} \\ \mathbf{H}_{21} & \mathbf{0} \end{pmatrix} \tag{6.13}$$

In the one-dimensional setting, the components (i, j), $i, j = 1, \ldots, N_0$, of the blocks of matrices $\mathbf{M}$ and $\mathbf{H}$, already defined in the general case in equations (5.34) and (5.35), are given by

$$(\mathbf{M}^v)_{i,j} = c(\phi_j, \phi_i) = \int_\Omega \rho\, \phi_j\, \phi_i\, dx, \qquad (\mathbf{M}^u)_{i,j} = a(\phi_j, \phi_i) = \int_\Omega \lambda_{\text{el}}\, \frac{d\phi_j}{dx}\, \frac{d\phi_i}{dx}\, dx \tag{6.14}$$

and

$$(\mathbf{H}_{11})_{i,j} = \quad b(\phi_j, \phi_i) = \quad \int_\Omega \lambda_{\text{vi}}\, \frac{d\phi_j}{dx}\, \frac{d\phi_i}{dx}\, dx, \tag{6.15a}$$

$$(\mathbf{H}_{12})_{i,j} = \quad a(\phi_j, \phi_i) = \quad \int_\Omega \lambda_{\text{el}}\, \frac{d\phi_j}{dx}\, \frac{d\phi_i}{dx}\, dx, \tag{6.15b}$$

$$(\mathbf{H}_{21})_{i,j} = -a(\phi_j, \phi_i) = -\int_\Omega \lambda_{\text{el}}\, \frac{d\phi_j}{dx}\, \frac{d\phi_i}{dx}\, dx. \tag{6.15c}$$

Having used the same basis functions for the space approximation of u and v, one can easily see that $\mathbf{M}^u = \mathbf{H}_{12} = -\mathbf{H}_{21}$. Therefore, we can simplify the notation and rewrite the matrices $\mathbf{M}$ and $\mathbf{H}$ in relations (6.13) as

$$\mathbf{M} = \begin{pmatrix} \mathbf{C} & \mathbf{0} \\ \mathbf{0} & \mathbf{A} \end{pmatrix} \qquad \mathbf{H} = \begin{pmatrix} \mathbf{B} & \mathbf{A} \\ -\mathbf{A} & \mathbf{0} \end{pmatrix},$$

where

$$\begin{aligned} \mathbf{C}_{i,j} &= c(\phi_j, \phi_i) = \int_\Omega \rho\, \phi_j\, \phi_i\, dx, \\ \mathbf{B}_{i,j} &= b(\phi_j, \phi_i) = \int_\Omega \lambda_{\text{vi}}\, \frac{d\phi_j}{dx}\, \frac{d\phi_i}{dx}\, dx, \\ \mathbf{A}_{i,j} &= a(\phi_j, \phi_i) = \int_\Omega \lambda_{\text{el}}\, \frac{d\phi_j}{dx}\, \frac{d\phi_i}{dx}\, dx. \end{aligned} \tag{6.16}$$

Finally, the forcing vector $\boldsymbol{F}$ is defined as

$$\boldsymbol{F} := \boldsymbol{F}^{ext} + \boldsymbol{F}^{neu} + \boldsymbol{F}^{dir},$$

where $\boldsymbol{F}^{ext}$ is the contribution of the external forcing function f_{ext} in definition (6.1),

$$\boldsymbol{F}_i^{ext} := \begin{cases} \int_\Omega f_{ext}\, \phi_i\, dx, & i = 1, \dots, N_0, \\ 0, & i = N_0 + 1, \dots, 2N_0, \end{cases}$$

$\boldsymbol{F}^{neu}$ is the contribution due to the time-dependent Neumann boundary condition imposed on $x = b$,

$$\boldsymbol{F}_i^{neu} := \begin{cases} s(t)\, \phi_i(b), & i = 1, \dots, N_0, \\ 0, & i = N_0 + 1, \dots, 2N_0, \end{cases}$$

and $\boldsymbol{F}^{dir}$ is the contribution given by the lifting of the Dirichlet boundary condition imposed on $x = a$,

$$\boldsymbol{F}_i^{dir} := \begin{cases} \int_\Omega - \left(\lambda_{\text{el}}\, (\mathcal{L} u_D)' + \lambda_{\text{vi}}\, (\mathcal{L} \dot{u}_D)'\right) \phi_i' - \rho \mathcal{L}_D \ddot{u}_D\, \phi_i\, dx & i = 1, 2, \dots, N_0, \\ 0 & i = N_0 + 1, \dots, 2N_0. \end{cases}$$

Using the expressions (6.10), the vector $\boldsymbol{F}^{dir}$ can be computed as follows

$$\boldsymbol{F}^{dir} = - \begin{pmatrix} \mathbf{S}_1 & \mathbf{S}_2 \\ \mathbf{0} & \mathbf{0} \end{pmatrix} \begin{pmatrix} \dot{\boldsymbol{\theta}}_D \\ \boldsymbol{\theta}_D \end{pmatrix} - \begin{pmatrix} \mathbf{N}\, \ddot{\boldsymbol{\theta}}_D \\ \mathbf{0} \end{pmatrix}$$

where, for any $i = 1, \dots, N_0$ and $j = 1, \dots, N$, we set

$$\begin{aligned} (\mathbf{S}_1)_{i,j} &= b(\hat{\phi}_j, \phi_i) = \int_\Omega \lambda_{\text{vi}}\, \hat{\phi}_j\, \phi_i\, dx, \\ (\mathbf{S}_2)_{i,j} &= a(\hat{\phi}_j, \phi_i) = \int_\Omega \lambda_{\text{el}}\, \hat{\phi}_j\, \phi_i\, dx, \\ \mathbf{N}_{i,j} &= c(\hat{\phi}_j, \phi_i) = \int_\Omega \rho\, \hat{\phi}_j\, \phi_i\, dx. \end{aligned} \tag{6.17}$$

The initial conditions

$$u(x, 0) = u_0(x) \quad \text{and} \quad v(x, 0) = v_0(x) \quad \text{in } \Omega$$

are imposed in weak form, that is

$$\left(\begin{pmatrix} v_N|_{t=0} \\ u_N|_{t=0} \end{pmatrix}, \phi \right)_{V_m} = \left(\begin{pmatrix} v_0 \\ u_0 \end{pmatrix}, \phi \right)_{V_m}, \qquad \forall \phi \in \mathcal{V}_{N_0}. \tag{6.18}$$

where, for all $\Phi = (\phi^v, \phi^u)$, $\Psi = (\psi^v, \psi^u) \in \mathcal{V}_{N_0}$, the scalar product $(\cdot, \cdot)_{V_m}$ is defined as

$$(\Phi, \Psi)_{V_m} := c(\phi^v, \phi^u) + a(\psi^v, \psi^u) = \int_\Omega \rho\, \phi^v\, \psi^v\, dx + \int_\Omega \lambda_{\text{el}} \frac{d\phi^u}{dx} \frac{d\psi^u}{dx}\, dx.$$

equation (6.18) is equivalent to

$$\boldsymbol{\xi}(0) = \begin{pmatrix} \boldsymbol{\eta}(0) \\ \boldsymbol{\theta}(0) \end{pmatrix} = \mathbf{M}^{-1}\boldsymbol{m} =: \boldsymbol{\xi}_0,$$

where

$$\boldsymbol{m}_i := \begin{cases} \displaystyle\int_\Omega \rho\, \phi_j\, v_0\, dx, & i = j = 1, \dots, N_0, \\ \displaystyle\int_\Omega \sigma_{\text{el}}(\phi_j)\, \frac{du_0}{dx}\, dx & i = N_0 + 1, \dots, 2N_0,\ j = i - N_0. \end{cases}$$

6.1.2 Basis Functions Definition

We now show how to construct the sets $\mathcal{B}_N$ and $\mathcal{B}_{N_0}$ of linearly independent basis functions for the finite dimensional spaces V_N and V_{N_0}, respectively. In particular, we build these two sets in such a way they satisfy the condition $\mathcal{B}_{N_0} \subset \mathcal{B}_N$. This is a common choice that is usually adopted to facilitate the computation of the matrices $\mathbf{M}$ and $\mathbf{H}$ and of the forcing vector $\boldsymbol{F}^{dir}$ from the implementation perspective. For example, let us suppose that we have computed the matrix $\hat{\mathbf{C}}$ whose component (i, j) is defined as follows

$$\hat{\mathbf{C}}_{i,j} := \int_\Omega \rho\, \hat{\phi}_j\, \hat{\phi}_i\, dx, \quad \text{where} \quad \hat{\phi}_i, \hat{\phi}_j \in \mathcal{B}_N,\ i, j = 1, \dots, N.$$

Then, if $\mathcal{B}_{N_0} \subset \mathcal{B}_N$, the matrix $\mathbf{N}$ defined in equation (6.17) is obtained from $\hat{\mathbf{C}}$ by removing the rows associated to those basis functions that are in $\mathcal{B}_N$ but not in $\mathcal{B}_{N_0}$, whereas the matrix $\mathbf{C}$ defined in equation (6.16) is obtained by removing from $\hat{\mathbf{C}}$ both the rows and the columns associated to the basis functions $\hat{\phi} \in \mathcal{B}_N \backslash \mathcal{B}_{N_0}$. The same reasoning can also be applied to matrices $\mathbf{B}$ (resp. $\mathbf{A}$) and $\mathbf{S}_1$ (resp. $\mathbf{S}_2$). As a consequence, we describe how to define the set $\mathcal{B}_N$ and subsequently we show that it also contains the set $\mathcal{B}_{N_0}$. Moreover, we only discuss the computation of the following matrices

$$\hat{\mathbf{C}}_{i,j} = c(\hat{\phi}_j, \hat{\phi}_i) = \int_\Omega \rho\, \hat{\phi}_j\, \hat{\phi}_i\, dx, \tag{6.19a}$$

$$\hat{\mathbf{B}}_{i,j} = b(\hat{\phi}_j, \hat{\phi}_i) = \int_\Omega \lambda_{\text{vi}}\, \frac{d\hat{\phi}_j}{dx}\, \frac{d\hat{\phi}_i}{dx}\, dx, \tag{6.19b}$$

$$\hat{\mathbf{A}}_{i,j} = a(\hat{\phi}_j, \hat{\phi}_i) = \int_\Omega \lambda_{\text{el}}\, \frac{d\hat{\phi}_j}{dx}\, \frac{d\hat{\phi}_i}{dx}\, dx, \tag{6.19c}$$

where $\hat{\phi}_i, \hat{\phi}_j \in \mathcal{B}_N$, $i, j = 1, \dots, N$ and then compute the other matrices as

$$\mathbf{C} = \hat{\mathbf{C}}(dir, dir), \qquad \mathbf{B} = \hat{\mathbf{B}}(dir, dir), \qquad \mathbf{A} = \hat{\mathbf{A}}(dir, dir)$$
$$\mathbf{N} = \hat{\mathbf{C}}(dir, :), \qquad \mathbf{S}_1 = \hat{\mathbf{B}}(dir, :), \qquad \mathbf{S}_2 = \hat{\mathbf{A}}(dir, :),$$

where *dir* denotes the set of indices associated to those basis functions that are both in $\mathcal{B}_N$ and $\mathcal{B}_{N_0}$. In the first part of this section we start by introducing the class of piecewise boundary-adapted polynomial basis functions, which includes both nodal and modal basis functions and that provides a general framework in which a wide range of Galerkin methods, such as the spectral-Galerkin, the Spetral Element Method, the Finite Element Method and the $p-$version of the Finite Element Method, are based. Finally, in the last part of this section, we focus on the definition the basis functions for the spectral-Galerkin method and we subsequently define the linear Lagrangian basis functions used in the Finite Element Method.

Polynomial Boundary-Adapted Basis Functions

We start by performing a partition the domain $\Omega = (a, b)$ into a set of $M \geq 1$ disjoint subintervals, also called *elements*, $\Omega_m = (x_{m-1}, x_m)$, $m = 1, \dots, M$, with $a = x_0 < x_1 < \cdots < x_M = b$. Then, we

define the finite dimensional subspace V_N of $H^1(\Omega)$ as the space containing all the functions that are polynomials of degree $N_m \geq 1$ on the element Ω_m and that are continuous at the interval endpoints, i.e.,

$$V_N = \left\{ v \in \mathcal{C}^0(\Omega) \ : \ v_{|\Omega_m} \in \mathbb{P}_{N_m}(\Omega_m), \ m = 1, \ldots, M \right\}.$$

To define the set $\mathcal{B}_N$ of basis functions generating this space, we proceed as follows.

1. We start by choosing a suitable set of reference polynomial basis functions $\hat{\varphi}$ defined on a reference interval, that we denote by $\hat{\Omega}$.

2. Subsequently, we define a set of basis functions on each subdomain Ω_m, $m = 1, \ldots, M$, by mapping the reference basis from the reference interval $\hat{\Omega}$ to the subdomain Ω_m.

3. Finally, we define global continuous basis functions on Ω by "glueing" the local basis functions at the interface points x_m, $m = 1, \ldots, M-1$.

The main difficulty in this procedure consists in esuring the continuity of the global basis functions at the interface points x_m, $m = 1, \ldots, M-1$. For intance, let us suppose that the interval $(-1, +1)$ is a subdomain of a wider interval and let us consider the Legendre polynomials as reference basis functions. Then, it is evident that this set of polynomial bases is inappropriate to produce global basis made up of continuous functions, given that each Legendre polynomial is nonzero at both endpoints of the interval. Therefore, the choice of the reference polynomial basis is of paramount importance, as the local bases defined within each subdomain must allow straightforward matching at the interface points in order to form global bases. The class of polynomials bases having the properties that we are looking for are referred to as *boundary-adapted bases*. Having denoted by $\mathbb{P}_N(-1, +1)$ the space of polynomials defined on the interval $(-1, +1)$ and having degree less than or equal to N, we recall that a basis for $\mathbb{P}_N(-1, +1)$ is termed boundary-adapted if it contains two functions, called *vertex basis functions*, that are nonzero at precisely one endpoint of the interval and $N-1$ functions, called *bubble functions* or *internal basis functions*, vanishing at both the endpoints. It is worth noting that, if we drop the two vertex functions from a boundary-adapted basis, we get a basis for the subspace $\mathbb{P}_N^0(-1, +1)$ of the polynomials vanishing at both the endpoints. Polynomial boundary-adapted basis can be either of *modal* or *nodal* type. In a nodal basis each function is responsible for reproducing the value of the polynomial at one particular node in the interval. An example of a widely used nodal boundary-adapted basis is provided by the Lagrange basis ψ_i, $i = 0, \ldots, N$, associated with a set of Jacobi Gauss-Lobatto points in the interval $[-1, +1]$. The vertex functions are ψ_0 and ψ_N, i.e., the Lagrange polynomials associated with the endpoints, whereas the bubble functions are the ψ_i's for $i = 1, \ldots, N-1$, i.e., the Lagrange polynomials associated to the internal nodes. Nodal basis functions based on Lagrange polynomials defined at the Jacobi Gauss-Lobatto quadrature points are mainly used in the context of Spectral Element Method (SEM) [153, 154]. On the other hand, in a boundary-adapted basis of modal type each basis function provides one particular pattern of oscillation of higher and higher frequency. These basis can be constructed, for example, by considering suitable linear combinations of orthogonal polynomials of Jacobi type, such as the Legendre or Chebyshev polynomials. For example, having denoted by $L_k(x)$ the Legendre polynomial of degree k, the Legendre boundary-adapted basis functions having degree up to N are defined as

$$\begin{aligned}
&\text{left vertex function:} && \hat{\varphi}_0(x) = \frac{1}{2}\left(L_0(x) - L_1(x)\right) = \frac{1-x}{2}, \\
&\text{bubble basis functions:} && \hat{\varphi}_k(x) = \frac{1}{\sqrt{2(2k+1)}}\left(L_{k-1}(x) - L_{k+1}(x)\right), \qquad 1 \leq k \leq N-1, \\
&\text{right vertex function:} && \hat{\varphi}_N(x) = \frac{1}{2}\left(L_0(x) + L_1(x)\right) = \frac{1+x}{2}.
\end{aligned}$$

For further details concerning the definition of Legendre or Chebyshev boundary-adapted basis and the computation of integrals involving their products, we refer the reader to Sections 4.3.1 and 4.4.1, respectively. The usage of modal basis functions is in general associated to the $p-$ or $hp-$version of the Finite Element Method. Indeed, modal boundary-adapted basis using Legendre polynomials where proposed for the first time by Babuska and co-workers, who employed this type of basis in the

$p-$version of the Finite Element Method they developed [246–249]. Subsequently, Shen proposed to use boundary-adapted modal basis functions based on either Legendre or Chebyshev polynomials of the first kind in the context of spectral-Galerkin methods [250, 251]. These modal basis functions are also said to be *hierarchical* because the set of basis used to generate $\mathbb{P}_{N-1}(-1,+1)$, $N \geq 2$, is fully contained into the set of basis generating $\mathbb{P}_N(-1,+1)$, while this is not the case when using Lagrange polynomials as they all have the same degree.

Before proceeding, it is worth emphasizing once again that the procedure we are about to describe for the construction of the set $\mathcal{B}_N$ is entirely general, in the sense that it does not depend on a specific type of boundary-adapted basis functions (i.e., it can be applied to both modal and nodal basis functions). Let us consider boundary-adapted polynomials $\hat{\varphi}_i(x)$, $i = 0,\dots,\bar{N}$, where $\bar{N} := \max_{m=1}^{M} N_m$, defined on the reference element $\hat{\Omega} = (-1,+1)$. Then, for all $m = 1,\dots,M$, we define basis functions $\varphi_i^{(m)}(x)$ in $\Omega_m = (x_{m-1}, x_m)$ by mapping $\hat{\varphi}_i(x)$ from $\hat{\Omega}$ to Ω_m. More precisely, for all $x \in \Omega_m$, we set

$$\varphi_i^{(m)}(x) := \hat{\varphi}_i(F_m^{-1}(x)), \qquad i = 0,\dots,N_m, \tag{6.20}$$

where F_m is the affine function that maps the reference interval $\hat{\Omega}$ into $\Omega_m = (x_{m-1}, x_m)$, i.e.,

$$\begin{aligned} F_m &: \hat{\Omega} \to \Omega_m \\ \hat{x} &\mapsto F_m(\hat{x}) := \frac{x_m - x_{m-1}}{2}\hat{x} + \frac{x_m + x_{m-1}}{2}. \end{aligned}$$

The functions defined in expression (6.20) form a boundary-adapted basis in each element Ω_m, which means that on each element Ω_m a polynomial $v \in \mathbb{P}_N(\Omega_m)$ is represented in terms of the basis functions (6.20) as follows

$$v(x) = \textstyle\sum_{i=0}^{N_m} v_i^{(m)} \varphi_i^{(m)}(x), \qquad x \in \Omega_m,$$

where $u_i^{(m)}$ represents the modal or nodal coefficients, depending on the type of basis being chosen. Then, a global representation of u_N can be obtained by generating a set of global basis for V_N as follows. For every $m = 1,\dots,M$ and every $i = 1,\dots,N_m - 1$, each local bubble basis function $\varphi_i^{(m)}(x)$ is extended by zero outside the subdomain Ω_m, generating a global continuous basis function $\tilde{\varphi}_i^{(m)}(x)$ supported over Ω_m. More precisely we define the function

$$\tilde{\varphi}_i^{(m)}(x) := \begin{cases} \varphi_i^{(m)}(x), & \text{for } x \in \bar{\Omega}_m, \\ 0 & \text{otherwise.} \end{cases}$$

Moreover, for every interface node x_m, $m = 1,\dots,M-1$, we define the continuous function $\varphi_m^*(x)$ supported over the interval $\bar{\Omega}_m \cup \bar{\Omega}_{m+1} = (x_{m-1}, x_{m+1})$ by "glueing" the two vertex functions $\varphi_{N_m}^{(m)}(x)$ and $\varphi_0^{(m+1)}$ defined over the contiguous subdomains Ω_m and Ω_{m+1}, respectively. So, we have

$$\varphi_m^*(x) := \begin{cases} \varphi_{N_m}^{(m)}(x), & \text{for } x \in \bar{\Omega}_m, \\ \varphi_0^{(m+1)}(x), & \text{for } x \in \bar{\Omega}_{m+1}, \\ 0, & \text{otherwise.} \end{cases}$$

Finally, we define the two (global) boundary basis functions $\varphi_1^{(\Gamma)}$ and $\varphi_M^{(\Gamma)}$ by extending to zero the two vertex functions $\varphi_0^{(1)}$ and $\varphi_{N_M}^{(M)}$ outside the subdomains Ω_1 and Ω_M, respectively:

$$\varphi_1^{(\Gamma)} = \begin{cases} \varphi_0^{(1)}, & \text{for } x \in \bar{\Omega}_1, \\ 0, & \text{otherwise,} \end{cases} \qquad \varphi_M^{(\Gamma)} = \begin{cases} \varphi_{N_M}^{(M)}, & \text{for } x \in \bar{\Omega}_M, \\ 0, & \text{otherwise.} \end{cases}$$

In such a way we obtain $n_I = \sum_{m=1}^{M}(N_m - 1)$ internal (bubble) basis functions plus $n_{VI} = M - 1$ (vertex) interface basis functions and $n_{VB} = 2$ (vertex) boundary basis functions, yielding $N = n_I + n_{VI} + n_{VB} = \sum_{m=1}^{M} N_m + 1$ basis functions defining the set $\mathcal{B}_N$:

$$\mathcal{B}_N := \underbrace{\{\varphi_1^{(\Gamma)}, \varphi_M^{(\Gamma)}\}}_{\text{boundary basis}} \cup \underbrace{\{\varphi_m^*,\ m = 1,\dots,M-1\}}_{\text{interface basis}} \cup \underbrace{\{\tilde{\varphi}_i^{(m)},\ m = 1\dots,M,\ i = 1,\dots,N_m - 1\}}_{\text{bubble basis}}. \tag{6.21}$$

Therefore, for every $x \in \Omega = (a, b)$, a function $v \in V_N$ can be represented as

$$v(x) = \sum_{m=1}^{M-1} v_m^* \varphi_m^*(x) + \sum_{m=1}^{M} \sum_{i=1}^{N_m-1} v_i^{(m)} \tilde{\varphi}_i^{(m)}(x) + v_1^{(\Gamma)} \varphi_1^{(\Gamma)}(x) + v_M^{(\Gamma)} \varphi_M^{(\Gamma)}(x).$$

It is worth noting that all the (global) interface and bubble basis functions vanish at both the boundary nodes a and b. This means that the set $\mathcal{B}_{N_0}$ of basis functions generating the space V_{N_0} can be obtained from $\mathcal{B}_N$ by simply disregarding the boundary basis function(s) associated to the boundary node(s) where Dirichlet boundary conditions are imposed. Since in the initial-boundary value problem (6.3) we have considered Dirichlet boundary conditions imposed only on the left endpoint of Ω, it is suffcient to remove the basis function $\varphi_1^{(\Gamma)}$ from $\mathcal{B}_N$ to obtain the set $\mathcal{B}_{N_0}$. Finally, we have to define the ordering of the global basis functions in $\mathcal{B}_N$. So we identify the basis functions of $\mathcal{B}_N$ with $\hat{\phi}_i$, $i = 0, 1, \ldots, N := \sum_{m=1}^{M} N_m$, as we have done in Section 6.1.1 and at the beginning of Section 6.1.2 and we define the following relation between them and the boundary, bubble and interface basis functions defined above:

$$\begin{aligned}
&\hat{\phi}_0 \equiv \varphi_1^{(\Gamma)}, \\
&\hat{\phi}_i \equiv \tilde{\varphi}_i^{(1)}, && i = 1, \ldots, N_1 - 1 \\
&\hat{\phi}_{N_1} \equiv \varphi_1^*, \\
&\hat{\phi}_{N_1+i} \equiv \tilde{\varphi}_i^{(2)}, && i = 1, \ldots, N_2 - 1 \\
&\hat{\phi}_{N_1+N_2} \equiv \varphi_2^* \\
&\vdots \\
&\hat{\phi}_{\sum_{m=1}^{M} N_m} \equiv \varphi_M^{(\Gamma)}.
\end{aligned}$$

The ordering is important in the construction of the matrices arising from the semi-discretisation of the weak formulation.

Spectral-Galerkin Basis Functions

Let us recall that, at the beginning of Section 6.1.1, we have defined the density $\rho = \rho(x)$, the Young modulus $\lambda_{\text{el}} = \lambda_{\text{el}}(x)$ and the dynamic viscosity $\lambda_{\text{vi}} = \lambda_{\text{vi}}(x)$ as piecewise positive constant functions, thereby identifying the domain Ω with a material that is made by the union of several homogeneous materials next to each other. In the spectral-Galerkin approach that we propose, the partition of the domain Ω is defined in such a way that each subinterval Ω_m, $m = 1, \ldots, M$, is associated to a different homogeneous material. Therefore, each subinterval Ω_m is characterised by a different triplet $(\rho_m, \lambda_{el,m}, \lambda_{vi,m})$ of constant material parameters. Clearly, in the case of homogeneous material, the support of all the basis functions is given by the whole domain Ω. Moreover, within this approach we also allow the number of basis functions associated to each subdomain Ω_m, $m = 1, \ldots, M$, to be different. Polynomial boundary-adapted modal basis functions based either on Legendre polynomials or Chebyshev polynomials of the first kind are the type of bases that we have considered for the spectral-Galerkin method. Details about the computation of the components of matrices $\hat{\mathbf{A}}$, $\hat{\mathbf{B}}$ and $\hat{\mathbf{C}}$, defined in expressions (6.19), can be found in Chapter 4 (§4.3.1 for Legendre polynomials and §4.4.1 for Chebyshev polynomials) for the case of single domain problems (i.e., problems in which the material is homogeneous). On the other hand, for multi-domains problems (as when dealing with heterogeneous materials) the components of the matrices defined in expressions (6.19) can be computed by replacing the integral over Ω with a sum of integrals over the disjoint elements Ω_m, with $m = 1, \ldots, M$. Then, each of these integrals can be computed by relying again on the results presented in Chapter 4. Moreover, since the boundary-adapted polynomial basis functions defined in the previous section are formed by boundary and bubble basis functions supported over one subdomain and interface basis functions supported by two contiguous subdomains, it follows that the only entries whose value is determined by more than one subdomain are those associated to the interface basis functions.

Linear Galerkin Finite Element Basis Functions

In the context of the Finite Element Method, one usually considers a partition of the domain into a number of elements $M > 1$ such that the physical parameters ρ, λ_{el} and λ_{vi} are constant within each of them. Therefore, in this case the partition of the domain Ω is not related to the number of materials involved. The size of the elements $\Omega_m = (x_{m-1}, x_m)$, $m = 1, \ldots, M$, is allowed to vary from one element to another and is denoted by h_m, i.e., $h_m := x_m - x_{m-1}$. Moreover, we define the mesh size parameter $h := \max_m h_m$. Within this work, we consider the finite-dimensional space $V_N \subset H^1(\Omega)$ (hereafter denoted by V_h, as it is usually done in the context of Finite Elements) to be constituted by continuous and piecewise linear functions. Since only one straight line can connect two different points and the basis functions are required to be continuous over Ω, the number of degrees of freedom of the functions in V_h, i.e., the values that must be assigned to uniquely define the functions themselves, is equal to the number of vertices $(M + 1)$ of the partition. As a consequence we only need to define $M + 1$ linearly independent basis functions. A typical choice is given by the characteristic Lagrangian basis functions ψ_m, which we recall that are characterised by the following property

$$\psi_m(x_n) = \delta_{mn}, \qquad m, n = 0, 1, \ldots, M,$$

δ_{mn} being the Kronecker delta. The nodal function ψ_m is therefore piecewise linear and equal to one at x_m and zero in the remaining nodes of the partition. More precisely, the linear Lagrangian basis function ψ_m associated to node x_m is defined as

$$\psi_m(x) = \begin{cases} \dfrac{x - x_{m-1}}{x_m - x_{m-1}}, & \text{for } x_{m-1} \le x \le x_m, \\ \dfrac{x_{m+1} - x}{x_{m+1} - x_m}, & \text{for } x_m \le x \le x_{m+1}, \\ 0, & \text{otherwise.} \end{cases}$$

When $m \neq 0$ and $m \neq M$ the basis function ψ_m has as support the union of the intervals $\bar{\Omega}_m = (x_{m-1}, x_m]$ and $\bar{\Omega}_{m+1} = [x_m, x_{m+1})$. On the other hand, for $m = 0$ and $m = M$ the support is limited to the first and last intervals, i.e., to $\bar{\Omega}_1 = (x_0, x_1]$ and $\bar{\Omega}_M = [x_{M-1}, x_M)$, respectively. In other words, in the context of linear Finite Elements, the set of basis functions $\mathcal{B}_N$ defined in (6.21) is formed only by boundary and interface basis functions, whereas bubble functions are not included (due to the low polynomial degree). Moreover, the set of basis functions $\mathcal{B}_{N_0}$ is obtained, as already mentioned, from $\mathcal{B}_N$ by disregarding the linear Lagrangian basis function ψ_0 associated to the node $x_0 = a$ where Dirichlet boundary conditions are imposed. Owing to the fact that the only basis functions whose support overlaps with that of ψ_m are ψ_{m-1} and ψ_{m+1}, it follows that the matrices defined by expressions (6.19) are tridiagonal. In particular, taking $\hat{\phi}_i \equiv \psi_i$, $i = 0, \ldots, M$, we have:

$$\mathbf{C}_{i,j} = c(\hat{\phi}_j, \hat{\phi}_i) = \int_\Omega \rho\, \hat{\phi}_j\, \hat{\phi}_i\, dx = \sum_{m=1}^{M} \rho_m \int_{\Omega_m} \hat{\phi}_j\, \hat{\phi}_i\, dx = \begin{cases} \rho_{i+1} \dfrac{h_{i+1}}{6}, & j = i + 1, \\ \rho_i \dfrac{h_i}{3} + \rho_{i+1} \dfrac{h_{i+1}}{3}, & i = j \\ \rho_i \dfrac{h_i}{6}, & j = i - 1, \\ 0, & \text{otherwise.} \end{cases}$$

$$\mathbf{B}_{i,j} = b(\hat{\phi}_j, \hat{\phi}_i) = \int_\Omega \lambda_{\text{vi}} \frac{d\hat{\phi}_j}{dx} \frac{d\hat{\phi}_i}{dx}\, dx = \sum_{m=1}^{M} \lambda_{vi,m} \int_{\Omega_m} \frac{d\hat{\phi}_j}{dx} \frac{d\hat{\phi}_i}{dx}\, dx = \begin{cases} -\dfrac{\lambda_{vi,i+1}}{h_{i+1}}, & j = i + 1, \\ \dfrac{\lambda_{vi,i}}{h_i} + \dfrac{\lambda_{vi,i+1}}{h_{i+1}}, & i = j \\ -\dfrac{\lambda_{vi,i}}{h_i}, & j = i - 1, \\ 0, & \text{otherwise.} \end{cases}$$

$$\mathbf{A}_{i,j} = a(\hat{\phi}_j, \hat{\phi}_i) = \int_\Omega \lambda_{\text{el}} \frac{d\hat{\phi}_j}{dx} \frac{d\hat{\phi}_i}{dx}\, dx = \sum_{m=1}^{M} \lambda_{el,m} \int_{\Omega_m} \frac{d\hat{\phi}_j}{dx} \frac{d\hat{\phi}_i}{dx}\, dx = \begin{cases} -\dfrac{\lambda_{el,i+1}}{h_{i+1}}, & j = i+1, \\ \dfrac{\lambda_{el,i}}{h_i} + \dfrac{\lambda_{el,i+1}}{h_{i+1}}, & i = j \\ -\dfrac{\lambda_{el,i}}{h_i}, & j = i-1, \\ 0, & \text{otherwise.} \end{cases}$$

These three matrices and the matrices obtained from them by removing the first row and/or the first column (which are associated to the basis function defined on $x_0 \equiv a$) are sufficient to build all the block matrices arising from the Galerkin Finite Element discretisation with linear basis functions.

6.1.3 Convergence of the Semi-Discrete Solution

In this section we derive the convergence rate for the V_m-norm of the error $U(t) - U_N(t)$, where $U(t)$ is the solution of the continuous problem (6.7) at time t and $U_N(t)$ is the solution of the semi-discrete problem (6.12) at time t obtained by using either the Spectral or the Linear Finite Element Method. We start by recalling the result given by Corollary 5.1, which states that, for any $t \geq 0$, the following error estimate holds:

$$\|U(t) - U_N(t)\|_{V_m} \lesssim \inf\{\|U(t) - \Phi\|_{V_\ell} \ : \ \Phi \in \mathcal{V}_{N_0}\} + e^{\lambda t} \int_0^t \inf\{\|\partial_s(e^{-\lambda s}U(s)) - \Phi\|_{V_\ell} \ : \ \Phi \in \mathcal{V}_{N_0}\}\, ds. \quad (6.22)$$

The convergence rate for both the Spectral and Finite Element Method is then obtained by providing an appropriate upper bound for the quantity

$$\inf\{\|U(t) - \Phi\|_{V_\ell} \ : \ \Phi \in \mathcal{V}_{N_0}\}.$$

In particular, the upper bound will depend on the discretisation parameter, which we recall is the polynomial degree N, in the case of the Spectral Method, and the mesh size h for the Finite Element Method.

Spectral Method Using the results from orthogonal polynomials approximation theory preseted in Section 4.6 and, in particular, equations (4.28) and (4.29), we obtain that, for all $v \in H^2(\Omega)$, the following estimate holds:

$$\inf\{\|u - \phi\|_{H^1} \ : \ \phi \in \mathbb{P}_N\} \leq CN^{-1}|u|_{H^2}.$$

Therefore, in the Spectral method, when using Legendre polynomials defined over the whole domain Ω, the estimate (6.22) becomes

$$\begin{aligned} \|U(t) - U_N(t)\|_{V_m} &\leq CN^{-1}\left(|U(t)|_{H^2(\Omega)^2} + e^{\lambda t}\int_0^t |\partial_s(e^{-\lambda s}U(s))|_{H^2(\Omega)^2}\, ds\right) \\ &\leq CN^{-1}\left(|U(t)|_{H^2(\Omega)^2} + e^{\lambda t}\max_{s\in(0,t)} e^{-\lambda s}\left(\lambda|U(s)|_{H^2(\Omega)^2} + |\dot{U}(s)|_{H^2(\Omega)^2}\right)\right). \end{aligned} \quad (6.23)$$

Finite Element Method Within the Linear Finite Element framework, from (3.17) and (3.18) we obatin that, for all $v \in H^2(\Omega)$, the following estimate holds

$$\inf\{\|v - \phi\|_{H^1(\Omega)} \ : \ \phi \in V_{N_0}\} \leq Ch|v|_{H^2(\Omega)}.$$

Substituting this estimate into the estimate (6.22) yields

$$\begin{aligned} \|U(t) - U_N(t)\|_{V_m} &\leq Ch\left(|U(t)|_{H^2(\Omega)^2} + e^{\lambda t}\int_0^t |\partial_s(e^{-\lambda s}U(s))|_{H^2(\Omega)^2}\, ds\right) \\ &\leq Ch\left(|U(t)|_{H^2(\Omega)^2} + e^{\lambda t}\max_{s\in(0,t)} e^{-\lambda s}\left(\lambda|U(s)|_{H^2(\Omega)^2} + |\dot{U}(s)|_{H^2(\Omega)^2}\right)\right). \end{aligned} \quad (6.24)$$

6.1.4 Numerical Simulations

In this section we discuss some results that we have obtained by applying the proposed numerical approach to one-dimensional problems. We first study the convergence in space of the schemes by solving some problems with manufactured solution and then we investigate the propagation of 1D waves in both homogeneous and heterogeneous materials.

Numerical Convergence

We investivage the convergence of the Spectral and Finite Element methods by solving two problems having exact solution. The first problem has the purpose of showing the capability of the Spectral method to achieve exponential convergence when the solution exibiths high regularity; in this case no forcing term is present. The second problem features a solution with low regularity and aims at experimentally deriving some convergence rates for both the Spectral and the Finite Element methods; in this case an external forcing terms is added to the displacement equations of motion. As is usually done in this type of experiment, we solve both the problems by using several values of the discretisation parameter (i.e., the basis functions polynomial degree N for the Spectral method and the mesh parameter h for the Finite Element Method) and we then look at the behaviour of the norm of the error computed at time t as a function of this parameter. In particular, we report the bahaviour of the relative error computed using both the L^2 and the V_m norms, which are expressed by

$$\varepsilon_{L^2}(t) = \frac{\|U(t) - U_N(t)\|_{L^2(\Omega)}}{\|U(t)\|_{L^2(\Omega)}} \qquad \varepsilon_{V_m}(t) = \frac{\|U(t) - U_N(t)\|_{V_m}}{\|U(t)\|_{V_m}}$$

Without source term We consider a displacement function having the form

$$u(x,t) = u_0 \exp(i\omega t - ikx) \tag{6.25}$$

where $u_0 \in \mathbb{R}$ is the amplitude, ω is the angular frequency and k is the wave number. Substituting expression (6.25) into the displacement equation of motion (6.1) with Kelvin-Voigt constitutive model (6.2), we find that the following equation must be satisfied for the displacement (6.25) to be solution of (6.1)-(6.2):

$$\rho\omega^2 = k^2\lambda_{\text{el}} + i\omega k^2 \lambda_{\text{vi}}$$

Clearly, we have two possibilities for solving this equation: either we fix a value for ω and compute k or we fix the value of k and compute ω. We consider both these two scenarios, as we will see that they lead to different types of propagating waves. Let us first consider the case in which the angular frequency is given, i.e., $\omega \equiv \omega_0 \in \mathbb{R}$. Then, the wavenumber k is given by:

$$k = \sqrt{\frac{\rho\omega_0^2}{\lambda_{\text{el}} + i\omega_0\lambda_{\text{vi}}}} = \sqrt{\frac{\rho\omega_0^2\lambda_{\text{el}}}{\lambda_{\text{el}}^2 + \omega_0^2\lambda_{\text{vi}}^2} - i\frac{\rho\omega_0^3\lambda_{\text{vi}}}{\lambda_{\text{el}}^2 + \omega_0^2\lambda_{\text{vi}}^2}} \tag{6.26}$$

Note that k is a complex number whose imaginary part is negative when $\omega > 0$. Then, writing (6.25) as

$$u(x,t) = \exp(\Im(k)x)\exp(i\omega_0 t - i\Re(k)x) \tag{6.27}$$

we clearly see that $\Im(k)$ is responsible for the attenuation of the wave in space. On the other hand, if we fix the value of the wavenumber and assume it to be real, i.e., $k \equiv k_0 \in \mathbb{R}$, we obtain the following values for the anguar frequency ω:

$$\omega = \frac{i\lambda_{\text{vi}}k_0^2 \pm \sqrt{(i\lambda_{\text{vi}}k_0^2)^2 + 4\rho k_0^2\lambda_{\text{el}}}}{2\rho}. \tag{6.28}$$

The two solutions turn out to be complex and with opposite nonzero real part provided that $4\rho\lambda_{\text{el}} - \lambda_{\text{vi}}^2 k_0^2 > 0$. In this case the imaginary part is responsible for the attenuation of the propagating wave

Problem type	ρ [kg m^{-1}]	λ_{el} [kg m s^{-2}]	λ_{vi} [kg m s^{-1}]	ω [rad s^{-1}]	k [rad m^{-1}]
space attenuation	1	0.5	0.01	3.5	$4.9407 - 0.1727i$
time attenuation	1	0.5	0.1	$3.3072 + 1.2500i$	5

Table 6.1: Parameters used to solve the two problems with exact solution given by (6.25).

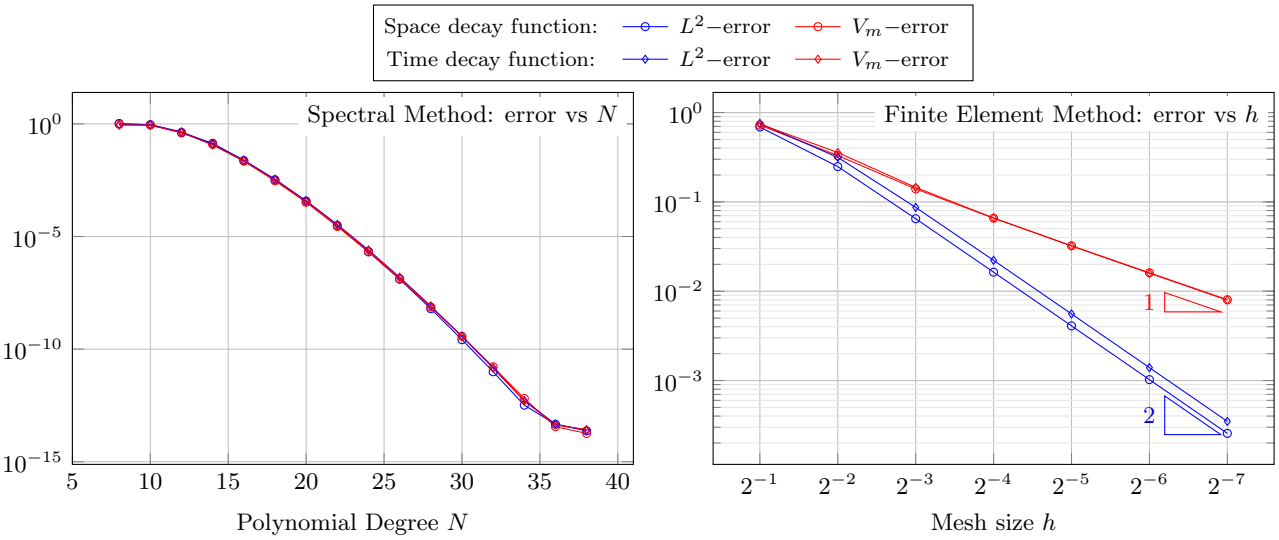


Figure 6.1: Behaviour of the relative errors ε_{L^2} (blue line) and ε_{V_m} (red line) for the problem whose exact solution is given by (6.25). The errors are computed at time $t = 1\,\text{s}$. The left panel shows the errors obtained with the Spectral Method as a function of the basis polynomial degree N: for both norms, exponential convergence of the numerical solution to the exact solution is achieved. The right panel shows the errors obtained with the Finite Element Method as functions of the mesh size h: linear and quadratic convergence are achieved for the V_m and L^2 norms, respectively.

in time. Indeed, the contribution given by the real and imaginary part of ω can be highlighted again by rewriting (6.25) as follows:

$$u(x,t) = \exp(-\Im(\omega)t)\exp(i\Re(\omega)t - ik_0x) \tag{6.29}$$

We solve both the problems on the domain $\Omega = (0,5)$ with homogeneous physical properties defined by the parameters $\rho = 1\,\text{kg m}^{-1}$, $\lambda_{\text{el}} = 0.5\,\text{kg m s}^{-2}$ and $\lambda_{\text{vi}} = 0.01\,\text{kg m s}^{-1}$ for the problem with attenuation in space and parameters $\rho = 1\,\text{kg m}^{-1}$, $\lambda_{\text{el}} = 0.5\,\text{kg m s}^{-2}$ and $\lambda_{\text{vi}} = 0.1\,\text{kg m s}^{-1}$ for the problem with attenuation in time. Moreover, in the first case we choose $\omega_0 = 3.5\,\text{rad s}^{-1}$ and compute $k \in \mathbb{C}$ using (6.26), whereas in the second case and we choose $k_0 = 5\,\text{rad m}^{-1}$ and compute $\omega \in \mathbb{C}$ using (6.28). All the parameters used to define the two problems are also listed in Table 6.1. The initial conditions and the boundary conditions are computed using the exact solution. In particular, we impose time-dependent Dirichlet boundary conditions on the left endpoint (i.e., $x = 0$) and time-dependent Neumann boundary conditions on the right endpoint (i.e., $x = 5$). The relative errors ε_{L^2} and ε_{V_m} are computed at time $t = 1\,\text{s}$. The problems are solved exactly in time by using the procedure based on eigenvalue decomposition and matrix exponential explained in Section 5.3.3. Therefore, we are not introducing any additional error as instead would be the case if a time stepping procedure were employed. Figure 6.1 shows the behaviour of the relative errors ε_{L^2} and ε_{V_m} obtained by solving the two problems by means of the Spectral Method (left panel) and of the Linear Finite Element Method (right panel). More precisely, the red line shows the behaviour of ε_{V_m} whereas the blue line displays the behavuour of ε_{L^2}. Moreover, different marker types are used to distinguish the two problems: the diamond is associated to the problem charactersised by attenuation in space, i.e., the problem whose solution is given by (6.27), whereas the cirle identifies the problem characterised by attenuation in time, i.e., the problem whose solution has the form (6.29). In the left panel (Spectral Method) the errors are plotted against the basis functions polynomial degree N. For both the problems and both

the norms we observe exponential convergence of the numerical solution to the exact one, a result that is expected when using spectral methods to solve problems with very smooth solutions. On the other hand, the right panel (Finite Element Method) shows the relative errors as functions of the mesh size h. In this case, the logarithmic plot clearly displays different convergence rates depending on the type of norm being used to compute the errors. In particular, we observe that quadratic convergence in the mesh parameter h is achieved for the L^2 norm of the solution, whereas the convergence is linear for the V_m-norm of the error. The results about the V_m norm validates the error estimate derived in (6.24). The errors are also listed in Tables 6.2 (Spectral Method), 6.3 and 6.4 (FEM).

	Space decay function		Time decay function	
polynomial degree	relative error L^2	relative error V_m	relative error L^2	relative error V_m
8	$1.04712e+00$	$9.68838e-01$	$9.02938e-01$	$8.97609e-01$
12	$3.99430e-01$	$4.21055e-01$	$4.42207e-01$	$4.09441e-01$
16	$2.35277e-02$	$2.21886e-02$	$2.47478e-02$	$2.24450e-02$
20	$3.73798e-04$	$3.29808e-04$	$3.86025e-04$	$3.56166e-04$
24	$2.15211e-06$	$2.05490e-06$	$2.51784e-06$	$2.36546e-06$
28	$6.21826e-09$	$7.42946e-09$	$8.18977e-09$	$7.80799e-09$
32	$9.88331e-12$	$1.64274e-11$	$1.47869e-11$	$1.42921e-11$
36	$4.60316e-14$	$3.60499e-14$	$4.70063e-14$	$4.25595e-14$

Table 6.2: Spectral Method: relative errors, at $t = 1\,\mathrm{s}$, for the two problems with exact solution given by expression (6.25).

#ref	#elements	h	relative error L^2	rate L^2	relative error V_m	rate V_m
-	5	2^0	$1.42378e+00$	-	$1.24105e+00$	-
1	10	2^{-1}	$6.89119e-01$	1.04690	$7.23111e-01$	0.77927
2	20	2^{-2}	$2.48420e-01$	1.47197	$3.30043e-01$	1.13156
3	40	2^{-3}	$6.48180e-02$	1.93832	$1.39778e-01$	1.23952
4	80	2^{-4}	$1.63376e-02$	1.98820	$6.57207e-02$	1.08871
5	160	2^{-5}	$4.09216e-03$	1.99726	$3.23000e-02$	1.02481
6	320	2^{-6}	$1.02352e-03$	1.99933	$1.60787e-02$	1.00639
7	640	2^{-7}	$2.55908e-04$	1.99983	$8.03037e-03$	1.00161

Table 6.3: FEM: relative errors, at time $t = 1\,\mathrm{s}$, for the problem with attenuation in space.

#ref	#elements	h	relative error L^2	rate L^2	relative error V_m	rate V_m
-	5	2^0	$2.89740e+00$	-	$2.17330e+00$	-
1	10	2^{-1}	$7.55575e-01$	1.93911	$7.43052e-01$	1.54835
2	20	2^{-2}	$3.15208e-01$	1.26127	$3.57210e-01$	1.05669
3	40	2^{-3}	$8.67431e-02$	1.86148	$1.45250e-01$	1.29823
4	80	2^{-4}	$2.21564e-02$	1.96902	$6.60212e-02$	1.13754
5	160	2^{-5}	$5.56803e-03$	1.99248	$3.20702e-02$	1.04169
6	320	2^{-6}	$1.39381e-03$	1.99814	$1.59134e-02$	1.01099
7	640	2^{-7}	$3.48565e-04$	1.99953	$7.94137e-03$	1.00279

Table 6.4: FEM: relative errors, at time $t = 1\,\mathrm{s}$, for the problem with attenuation in time.

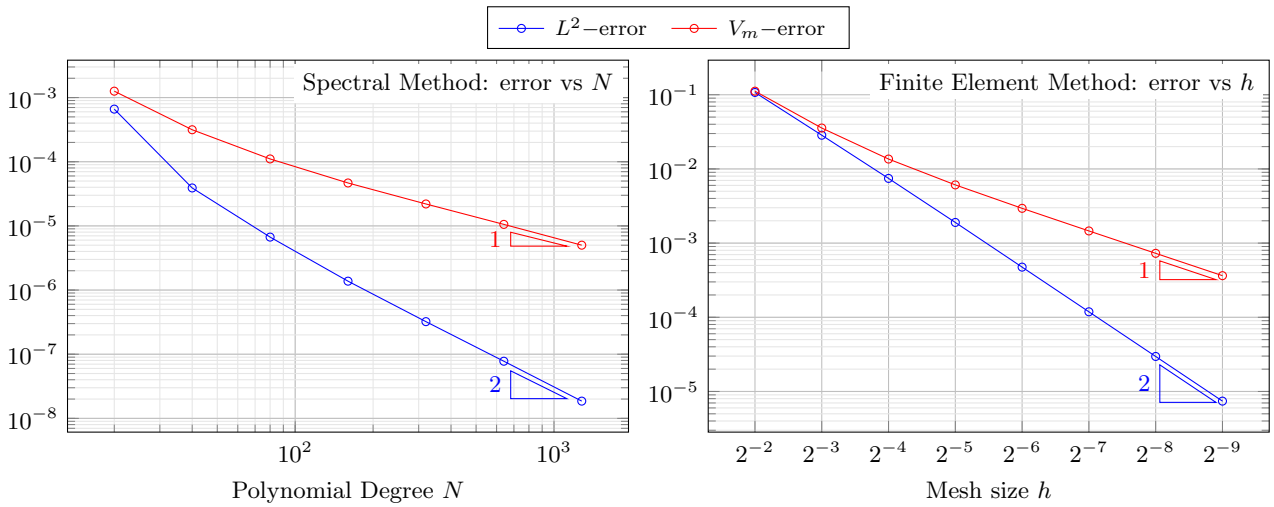


Figure 6.2: Behaviour of the relative errors ε_{L^2} (blue line) and ε_{V_m} (red line) obtained by solving a manufactured problem with non-zero forcing function by means of the Spectral Method (left panel) and of the Linear Finite Element Method (right panel). The problem has exact solution given by $u(x,t) := s(t)r(x)$, where s and r are defined in (6.30). The errors are computed at time $t = 0.1\,\mathrm{s}$ and are shown as a function of the discretisation parameters, i.e., the polynomial degree N (Spectral Method) and the mesh size h (FEM).

With source term We consider a displacement function $u\colon \Omega \times [0,\infty) \to \mathbb{R}$, with $\Omega = (-1,+1)$, that can be written in the form $u(x,t) = s(x)r(t)$, where the functions r and s are defined as follows

$$s\colon [0,\infty) \to \mathbb{R} \qquad t \mapsto s(t) := \sin(2\pi k t), \tag{6.30a}$$

$$r\colon \Omega \to \mathbb{R} \qquad x \mapsto r(x) := \begin{cases} 2x^2 + x, & \text{if } -1 \le x \le 0, \\ \frac{16}{21}x^{7/4} + x, & \text{if } 0 < x \le 1. \end{cases} \tag{6.30b}$$

The function $r(x)$ is only $C^1(\Omega)$ with its second derivative being constant on $\Omega_- := (-1,0)$ and equal to $x^{-1/4}$ in $\Omega_+ := (0,+1)$. Therefore, we have $u(t) \in H^2(\Omega)$ for any $t \ge 0$. For the displacement function u defined above to be solution of the Cauchy momentum equations (6.1) with Kelvin-Voigt constitutive model (6.2), we need to consider a suitable non-zero external forcing term f_{ext}. This term is obtained by substituting the expression of $u(x,t)$ (and the expressions of its derivatives in space and time) into Equation (6.3a). The initial conditions and the boundary conditions are computed using the exact solution. In particular, we impose time-dependent Dirichlet boundary conditions on both the endpoints of the domain. The material is assumed to be homogeneous and characterised by the following material parameters: $\rho = 1\,\mathrm{kg\,m^{-1}}$, $\lambda_{\mathrm{el}} = 1\,\mathrm{kg\,m\,s^{-2}}$ and $\lambda_{\mathrm{vi}} = 0.002\,\mathrm{kg\,m\,s^{-1}}$. As in the previous problem, the system of ODEs is solved exactly (up to machine precision) in time by using the procedure based on eigenvalue decomposition and matrix exponential discussed in §5.3.3. The relative errors ε_{L^2} and ε_{V_m} are computed at time $t = 0.1\,\mathrm{s}$. Figure 6.2 shows the behaviour of the relative errors for both the Spectral method (left panel) and the Finite Element Method (right panel) against the discretisation parameters N and h, respectively. As expected, the Finite Element solution exhibits the same convergence rates that we have already observed in the previous problem, i.e., linear for the V_m norm and quadratic for the L^2 norm. More interesting are the results obtained with the Spectral Method: indeed, owing to the lower regularity of the displacement function u, we do not achieve the exponential convergence of the numerical solution to the exact one that was observed in Figure 6.1 and related to the problem whose exact solution was given by (6.25). More precisely, we observe a linear convergence in N for the V_m norm and a quadratic convergence in N for the L^2 norm, thus validating the convergence rates derived in (6.23) when $u(t) \in H^2(\Omega)$ for all $t \ge 0$. The errors are also listed in Tables 6.5 (Spectral Method), 6.6 (FEM).

N	relative error L^2	rate L^2	relative error V_m	rate V_m
20	$6.61013e-04$	-	$1.25882e-03$	-
40	$3.90452e-05$	4.08146	$3.15240e-04$	1.99755
80	$6.69104e-06$	2.54484	$1.10593e-04$	1.51119
160	$1.37552e-06$	2.28225	$4.66777e-05$	1.24446
320	$3.21836e-07$	2.09558	$2.19670e-05$	1.08740
640	$7.77635e-08$	2.04916	$1.05579e-05$	1.05701
1280	$1.85724e-08$	2.06593	$5.00545e-06$	1.07676

Table 6.5: Spectral Method: relative errors, at time $t = 1\,\mathrm{s}$, for the problem with forcing function.

#ref	#elements	h	relative error L^2	rate L^2	relative error V_m	rate V_m
0	8	2^{-2}	$1.07452e-01$	-	$1.11770e-01$	-
1	16	2^{-3}	$2.84816e-02$	1.91559	$3.55939e-02$	1.65083
2	32	2^{-4}	$7.45144e-03$	1.93444	$1.35907e-02$	1.38901
3	64	2^{-5}	$1.89938e-03$	1.97199	$6.09255e-03$	1.15750
4	128	2^{-6}	$4.74616e-04$	2.00069	$2.94452e-03$	1.04901
5	256	2^{-7}	$1.18620e-04$	2.00042	$1.45947e-03$	1.01259
6	512	2^{-8}	$2.96521e-05$	2.00014	$7.28275e-04$	1.00288
7	1024	2^{-9}	$7.41262e-06$	2.00008	$3.64008e-04$	1.00051

Table 6.6: FEM: relative errors, at time $t = 1\,\mathrm{s}$, for the problem with forcing function.

Application Example: Homogeneous and Heterogeneous Materials

In this numerical example we compare the propagation of 1D displacement waves on homogeneous and heterogeneous materials. The problem is defined on the domain $\Omega = \bar{\Omega}_1 \cup \bar{\Omega}_2$, where $\Omega_1 = (0, 2)$ and $\Omega_2 = (2, 4)$. Concerning the material parameters, we consider three different scenarios (see also Table 6.7):

(i) homogeneous material having density $\rho^0 = 1\,\mathrm{kg\,m^{-1}}$, elasticity $\lambda^0_{\mathrm{el}} = 1\,\mathrm{kg\,m\,s^{-2}}$ and viscosity $\lambda^0_{\mathrm{vi}} = 7.5 \times 10^{-4}\,\mathrm{kg\,m\,s^{-1}}$ on Ω;

(ii) heterogeneous material with constant density ρ^0 and elasticity λ^0_{el} on Ω and piecewise constant viscosity given by $\lambda_{\mathrm{vi}} = \lambda^0_{\mathrm{vi}}$ on Ω_1 and $\lambda_{\mathrm{vi}} = 20\lambda^0_{\mathrm{vi}}$ on Ω_2;

(iii) heterogeneous material with constant density ρ^0 and viscosity λ^0_{vi} on Ω and piecewise constant elasticity given by $\lambda_{\mathrm{el}} = \lambda^0_{\mathrm{el}}$ on Ω_1 and $\lambda_{\mathrm{el}} = 3\lambda^0_{\mathrm{el}}$ on Ω_2.

We consider zero initial condition for both the displacement and the velocity. On the left endpoint of the domain (i.e., $x = 0\,\mathrm{m}$), we impose time-dependent Dirichlet boundary conditions defined by the function $u_D(t) = A\sin(2\pi kt)$, where $A = 1\,\mathrm{m}$ and $k = 3\,\mathrm{Hz}$, whereas on the right endpoint of the domain (i.e., $x = 4\,\mathrm{m}$), we impose zero Neumann boundary conditions. Moreover, as when we investigated the numerical convergence of the scheme, the problem is solved exactly in time by using the procedure explained in Section 5.3.3. We solve the problem by means of the Spectral Method and we consider boundary-adapted Legendre bases having degree up to 100 on both the subdomains Ω_1 and Ω_2. The numerical results are shown in Figure 6.3. Each row refers to a different time, whereas the three columns refer to the three different material configurations described above. A vertical green line is used to highlight the location of the material interface in the second and third cases with varying viscosity and elasticity, while it is used only as a help line in the first case with the aim of facilitating the comparison with the other two material configurations. Looking at the first two rows of Figure 6.3, we see that the results are the same for all the material configurations. This was expected since the displacement wave, that started to propagate due to the time-dependent Dirichlet boundary conditions imposed on $x = 0$, is still confined in left subdomain (Ω_1), where the material properties are the same

Material configuration	Ω_1	Ω_2
Case (i): homoegeneous material	ρ_0, λ^0_{el}, λ^0_{vi}	ρ_0, λ^0_{el}, λ^0_{vi}
Case (ii): heterogeneous material (varying viscosity)	ρ_0, λ^0_{el}, λ^0_{vi}	ρ_0, λ^0_{el}, $20\lambda^0_{\text{vi}}$
Case (iii): heterogeneous material (varying elasticity)	ρ_0, λ^0_{el}, λ^0_{vi}	ρ_0, $3\lambda^0_{\text{el}}$, λ^0_{vi}

Table 6.7: Summary of the different material configurations considered in the numerical example.

for all the material configurations. Starting from the thrid row we see that the numerical results depend on the material configuration, since the wave is now propagating on Ω_2. More precisely, in the second column plot, which refers to the problem with higher viscosity in Ω_2, we observe a stronger attenuation of the propagating displacement wave, whereas in the third column plot, which refers to the problem with higher elasticity on Ω_2, we observe that the wave is moving with an higher phase velocity. Furthermore, in this case we also observe a reflecting wave that originated at the material interface and is propagating towards the left endpoint. This considerations are even more evident in the plots shown in the fourth row, where we can see that the displacement wave shown in the third column has almost reached the right endpoint of the domain, whereas in the other two cases it is still behind. In the plots shown in the fifth row we see that even the displacement waves related to the first and second material configurations have now reached the right endpoint of the domain where zero Neumann boundary condition is imposed. Owing to this boundary condition, we observe in the plot in the third column a reflecting wave that propagates towards left producing an increase in the wave amplitude. Finally, looking at the results in the sixth row, we can observe the effect of zero Neumann boundary conditions also in the case of homogeneous material (first column), whereas it is almost impossible to observe this behaviour in the second column because of the high viscosity that dampens the amplitude of the wave.

6.2 Two-dimensional Cartesian Coordinates

In this section we discuss the numerical solution of the displacement equations of motion with Kelvin-Voigt constitutive model in a two-dimensional domain using Cartesian Coordinates. We start by showing in Section 6.2.1 that the two-dimensional problem to be solved can be obtained by assuming that the three-dimensional motion is independent of one space dimension, say y. Indeed, under this assumption, the displacement equations of motion can be decoupled into a scalar partial differential equation for the displacement $u_y(x, z)$, which describes the propagation of SH-waves, and a vector partial differential equation for the displacement field $(u_x(x, z), u_z(x, z))$, which describes the propagation of P-SV waves. The latter will be the focus of this section. In Section 6.2.2 we show how to construct the sets of basis functions employed in the Galerkin discretisation in space of the weak formulation when applying the Spectral (Element) Method and the Finite Element Method. More specifically, for the Spectral (Element) Method we consider a partition of the domain into rectangular elements, each one characterised by different material properties, and we define globally continuous basis functions by glueing boundary-adapted polynomials defined within each element by tensorization of two families of one-dimensional polynomial bases. For the Finite Element Method we consider linear Lagrangian basis functions defined at the nodes of a regular triangulation of the domain. Finally, in Section 6.2.3 we present some results that have been obtained by employing the discussed numerical approaches to solve the weak formulation of the two-dimensional initial-boundary value problem. As in the one-dimensional setting, we first show the convergence of the implemented numerical algorithms by solving some problems with manufactured solution and subsequently we simulate the propagation of waves generated by the action of a point load in both homogeneous and heterogeneous materials.

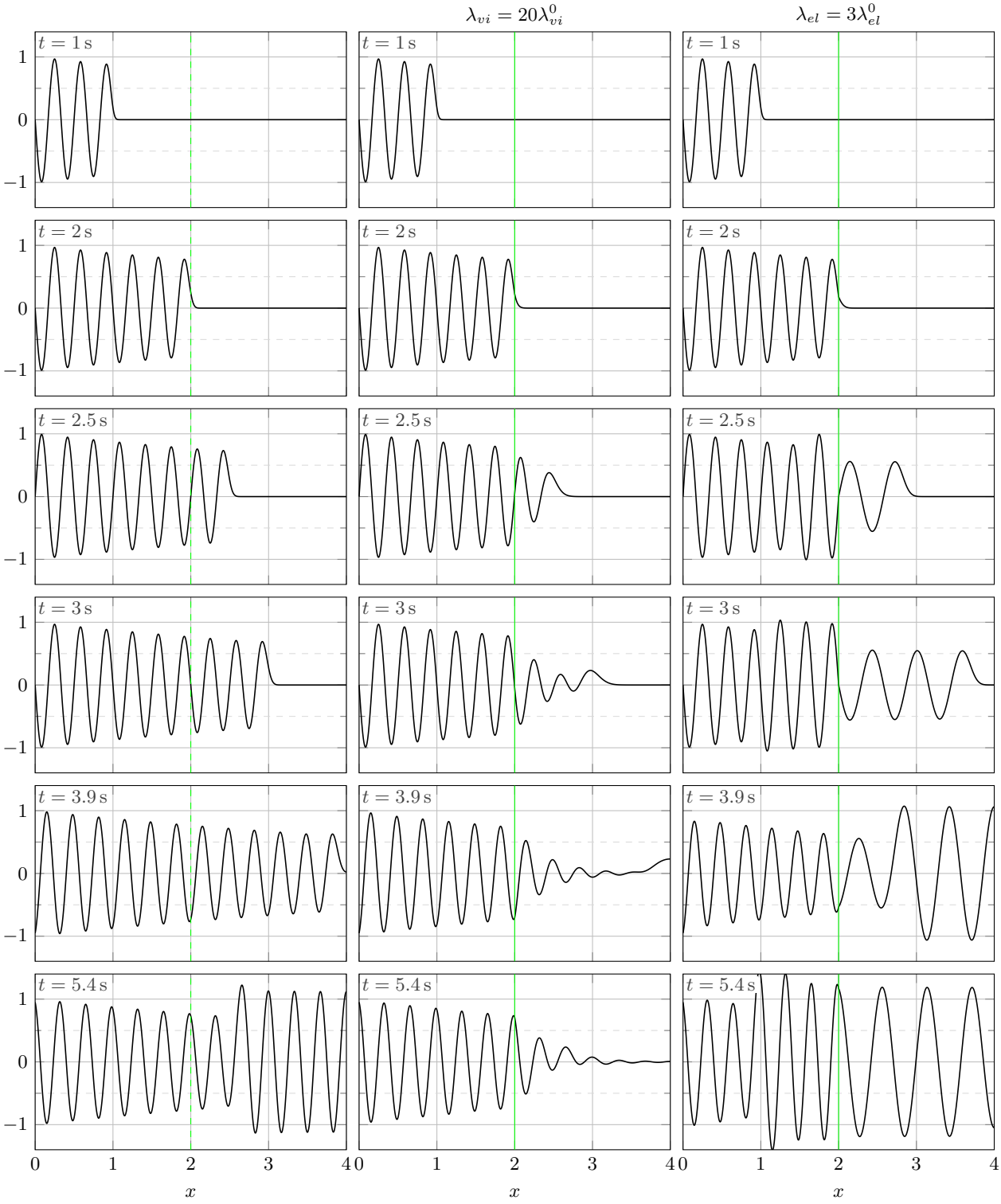


Figure 6.3: Numerical example comparing the propagation of one-dimensional waves on homogeneous and heterogenous materials. Each row refer to a different time, whereas each column refers to a different material configuration. The material in the first column is homogeneous and characterised by density $\rho^0 = 1\,\mathrm{kg\,m^{-1}}$, elasticity $\lambda_{\mathrm{el}} = 1\,\mathrm{kg\,m\,s^{-2}}$ and viscosity $\lambda_{\mathrm{vi}} = 7.5 \times 10^{-4}\,\mathrm{kg\,m\,s^{-1}}$. In the second column, we consider an heterogeneous material with a viscosity that is 20 times higher in $\Omega_2 = (2, 4)$, whereas in the third column we consider an heterogeneous material with an elasticity that is three times higher in Ω_2.

6.2.1 Problem Formulation

In the three-dimensional case, the gradient of the displacement field is given by:

$$\nabla \boldsymbol{u} = \begin{bmatrix} \dfrac{\partial u_x}{\partial x} & \dfrac{\partial u_x}{\partial y} & \dfrac{\partial u_x}{\partial z} \\ \dfrac{\partial u_y}{\partial x} & \dfrac{\partial u_y}{\partial y} & \dfrac{\partial u_y}{\partial z} \\ \dfrac{\partial u_z}{\partial x} & \dfrac{\partial u_z}{\partial y} & \dfrac{\partial u_z}{\partial z} \end{bmatrix}$$

From (5.5), it follows that the three-dimensional displacement equations of motion have the following explicit expression:

$$\begin{aligned}
\rho \ddot{u}_x &= (\lambda_{\text{el}} + \mu) \frac{\partial}{\partial x} \left(\frac{\partial u_x}{\partial x} + \frac{\partial u_y}{\partial y} + \frac{\partial u_z}{\partial z} \right) + \mu \left(\frac{\partial^2 u_x}{\partial x^2} + \frac{\partial^2 u_x}{\partial y^2} + \frac{\partial^2 u_x}{\partial z^2} \right) \\
&\quad + (\lambda_{\text{vi}} + \eta) \frac{\partial}{\partial x} \left(\frac{\partial \dot{u}_x}{\partial x} + \frac{\partial \dot{u}_y}{\partial y} + \frac{\partial \dot{u}_z}{\partial z} \right) + \eta \left(\frac{\partial^2 \dot{u}_x}{\partial x^2} + \frac{\partial^2 \dot{u}_x}{\partial y^2} + \frac{\partial^2 \dot{u}_x}{\partial z^2} \right) + f_x \\
\rho \ddot{u}_y &= (\lambda_{\text{el}} + \mu) \frac{\partial}{\partial y} \left(\frac{\partial u_x}{\partial x} + \frac{\partial u_y}{\partial y} + \frac{\partial u_z}{\partial z} \right) + \mu \left(\frac{\partial^2 u_y}{\partial x^2} + \frac{\partial^2 u_y}{\partial y^2} + \frac{\partial^2 u_y}{\partial z^2} \right) \\
&\quad + (\lambda_{\text{vi}} + \eta) \frac{\partial}{\partial y} \left(\frac{\partial \dot{u}_x}{\partial x} + \frac{\partial \dot{u}_y}{\partial y} + \frac{\partial \dot{u}_z}{\partial z} \right) + \eta \left(\frac{\partial^2 \dot{u}_y}{\partial x^2} + \frac{\partial^2 \dot{u}_y}{\partial y^2} + \frac{\partial^2 \dot{u}_y}{\partial z^2} \right) + f_y \\
\rho \ddot{u}_z &= (\lambda_{\text{el}} + \mu) \frac{\partial}{\partial z} \left(\frac{\partial u_x}{\partial x} + \frac{\partial u_y}{\partial y} + \frac{\partial u_z}{\partial z} \right) + \mu \left(\frac{\partial^2 u_z}{\partial x^2} + \frac{\partial^2 u_z}{\partial y^2} + \frac{\partial^2 u_z}{\partial z^2} \right) \\
&\quad + (\lambda_{\text{vi}} + \eta) \frac{\partial}{\partial x} \left(\frac{\partial \dot{u}_x}{\partial x} + \frac{\partial \dot{u}_y}{\partial y} + \frac{\partial \dot{u}_z}{\partial z} \right) + \eta \left(\frac{\partial^2 \dot{u}_z}{\partial x^2} + \frac{\partial^2 \dot{u}_z}{\partial y^2} + \frac{\partial^2 \dot{u}_z}{\partial z^2} \right) + f_z
\end{aligned}$$

Now assuming the displacement field to be independent of the space variable y, we see that some terms vanish

$$\begin{aligned}
\rho \ddot{u}_x &= (\lambda_{\text{el}} + \mu) \frac{\partial}{\partial x} \left(\frac{\partial u_x}{\partial x} + \cancel{\frac{\partial u_y}{\partial y}} + \frac{\partial u_z}{\partial z} \right) + \mu \left(\frac{\partial^2 u_x}{\partial x^2} + \cancel{\frac{\partial^2 u_x}{\partial y^2}} + \frac{\partial^2 u_x}{\partial z^2} \right) \\
&\quad + (\lambda_{\text{vi}} + \eta) \frac{\partial}{\partial x} \left(\frac{\partial \dot{u}_x}{\partial x} + \cancel{\frac{\partial \dot{u}_y}{\partial y}} + \frac{\partial \dot{u}_z}{\partial z} \right) + \eta \left(\frac{\partial^2 \dot{u}_x}{\partial x^2} + \cancel{\frac{\partial^2 \dot{u}_x}{\partial y^2}} + \frac{\partial^2 \dot{u}_x}{\partial z^2} \right) + f_x \\
\rho \ddot{u}_y &= \cancel{(\lambda_{\text{el}} + \mu) \frac{\partial}{\partial y} \left(\frac{\partial u_x}{\partial x} + \frac{\partial u_y}{\partial y} + \frac{\partial u_z}{\partial z} \right)} + \mu \left(\frac{\partial^2 u_y}{\partial x^2} + \cancel{\frac{\partial^2 u_y}{\partial y^2}} + \frac{\partial^2 u_y}{\partial z^2} \right) \\
&\quad + \cancel{(\lambda_{\text{vi}} + \eta) \frac{\partial}{\partial y} \left(\frac{\partial \dot{u}_x}{\partial x} + \frac{\partial \dot{u}_y}{\partial y} + \frac{\partial \dot{u}_z}{\partial z} \right)} + \eta \left(\frac{\partial^2 \dot{u}_y}{\partial x^2} + \cancel{\frac{\partial^2 \dot{u}_y}{\partial y^2}} + \frac{\partial^2 \dot{u}_y}{\partial z^2} \right) + f_y \\
\rho \ddot{u}_z &= (\lambda_{\text{el}} + \mu) \frac{\partial}{\partial z} \left(\frac{\partial u_x}{\partial x} + \cancel{\frac{\partial u_y}{\partial y}} + \frac{\partial u_z}{\partial z} \right) + \mu \left(\frac{\partial^2 u_z}{\partial x^2} + \cancel{\frac{\partial^2 u_z}{\partial y^2}} + \frac{\partial^2 u_z}{\partial z^2} \right) \\
&\quad + (\lambda_{\text{vi}} + \eta) \frac{\partial}{\partial x} \left(\frac{\partial \dot{u}_x}{\partial x} + \cancel{\frac{\partial \dot{u}_y}{\partial y}} + \frac{\partial \dot{u}_z}{\partial z} \right) + \eta \left(\frac{\partial^2 \dot{u}_z}{\partial x^2} + \cancel{\frac{\partial^2 \dot{u}_z}{\partial y^2}} + \frac{\partial^2 \dot{u}_z}{\partial z^2} \right) + f_z
\end{aligned}$$

thus leading to the following system of partial differential equations

$$\rho\ddot{u}_x = (\lambda_{\text{el}}+\mu)\frac{\partial}{\partial x}\left(\frac{\partial u_x}{\partial x}+\frac{\partial u_z}{\partial z}\right)+\mu\left(\frac{\partial^2 u_x}{\partial x^2}+\frac{\partial^2 u_x}{\partial z^2}\right)+ \tag{6.31a}$$
$$+(\lambda_{\text{vi}}+\eta)\frac{\partial}{\partial x}\left(\frac{\partial \dot{u}_x}{\partial x}+\frac{\partial \dot{u}_z}{\partial z}\right)+\eta\left(\frac{\partial^2 \dot{u}_x}{\partial x^2}+\frac{\partial^2 \dot{u}_x}{\partial z^2}\right)+f_x$$
$$\rho\ddot{u}_y = \mu\left(\frac{\partial^2 u_y}{\partial x^2}+\frac{\partial^2 u_y}{\partial z^2}\right)+\eta\left(\frac{\partial^2 \dot{u}_y}{\partial x^2}+\frac{\partial^2 \dot{u}_y}{\partial z^2}\right)+f_y \tag{6.31b}$$
$$\rho\ddot{u}_z = (\lambda_{\text{el}}+\mu)\frac{\partial}{\partial z}\left(\frac{\partial u_x}{\partial x}+\frac{\partial u_z}{\partial z}\right)+\mu\left(\frac{\partial^2 u_z}{\partial x^2}+\frac{\partial^2 u_z}{\partial z^2}\right)+ \tag{6.31c}$$
$$+(\lambda_{\text{vi}}+\eta)\frac{\partial}{\partial z}\left(\frac{\partial \dot{u}_x}{\partial x}+\frac{\partial \dot{u}_z}{\partial z}\right)+\eta\left(\frac{\partial^2 \dot{u}_z}{\partial x^2}+\frac{\partial^2 \dot{u}_z}{\partial z^2}\right)+f_z.$$

It is easy to see that equation (6.31b) is decoupled from equations (6.31a) and (6.31c). Having denoted by ∇_2 the gradient with respect to the x and z space variables and by $\boldsymbol{u}_2$ the component of the displacement field $\boldsymbol{u}$ on the $xz-$plane, i.e., $\boldsymbol{u}_2 := (u_x, u_z)$, we can rewrite the system of partial differential equations (6.31) as follows:

$$\rho\ddot{\boldsymbol{u}}_2 = (\lambda_{\text{el}}+\mu)\nabla_2(\nabla_2\cdot\boldsymbol{u}_2)+\mu\Delta_2\boldsymbol{u}_2+(\lambda_{\text{vi}}+\eta)\nabla_2(\nabla_2\cdot\dot{\boldsymbol{u}}_2)+\eta\Delta_2\dot{\boldsymbol{u}}_2 \tag{P-SV}$$
$$\rho\ddot{u}_y = \mu\Delta_2 u_y+\eta\Delta_2\dot{u}_y \tag{SH}$$

The vector equation (P-SV) describes the propagation of P-SV waves, whereas the scalar equation (SH) describes the propagation of SH-waves. In this section we will focus on equation (P-SV) and simplify the notation by neglecting the subscript 2 appearing in $\boldsymbol{u}_2$ and ∇_2. It is worth noting that this equation is equal to the one discussed in Section 5.2 and therefore the weak formulation and the Galerkin semi-discretisation developed in that section apply here as well.

6.2.2 Basis Functions Definition

The weak formulation of the two-dimensional initial-boundary value problem governing the propagation of P-SV waves on Kelvin-Voigt materials is discretised in space by means of both the Galerkin Spectral (Element) Method and the Finite Element Method. In this subsection we introduce the basis functions that have been used and show how to compute the matrices arising from the semi-discretisation of the weak formulation.

Spectral-Galerkin Basis Functions

To define the Spectral-Galerkin basis functions on a domain $\Omega\subset\mathbb{R}^2$, we follow a procedure similar to the one described in Section 6.1.2, where we have defined one-dimensional polynomial basis functions.

1. We perform a partition of the domain $\Omega\subset\mathbb{R}^2$ into M disjoint subdomains (or elements) $\Omega_1,\dots,\Omega_M$, each one associated to a different material.

2. We choose a set of reference polynomial basis functions defined on the reference element $\hat{\Omega} = (-1,+1)^2$.

3. We define a set of basis functions on each element of the partition by mapping the reference basis from the reference domain $\hat{\Omega}$ to the actual element Ω_m, $m=1,\dots,M$.

4. We define global continuous basis functions by *glueing* the local basis functions at the interfaces.

5. We construct vector basis functions in such a way each scalar component is globally continuous and defined using the procedure in 2 – 4.

Partition of the domain As we have done the one-dimensional setting, when dealing with heterogeneous layered materials, we introduce a geometrically conforming partition (or decomposition) $\mathcal{T}(\Omega) = \{\Omega_m,\, m = 1, \dots, M\}$ of the domain Ω and we set $h_m := \mathrm{diam}(\Omega_m)$. In particular, we consider the number of elements M to be equal to the number of materials, so that each Ω_m has a different set of positive and constant parameters $(\rho_m, \lambda_{\mathrm{el},m}, \mu_m, \lambda_{\mathrm{vi},m}, \eta_m)$ associated to it. We assume that each element Ω_m, with $m = 1, \dots, M$, and is obtained by a transformation F_m from a reference (or parent) element $\hat{\Omega} = (-1, +1)^2$, i.e., $F_m \colon \hat{\Omega} \to \Omega_m$. The transformation F_m must be bijective and differentiable with its inverse. In this section the elements Ω_m are assumed to be rectangular elements, for which the transformation F_m is a bilinear affine map. Then, $\bar{\Omega} = \cup_m \bar{\Omega}_m$, and, for $m \neq k$, $\bar{\Omega}_m \cap \bar{\Omega}_k$ is either empty, or a vertex or a complete edge for both the elements.

Reference polynomial basis On the reference element $\hat{\Omega}$ we introduce the following polynomial space:

$$\mathbb{Q}_N = \mathbb{P}_{N_x}(-1, +1) \otimes \mathbb{P}_{N_z}(-1, +1), \qquad N = (N_x, N_z), \tag{6.32}$$

which denotes the space of polynomials having degree less than or equal to N_x in variable x and degree less than or equal to N_z in variable z. We now construct boundary-adapted polynomial modal bases for $\mathbb{Q}_N$ by taking the tensor product of one-dimensional boundary-adapted (Legendre or Chebyshev) polynomials. So, let $\{\hat{\varphi}^x_{k_x},\, k_x = 0, \dots, N_x\}$ and $\{\hat{\varphi}^z_{k_z},\, k_z = 0, \dots, N_z\}$ denote two families of one-dimensional boundary-adapted polynomials defined on the reference interval $(-1, +1)$. Then, the family of functions $\{\hat{\varphi}_{\boldsymbol{k}}\}$ defined as

$$\hat{\varphi}_{\boldsymbol{k}}(\hat{\boldsymbol{x}}) = \hat{\varphi}^x_{k_x}(\hat{x})\hat{\varphi}^z_{k_z}(\hat{z}), \qquad \boldsymbol{k} = (k_x, k_z), \qquad \hat{\boldsymbol{x}} = (\hat{x}, \hat{z}),$$

is a two-dimensional boundary-adapted basis on the domain $\hat{\Omega}$. In particular, this basis is formed by

- $(N_x - 1)(N_z - 1)$ *bubble functions* vanishing on $\partial\hat{\Omega}$ (for $1 \le k_x \le N_x - 1$ and $1 \le k_z \le N_z - 1$),
- 4 *vertex functions* not vanishing at precisely one vertex (for $k_x \in \{0, N_x\}$ and $k_z \in \{0, N_z\}$),
- $2(N_x + N_z - 2)$ *edge functions* not vanishing at precisely one edge (for $k_x \in \{0, N_x\}$, $1 \le k_z \le N_z - 1$ and $k_z \in \{0, N_z\}$, $1 \le k_x \le N_x - 1$).

Hereafter, we will often adopt the single-index notation based on the lexicographic ordering for the multi-dimensional basis $\hat{\varphi}_{\boldsymbol{k}}(\hat{\boldsymbol{x}})$, i.e., we will write $\hat{\varphi}_i(\hat{\boldsymbol{x}})$, where the index i is defined as follows

$$\{0, \dots, N_x\} \times \{0, \dots, N_z\} \ni (k_x, k_z) \mapsto i = k_x + k_z(N_x + 1) \in \{1, \dots, \bar{N}\},$$

with $\bar{N} = (N_x + 1)(N_z + 1)$. On the other hand, when referring to the indices of the pair (k_x, k_z) associated to the single-index i, we will use the notation $k_x(i)$ and $k_z(i)$.

Mapping of the reference basis For every $\Omega_m = (x_{0,m}, x_{1,m}) \times (z_{0,m}, z_{1,m})$, with $m = 1, \dots, M$, let $N_m = (N_{m,x}, N_{m,z})$. Then, we define the space

$$V_{N_m}(\Omega_m) = \{v \ : \ v = \hat{v} \circ F_m^{-1} \text{ for some } \hat{v} \in \mathbb{Q}_{N_m}\},$$

whose elements are images, through F_m, of polynomial functions $\hat{v} \in \mathbb{Q}_{N_m}$ in $\hat{\Omega}$. Let us first denote by $\hat{B}_{N_m}$ a suitably chosen boundary-adapted modal basis of $\mathbb{Q}_{N_m}$:

$$\hat{B}_{N_m} = \left\{\hat{\varphi}^{(m)}_i,\, i = 1, \dots, \bar{N}_m\right\}, \tag{6.33}$$

where $\bar{N}_m := (N_{m,x} + 1)(N_{m,z} + 1)$ is the total number of two-dimensional basis functions, i.e., $\bar{N}_m = |B_{N_m}|$. Then, a basis B_{N_m} for V_{N_m}, where

$$B_{N_m} = \left\{\varphi^{(m)}_i,\, i = 1, \dots, \bar{N}_m\right\}, \tag{6.34}$$

is obtained as the image of $\hat{B}_{N_m}$ through F_m, that is, $\forall i = 1, \ldots, \bar{N}_m$,

$$\varphi_i^{(m)} = \hat{\varphi}_i^{(m)} \circ F_m^{-1}. \tag{6.35}$$

Since in this work we consider only rectangular elements, (6.35) can be also written as

$$\varphi_i^{(m)}(\boldsymbol{x}) = \varphi_{k_x(i)}^{m,x}(x)\varphi_{k_z(i)}^{m,z}(z) = \hat{\varphi}_{k_x(i)}^{m,x}(F_{x,m}^{-1}(x))\hat{\varphi}_{k_z(i)}^{m,z}(F_{z,m}^{-1}(z)), \tag{6.36}$$

where $F_{x,m}$ and $F_{z,m}$ are affine functions that map the reference interval $(-1, +1)$ into the two intervals $(x_{0,m}, x_{1,m})$ and $(z_{0,m}, z_{1,m})$ defining the domain Ω_m, i.e.,

$$\begin{aligned} F_{x,m}\colon (-1,+1) &\to (x_{0,m}, x_{1,m}) \qquad \hat{x} \mapsto F_{x,m}(\hat{x}) := \frac{x_{1,m} - x_{0,m}}{2}\hat{x} + \frac{x_{0,m} + x_{1,m}}{2}, \\ F_{z,m}\colon (-1,+1) &\to (z_{0,m}, z_{1,m}) \qquad \hat{z} \mapsto F_{z,m}(\hat{z}) := \frac{z_{1,m} - z_{0,m}}{2}\hat{z} + \frac{z_{0,m} + z_{1,m}}{2}. \end{aligned}$$

while $\varphi_{k_x}^{m,x}$ (resp. $\varphi_{k_z}^{m,z}$) is the image of the reference one-dimensional basis function $\hat{\varphi}_{k_x}^{m,x}$ (resp. $\hat{\varphi}_{k_z}^{m,z}$) through the affine map $F_{x,m}$ (resp. $F_{z,m}$).

Global basis functions Finally, we define the space

$$V_\delta = \{v \in C^0(\bar{\Omega}) \ : \ v|_{\Omega_m} \in V_{N_m}(\Omega_m), \forall \Omega_m \in \mathcal{T}(\Omega)\}, \tag{6.37}$$

where the subindex δ is an abridged notation for "discrete", borrowed from [154], that takes into account both the geometric dicretisation of the domain $\Omega = \cup_m \Omega_m$ and the multiple polynomial degrees $\{N_m\}$ used on each element. The space V_δ contains all the functions that are globally continuous over Ω and that are polynomials of degree less than or equal to $N_{m,x}$ with respect to variable x and of degree less than or equal to $N_{m,z}$ with respect to variable z when restricted to element Ω_m. A basis for the whole space V_δ is then obtained by "glueing" together the elemental basis functions defined on each element Ω_m, thereby guaranteeing global continuity over Ω. As in the one-dimensional case, each bubble basis function, say $\varphi_i^{(m)} \in V_{N_m}(\Omega_m)$, immediately generates a global basis function $\tilde{\varphi}_i^{(m)} \in V_\delta$ by extending it by zero outside the element Ω_m where it was originally defined, i.e.,

$$\tilde{\varphi}_i^{(m)}(\boldsymbol{x}) := \begin{cases} \varphi_i^{(m)}(\boldsymbol{x}), & \text{for } \boldsymbol{x} \in \Omega_m, \\ 0, & \text{otherwise.} \end{cases} \tag{6.38}$$

Vertex and edge basis functions living in contiguous elements are properly matched to generate global basis functions. The matching is fairly trivial if the polynomial degree is the same for both the variables x and z on both the contiguous domain. Let us consider subdomains Ω_m and Ω_k sharing a common edge denoted by $\Gamma_{km} = \partial\bar{\Omega}_m \cap \partial\bar{\Omega}_k$. Then, two edge basis functions, say $\varphi_i^{(m)}$ living in Ω_m and $\varphi_j^{(k)}$ living in Ω_k, coinciding on the interface Γ_{km}, i.e., $\varphi_i^{(m)}|_{\Gamma_{km}} \equiv \varphi_j^{(m)}|_{\Gamma_{km}}$, give rise to a function $\varphi^{(\Gamma_{km})}$ that is continuous across Γ_{km}:

$$\varphi^{(\Gamma_{km})} = \begin{cases} \varphi_i^{(m)}, & \text{in } \bar{\Omega}_m, \\ \varphi_j^{(k)}, & \text{in } \bar{\Omega}_k, \\ 0, & \text{elsewhere.} \end{cases} \tag{6.39}$$

This matching procedure still applies if on each contiguous element one allows for a different polynomial degree along each direction (x and z), provided that the polynomial degrees along an interface between two elements agree on both sides. To fix ideas, suppose that $\Omega_1 := (0,1)\times(0,1)$ and $\Omega_2 := (1,2)\times(0,1)$. Then, the interface Γ_{12} between the two elements is given by $\Gamma_{12} = \partial\bar{\Omega}_1 \cap \partial\bar{\Omega}_2 = \{1\}\times(0,1)$. In this case, easy matching of the basis functions at the interface is obtained by considering the same polynomial degree for variable z on both Ω_1 and Ω_2, i.e., $N_{1,z} \equiv N_{2,z}$, whereas the polynomial degrees $N_{1,x}$ and $N_{2,x}$ for variable x might be different. Clearly, in the case of horizontal interface, the polynomial degrees must be the same in x and are allowed to be different on z. For vertex basis functions the procedure is basically the same and the global basis is obtained by glueing together all the local vertex basis functions associated with that specific vertex and extending the resulting function by zero outside the patch of elements containing the vertex.

Vector basis functions We define vector basis functions in such a way that each scalar component belongs to the space V_δ defined in (6.37). In other words, we define the space V_N used in Section 5.3 by setting $V_N := [V_\delta]^2$. Similarly, we can define the space $V_{N_0} := [V_{0,\delta}]^2$, where $V_{0,\delta} \subset V_\delta$ contains all the functions in V_δ vanishing on Γ_D, i.e., the portion of $\partial\Omega$ where Dirichlet boundary conditions are imposed. Following Section 5.3 and assuming that the basis functions used for the approximation in space of the displacement field $\boldsymbol{u}$ and of the velocity field $\boldsymbol{v}$ are the same, we can define the sets of basis functions $\mathcal{B}_N$ and $\mathcal{B}_{N_0} \subset \mathcal{B}_N$ such that:

$$\mathcal{B}_N := \{\hat{\boldsymbol{\phi}}_1, \dots, \hat{\boldsymbol{\phi}}_N\}, \quad V_N = \text{span}(\mathcal{B}_N), \quad \dim(V_N) = N, \tag{6.40a}$$

$$\mathcal{B}_{N_0} := \{\boldsymbol{\phi}_1, \dots, \boldsymbol{\phi}_{N_0}\}, \quad V_{N_0} = \text{span}(\mathcal{B}_{N_0}), \quad \dim(V_{N_0}) = N_0 < N. \tag{6.40b}$$

The numbering of the basis functions $\hat{\boldsymbol{\phi}}_i$, $i = 1, \dots, N_0$, is such that we first have all the basis functions for the x component of the vector field and then we have all the basis functions for the z component, which means

$$\hat{\boldsymbol{\phi}}_i(\boldsymbol{x}) := \begin{cases} \hat{\boldsymbol{\phi}}_{x,i}, & \text{for } i = j = 1, \dots, N_x, \\ \hat{\boldsymbol{\phi}}_{z,j}, & \text{for } i = N_x + 1, \dots, N, \ j = i - N_x, \ N = N_x + N_z. \end{cases} \tag{6.41}$$

where

$$\hat{\boldsymbol{\phi}}_{x,i} = \begin{pmatrix} \hat{\phi}_{x,i} \\ 0 \end{pmatrix} \qquad \hat{\boldsymbol{\phi}}_{z,i} = \begin{pmatrix} 0 \\ \hat{\phi}_{z,i} \end{pmatrix}. \tag{6.42}$$

The same reasoning clearly applies to $\boldsymbol{\phi}_i$, $i = 1, \dots, N$, since $\mathcal{B}_{N_0} \subset \mathcal{B}_N$. It is worth noting that in (6.41) we have used N_x (resp. N_z) to denote the total number of (global) two-dimensional basis functions used for the x (resp. z) component of the vector field, whereas in (6.32) it was used to denote the maximum degree of the one-dimensional polynomial basis functions defined on the reference interval $(-1, +1)$ and associated to variable x (resp. z). In what follows, the meaning will be clear from the context. Moreover, we want to highlight that the scalar basis functions $\hat{\phi}_{x,i} \in V_\delta$ and $\hat{\phi}_{z,i} \in V_\delta$ in (6.42) are the global basis functions defined by extending bubble functions to the whole domain Ω or by glueing edge/vertex basis functions as in (6.38) and (6.39), respectively. For the computation of the matrices arising in the Galerkin semi-discretisation of the weak formulation, we will see that it is useful to consider the restriction of the global basis functions defined above to the elements Ω_m and to define a proper local numbering of these local basis functions. Then, we use the superscript m to denote the restriction of the vector basis functions $\hat{\boldsymbol{\phi}}_j$ and $\hat{\boldsymbol{\phi}}_{\alpha,j}$, with $\alpha = x, z$, to the domain Ω_m, i.e., we write $\hat{\boldsymbol{\phi}}^m := \hat{\boldsymbol{\phi}}|_{\Omega_m}$ and $\hat{\boldsymbol{\phi}}^m_\alpha := \hat{\boldsymbol{\phi}}_\alpha|_{\Omega_m}$. Moreover, we define the following local ordering

$$\hat{\boldsymbol{\phi}}^m_i := \begin{cases} \hat{\boldsymbol{\phi}}^m_{x,j}, & \text{for } j = i = 1, \dots, \bar{N}^x_m, \\ \hat{\boldsymbol{\phi}}^m_{z,j}, & \text{for } j = 1, \dots, \bar{N}^z_m, \ i = j + \bar{N}^x_m. \end{cases} \tag{6.43}$$

where $\bar{N}^x_m = (N^x_{x,m} + 1)(N^x_{z,m} + 1)$, $\bar{N}^z_m = (N^z_{x,m} + 1)(N^z_{z,m} + 1)$ and

$$\hat{\boldsymbol{\phi}}^m_{x,i} = \begin{pmatrix} \hat{\varphi}^{(m)}_{x,i} \\ 0 \end{pmatrix} \qquad \hat{\boldsymbol{\phi}}^m_{z,i} = \begin{pmatrix} 0 \\ \hat{\varphi}^{(m)}_{z,i} \end{pmatrix}. \tag{6.44}$$

with $\hat{\varphi}^{(m)}_{\alpha,i}$, $\alpha = x, z$, being the restriction of $\hat{\phi}_\alpha$, in (6.42) to Ω_m. These are the local basis functions defining the set B_{N_m} in (6.34) and that have been used to build globally continuous basis. Here we have used the additional index $\alpha \in \{x, z\}$ to distinguish the component of the vector field to which the scalar basis belongs. Then, using (6.36) we can write

$$\hat{\varphi}^{(m)}_{\alpha,j}(x, z) = \hat{\varphi}^{m,x}_{\alpha,k_x(j)}(x)\, \hat{\varphi}^{m,z}_{\alpha,k_z(j)}(z). \tag{6.45}$$

Finally, it is worth emphasizing that the hat symbol used in (6.45) has a different meaning compared to the one used in, e.g., (6.33). Indeed, in (6.45) it refers to scalar basis functions related to the set $\mathcal{B}_N$, whereas in (6.33) it was used to denote scalar basis defined on the reference domain $(-1, +1)^2$. Since reference basis functions will not be used in the remaining part of this section, the change of meaning should be clear to the reader.

Computation of matrices Having chosen the same basis functions for the semi-discrete approximation of $\boldsymbol{u}$ and $\boldsymbol{v}$ and having defined $\mathcal{B}_N$ and $\mathcal{B}_{N_0}$ in such a way $\mathcal{B}_{N_0} \subset \mathcal{B}_N$, the computation of all the matrices arising in the Galerkin semi-discrete approximation developed in Section 5.3 reduces to the computation of three matrices based on the bilinear forms $a(\cdot,\cdot)$, $b(\cdot,\cdot)$ and $c(\cdot,\cdot)$ defined in (5.16), i.e.,

$$\hat{\mathbf{C}}_{i,j} = c(\hat{\boldsymbol{\phi}}_j, \hat{\boldsymbol{\phi}}_i) = \int_\Omega \rho\, \hat{\boldsymbol{\phi}}_j \cdot \hat{\boldsymbol{\phi}}_i \, d\boldsymbol{x}, \tag{6.46a}$$

$$\hat{\mathbf{B}}_{i,j} = b(\hat{\boldsymbol{\phi}}_j, \hat{\boldsymbol{\phi}}_i) = \int_\Omega \boldsymbol{\sigma}_{\mathrm{vi}}(\hat{\boldsymbol{\phi}}_j) : \boldsymbol{\varepsilon}(\hat{\boldsymbol{\phi}}_i)\, d\boldsymbol{x}, \tag{6.46b}$$

$$\hat{\mathbf{A}}_{i,j} = a(\hat{\boldsymbol{\phi}}_j, \hat{\boldsymbol{\phi}}_i) = \int_\Omega \boldsymbol{\sigma}_{\mathrm{el}}(\hat{\boldsymbol{\phi}}_j) : \boldsymbol{\varepsilon}(\hat{\boldsymbol{\phi}}_i)\, d\boldsymbol{x}. \tag{6.46c}$$

Indeed, the matrices used in (5.33) to define the block matrices $\mathbf{M}$ and $\mathbf{H}$ and the ones used in (5.36) to define the Dirichlet contribution to the forcing vector $\boldsymbol{F}$ can be computed as in the one-dimensional case, i.e., we have

$$\mathbf{M}^v = \hat{\mathbf{C}}(dir, dir), \qquad \mathbf{H}_{11} = \hat{\mathbf{B}}(dir, dir), \qquad \mathbf{M}^u = \mathbf{H}_{12} = -\mathbf{H}_{21} = \hat{\mathbf{A}}(dir, dir)$$
$$\mathbf{N}_{11} = \hat{\mathbf{C}}(dir, :), \qquad \mathbf{B}_{11} = \hat{\mathbf{B}}(dir, :), \qquad \mathbf{B}_{12} = \hat{\mathbf{A}}(dir, :),$$

where dir denotes the set of indices associated to those basis functions that are both in $\mathcal{B}_N$ and $\mathcal{B}_{N_0}$. The component (i,j) of matrices $\hat{\mathbf{C}}$, $\hat{\mathbf{B}}$ and $\hat{\mathbf{A}}$ defined in (6.46) can be computed as follows

$$\hat{\mathbf{C}}_{i,j} = \int_\Omega \rho\, \hat{\boldsymbol{\phi}}_j \cdot \hat{\boldsymbol{\phi}}_i \, d\boldsymbol{x} = \sum_{m=1}^{M} \int_{\Omega_m} \rho_m\, \hat{\boldsymbol{\phi}}_j^m \cdot \hat{\boldsymbol{\phi}}_i^m \, d\boldsymbol{x} = \sum_{m \in \mathcal{A}(i,j)} \int_{\Omega_m} \rho_m\, \hat{\boldsymbol{\phi}}_j^m \cdot \hat{\boldsymbol{\phi}}_i^m \, d\boldsymbol{x} = \sum_{m \in \mathcal{A}(i,j)} \left(\hat{\mathbf{C}}^m\right)_{k,l}$$

$$\hat{\mathbf{B}}_{i,j} = \int_\Omega \boldsymbol{\sigma}_{\mathrm{vi}}(\hat{\boldsymbol{\phi}}_i) : \boldsymbol{\varepsilon}(\hat{\boldsymbol{\phi}}_i)\, d\boldsymbol{x} = \sum_{m=1}^{M} \int_{\Omega_m} \boldsymbol{\sigma}_{\mathrm{vi}}(\hat{\boldsymbol{\phi}}_i^m) : \boldsymbol{\varepsilon}(\hat{\boldsymbol{\phi}}_i^m)\, d\boldsymbol{x} = \sum_{m \in \mathcal{A}(i,j)} \int_{\Omega_m} \boldsymbol{\sigma}_{\mathrm{vi}}(\hat{\boldsymbol{\phi}}_i^m) : \boldsymbol{\varepsilon}(\hat{\boldsymbol{\phi}}_i^m)\, d\boldsymbol{x} = \sum_{m \in \mathcal{A}(i,j)} \left(\hat{\mathbf{B}}^m\right)_{k,l}$$

$$\hat{\mathbf{A}}_{i,j} = \int_\Omega \boldsymbol{\sigma}_{\mathrm{el}}(\hat{\boldsymbol{\phi}}_i) : \boldsymbol{\varepsilon}(\hat{\boldsymbol{\phi}}_i)\, d\boldsymbol{x} = \sum_{m=1}^{M} \int_{\Omega_m} \boldsymbol{\sigma}_{\mathrm{el}}(\hat{\boldsymbol{\phi}}_i^m) : \boldsymbol{\varepsilon}(\hat{\boldsymbol{\phi}}_i^m)\, d\boldsymbol{x} = \sum_{m \in \mathcal{A}(i,j)} \int_{\Omega_m} \boldsymbol{\sigma}_{\mathrm{el}}(\hat{\boldsymbol{\phi}}_i^m) : \boldsymbol{\varepsilon}(\hat{\boldsymbol{\phi}}_i^m)\, d\boldsymbol{x} = \sum_{m \in \mathcal{A}(i,j)} \left(\hat{\mathbf{A}}^m\right)_{k,l}.$$

For all the three matrices, the integral over the domain Ω is computed by summing the contributions given by all the subdomains Ω_m, $m = 1, \ldots, M$. Actually, the subdomains that provide a non-zero contribution to the compontent (i,j) of the three matrices defined in (6.46) are only those being part of the support of both basis functions $\hat{\boldsymbol{\phi}}_i$ and $\hat{\boldsymbol{\phi}}_j$. Then, the set of indices associated to subdomains contributing to the entry (i,j) is denoted by $\mathcal{A}(i,j) \subseteq \{1, \ldots, M\}$. Thus, in practice one calculates the element matrices $\hat{\mathbf{C}}^m$, $\hat{\mathbf{B}}^m$ and $\hat{\mathbf{A}}^m$, for all $m = 1, \ldots, M$, and then adds these local contributions to the global matrices $\hat{\mathbf{C}}$, $\hat{\mathbf{B}}$ and $\hat{\mathbf{A}}$, respectively. This assembly procedures requires the definition of a *map* that relates the indices of the (local) polynomial basis functions defined on each element Ω_m to the indices of the (global) continuous basis defined over the whole domain Ω. In the expressions above, the global indices are (i,j) and the local indices are (k,l). So, the map must tell that the polynomial basis function of local index k defined on element Ω_m has been used to build the global basis function having index i. Clearly, same reasoning applies to indices j and l. Note that, for bubble functions extended to zero outside the domain in which they have been defined there is a one-to-one correspondence between local and global indices, whereas the global index of a function obtained by glueing vertex/edge bases is associated to multiple local indices, one for each local polynomial being part of the glueing process. We now discuss the computation of the components of the element matrices and start with matrix $\hat{\mathbf{C}}^m$. From (6.43) and (6.44) we see that $\hat{\mathbf{C}}^m$ is a 2×2 block matrix with the following structure

$$\hat{\mathbf{C}}^m = \begin{pmatrix} \mathbf{C}_m^x & \mathbf{0} \\ \mathbf{0} & \mathbf{C}_m^z \end{pmatrix},$$

where the component (i,j) of $\mathbf{C}_m^\alpha$, with $\alpha = x, z$, is given by

$$(\mathbf{C}_m^\alpha)_{i,j} \overset{(6.45)}{=} \int_{\Omega_m} \rho_m\, \hat{\varphi}_{\alpha,j}^{(m)}\, \hat{\varphi}_{\alpha,i}^{(m)}\, d\boldsymbol{x} = \rho_m \left(\int_{x_{0,m}}^{x_{1,m}} \hat{\varphi}_{\alpha,k_x(j)}^{m,x}(x) \hat{\varphi}_{\alpha,k_x(i)}^{m,x}(x)\, dx \right) \left(\int_{z_{0,m}}^{z_{1,m}} \hat{\varphi}_{\alpha,k_z(j)}^{m,z}(z) \hat{\varphi}_{\alpha,k_z(i)}^{m,z}(z)\, dz \right).$$

The one-dimensional integrals can be computed as shown in Section 4.3.1 (for boundary-adapted Legendre polynomials) or Section 4.4.1 (for boundary-adapted Chebyshev polynomials). We now discuss the computation of matrices $\hat{\mathbf{B}}^m$ and $\hat{\mathbf{A}}^m$. From the definition of $\boldsymbol{\sigma}_{\text{vi}}$ we see that

$$\left(\hat{\mathbf{B}}^m\right)_{i,j} = \int_{\Omega_m} \boldsymbol{\sigma}_{\text{vi}}(\hat{\boldsymbol{\phi}}_j^m) : \boldsymbol{\varepsilon}(\hat{\boldsymbol{\phi}}_i^m)\, d\boldsymbol{x} = \int_{\Omega_m} \lambda_{\text{vi},m}\, \text{tr}(\boldsymbol{\varepsilon}(\hat{\boldsymbol{\phi}}_j^m))\, \text{tr}(\boldsymbol{\varepsilon}(\hat{\boldsymbol{\phi}}_i^m))\, d\boldsymbol{x} + \int_{\Omega_m} 2\eta_m\, \boldsymbol{\varepsilon}(\hat{\boldsymbol{\phi}}_j^m) : \boldsymbol{\varepsilon}(\hat{\boldsymbol{\phi}}_i^m)\, d\boldsymbol{x}$$

while from the definition of $\boldsymbol{\sigma}_{\text{el}}$ we have that

$$\left(\hat{\mathbf{A}}^m\right)_{i,j} = \int_{\Omega_m} \boldsymbol{\sigma}_{\text{el}}(\hat{\boldsymbol{\phi}}_j^m) : \boldsymbol{\varepsilon}(\hat{\boldsymbol{\phi}}_i^m)\, d\boldsymbol{x} = \int_{\Omega_m} \lambda_{\text{el},m}\, \text{tr}(\boldsymbol{\varepsilon}(\hat{\boldsymbol{\phi}}_j^m))\, \text{tr}(\boldsymbol{\varepsilon}(\hat{\boldsymbol{\phi}}_i^m))\, d\boldsymbol{x} + \int_{\Omega_m} 2\mu_m\, \boldsymbol{\varepsilon}(\hat{\boldsymbol{\phi}}_j^m) : \boldsymbol{\varepsilon}(\hat{\boldsymbol{\phi}}_i^m)\, d\boldsymbol{x}.$$

Therefore, the element matrices $\hat{\mathbf{B}}^m$ and $\hat{\mathbf{A}}^m$ can be rewritten as

$$\hat{\mathbf{B}}^m = \lambda_{\text{vi},m}\mathbf{T}_m + 2\eta_m\mathbf{G}_m, \qquad \hat{\mathbf{A}}^m = \lambda_{\text{el},m}\mathbf{T}_m + 2\mu_m\mathbf{G}_m,$$

where $\mathbf{T}_m$ and $\mathbf{G}_m$ are 2×2 block matrices with the following structure:

$$\mathbf{T}_m = \begin{pmatrix} \mathbf{T}_m^{xx} & \mathbf{T}_m^{xz} \\ \mathbf{T}_m^{zx} & \mathbf{T}_m^{zz} \end{pmatrix}, \qquad \mathbf{G}_m = \begin{pmatrix} \mathbf{G}_m^{xx} & \mathbf{G}_m^{xz} \\ \mathbf{G}_m^{zx} & \mathbf{G}_m^{zz} \end{pmatrix}.$$

The component (i,j) of each block of matrix $\mathbf{T}_m$ is given by

$$\left(\mathbf{T}_m^{\alpha\beta}\right)_{i,j} = \int_{\Omega_m} \text{tr}\left(\boldsymbol{\varepsilon}\left(\hat{\boldsymbol{\phi}}_{\beta,j}^m\right)\right) \text{tr}\left(\boldsymbol{\varepsilon}\left(\hat{\boldsymbol{\phi}}_{\alpha,i}^m\right)\right)\, d\boldsymbol{x} = \int_{\Omega_m} \frac{\partial\hat{\varphi}_{\beta,j}^{(m)}}{\partial\beta}\frac{\partial\hat{\varphi}_{\alpha,i}^{(m)}}{\partial\alpha}\, d\boldsymbol{x}, \qquad \alpha,\beta = x,z,$$

and the component (i,j) of each block of matrix $\mathbf{G}_m$ is given by

$$(\mathbf{G}_m^{xx})_{i,j} = \int_{\Omega_m} \boldsymbol{\varepsilon}\left(\hat{\boldsymbol{\phi}}_{x,j}^m\right) : \boldsymbol{\varepsilon}\left(\hat{\boldsymbol{\phi}}_{x,i}^m\right)\, d\boldsymbol{x} = \int_{\Omega_m} \frac{\partial\hat{\varphi}_{x,j}^{(m)}}{\partial x}\frac{\partial\hat{\varphi}_{x,i}^{(m)}}{\partial x}\, d\boldsymbol{x} + \frac{1}{2}\int_{\Omega_m} \frac{\partial\hat{\varphi}_{x,j}^{(m)}}{\partial z}\frac{\partial\hat{\varphi}_{x,i}^{(m)}}{\partial z}\, d\boldsymbol{x} \tag{6.47a}$$

$$(\mathbf{G}_m^{zz})_{i,j} = \int_{\Omega_m} \boldsymbol{\varepsilon}\left(\hat{\boldsymbol{\phi}}_{z,j}^m\right) : \boldsymbol{\varepsilon}\left(\hat{\boldsymbol{\phi}}_{z,i}^m\right)\, d\boldsymbol{x} = \int_{\Omega_m} \frac{\partial\hat{\varphi}_{z,j}^{(m)}}{\partial z}\frac{\partial\hat{\varphi}_{z,i}^{(m)}}{\partial z}\, d\boldsymbol{x} + \frac{1}{2}\int_{\Omega_m} \frac{\partial\hat{\varphi}_{z,j}^{(m)}}{\partial x}\frac{\partial\hat{\varphi}_{z,i}^{(m)}}{\partial x}\, d\boldsymbol{x} \tag{6.47b}$$

$$(\mathbf{G}_m^{xz})_{i,j} = \int_{\Omega_m} \boldsymbol{\varepsilon}\left(\hat{\boldsymbol{\phi}}_{z,j}^m\right) : \boldsymbol{\varepsilon}\left(\hat{\boldsymbol{\phi}}_{x,i}^m\right)\, d\boldsymbol{x} = \frac{1}{2}\int_{\Omega_m} \frac{\partial\hat{\varphi}_{z,j}^{(m)}}{\partial x}\frac{\partial\hat{\varphi}_{x,i}^{(m)}}{\partial z}\, d\boldsymbol{x} \tag{6.47c}$$

Using (6.45), the integrals appearing in (6.47) becomes:

$$\int_{\Omega_m} \frac{\partial\hat{\varphi}_{\alpha,j}^{(m)}}{\partial x}\frac{\partial\hat{\varphi}_{\alpha,i}^{(m)}}{\partial x}\, d\boldsymbol{x} = \left(\int_{x_{0,m}}^{x_{1,m}} \hat{\varphi}_{\alpha,k_x(j)}^{m,x}{}'(x)\, \hat{\varphi}_{\alpha,k_x(i)}^{m,x}{}'(x)\, dx\right)\left(\int_{z_{0,m}}^{z_{1,m}} \hat{\varphi}_{\alpha,k_z(j)}^{m,z}(z)\, \hat{\varphi}_{\alpha,k_z(i)}^{m,z}(z)\, dz\right),$$

$$\int_{\Omega_m} \frac{\partial\hat{\varphi}_{\alpha,j}^{(m)}}{\partial z}\frac{\partial\hat{\varphi}_{\alpha,i}^{(m)}}{\partial z}\, d\boldsymbol{x} = \left(\int_{x_{0,m}}^{x_{1,m}} \hat{\varphi}_{\alpha,k_x(j)}^{m,x}(x)\, \hat{\varphi}_{\alpha,k_x(i)}^{m,x}(x)\, dx\right)\left(\int_{z_{0,m}}^{z_{1,m}} \hat{\varphi}_{\alpha,k_z(j)}^{m,z}{}'(z)\, \hat{\varphi}_{\alpha,k_z(i)}^{m,z}{}'(z)\, dz\right),$$

$$\int_{\Omega_m} \frac{\partial\hat{\varphi}_{z,j}^{(m)}}{\partial x}\frac{\partial\hat{\varphi}_{x,i}^{(m)}}{\partial z}\, d\boldsymbol{x} = \left(\int_{x_{0,m}}^{x_{1,m}} \hat{\varphi}_{x,k_x(j)}^{m,x}{}'(x)\, \hat{\varphi}_{z,k_x(i)}^{m,x}(x)\, dx\right)\left(\int_{z_{0,m}}^{z_{1,m}} \hat{\varphi}_{x,k_z(j)}^{m,z}(z)\, \hat{\varphi}_{z,k_z(i)}^{m,z}{}'(z)\, dz\right).$$

The one-dimensional integrals can be computed using the results presented in Sections 4.3.1 and 4.4.1.

Galerkin Finite Element Linear Basis Functions

In this section we define the basis functions used when computing the numerical solution of the two dimensional linear viscoelastic equations with Kelvin-Voigt consitutive model by means of linear triangular finite elements.

Triangulation We start by defining a partition of the domain $\Omega \subset \mathbb{R}^2$ and we call it *a computational mesh*. In particular, we define a *triangulation* $\mathcal{T}_h(\Omega)$ formed by the union of triangles such that:

- $\mathcal{T}_h(\Omega)$ is formed by n_v nodes (triangle vertices named N_i, $i = 1, \dots, n_v$, with given coordinates) and M triangles (identified by T_k , $k = 1, \dots, M$);
- $\Omega = \bigcup_{T_k \in \mathcal{T}_h(\Omega)} T_k = T_1 \cup T_2 \dots \cup T_M$;
- if non empty, $T_i \cap T_j = e_{ij}$, $i \neq j$, where e_{ij} denotes the edge shared by triangles T_i and T_j;
- no vertex N_i lies in the interior of a triangle edge;
- the boundary triangles have at least one vertex on the boundary.

Finally, we introduce the mesh parameter h, defined as:

$$h = \max_{T_i \in \mathcal{T}_h} \operatorname{diam}(T_i) = \max_{T_i \in \mathcal{T}_h} \max_{x,y \in T_i} |x - y|,$$

where the triangle diameter diam (T_i) is defined as the longest edge of T_i. As in the one-dimensional Finite Element setting, we now assume the material parameters (ρ, λ_{el}, μ, λ_{vi} and η) to be piecewise positive constant function over Ω and, in particular, we assume them to be constant within each element of the triangulation. In other words, the material interfaces must coincide with the edges of the triangles in the computational mesh. We denote by ρ_T, $\lambda_{\text{el},T}$, μ_T, $\lambda_{\text{vi},T}$ and η_T the value of the material parameters associated to triangle T.

Linear Lagrangian basis functions Then, we proceed by defining the finite dimensional space

$$\mathcal{P}_h^1 := \left\{ v \in C^0(\overline{\Omega}) : v|_T \in \mathbb{P}_1(T), \forall T \in \mathcal{T}_h(\Omega) \right\},$$

which is the space of globally continuous scalar functions that are polynomials of degree 1 on the triangles (elements) of the triangulation $\mathcal{T}_h(\Omega)$. Moreover, we define the space

$$\mathcal{P}_{0,h}^1 := \left\{ v \in \mathcal{P}_h^1 : v|_{\Gamma_D} = 0 \right\}.$$

We now want to define a set of linear Lagrangian basis functions for the finite dimensional spaces defined above. We use nodes N_i of the triangulation, denote the coordinates of N_i as $\boldsymbol{x}_i = (x_i, z_i)$ and build a set of basis functions $\{\varphi_i(\boldsymbol{x}),\ i = 1, \dots, n_v\}$ for the space $\mathcal{P}_h^1$ such that:

$$\varphi_i(\boldsymbol{x}_j) = \delta_{ij}, \qquad \forall i, j = 1, \dots, n_v.$$

These are piecewise linear functions of pyramidal shape and with support given by the unions of all triangles sharing node N_i. Thus, we can express a generic function $v \in \mathcal{P}_h^1$ as a linear combination of the basis functions

$$v(\boldsymbol{x}) = \sum_{j=1}^{n_v} v_j \varphi_j(\boldsymbol{x}) = \sum_{j=1}^{n_v} v(\boldsymbol{x}_j)\, \varphi_j(\boldsymbol{x}) \qquad \forall \boldsymbol{x} \in \mathcal{T}_h(\Omega).$$

Clearly, considering only those basis functions associated to vertices not lying on the Dirichlet boundary Γ_D we obtain a set of basis functions for the finite dimensional space $\mathcal{P}_{0,h}^1$ of piecewise linear functions vanishing on Γ_D. Let us now consider a triangular element T with nodes i, j and m. As we have seen above, the linear basis function $\varphi_i^T(x, z)$, relative to node i and finite element T, must assume value equal to one on i and equal to zero on j and m. Since there are three conditions to determine the basis function, this must have the form:

$$\varphi_i^T(x, z) = c_0 + c_1 x + c_2 z.$$

Coefficients c_0, c_1 and c_2 are determined solving the system given by the previous conditions:

$$\begin{cases} c_0 + c_1 x_i + c_2 z_i = 1 \\ c_0 + c_1 x_j + c_2 z_j = 0 \\ c_0 + c_1 x_m + c_2 z_m = 0 \end{cases} \implies \begin{bmatrix} 1 & x_i & z_i \\ 1 & x_j & z_j \\ 1 & x_m & z_m \end{bmatrix} \begin{pmatrix} c_0 \\ c_1 \\ c_2 \end{pmatrix} = \begin{pmatrix} 1 \\ 0 \\ 0 \end{pmatrix} \implies A\mathbf{c} = \mathbf{e}_1$$

where matrix C is always invertible if i, j and m are not aligned. Then it results:

$$\mathbf{c} = A^{-1}\mathbf{e}_1, \qquad A^{-1} = \frac{1}{\det(A)} \begin{bmatrix} x_j z_m - x_m z_j & x_m z_i - x_i z_m & x_i z_j - x_j z_i \\ z_j - z_m & z_m - z_i & z_i - z_j \\ x_m - x_j & x_i - x_m & x_j - x_i \end{bmatrix},$$

with $\det(A) = 2\Delta_T$ and $|\Delta_T|$ being the area of the triangle T. Finally, basis function $\varphi_i^T(x, y)$ can be written as:

$$\varphi_k^T(x, z) = \frac{a_k + b_k x + c_k z}{2\Delta_T}, \qquad k = i, j, m, \tag{6.48}$$

where the coefficients are:

$$\begin{aligned} a_i &= x_j z_m - x_m z_j, & b_i &= z_j - z_m, & c_i &= x_m - x_j, \\ a_j &= x_m z_i - x_i z_m, & b_j &= z_m - z_i, & c_j &= x_i - x_m, \\ a_m &= x_i z_j - x_j z_i, & b_m &= z_i - z_j, & c_m &= x_j - x_i. \end{aligned}$$

Returning to our initial issue, we have that the solution $(\boldsymbol{v}_h(t), \boldsymbol{u}_h(t))$ of the Galerkin problem (5.31) consists of approximating in space of the velocity and displacement fields at time $t \geq 0$. Then, for any $t \geq 0$, we write both the components of these two vector fields by using piecewise linear functions, i.e., $\boldsymbol{u}_h(t), \boldsymbol{v}_h(t) \in V_h := [P_h^1]^2$. Thus, the components of the displacement field can be written using basis function in $\mathcal{P}_h^1$ as

$$u_h^x(t, \boldsymbol{x}) = \sum_{i=1}^{n_v} u_i^x(t)\varphi_i(\boldsymbol{x}), \qquad u_h^z(t, \boldsymbol{x}) = \sum_{i=1}^{n_v} u_i^z(t)\varphi_i(\boldsymbol{x}).$$

Then we define a nodal basis $\{\boldsymbol{\phi}_i,\, i = 1, 2, \ldots, 2n_v\}$ for V_h as

$$\boldsymbol{\phi}_{2i-1}(\boldsymbol{x}) = \varphi_i(\boldsymbol{x})\boldsymbol{e}_1, \qquad \boldsymbol{\phi}_{2i}(\boldsymbol{x}) = \varphi_i(\boldsymbol{x})\boldsymbol{e}_2, \qquad i = 1, 2, \ldots, n_v,$$

where $\boldsymbol{e}_i$ denotes the i-th unit vector. Furthermore, we define $\mathbf{u}\colon \mathbb{R}_+ \to \mathbb{R}^{2n_v}$ such that

$$u_{2i-1}(t) = u_i^x(t), \qquad u_{2i}(t) = u_i^z(t), \qquad i = 1, 2, \ldots, n_v. \tag{6.49}$$

Finally $\boldsymbol{u}_h(t, \boldsymbol{x}) \in V_h$ takes the form

$$\boldsymbol{u}_h(t, \boldsymbol{x}) = u_h^x(t, \boldsymbol{x})\boldsymbol{e}_1 + u_h^z(t, \boldsymbol{x})\boldsymbol{e}_2 = \sum_{i=1}^{n_v} u_i^x(t)\varphi_i(\boldsymbol{x})\boldsymbol{e}_1 + \sum_{i=1}^{n_v} u_i^z(t)\varphi_i(\boldsymbol{x})\boldsymbol{e}_2 = \sum_{i=1}^{2n_v} u_i(t)\boldsymbol{\phi}_i(\boldsymbol{x}). \tag{6.50}$$

The ordering of the global degrees of freedom introduced in (6.49) shows that the components of $\mathbf{u}$ with odd index represent the displacements along the x direction while the ones with even index are the displacements along z. Therefore, the index of the node associated to the global degree of freedom i, $i = 1, 2, \ldots, 2n_v$, is given by $\lceil i/2 \rceil$, where $\lceil p \rceil := \min\{n \in \mathbb{N} : n \geq p\}$. Similarly, the velocity field $\boldsymbol{v}_h(t) \in V_h$ which can be written as

$$\boldsymbol{v}_h(t, \boldsymbol{x}) = v_h^x(t, \boldsymbol{x})\boldsymbol{e}_1 + v_h^z(t, \boldsymbol{x})\boldsymbol{e}_2 = \sum_{i=1}^{n_v} v_i^x(t)\varphi_i(\boldsymbol{x})\boldsymbol{e}_1 + \sum_{i=1}^{n_v} v_i^z(t)\varphi_i(\boldsymbol{x})\boldsymbol{e}_2 = \sum_{i=1}^{2n_v} v_i(t)\boldsymbol{\phi}_i(\boldsymbol{x}).$$

Computation of matrices Having defined the triangular linear basis functions, we now address the computation of the Finite Element matrices arising from the Galerkin semi-discretisation of the weak-formulation. The matrix associated to the bilinear form $c(\cdot\,,\cdot)$ defined in (5.16a) can be computed as follows:

$$\hat{\mathbf{C}}_{i,j} = c(\hat{\boldsymbol{\phi}}_j, \hat{\boldsymbol{\phi}}_i) = \int_\Omega \rho\, \hat{\boldsymbol{\phi}}_j \cdot \hat{\boldsymbol{\phi}}_i \, d\boldsymbol{x} \tag{6.51a}$$

$$= \sum_{T \in \mathcal{T}_h(\Omega)} \rho_T \int_T \hat{\boldsymbol{\phi}}_j \cdot \hat{\boldsymbol{\phi}}_i \, d\boldsymbol{x} \tag{6.51b}$$

$$= \sum_{T \in \mathcal{A}(i,j)} \rho_T \int_T \hat{\boldsymbol{\phi}}_j \cdot \hat{\boldsymbol{\phi}}_i \, d\boldsymbol{x} \tag{6.51c}$$

$$= \sum_{T \in \mathcal{A}(i,j)} C_{k,l}^{(T)} \tag{6.51d}$$

In particular, the integral over the computational domain Ω in (6.51a) is calculated by summing the contributions given by all the triangles T in the triangulation $\mathcal{T}_h(\Omega)$, thus obtaining (6.51b). Actually, owing to the local support of the linear Lagrangian basis functions, most of the triangles in $\mathcal{T}_h(\Omega)$ do not provide any contribution to the component (i,j) of the matrix $\hat{\mathbf{C}}$. Therefore, the sum over all the triangles in $\mathcal{T}_h(\Omega)$ can be replaced as done in (6.51c) with the sum over the triangles in $\mathcal{A}(i,j)$, which denotes the set of triangles in $\mathcal{T}_h(\Omega)$ sharing both the vertices associated to the global degrees of freedom i and j. So, the set $\mathcal{A}(i,j)$, when non-empty, contains either two triangles sharing and edge (when $i \neq j$) or all the triangles sharing a node (when $i = j$). Then, the local contribution given by triangle T to matrix C is a 6-by-6 matrix denoted by $C^{(T)}$. The dimension of this matrix is equal to the number of vertices in a triangle times the number of degrees of freedom associated to each vertex (i.e., the two vector field components x and z). The indices k and l appearing in (6.51d) are the local indices, so $k,l \in \{1,2,\dots,6\}$, associated to the global indices $i,j \in \{1,2,\dots,2n_v\}$ in triangle T. Before proceeding with the computation of the element mass matrix $C^{(T)}$, it is important to specify the ordering of the local degrees of freedom within triangle T. We decide to first consider the dofs associated to the vector field component x and then the dofs associated to the component z. For example, let us suppose that the triangle T has vertices $\{10,7,18\}$. Then, the global degrees of freedom associated to these vertices have indices $\{19,10,13,14,35,36\}$ (see (6.49) for an explanation of the ordering of global degrees of freedom) and their local indices are $\{1,4,2,5,3,6\}$. In other words, having denoted by $g_x(i)$ and $g_z(i)$ the global dofs associated to the x and z components of the field and to vertex i, with $i \in \{1,2,\dots,n_v\}$, and having denoted by $\ell_T(j)$ the local index associated to the global index $j \in \{1,2,\dots,2n_v\}$ within triangle T, we have

$$10 \begin{cases} g_x(10) = 19 \;\to\; \ell_T(19) = 1, \\ g_z(10) = 20 \;\to\; \ell_T(20) = 4, \end{cases} \quad 7 \begin{cases} g_x(7) = 13 \;\to\; \ell_T(13) = 2, \\ g_z(7) = 14 \;\to\; \ell_T(14) = 5, \end{cases} \quad 18 \begin{cases} g_x(18) = 35 \;\to\; \ell_T(35) = 3, \\ g_z(18) = 36 \;\to\; \ell_T(36) = 6. \end{cases}$$

The local contribution $C^{(T)}$ given by triangle T to the global mass matrix C in (6.51) has the form

$$C^{(T)} = \begin{bmatrix} M^{(T)} & \mathbb{O} \\ \mathbb{O} & M^{(T)} \end{bmatrix}$$

where $\mathbb{O} \in \mathbb{R}^{3\times 3}$ is the null matrix and

$$M^{(T)} = \rho_T |\Delta_T| \begin{bmatrix} \frac{1}{6} & \frac{1}{12} & \frac{1}{12} \\ \frac{1}{12} & \frac{1}{6} & \frac{1}{12} \\ \frac{1}{12} & \frac{1}{12} & \frac{1}{6} \end{bmatrix}.$$

Similarly to what we have seen in (6.51), the matrices associated to the bilinear forms $b(\cdot\,,\cdot)$ and $a(\cdot\,,\cdot)$ defined in (5.16b) and (5.16c), respectively, can be computed as:

$$\hat{\mathbf{B}}_{i,j} = b(\hat{\boldsymbol{\phi}}_j, \hat{\boldsymbol{\phi}}_i) = \int_\Omega \boldsymbol{\sigma}_{\mathrm{vi}}(\hat{\boldsymbol{\phi}}_j) : \boldsymbol{\varepsilon}(\hat{\boldsymbol{\phi}}_i)\, d\boldsymbol{x} = \sum_{T\in\mathcal{A}(i,j)} \int_T \boldsymbol{\sigma}_{\mathrm{vi}}(\hat{\boldsymbol{\phi}}_j) : \boldsymbol{\varepsilon}(\hat{\boldsymbol{\phi}}_i)\, d\boldsymbol{x} = \sum_{T\in\mathcal{A}(i,j)} B^{(T)}_{k,l} \tag{6.52}$$

$$\hat{\mathbf{A}}_{i,j} = a(\hat{\boldsymbol{\phi}}_j, \hat{\boldsymbol{\phi}}_i) = \int_\Omega \boldsymbol{\sigma}_{\mathrm{el}}(\hat{\boldsymbol{\phi}}_j) : \boldsymbol{\varepsilon}(\hat{\boldsymbol{\phi}}_i)\, d\boldsymbol{x} = \sum_{T\in\mathcal{A}(i,j)} \int_T \boldsymbol{\sigma}_{\mathrm{el}}(\hat{\boldsymbol{\phi}}_j) : \boldsymbol{\varepsilon}(\hat{\boldsymbol{\phi}}_i)\, d\boldsymbol{x} = \sum_{T\in\mathcal{A}(i,j)} A^{(T)}_{k,l} \tag{6.53}$$

We now show how to compute the local contribution $A^{(T)}$ given by triangle T to the global elastic stiffness matrix A in (6.53). We use the Voigt representation of the symmetric strain tensor, which reads

$$\gamma(\boldsymbol{u}_h) := \begin{bmatrix} \partial u_x/\partial x \\ \partial u_z/\partial z \\ \partial u_z/\partial x + \partial u_x/\partial z \end{bmatrix} = \begin{bmatrix} \varepsilon_{11}(\boldsymbol{u}_h) \\ \varepsilon_{22}(\boldsymbol{u}_h) \\ 2\varepsilon_{12}(\boldsymbol{u}_h) \end{bmatrix}.$$

Now let $\mathbf{u}_T$ be the vector whose components are the nodal values of $\boldsymbol{u}_h$ on triangle T, i.e.,

$$\mathbf{u}_T = \begin{bmatrix} u_1^x & u_2^x & u_3^x & u_1^z & u_2^z & u_3^z \end{bmatrix}^\top,$$

where the subscripts denote the local index of the triangle vertices. Using the expression of $\boldsymbol{u}_h$ given in (6.50), $\gamma(\boldsymbol{u}_h)$ becomes:

$$\gamma(\boldsymbol{u}_h) = \begin{bmatrix} \partial_x\varphi_i & \partial_x\varphi_j & \partial_x\varphi_k & 0 & 0 & 0 \\ 0 & 0 & 0 & \partial_z\varphi_i & \partial_z\varphi_j & \partial_z\varphi_k \\ \partial_z\varphi_i & \partial_z\varphi_j & \partial_z\varphi_k & \partial_x\varphi_i & \partial_x\varphi_j & \partial_x\varphi_k \end{bmatrix} \begin{bmatrix} u_1^x \\ \vdots \\ u_3^z \end{bmatrix}$$

Then, recalling that $\varphi_i^T(x,y) = (a_i + b_i x + c_i y)/2\Delta_T$, we obtain

$$\gamma(\boldsymbol{u}_h) = \frac{1}{2\Delta_T} R\mathbf{u}, \qquad \text{where} \qquad R := \begin{bmatrix} b_i & b_j & b_k & 0 & 0 & 0 \\ 0 & 0 & 0 & c_i & c_j & c_k \\ c_i & c_j & c_k & b_i & b_j & b_k \end{bmatrix}. \tag{6.54}$$

Using again Voigt notation, the constitutive equations $\boldsymbol{\sigma}_{\text{el}}(\boldsymbol{u}_h) = \mathbb{C}_{\text{el}}\boldsymbol{\varepsilon}(\boldsymbol{u}_h)$ become

$$\begin{bmatrix} \sigma_{11}(\boldsymbol{u}_h) \\ \sigma_{22}(\boldsymbol{u}_h) \\ \sigma_{12}(\boldsymbol{u}_h) \end{bmatrix} = \begin{bmatrix} \lambda_{\text{el},T} + 2\mu_T & \lambda_{\text{el},T} & 0 \\ \lambda_{\text{el},T} & \lambda_{\text{el},T} + 2\mu_T & 0 \\ 0 & 0 & \mu_T \end{bmatrix} \begin{bmatrix} \varepsilon_{11}(\boldsymbol{u}_h) \\ \varepsilon_{22}(\boldsymbol{u}_h) \\ 2\varepsilon_{12}(\boldsymbol{u}_h) \end{bmatrix} =: C_{\text{el}}\gamma(\boldsymbol{u}_h)$$

and then we obtain

$$\boldsymbol{\varepsilon}(v_h) : \boldsymbol{\sigma}_{\text{el}}(\boldsymbol{u}_h) = \sigma_{11}\varepsilon_{11} + \sigma_{22}\varepsilon_{22} + \underbrace{\sigma_{12}\varepsilon_{12} + \sigma_{21}\varepsilon_{21}}_{=2\sigma_{12}\varepsilon_{12}} = \gamma(v_h)^\top C_{\text{el}}\gamma(\boldsymbol{u}_h) = \mathbf{v}^\top R^\top C_{\text{el}} R\mathbf{u}.$$

From this chain of equalities and using the fact that all the matrices have constant coefficients, it follows that

$$\int_T \boldsymbol{\varepsilon}(\boldsymbol{v}_h) : \boldsymbol{\sigma}_{\text{el}}(\boldsymbol{u}_h)\, d\boldsymbol{x} = \int_T \mathbf{v}^\top R^\top C_{\text{el}} R\mathbf{u}\, d\boldsymbol{x} = |\Delta_T| \mathbf{v}^\top R^\top C_{\text{el}} R\mathbf{u}, \tag{6.55}$$

where the element elastic stiffness matrix is given by

$$A^{(T)} = |\Delta_T| R^\top C_{\text{el}} R.$$

Finaly, we want to provide an explicit expression for the components of the local elastic stiffness matrix $A^{(T)}$. After having introduced the following vectors

$$\mathbf{b} = \frac{1}{2|\Delta_T|}\begin{bmatrix} b_i \\ b_j \\ b_k \end{bmatrix}, \qquad \mathbf{c} = \frac{1}{2|\Delta_T|}\begin{bmatrix} c_i \\ c_j \\ c_k \end{bmatrix}, \qquad \mathbf{0} = \begin{bmatrix} 0 \\ 0 \\ 0 \end{bmatrix},$$

the matrix R, defined in (6.54), takes the form

$$R = \begin{bmatrix} \mathbf{b}^\top & \mathbf{0}^\top \\ \mathbf{0}^\top & \mathbf{c}^\top \\ \mathbf{c}^\top & \mathbf{b}^\top \end{bmatrix},$$

and the matrix multiplication $R^\top C_{\text{el}} R$ gives

$$\begin{aligned} \frac{A^{(T)}}{|\Delta_T|} = R^\top C_{\text{el}} R &= \begin{bmatrix} \mathbf{b} & \mathbf{0} & \mathbf{c} \\ \mathbf{0} & \mathbf{c} & \mathbf{b} \end{bmatrix} \begin{bmatrix} 2\mu_T + \lambda_{\text{el},T} & \lambda_{\text{el},T} & 0 \\ \lambda_{\text{el},T} & 2\mu_T + \lambda_{\text{el},T} & 0 \\ 0 & 0 & \mu_T \end{bmatrix} \begin{bmatrix} \mathbf{b}^\top & \mathbf{0}^\top \\ \mathbf{0}^\top & \mathbf{c}^\top \\ \mathbf{c}^\top & \mathbf{b}^\top \end{bmatrix} \\ &= \begin{bmatrix} \mathbf{b} & \mathbf{0} & \mathbf{c} \\ \mathbf{0} & \mathbf{c} & \mathbf{b} \end{bmatrix} \begin{bmatrix} (2\mu_T + \lambda_{\text{el},T})\mathbf{b}^\top & \lambda_{\text{el},T}\mathbf{c}^\top \\ \lambda_{\text{el},T}\mathbf{b}^\top & (2\mu_T + \lambda_{\text{el},T})\mathbf{c}^\top \\ \mu_T\mathbf{c}^\top & \mu_T\mathbf{b}^\top \end{bmatrix} \\ &= \begin{bmatrix} (2\mu_T + \lambda_{\text{el},T})\mathbf{b}\mathbf{b}^\top + \mu_T\mathbf{c}\mathbf{c}^\top & \lambda_{\text{el},T}\mathbf{b}\mathbf{c}^\top + \mu_T\mathbf{c}\mathbf{b}^\top \\ \lambda_{\text{el},T}\mathbf{c}\mathbf{b}^\top + \mu_T\mathbf{b}\mathbf{c}^\top & (2\mu_T + \lambda_{\text{el},T})\mathbf{c}\mathbf{c}^\top + \mu_T\mathbf{b}\mathbf{b}^\top \end{bmatrix}. \end{aligned}$$

It is more convenient to express the element elastic stiffness matrix in the form

$$A^{(T)} = \lambda_{\text{el},T} F^{(T)} + \mu_T G^{(T)},$$

where

$$F^{(T)} = |\Delta_T| \begin{bmatrix} \mathbf{b}\mathbf{b}^\top & \mathbf{b}\mathbf{c}^\top \\ \mathbf{c}\mathbf{b}^\top & \mathbf{c}\mathbf{c}^\top \end{bmatrix} \qquad \text{and} \qquad G^{(T)} = |\Delta_T| \begin{bmatrix} 2\mathbf{b}\mathbf{b}^\top + \mathbf{c}\mathbf{c}^\top & \mathbf{c}\mathbf{b}^\top \\ \mathbf{b}\mathbf{c}^\top & 2\mathbf{c}\mathbf{c}^\top + \mathbf{b}\mathbf{b}^\top \end{bmatrix},$$

which highlights the separate contributions given by the elastic Lamè parameters λ_{el} and μ. The computation of the element viscous stiffness matrix $B^{(T)}$ in (6.52) follows exactly the same procedure outlined for matrix $A^{(T)}$. Then, we have:

$$B^{(T)} = \lambda_{\text{vi},T} F^{(T)} + \eta_T G^{(T)},$$

which shows that the computation of the two element matrices $F^{(T)}$ and $G^{(T)}$ is sufficient to calculate both the element stiffness matrices $A^{(T)}$ and $B^{(T)}$.

6.2.3 Numerical Simulations

In this section we first investigate the numerical convergence of the Galerkin Spectral and Finite Element methods and then we solve two problems that are similar to the Lamb's problem discussed in 2.2.2.

Numerical Convergence

We now investigate the numerical convergence of the proposed numerical approaches by solving two problems with known smooth solution. More precisely, the first problem does not include a source term in the diplacement equations of motion, whereas the second does.

Convergence without source term A displacement function solution of the equations of motion with viscoelastic Kelvin-Voigt constitutive model and without additional source terms is computed using an approach similar to the one used in [252–254]. We start by assuming that the displacement and velocity have the form

$$u_x(x,z,t) = u_x^0 \exp(i\omega t + ik_x x + ik_z z), \tag{6.56a}$$
$$u_z(x,z,t) = u_z^0 \exp(i\omega t + ik_x x + ik_z z), \tag{6.56b}$$
$$v_x(x,z,t) = v_x^0 \exp(i\omega t + ik_x x + ik_z z), \tag{6.56c}$$
$$v_z(x,z,t) = v_z^0 \exp(i\omega t + ik_x x + ik_z z), \tag{6.56d}$$

where k_x and k_z are known real numbers, whereas the angular frequency ω and the amplitudes u_x^0, u_z^0, v_x^0 and v_z^0 are complex numbers to be computed using the procedure we are about to describe. Since the velocity is the time derivative of the displacement, we expect the amplitudes v_x^0 and v_z^0 to be defined by $v_x^0 = i\omega u_x^0$ and $v_z^0 = i\omega u_z^0$, respectively. Substituting the expressions in (6.56) into the following system of equations

$$\rho\, \dot{\boldsymbol{v}} = \operatorname{div}(\boldsymbol{\sigma}_{\text{vi}}(\boldsymbol{v}) + \boldsymbol{\sigma}_{\text{el}}(\boldsymbol{u}))$$
$$\dot{\boldsymbol{u}} = \boldsymbol{v}$$

and dividing both sides of each equation by the term $\exp(i\omega t + ik_x x + ik_z z)$, we obtain the eigenvalue problem

$$\begin{pmatrix} \frac{ik_z^2\eta + k_x^2(\lambda_{\text{vi}}+2\eta)}{\rho} & \frac{ik_xk_z(\lambda_{\text{vi}}+\eta)}{\rho} & \frac{ik_z^2\mu + k_x^2(\lambda_{\text{el}}+2\mu)}{\rho} & \frac{ik_xk_z(\lambda_{\text{el}}+\mu)}{\rho} \\ \frac{ik_xk_z(\lambda_{\text{vi}}+\eta)}{\rho} & \frac{ik_x^2\eta + k_z^2(\lambda_{\text{vi}}+2\eta)}{\rho} & \frac{ik_xk_z(\lambda_{\text{el}}+\mu)}{\rho} & \frac{ik_x^2\mu + k_z^2(\lambda_{\text{el}}+2\mu)}{\rho} \\ -i & 0 & 0 & 0 \\ 0 & -i & 0 & 0 \end{pmatrix} \begin{pmatrix} v_x^0 \\ v_z^0 \\ u_x^0 \\ u_z^0 \end{pmatrix} = \omega \begin{pmatrix} v_x^0 \\ v_z^0 \\ u_x^0 \\ u_z^0 \end{pmatrix}, \tag{6.57}$$

where the angular frequency is the eigenvalue and the amplitudes of the displacement and velocity fields are the components of the eigenvector. Solving the problem we obtain two pairs of eigenvalues,

with the two eigenvalues of each pair having opposite real part and equal imaginary part. Since the real part of ω is not responsible for the attenuation of the wave but it only determines how it propagates, we consider the two eigenvalues with positive real part, say $\omega^{(1)}$ and $\omega^{(2)}$, and neglect the others. Having denoted by $\mathbf{a}^{(1)}$ and $\mathbf{a}^{(2)}$ the eigenvectors associated to $\omega^{(1)}$ and $\omega^{(2)}$, we have that one of them, say $\mathbf{a}^{(1)}$, describes the propagation of a P wave whereas the other ($\mathbf{a}^{(2)}$) described the propagation of an S wave. Therefore, we can rewrite the displacement and velocity fields as a linear combination of these two type of waves solution of the eigenvalue problem (6.57), obtaining

$$v_x(x,z,t) = \alpha a_1^{(1)} \exp(i\omega^{(1)}t + ik_x x + ik_z z) + \beta a_1^{(2)} \exp(i\omega^{(2)}t + ik_x x + ik_z z) \tag{6.58a}$$

$$v_z(x,z,t) = \alpha a_2^{(1)} \exp(i\omega^{(1)}t + ik_x x + ik_z z) + \beta a_2^{(2)} \exp(i\omega^{(2)}t + ik_x x + ik_z z) \tag{6.58b}$$

$$u_x(x,z,t) = \alpha a_3^{(1)} \exp(i\omega^{(1)}t + ik_x x + ik_z z) + \beta a_3^{(2)} \exp(i\omega^{(2)}t + ik_x x + ik_z z) \tag{6.58c}$$

$$u_z(x,z,t) = \alpha a_4^{(1)} \exp(i\omega^{(1)}t + ik_x x + ik_z z) + \beta a_4^{(2)} \exp(i\omega^{(2)}t + ik_x x + ik_z z). \tag{6.58d}$$

By construction, the displacement defined by (6.58c) and (6.58d) is solution of the Cacuchy equations of motion with Kelvin-Voigt constitutive model when suitable initial and boundary conditions are considered. We numerically solve the initial-boundary value problem defined on the squared domain $(-2,+2)^2$ and consider an homogeneous material having density $\rho = 1\,\mathrm{kg\,m^{-3}}$, elastic Lamè parameters $\lambda_{\mathrm{el}} = \mu_{el} = 0.4\,\mathrm{Pa}$ and viscous parameters $\lambda_{\mathrm{vi}} = \eta = 0.005\,\mathrm{Pa\,s}$. Moreover, we consider displacement and velocity fields with wavenumbers $k_x = k_z = \pi$. The eigenvalues with positive real part obtained solving the eigenvalue problem (6.57) are $\omega^{(1)} \approx 4.86468 + 0.148044i$ and $\omega^{(2)} \approx 2.80949 + 0.049348i$. In accordance with what we have said above, the components of $\mathbf{a}^{(1)}$ are such that $a_1^{(1)} = a_2^{(1)}$ and $a_3^{(1)} = a_4^{(1)}$, which means that the direction of the motion is given by the wavenumber vector $\mathbf{k} = (k_x, k_z) = (\pi, \pi)$ (P-wave), whereas the components of $\mathbf{a}^{(2)}$ are such that $a_1^{(2)} = -a_2^{(2)}$ and $a_3^{(2)} = -a_4^{(2)}$, i.e., the motion develops along the direction orthogonal to the one defined by the wavenumber vector (S-wave). Then, we choose coefficients α and β in (6.58) so that $\alpha a_3^{(1)} = \alpha a_4^{(1)} = 1$ and $\beta a_3^{(2)} = -\beta a_4^{(2)} = 1$. Furthermore, we choose initial condition given by the real part of the expressions in (6.58) evaluated at time $t = 0\,\mathrm{s}$; in this way the solution is real as well and the displacement field has the form:

$$u_x(x,z,t) = \exp(-\Im\omega^{(1)}t)\cos(\Re\omega^{(1)}t + k_x x + k_z z) + \exp(-\Im\omega^{(2)}t)\cos(\Re\omega^{(2)}t + k_x x + k_z z) \tag{6.59a}$$

$$u_z(x,z,t) = \exp(-\Im\omega^{(1)}t)\cos(\Re\omega^{(1)}t + k_x x + k_z z) - \exp(-\Im\omega^{(2)}t)\cos(\Re\omega^{(2)}t + k_x x + k_z z) \tag{6.59b}$$

We impose time-dependent Dirichlet boundary conditions on the left and right boundaries and time-dependent Neumann boundary conditions on the top and bottom boundaries. The solution in time is computed again by means of eigenvalue decomposition and exact integration as described in §5.3.3. The relative errors of the solution in the L^2 and V_m norms are computed at time $t = 1\,\mathrm{s}$. These erros are shown in Figure 6.4 and listed in Table 6.8. The left panel of Figure 6.5 shows the behaviour of the relative errors obtained by solving the problem with the Spectral Method. The errors are plotted against the basis functions polynomial degree N. Due to the regularity of the solution, we observe that exponential convergence of the numerical solution to the exact one is achieved using both the L^2 and V_m norms. The right panel of Figure 6.5 shows the behaviour of the relative errors obtained solving the problem with the Finite Element Method. The errors are plotted as functions of the mesh parameter h. As expected, we achieve quadratic convergence for the error in L^2-norm and linear convergence for the error in the V_m-norm.

Convergence with source term We also investigate the numerical convergence for a problem with manufactured solution and source term. In particular, the source term is defined in such a way that the solution of the displacement equations with viscoelastic Kelvin-Voigt constitutive model is given by:

$$u_x(x,z,t) = \sin^3(\pi x)\cos^3\left(\frac{\pi}{2}z\right)\sin^3(2\pi t) \tag{6.60a}$$

$$u_z(x,z,t) = \cos^3\left(\frac{\pi}{2}x\right)\sin^3(\pi z)\sin^3(2\pi t). \tag{6.60b}$$

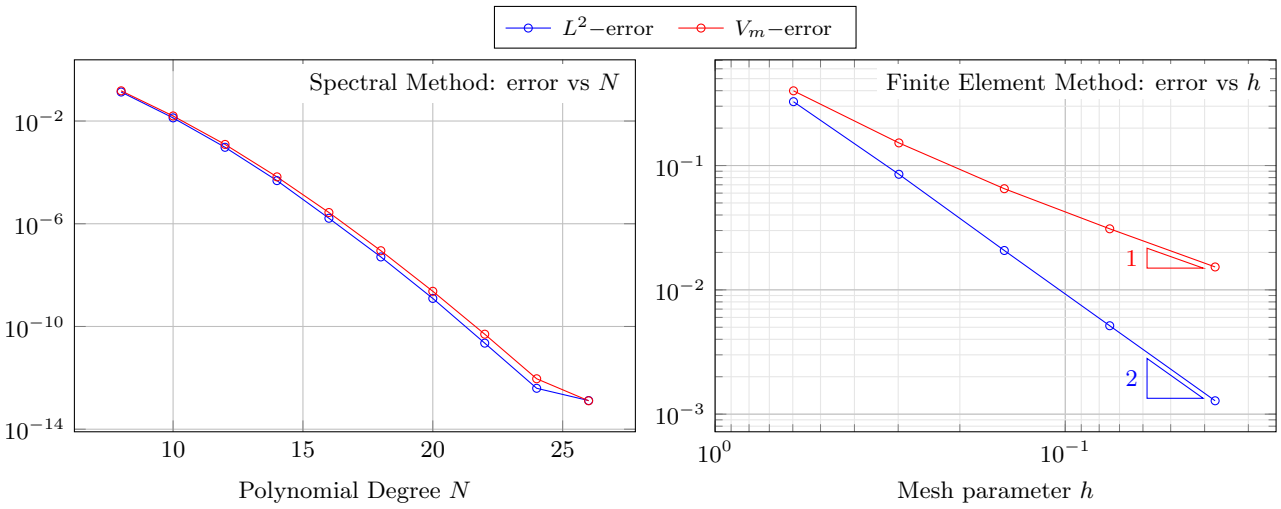


Figure 6.4: Relative errors, at $t = 0.35\,\mathrm{s}$, for the manufactured problem with exact solution (6.59).

Spectral Method			Finite Element Method					
N	rel error L^2	rel error V_m	h	elements	rel error L^2	rate L^2	rel error V_m	rate V_m
8	$1.34e-01$	$1.50e-01$	$5.973e-01$	160	$3.26e-01$		$3.99e-01$	
12	$9.48e-04$	$1.23e-03$	$2.986e-01$	640	$8.51e-02$	1.940	$1.52e-01$	1.392
16	$1.64e-06$	$2.74e-06$	$1.493e-01$	2560	$2.07e-02$	2.037	$6.51e-02$	1.224
20	$1.24e-09$	$2.34e-09$	$7.466e-02$	10240	$5.14e-03$	2.011	$3.10e-02$	1.072
24	$3.92e-13$	$9.20e-13$	$3.733e-02$	40960	$1.28e-03$	2.005	$1.53e-02$	1.019

Table 6.8: Relative errors, at $t = 0.35\,\mathrm{s}$, for the manufactured problem with exact solution (6.59).

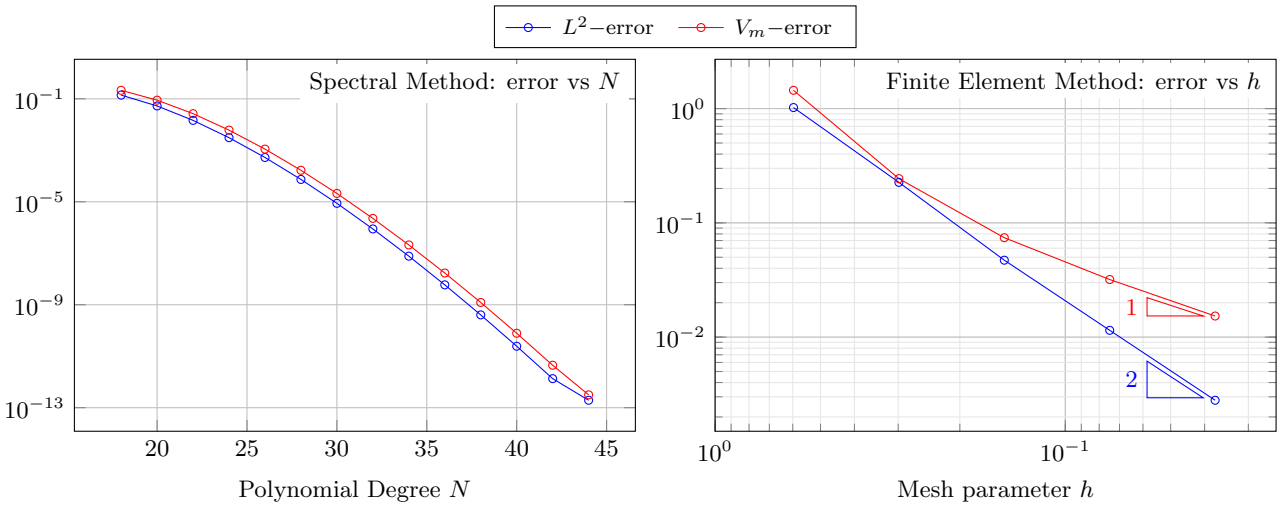


Figure 6.5: Relative errors, at $t = 0.35\,\mathrm{s}$, for the manufactured problem with exact solution (6.60).

Spectral Method			Finite Element Method					
N	rel error L^2	rel error V_m	h	elements	rel error L^2	rate L^2	rel error V_m	rate V_m
22	$1.46e-02$	$2.65e-02$	5.973e-01	160	1.02e+00	-	1.45e+00	-
26	$5.27e-04$	$1.12e-03$	2.986e-01	640	2.26e-01	2.176	2.44e-01	2.569
30	$8.73e-06$	$2.11e-05$	1.493e-01	2560	4.71e-02	2.263	7.41e-02	1.717
34	$7.73e-08$	$2.11e-07$	7.466e-02	10240	1.15e-02	2.040	3.19e-02	1.216
38	$4.03e-10$	$1.23e-09$	3.733e-02	40960	2.80e-03	2.033	1.53e-02	1.061

Table 6.9: Relative errors, at $t = 0.35\,\mathrm{s}$, for the manufactured problem with exact solution (6.60).

We solve the problem in the squared domain $(-2,+2)^2$ and we consider an homogeneous material having density $\rho = 1\,\mathrm{kg\,m^{-3}}$, elastic Lamè parameters $\lambda_{\mathrm{el}} = \mu_{el} = 1\,\mathrm{Pa}$ and viscous parameters $\lambda_{\mathrm{vi}} = \eta = 0.1\,\mathrm{Pa\,s}$. We impose time-dependent Dirichlet boundary conditions on the left and right boundaries and time-dependent Neumann boundary conditions on the top and bottom boundaries. The solution in time is computed again by means of eigenvalue decomposition and exact integration as described in §5.3.3. The relative errors of the solution in the L^2 and V_m norms are computed at time $t = 0.35\,\mathrm{s}$. These erros are listed in Table 6.9 and plotted in Figure 6.5. The left panel of Figure 6.5 shows the behaviour of the relative errors (blue line for the L^2-norm and and red line for the V_m-norm) obtained with the Spectral Method. Even with source term, due to the regularity of the solution, we see that the convergence of the numerical solution to the exact one is exponential in the basis functions polynomial degree N. The right panel of Figure 6.5 shows the behaviour of the relative errors obtained solving the problem with the Finite Element Method. The errors are plotted against the mesh parameter: again, we achieve quadratic convergence for the error in L^2-norm and linear convergence for the error in the V_m-norm.

Application Example: A variant of Lamb's Plane Strain Problem

In this section we consider the numerical solution of a variant of the well-known Lamb's problem described in Section 2.2.2. Let us recall that this problem, formulated for the first time by Lamb in 1903 [122], consists of studying the dynamic response in a homogeneous and isotropic elastic half-space due to the action of an applied vertical or horizontal point load. Since the first contribution given by Lamb, the problem has been studied by several researchers who provided closed-form solutions describing the motion of the free-surface of an elastic half-space in the particular case of a vertical point load acting on it. Here we clearly focus on the plane-strain version of the Lamb's problem, whose exact solution is discussed in Section 2.2.2. Moreover, the problem that we address is a variant of the original one, in the sense that, instead of considering an half-space, we simulate the dynamic response due to the application of a vertical point load onto the upper horizontal boundary of a squared domain $\Omega = (-1/2,+1/2)^2$. Furthermore, we simulate the propagation of waves on both elastic and linear viscoelastic Kelvin-Voigt materials. Concerning the boundary conditions, we impose zero Neumann boundary conditions on the vertical boundaries of the square and zero Dirichlet boundary conditions on the bottom horizontal boundary. We first test the numerical solution obtained in the purely elastic case against the exact solution of the Lamb's problem. The elastic material is characterised by density $\rho = 1\,\mathrm{kg\,m^{-3}}$ and Lamè parameters $\lambda_{\mathrm{el}} = 0.27\,\mathrm{Pa}$ and $\mu = 0.033\,\mathrm{Pa}$. The source is defined as the product between a Dirac delta in space, which is acting on the point of the upper boundary having coordinates $(0, 1/2)$, and a Ricker-type wavelet in time, i.e., a function having the form $f(t) = A(1 - 2(\pi f_0(t-t_0))^2)\exp(-(\pi f_0(t-t_0))^2)$ where $A = 1\,\mathrm{m}$, $f_0 = 2\,\mathrm{Hz}$ and $t_0 = 1\,\mathrm{s}$. We consider the receiver to be located at the upper boundary as well and at $0.1\,\mathrm{m}$ from the source. The problem is solved by using polynomial basis functions having degree up to 80 in each coordinate (x and z). Figure 6.6 shows the comparison between the exact solution (black line) and the numerical solution (red line) over the time interval $t \in [0,3]\mathrm{s}$ for the horizontal and vertical components of the displacement (first row) and the horizontal and vertical components of the velocity (second row). We can clearly see that in all the four panels the numerical solution is in good agreement with the exact one. Then, we proceed to compute the numerical solution of a problem that differs from the previous one only by the choice of the constitutive law, which is now of Kelvin-Voigt type. In particular, we solve the problem for different values of the quality factors Q_P and Q_S, whose expressions have been defined, in the case of Kelvin-Voigt materials, in Equation (2.35). The set of values considered for the quality factors has been obtained by varying the viscosity parameters λ_{vi} and η and keeping the Lamè elasticity parameters fixed to the values $\lambda_{\mathrm{el}} = 0.27\,\mathrm{Pa}$ and $\mu = 0.033\,\mathrm{Pa}$. Then, the numerical solutions obtained for different values of the quality factors have been compared with the aim of highlighting how the viscosity affects the dynamic response to the applied load. Figure 6.7 shows the horizontal and vertical component of the displacement (first row) and the horizontal and vertical component of the velocity (second row). Each curve shows the solution associated to a different value of the quality factors. Since in the viscoelastic case the exact solution is not available, we also plot for reference the exact solution of the original elastic Lamb's problem (black thicker line). As expected, the results show that decreasing

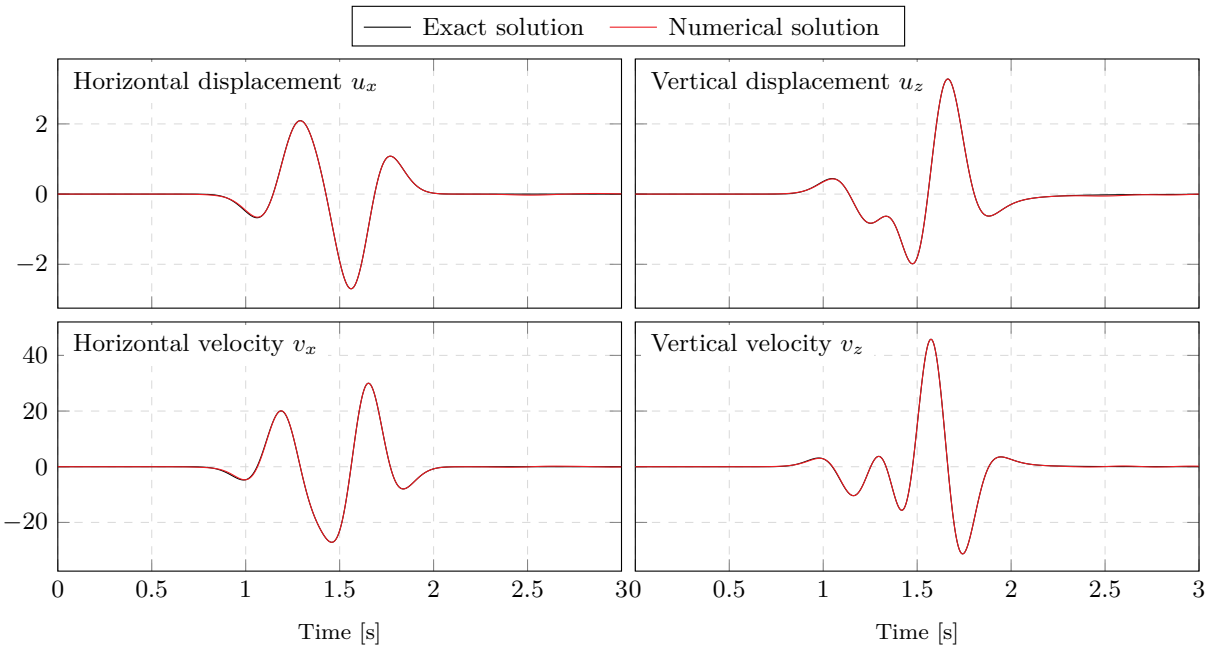


Figure 6.6: Lamb's plane-strain problem: comparison between the exact solution (black line) and the numerical solution (red line) for the horizontal and vertical components of the displacement (first row) and the of the velocity (second row) over the time interval $t \in [0, 3]$s. The vertical point load source is located at $x = 0\,\mathrm{m}$ and $z = 0\,\mathrm{m}$ and has a dependence on time defined by a Ricker-type wavelet having dominant frequency $2\,\mathrm{Hz}$. The receiver is located at the boundary point having coordinates $x = 0.1\,\mathrm{m}$ and $z = 0\,\mathrm{m}$. The medium is purely elastic, with density $\rho = 1\,\mathrm{kg\,m^{-3}}$ and Lamè parameters $\lambda_{el} = 0.27\,\mathrm{Pa}$ and $\mu = 0.033\,\mathrm{Pa}$.

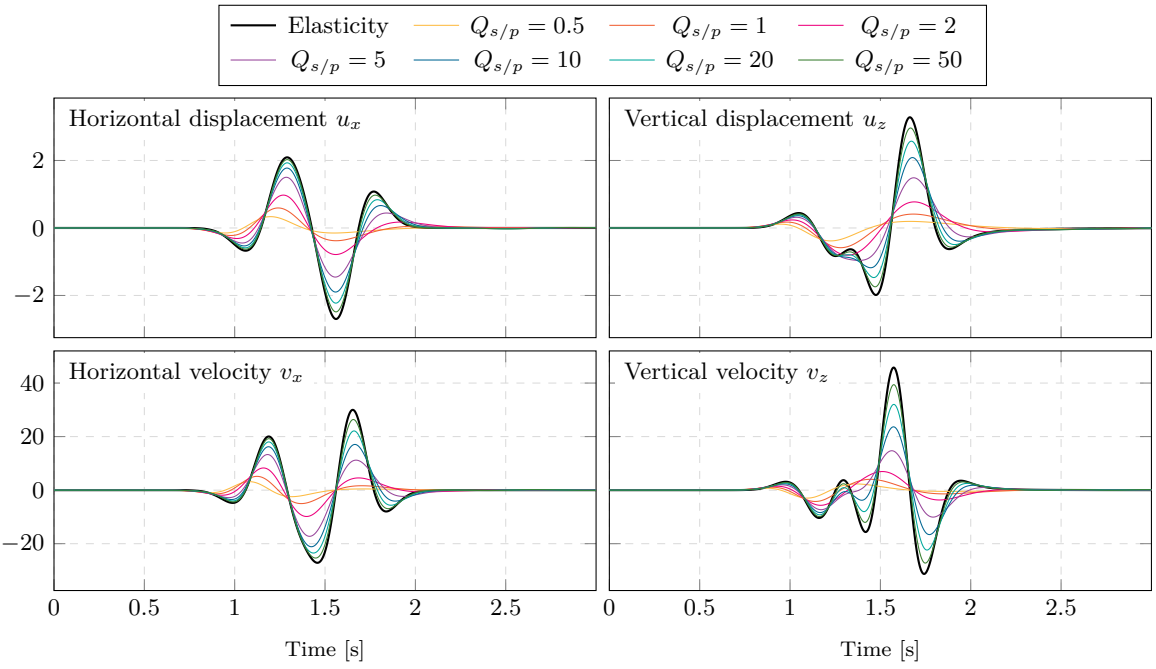


Figure 6.7: Variant of Lamb's plane-strain Problem. Comparison between the exact solution (black line) in the lossless case and the numerical solutions (coloured lines) in the Kelvin-Voigt viscoelastic case for different values of the quality factor Q_P and Q_S. The displacement is shown in the first row, while the velocity is shown in the second row. The horizontal and vertical components of the displacement and velocity fields are showns in the left and right column, respectively.

the value of the quality factors (which means that, at constant elasticity, we increase the value of the viscosity), the attenuation becomes stronger and therefore the amplitude of the waves decreases. Finally, the panels in Figure 6.8 show the displacement magnitude at four different times (rows) and for three different material properties (columns). In particular, the first column shows the numerical solution in the lossless case (purely elastic material), whereas the second and third columns show the numerical solution in the Kelvin-Voigt viscoelastic case, with different values of the quality factors. The panels in the first row show the displacement wave 2 seconds after that it started to propagate from the point on the upper horizontal boundary where the vertical load (the white arrow on the panels) is applied. In the second row, the first wave has reached the boundary of the computational domain and, owing to the imposed zero Dirichlet and zero Neumann boundary conditions, it has been reflected. Moreover, the main displacement wave (the one with greater amplitude) has reached the lateral boundary of the domain and, as expected, we can clearly see that its amplitude is smaller for smaller values of the quality factors (i.e., higher values of the viscosity). In the third and fourth rows the waves continue to propagate and to reflect once they reach the boundaries. Furthermore, as time goes by, the difference, in terms of amplitude value, between the propagating displacement waves increases, thus showing once again the dissipative nature characterising Kelvin-Voigt materials.

Application Example: Homogeneous and Heterogeneous Materials

We now simulate the propagation of displacement waves on heterogeneous materials and compare the viscoelastic solution with the elastic one. As in the previous example we consider the domain $\Omega = (-1/2, +1/2)^2$. However, the waves are now generated by the application of an horizontal buried point load acting on the point having coordinates $(0, 0.2)$. The time dependent behaviour of the point load is described by the same Ricker wavelet considered in the previous problem. We also impose the same boundary conditions, i.e., zero Dirichlet boundary conditions on the lower horizontal boundary and zero Neumann boundary conditions otherwise. Concerning the material properties, we consider three different cases. In the first case, the material is purely elastic and homogeneous, with density $\rho = 1\,\mathrm{kg\,m^{-3}}$ and Lamè parameters $\lambda_{el} = 0.27\,\mathrm{Pa}$ and $\mu = 0.033\,\mathrm{Pa}$, whereas in the other two cases the material is viscoelastic and heterogeneous. In the heterogeneous setting, we divide the domain into two subdomains $\Omega_+ := \{(x, z) \in \Omega \ : \ z > 0\}$ and $\Omega_- := \{(x, z) \in \Omega \ : \ z < 0\}$. Then we assign different material properties to Ω_+ and Ω_-. In particular, in the second case the elasticity is kept constant in the whole domain Ω, while the viscosity in Ω_- is 500 times higher than the viscosity in Ω_+. In the third case, the viscosity is kept constant Ω, whereas the elasticity in Ω_- is 4 times lower compared to the elasticity of Ω_+. The numerical results are shown in Figure 6.9. Each panel shows the displacement magnitude at four different times (rows) and for three different material properties (columns). The continuous horizontal green line in the panels of the second and third column is used to denote the interface between different materials. The dashed green line in the panels of the first column is used as a guide line to facilitate the comparison with the results obtained in the case of heterogeneous materials but does not denote any material interface (we remark that the medium is indeed homogeneous). The figures show how the material heterogeneity and the presence of viscosity affects the propagation of waves, resulting in different attenuation and reflections at material interfaces. In particular, the first thing we can notice is that the solutions at time $t = 1.8\,\mathrm{s}$ (first row panels) are very similar on Ω_+ and do not manifest dependence on the material parameters characterising the materials. This is due to the fact that the main displacement wave, that has originated from the point having coordinates $(0, 0.2)$, has not reached the material interface yet and is still propagating on Ω_+. We recall that the three upper subdomains are all characterised by the same elastic properties and that the ones of the second and third column also have the same viscous parameters λ_{vi} and η. Moreover, the values of the viscous parameters are very small, which implies that the quality factors Q_P and Q_S are very high and that the attenuation of the amplitude of the waves is very low. As a consequence, the viscoelastic solution turns out to be really similar to the one obtained in the lossless case. On the other hand we also notice that there is another wave, having a much smaller amplitude that has already reached the material interface and is propagating on Ω_- with different speed depending on the material configuration. Looking now at the solutions at time $t = 2.8\,\mathrm{s}$, i.e., the panels in the second row, we can see that in all the cases the main wave has reached the upper horizontal boundary and a reflected wave

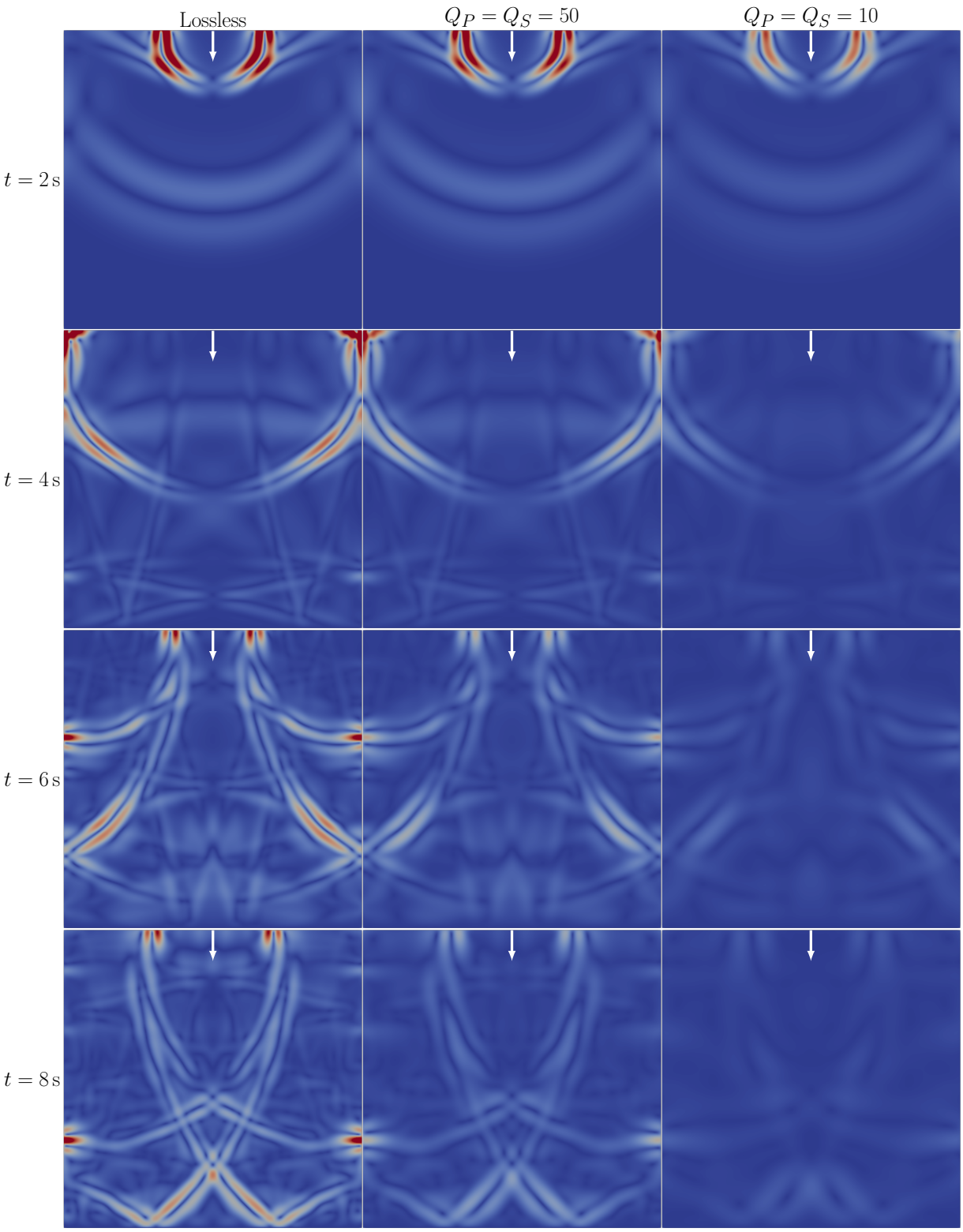


Figure 6.8: Variant of Lamb's plane-strain problem. Each panel shows the displacement magnitude at different times (rows) and for different material properties (columns). The waves propagate due to the presence of a vertical point load acting at the point of the horizontal boundary having coordinates $(0, 0.5)$. The panels show how higher values of the viscosity parameters result in a stronger dissipation of the propagating waves.

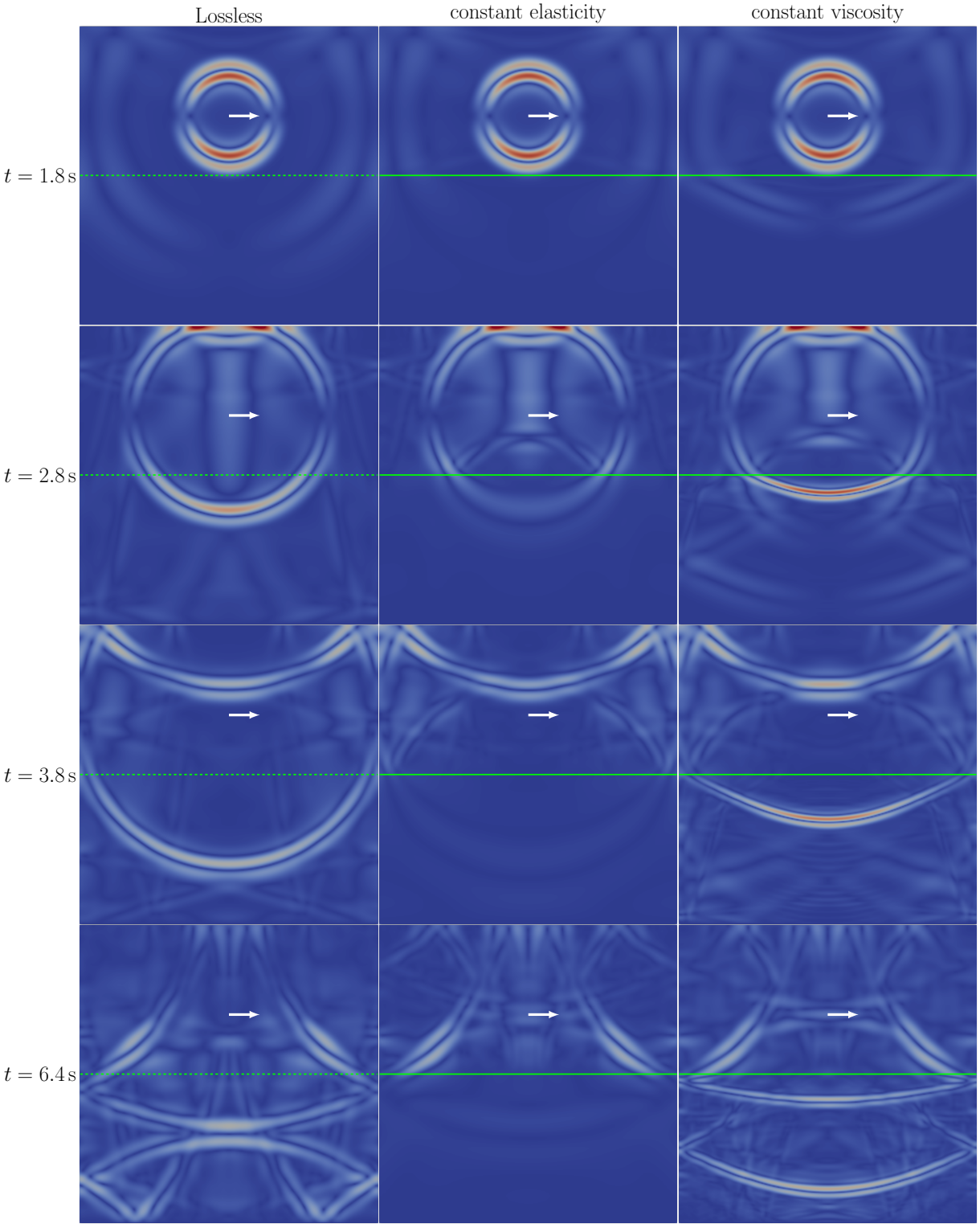


Figure 6.9: Each panel shows the displacement magnitude at different times (rows) and for different material properties (columns). The waves propagates due to the presence of an horizontal point load (white arrow) acting at the point of the domain $\Omega = (-1/2, +1/2)^2$ having coordinate $(0, 0.2)$. The continuous green line in the panels of the second and third column is used to denote the interface between different materials. The dashed green line in the panels of the lossless case is used as a reference line for easier comparison with the results obtained with heterogeneous materials. The figures show how the material heterogeneity and the presence of viscosity affects the propagation of waves, resulting in different attenuation and reflections at material interfaces.

is starting to propagate due to the imposition of zero Neumann boundary conditions. Furthermore, since the main propagating wave has also reached the material interface, we clearly observe the effect of the change in material parameters. In particular, in the panel of the second column, we observe a much higher attenuation of the wave as a consequence of the viscosity being 500 times higher in Ω_- compared to Ω_+. On the other hand, looking at the panel in the third column, we notice that the displacement wave travels with a lower phase velocity in Ω_- than in Ω_+, this also affecting the shape of the wavefront, which is observed to be much more flat in this case than in the other two scenarios. This is a consequence of the fact that the Lamè elastic parameters in Ω_- are four times smaller than the ones in Ω_+. Moreover, in the two heterogeneous cases we also observe that a reflection at the material interface has occurred: indeed, a wave with small amplitude has appeared at the material iterface and is moving towards the upper horizontal boundary. At time $t = 3.8\,\mathrm{s}$, we observe that in all the scenarios the wave generated from the reflection against the upper horizontal boundary is propagating towards the bottom of the squared domain. Owing to the fact that in Ω_+ the elastic parameters are the same and that the quality factors are very high, the phase velocity and the shape of the wavefront are almost the same in all the three cases, with small differences mainly due to the interaction between this wave and other waves generated by other reflections at the vertical boundaries or at the material interaface and having different amplitudes depending on the material parameters. Moreover, the wave on Ω_- is still moving towards the bottom horizontal boundary. Owing to the much higher viscosity, this wave can be only barely seen in the second case, whereas the difference in phase velocity between the wave on first panel and the one on the third panel is even more evident than it was at $t = 2.8\,\mathrm{s}$. Finally, at time $t = 8.49\,\mathrm{s}$, we see that, in the lossless case, the initial wave has reached the bottom horizontal surface and has been reflected. On the other hand, in the third case we do not observe this reflection, as the phase velocity is much lower and the wave have not reached the bottom boundary yet. Moreover, in both these two cases we observe that the wave generated from the reflection with the upper horizontal boundary at time $t = 2.8\,\mathrm{s}$ has reached the subdomain Ω_-. Finally, in the second panel we still do not observe any wave on Ω_- due to the very high viscosity parameters characterising this subdomain.

6.3 Axisymmetric Cylindrical Coordinates

In this Section we discuss the numerical computation of *axisymmetric* solutions of the displacement equations governing the propagation of waves on Kelvin-Voigt viscoelastic materials. In Section 6.3.1 we introduce the Cauchy momentum equations in cylindrical coordinates (r, θ, z) and we show how they simplify under the assumption of axial symmetry. Under this assumption, the displacement field has only radial and axial components, which are both independent of the angle θ. In Section 6.3.2 we construct the set of basis functions used in the Galerkin semi-discrete approximation of the weak formulation when applying the Spectral (Element) Method. In particular, we follow the same procedure that has been outlined in Section 6.2.2, where we have defined continuous basis functions that are boundary-adapted polynomials within each material domain. However, owing to the assumption of cylindrical symmetry, special attention must be devoted to the definition of the radial component of the vector basis functions, which must be zero at $r = 0$. Finally, in Section 6.3.3 we present some results. As in the one-dimensional and in the two-dimensional Cartesian frameworks, we first show the convergence of the implemented numerical scheme by solving a problem with manufactured solution and subsequently we simulate the propagation of axisymmetric waves generated by the action of a point load in both homogeneous and heterogeneous materials.

6.3.1 Problem Formulation

When using cylindrical coordinates (r, θ, z), the displacement field is written as

$$\boldsymbol{u} = (u_r(r, \theta, z), u_\theta(r, \theta, z), u_z(r, \theta, z)),$$

where u_r is the radial component, u_θ is the tangential component and u_z is the axial component. Within this setting, the gradient of the displacement field is given by

$$\nabla \boldsymbol{u} = \begin{bmatrix} \dfrac{\partial u_r}{\partial r} & \dfrac{1}{r}\dfrac{\partial u_r}{\partial \theta} - \dfrac{u_\theta}{r} & \dfrac{\partial u_r}{\partial z} \\ \dfrac{\partial u_\theta}{\partial r} & \dfrac{1}{r}\dfrac{\partial u_\theta}{\partial \theta} + \dfrac{u_r}{r} & \dfrac{\partial u_\theta}{\partial z} \\ \dfrac{\partial u_z}{\partial r} & \dfrac{1}{r}\dfrac{\partial u_z}{\partial \theta} & \dfrac{\partial u_z}{\partial z} \end{bmatrix}$$

and the Cauchy momentum equations have the following form:

$$\rho \frac{\partial^2 u_r}{\partial t^2} = \frac{\partial \sigma_{rr}}{\partial r} + \frac{1}{r}\frac{\partial \sigma_{r\theta}}{\partial \theta} + \frac{\partial \sigma_{rz}}{\partial z} + \frac{\sigma_{rr} - \sigma_{\theta\theta}}{r} + f_r, \tag{6.61a}$$

$$\rho \frac{\partial^2 u_\theta}{\partial t^2} = \frac{\partial \sigma_{r\theta}}{\partial r} + \frac{1}{r}\frac{\partial \sigma_{\theta\theta}}{\partial \theta} + \frac{\partial \sigma_{\theta z}}{\partial z} + \frac{\sigma_{r\theta} + \sigma_{\theta r}}{r} + f_\theta, \tag{6.61b}$$

$$\rho \frac{\partial^2 u_z}{\partial t^2} = \frac{\partial \sigma_{zr}}{\partial r} + \frac{1}{r}\frac{\partial \sigma_{z\theta}}{\partial \theta} + \frac{\partial \sigma_{zz}}{\partial z} + \frac{\sigma_{zr}}{r} + f_z. \tag{6.61c}$$

We now assume the problem to be axisymmetric. This is equivalent to say that the tangential component of the displacement, u_θ, is equal to zero and that the remaining components, i.e., the radial and axial displacements, does not depend on the angle θ. Under this assumption, the gradient and the strain tensor associated to the displacement field $\boldsymbol{u} = (u_r(r,z), u_z(r,z))$ are given by:

$$\nabla \boldsymbol{u} = \begin{bmatrix} \dfrac{\partial u_r}{\partial r} & 0 & \dfrac{\partial u_r}{\partial z} \\ 0 & \dfrac{u_r}{r} & 0 \\ \dfrac{\partial u_z}{\partial r} & 0 & \dfrac{\partial u_z}{\partial z} \end{bmatrix} \qquad \boldsymbol{\varepsilon}(\boldsymbol{u}) = \begin{bmatrix} \dfrac{\partial u_r}{\partial r} & 0 & \dfrac{1}{2}\left(\dfrac{\partial u_r}{\partial z} + \dfrac{\partial u_z}{\partial r}\right) \\ 0 & \dfrac{u_r}{r} & 0 \\ \dfrac{1}{2}\left(\dfrac{\partial u_z}{\partial r} + \dfrac{\partial u_r}{\partial z}\right) & 0 & \dfrac{\partial u_z}{\partial z} \end{bmatrix}. \tag{6.62}$$

The Cauchy momentum equations simplify as well in the case of axisymmetric problem. Indeed, the second equation (6.61b) is not present and all the derivatives with respect the angle θ vanish. However, it is worth noting that $\sigma_{\theta\theta}$ is not zero, since the radial displacement produces a non-vanishing term in $\varepsilon_{\theta\theta}$. Then, for an axisymmetric problem, we obtain the following Cauchy equations:

$$\rho \frac{\partial^2 u_r}{\partial t^2} = \frac{\partial \sigma_{rr}}{\partial r} + \frac{\partial \sigma_{rz}}{\partial z} + \frac{\sigma_{rr} - \sigma_{\theta\theta}}{r} + f_r, \tag{6.63a}$$

$$\rho \frac{\partial^2 u_z}{\partial t^2} = \frac{\partial \sigma_{zr}}{\partial r} + \frac{\partial \sigma_{zz}}{\partial z} + \frac{\sigma_{zr}}{r} + f_z. \tag{6.63b}$$

6.3.2 Basis Functions Definition

The weak formulation of initial-boundary value problem obtained by combining the axisymmetric Cauchy momentum equations (6.63) with the Kelvin-Voigt constitutive model is discretised in space by means of the Galerkin Spectral (Element) Method. In this Section we define Spectral-Galerkin basis functions on a cylindrical domain $\Omega \subset \mathbb{R}^3$ by following a procedure similar to the one described Section 6.1.2, where piecewise boundary-adapted polynomial basis functions depending on the Cartesian coordinates (x, z) have been defined.

1. We perform a partition of the cylindrical domain $\Omega \subset \mathbb{R}^3$ into M disjoint subdomains (or elements) $\Omega_1, \ldots, \Omega_M$, each one associated to a different material.

2. We choose a set of one-dimensional polynomial basis functions defined on the reference interval $(-1, +1)$.

3. We define a set of two-dimensional basis functions on each element Ω_m of the partition by tensorization of mapped one-dimensional reference polynomial bases.

4. We define global continuous basis functions by *glueing* the local basis functions at the interfaces.

5. We construct vector basis functions in such a way each scalar component is globally continuous and defined using the procedure in 2 – 4.

6. We deal with the singularity introduced by the cylindrical coordinates at $r = 0$ by removing vector basis functions whose radial component is not equal to zero at $r = 0$.

Partition of the domain The cylindrical domain $\Omega \subset \mathbb{R}^3$ is partitioned into a number $M \geq 1$ of subdomains (or elements) denoted by Ω_m, with $m = 1, \ldots, M$. As in the one-dimensional and in the two-dimensional Cartesian frameworks, each subdomain Ω_m represents a different material, characterized by density ρ_m, elastic Lamè parameters $\lambda_{\text{el},m}$ and μ_m, and viscous Lamè parameters $\lambda_{\text{vi},m}$ and η_m. In particular, the subdomains Ω_m are obtained by taking a cylinder whose axis is the $z-$axis of a Cartesian reference frame and then considering the two following ways of partitioning (or a combination of them):

1. cutting the cylinder with horizontal planes (i.e. such that $z = const$),

2. considering the cylinder as made by a "true" cylinder plus a certain number of *hollow cylinders* (or cylindrical shells).

Using cyldrical coordinates (r, θ, z) and assuming (as we have done in Section 6.3.1) that the solution of the displacement equations of motion has circular symmetry around the axis of the cylinder, we can solve the problem on a two-dimensional rectangular domain $\Omega \subset \{(r, z) \ : \ r \geq 0\}$. Therefore, as in the two-dimensional Cartesian setting, the elements Ω_m are rectangular, i.e., for all $m = 1, \ldots, M$, $\Omega_m = (r_{0,m}, r_{1,m}) \times (z_{0,m}, z_{1,m})$.

Scalar basis functions For all $m = 1, \ldots, M$, let $\{\hat{\varphi}^{m,r}_{k_r}, \ k_r = 0, \ldots, N_{m,r}\}$ and $\{\hat{\varphi}^{m,z}_{k_z}, \ k_z = 0, \ldots, N_{m,z}\}$ be two families of one-dimensional boundary-adapted polynomials defined on the reference interval $(-1, +1)$. Moreover, let $F_{r,m}$ and $F_{z,m}$ be two affine functions that map the reference interval $(-1, +1)$ into the intervals $(r_{0,m}, r_{1,m})$ and $(z_{0,m}, z_{1,m})$ defining the rectangular element $\Omega_m := (r_{0,m}, r_{1,m}) \times (z_{0,m}, z_{1,m})$, i.e.,

$$F_{r,m} \colon (-1, +1) \to (r_{0,m}, r_{1,m}) \qquad F_{z,m} \colon (-1, +1) \to (z_{0,m}, z_{1,m}).$$

Then, we denote by $\varphi^{m,r}_{k_r}$, $k_r = 0, \ldots, N_{m,r}$, and $\varphi^{m,z}_{k_z}$, $k_z = 0, \ldots, N_{m,z}$, the images of the reference one-dimensional polynomial basis $\hat{\varphi}^{m,r}_{k_r}$ and $\hat{\varphi}^{m,z}_{k_z}$ under the affine maps $F_{r,m}$ and $F_{z,m}$, i.e.,

$$\varphi^{m,r}_{k_r}(r) = \hat{\varphi}^{m,r}_{k_r}(F^{-1}_{r,m}(r)) \qquad \varphi^{m,z}_{k_z}(z) = \hat{\varphi}^{m,z}_{k_z}(F^{-1}_{z,m}(z)).$$

These two families of mapped basis functions tensorize to produce a set of boundary-adapted polynomial basis on the element Ω_m:

$$\varphi^{(m)}_j(r, z) = \varphi^{m,r}_{k_r(j)}(r)\varphi^{m,z}_{k_z(j)}(z), \qquad j = 1, \ldots, \bar{N}_m,$$

where $\bar{N}_m := (N_{m,r} + 1)(N_{m,z} + 1)$. Note that the indices $k_{m,r}$ and $k_{m,z}$ of the one-dimensional bases are now functions of the index j, i.e., a one-to-one map

$$\{1, 2, \ldots, \bar{N}_m\} \ni j \mapsto (k_r(j), k_z(j)) \in \{0, 1, \ldots, N_{m,r}\} \times \{0, 1, \ldots, N_{m,z}\}$$

has been introduced for each element Ω_m with the aim of providing an ordering of multi-indices $(k_{m,r}, k_{m,z})$. The set $\{\varphi^{(m)}_j, \ j = 1, \ldots, \bar{N}_m\}$ is formed by *bubble*, *vertex* and *edge* functions and generates the space $V_{N_m}(\Omega_m)$, with $N_m = (N_{m,r}, N_{m,z})$ of tensor product polynomials defined on Ω_m, i.e.,

$$V_{N_m}(\Omega_m) := \text{span}\{\varphi^{(m)}_j \ : \ j = 1, \ldots, \bar{N}_m\}.$$

Finally, we introduce continuous basis functions defined over the whole domain Ω. So, we define the space

$$V_\delta = \{v \in C^0(\bar{\Omega}) \ : \ v|_{\Omega_m} \in V_{N_m}(\Omega_m), \ m = 1, \dots, M\}, \tag{6.64}$$

where we recall that the subindex δ is an abridged notation for "discrete" taking into account both the geometric dicretisation of the domain $\Omega = \cup_m \Omega_m$ and the different polynomial degrees $N_m = (N_{m,r}, N_{m,z})$ used on each element. The space V_δ contains all the functions that are globally continuous over Ω and that are polynomials of degree less than or equal to $N_{m,r}$ with respect to variable r and of degree less than or equal to $N_{m,z}$ with respect to variable z when restricted to element Ω_m. A basis for the whole space V_δ is obtained as discussed in Section 6.2.2 by extending bubble functions to zero in the region of the domain outside the element where they were originally defined and by "glueing" together vertex (resp. edge) basis functions defined on continguous elements and matching at the common vertex (resp. edge), thereby guaranteeing global continuity over Ω.

Vector basis functions As we have done in the two-dimensional Cartesian setting (§6.2.2), we define vector basis functions in such a way that each scalar component belongs to the space V_δ defined in (6.64), i.e., we define the space V_N used in Section 5.3 by setting $V_N := [V_\delta]^2$. Similarly, we can define the space $V_{N_0} := [V_{0,\delta}]^2$, where $V_{0,\delta} \subset V_\delta$ contains all the functions in V_δ vanishing on Γ_D. Following Section 5.3 and assuming as usual that the basis functions used for the approximation in space of the displacement field $\boldsymbol{u}$ and of the velocity field $\boldsymbol{v}$ are the same, we can define the sets of basis functions $\mathcal{B}_N$ and $\mathcal{B}_{N_0} \subset \mathcal{B}_N$ such that:

$$\begin{aligned} \mathcal{B}_N &:= \{\hat{\boldsymbol{\phi}}_1, \dots, \hat{\boldsymbol{\phi}}_N\}, \quad V_N = \operatorname{span}(\mathcal{B}_N), \quad \dim(V_N) = N, \\ \mathcal{B}_{N_0} &:= \{\boldsymbol{\phi}_1, \dots, \boldsymbol{\phi}_{N_0}\}, \quad V_{N_0} = \operatorname{span}(\mathcal{B}_{N_0}), \quad \dim(V_{N_0}) = N_0 < N. \end{aligned}$$

The numbering of the basis functions $\hat{\boldsymbol{\phi}}_i$, $i = 1, \dots, N_0$, is such that we first have all the basis functions for the r component of the vector field and then we have all the basis functions for the z component, which means

$$\hat{\boldsymbol{\phi}}_i(\boldsymbol{x}) := \begin{cases} \hat{\boldsymbol{\phi}}_{r,i}, & \text{for } i = j = 1, \dots, N_r, \\ \hat{\boldsymbol{\phi}}_{z,j}, & \text{for } i = N_r + 1, \dots, N, \ j = i - N_r, \ N = N_r + N_z. \end{cases}$$

where

$$\hat{\boldsymbol{\phi}}_{r,i} = \begin{pmatrix} \hat{\phi}_{r,i} \\ 0 \end{pmatrix} \qquad \hat{\boldsymbol{\phi}}_{z,i} = \begin{pmatrix} 0 \\ \hat{\phi}_{z,i} \end{pmatrix}. \tag{6.66}$$

The same reasoning clearly applies to $\boldsymbol{\phi}_i$, $i = 1, \dots, N$, since $\mathcal{B}_{N_0} \subset \mathcal{B}_N$. As explained in Section 6.2.2, for the computation of the matrices arising in the Spectral-Galerkin semi-discretisation of the weak formulation it is useful to define a proper numbering of the local polynomials used to define the globally continuous basis and a map relating, for each element, the local indices to the global ones. Then, we use again the superscript m to denote the restriction of the vector basis functions $\hat{\boldsymbol{\phi}}_j$ and $\hat{\boldsymbol{\phi}}_{\alpha,j}$, with $\alpha = r, z$, to the domain Ω_m, i.e., we write $\hat{\boldsymbol{\phi}}^m := \hat{\boldsymbol{\phi}}|_{\Omega_m}$ and $\hat{\boldsymbol{\phi}}^m_\alpha := \hat{\boldsymbol{\phi}}_\alpha|_{\Omega_m}$. Moreover, we define the following local ordering

$$\hat{\boldsymbol{\phi}}^m_i := \begin{cases} \hat{\boldsymbol{\phi}}^m_{r,j}, & \text{for } j = i = 1, \dots, \bar{N}^r_m, \\ \hat{\boldsymbol{\phi}}^m_{z,j}, & \text{for } j = 1, \dots, \bar{N}^z_m, \ i = j + \bar{N}^r_m. \end{cases} \tag{6.67}$$

where

$$\hat{\boldsymbol{\phi}}^m_{r,i} = \begin{pmatrix} \hat{\varphi}^{(m)}_{r,i} \\ 0 \end{pmatrix} \qquad \hat{\boldsymbol{\phi}}^m_{z,i} = \begin{pmatrix} 0 \\ \hat{\varphi}^{(m)}_{z,i} \end{pmatrix}. \tag{6.68}$$

with $\hat{\varphi}^{(m)}_{\alpha,i}$, $\alpha = r, z$, being the restriction of $\hat{\phi}_\alpha$, in (6.66) to Ω_m. We emphasize that these are the local basis functions that have been used to build globally continuous basis. Here we have used the additional subscript $\alpha \in \{x, z\}$ to distinguish the component of the vector field to which the scalar basis belongs. Then, using (6.36) we can write

$$\hat{\varphi}^{(m)}_{\alpha,j}(r, z) = \hat{\varphi}^{m,r}_{\alpha,k_r(j)}(r)\, \hat{\varphi}^{m,z}_{\alpha,k_z(j)}(z). \tag{6.69}$$

Let us recall that the space V_N (resp. V_{N_0}) must be a finite dimensional subspace of $H^1(\Omega)^2$ (resp. $H^1_D(\Omega)^2$). However, the spaces generated by the vector basis functions in $\mathcal{B}_N$ and $\mathcal{B}_{N_0}$ do not satisfy this condition. This can be shown by computing the $H^1(\Omega_m)^2$ norm of the basis functions $\hat{\boldsymbol{\phi}}^m_{\alpha,j}$, $\alpha = r, z$, namely

$$\left\|\hat{\boldsymbol{\phi}}^m_{\alpha,j}\right\|^2_{H^1(\Omega_m)} = \left\|\hat{\boldsymbol{\phi}}^m_{\alpha,j}\right\|^2_{L^2(\Omega_m)} + \left\|\nabla\hat{\boldsymbol{\phi}}^m_{\alpha,j}\right\|^2_{L^2(\Omega_m)}, \qquad \alpha = r, z,$$

where

$$\left\|\hat{\boldsymbol{\phi}}^m_{\alpha,j}\right\|^2_{L^2(\Omega_m)} = \int_{\Omega_m}\left|\hat{\varphi}^{(m)}_{\alpha,j}\right|^2 rdrdz = \left(\int_{r_{0,m}}^{r_{1,m}} \varphi^{m,r}_{\alpha,k_r(j)}(r)\varphi^{m,r}_{\alpha,k_r(j)}(r)\, rdr\right)\left(\int_{z_{0,m}}^{z_{1,m}} \varphi^{m,z}_{\alpha,k_z(j)}(z)\varphi^{m,z}_{\alpha,k_z(j)}(z)\, dz\right)$$

and

$$\begin{aligned}\left\|\nabla\hat{\boldsymbol{\phi}}^m_{z,j}\right\|^2_{L^2(\Omega_m)} &= \int_{\Omega_m}\left|\nabla\hat{\boldsymbol{\phi}}^m_{z,j}\right|^2 rdrdz = \int_{\Omega_m}\left|\frac{\partial\hat{\varphi}^{(m)}_{z,j}}{\partial r}\right|^2 + \left|\frac{\partial\hat{\varphi}^{(m)}_{z,j}}{\partial z}\right|^2 rdrdz \\ &= \int_{\Omega_m}\left[\hat{\varphi}^{m,r}_{z,k_r(j)}{}'(r)\hat{\varphi}^{m,z}_{z,k_z(j)}(z)\right]^2 rdrdz + \int_{\Omega_m}\left[\hat{\varphi}^{m,r}_{z,k_r(j)}(r)\hat{\varphi}^{m,z}_{z,k_z(j)}{}'(z)\right]^2 rdrdz,\end{aligned}$$

$$\begin{aligned}\left\|\nabla\hat{\boldsymbol{\phi}}^m_{r,j}\right\|^2_{L^2(\Omega_m)} &= \int_{\Omega_m}\left|\nabla\hat{\boldsymbol{\phi}}^m_{r,j}\right|^2 rdrdz = \int_{\Omega_m}\left|\frac{\partial\hat{\varphi}^{(m)}_{r,j}}{\partial r}\right|^2 + \left|\frac{\partial\hat{\varphi}^{(m)}_{r,j}}{\partial z}\right|^2 + \left|\frac{\hat{\varphi}^{(m)}_{r,j}}{r}\right|^2 rdrdz \\ &= \int_{\Omega_m}\left[\hat{\varphi}^{m,r}_{r,k_r(j)}{}'(r)\hat{\varphi}^{m,z}_{r,k_z(j)}(z)\right]^2 rdrdz + \int_{\Omega_m}\left[\hat{\varphi}^{m,r}_{r,k_r(j)}(r)\hat{\varphi}^{m,z}_{r,k_z(j)}{}'(z)\right]^2 rdrdz \\ &\quad + \int_{\Omega_m}\left[\frac{\hat{\varphi}^{m,r}_{r,k_r(j)}(r)\hat{\varphi}^{m,z}_{r,k_z(j)}(z)}{r}\right]^2 rdrdz. \qquad (6.70)\end{aligned}$$

It is clear that $\|\hat{\boldsymbol{\phi}}^m_{r,j}\|^2_{L^2(\Omega_m)}$, $\|\hat{\boldsymbol{\phi}}^m_{z,j}\|^2_{L^2(\Omega_m)}$ and $\|\nabla\hat{\boldsymbol{\phi}}^m_{z,j}\|^2_{L^2(\Omega_m)}$ are all finite, as they involve the computation of integrals of polynomials (or their derivatives) on bounded domains. The same reasoning holds for the first two integrals in (6.70). Let us now look at the last integral in (6.70), which can be written as:

$$\int_{\Omega_m}\left[\frac{\hat{\varphi}^{m,r}_{r,k_r(j)}(r)\hat{\varphi}^{m,z}_{r,k_z(j)}(z)}{r}\right]^2 rdrdz = \left(\int_{r_{0,m}}^{r_{1,m}}\frac{\hat{\varphi}^{m,r}_{r,k_r(j)}(r)\hat{\varphi}^{m,r}_{r,k_r(j)}(r)}{r}\, dr\right)\left(\int_{z_{0,m}}^{z_{1,m}}\hat{\varphi}^{m,z}_{r,k_z(j)}(z)\hat{\varphi}^{m,z}_{r,k_z(j)}(z)\, dz\right).$$

The integral with respect to variable r is not finite for all the indices j when $r_{0,m} = 0$. Indeed, we recall that mapped one-dimensional boundary-adapted basis functions $\hat{\varphi}^{m,r}_{r,k_r}$ based on linear combinations of either Legendre or Chebyshev polynomials do not vanish at the left endpoint of the domain where they have been defined for $k_r = 0$. Therefore, the integral does not convergence for all the indices j such that $k_r(j) = 0$ and, consequently, the $H^1(\Omega)^2-$norm of all those vector basis functions $\hat{\boldsymbol{\phi}}_{r,j}$ such that their restriction on Ω_m is given by $\hat{\boldsymbol{\phi}}^m_{r,j}$ is not finite. So, these basis functions must be removed from $\mathcal{B}_N$ and $\mathcal{B}_{N_0}$ in order for these sets to generate finite dimensional subspaces of $H^1(\Omega)^2$ and $H^1_D(\Omega)^2$, respectively.

Computation of matrices Having chosen the same basis functions for the semi-discrete approximation of $\boldsymbol{u}$ and $\boldsymbol{v}$ and having defined $\mathcal{B}_N$ and $\mathcal{B}_{N_0}$ in such a way $\mathcal{B}_{N_0} \subset \mathcal{B}_N$, the computation of all the matrices arising in the Galerkin semi-discrete approximation developed in Section 5.3 reduces once again to the computation of three matrices based on the bilinear forms $a(\cdot,\cdot)$, $b(\cdot,\cdot)$ and $c(\cdot,\cdot)$ defined in (5.16), i.e.,

$$\hat{\mathbf{C}}_{i,j} = c(\hat{\boldsymbol{\phi}}_j, \hat{\boldsymbol{\phi}}_i) = \int_\Omega \rho\,\hat{\boldsymbol{\phi}}_j\cdot\hat{\boldsymbol{\phi}}_i\, d\boldsymbol{x}, \qquad (6.71a)$$

$$\hat{\mathbf{B}}_{i,j} = b(\hat{\boldsymbol{\phi}}_j, \hat{\boldsymbol{\phi}}_i) = \int_\Omega \boldsymbol{\sigma}_{\text{vi}}(\hat{\boldsymbol{\phi}}_j) : \boldsymbol{\varepsilon}(\hat{\boldsymbol{\phi}}_i)\, d\boldsymbol{x}, \qquad (6.71b)$$

$$\hat{\mathbf{A}}_{i,j} = a(\hat{\boldsymbol{\phi}}_j, \hat{\boldsymbol{\phi}}_i) = \int_\Omega \boldsymbol{\sigma}_{\text{el}}(\hat{\boldsymbol{\phi}}_j) : \boldsymbol{\varepsilon}(\hat{\boldsymbol{\phi}}_i)\, d\boldsymbol{x}. \qquad (6.71c)$$

Indeed, as we have explained in Section 6.1.2 and Section 6.2.2, the matrices defining $\mathbf{M}$ and $\mathbf{H}$ in (5.33) and the matrices defining the Dirichlet contribution to the forcing vector $\boldsymbol{F}$ in (5.36) can be computed as follows

$$\mathbf{M}^v = \hat{\mathbf{C}}(dir, dir), \qquad \mathbf{H}_{11} = \hat{\mathbf{B}}(dir, dir), \qquad \mathbf{M}^u = \mathbf{H}_{12} = -\mathbf{H}_{21} = \hat{\mathbf{A}}(dir, dir),$$
$$\mathbf{N}_{11} = \hat{\mathbf{C}}(dir, :), \qquad \mathbf{B}_{11} = \hat{\mathbf{B}}(dir, :), \qquad \mathbf{B}_{12} = \hat{\mathbf{A}}(dir, :),$$

where dir denotes the set of indices associated to those basis functions that are both in $\mathcal{B}_N$ and $\mathcal{B}_{N_0}$. Moreover, we recall that the component (i, j) of matrices $\hat{\mathbf{C}}$, $\hat{\mathbf{B}}$ and $\hat{\mathbf{A}}$ in (6.71) are given by

$$\hat{\mathbf{C}}_{i,j} = \int_\Omega \rho\, \hat{\boldsymbol{\phi}}_j \cdot \hat{\boldsymbol{\phi}}_i \, d\boldsymbol{x} = \sum_{m=1}^{M} \int_{\Omega_m} \rho_m\, \hat{\boldsymbol{\phi}}_j^m \cdot \hat{\boldsymbol{\phi}}_i^m \, d\boldsymbol{x} = \sum_{m \in \mathcal{A}(i,j)} \int_{\Omega_m} \rho_m\, \hat{\boldsymbol{\phi}}_j^m \cdot \hat{\boldsymbol{\phi}}_i^m \, d\boldsymbol{x} = \sum_{m \in \mathcal{A}(i,j)} \left(\hat{\mathbf{C}}^m\right)_{k,l}$$

$$\hat{\mathbf{B}}_{i,j} = \int_\Omega \boldsymbol{\sigma}_{\mathrm{vi}}(\hat{\boldsymbol{\phi}}_i) : \boldsymbol{\varepsilon}(\hat{\boldsymbol{\phi}}_i) \, d\boldsymbol{x} = \sum_{m=1}^{M} \int_{\Omega_m} \boldsymbol{\sigma}_{\mathrm{vi}}(\hat{\boldsymbol{\phi}}_i^m) : \boldsymbol{\varepsilon}(\hat{\boldsymbol{\phi}}_i^m) \, d\boldsymbol{x} = \sum_{m \in \mathcal{A}(i,j)} \int_{\Omega_m} \boldsymbol{\sigma}_{\mathrm{vi}}(\hat{\boldsymbol{\phi}}_i^m) : \boldsymbol{\varepsilon}(\hat{\boldsymbol{\phi}}_i^m) \, d\boldsymbol{x} = \sum_{m \in \mathcal{A}(i,j)} \left(\hat{\mathbf{B}}^m\right)_{k,l}$$

$$\hat{\mathbf{A}}_{i,j} = \int_\Omega \boldsymbol{\sigma}_{\mathrm{el}}(\hat{\boldsymbol{\phi}}_i) : \boldsymbol{\varepsilon}(\hat{\boldsymbol{\phi}}_i) \, d\boldsymbol{x} = \sum_{m=1}^{M} \int_{\Omega_m} \boldsymbol{\sigma}_{\mathrm{el}}(\hat{\boldsymbol{\phi}}_i^m) : \boldsymbol{\varepsilon}(\hat{\boldsymbol{\phi}}_i^m) \, d\boldsymbol{x} = \sum_{m \in \mathcal{A}(i,j)} \int_{\Omega_m} \boldsymbol{\sigma}_{\mathrm{el}}(\hat{\boldsymbol{\phi}}_i^m) : \boldsymbol{\varepsilon}(\hat{\boldsymbol{\phi}}_i^m) \, d\boldsymbol{x} = \sum_{m \in \mathcal{A}(i,j)} \left(\hat{\mathbf{A}}^m\right)_{k,l}.$$

As already explained in detail in Section 6.2.2, matrices $\hat{\mathbf{A}}$, $\hat{\mathbf{B}}$ and $\hat{\mathbf{C}}$ are constructed by assembling the local matrices $\hat{\mathbf{A}}^m$, $\hat{\mathbf{B}}^m$ and $\hat{\mathbf{C}}^m$, which represent the contribution given by each element Ω_m, $m = 1, \dots, M$. We now discuss the computation of the components of the three element matrices $\hat{\mathbf{C}}^m$, $\hat{\mathbf{B}}^m$ and $\hat{\mathbf{A}}^m$. From (6.67) and (6.68) we see that $\hat{\mathbf{C}}^m$ is a 2×2 block matrix with the following structure

$$\hat{\mathbf{C}}^m = \begin{pmatrix} \mathbf{C}_m^r & \mathbf{0} \\ \mathbf{0} & \mathbf{C}_m^z \end{pmatrix},$$

where the component (i, j) of $\mathbf{C}_m^\alpha$, with $\alpha = r, z$, is given by

$$(\mathbf{C}_m^\alpha)_{i,j} \overset{(6.69)}{=} \int_{\Omega_m} \rho_m\, \hat{\varphi}_{\alpha,j}^{(m)}\, \hat{\varphi}_{\alpha,i}^{(m)} \, d\boldsymbol{x} = \rho_m \left(\int_{r_{0,m}}^{r_{1,m}} \hat{\varphi}_{\alpha,k_r(j)}^{m,r}(r) \hat{\varphi}_{\alpha,k_r(i)}^{m,r}(r)\, r dr \right) \left(\int_{z_{0,m}}^{z_{1,m}} \hat{\varphi}_{\alpha,k_z(j)}^{m,z}(z) \hat{\varphi}_{\alpha,k_z(i)}^{m,z}(z)\, dz \right).$$

The one-dimensional integrals can be computed as shown in Section 4.3.1 (for boundary-adapted Legendre polynomials) or Section 4.4.1 (for boundary-adapted Chebyshev polynomials). We now discuss the computation of matrices $\hat{\mathbf{B}}^m$ and $\hat{\mathbf{A}}^m$. From the definition of $\boldsymbol{\sigma}_{\mathrm{vi}}$ we see that

$$\left(\hat{\mathbf{B}}^m\right)_{i,j} = \int_{\Omega_m} \boldsymbol{\sigma}_{\mathrm{vi}}(\hat{\boldsymbol{\phi}}_j^m) : \boldsymbol{\varepsilon}(\hat{\boldsymbol{\phi}}_i^m) \, d\boldsymbol{x} = \int_{\Omega_m} \lambda_{\mathrm{vi},m}\, \mathrm{tr}(\boldsymbol{\varepsilon}(\hat{\boldsymbol{\phi}}_j^m))\, \mathrm{tr}(\boldsymbol{\varepsilon}(\hat{\boldsymbol{\phi}}_i^m)) \, d\boldsymbol{x} + \int_{\Omega_m} 2\eta_m\, \boldsymbol{\varepsilon}(\hat{\boldsymbol{\phi}}_j^m) : \boldsymbol{\varepsilon}(\hat{\boldsymbol{\phi}}_i^m) \, d\boldsymbol{x}$$

while from the definition of $\boldsymbol{\sigma}_{\mathrm{el}}$ we have that

$$\left(\hat{\mathbf{A}}^m\right)_{i,j} = \int_{\Omega_m} \boldsymbol{\sigma}_{\mathrm{el}}(\hat{\boldsymbol{\phi}}_j^m) : \boldsymbol{\varepsilon}(\hat{\boldsymbol{\phi}}_i^m) \, d\boldsymbol{x} = \int_{\Omega_m} \lambda_{\mathrm{el},m}\, \mathrm{tr}(\boldsymbol{\varepsilon}(\hat{\boldsymbol{\phi}}_j^m))\, \mathrm{tr}(\boldsymbol{\varepsilon}(\hat{\boldsymbol{\phi}}_i^m)) \, d\boldsymbol{x} + \int_{\Omega_m} 2\mu_m\, \boldsymbol{\varepsilon}(\hat{\boldsymbol{\phi}}_j^m) : \boldsymbol{\varepsilon}(\hat{\boldsymbol{\phi}}_i^m) \, d\boldsymbol{x}.$$

Therefore, the element matrices $\hat{\mathbf{B}}^m$ and $\hat{\mathbf{A}}^m$ can be rewritten as

$$\hat{\mathbf{B}}^m = \lambda_{\mathrm{vi},m} \mathbf{T}_m + 2\eta_m \mathbf{G}_m, \qquad \hat{\mathbf{A}}^m = \lambda_{\mathrm{el},m} \mathbf{T}_m + 2\mu_m \mathbf{G}_m,$$

where $\mathbf{T}_m$ and $\mathbf{G}_m$ are 2×2 block matrices with the following structure:

$$\mathbf{T}_m = \begin{pmatrix} \mathbf{T}_m^{rr} & \mathbf{T}_m^{rz} \\ \mathbf{T}_m^{zr} & \mathbf{T}_m^{zz} \end{pmatrix}, \qquad \mathbf{G}_m = \begin{pmatrix} \mathbf{G}_m^{rr} & \mathbf{G}_m^{rz} \\ \mathbf{G}_m^{zr} & \mathbf{G}_m^{zz} \end{pmatrix}.$$

From (6.62) and (6.68), we have the following expressions for the strain tensor of basis functions $\hat{\boldsymbol{\phi}}_{r,j}^m$ and $\hat{\boldsymbol{\phi}}_{z,j}^m$:

$$\boldsymbol{\varepsilon}(\hat{\boldsymbol{\phi}}_{r,j}^m) = \begin{bmatrix} \dfrac{\partial \hat{\varphi}_{r,j}^{(m)}}{\partial r} & 0 & \dfrac{1}{2} \dfrac{\partial \hat{\varphi}_{r,j}^{(m)}}{\partial z} \\ 0 & \dfrac{\hat{\varphi}_{r,j}^{(m)}}{r} & 0 \\ \dfrac{1}{2} \dfrac{\partial \hat{\varphi}_{r,j}^{(m)}}{\partial z} & 0 & 0 \end{bmatrix} \qquad \boldsymbol{\varepsilon}(\hat{\boldsymbol{\phi}}_{z,j}^m) = \begin{bmatrix} 0 & 0 & \dfrac{1}{2} \dfrac{\partial \hat{\varphi}_{z,j}^{(m)}}{\partial r} \\ 0 & 0 & 0 \\ \dfrac{1}{2} \dfrac{\partial \hat{\varphi}_{z,j}^{(m)}}{\partial r} & 0 & \dfrac{\partial \hat{\varphi}_{z,j}^{(m)}}{\partial z} \end{bmatrix}$$

Using this result we see that the components (i,j) of each block of matrix $\mathbf{T}_m$ are given by

$$(\mathbf{T}_m^{rr})_{i,j} = \int_{\Omega_m} \mathrm{tr}\left(\boldsymbol{\varepsilon}\left(\hat{\boldsymbol{\phi}}_{r,j}^m\right)\right)\mathrm{tr}\left(\boldsymbol{\varepsilon}\left(\hat{\boldsymbol{\phi}}_{r,i}^m\right)\right)\,d\boldsymbol{x} = \int_{\Omega_m}\left(\frac{\partial\hat{\varphi}_{r,j}^{(m)}}{\partial r}+\frac{\hat{\varphi}_{r,j}^{(m)}}{r}\right)\left(\frac{\partial\hat{\varphi}_{r,i}^{(m)}}{\partial r}+\frac{\hat{\varphi}_{r,i}^{(m)}}{r}\right)\,d\boldsymbol{x}, \tag{6.72a}$$

$$(\mathbf{T}_m^{rz})_{i,j} = \int_{\Omega_m} \mathrm{tr}\left(\boldsymbol{\varepsilon}\left(\hat{\boldsymbol{\phi}}_{z,j}^m\right)\right)\mathrm{tr}\left(\boldsymbol{\varepsilon}\left(\hat{\boldsymbol{\phi}}_{r,i}^m\right)\right)\,d\boldsymbol{x} = \int_{\Omega_m}\frac{\partial\hat{\varphi}_{z,j}^{(m)}}{\partial z}\left(\frac{\partial\hat{\varphi}_{r,i}^{(m)}}{\partial r}+\frac{\hat{\varphi}_{r,i}^{(m)}}{r}\right)\,d\boldsymbol{x}, \tag{6.72b}$$

$$(\mathbf{T}_m^{zr})_{i,j} = \int_{\Omega_m} \mathrm{tr}\left(\boldsymbol{\varepsilon}\left(\hat{\boldsymbol{\phi}}_{r,j}^m\right)\right)\mathrm{tr}\left(\boldsymbol{\varepsilon}\left(\hat{\boldsymbol{\phi}}_{z,i}^m\right)\right)\,d\boldsymbol{x} = \int_{\Omega_m}\left(\frac{\partial\hat{\varphi}_{r,j}^{(m)}}{\partial r}+\frac{\hat{\varphi}_{r,j}^{(m)}}{r}\right)\frac{\partial\hat{\varphi}_{z,i}^{(m)}}{\partial z}\,d\boldsymbol{x}, \tag{6.72c}$$

$$(\mathbf{T}_m^{zz})_{i,j} = \int_{\Omega_m} \mathrm{tr}\left(\boldsymbol{\varepsilon}\left(\hat{\boldsymbol{\phi}}_{z,j}^m\right)\right)\mathrm{tr}\left(\boldsymbol{\varepsilon}\left(\hat{\boldsymbol{\phi}}_{z,i}^m\right)\right)\,d\boldsymbol{x} = \int_{\Omega_m}\frac{\partial\hat{\varphi}_{z,j}^{(m)}}{\partial z}\frac{\partial\hat{\varphi}_{z,i}^{(m)}}{\partial z}\,d\boldsymbol{x}, \tag{6.72d}$$

and the components (i,j) of each block of matrix $\mathbf{G}_m$ are given by

$$(\mathbf{G}_m^{rr})_{i,j} = \int_{\Omega_m}\boldsymbol{\varepsilon}\left(\hat{\boldsymbol{\phi}}_{r,j}^m\right):\boldsymbol{\varepsilon}\left(\hat{\boldsymbol{\phi}}_{r,i}^m\right)\,d\boldsymbol{x} = \int_{\Omega_m}\frac{\partial\hat{\varphi}_{r,j}^{(m)}}{\partial r}\frac{\partial\hat{\varphi}_{r,i}^{(m)}}{\partial r}\,d\boldsymbol{x}+\int_{\Omega_m}\frac{\hat{\varphi}_{r,j}^{(m)}}{r}\frac{\hat{\varphi}_{r,i}^{(m)}}{r}\,d\boldsymbol{x}+\frac{1}{2}\int_{\Omega_m}\frac{\partial\hat{\varphi}_{r,j}^{(m)}}{\partial z}\frac{\partial\hat{\varphi}_{r,i}^{(m)}}{\partial z}\,d\boldsymbol{x}, \tag{6.73a}$$

$$(\mathbf{G}_m^{zz})_{i,j} = \int_{\Omega_m}\boldsymbol{\varepsilon}\left(\hat{\boldsymbol{\phi}}_{z,j}^m\right):\boldsymbol{\varepsilon}\left(\hat{\boldsymbol{\phi}}_{z,i}^m\right)\,d\boldsymbol{x} = \int_{\Omega_m}\frac{\partial\hat{\varphi}_{z,j}^{(m)}}{\partial z}\frac{\partial\hat{\varphi}_{z,i}^{(m)}}{\partial z}\,d\boldsymbol{x}+\frac{1}{2}\int_{\Omega_m}\frac{\partial\hat{\varphi}_{z,j}^{(m)}}{\partial r}\frac{\partial\hat{\varphi}_{z,i}^{(m)}}{\partial r}\,d\boldsymbol{x}, \tag{6.73b}$$

$$(\mathbf{G}_m^{rz})_{i,j} = \int_{\Omega_m}\boldsymbol{\varepsilon}\left(\hat{\boldsymbol{\phi}}_{z,j}^m\right):\boldsymbol{\varepsilon}\left(\hat{\boldsymbol{\phi}}_{r,i}^m\right)\,d\boldsymbol{x} = \frac{1}{2}\int_{\Omega_m}\frac{\partial\hat{\varphi}_{z,j}^{(m)}}{\partial r}\frac{\partial\hat{\varphi}_{r,i}^{(m)}}{\partial z}\,d\boldsymbol{x}, \tag{6.73c}$$

$$(\mathbf{G}_m^{zr})_{i,j} = \int_{\Omega_m}\boldsymbol{\varepsilon}\left(\hat{\boldsymbol{\phi}}_{r,j}^m\right):\boldsymbol{\varepsilon}\left(\hat{\boldsymbol{\phi}}_{z,i}^m\right)\,d\boldsymbol{x} = \frac{1}{2}\int_{\Omega_m}\frac{\partial\hat{\varphi}_{r,j}^{(m)}}{\partial z}\frac{\partial\hat{\varphi}_{z,i}^{(m)}}{\partial r}\,d\boldsymbol{x} \tag{6.73d}$$

Finally, using (6.45), the integrals appearing in (6.72) and (6.73) becomes:

$$\int_{\Omega_m}\frac{\partial\hat{\varphi}_{\alpha,j}^{(m)}}{\partial r}\frac{\partial\hat{\varphi}_{\alpha,i}^{(m)}}{\partial r}\,d\boldsymbol{x} = \left(\int_{r_{0,m}}^{r_{1,m}}\hat{\varphi}_{\alpha,k_r(j)}^{m,r}{}'(x)\,\hat{\varphi}_{\alpha,k_r(i)}^{m,r}{}'(x)\,r dr\right)\left(\int_{z_{0,m}}^{z_{1,m}}\hat{\varphi}_{\alpha,k_z(j)}^{m,z}(z)\,\hat{\varphi}_{\alpha,k_z(i)}^{m,z}(z)\,dz\right),$$

$$\int_{\Omega_m}\frac{\partial\hat{\varphi}_{\alpha,j}^{(m)}}{\partial z}\frac{\partial\hat{\varphi}_{\alpha,i}^{(m)}}{\partial z}\,d\boldsymbol{x} = \left(\int_{r_{0,m}}^{r_{1,m}}\hat{\varphi}_{\alpha,k_r(j)}^{m,r}(r)\,\hat{\varphi}_{\alpha,k_r(i)}^{m,r}(r)\,r dr\right)\left(\int_{z_{0,m}}^{z_{1,m}}\hat{\varphi}_{\alpha,k_z(j)}^{m,z}{}'(z)\,\hat{\varphi}_{\alpha,k_z(i)}^{m,z}{}'(z)\,dz\right),$$

$$\int_{\Omega_m}\frac{\partial\hat{\varphi}_{\alpha,j}^{(m)}}{\partial r}\frac{\partial\hat{\varphi}_{\beta,i}^{(m)}}{\partial z}\,d\boldsymbol{x} = \left(\int_{r_{0,m}}^{r_{1,m}}\hat{\varphi}_{\alpha,k_r(j)}^{m,r}{}'(r)\,\hat{\varphi}_{\beta,k_r(i)}^{m,r}(r)\,r dr\right)\left(\int_{z_{0,m}}^{z_{1,m}}\hat{\varphi}_{\alpha,k_z(j)}^{m,z}(z)\,\hat{\varphi}_{\beta,k_z(i)}^{m,z}{}'(z)\,dz\right),$$

$$\int_{\Omega_m}\frac{\hat{\varphi}_{r,j}^{(m)}}{r}\frac{\hat{\varphi}_{r,i}^{(m)}}{r}\,d\boldsymbol{x} = \left(\int_{r_{0,m}}^{r_{1,m}}\frac{\hat{\varphi}_{r,k_r(j)}^{m,r}(r)\,\hat{\varphi}_{r,k_r(i)}^{m,r}(r)}{r}\,dr\right)\left(\int_{z_{0,m}}^{z_{1,m}}\hat{\varphi}_{r,k_z(j)}^{m,z}(z)\,\hat{\varphi}_{r,k_z(i)}^{m,z}(z)\,dz\right),$$

$$\int_{\Omega_m}\frac{\partial\hat{\varphi}_{r,j}^{(m)}}{\partial r}\frac{\hat{\varphi}_{r,i}^{(m)}}{r}\,d\boldsymbol{x} = \left(\int_{r_{0,m}}^{r_{1,m}}\hat{\varphi}_{r,k_r(j)}^{m,r}{}'(r)\,\hat{\varphi}_{r,k_r(i)}^{m,r}(r)\,dr\right)\left(\int_{z_{0,m}}^{z_{1,m}}\hat{\varphi}_{\alpha,k_z(j)}^{m,z}(z)\,\hat{\varphi}_{\alpha,k_z(i)}^{m,z}(z)\,dz\right),$$

$$\int_{\Omega_m}\frac{\partial\hat{\varphi}_{z,j}^{(m)}}{\partial z}\frac{\hat{\varphi}_{r,i}^{(m)}}{r}\,d\boldsymbol{x} = \left(\int_{r_{0,m}}^{r_{1,m}}\hat{\varphi}_{r,k_r(j)}^{m,r}(r)\,\hat{\varphi}_{r,k_r(i)}^{m,r}(r)\,dr\right)\left(\int_{z_{0,m}}^{z_{1,m}}\hat{\varphi}_{\alpha,k_z(j)}^{m,z}{}'(z)\,\hat{\varphi}_{\alpha,k_z(i)}^{m,z}(z)\,dz\right).$$

The one-dimensional integrals can be computed using the results presented in Sections 4.3.1 and 4.4.1.

6.3.3 Numerical Simulations

In this section we first investigate the numerical convergence and we then show the results that we have obtained by applying our numerical approach to two test cases. The first example considers an homogeneous material whereas the second compares the propagation of waves on different heterogeneous materials.

Numerical Convergence

As we have done for the two-dimensional system of equations depending on Cartesian coordinates, we investigate the numerical convergence by computing the numerical solution of a problem defined using

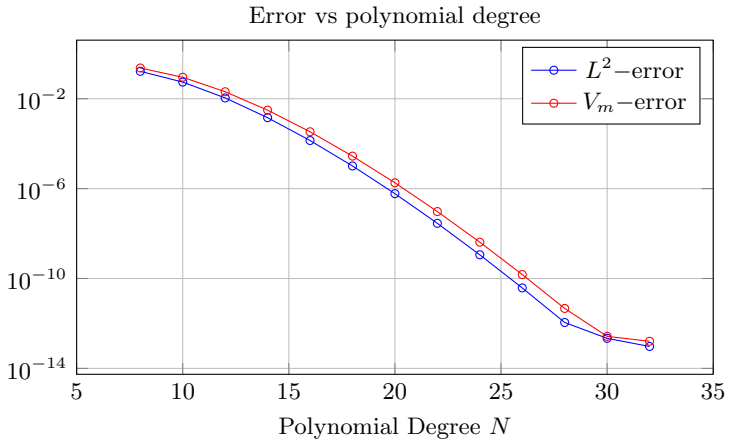


Figure 6.10: Behaviour of the relative errors in the L^2 and V_m norms, computed at time $t = 0.35\,\mathrm{s}$ and shown against the basis functions polynomial degree N, for the problem with exact solution (6.74).

polynomial degree N	relative error L^2	relative error V_m
8	1.66713e-01	2.33952e-01
12	1.08885e-02	2.05423e-02
16	1.38582e-04	3.39178e-04
20	5.98146e-07	1.81916e-06
24	1.13352e-09	4.12977e-09
28	1.10280e-12	4.65942e-12
32	9.45887e-14	1.60819e-13

Table 6.10: Relative errors, at $t = 0.35\,\mathrm{s}$, for the manufactured problem with exact solution (6.74).

a manufactured solution and having a source term. In particular, the source term is defined in such a way the solution of the displacement equations with viscoelastic Kelvin-Voigt model is given by:

$$u_r(r,z,t) = r\sin^3(\pi r)\cos^3\left(\frac{\pi}{2}z\right)\sin^3(2\pi t) \tag{6.74a}$$

$$u_z(r,z,t) = \cos^3\left(\frac{\pi}{2}r\right)\sin^3(\pi z)\sin^3(2\pi t). \tag{6.74b}$$

We solve the problem in the cylindrical domain $\Omega := [0,1]\times[-1,+1]$ and we consider density $\rho = 1\,\mathrm{kg\,m^{-3}}$, elastic parameters $\lambda_{\mathrm{el}} = \mu_{el} = 1\,\mathrm{Pa}$ and viscous parameters $\lambda_{\mathrm{vi}} = \eta = 0.1\,\mathrm{Pa\,s}$. We impose zero Dirichlet boundary conditions on the two base surfaces and zero Neumann boundary conditions on the lateral surface of the cylindrical domain. The solution in time is again computed by means of eigenvalue decomposition and exact integration as described in Section 5.3.3. The relative errors of the solution in the L^2 and V_m norms are computed at time $t = 0.35\,\mathrm{s}$. The behaviour of the errors in shown against the polynomial degree N in Figure 6.10. The values on the x axis of Figure 6.10 denote the polynomial degrees that have been used for both the dependent variables (r and z) of all the components of the unknown displacement and velocity fields (i.e., u_r, u_z, v_r and v_z). Even in this case we see that the convergence of the numerical solution to the exact one is exponential in the polynomial degree of the basis functions. The errors are also listed in Table 6.10.

Application Example: a Variant of Lamb's Axisymmetric Problem

In this section we consider the numerical solution of the 3D Lamb's problem described in Section 2.2.2. We proceed as we have already done when solving the two-dimensional plane-strain problem (§6.2.3), namely by considering a variant of the original problem formulated by Lamb. More precisely, instead of defining the preblem on a half-space, we compute numerically the dynamic response due to the

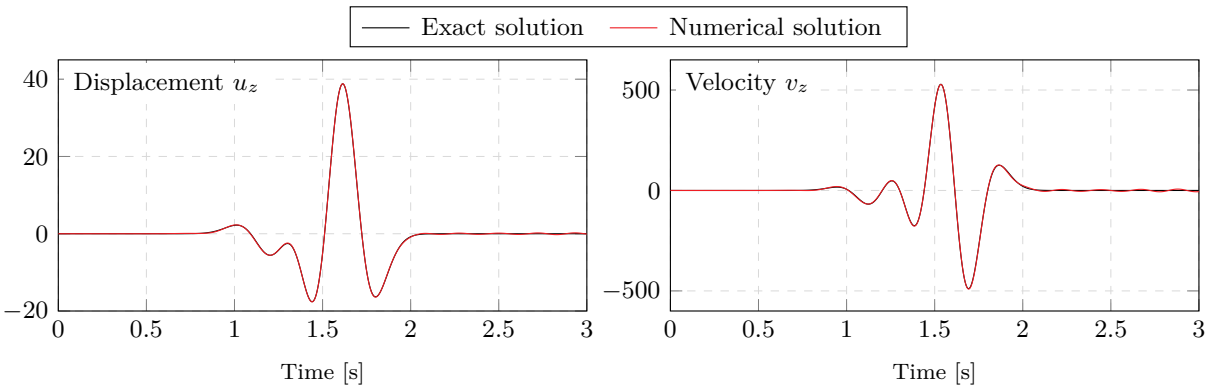


Figure 6.11: Lamb's problem: comparison between the exact solution (black line) and the numerical solution (red line) for the vertical component of the displacement (left panel) and the vertical component of the velocity (right panel) over the time interval $t \in [0, 3]$s. The source is a vertical point load located at $r = 0\,\mathrm{m}$ and $z = 1\,\mathrm{m}$ and has a dependence on time defined by a Ricker-type wavelet having dominant frequency $2\,\mathrm{Hz}$. The cylindrical medium is purely elastic, with density $\rho = 1\,\mathrm{kg\,m^{-3}}$ and Lamè parameters $\lambda_{el} = 0.27\,\mathrm{Pa}$ and $\mu = 0.033\,\mathrm{Pa}$.

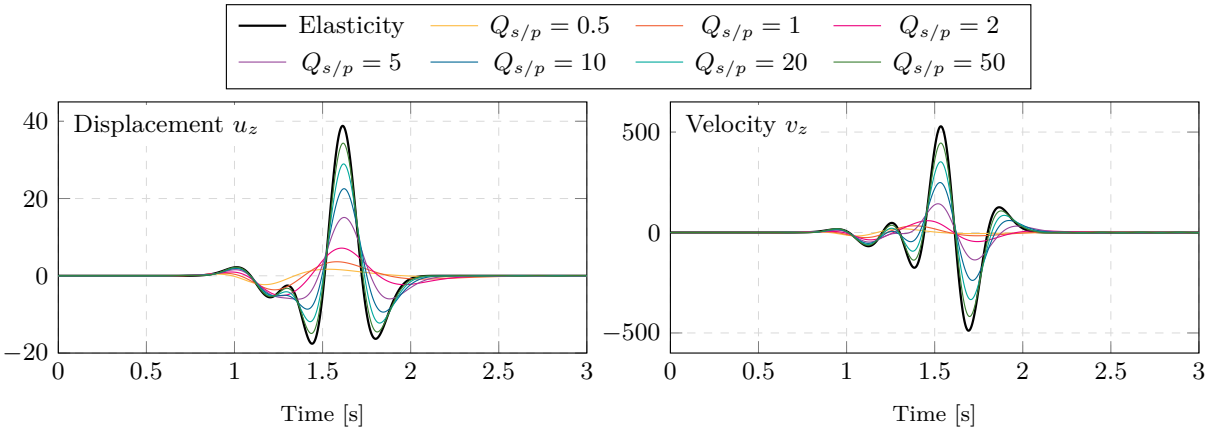


Figure 6.12: Variant of Lamb's Problem. Comparison between the analytical solution (black line) in the lossless case and the numerical solutions (coloured lines) in the Kelvin-Voigt viscoelastic case for different values of the quality factor Q_P and Q_S. The vertical components of the displacement and the velocity are shown in panels left and right, respectively.

application of a vertical point load onto the upper horizontal surface of a cylindrical domain having unit radius and height, i.e., $\Omega = (0, 1) \times [0, 2\pi) \times (0, 1)$. Furthermore, we simulate the propagation of waves on both elastic and Kelvin-Voigt viscoelastic materials. Clearly the vertical load is applied at $r = 0$ (i.e., on the axis of the cylindrical domain), as in this case the problem is axisymmetric and it can be solved by means of the numerical framework developed in this section. Polynomial basis functions having degree up to 80 in each coordinate (r and z) have been considered. We impose zero Neumann boundary conditions on the lateral surface of the cylinder and zero Dirichlet boundary conditions on the bottom horizontal surface. We first test the numerical solution obtained in the purely elastic case against the exact solution of the Lamb's problem. We consider the same material parameters used for the plane-strain problem. The elastic material is characterised by density $\rho = 1\,\mathrm{kg\,m^{-3}}$ and Lamè parameters $\lambda_{\mathrm{el}} = 0.27\,\mathrm{Pa}$ and $\mu = 0.033\,\mathrm{Pa}$. The source is defined as a Dirac delta in space and as a Ricker-type wavelet in time, i.e., a function having the form $f(t) = A(1-2(\pi f_0(t-t_0))^2)\exp(-(\pi f_0(t-t_0))^2)$ where $A = 1\,\mathrm{m}$, $f_0 = 2\,\mathrm{Hz}$ and $t_0 = 1\,\mathrm{s}$. The receiver is located at the upper surface and at $0.15\,\mathrm{m}$ from the source. Figure 6.11 shows the comparison between the exact solution (black line) and the numerical solution (red line) over the time interval $t \in [0, 3]$s for the vertical component of the displacement (left panel) and the vertical component of the velocity (right panel). In both cases, we can clearly see that there is a quite good agreement between the numerical solution and the exact one, the main difference

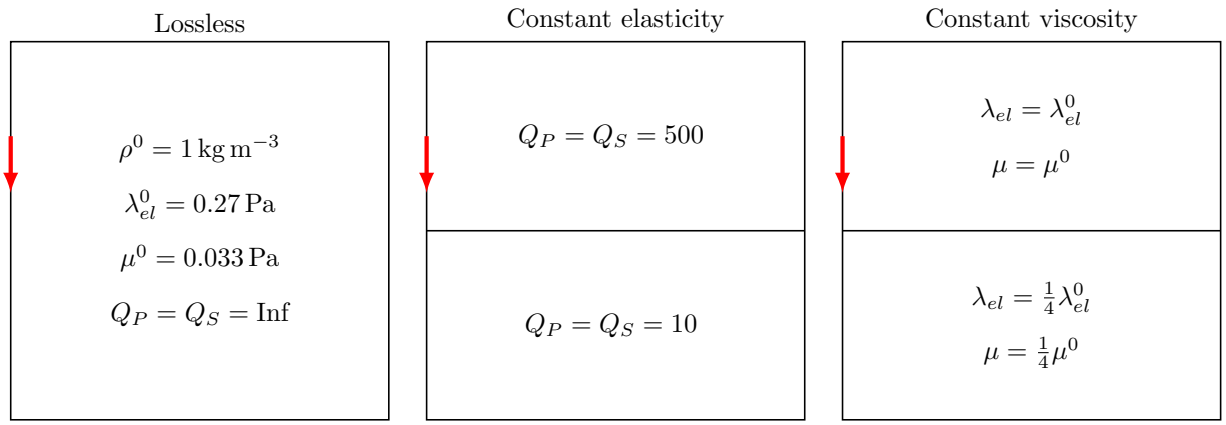


Figure 6.13: Three different scenarios in terms of materials considered for the solution of the problem with vertical buried point load applied at the point of the axis of the cylinder having coordinate $z = 0.75\,\mathrm{m}$ (see red arrows). In the first case (left panel), the material is purely elastic and homogeneous, whereas in the other two cases (middle and right panels) the material is viscoelastic and heterogeneous. In particular, in the case shown in the middle panel the elasticity is constant in the whole domain and the viscosity changes, while in the example displayed in the right panel the viscosity is constant and the elasticity varies.

consisting in some oscillations that are observed in the numerical solution after the surface wave has reached the receiver. However, these oscillations are very small compared to the amplitude of the wave. Then, we proceed to examine the same problem but with the material being now viscoelastic of Kelvin-Voigt type rather than purely elastic. We solve the problem by using different values of the quality factors Q_P and Q_S that have been obtained by varying the viscosity parameters and keeping the elastic parameters fixed. Then, we compare the numerical solutions with the aim of highlighting how the viscosity affects the dynamic response to the applied load. Figure 6.12 shows the vertical component of the displacement (left panel) and the vertical component of the velocity (right panel). Each curve shows the solution associated to a different value of the quality factors. Since in this case the exact solution is not available, we also plot for reference the exact solution of the original (elastic) Lamb's problem (black thicker line). As expected, the results clearly show that decreasing the value of the quality factors (which means that, at constant elasticity, we increase the value of the viscosity), the attenuation becomes stronger and therefore the amplitude of the waves decreases.

Application Example: Homogeneous and Heterogeneous Materials

In the second numerical example, we simulate the propagation of waves on heterogeneous materials and compare the viscoelastic solution with the lossless one. As in the previous example, the propagating waves are generated by the application of a vertical point load acting on the axis of symmetry of the cylindrical domain $\Omega = (0,1) \times [0, 2\pi) \times (0,1)$. However, we now consider a buried force, i.e., we consider the point load not acting on the upper surface of the cylindrical domain but on the point of the $z-$axis for which $z = 0.75\,\mathrm{m}$. The time dependent behaviour of the point load is described by the same Ricker wavelet considered in the previous problem. We also impose the same boundary conditions, i.e., zero Dirichlet boundary conditions on the base surface and zero Neumann boundary conditions otherwise. Concerning the material properties, we analyse three different scenarios, which are shown in Figure 6.13. In the first case (left panel), the material is purely elastic and homogeneous, with density $\rho = 1\,\mathrm{kg\,m^{-3}}$ and Lamè parameters $\lambda_{el} = 0.27\,\mathrm{Pa}$ and $\mu = 0.033\,\mathrm{Pa}$, whereas in the other two cases (middle and right panels) the material is viscoelastic and heterogeneous. In the heterogeneous setting, we divide the domain into two subdomains denoted by $\Omega_\pm$ and obtained by intersecting the cylindrical domain Ω with the plane $z = 0.5$, i.e., we have $\Omega_+ := \{(r,\theta,z) \in \Omega \ : \ z > 0.5\}$ and $\Omega_- := \{(r,\theta,z) \in \Omega \ : \ z < 0.5\}$. Then we assign different material properties to Ω_+ and Ω_-. In particular, in the case shown in the middle panel the elasticity is kept constant in the whole domain Ω, while the viscosity in Ω_- is 50 times higher than the viscosity in Ω_+. In the example displayed

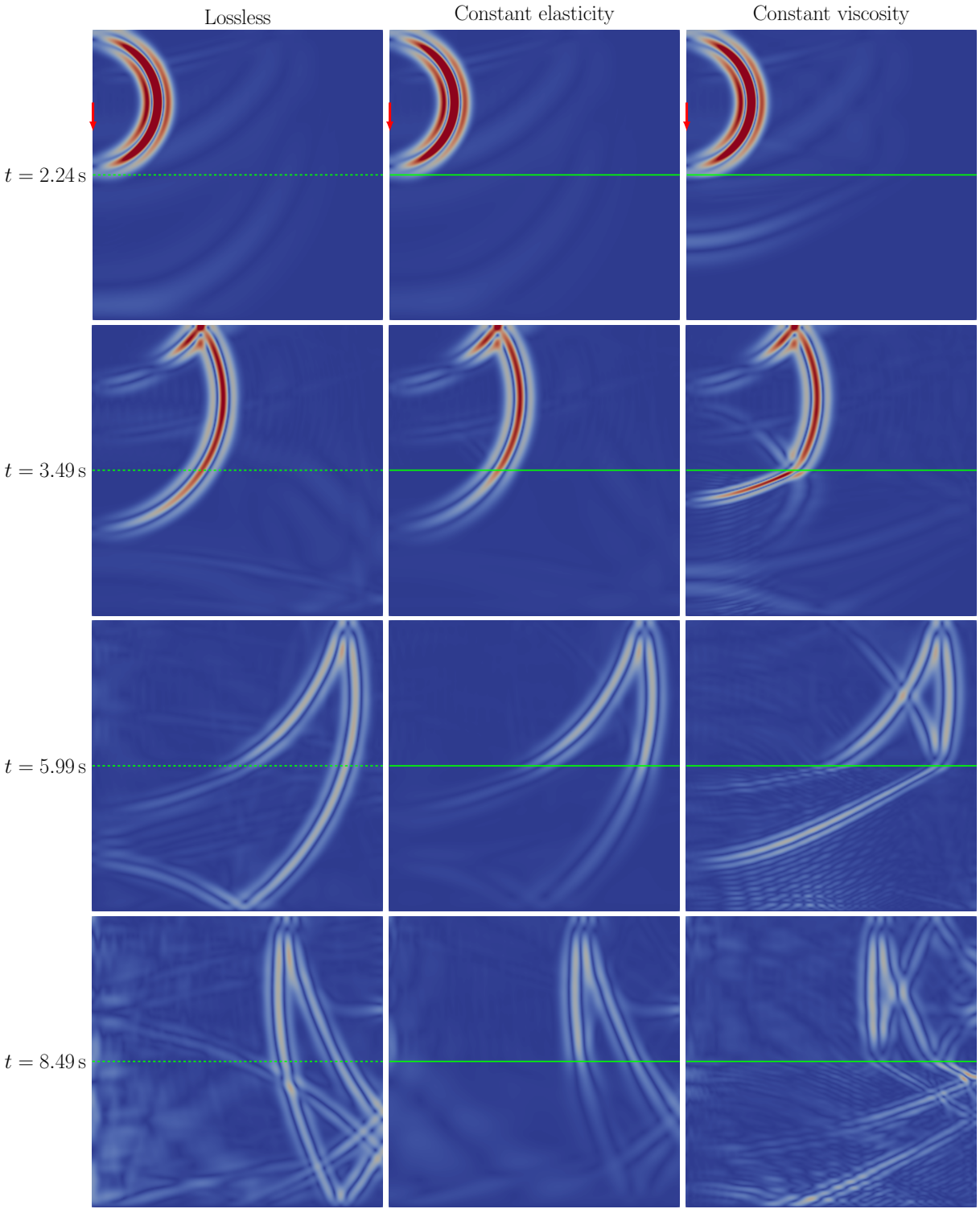


Figure 6.14: Each panel shows the displacement magnitude at different times (rows) and for different material properties (columns). The waves propagates due to the presence of a vertical point load acting at the point of the axis of a cylindrical domain having coordinate $z = 0.75\,\mathrm{m}$. The continuous green line in the panels of the second and third column is used to denote the interface between different materials. The dashed green line in the panels of the lossless case is used as an help line for easier comparison with the results obtained with heterogeneous materials. The figures show how the material heterogeneity and the presence of viscosity affects the propagation of waves, resulting in different attenuation and reflections at material interfaces.

in the right panel, the viscosity is now kept constant Ω, whereas the elasticity in Ω_- is 4 times lower compared to the elasticity of Ω_+. The numerical results are shown in Figure 6.14. Each panel shows the displacement magnitude at four different times (rows) and for different material properties (columns). The continuous horizontal green line in the panels of the second and third column is used to denote the interface between different materials. The dashed green line in the panels of the first column is used as a guide line to facilitate the comparison with the results obtained with heterogeneous materials but does not denote any material interface (we remark that the medium is indeed homogeneous). The figures show how the material heterogeneity and the presence of viscosity affects the propagation of waves, resulting in different attenuation and reflections at material interfaces. In particular, the first thing we can notice is that the solutions at time $t = 2.24\,\mathrm{s}$ (first row panels) are very similar and do not manifest strong dependence on the material parameters characterising the materials. This is due to the fact that waves that start to propagate from the point of the $z-$axis having coordinate $z = 0.75\,\mathrm{m}$ have not yet reached the material interfaces. Moreover, we recall that the upper subdomains of the problems in the second and third column have the same viscoelastic properties and, in particular, they are characterised by very high quality factors, which implies that the attenuation is very low. As a consequence, the viscoelastic solution turns out to be really similar to the one obtained in the lossless case. Looking at the solutions at time $t = 3.49\,\mathrm{s}$, i.e., the panels in the second row, we can see that in all the cases there is a reflected wave that started to propagate from the upper base surface due to the imposition of zero Neumann boundary conditions. Furthermore, since the first propagating wave has reached the material interface, we observe the effect of the change in material parameters. In particular, in the panel of the second column, we observe a much higher attenuation of the wave as a consequence of the viscosity being 50 times higher in Ω_- compared to Ω_+. On the other hand, looking at the panel in the third column, we notice that the phase velocity at which the wave travels is affected by the much lower elasticity of Ω_- compared to Ω_+ and this results in a different direction of propagation of the wave. Similar conclusions can be drawn from the panels in the third row, which show the numerical solution at time $t = 5.99\,\mathrm{s}$. In particular, in the lossless case we observe a reflected wave that started to popagate from the base surface of the cylindrical domain, whereas, owing to the much higher viscosity, it can be only barely seen in the second case. In the third case we do not observe this reflected wave, as the phase velocity is much lower and the original wave have not yet reached the bottom surface. However, in this case we notice a reflected wave that has started to propagate from the material interface and that travels towards the upper base surface. Finally, at time $t = 8.49\,\mathrm{s}$, we see that, in all the cases, the initial wave has reached the lateral surface and has been reflected. Moreover, in the lossless case we observe multiple reflections at the base surface of the domain, whereas, in the case of varying viscosity, only few of them can be distinguished and, in the case of varying elastic, the waves pattern is much different due to the lower phase velocity.

6.4 Full 3D Cylindrical Coordinates

In this section we describe a Spectral-Galerkin numerical approach for the solution of the three-dimensional displacement equations of motion with Kelvin-Voigt constitutive model on cylindrical domains. We continue to adopt the geometrical setting introduced in Section 6.3 and briefly summarised in Section 6.4.1, thereby defining displacement and velocity fields using cylindrical coordinates (r, θ, z). However, in this Section we do not assume any a priori symmetry of the solution, which therefore depends, in the general case, on all the three coordinates (r, θ, z). Moreover, in this section we write the vector field function $\boldsymbol{u}$ in the form

$$\boldsymbol{u}(r, \theta, z) = u_x(r, \theta, z)\boldsymbol{e}_x + u_y(r, \theta, z)\boldsymbol{e}_y + u_z(r, \theta, z)\boldsymbol{e}_x,$$

where $\{\boldsymbol{e}_x, \boldsymbol{e}_y, \boldsymbol{e}_z\}$ is the canonical basis of the euclidean space $\mathbb{R}^3$, instead of using the radial, tangential and axial components $\{\boldsymbol{e}_r, \boldsymbol{e}_\theta, \boldsymbol{e}_Z\}$. This choice allows to define the basis functions even on the cylinder axis ($r = 0$) without particular issues. In Section 6.4.2 we define the sets of basis functions to be used in the Galerkin discretisation in space of the weak formulation. As usual, we partition the domain in material subdomains and define local basis functions by tensorization of one-dimensional bases. However, in contrast with what we have done in the previous sections, where the use of boundary-

adapted polynomial allowed a straightforward matching of the local basis functions at the material interfaces and thus the definition of globally continuous basis, we now consider a more general approach which imposes weak continuity in L^2 of the basis functions at each material interface (§6.4.3). Finally, in Section 6.4.4 we show how to compute the matrices arising in the semi-discretisation of the weak formulation.

6.4.1 Geometrical Setting

The geometrical setting is the one described in Section 6.3, i.e., we consider a cylindrical domain $\Omega \subset \mathbb{R}^3$ that is partitioned into a number $D \geq 1$ of subdomains (or elements) denoted by Ω_ℓ, with $\ell = 1, \dots, D$. The partition of Ω is obtained by cutting the cylinder with planes that are orthogonal to its axis and by considering the cylinder as made by a "true" cylinder plus a certain number of cylindrical shells. As in the previous sections, each subdomain Ω_ℓ represents a different material, characterized by density ρ_ℓ, elastic Lamè parameters $\lambda_{\text{el},\ell}$ and μ_ℓ, and viscous Lamè parameters $\lambda_{\text{vi},\ell}$ and η_ℓ. Since we are not assuming a priori any symmetry of the solution, the basis functions depend on all the cylindrical coordinates r, θ and z and the elements Ω_ℓ, with $\ell = 1, \dots, D$, have the form $\Omega_\ell := (r_{0,\ell}, r_{1,\ell}) \times [0, 2\pi) \times (z_{0,\ell}, z_{1,\ell})$. Moreover, we define the function $\chi_\ell(r, \theta, z)$ as

$$\chi_\ell(r, \theta, z) := \begin{cases} 1, & \text{if } (r, \theta, z) \in \Omega_\ell, \\ 0, & \text{if } (r, \theta, z) \notin \Omega_\ell, \end{cases} \qquad \ell = 1, 2, \dots, D. \tag{6.75}$$

6.4.2 Basis Functions Definition

As we have already seen, in order to numerically solve problem (5.31) we have to define a finite dimensional subspace $\mathcal{V}_{N_0}$ of $H^1_D(\Omega)^6$ and a finite dimensional subspace $\mathcal{V}_N \geq \mathcal{V}_{N_0}$ of $H^1(\Omega)^6$. As usual, we proceed by defining two sets of continuous basis functions such that $\mathcal{V}_{N_0} = \text{span}(\boldsymbol{\Phi}_1, \dots, \boldsymbol{\Phi}_{2N_0})$ and $\mathcal{V}_N = \text{span}(\hat{\boldsymbol{\Phi}}_1, \dots, \hat{\boldsymbol{\Phi}}_{2N})$. In contrast to what we have done in the previous sections, the basis functions considered here are defined in a slightly different way. The first difference is related to the presence of the angle θ. The basis functions depending on this variabale will be Fourier characters (or, in general, trigonometric functions), as they are commonly adopted within the context of spectral methods for the numerical approximation of functions defined on periodic domains. The second difference concerns the continuity of the basis functions across the material interfaces. In the previous sections global continuity on Ω was achieved by considering suitable linear combinations of orthogonal polynomials, i.e., the so-called boundary-adapted orthogonal polynomials. Here, we relax this requirement, in the sense we consider this kind of polynomials only within those subdomains Ω_ℓ where Dirichlet boundary conditions are imposed and require weak continuity at the material interfaces. Thus, to build the subspaces $\mathcal{V}_{N_0}$ and $\mathcal{V}_N$, we have proceeded as follows.

1. First, on each domain Ω_ℓ, $\ell = 1, \dots, D$, we have picked two sets of basis functions $\boldsymbol{\Psi}$ and $\hat{\boldsymbol{\Psi}}$ that are separately $\mathcal{C}^1$ with respect to each variable r, θ and z. It is worth emphasizing that this does not imply that these functions are jointly $\mathcal{C}^1(\Omega_\ell)$, due to the singularity of the cylindrical coordinates system on the z-axis.

2. Then, we have considered only those basis functions $\boldsymbol{\Psi}_i$, $i = 1, \dots, M_0$, and $\hat{\boldsymbol{\Psi}}_i$, $i = 1, \dots, M$, such that the finite dimensional vector space they generate is a subspace of $H^1_D(\Omega_\ell)^6$ and $H^1(\Omega_\ell)^6$, respectively. These basis functions have been used for the computation of the mass and stiffness matrices, as this choice basically guarantees an easy computation of integrals and derivatives in domains with different physical properties.

3. Finally, we have built $\boldsymbol{\Phi}$ and $\hat{\boldsymbol{\Phi}}$ by "gluing" $\boldsymbol{\Psi}$ and $\hat{\boldsymbol{\Psi}}$ at the interface Σ_{ij} between Ω_i and Ω_j, with $i, j = 1, 2, \dots, D$, i.e., enforcing the continuity at the interfaces and thus building basis functions that are globally continuous in Ω (see Section 6.4.3 for further details).

We consider the vector basis functions $\boldsymbol{\Phi}_i$ and $\hat{\boldsymbol{\Phi}}_i$ as subdivided into two blocks, i.e., $\boldsymbol{\Phi}_i = (\boldsymbol{\Phi}_i^v, \boldsymbol{\Phi}_i^u)^\mathsf{T}$ and $\hat{\boldsymbol{\Phi}}_i = (\hat{\boldsymbol{\Phi}}_i^v, \hat{\boldsymbol{\Phi}}_i^u)^\mathsf{T}$, the first one referring to $\boldsymbol{v}_N$ and the second one to $\boldsymbol{u}_N$, with $\boldsymbol{\Phi}_i^u = (\Phi_i^{u_x}, \Phi_i^{u_y}, \Phi_i^{u_z})^\mathsf{T}$. The numbering of both the two blocks $\boldsymbol{\Psi}^v$ and $\boldsymbol{\Psi}^u$ follows the numbering of the domains Ω_ℓ where they

are defined. In other words, denoting by $3\hat{m}_\ell$ the number of vector basis functions on each domain Ω_ℓ, we have

$$\hat{\mathbf{\Psi}}^v = \left(\hat{\mathbf{\Psi}}_1^{v,1}, \dots, \hat{\mathbf{\Psi}}_{3\hat{m}_1}^{v,1}, \hat{\mathbf{\Psi}}_1^{v,2}, \dots, \hat{\mathbf{\Psi}}_{3\hat{m}_2}^{v,2}, \dots, \hat{\mathbf{\Psi}}_1^{v,D}, \dots, \hat{\mathbf{\Psi}}_{3\hat{m}_D}^{v,D}\right). \tag{6.76}$$

Then, each of these vector basis functions $\hat{\mathbf{\Psi}}_j^{v,\ell}$, with $\ell = 1, \dots, D$ and $j = 1, \dots, \hat{m}_\ell$ are defined as:

$$\hat{\mathbf{\Psi}}_i^{v,\ell} = \begin{cases} \hat{\mathbf{\Psi}}_j^{v_x,\ell}, & \text{for } i = 1, \dots, \hat{m}_\ell,\ j = i, \\ \hat{\mathbf{\Psi}}_j^{v_y,\ell}, & \text{for } i = \hat{m}_\ell + 1, \dots, 2\hat{m}_\ell,\ j = i - \hat{m}_\ell, \\ \hat{\mathbf{\Psi}}_j^{v_z,\ell}, & \text{for } i = 2\hat{m}_\ell + 1, \dots, 3\hat{m}_\ell,\ j = i - 2\hat{m}_\ell, \end{cases} \tag{6.77}$$

where, for a suitable choice of scalar basis functions $\psi_{\alpha,j}^\ell \in H^1(\Omega_\ell)$, with $\alpha = x, y, z$, we set

$$\hat{\mathbf{\Psi}}_j^{v_x,\ell} = \begin{pmatrix} \hat{\psi}_{x,j}^\ell \\ 0 \\ 0 \end{pmatrix}, \qquad \hat{\mathbf{\Psi}}_j^{v_y,\ell} = \begin{pmatrix} 0 \\ \hat{\psi}_{y,j}^\ell \\ 0 \end{pmatrix}, \qquad \hat{\mathbf{\Psi}}_j^{v_z,\ell} = \begin{pmatrix} 0 \\ 0 \\ \hat{\psi}_{z,j}^\ell \end{pmatrix}, \qquad j = 1, \dots, \hat{m}_\ell. \tag{6.78}$$

Owing to the cylindrical shape of the domain Ω_ℓ, one may define the basis functions $\hat{\psi}_{\alpha,j}^\ell$, $\alpha = x, y, z$, $\ell = 1, 2, \dots, D$, by tensor products of Fourier functions in θ, polynomials in r, and polynomials in z. Unfortunately, the requirement $\hat{\psi}_{\alpha,j}^\ell \in H^1(\Omega_\ell)$, for all $\alpha = x, y, z$, is not in general satisfied by such a choice when $\Omega_\ell \cap \{r = 0\} \neq \emptyset$, due to the singularity of cylindrical coordinates on the z-axis. Thus, we need to proceed with the following two steps: first, we define the scalar functions $\underline{\psi_{\alpha,j}^\ell}$ as above and second we compute a basis $\{\hat{\psi}_{\alpha,j}^\ell\}$ for the intersection between the space generated by $\underline{\psi_{\alpha,j}^\ell}$ and $H^1(\Omega_\ell)$. Namely, given a spectral discretisation parameter $n \in \mathbb{N}$, we denote by $\mathbb{P}_n$ the space of polynomials of degree not larger than n and by $\mathcal{F}_n$ the space of Fourier sums with frequencies in the set $\{-\lfloor n/2 \rfloor, \dots, -1, 0, 1, \dots, \lfloor n/2 \rfloor\}$, where the floor function is defined as $\lfloor p \rfloor = \max\{n \in \mathbb{N}, n \leq p\}$. Then we construct a basis for the local tensor product space $\mathcal{F}_n \otimes \mathbb{P}_n \otimes \mathbb{P}_n$ by products of the standard Fourier basis, a basis for the r-polynomials, and a basis for the z-polynomials. We remark that, in order to improve the flexibility of our method, we allow to use different basis on each subdomain Ω_ℓ and for the two variables r and z. Thus, for any $\alpha = x, y, z$ and any $\ell = 1, 2, \dots, D$, we pick a basis $\{p_{\alpha,0}^\ell, p_{\alpha,1}^\ell, \dots, p_{\alpha,n}^\ell\}$ and a basis $\{q_{\alpha,0}^\ell, q_{\alpha,1}^\ell, \dots, q_{\alpha,n}^\ell\}$ of $\mathbb{P}_n$. We choose such polynomial basis $\{p_{\alpha,s}^\ell\}$ and $\{q_{\alpha,t}^\ell\}$ in a way that simplifies the imposition of the Dirichlet boundary conditions: we assume that, for any ℓ such that $\partial\Omega_\ell \cap \Gamma_D \neq \emptyset$ and for any $\alpha = x, y, z$,

$$\text{if } \partial\Omega_\ell \cap \Gamma_D \supseteq \{\boldsymbol{x} \in \partial\Omega_\ell : z = \hat{z}\}, \text{ then } q_{\alpha,t}^\ell(\hat{z}) = 0, \forall t = 1, 2, \dots, n, \tag{6.79a}$$

$$\text{if } \partial\Omega_\ell \cap \Gamma_D \supseteq \{\boldsymbol{x} \in \partial\Omega_\ell : r = \hat{r}\}, \text{ then } p_{\alpha,s}^\ell(\hat{r}) = 0, \forall s = 1, 2, \dots, n. \tag{6.79b}$$

Also, for handling the singularity introduced by the use of cylindrical coordinates, we assume, for any ℓ such that $r_{0,\ell} = 0$,

$$p_{\alpha,s}^\ell(0) = 0,\ \forall s = 1, 2, \dots, n. \tag{6.80}$$

When dealing with the tensor product $\mathcal{F}_n \otimes \mathbb{P}_n \otimes \mathbb{P}_n$, we need to introduce an ordering of multi-indices, i.e., a one-to-one map

$$\{1, 2, \dots, m\} \ni j \mapsto (k(j), s(j), t(j)) \in \{-\lfloor n/2 \rfloor, \dots, \lfloor n/2 \rfloor\} \times \{0, 1, \dots, n\} \times \{0, 1, \dots, n\} =: Q_\ell,$$

where $m = m(n) := (n+1)^2(2\lfloor n/2 \rfloor + 1)$. For the sake of simplicity, in our implementation we have chosen to use the graded inverse lexicographic ordering of multi-indices. Thus we consider scalar basis functions having the form:

$$\underline{\psi_{\alpha,j}^\ell}(r, \theta, z) = e^{ik(j)\theta} p_{\alpha,s(j)}^\ell(r) q_{\alpha,t(j)}^\ell(z) \chi_\ell(r, \theta, z),\ \ j = 1, 2, \dots, m,\ \alpha = x, y, z,\ \ell = 1, 2, \dots, N_l,$$

where $\chi_\ell(r, \theta, z)$ is defined as in (6.75). Now the goal is to compute a basis for the following linear spaces

$$W_{n,\ell} := \operatorname{span}\left\{\underline{\psi_{\alpha,j}^\ell} \boldsymbol{e}_\alpha : \alpha = x, y, z,\ j = 1, 2, \dots, m(n)\right\} \cap H^1(\Omega_\ell)^3 \tag{6.81}$$

where $\ell = 1, 2, \dots, D$. So, let us consider the following function:

$$\boldsymbol{\Psi}^\ell = \underline{\psi_x^\ell}\boldsymbol{e}_x + \underline{\psi_y^\ell}\boldsymbol{e}_y + \underline{\psi_z^\ell}\boldsymbol{e}_z,$$

where

$$\begin{aligned}
\underline{\psi_x^\ell}(r,\theta,z) &= e^{ik\theta} p_{x,s}^\ell(r) q_{x,t}^\ell(z) \chi_\ell(r,\theta,z),\\
\underline{\psi_y^\ell}(r,\theta,z) &= e^{ik\theta} p_{y,s}^\ell(r) q_{y,t}^\ell(z) \chi_\ell(r,\theta,z),\\
\underline{\psi_z^\ell}(r,\theta,z) &= e^{ik\theta} p_{z,s}^\ell(r) q_{z,t}^\ell(z) \chi_\ell(r,\theta,z)
\end{aligned}$$

and compute the $H^1(\Omega)^3$-norm, namely $\|\boldsymbol{\Psi}^\ell\|^2_{H^1(\Omega)} = \|\boldsymbol{\Psi}^\ell\|_{L^2(\Omega)} + \|\nabla\boldsymbol{\Psi}^\ell\|_{L^2(\Omega)}$, where

$$\begin{aligned}
\|\boldsymbol{\Psi}^\ell\|^2_{L^2(\Omega)} &= \int_\Omega \boldsymbol{\Psi}^\ell \cdot \overline{\boldsymbol{\Psi}}^\ell \, d\boldsymbol{x} = \sum_{\alpha=x,y,z} \int_{\Omega_\ell} |\underline{\psi_\alpha^\ell}|^2 \, d\boldsymbol{x} = \\
&= 2\pi \sum_{\alpha=x,y,z} \left(\int_{r_{0,\ell}}^{r_{1,\ell}} p_{\alpha,s}^\ell(r) p_{\alpha,s}^\ell(r)\, r dr \right) \left(\int_{z_{0,\ell}}^{z_{1,\ell}} q_{\alpha,t}^\ell(z) q_{\alpha,t}^\ell(z)\, dz \right)
\end{aligned}$$

and

$$\begin{aligned}
\|\nabla\boldsymbol{\Psi}^\ell\|^2_{L^2(\Omega)} &= \int_\Omega \nabla\boldsymbol{\Psi}^\ell : \nabla\boldsymbol{\Psi}^\ell \, d\boldsymbol{x} = \sum_{\alpha,\beta=x,y,z} \int_{\Omega_\ell} \left| \partial \underline{\psi_\alpha^\ell} / \partial\beta \right|^2 \, d\boldsymbol{x} = \\
&\sum_{\alpha,\beta=x,y,z} \left(\int_{\Omega_\ell} \left[p_{\alpha,s}^{\ell\,\prime}(r) q_{\alpha,t}^\ell(z) \right]^2 d\boldsymbol{x} + \int_{\Omega_\ell} \left[p_{\alpha,s}^\ell(r) q_{\alpha,t}^{\ell\,\prime}(z) \right]^2 d\boldsymbol{x} + \int_{\Omega_\ell} \left[\frac{k p_{\alpha,s}^\ell(r) q_{\alpha,t}^\ell(z)}{r} \right]^2 d\boldsymbol{x} \right).
\end{aligned} \tag{6.82}$$

It is clear that $\|\boldsymbol{\Psi}^\ell\|^2_{L^2(\Omega)}$ is always finite, as it involves the sum of integrals of polynomials on bounded domains. The same holds for the first two integrals in (6.82). Let us now rewrite the third integral as

$$\int_{\Omega_\ell} \left[\frac{k p_{\alpha,s}^\ell(r) q_{\alpha,t}^\ell(z)}{r} \right]^2 d\boldsymbol{x} = 2\pi k \left(\int_{r_{0,\ell}}^{r_{1,\ell}} \frac{p_{\alpha,s}^\ell(r) p_{\alpha,s}^\ell(r)}{r} \, dr \right) \left(\int_{z_{0,\ell}}^{z_{1,\ell}} q_{\alpha,t}^\ell(z) q_{\alpha,t}^\ell(z)\, dz \right).$$

Then, we can see that the integral with respect to the variable r may not always be finite: indeed, if we consider an index ℓ such that $r_{0,\ell} = 0$ and take $s = 0$ (so that p_α^ℓ does not vanish in 0, see (6.80)), the integral does not converge. Therefore, for all the domains Ω_ℓ such that $r_{0,\ell} = 0$ we need to require

$$k \neq 0 \;\Rightarrow\; s \neq 0. \tag{6.83}$$

Thus we have, for all $\ell = 1, 2, \dots, D$,

$$W_{n,\ell} = \begin{cases} \operatorname{span}\left\{ \underline{\psi_{\alpha,j}^\ell} \boldsymbol{e}_\alpha : \alpha = x,y,z,\ j = 1,2,\dots,m \right\} & r_{0,\ell} \neq 0 \\ \operatorname{span}\left\{ \underline{\psi_{\alpha,j}^\ell} \boldsymbol{e}_\alpha : \alpha = x,y,z,\ j = 1,2,\dots,m :\ s(j) \neq 0 \text{ if } k(j) \neq 0 \right\} & r_{0,\ell} = 0 \end{cases}.$$

Note that in particular the above expression provides an implicit definition of the basis functions $\hat{\boldsymbol{\Psi}}$. More explicitly, for any $\ell = 1, 2, \dots, D$, we can introduce a new local basis ordering

$$j \mapsto (k^\ell(j), s^\ell(j), t^\ell(j))$$

which coincides with the original ordering if $r_{0,\ell} \neq 0$, while, if $r_{0,\ell} = 0$, is obtained by relabelling (according the old ordering) the multi-indices sequence obtained by discarding the multi-indices not satisfying the condition stated in (6.83). Then we set

$$\hat{\psi}_{\alpha,j}^\ell = e^{ik^\ell(j)} p_{\alpha,s^\ell(j)}^\ell(r) q_{\alpha,t^\ell(j)}^\ell(z) \chi_\ell(r,z), \tag{6.84}$$

and the basis $\hat{\mathbf{\Psi}}$ is defined by (6.76–6.78). We report the set of multi-indices that we consider when defining $\hat{\psi}^{\ell}_{\alpha,j}$ in Figure 6.15: if $r_{0,\ell} \neq 0$, then the considered multi-indices are as in Panel a. If instead $r_{0,\ell} = 0$, then we consider multi-indices as in Panel b. Note in particular that

$$\hat{m}_\ell = \begin{cases} (n+1)^2(2\lfloor n/2 \rfloor + 1), & \text{if } r_{0,\ell} \neq 0 \\ (n+1)[(2\lfloor n/2 \rfloor + 1)n + 1], & \text{otherwise} \end{cases}. \tag{6.85}$$

In order to define the basis $\mathbf{\Psi}$, i.e., those generating a finite dimensional subspace of $H^1_D(\Omega)^6$, we can work in an analogous way. Indeed, for any ℓ such that $\partial\Omega_\ell \cap \Gamma_D \neq \emptyset$ we consider only the multi-indices (k^ℓ, s^ℓ, t^ℓ) such that $t^\ell \neq 0$ or/and $s^\ell \neq 0$ (depending whether $\partial\Omega_\ell \cap \Gamma_D$ is a lateral surface or a base surface or the union of both) and define the local multi-index ordering

$$\{1, 2, \dots, m_\ell\} \ni j \mapsto (k^\ell_d(j), s^\ell_d(j), t^\ell_d(j)) \in Q_\ell \tag{6.86}$$

as above. In other words,

$$(k^\ell_d(j), s^\ell_d(j), t^\ell_d(j)) = (k^\ell(j), s^\ell(j), t^\ell(j)) \in Q_\ell \qquad \text{if } \partial\Omega_\ell \cap \Gamma_D = \emptyset, \tag{6.87a}$$

$$(k^\ell_d(j), s^\ell_d(j), t^\ell_d(j)) \in \{(k,s,t) \in Q_\ell : t \neq 0\} \qquad \text{if } \partial\Omega_\ell \cap \Gamma_D = \{\boldsymbol{x} \in \partial\Omega_\ell \ : \ z = \hat{z}\}, \tag{6.87b}$$

$$(k^\ell_d(j), s^\ell_d(j), t^\ell_d(j)) \in \{(k,s,t) \in Q_\ell : s \neq 0\} \qquad \text{if } \partial\Omega_\ell \cap \Gamma_D = \{\boldsymbol{x} \in \partial\Omega_\ell \ : \ r = \hat{r}\}, \tag{6.87c}$$

$$(k^\ell_d(j), s^\ell_d(j), t^\ell_d(j)) \in \{(k,s,t) \in Q_\ell : s \neq 0, t \neq 0\} \qquad \text{if } \partial\Omega_\ell \cap \Gamma_D = \{\boldsymbol{x} \in \partial\Omega_\ell \ : \ r = \hat{r} \text{ and } z = \hat{z}\}. \tag{6.87d}$$

Summarising and considering, without loss of generality, the case in (6.87b), we have:

a) if $\partial\Omega_\ell \cap \Gamma_D = \emptyset$ and $r_{0,\ell} \neq 0$, we consider the multi-indices set Q_ℓ as in Panel a Figure 6.15,

b) if $\partial\Omega_\ell \cap \Gamma_D = \emptyset$ and $r_{0,\ell} = 0$, we consider the multi-indices set Q_ℓ as in Panel b of Figure 6.15

c) if $\partial\Omega_\ell \cap \Gamma_D \neq \emptyset$ and $r_{0,\ell} \neq 0$, we consider the multi-indices set Q_ℓ as in Panel c of Figure 6.15,

d) if $\partial\Omega_\ell \cap \Gamma_D \neq \emptyset$ and $r_{0,\ell} = 0$, we consider the multi-indices set Q_ℓ as in Panel d of Figure 6.15.

Moreover, the number of basis functions is given by

$$m_\ell = \begin{cases} (n+1)^2(2\lfloor n/2 \rfloor + 1), & \text{if } \partial\Omega_\ell \cap \Gamma_D = \emptyset \text{ and } r_{0,\ell} \neq 0 \\ (n+1)[(2\lfloor n/2 \rfloor + 1)n + 1], & \text{if } \partial\Omega_\ell \cap \Gamma_D = \emptyset \text{ and } r_{0,\ell} = 0 \\ n(n+1)(2\lfloor n/2 \rfloor + 1), & \text{if } \partial\Omega_\ell \cap \Gamma_D \neq \emptyset \text{ and } r_{0,\ell} \neq 0 \\ n[(2\lfloor n/2 \rfloor + 1)n + 1], & \text{if } \partial\Omega_\ell \cap \Gamma_D \neq \emptyset \text{ and } r_{0,\ell} = 0 \end{cases}. \tag{6.88}$$

It is worth highlighting that, due to the property stated in (6.79) of the polynomials basis that we are using for the dependence on the space variables r and z, if $\partial\Omega_\ell \cap \Gamma_D \neq \emptyset$, then the functions

$$\psi^\ell_{\alpha,j} = e^{ik^\ell_d(j)} p^\ell_{\alpha,s^\ell_d(j)}(r) q^\ell_{\alpha,t^\ell_d(j)}(z) \chi_\ell(r,z) \tag{6.89}$$

vanish on Γ_D. Therefore we define the basis $\mathbf{\Psi}$ as in (6.76–6.78), but using the scalar basis $\psi^\ell_{\alpha,j}$ instead of the scalar basis $\hat{\psi}^\ell_{\alpha,j}$. Precisely we set

$$\mathbf{\Psi}^v = \left(\mathbf{\Psi}^{v,1}_1, \dots, \mathbf{\Psi}^{v,1}_{3m_1}, \mathbf{\Psi}^{v,2}_1, \dots, \mathbf{\Psi}^{v,2}_{3m_2}, \dots, \mathbf{\Psi}^{v,D}_1, \dots, \mathbf{\Psi}^{v,D}_{3m_D} \right),$$

where, each of these vector basis functions $\mathbf{\Psi}^{v,\ell}_j$, with $\ell = 1, \dots, D$ and $j = 1, \dots, m_\ell$ are defined as:

$$\mathbf{\Psi}^{v,\ell}_i = \begin{cases} \mathbf{\Psi}^{v_x,\ell}_j, & \text{for } i = 1, \dots, m_\ell, \ j = i, \\ \mathbf{\Psi}^{v_y,\ell}_j, & \text{for } i = m_\ell + 1, \dots, 2m_\ell, \ j = i - m_\ell, \\ \mathbf{\Psi}^{v_z,\ell}_j, & \text{for } i = 2m_\ell + 1, \dots, 3m_\ell, \ j = i - 2m_\ell, \end{cases}$$

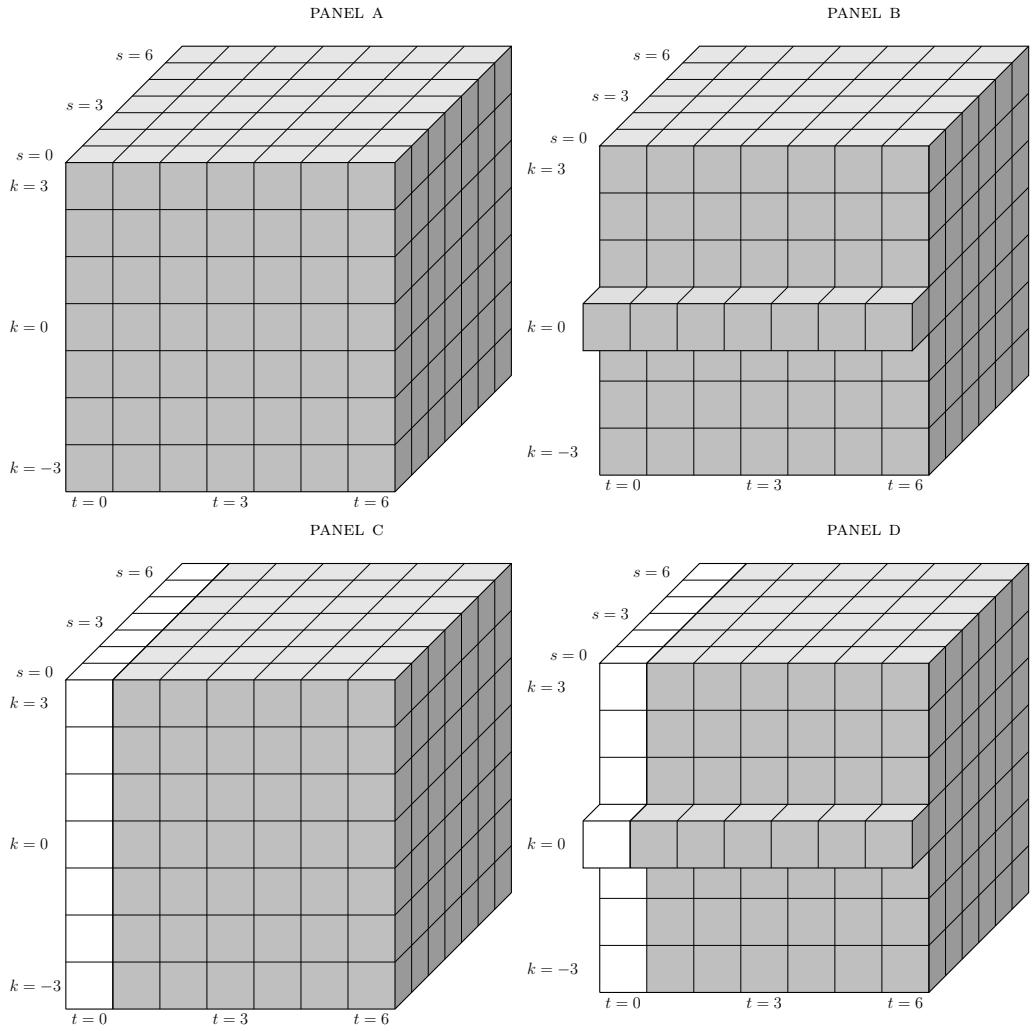


Figure 6.15: Different sets of multi-indices used in the construction of the scalar basis $\underline{\psi^{\ell}_{\alpha,j}}$, $\hat{\psi}^{\ell}_{\alpha,j}$, and $\psi^{\ell}_{\alpha,j}$ in the easy case of $n = 3$.

and

$$\boldsymbol{\Psi}_j^{v_x,\ell} = \begin{pmatrix} \psi^{\ell}_{x,j} \\ 0 \\ 0 \end{pmatrix}, \qquad \boldsymbol{\Psi}_j^{v_y,\ell} = \begin{pmatrix} 0 \\ \psi^{\ell}_{y,j} \\ 0 \end{pmatrix}, \qquad \boldsymbol{\Psi}_j^{v_z,\ell} = \begin{pmatrix} 0 \\ 0 \\ \psi^{\ell}_{z,j} \end{pmatrix}, \qquad j = 1, \dots, m_\ell.$$

In the following subsections, we will often consider the case in which both $\boldsymbol{v}$ and $\boldsymbol{u}$ have the same basis functions and therefore we will simplify the notation writing $\boldsymbol{\Psi}_j^{\alpha,\ell}$ (resp. $\hat{\boldsymbol{\Psi}}_j^{\alpha,\ell}$) to denote both $\boldsymbol{\Psi}_j^{v_\alpha,\ell}$ and $\boldsymbol{\Psi}_j^{u_\alpha,\ell}$ (resp. $\hat{\boldsymbol{\Psi}}_j^{v_\alpha,\ell}$ and $\hat{\boldsymbol{\Psi}}_j^{u_\alpha,\ell}$), for all $\alpha = x, y, z$. Moreover, when the basis are the same for all the components x, y and z, we will write $\boldsymbol{\Psi}_j^{\ell}$ instead of $\boldsymbol{\Psi}_j^{\alpha,\ell}$.

6.4.3 Imposition of Continuity Conditions at Material Interfaces

The space $W_n := W_{n,1} + W_{n,2} + \cdots + W_{n,D}$, with $W_{n,1}, W_{n,2}, \dots, W_{n,D}$, defined as in (6.81), is a finite dimensional subspace of $H^1(\Omega)^3$ containing also functions that are non-continuous at the material interfaces $\Sigma_{ij} := \partial\Omega_i \cap \partial\Omega_j$, $i, j = 1, \dots, D$. We now want to consider only those functions that are globally continuous on Ω, i.e. we want to define a finite dimensional space $\mathcal{V}_N \subset H^1(\Omega)^6$ consisting of continuous vector basis functions having non-zero value in Γ_D

$$\mathcal{V}_N := \left\{ W_n^2 \ni \hat{\boldsymbol{\Phi}} = (\hat{\boldsymbol{\Phi}}^v, \hat{\boldsymbol{\Phi}}^u)^{\mathsf{T}} = (\hat{\Phi}^{v_x}, \hat{\Phi}^{v_y}, \hat{\Phi}^{v_z}, \hat{\Phi}^{u_x}, \hat{\Phi}^{u_y}, \hat{\Phi}^{u_z})^{\mathsf{T}} \ : \ (\hat{\boldsymbol{\Phi}})_j \in \mathcal{C}(\Omega),\ j = 1, \dots, 6 \right\}.$$

and a finite dimensional space $\mathcal{V}_{N_0} \subset H^1_D(\Omega)^6$ of continuous vector basis functions vanishing in Γ_D

$$\mathcal{V}_{N_0} := \{ \boldsymbol{\Phi} \in \mathcal{V}_N \ : \ T_D \boldsymbol{\Phi} = 0 \}.$$

Roughly speaking, the idea here is to build a set of continuous scalar basis functions by "gluing" the scalar basis defined by (6.84) at the interfaces between the different domains where they are defined. In particular, new set of continuous basis is obtained by computing a matrix imposing the continuity constraint, performing a `QR` decomposition of its transpose and finally extracting the matrix for the change of basis from the orthogonal matrix Q. Since the three-dimensional problem involves six unknowns (both displacement and velocity along x, y and z), we need a change of basis matrix for each of them. Actually, this does not always imply that we need to repeat all the computations for each unknown: indeed, if the scalar basis functions used to approximate all the six unknowns are the same, then the matrix for the change of basis is also the same. So, let us denote by $\delta = \delta(r, \theta, z)$ one of the six unknown fields and let us consider the continuity of basis functions $\hat{\psi}_j^\ell$, with $\ell = 1, 2, \ldots, D$ not vanishing on Γ_D. We know that $\delta(r, \theta, z)$ can be written as

$$\delta(r, \theta, z) = \sum_{\ell=1}^{D} \sum_{j=1}^{\hat{m}_\ell} \delta_j^\ell \hat{\psi}_j^\ell(r, \theta, z). \tag{6.90}$$

Moreover, let us denote with $\boldsymbol{\delta} = (\boldsymbol{\delta}^1, \ldots, \boldsymbol{\delta}^D)^\mathsf{T} = (\delta_1^1, \ldots, \delta_{m_1}^1, \ldots, \delta_1^D, \ldots, \delta_{\hat{m}_D}^D)^\mathsf{T}$ the coefficients of the expansion in (6.90) and let us now consider two domains Ω_k and Ω_h such that $\partial\Omega_k \cap \partial\Omega_h = \Sigma_{kh}$. Therefore, we impose the continuity of δ at the interface Σ_{kh} by requiring that

$$\mathbf{c}_{kh} \begin{pmatrix} \boldsymbol{\delta}^k \\ \boldsymbol{\delta}^h \end{pmatrix} = \mathbf{0},$$

where $\mathbf{c}_{kh}$ is continuity constraint matrix at Σ_{kh}. This is the algebraic form of the following condition

$$\int_{\Sigma_{kh}^+} \delta|_{\Sigma_{hk}^+} \varphi \, dS = \int_{\Sigma_{kh}^-} \delta|_{\Sigma_{hk}^-} \varphi \, dS, \qquad \forall \varphi \in \mathcal{T}_n(\Sigma_{kh}),$$

where the space $\mathcal{T}_n(\Sigma_{kh})$ is defined as

$$T_n(\Sigma_{kh}) := \text{span}\left\{ t^+, \, t^- \;:\; \exists \hat{\psi}_i^k, \hat{\psi}_j^h \text{ such that } \hat{\psi}_j^k\big|_{\Sigma_{kh}^+} = t^+, \; \hat{\psi}_j^h\big|_{\Sigma_{kh}^-} = t^- \right\}.$$

Therefore, having denoted by $\mathcal{B}_n(\Sigma_{kh})$ a basis of $\mathcal{T}_n(\Sigma_{kh})$ and assuming that Σ_{kh} is a vertical surface such that $r_{1,k} \equiv r_{0,h}$, we have, $\forall \varphi_i \in \mathcal{B}_n(\Sigma_{kh})$,

$$\sum_{j=1}^{\hat{m}_k} \delta_j^k \underbrace{\int_{\Sigma_{kh}^+} \psi_j^k(r_{1,k}, \theta, z) \overline{\varphi}_i(\theta, z) \, r_{1,k} \, d\theta dz}_{\left(C_{\Sigma_{kh}^+}\right)_{i,j}} = \sum_{j=1}^{\hat{m}_h} \delta_j^h \underbrace{\int_{\Sigma_{kh}^-} \psi_j^h(r_{0,h}, \theta, z) \overline{\varphi}_i(\theta, z) \, r_{0,h} \, d\theta dz}_{-\left(C_{\Sigma_{kh}^-}\right)_{i,j}},$$

which can be written in matrix form as

$$C_{\Sigma_{kh}^+} \boldsymbol{\delta}^k + C_{\Sigma_{kh}^-} \boldsymbol{\delta}^h = \mathbf{0}, \qquad \boldsymbol{c}_{kh} = \begin{pmatrix} C_{\Sigma_{kh}^+} & C_{\Sigma_{kh}^-} \end{pmatrix} \tag{6.91}$$

On the other hand, assuming that Σ_{kh} is an horizontal surface such that $z_{1,k} \equiv z_{0,h}$ and

$$\sum_{j=1}^{\hat{m}_k} \delta_j^k \int_{\Sigma_{kh}^+} \psi_j^k(r, \theta, z_{1,k}) \overline{\varphi}_i(r, \theta) \, r dr d\theta = \sum_{j=1}^{\hat{m}_h} \delta_j^h \int_{\Sigma_{kh}^-} \psi_j^h(r, \theta, z_{0,h}) \overline{\varphi}_i(r, \theta) \, r dr d\theta, \quad \forall \overline{\varphi}_i \in \mathcal{B}_n(\Sigma_{kh}).$$

for which the matrix form is again as in (6.91) but obviously with different components for $C_{\Sigma_{kh}^+}$ and $C_{\Sigma_{kh}^-}$. The continuity constraint matrix $\mathbf{c}_{kh}$ enforces continuity of basis functions only at the interface Σ_{kh}. Then we need to assembly a block matrix $\mathbf{C}$ to compute a new basis that is continuous over all the interfaces. For example, looking at the partitioning of Ω in Figure 6.16 we obtain a matrix with the following structure:

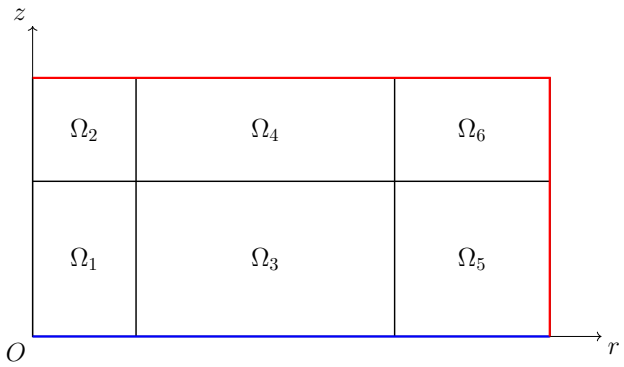


Figure 6.16: Section of cylindrical domain Ω with a possible partition

$$\mathbf{C} = \begin{pmatrix} C_{\Sigma_{12}^+} & C_{\Sigma_{12}^-} & 0 & 0 & 0 & 0 \\ 0 & 0 & C_{\Sigma_{34}^+} & C_{\Sigma_{34}^-} & 0 & 0 \\ 0 & 0 & 0 & 0 & C_{\Sigma_{56}^+} & C_{\Sigma_{56}^-} \\ C_{\Sigma_{13}^+} & 0 & C_{\Sigma_{13}^-} & 0 & 0 & 0 \\ 0 & C_{\Sigma_{24}^+} & 0 & C_{\Sigma_{24}^-} & 0 & 0 \\ 0 & 0 & C_{\Sigma_{35}^+} & 0 & C_{\Sigma_{35}^-} & 0 \\ 0 & 0 & 0 & C_{\Sigma_{46}^+} & 0 & C_{\Sigma_{46}^-} \end{pmatrix},$$

where each row block represents the continuity constraint of a given interface and each column block represent a different domain Ω_ℓ, $\ell = 1, 2, \ldots, D$. It is worth emphasizing that the order of the rows imposing the continuity constraint is not important, while the ordering of the columns must obviously follow the numbering of the domains Ω_ℓ. Having built the matrix imposing the continuity constraint, we now perform the `QR` decomposition of $\mathbf{C}^\mathsf{T}$, that is

$$\mathbf{C} = \begin{pmatrix} \tilde{\mathbf{R}}_0^\mathsf{T} & \mathbf{0} \end{pmatrix} \begin{pmatrix} \tilde{\mathbf{Q}}_0^\mathsf{T} \\ \tilde{\mathbf{Q}}_1^\mathsf{T} \end{pmatrix},$$

where $\tilde{\mathbf{Q}}_1$ is the matrix for the change of basis. In other words each column of matrix $\tilde{\mathbf{Q}}_1$ is a new *continuous* basis function used to approximate one of the six unknowns and it is given as a linear combination of the old (non-continuous) basis functions. Generalizing to the case in which basis functions for unknowns v_x, v_y, v_z, u_x, u_y and u_z are all different (and therefore assuming to compute a matrix $\mathbf{C}$ and to perform the `QR` decomposition for each of them), we can build the matrix for the change of basis as follows:

$$\hat{\mathbf{Q}}_c = \begin{pmatrix} \mathbf{Q}_1^{v_x} & 0 & 0 & 0 & 0 & 0 \\ 0 & \mathbf{Q}_1^{v_y} & 0 & 0 & 0 & 0 \\ 0 & 0 & \mathbf{Q}_1^{v_z} & 0 & 0 & 0 \\ 0 & 0 & 0 & \mathbf{Q}_1^{u_x} & 0 & 0 \\ 0 & 0 & 0 & 0 & \mathbf{Q}_1^{u_y} & 0 \\ 0 & 0 & 0 & 0 & 0 & \mathbf{Q}_1^{u_z} \end{pmatrix}$$

Now the problem is that the ordering of the rows in matrix $\hat{\mathbf{Q}}_c$ is not compatible with the numbering of the (old) basis functions described in (6.76) and (6.77): indeed notice that in the change of basis matrix the rows are ordered by vector field component instead of being divided by considering the different domains in which they are defined. Then, after a suitable permutation of the rows of matrix $\hat{\mathbf{Q}}_c$ we can write the new continuous basis as

$$\hat{\mathbf{\Phi}}_i = \textstyle\sum_{j=1}^{M_0} (\hat{\mathbf{Q}}_c)_{j,i} \hat{\mathbf{\Psi}}_j, \qquad i = 1, \ldots, N_0.$$

Finally, notice that this procedure must be performed for the computation of both $\mathbf{\Phi}$ and $\hat{\mathbf{\Phi}}$: indeed, even though we start from non continuous basis functions satisfying $\{\mathbf{\Psi}_i,\, i = 1, \ldots, M_0\} \subset \{\hat{\mathbf{\Psi}}_i,\, i = 1, \ldots, M\}$, we obtain continuous basis such that $\{\mathbf{\Phi}_i,\, i = 1, \ldots, N_0\} \not\subset \{\hat{\mathbf{\Phi}}_i,\, i = 1, \ldots, N\}$. Then, we denote by $\mathbf{Q}_c$ the matrix for the change of basis from $\mathbf{\Phi}$ to $\mathbf{\Psi}$.

6.4.4 Computation of Matrices

Computation of the mass matrix

We recall that, when using continuous basis functions $\boldsymbol{\Phi}$ vanishing on Γ_D, the mass matrix is denoted by $\mathbf{M}$ and has the form

$$\mathbf{M} = \begin{pmatrix} \mathbf{M}^v & 0 \\ 0 & \mathbf{M}^u \end{pmatrix},$$

where the blocks have dimension $N_0 \times N_0$ with elements (i,j) defined by:

$$(\mathbf{M}^v)_{i,j} = \int_\Omega \boldsymbol{\Phi}_i^v \cdot \boldsymbol{\Phi}_j^v \, d\boldsymbol{x}\,, \quad (\mathbf{M}^u)_{i,j} = \int_\Omega \boldsymbol{\sigma}_{\mathrm{el}}(\boldsymbol{\Phi}_j^u) : \boldsymbol{\varepsilon}(\boldsymbol{\Phi}_i^u) \, d\boldsymbol{x} \tag{6.92}$$

On the other hand, when considering continuous basis functions $\hat{\boldsymbol{\Phi}}$ *not* vanishing on Γ_D, the mass matrix is denoted by $\hat{\mathbf{M}}$ and has the form

$$\hat{\mathbf{M}} = \begin{pmatrix} \hat{\mathbf{M}}^v & 0 \\ 0 & \hat{\mathbf{M}}^u \end{pmatrix},$$

where the blocks have dimension $N \times N$ with elements (i,j) defined by:

$$\left(\hat{\mathbf{M}}^v\right)_{i,j} = \int_\Omega \hat{\boldsymbol{\Phi}}_i^v \cdot \hat{\boldsymbol{\Phi}}_j^v \, d\boldsymbol{x}\,, \quad \left(\hat{\mathbf{M}}^u\right)_{i,j} = \int_\Omega \boldsymbol{\sigma}_{\mathrm{el}}(\hat{\boldsymbol{\Phi}}_j^u) : \boldsymbol{\varepsilon}(\hat{\boldsymbol{\Phi}}_i^u) \, d\boldsymbol{x} \tag{6.93}$$

Furthermore, one can also consider different basis functions for rows and columns: for instance, let us consider basis functions $\boldsymbol{\Phi}$ for rows and basis functions $\hat{\boldsymbol{\Phi}}$ for columns. Then, we define the following matrix

$$\mathbf{N} = \begin{pmatrix} \mathbf{N}^v & 0 \\ 0 & \mathbf{N}^u \end{pmatrix},$$

where the blocks have dimension $N_0 \times N$ and the element (i,j) is defined as:

$$(\mathbf{N}^{v,u})_{i,j} = \int_\Omega \hat{\boldsymbol{\Phi}}_j^{v,u} \cdot \boldsymbol{\Phi}_i^{v,u} \, d\boldsymbol{x}. \tag{6.94}$$

Actually, we do not obtain matrix $\mathbf{M}$, $\hat{\mathbf{M}}$ and $\mathbf{N}$ by computing directly integrals in (6.92–6.94). Instead, we first compute integrals involving non continuous basis functions $\boldsymbol{\Psi}$ and $\hat{\boldsymbol{\Psi}}$ and then we obtain integrals with respect to $\boldsymbol{\Phi}$ and $\hat{\boldsymbol{\Phi}}$ by applying the change of basis matrices $\mathbf{Q}$ and $\hat{\mathbf{Q}}$ computed in Section 6.4.3. More specifically, we have:

$$\mathbf{M} = \mathbf{Q}_c^\top \tilde{\mathbf{M}} \mathbf{Q}_c, \quad \tilde{\mathbf{M}} = \begin{pmatrix} \tilde{\mathbf{M}}^v & 0 \\ 0 & \tilde{\mathbf{M}}^u \end{pmatrix}, \quad \left(\tilde{\mathbf{M}}^v\right)_{i,j} = \int_\Omega \boldsymbol{\Psi}_i^v \cdot \boldsymbol{\Psi}_j^v \, d\boldsymbol{x}, \quad \left(\hat{\mathbf{M}}^u\right)_{i,j} = \int_\Omega \boldsymbol{\sigma}_{\mathrm{el}}(\boldsymbol{\Psi}_j^u) : \boldsymbol{\varepsilon}(\boldsymbol{\Psi}_i^u) \, d\boldsymbol{x}$$

$$\hat{\mathbf{M}} = \hat{\mathbf{Q}}_c^\top \tilde{\tilde{\mathbf{M}}} \hat{\mathbf{Q}}_c, \quad \tilde{\tilde{\mathbf{M}}} = \begin{pmatrix} \tilde{\tilde{\mathbf{M}}}^v & 0 \\ 0 & \tilde{\tilde{\mathbf{M}}}^u \end{pmatrix}, \quad \left(\tilde{\tilde{\mathbf{M}}}^v\right)_{i,j} = \int_\Omega \hat{\boldsymbol{\Psi}}_j^v \cdot \hat{\boldsymbol{\Psi}}_i^v \, d\boldsymbol{x}, \quad \left(\tilde{\tilde{\mathbf{M}}}^u\right)_{i,j} = \int_\Omega \boldsymbol{\sigma}_{\mathrm{el}}(\boldsymbol{\Psi}_j^u) : \boldsymbol{\varepsilon}(\hat{\boldsymbol{\Psi}}_i^u) \, d\boldsymbol{x}$$

$$\mathbf{N} = \mathbf{Q}_c^\top \tilde{\mathbf{N}} \hat{\mathbf{Q}}_c, \quad \tilde{\mathbf{N}} = \begin{pmatrix} \tilde{\mathbf{N}}^v & 0 \\ 0 & \tilde{\mathbf{N}}^u \end{pmatrix}, \quad \left(\tilde{\mathbf{N}}^{v,u}\right)_{i,j} = \int_\Omega \hat{\boldsymbol{\Psi}}_j^{v,u} \cdot \boldsymbol{\Psi}_i^{v,u} \, d\boldsymbol{x}.$$

We now show how to compute $\tilde{\tilde{\mathbf{M}}}$, which is, among the matrices defined above, the only one we actually have to compute: indeed, basis functions $\hat{\boldsymbol{\Psi}}$ and $\boldsymbol{\Psi}$ have been defined in such a way that mass matrix $\tilde{\mathbf{M}}$ can be obtained from $\tilde{\tilde{\mathbf{M}}}$ by removing those rows and columns associated to basis functions $\hat{\boldsymbol{\Psi}}_j^{v,\ell}$ and $\hat{\boldsymbol{\Psi}}_j^{u,\ell}$ not vanishing on $\partial\Omega_\ell \cap \Gamma_D \neq \emptyset$. Similarly, removing only the rows satisfying the conditions above we obtain matrix $\tilde{\mathbf{N}}$. So, let us consider matrix $\tilde{\tilde{\mathbf{M}}}^v$ and notice that it is a block diagonal matrix, since integrals of basis functions having support on different subdomains Ω_m, with $\ell = 1, 2, \ldots, D$, are zero. So, we can write:

$$\tilde{\tilde{\mathbf{M}}}^v = \begin{pmatrix} \tilde{\tilde{\mathbf{M}}}_1^v & & & 0 \\ & \tilde{\tilde{\mathbf{M}}}_2^v & & \\ & & \ddots & \\ 0 & & & \tilde{\tilde{\mathbf{M}}}_\ell^v \end{pmatrix}$$

Again, how we build matrices $\tilde{\tilde{\mathbf{M}}}^v_\ell$, $\ell = 1, 2, \dots, D$, does not depend on the subscript m, the only difference being that the computation of the integrals is performed over a different domain Ω_ℓ. Furthermore, the numbering of the basis functions is so that even these matrices are block-diagonal:

$$\tilde{\tilde{\mathbf{M}}}^v_\ell = \begin{pmatrix} \tilde{\tilde{\mathbf{M}}}^{vx}_\ell & 0 & 0 \\ 0 & \tilde{\tilde{\mathbf{M}}}^{vy}_\ell & 0 \\ 0 & 0 & \tilde{\tilde{\mathbf{M}}}^{vz}_\ell \end{pmatrix}$$

where each block is related to a different component $(x,\, y,\, z)$ of the vector field $\boldsymbol{v}$. Assuming that the basis functions are the same for each component x, y and z, the computation of the component (i, j) of one of this matrices, for example $\tilde{\tilde{\mathbf{M}}}^{vx}_\ell$, is performed as follows

$$\begin{aligned}
\left(\tilde{\tilde{\mathbf{M}}}^{vx}_\ell\right)_{hj} &= \int_\Omega \hat{\psi}^\ell_j \overline{\hat{\psi}^\ell_h}\, r dr d\theta dz \\
&= \int_{\Omega_\ell} e^{ik^\ell(j)\theta} p^\ell_{s^\ell(j)}(r) q^\ell_{t^\ell(j)}(z) e^{-ik^\ell(h)\theta} p^\ell_{s^\ell(h)}(r) q^\ell_{t^\ell(h)}(z)\, r dr d\theta dz \\
&= \left(\int_0^{2\pi} e^{i(k^\ell(j) - k^\ell(h))\theta}\, d\theta\right) \left(\int_{r_{0,\ell}}^{r_{1,\ell}} p^\ell_{s^\ell(j)}(r) p^\ell_{s^\ell(h)}(r)\, r dr\right) \left(\int_{z_{0,\ell}}^{z_{1,\ell}} q^\ell_{t^\ell(j)}(z) q^\ell_{t^\ell(h)}(z)\, dz\right).
\end{aligned}$$

Finally, notice that the computation of the first integral is straightforward and it is equal to $2\pi\delta_{k(j),k(h)}$, δ being the Kronecker delta, whereas the others depend on the type of polynomials we are considering. The computation of the second and third integral, when $p(r)$ and $q(z)$ involve linear combinations of Chebyshev polynomials of the first kind, is discussed in Section 4.4.1.

Computation of the stiffness matrix

We recall that, when using continuous basis functions $\boldsymbol{\Phi}$ vanishing on Γ_D, the stiffness matrix is denoted by $\mathbf{H}$ and has the form

$$\mathbf{H} = \begin{pmatrix} \mathbf{H}_{11} & \mathbf{H}_{12} \\ \mathbf{H}_{21} & \mathbf{H}_{22} \end{pmatrix},$$

where the blocks have dimension $N_0 \times N_0$ and their elements (i, j) are defined as:

$$\begin{aligned}
(\mathbf{H}_{11})_{i,j} &= \int_\Omega \boldsymbol{\sigma}_{\text{vi}}\left(\boldsymbol{\Phi}^v_j\right) : \boldsymbol{\varepsilon}(\boldsymbol{\Phi}^v_i)\, d\boldsymbol{x} & (\mathbf{H}_{12})_{i,j} &= \int_\Omega \boldsymbol{\sigma}_{\text{el}}\left(\boldsymbol{\Phi}^u_j\right) : \boldsymbol{\varepsilon}(\boldsymbol{\Phi}^v_i)\, d\boldsymbol{x} \\
(\mathbf{H}_{21})_{i,j} &= -\int_\Omega \overline{\boldsymbol{\sigma}_{\text{el}}\left(\boldsymbol{\Phi}^v_j\right) : \boldsymbol{\varepsilon}(\boldsymbol{\Phi}^u_i)}\, d\boldsymbol{x} & (\mathbf{H}_{22})_{i,j} &= 0,
\end{aligned}$$

On the other hand, when considering continuous basis functions $\hat{\boldsymbol{\Phi}}$ *not* vanishing on Γ_D, the stiffness matrix is denoted by $\hat{\mathbf{H}}$ and has the form:

$$\hat{\mathbf{H}} = \begin{pmatrix} \hat{\mathbf{H}}_{11} & \hat{\mathbf{H}}_{12} \\ \hat{\mathbf{H}}_{21} & \hat{\mathbf{H}}_{22} \end{pmatrix},$$

where the blocks have dimension $N \times N$ and their elements (i, j) are defined as:

$$\begin{aligned}
\left(\hat{\mathbf{H}}_{11}\right)_{i,j} &= \int_\Omega \boldsymbol{\sigma}_{\text{vi}}(\hat{\boldsymbol{\Phi}}^v_j) : \boldsymbol{\varepsilon}(\hat{\boldsymbol{\Phi}}^v_i)\, d\boldsymbol{x} & \left(\hat{\mathbf{H}}_{12}\right)_{i,j} &= \int_\Omega \boldsymbol{\sigma}_{\text{el}}(\hat{\boldsymbol{\Phi}}^u_j) : \boldsymbol{\varepsilon}(\hat{\boldsymbol{\Phi}}^v_i)\, d\boldsymbol{x} \\
\left(\hat{\mathbf{H}}_{21}\right)_{i,j} &= -\int_\Omega \overline{\boldsymbol{\sigma}_{\text{el}}(\hat{\boldsymbol{\Phi}}^v_j) : \boldsymbol{\varepsilon}(\hat{\boldsymbol{\Phi}}^u_i)}\, d\boldsymbol{x} & \left(\hat{\mathbf{H}}_{22}\right)_{i,j} &= 0,
\end{aligned}$$

Furthermore, one can also consider different basis functions for rows and columns: for instance, let us consider basis functions $\boldsymbol{\Phi}$ for rows and basis functions $\hat{\boldsymbol{\Phi}}$ for columns. Then, we define the following matrix

$$\mathbf{B} = \begin{pmatrix} \mathbf{B}_{11} & \mathbf{B}_{12} \\ \mathbf{B}_{21} & \mathbf{B}_{22} \end{pmatrix},$$

where the blocks have dimension $N_0 \times N$ and their elements (i,j) are defined as:

$$(\mathbf{B}_{11})_{i,j} = \int_\Omega \boldsymbol{\sigma}_{\text{vi}}(\hat{\boldsymbol{\Phi}}_j^v) : \boldsymbol{\varepsilon}(\boldsymbol{\Phi}_i^v)\, d\boldsymbol{x} \qquad (\mathbf{B}_{12})_{i,j} = \int_\Omega \boldsymbol{\sigma}_{\text{el}}(\hat{\boldsymbol{\Phi}}_j^u) : \boldsymbol{\varepsilon}(\boldsymbol{\Phi}_i^v)\, d\boldsymbol{x}$$
$$(\mathbf{B}_{21})_{i,j} = \int_\Omega \hat{\boldsymbol{\Phi}}_j^v \cdot \boldsymbol{\Phi}_i^u\, d\boldsymbol{x} \qquad (\mathbf{B}_{22})_{i,j} = 0,$$

As we have done for the mass matrix, we compute the stiffness matrices $\mathbf{H}$, $\hat{\mathbf{H}}$ and $\mathbf{B}$ by evaluating integrals with respect to *non* continuous basis functions $\boldsymbol{\Psi}$ and $\hat{\boldsymbol{\Psi}}$ and then obtaining the integrals with respect to $\boldsymbol{\Phi}$ and $\hat{\boldsymbol{\Phi}}$ by applying the matrices for the change of basis $\mathbf{Q}_c$ and $\hat{\mathbf{Q}}_c$. More specifically, we have:

$$\mathbf{H} = \mathbf{Q}_c^\top \tilde{\mathbf{H}} \mathbf{Q}_c, \qquad \hat{\mathbf{H}} = \hat{\mathbf{Q}}_c^\top \tilde{\hat{\mathbf{H}}} \hat{\mathbf{Q}}_c, \qquad \mathbf{B} = \mathbf{Q}_c^\top \tilde{\mathbf{B}} \hat{\mathbf{Q}}_c,$$

where

$$\tilde{\mathbf{H}} = \begin{pmatrix} \tilde{\mathbf{H}}_{11} & \tilde{\mathbf{H}}_{12} \\ \tilde{\mathbf{H}}_{21} & \tilde{\mathbf{H}}_{22} \end{pmatrix}, \qquad \tilde{\hat{\mathbf{H}}} = \begin{pmatrix} \tilde{\hat{\mathbf{H}}}_{11} & \tilde{\hat{\mathbf{H}}}_{12} \\ \tilde{\hat{\mathbf{H}}}_{21} & \tilde{\hat{\mathbf{H}}}_{22} \end{pmatrix}, \qquad \tilde{\mathbf{B}} = \begin{pmatrix} \tilde{\mathbf{B}}_{11} & \tilde{\mathbf{B}}_{12} \\ \tilde{\mathbf{B}}_{21} & \tilde{\mathbf{B}}_{22} \end{pmatrix},$$

and

$$\left(\tilde{\mathbf{H}}_{11}\right)_{i,j} = \int_\Omega \boldsymbol{\sigma}_{\text{vi}}(\boldsymbol{\Psi}_j^v) : \boldsymbol{\varepsilon}(\boldsymbol{\Psi}_i^v)\, d\boldsymbol{x} \qquad \left(\tilde{\hat{\mathbf{H}}}_{11}\right)_{i,j} = \int_\Omega \boldsymbol{\sigma}_{\text{vi}}(\hat{\boldsymbol{\Psi}}_j^v) : \boldsymbol{\varepsilon}(\hat{\boldsymbol{\Psi}}_i^v)\, d\boldsymbol{x} \qquad \left(\tilde{\mathbf{B}}_{11}\right)_{i,j} = \int_\Omega \boldsymbol{\sigma}_{\text{vi}}(\hat{\boldsymbol{\Psi}}_j^v) : \boldsymbol{\varepsilon}(\boldsymbol{\Psi}_i^v)\, d\boldsymbol{x},$$
$$\left(\tilde{\mathbf{H}}_{12}\right)_{i,j} = \int_\Omega \boldsymbol{\sigma}_{\text{el}}(\boldsymbol{\Psi}_j^u) : \boldsymbol{\varepsilon}(\boldsymbol{\Psi}_i^v)\, d\boldsymbol{x} \qquad \left(\tilde{\hat{\mathbf{H}}}_{12}\right)_{i,j} = \int_\Omega \boldsymbol{\sigma}_{\text{el}}(\hat{\boldsymbol{\Psi}}_j^u) : \boldsymbol{\varepsilon}(\hat{\boldsymbol{\Psi}}_i^v)\, d\boldsymbol{x} \qquad \left(\tilde{\mathbf{B}}_{12}\right)_{i,j} = \int_\Omega \boldsymbol{\sigma}_{\text{el}}(\hat{\boldsymbol{\Psi}}_j^u) : \boldsymbol{\varepsilon}(\boldsymbol{\Psi}_i^v)\, d\boldsymbol{x},$$
$$\left(\tilde{\mathbf{H}}_{21}\right)_{i,j} = -\int_\Omega \overline{\boldsymbol{\sigma}_{\text{el}}(\boldsymbol{\Psi}_j^v) : \boldsymbol{\varepsilon}(\boldsymbol{\Psi}_i^u)}\, d\boldsymbol{x} \qquad \left(\tilde{\hat{\mathbf{H}}}_{21}\right)_{i,j} = -\int_\Omega \overline{\boldsymbol{\sigma}_{\text{el}}(\hat{\boldsymbol{\Psi}}_j^v) : \boldsymbol{\varepsilon}(\hat{\boldsymbol{\Psi}}_i^u)}\, d\boldsymbol{x} \qquad \left(\tilde{\mathbf{B}}_{21}\right)_{i,j} = \int_\Omega \hat{\boldsymbol{\Psi}}_j^v \cdot \boldsymbol{\Psi}_i^u\, d\boldsymbol{x}$$
$$\left(\tilde{\mathbf{H}}_{22}\right)_{i,j} = 0, \qquad \left(\tilde{\hat{\mathbf{H}}}_{22}\right)_{i,j} = 0, \qquad \left(\tilde{\mathbf{B}}_{22}\right)_{i,j} = 0.$$

We now show how to compute the stiffness matrix $\tilde{\hat{\mathbf{H}}}$, i.e. the one defined using basis functions $\hat{\boldsymbol{\Psi}}$, as the others ($\tilde{\mathbf{H}}$ and $\tilde{\mathbf{B}}$) are simply obtained by removing some rows and/or columns. Since the computation of block $\tilde{\hat{\mathbf{H}}}_{21}$ is equal to the one of block $\tilde{\hat{\mathbf{H}}}_{12}$, we now focus on the block diagonal matrices $\tilde{\hat{\mathbf{H}}}_{11}$ and $\tilde{\hat{\mathbf{H}}}_{12}$, where each block on the diagonal refers to a different domain Ω_ℓ, $\ell = 1, \dots, D$:

$$\tilde{\hat{\mathbf{H}}}_{11} = \begin{pmatrix} \tilde{\hat{\mathbf{H}}}_{11}^1 & & & 0 \\ & \tilde{\hat{\mathbf{H}}}_{11}^2 & & \\ & & \ddots & \\ 0 & & & \tilde{\hat{\mathbf{H}}}_{11}^D \end{pmatrix}, \qquad \tilde{\hat{\mathbf{H}}}_{12} = \begin{pmatrix} \tilde{\hat{\mathbf{H}}}_{12}^1 & & & 0 \\ & \tilde{\hat{\mathbf{H}}}_{12}^2 & & \\ & & \ddots & \\ 0 & & & \tilde{\hat{\mathbf{H}}}_{12}^D \end{pmatrix}.$$

From the definition of $\boldsymbol{\sigma}_{\text{vi}}$ we see that

$$\begin{aligned}
\left(\tilde{\hat{\mathbf{H}}}_{11}\right)_{i,j} &= \int_\Omega \boldsymbol{\sigma}_{\text{vi}}\left(\hat{\boldsymbol{\Psi}}_j^v\right) : \boldsymbol{\varepsilon}\left(\hat{\boldsymbol{\Psi}}_i^v\right)\, r dr d\theta dz \\
&= \int_\Omega \left[\lambda_{\text{vi}} \operatorname{tr}\left(\boldsymbol{\varepsilon}\left(\hat{\boldsymbol{\Psi}}_j^v\right)\right) \mathbb{I} + 2\eta \boldsymbol{\varepsilon}\left(\hat{\boldsymbol{\Psi}}_j^v\right)\right] : \boldsymbol{\varepsilon}\left(\hat{\boldsymbol{\Psi}}_i^v\right)\, r dr d\theta dz \\
&= \int_\Omega \lambda_{\text{vi}} \operatorname{tr}\left(\boldsymbol{\varepsilon}\left(\hat{\boldsymbol{\Psi}}_j^v\right)\right) \mathbb{I} : \boldsymbol{\varepsilon}\left(\hat{\boldsymbol{\Psi}}_i^v\right)\, r dr d\theta dz + \int_\Omega 2\eta \boldsymbol{\varepsilon}\left(\hat{\boldsymbol{\Psi}}_j^v\right) : \boldsymbol{\varepsilon}\left(\hat{\boldsymbol{\Psi}}_i^v\right)\, r dr d\theta dz \\
&= \int_\Omega \lambda_{\text{vi}} \operatorname{tr}\left(\boldsymbol{\varepsilon}\left(\hat{\boldsymbol{\Psi}}_j^v\right)\right) \operatorname{tr}\left(\boldsymbol{\varepsilon}\left(\hat{\boldsymbol{\Psi}}_i^v\right)\right)\, r dr d\theta dz + \int_\Omega 2\eta \boldsymbol{\varepsilon}\left(\hat{\boldsymbol{\Psi}}_j^v\right) : \boldsymbol{\varepsilon}\left(\hat{\boldsymbol{\Psi}}_i^v\right)\, r dr d\theta dz
\end{aligned}$$

while from the definition of $\boldsymbol{\sigma}_{\text{el}}$ we have

$$\begin{aligned}
\left(\tilde{\hat{\mathbf{H}}}_{12}\right)_{i,j} &= \int_\Omega \boldsymbol{\sigma}_{\text{el}}\left(\hat{\boldsymbol{\Psi}}_j^u\right) : \nabla \hat{\boldsymbol{\Psi}}_i^v\, r dr d\theta dz \\
&= \int_\Omega \left[\lambda_{\text{el}} \operatorname{tr}\left(\nabla \hat{\boldsymbol{\Psi}}_j^u\right) \mathbf{I} + 2\mu \boldsymbol{\varepsilon}\left(\hat{\boldsymbol{\Psi}}_j^u\right)\right] : \nabla \hat{\boldsymbol{\Psi}}_i^v\, r dr d\theta dz \\
&= \int_\Omega \lambda_{\text{el}} \operatorname{tr}\left(\nabla \hat{\boldsymbol{\Psi}}_j^u\right) \mathbf{I} : \nabla \hat{\boldsymbol{\Psi}}_i^v\, r dr d\theta dz + \int_\Omega 2\mu \boldsymbol{\varepsilon}\left(\hat{\boldsymbol{\Psi}}_j^u\right) : \nabla \hat{\boldsymbol{\Psi}}_i^v\, r dr d\theta dz \\
&= \int_\Omega \lambda_{\text{el}} \operatorname{tr}\left(\nabla \hat{\boldsymbol{\Psi}}_j^u\right) \operatorname{tr}\left(\nabla \hat{\boldsymbol{\Psi}}_i^v\right)\, r dr d\theta dz + \int_\Omega 2\mu \boldsymbol{\varepsilon}\left(\hat{\boldsymbol{\Psi}}_j^u\right) : \boldsymbol{\varepsilon}\left(\hat{\boldsymbol{\Psi}}_i^v\right)\, r dr d\theta dz
\end{aligned}$$

Now assuming that basis functions for variable $\boldsymbol{v}$ (i.e. $\hat{\boldsymbol{\Psi}}^v$) are equals to basis functions for variable $\boldsymbol{u}$ (i.e. $\hat{\boldsymbol{\Psi}}^u$), we can rewrite matrices $\tilde{\tilde{\mathbf{H}}}_{11}^{\ell}$ and $\tilde{\tilde{\mathbf{H}}}_{12}^{\ell}$ as follows

$$\tilde{\tilde{\mathbf{H}}}_{11}^{\ell} = \lambda_{\mathrm{vi}}\mathbf{T}_{\ell} + 2\eta\mathbf{G}_{\ell}, \qquad \tilde{\tilde{\mathbf{H}}}_{12}^{\ell} = \lambda_{\mathrm{el}}\mathbf{T}_{\ell} + 2\mu\mathbf{G}_{\ell}.$$

where $\mathbf{T}_{\ell}$ and $\mathbf{G}_{\ell}$ are block matrices with the following structure:

$$\mathbf{T}_{\ell} = \begin{pmatrix} \mathbf{T}_{\ell}^{xx} & \mathbf{T}_{\ell}^{xy} & \mathbf{T}_{\ell}^{xz} \\ \mathbf{T}_{\ell}^{yx} & \mathbf{T}_{\ell}^{yy} & \mathbf{T}_{\ell}^{yz} \\ \mathbf{T}_{\ell}^{zx} & \mathbf{T}_{\ell}^{zy} & \mathbf{T}_{\ell}^{zz} \end{pmatrix}, \qquad \mathbf{G}_{\ell} = \begin{pmatrix} \mathbf{G}_{\ell}^{xx} & \mathbf{G}_{\ell}^{xy} & \mathbf{G}_{\ell}^{xz} \\ \mathbf{G}_{\ell}^{yx} & \mathbf{G}_{\ell}^{yy} & \mathbf{G}_{\ell}^{yz} \\ \mathbf{G}_{\ell}^{zx} & \mathbf{G}_{\ell}^{zy} & \mathbf{G}_{\ell}^{zz} \end{pmatrix}.$$

Moreover, both $\mathbf{T}_{\ell}$ and $\mathbf{G}_{\ell}$ are Hermitian matrices, which means that $(\mathbf{T}_{\ell}^{\alpha\beta})_{i,j} = (\overline{\mathbf{T}_{\ell}^{\beta\alpha}})_{j,i}$ and $(\mathbf{G}_{\ell}^{\alpha\beta})_{i,j} = (\overline{\mathbf{G}_{\ell}^{\beta\alpha}})_{j,i}$. Then, we recall that, for $\alpha = x, y, z$, the symmetric gradient $\boldsymbol{\varepsilon}(\hat{\boldsymbol{\Psi}}_j^{\alpha,\ell})$ is given by

$$\boldsymbol{\varepsilon}\left(\hat{\boldsymbol{\Psi}}_j^{x,\ell}\right) = \begin{pmatrix} \dfrac{\partial\hat{\psi}_{x,j}^{\ell}}{\partial x} & \dfrac{1}{2}\dfrac{\partial\hat{\psi}_{x,j}^{\ell}}{\partial y} & \dfrac{1}{2}\dfrac{\partial\hat{\psi}_{x,j}^{\ell}}{\partial z} \\ \dfrac{1}{2}\dfrac{\partial\hat{\psi}_{x,j}^{\ell}}{\partial y} & 0 & 0 \\ \dfrac{1}{2}\dfrac{\partial\hat{\psi}_{x,j}^{\ell}}{\partial z} & 0 & 0 \end{pmatrix}$$

$$\boldsymbol{\varepsilon}\left(\hat{\boldsymbol{\Psi}}_j^{y,\ell}\right) = \begin{pmatrix} 0 & \dfrac{1}{2}\dfrac{\partial\hat{\psi}_{y,j}^{\ell}}{\partial x} & 0 \\ \dfrac{1}{2}\dfrac{\partial\hat{\psi}_{y,j}^{\ell}}{\partial x} & \dfrac{\partial\hat{\psi}_{y,j}^{\ell}}{\partial y} & \dfrac{1}{2}\dfrac{\partial\hat{\psi}_{y,j}^{\ell}}{\partial z} \\ 0 & \dfrac{1}{2}\dfrac{\partial\hat{\psi}_{y,j}^{\ell}}{\partial z} & 0 \end{pmatrix}$$

$$\boldsymbol{\varepsilon}\left(\hat{\boldsymbol{\Psi}}_j^{z,\ell}\right) = \begin{pmatrix} 0 & 0 & \dfrac{1}{2}\dfrac{\partial\hat{\psi}_{z,j}^{\ell}}{\partial x} \\ 0 & 0 & \dfrac{1}{2}\dfrac{\partial\hat{\psi}_{z,j}^{\ell}}{\partial y} \\ \dfrac{1}{2}\dfrac{\partial\hat{\psi}_{z,j}^{\ell}}{\partial x} & \dfrac{1}{2}\dfrac{\partial\hat{\psi}_{z,j}^{\ell}}{\partial y} & \dfrac{\partial\hat{\psi}_{z,j}^{\ell}}{\partial z} \end{pmatrix}$$

Therefore, the component (i,j) of each block of matrix $\mathbf{T}_{\ell}$ is given by

$$\left(\mathbf{T}_{\ell}^{\alpha\beta}\right)_{i,j} = \int_{\Omega} \mathrm{tr}\left(\boldsymbol{\varepsilon}\left(\hat{\boldsymbol{\Psi}}_j^{\beta,\ell}\right)\right) \mathrm{tr}\left(\boldsymbol{\varepsilon}\left(\hat{\boldsymbol{\Psi}}_i^{\alpha,\ell}\right)\right)\, d\boldsymbol{x} = \int_{\Omega} \frac{\partial\hat{\psi}_{\beta,j}^{\ell}}{\partial\beta}\overline{\frac{\partial\hat{\psi}_{\alpha,i}^{\ell}}{\partial\alpha}}\, d\boldsymbol{x}, \qquad \alpha,\beta = x,y,z,$$

and the component (i,j) of each block of matrix $\mathbf{G}_{\ell}$ is given by

$$(\mathbf{G}_{\ell}^{xx})_{i,j} = \int_{\Omega} \boldsymbol{\varepsilon}\left(\hat{\boldsymbol{\Psi}}_j^{x,\ell}\right) : \boldsymbol{\varepsilon}\left(\hat{\boldsymbol{\Psi}}_i^{x,\ell}\right)\, d\boldsymbol{x} = \int_{\Omega} \frac{\partial\hat{\psi}_{x,j}^{\ell}}{\partial x}\overline{\frac{\partial\hat{\psi}_{x,i}^{\ell}}{\partial x}}\, d\boldsymbol{x} + \frac{1}{2}\int_{\Omega} \frac{\partial\hat{\psi}_{x,j}^{\ell}}{\partial y}\overline{\frac{\partial\hat{\psi}_{x,i}^{\ell}}{\partial y}}\, d\boldsymbol{x} + \frac{1}{2}\int_{\Omega} \frac{\partial\hat{\psi}_{x,j}^{\ell}}{\partial z}\overline{\frac{\partial\hat{\psi}_{x,i}^{\ell}}{\partial z}}\, d\boldsymbol{x}$$

$$(\mathbf{G}_{\ell}^{yy})_{i,j} = \int_{\Omega} \boldsymbol{\varepsilon}\left(\hat{\boldsymbol{\Psi}}_j^{y,\ell}\right) : \boldsymbol{\varepsilon}\left(\hat{\boldsymbol{\Psi}}_i^{y,\ell}\right)\, d\boldsymbol{x} = \int_{\Omega} \frac{\partial\hat{\psi}_{y,j}^{\ell}}{\partial x}\overline{\frac{\partial\hat{\psi}_{y,i}^{\ell}}{\partial x}}\, d\boldsymbol{x} + \frac{1}{2}\int_{\Omega} \frac{\partial\hat{\psi}_{y,j}^{\ell}}{\partial y}\overline{\frac{\partial\hat{\psi}_{y,i}^{\ell}}{\partial y}}\, d\boldsymbol{x} + \frac{1}{2}\int_{\Omega} \frac{\partial\hat{\psi}_{y,j}^{\ell}}{\partial z}\overline{\frac{\partial\hat{\psi}_{y,i}^{\ell}}{\partial z}}\, d\boldsymbol{x}$$

$$(\mathbf{G}_{\ell}^{zz})_{i,j} = \int_{\Omega} \boldsymbol{\varepsilon}\left(\hat{\boldsymbol{\Psi}}_j^{z,\ell}\right) : \boldsymbol{\varepsilon}\left(\hat{\boldsymbol{\Psi}}_i^{z,\ell}\right)\, d\boldsymbol{x} = \int_{\Omega} \frac{\partial\hat{\psi}_{z,j}^{\ell}}{\partial x}\overline{\frac{\partial\hat{\psi}_{z,i}^{\ell}}{\partial x}}\, d\boldsymbol{x} + \frac{1}{2}\int_{\Omega} \frac{\partial\hat{\psi}_{z,j}^{\ell}}{\partial y}\overline{\frac{\partial\hat{\psi}_{z,i}^{\ell}}{\partial y}}\, d\boldsymbol{x} + \frac{1}{2}\int_{\Omega} \frac{\partial\hat{\psi}_{z,j}^{\ell}}{\partial z}\overline{\frac{\partial\hat{\psi}_{z,i}^{\ell}}{\partial z}}\, d\boldsymbol{x}$$

$$(\mathbf{G}_{\ell}^{xy})_{i,j} = \int_{\Omega} \boldsymbol{\varepsilon}\left(\hat{\boldsymbol{\Psi}}_j^{y,\ell}\right) : \boldsymbol{\varepsilon}\left(\hat{\boldsymbol{\Psi}}_i^{x,\ell}\right)\, d\boldsymbol{x} = \frac{1}{2}\int_{\Omega} \frac{\partial\hat{\psi}_{y,j}^{\ell}}{\partial x}\overline{\frac{\partial\hat{\psi}_{x,i}^{\ell}}{\partial y}}\, d\boldsymbol{x}$$

$$(\mathbf{G}_{\ell}^{xz})_{i,j} = \int_{\Omega} \boldsymbol{\varepsilon}\left(\hat{\boldsymbol{\Psi}}_j^{z,\ell}\right) : \boldsymbol{\varepsilon}\left(\hat{\boldsymbol{\Psi}}_i^{x,\ell}\right)\, d\boldsymbol{x} = \frac{1}{2}\int_{\Omega} \frac{\partial\hat{\psi}_{z,j}^{\ell}}{\partial x}\overline{\frac{\partial\hat{\psi}_{x,i}^{\ell}}{\partial z}}\, d\boldsymbol{x}$$

$$(\mathbf{G}_{\ell}^{yz})_{i,j} = \int_{\Omega} \boldsymbol{\varepsilon}\left(\hat{\boldsymbol{\Psi}}_j^{z,\ell}\right) : \boldsymbol{\varepsilon}\left(\hat{\boldsymbol{\Psi}}_i^{y,\ell}\right)\, d\boldsymbol{x} = \frac{1}{2}\int_{\Omega} \frac{\partial\hat{\psi}_{z,j}^{\ell}}{\partial y}\overline{\frac{\partial\hat{\psi}_{y,i}^{\ell}}{\partial z}}\, d\boldsymbol{x}$$

So, the computation of matrices $\mathbf{T}$ and $\mathbf{G}$ (and therefore of matrices $\tilde{\tilde{\mathbf{H}}}_{11}$ and $\tilde{\tilde{\mathbf{H}}}_{12}$) requires the integration of products of partial derivatives of basis functions. We now show only the explicit form of the integrals to be computed.

$$\begin{aligned}
&\int_\Omega \frac{\partial \hat{\psi}_j^\ell}{\partial x}\overline{\frac{\partial \hat{\psi}_h^\ell}{\partial x}} r\,dr d\theta dz = \\
&+\left(\int_0^{2\pi} \cos^2\theta e^{ik^\ell(j)\theta} e^{-ik^\ell(h)\theta}\,d\theta\right)\left(\int_{r_{0,\ell}}^{r_{1,\ell}} p_{s^\ell{}'(j)}^\ell(r) p_{s^\ell(h)}^{\ell\,\prime}(r) r\,dr\right)\left(\int_{z_{0,\ell}}^{z_{1,\ell}} q_{t^\ell(j)}^\ell(z) q_{t^\ell(h)}^\ell(z)\,dz\right) \\
&-\left(\int_0^{2\pi} \sin\theta\cos\theta e^{ik^\ell(j)\theta}(-ik^\ell(h)) e^{-ik^\ell(h)\theta}\,d\theta\right)\left(\int_{r_{0,\ell}}^{r_{1,\ell}} p_{s^\ell{}'(j)}^\ell(r) p_{s^\ell(h)}^\ell(r)\,dr\right)\left(\int_{z_{0,\ell}}^{z_{1,\ell}} q_{t^\ell(j)}^\ell(z) q_{t^\ell(h)}^\ell(z)\,dz\right) \\
&-\left(\int_0^{2\pi} \sin\theta\cos\theta(ik^\ell(j)) e^{ik^\ell(j)\theta} e^{-ik^\ell(h)\theta}\,d\theta\right)\left(\int_{r_{0,\ell}}^{r_{1,\ell}} p_{s^\ell(j)}^\ell(r) p_{s^\ell{}'(h)}^\ell(r)\,dr\right)\left(\int_{z_{0,\ell}}^{z_{1,\ell}} q_{t^\ell(j)}^\ell(z) q_{t^\ell(h)}^\ell(z)\,dz\right) \\
&+\left(\int_0^{2\pi} \sin^2\theta(ik^\ell(j)) e^{ik^\ell(j)\theta}(-ik^\ell(h)) e^{-ik^\ell(h)\theta}\,d\theta\right)\left(\int_{r_{0,\ell}}^{r_{1,\ell}} \frac{p_{s^\ell(j)}^\ell(r) p_{s^\ell(h)}^\ell(r)}{r}\,dr\right)\left(\int_{z_{0,\ell}}^{z_{1,\ell}} q_{t^\ell(j)}^\ell(z) q_{t^\ell(h)}^\ell(z)\,dz\right)
\end{aligned}$$

$$\begin{aligned}
&\int_\Omega \frac{\partial \hat{\psi}_j^\ell}{\partial x}\overline{\frac{\partial \hat{\psi}_h^\ell}{\partial y}} r\,dr d\theta dz = \\
&+\left(\int_0^{2\pi} \sin\theta\cos\theta e^{ik^\ell(j)\theta} e^{-ik^\ell(h)\theta}\,d\theta\right)\left(\int_{r_{0,\ell}}^{r_{1,\ell}} p_{s^\ell{}'(j)}^{\ell\,\prime}(r) p_{s^\ell{}'(h)}^{\ell\,\prime}(r) r\,dr\right)\left(\int_{z_{0,\ell}}^{z_{1,\ell}} q_{t^\ell(j)}^\ell(z) q_{t^\ell(h)}^\ell(z)\,dz\right) \\
&+\left(\int_0^{2\pi} \cos^2\theta e^{ik^\ell(j)\theta}(-ik^\ell(h)) e^{-ik^\ell(h)\theta}\,d\theta\right)\left(\int_{r_{0,\ell}}^{r_{1,\ell}} p_{s^\ell{}'(j)}^{\ell\,\prime}(r) p_{s^\ell(h)}^\ell(r)\,dr\right)\left(\int_{z_{0,\ell}}^{z_{1,\ell}} q_{t^\ell(j)}^\ell(z) q_{t^\ell(h)}^\ell(z)\,dz\right) \\
&-\left(\int_0^{2\pi} \sin^2\theta(ik^\ell(j)) e^{ik^\ell(j)\theta} e^{-ik^\ell(h)\theta}\,d\theta\right)\left(\int_{r_{0,\ell}}^{r_{1,\ell}} p_{s^\ell(j)}^\ell(r) p_{s^\ell{}'(h)}^{\ell\,\prime}(r)\,dr\right)\left(\int_{z_{0,\ell}}^{z_{1,\ell}} q_{t^\ell(j)}^\ell(z) q_{t^\ell(h)}^\ell(z)\,dz\right) \\
&-\left(\int_0^{2\pi} \sin\theta\cos\theta(ik^\ell(j)) e^{ik^\ell(j)\theta}(-ik^\ell(h)) e^{-ik^\ell(h)\theta}\,d\theta\right)\left(\int_{r_{0,\ell}}^{r_{1,\ell}} \frac{p_{s^\ell(j)}^\ell(r) p_{s^\ell(h)}^\ell(r)}{r}\,dr\right)\left(\int_{z_{0,\ell}}^{z_{1,\ell}} q_{t^\ell(j)}^\ell(z) q_{t^\ell(h)}^\ell(z)\,dz\right)
\end{aligned}$$

$$\begin{aligned}
&\int_\Omega \frac{\partial \hat{\psi}_j^\ell}{\partial x}\overline{\frac{\partial \hat{\psi}_h^\ell}{\partial z}} r\,dr d\theta dz = \\
&\left(\int_0^{2\pi} \cos\theta e^{ik^\ell(j)\theta} e^{-ik^\ell(h)\theta}\,d\theta\right)\left(\int_{r_{0,\ell}}^{r_{1,\ell}} p_{s^\ell{}'(j)}^\ell(r) p_{s^\ell(h)}^\ell(r) r\,dr\right)\left(\int_{z_{0,\ell}}^{z_{1,\ell}} q_{t^\ell(j)}^\ell(z) q_{t^\ell{}'(h)}^{\ell\,\prime}(z)\,dz\right) + \\
&-\left(\int_0^{2\pi} \sin\theta(ik^\ell(j)) e^{ik^\ell(j)\theta} e^{-ik^\ell(h)\theta}\,d\theta\right)\left(\int_{r_{0,\ell}}^{r_{1,\ell}} p_{s^\ell(j)}^\ell(r) p_{s^\ell(h)}^\ell(r)\,dr\right)\left(\int_{z_{0,\ell}}^{z_{1,\ell}} q_{t^\ell(j)}^\ell(z) q_{t^\ell{}'(h)}^{\ell\,\prime}(z)\,dz\right)
\end{aligned}$$

$$\begin{aligned}
&\int_\Omega \frac{\partial \hat{\psi}_j^\ell}{\partial y}\overline{\frac{\partial \hat{\psi}_h^\ell}{\partial y}} r\,dr d\theta dz = \\
&+\left(\int_0^{2\pi} \sin^2\theta e^{ik^\ell(j)\theta} e^{-ik^\ell(h)\theta}\,d\theta\right)\left(\int_{r_{0,\ell}}^{r_{1,\ell}} p_{s^\ell{}'(j)}^{\ell\,\prime}(r) p_{s^\ell{}'(h)}^{\ell\,\prime}(r) r\,dr\right)\left(\int_{z_{0,\ell}}^{z_{1,\ell}} q_{t^\ell(j)}^\ell(z) q_{t^\ell(h)}^\ell(z)\,dz\right) \\
&+\left(\int_0^{2\pi} \sin\theta\cos\theta e^{ik^\ell(j)\theta}(-ik^\ell(h)) e^{-ik^\ell(h)\theta}\,d\theta\right)\left(\int_{r_{0,\ell}}^{r_{1,\ell}} p_{s^\ell{}'(j)}^{\ell\,\prime}(r) p_{s^\ell(h)}^\ell(r)\,dr\right)\left(\int_{z_{0,\ell}}^{z_{1,\ell}} q_{t^\ell(j)}^\ell(z) q_{t^\ell(h)}^\ell(z)\,dz\right) \\
&+\left(\int_0^{2\pi} \sin\theta\cos\theta(ik^\ell(j)) e^{ik^\ell(j)\theta} e^{-ik^\ell(h)\theta}\,d\theta\right)\left(\int_{r_{0,\ell}}^{r_{1,\ell}} p_{s^\ell(j)}^\ell(r) p_{s^\ell{}'(h)}^{\ell\,\prime}(r)\,dr\right)\left(\int_{z_{0,\ell}}^{z_{1,\ell}} q_{t^\ell(j)}^\ell(z) q_{t^\ell(h)}^\ell(z)\,dz\right) \\
&+\left(\int_0^{2\pi} \cos^2\theta(ik^\ell(j)) e^{ik^\ell(j)\theta}(-ik^\ell(h)) e^{-ik^\ell(h)\theta}\,d\theta\right)\left(\int_{r_{0,\ell}}^{r_{1,\ell}} \frac{p_{s^\ell(j)}^\ell(r) p_{s^\ell(h)}^\ell(r)}{r}\,dr\right)\left(\int_{z_{0,\ell}}^{z_{1,\ell}} q_{t^\ell(j)}^\ell(z) q_{t^\ell(h)}^\ell(z)\,dz\right)
\end{aligned}$$

$$\begin{aligned}
&\int_\Omega \frac{\partial \hat{\psi}_j^\ell}{\partial y}\overline{\frac{\partial \hat{\psi}_h^\ell}{\partial z}} r\,dr d\theta dz = \\
&\left(\int_0^{2\pi} \sin\theta e^{ik^\ell(j)\theta} e^{-ik^\ell(h)\theta}\,d\theta\right)\left(\int_{r_{0,\ell}}^{r_{1,\ell}} p_{s^\ell{}'(j)}^\ell(r) p_{s^\ell(h)}^\ell(r) r\,dr\right)\left(\int_{z_{0,\ell}}^{z_{1,\ell}} q_{t^\ell(j)}^\ell(z) q_{t^\ell{}'(h)}^{\ell\,\prime}(z)\,dz\right) + \\
&+\left(\int_0^{2\pi} \cos\theta(ik^\ell(j)) e^{ik^\ell(j)\theta} e^{-ik^\ell(h)\theta}\,d\theta\right)\left(\int_{r_{0,\ell}}^{r_{1,\ell}} p_{s^\ell(j)}^\ell(r) p_{s^\ell(h)}^\ell(r)\,dr\right)\left(\int_{z_{0,\ell}}^{z_{1,\ell}} q_{t^\ell(j)}^\ell(z) q_{t^\ell{}'(h)}^{\ell\,\prime}(z)\,dz\right)
\end{aligned}$$

$$\int_{\Omega_1} \frac{\partial \hat{\psi}_j^\ell}{\partial z} \overline{\frac{\partial \hat{\psi}_h^\ell}{\partial z}} r\, dr d\theta dz = \left(\int_0^{2\pi} e^{i(k^\ell(j) - k^\ell(h))\theta}\, d\theta \right) \left(\int_{r_{0,\ell}}^{r_{1,\ell}} p^\ell_{s^\ell(j)}(r) p^\ell_{s^\ell(h)}(r) r\, dr \right) \left(\int_{z_{0,\ell}}^{z_{1,\ell}} q^{\ell\,\prime}_{t^\ell(j)}(z) q^{\ell\,\prime}_{t^\ell(h)}(z)\, dz \right)$$

As we have seen for the mass matrix, the computation of each volume integral reduces to the computation of three 1D integrals. The computation of these integrals, when $p(r)$ and $q(z)$ involve linear combinations of Chebyshev polynomials of the first kind, is discussed in Section 4.4.1.

Chapter 7

Conclusions

This doctoral thesis has been co-financed with resources from the *PON REACT-EU programme* (M.D. n. 1061/2021, Action IV.5 *"PhD programmes on Green related topics"*) and it aimed at the development and validation of mathematical and numerical tools capable of playing an important role in the minimization of the damage induced by landslides on civil infrastructures. As described in Section 1.3.1, Early Warning Systems based on the monitoring of high-frequency ground-generated stress waves (acoustic emissions) represent a recent and promising approach for the early detection of flow-like landslides, thereby reducing the possibility of harm or loss. Wave attenuation, mainly induced by material heterogeneity and inelastic material behaviour, represents one of the major technical challenges hindering application of such Early Warning System. Therefore, in this thesis we have decided to focus on the development of a mathematical and numerical approach to accurately simulate the propagation of waves in natural materials characterised by heterogeneous viscoelastic behaviour. In particular, we have decided to consider the Kelvin-Voigt viscoelastic model, as it is one of the most popular and widely used linear models describing the behavour of viscoelastic solid materials, whereas the analysis of other (possibly non-linear) models is left to future works.

We have first addressed the problem from a theoretical perspective, by studying the initial-boundary value problem obtained combining the Cauchy momentum equations with the Kelvin-Voigt constitutive model (see Chapter 5). The displacement equations of motion has been reduced from second order to first order in time by introducing an additional unknown, i.e., the velocity field. Instead of defining the relation between the displacement and the velocity by means of the classical L^2 approach, we have proceeded as in [182] and used the elastic operator. This formulation, that is used for the first time in combination with the Kelvin-Voigt constitutive model, has allowed to prove the existence and uniqueness of the solution of the initial-boundary value problem by using well-known results on first order linear evolution equations.

The weak formulation has been discretised in space by means of the Finite Element Method and of a spectral approach. The Finite Element Method has been used to compute the numerical solution of the initial-boundary value problem defined in the one-dimensional and two-dimensional settings with Cartesian coordinates. Linear Lagrangian basis functions have been used to discretise the displacement and velocity fields. In the case of homogeneous materials, the Spectral-Galerkin method has also been used to solve the initial-boundary value problem posed in the one-dimensional, two-dimensional and three-dimensional settings, the latter using cylindrical coordinates, with and without the assumption of axial symmetry of the solution. Within this method, the unknowns have been expanded using global boundary-adapted basis functions obtained by tensor product of one-dimensional bases. In particular, one-dimensional boundary-adapted modal basis functions, defined by means of linear combinations of Legendre and Chebyshev polynomials, have been used for the approximation of the solution in r and z, whereas trigonometric functions have been employed in θ. Both the numerical methods have been validated by solving some problems with exact solution and their convergence, with respect to the mesh parameter (for the Finite Element Method) and the basis functions polynomial degree (for the Spectral Method), has been investigated by experimentally deriving the convergence rates. In the case of smooth solution, the Spectral-Galerkin approach has achieved the expected exponential convergence.

In the case of heterogeneous layered materials, the spectral approach used in this work is similar

to the Spectral Element Method. Indeed, the domain has been partitioned into a set of elements, each one associated to a different material, and a set of local basis functions has been defined on each of them. The usage of boundary-adapted polynomials within each material subdomain has allowed a straightforward definition of globally continuous basis functions by glueing the local basis at the element interfaces. Compared to the classical Spectral Element Method, the numerical approach implemented in this thesis does not rely on any grid of points, as the solution is expanded by means modal basis functions. In the three-dimensional non-axisymmetric setting, an alternative strategy for the definition of globally continuous basis functions has been proposed. It enforces weak L^2 continuity of the local basis functions at the element interfaces. Despite the additional computational burden imposed by the QR factorizations, it is worth emphasizing that this method offers more freedom in the choice of polynomial basis functions, which do not necessarily have to be written in boundary-adapted form. Furthermore, this approach should also allow to consider non-matching material interfaces. The ability to handle non-matching material interfaces, and more generally to simulate wave propagation phenomena in more complex geometries than those considered in this thesis, is fundamental to understanding how waves propagate in the underground. A possible approach to dealing with complex geometries could be to use a more "classical" discretisation that is independent of the type of material. Moreover, this could be combined with an adaptive strategy that considers small elements in regions close to the boundaries, to the material interfaces or where source terms are applied, and large elements elsewhere. In this regard, the use of triangular elements and different polynomial degrees within each element is certainly helpful. All these aspects will be addressed in the future.

In this work, the system of Ordinary Differential Equations arising from the Galerkin discretisation in space of the weak formulation has been solved either by means of standard numerical time-stepping integration schemes or by exact integration via eigenvalue decomposition. The latter approach has the great advantage of providing the exact solution in time, which means that the only source of error in the numerical solution of the problem comes from the discretisation in space. Furthermore, once the eigenvalues have been determined, the solution can be immediately computed at any time with the same computational effort. However, it is worth highlighting that the computation of the eigenvalues may be prohibitively expensive if the dimension of the problem is very large. In this case, the use of time-stepping integration schemes represents the best approach, especially when the solution has to be computed at short times. Therefore, the strategy to be used depends on both the size of the problem and the time at which we have to compute the solution. Explicit schemes, such as the fourth-order Runge-Kutta method, are typically adopted in the numerical simulation of wave propagation phenomena. These schemes are usually employed in combination with some techniques that produce a diagonal mass matrix, such as mass lumping, in the Finite Element Method, and numerical integration at the Gauss-Legendre-Lobatto points where Lagrangian basis functions are defined, in the Spectral Element Method. The numerical approach discussed in this thesis does not provide a diagonal mass matrix for a twofold reason. Firstly, because of the use of modal basis functions and, secondly, because of the proposed weak formulation, which relates the velocity and the displacement in H^1 and not in L^2. For these reasons, we have adopted implicit time-stepping schemes, such as Backward Euler and Crank-Nicolson, which have the advantage of allowing the use of larger time steps.

Bibliography

[1] Centre for Research on the Epidemiology of Disasters (CRED). 2023 Disaster in Numbers: A Significant Year of Disaster Impact. https://files.emdat.be/reports/2023_EMDAT_report.pdf.

[2] K. B. Sim, M. L. Lee, and S. Y. Wong. A review of landslide acceptable risk and tolerable risk. *Geoenvironmental Disasters*, 9(1):3, 2022.

[3] S. Lacasse and F. Nadim. Landslide risk assessment and mitigation strategy. *Landslides–disaster risk reduction*, pages 31–61, 2009.

[4] D. J. Varnes. Landslide types and processes. *Landslides and engineering practice*, 24:20–47, 1958.

[5] D. J. Varnes. Slope movement types and processes. *Special report*, 176:11–33, 1978.

[6] D. M. Cruden and D. J. Varnes. Landslides: investigation and mitigation. *Transportation research board special report*, 247:36–75, 1996.

[7] J. N. Hutchinson. General report: Morphological and geotechnical parameters of landslides in relation to geology and hydrogeology. *International Journal of Rock Mechanics and Mining Sciences & Geomechanics Abstracts*, 26, 1988.

[8] O. Hungr, S. Evans, M. Bovis, and J. Hutchinson. A review of the classification of landslides of the flow type. *Environmental & Engineering Geoscience*, 8(1), 2002.

[9] O. Hungr, S. Leroueil, and L. Picarelli. The Varnes classification of landslide types, an update. *Landslides*, 11:167–194, 2014.

[10] S. B. Savage and K. Hutter. The motion of a finite mass of granular material down a rough incline. *Journal of fluid mechanics*, 199:177–215, 1989.

[11] A. Huber. *Schwallwellen in seen als folge von felsstürzen*. PhD thesis, ETH Zürich, 1980.

[12] S. B. Savage and K. Hutter. The dynamics of avalanches of granular materials from initiation to runout. Part I: Analysis. *Acta Mechanica*, 86(1-4):201–223, 1991.

[13] K. Hutter and T. Koch. Motion of a granular avalanche in an exponentially curved chute: experiments and theoretical predictions. *Philosophical Transactions of the Royal Society of London. Series A: Physical and Engineering Sciences*, 334(1633):93–138, 1991.

[14] R. Greve and K. Hutter. Motion of a granular avalanche in a convex and concave curved chute: experiments and theoretical predictions. *Philosophical Transactions of the Royal Society of London. Series A: Physical and Engineering Sciences*, 342(1666):573–600, 1993.

[15] K. Hutter, M. Siegel, S. Savage, and Y. Nohguchi. Two-dimensional spreading of a granular avalanche down an inclined plane. Part I. Theory. *Acta Mechanica*, 100:37–68, 1993.

[16] R. Greve, T. Koch, and K. Hutter. Unconfined flow of granular avalanches along a partly curved surface. I. Theory. *Proceedings of the Royal Society of London. Series A: Mathematical and Physical Sciences*, 445(1924):399–413, 1994.

[17] T. Koch, R. Greve, and K. Hutter. Unconfined flow of granular avalanches along a partly curved surface. II. Experiments and numerical computations. *Proceedings of the Royal Society of London. Series A: Mathematical and Physical Sciences*, 445(1924):415–435, 1994.

[18] K. Hutter, T. Koch, C. Pluüss, and S. Savage. The dynamics of avalanches of granular materials from initiation to runout. Part II. experiments. *Acta Mechanica*, 109:127–165, 1995.

[19] J. Gray, M. Wieland, and K. Hutter. Gravity-driven free surface flow of granular avalanches over complex basal topography. *Proceedings of the Royal Society of London. Series A: Mathematical, Physical and Engineering Sciences*, 455(1985):1841–1874, 1999.

[20] S. P. Pudasaini and K. Hutter. Rapid shear flows of dry granular masses down curved and twisted channels. *Journal of Fluid Mechanics*, 495:193–208, 2003.

[21] S. P. Pudasaini, W. Eckart, and K. Hutter. Gravity-driven rapid shear flows of dry granular masses in helically curved and twisted channels. *Mathematical Models and Methods in Applied Sciences*, 13(07):1019–1052, 2003.

[22] O. Hungr. A model for the runout analysis of rapid flow slides, debris flows, and avalanches. *Canadian geotechnical journal*, 32(4):610–623, 1995.

[23] J. S. Kwan and H. Sun. An improved landslide mobility model. *Canadian Geotechnical Journal*, 43(5):531–539, 2006.

[24] H. Chen and C. Lee. Numerical simulation of debris flows. *Canadian Geotechnical Journal*, 37(1):146–160, 2000.

[25] H. Chen and C. Lee. Runout analysis of slurry flows with Bingham model. *Journal of Geotechnical and Geoenvironmental Engineering*, 128(12):1032–1042, 2002.

[26] H. Chen and C. Lee. A dynamic model for rainfall-induced landslides on natural slopes. *Geomorphology*, 51(4):269–288, 2003.

[27] S. McDougall and O. Hungr. A model for the analysis of rapid landslide motion across three-dimensional terrain. *Canadian Geotechnical Journal*, 41(6):1084–1097, 2004.

[28] L. B. Lucy. A numerical approach to the testing of the fission hypothesis. *Astronomical Journal, vol. 82, Dec. 1977, p. 1013-1024.*, 82:1013–1024, 1977.

[29] R. A. Gingold and J. J. Monaghan. Smoothed Particle Hydrodynamics: theory and application to non-spherical stars. *Monthly notices of the royal astronomical society*, 181(3):375–389, 1977.

[30] A. Mangeney-Castelnau, J.-P. Vilotte, M.-O. Bristeau, B. Perthame, F. Bouchut, C. Simeoni, and S. Yerneni. Numerical modeling of avalanches based on Saint Venant equations using a kinetic scheme. *Journal of Geophysical Research: Solid Earth*, 108(B11), 2003.

[31] M. Pirulli. *Numerical modelling of landslide runout. A continuum mechanics approach.* PhD thesis, Politecnico di Torino, 2005.

[32] M. Pirulli, M.-O. Bristeau, A. Mangeney, and C. Scavia. The effect of the earth pressure coefficients on the runout of granular material. *Environmental modelling & software*, 22(10):1437–1454, 2007.

[33] M. Pirulli and A. Mangeney. Results of back-analysis of the propagation of rock avalanches as a function of the assumed rheology. *Rock Mechanics and Rock Engineering*, 41:59–84, 2008.

[34] M. Christen, P. Bartelt, and U. Gruber. RAMMS – a modeling system for snow avalanches, debris flows and rockfalls based on IDL. *Photogrammetrie Fernerkundung Geoinformation*, 2007(4):289, 2007.

[35] M. Christen, J. Kowalski, and P. Bartelt. RAMMS: Numerical simulation of dense snow avalanches in three-dimensional terrain. *Cold Regions Science and Technology*, 63(1-2):1–14, 2010.

[36] P. Bartelt, Y. Buehler, M. Christen, Y. Deubelbeiss, C. Graf, and B. McArdell. RAMMS – Rapid Mass Movement Simulation. A modeling system for debris flows in research and practice. User Manual v1.8.0, Debris Flow, Manuscript Update: July 2024. https://ramms.ch/wp-content/uploads/RAMMS_DBF_Manual.pdf.

[37] J. Kowalski. *Two-phase debris flow modeling.* PhD thesis, ETH Zürich, 2008.

[38] O. Hungr and S. Evans. Rock avalanche runout prediction using a dynamic model. In *Landslides*, pages 233–238, 1996.

[39] M. McKinnon, O. Hungr, and S. McDougall. Dynamic analyses of canadian landslides. In *Proceedings of the Fourth Canadian Conference on GeoHazards: From Causes to Management*, pages 20–24. Presse de l'Université de Laval, 2008.

[40] O. Hungr, H. Sun, and K. Ho. Mobility of selected landslides in hong kong-pilot back-analysis using a numerical model. *Report of the Geotechnical Engineering Office, Hong Kong SAR Government*, 1998.

[41] S. McDougall. *A new continuum dynamic model for the analysis of extremely rapid landslide motion across complex 3D terrain.* PhD thesis, University of British Columbia, 2006.

[42] P. Heinrich, G. Boudon, J. Komorowski, R. Sparks, R. Herd, and B. Voight. Numerical simulation of the December 1997 debris avalanche in Montserrat, Lesser Antilles. *Geophysical Research Letters*, 28(13):2529–2532, 2001.

[43] O. Pouliquen. On the shape of granular fronts down rough inclined planes. *Physics of fluids*, 11(7):1956–1958, 1999.

[44] O. Pouliquen and Y. Forterre. Friction law for dense granular flows: application to the motion of a mass down a rough inclined plane. *Journal of fluid mechanics*, 453:133–151, 2002.

[45] B. Voight, J.-C. Komorowski, G. Norton, M. Belousova, G. Boudon, P. Francis, W. Franz, P. Heinrich, R. Sparks, and S. Young. The 26 December (Boxing Day) 1997 sector collapse and debris avalanche at Soufriere Hills Volcano, Montserrat. *Geological Society, London, Memoirs*, 21:363–408, 11 2002.

[46] O. Pouliquen. Scaling laws in granular flows down rough inclined planes. *Physics of fluids*, 11(3):542–548, 1999.

[47] A. Voellmy. *On the destructive force of avalanches.* Alta Avalanche Study Center, 1964.

[48] B. Salm, A. Burkard, and H. Gubler. *Berechnung von Fliesslawinen: eine Anleitung für Praktiker mit Beispielen.* Eidgenössisches Institut für Schnee-und Lawinenforschung, Weissfluhjoch/Davos, 1990.

[49] B. Salm. Flow, flow transition and runout distances of flowing avalanches. *Annals of Glaciology*, 18:221–226, 1993.

[50] R. A. Bagnold. Experiments on a gravity-free dispersion of large solid spheres in a Newtonian fluid under shear. *Proceedings of the Royal Society of London. Series A. Mathematical and Physical Sciences*, 225(1160):49–63, 1954.

[51] C. Wendeler. *Debris-flow protection systems for mountain torrents: basics principles for planning and calculation of flexible barriers.* Swiss Federal Institute for Forest, Snow and Landscape Research WSL, 2016.

[52] J. Duffy and J. DeNatale. Debris flow mitigation using flexible barriers. In *Proceedings of the 47th Annual Highway Geology Symposium*, pages 243–252. Wyoming Department of Transportation Cody, WY, 1996.

[53] L. Castanon-Jano, E. Blanco-Fernandez, D. Castro-Fresno, and F. Ballester-Muñoz. Energy dissipating devices in falling rock protection barriers. *Rock Mechanics and Rock Engineering*, 50:603–619, 2017.

[54] J. S. DeNatale, R. M. Iverson, J. J. Major, R. G. LaHusen, G. L. Fliegel, and J. D. Duffy. Experimental testing of flexible barriers for containment of debris flows. Technical report, US Dept. of the Interior, US Geological Survey, 1999.

[55] C. Wendeler, A. Volkwein, A. Roth, M. Denk, and S. Wartmann. Field measurements and numerical modelling of flexible debris flow barriers. *Debris-Flow Hazards Mitig. Mech. Predict. Assess. Millpress, Rotterdam*, pages 681–687, 2007.

[56] C. Wendeler, A. Volkwein, A. Roth, B. Herzog, N. Hahlen, and M. Wenger. Hazard prevention using flexible multi-level debris flow barrier. In *11th Interpraevent Congress*, pages 547–554, 2008.

[57] C. Wendeler, B. McArdell, A. Volkwein, M. Denk, and E. Gröner. Debris flow mitigation with flexible ring net barriers—field tests and case studies. *WIT Trans Eng Sci*, 60:23–31, 2008.

[58] C. Wendeler and A. Volkwein. Laboratory tests for the optimization of mesh size for flexible debris-flow barriers. *Natural Hazards and Earth System Sciences*, 15(12):2597–2604, 2015.

[59] L. Canelli, A. M. Ferrero, M. Migliazza, and A. Segalini. Debris flow risk mitigation by the means of rigid and flexible barriers–experimental tests and impact analysis. *Natural Hazards and Earth System Sciences*, 12(5):1693–1699, 2012.

[60] Y. Huang, J. Yiu, J. Pappin, R. Sturt, J. S. Kwan, and K. K. Ho. Numerical investigation of landslide mobility and debris-resistant flexible barrier with LS-DYNA. In *Proceedings of the 13th international LS-DYNA users conference*, pages 8–10, 2014.

[61] J. Kwan, R. Koo, and C. W. W. Ng. Landslide mobility analysis for design of multiple debris-resisting barriers. *Canadian Geotechnical Journal*, 52(9):1345–1359, 2015.

[62] J. S. Kwan, E. H. Sze, and C. Lam. Finite element analysis for rockfall and debris flow mitigation works. *Canadian Geotechnical Journal*, 56(9):1225–1250, 2019.

[63] A. K. Cheung, J. Yiu, H. W. Lam, and E. H. Sze. Advanced numerical analysis of landslide debris mobility and barrier interaction. *HKIE Transactions*, 25(2):76–89, 2018.

[64] L. Zhao, J. He, Z. Yu, Y. Liu, Z. Zhou, and S. Chan. Coupled numerical simulation of a flexible barrier impacted by debris flow with boulders in front. *Landslides*, 17:2723–2736, 2020.

[65] H. W. Lam and A. L. Wong. Experimental and numerical study of dynamic soil debris impact load on reinforced concrete debris-resisting barriers. *Landslides*, 18(3):955–966, 2021.

[66] R. C. Koo, J. S. Kwan, C. Lam, S. R. Goodwin, C. Choi, C. Ng, J. Yiu, K. Ho, and W. Pun. Back-analysis of geophysical flows using three-dimensional runout model. *Canadian Geotechnical Journal*, 55(8):1081–1094, 2018.

[67] J. Sarrate, A. Huerta, and J. Donea. Arbitrary Lagrangian–Eulerian formulation for fluid–rigid body interaction. *Computer methods in applied mechanics and engineering*, 190(24-25):3171–3188, 2001.

[68] C. Liu, Z. Yu, and S. Zhao. Quantifying the impact of a debris avalanche against a flexible barrier by coupled DEM-FEM analyses. *Landslides*, 17:33–47, 2020.

[69] C. Liu and L. Liang. A coupled SPH–DEM–FEM approach for modeling of debris flow impacts on flexible barriers. *Arabian Journal of Geosciences*, 15(5):420, 2022.

[70] A. Albaba. *Discrete element modeling of the impact of granular debris flows on rigid and flexible structures*. PhD thesis, Université Grenoble Alpes, 2015.

[71] A. Leonardi, F. K. Wittel, M. Mendoza, R. Vetter, and H. J. Herrmann. Particle–fluid–structure interaction for debris flow impact on flexible barriers. *Computer-Aided Civil and Infrastructure Engineering*, 31(5):323–333, 2016.

[72] A. Leonardi, F. K. Wittel, M. Mendoza, and H. J. Herrmann. Lattice-Boltzmann method for geophysical plastic flows. *Recent advances in modeling landslides and debris flows*, pages 131–140, 2015.

[73] A. Pasqua, A. Leonardi, and M. Pirulli. Coupling Depth-Averaged and 3D numerical models for the simulation of granular flows. *Computers and Geotechnics*, 149:104879, 2022.

[74] H. H. Bui, R. Fukagawa, K. Sako, and S. Ohno. Lagrangian meshfree particles method (SPH) for large deformation and failure flows of geomaterial using elastic–plastic soil constitutive model. *International journal for numerical and analytical methods in geomechanics*, 32(12):1537–1570, 2008.

[75] H. H. Bui, R. Fukagawa, K. Sako, and J. C. Wells. Slope stability analysis and discontinuous slope failure simulation by elasto-plastic smoothed particle hydrodynamics (SPH). *Géotechnique*, 61(7):565–574, 2011.

[76] S. R. Idelsohn, J. Marti, P. Becker, and E. Oñate. Analysis of multifluid flows with large time steps using the particle finite element method. *International Journal for Numerical Methods in Fluids*, 75(9):621–644, 2014.

[77] P. Becker, S. Idelsohn, and E. Oñate. A unified monolithic approach for multi-fluid flows and fluid–structure interaction using the particle finite element method with fixed mesh. *Computational Mechanics*, 55:1091–1104, 2015.

[78] F. Salazar, J. Irazábal, A. Larese, and E. Oñate. Numerical modelling of landslide-generated waves with the particle finite element method (PFEM) and a non-Newtonian flow model. *International Journal for Numerical and Analytical Methods in Geomechanics*, 40(6):809–826, 2016.

[79] A. Larese, R. Rossi, E. Oñate, and S. Idelsohn. Validation of the particle finite element method (PFEM) for simulation of free surface flows. *Engineering Computations*, 25(4):385–425, 2008.

[80] I. Iaconeta, A. Larese, R. Rossi, and E. Oñate. A stabilized mixed implicit material point method for non-linear incompressible solid mechanics. *Computational Mechanics*, 63:1243–1260, 2019.

[81] I. Iaconeta, A. Larese, R. Rossi, and Z. Guo. Comparison of a material point method and a galerkin meshfree method for the simulation of cohesive-frictional materials. *Materials*, 10(10):1150, 2017.

[82] I. Iaconeta, A. Larese, R. Rossi, and E. Oñate. An implicit material point method applied to granular flows. *Procedia Engineering*, 175:226–232, 2017.

[83] S. Cuomo, A. D. Perna, and M. Martinelli. Material point method (MPM) hydro-mechanical modelling of flows impacting rigid walls. *Canadian Geotechnical Journal*, 58(11):1730–1743, 2021.

[84] D. Sulsky, S.-J. Zhou, and H. L. Schreyer. Application of a particle-in-cell method to solid mechanics. *Computer physics communications*, 87(1-2):236–252, 1995.

[85] B. Chandra, V. Singer, T. Teschemacher, R. Wüchner, and A. Larese. Nonconforming dirichlet boundary conditions in implicit material point method by means of penalty augmentation. *Acta Geotechnica*, 16(8):2315–2335, 2021.

[86] V. Singer, T. Teschemacher, A. Larese, R. Wüchner, and K.-U. Bletzinger. Lagrange multiplier imposition of non-conforming essential boundary conditions in implicit material point method. *Computational Mechanics*, 73(6):1311–1333, 2024.

[87] A. Larese, I. Iaconeta, B. Chandra, and V. Singer. Implicit MPM and coupled MPM–FEM in geomechanics. *Comput. Mech*, 175:226–232, 2019.

[88] V. Singer, K. B. Sautter, A. Larese, R. Wüchner, and K.-U. Bletzinger. A partitioned material point method and discrete element method coupling scheme. *Advanced Modeling and Simulation in Engineering Sciences*, 9(1):16, 2022.

[89] United Nations International Strategy for Disaster Reduction (UNISDR). Global Survey of Early Warning Systems: An assessment of capacities, gaps and opportunities towards building a comprehensive global early warning system for all natural hazards. https://www.unisdr.org/2006/ppew/info-resources/ewc3/Global-Survey-of-Early-Warning-Systems.pdf.

[90] M. Stähli, M. Sättele, C. Huggel, B. W. McArdell, P. Lehmann, A. Van Herwijnen, A. Berne, M. Schleiss, A. Ferrari, A. Kos, et al. Monitoring and prediction in early warning systems for rapid mass movements. *Natural Hazards and Earth System Science*, 15(4):905–917, 2015.

[91] M. Sättele, M. Bründl, and D. Straub. A classification of warning system for natural hazards. In *10th International Probabilistic Workshop, edited by: Moormann, C., Huber, M., and Proske, D., Stuttgart: Institut für Geotechnik der Universität Stuttgart*, pages 257–270, 2012.

[92] C. Michoud, S. Bazin, L. H. Blikra, M.-H. Derron, and M. Jaboyedoff. Experiences from site-specific landslide early warning systems. *Natural Hazards and Earth System Sciences*, 13(10):2659–2673, 2013.

[93] G. Pecoraro, M. Calvello, and L. Piciullo. Monitoring strategies for local landslide early warning systems. *Landslides*, 16:213–231, 2019.

[94] B. Thiebes, T. Glade, and R. Bell. Landslide analysis and integrative early warning-local and regional case studies. *Landslides and Engineered Slopes: Protecting Society through Improved Understanding, edited by: Eberhardt, E., Taylor & Francis Group, London*, 1921:2012, 1915.

[95] G. Michlmayr, D. Cohen, and D. Or. Sources and characteristics of acoustic emissions from mechanically stressed geologic granular media—A review. *Earth-Science Reviews*, 112(3-4):97–114, 2012.

[96] N. Berg, A. Smith, S. Russell, N. Dixon, D. Proudfoot, and W. A. Take. Correlation of acoustic emissions with patterns of movement in an extremely slow-moving landslide at Peace River, Alberta, Canada. *Canadian Geotechnical Journal*, 55(10):1475–1488, 2018.

[97] N. Dixon, M. Spriggs, A. Smith, P. Meldrum, and E. Haslam. Quantification of reactivated landslide behaviour using acoustic emission monitoring. *Landslides*, 12:549–560, 2015.

[98] N. Dixon, A. Smith, M. Spriggs, A. Ridley, P. Meldrum, and E. Haslam. Stability monitoring of a rail slope using acoustic emission. *Proceedings of the Institution of Civil Engineers-Geotechnical Engineering*, 168(5):373–384, 2015.

[99] N. Dixon, A. Smith, J. Flint, R. Khanna, B. Clark, and M. Andjelkovic. An acoustic emission landslide early warning system for communities in low-income and middle-income countries. *Landslides*, 15:1631–1644, 2018.

[100] J. Faillettaz, D. Or, and I. Reiweger. Codetection of acoustic emissions during failure of heterogeneous media: New perspectives for natural hazard early warning. *Geophysical Research Letters*, 43(3):1075–1083, 2016.

[101] J. M. Carcione. *Wave fields in real media: Wave propagation in anisotropic, anelastic, porous and electromagnetic media*. Elsevier, 2007.

[102] R. Christensen. *Theory of viscoelasticity: an introduction*. Elsevier, 2012.

[103] M. E. Gurtin and E. Sternberg. On the linear theory of viscoelasticity. *Arch. Ration. Mech. Anal.*, 11(1):291–356, 1962.

[104] J. M. Golden and G. A. Graham. *Boundary value problems in linear viscoelasticity*. Springer Science & Business Media, 2013.

[105] H. T. Banks, S. Hu, and Z. R. Kenz. A brief review of elasticity and viscoelasticity for solids. *Advances in Applied Mathematics and Mechanics*, 3(1):1–51, 2011.

[106] J. M. Carcione, F. Poletto, and D. Gei. 3-D wave simulation in anelastic media using the Kelvin–Voigt constitutive equation. *Journal of Computational Physics*, 196(1):282–297, 2004.

[107] K. R. Rajagopal. A note on a reappraisal and generalization of the Kelvin–Voigt model. *Mechanics research communications*, 36(2):232–235, 2009.

[108] M. Bulıcek, J. Málek, and K. Rajagopal. On Kelvin–Voigt model and its generalizations. *Evol. Equ. Control Theory*, 1(1):17–42, 2012.

[109] F. Mainardi. *Fractional calculus and waves in linear viscoelasticity: an introduction to mathematical models*. World Scientific, 2022.

[110] R. Koeller. Applications of fractional calculus to the theory of viscoelasticity. *Journal of Applied Mechanics*, 51:229–307, 06 1984.

[111] G. S. Blair. The role of psychophysics in rheology. *Journal of Colloid Science*, 2(1):21–32, 1947.

[112] F. Mainardi and S. Rogosin. George William Scott Blair – the pioneer of fractional calculus in rheology. *Comm in Applied and Industrial Math*, 6(1):e481, 2014.

[113] P. Nutting. A new general law of deformation. *Journal of the Franklin Institute*, 191(5):679–685, 1921.

[114] A. Gemant. A method of analyzing experimental results obtained from elasto-viscous bodies. *Journal of Applied Physics*, 7(8):311–317, 1936.

[115] G. Slonimsky. Laws of mechanical relaxation processes in polymers. *Journal of Polymer Science Part C: Polymer Symposia*, 16(3):1667–1672, 1967.

[116] Y. Wang. Generalized viscoelastic wave equation. *Geophysical Journal International*, 204(2):1216–1221, 2016.

[117] Q. Xu and Y. Wang. Determination of the viscoelastic parameters for the generalized viscoelastic wave equation. *Geophysical Journal International*, 233(2):875–884, 2023.

[118] H. Igel. *Computational seismology: a practical introduction*. Oxford University Press, 2017.

[119] J. C. Strikwerda. *Finite difference schemes and partial differential equations*. SIAM, 2004.

[120] P. Moczo, J. Kristek, and M. Gális. *The finite difference modelling of earthquake motions: Waves and ruptures*. Cambridge University Press, 2014.

[121] Z. Alterman and F. Karal Jr. Propagation of elastic waves in layered media by finite difference methods. *Bulletin of the Seismological Society of America*, 58(1):367–398, 1968.

[122] H. Lamb. On the Propagation of Tremors over the Surface of an Elastic Solid. *Proceedings of the royal society of London*, 72:128–130, 1903.

[123] D. M. Boore. Love waves in nonuniform wave guides: finite difference calculations. *Journal of Geophysical Research*, 75(8):1512–1527, 1970.

[124] R. Alford, K. Kelly, and D. M. Boore. Accuracy of finite difference modeling of the acoustic wave equation. *Geophysics*, 39(6):834–842, 1974.

[125] K. R. Kelly, R. W. Ward, S. Treitel, and R. M. Alford. Synthetic seismograms: a finite difference approach. *Geophysics*, 41(1):2–27, 1976.

[126] R. Madariaga. Dynamics of an expanding circular fault. *Bulletin of the Seismological Society of America*, 66(3):639–666, 1976.

[127] J. Virieux and R. Madariaga. Dynamic faulting studied by a finite difference method. *Bulletin of the Seismological Society of America*, 72(2):345–369, 1982.

[128] J. Virieux. SH-wave propagation in heterogeneous media: Velocity-stress finite difference method. *Geophysics*, 49(11):1933–1942, 1984.

[129] J. Virieux. P-SV wave propagation in heterogeneous media: velocity-stress finite difference method. *Geophysics*, 51(4):889–901, 1986.

[130] K. J. Marfurt. Accuracy of finite difference and finite element modeling of the scalar and elastic wave equations. *Geophysics*, 49(5):533–549, 1984.

[131] M. Dablain. The application of high-order differencing to the scalar wave equation. *Geophysics*, 51(1):54–66, 1986.

[132] A. Bayliss, K. Jordan, B. LeMesurier, and E. Turkel. A fourth-order accurate finite difference scheme for the computation of elastic waves. *Bulletin of the Seismological Society of America*, 76(4):1115–1132, 1986.

[133] A. R. Levander. Fourth-order finite difference P-SV seismograms. *Geophysics*, 53(11):1425–1436, 1988.

[134] P. Moczo, J. Kristek, and L. Halada. 3D fourth-order staggered-grid finite difference schemes: stability and grid dispersion. *Bulletin of the Seismological Society of America*, 90(3):587–603, 2000.

[135] E. Gottschammer and K. Olsen. Accuracy of the explicit planar free-surface boundary condition implemented in a fourth-order staggered-grid velocity-stress finite difference scheme. *Bulletin of the Seismological Society of America*, 91(3):617–623, 2001.

[136] J. Kristek, P. Moczo, and R. J. Archuleta. Efficient methods to simulate planar free surface in the 3D 4th-order staggered-grid finite difference schemes. *Studia Geophysica et Geodaetica*, 46:355–381, 2002.

[137] J. O. Robertsson. A numerical free-surface condition for elastic/viscoelastic finite difference modeling in the presence of topography. *Geophysics*, 61(6):1921–1934, 1996.

[138] M. Galis, P. Moczo, and J. Kristek. A 3-D hybrid finite difference – finite element viscoelastic modelling of seismic wave motion. *Geophysical Journal International*, 175(1):153–184, 2008.

[139] F. Muir, J. Dellinger, J. Etgen, and D. Nichols. Modeling elastic fields across irregular boundaries. *Geophysics*, 57(9):1189–1193, 1992.

[140] P. Moczo, J. Kristek, V. Vavrycuk, R. J. Archuleta, and L. Halada. 3D heterogeneous staggered-grid finite difference modeling of seismic motion with volume harmonic and arithmetic averaging of elastic moduli and densities. *Bulletin of the Seismological Society of America*, 92(8):3042–3066, 2002.

[141] J. Kristek and P. Moczo. Seismic-wave propagation in viscoelastic media with material discontinuities: a 3D fourth-order staggered-grid finite difference modeling. *Bulletin of the Seismological Society of America*, 93(5):2273–2280, 2003.

[142] E. Tessmer. Seismic finite difference modeling with spatially varying time steps. *Geophysics*, 65(4):1290–1293, 2000.

[143] C. Jastram and E. Tessmer. Elastic modelling on a grid with vertically varying spacing. *Geophysical prospecting*, 42(4):357–370, 1994.

[144] T. Bohlen. Parallel 3-D viscoelastic finite difference seismic modelling. *Computers & Geosciences*, 28(8):887–899, 2002.

[145] V. M. Sadovskii and O. V. Sadovskaya. A numerical algorithm for the analysis of viscoelastic waves in the Kelvin–Voigt medium. *Numerical methods and programming*, 15(1):98–108, 2014.

[146] G. Ivanov, Y. M. Volchkov, I. Bogulskii, S. Anisimov, and V. Kurguzov. Numerical Solution of Dynamic Elastic-Plastic Problems of Deformable Solids. *Sib. Univ. Izd., Novosibirsk*, 2002.

[147] V. K. Kalyani, Pallavika, and S. Chakraborty. Finite difference time-domain method for modelling of seismic wave propagation in viscoelastic media. *Applied Mathematics and Computation*, 237:133–145, 2014.

[148] J. J. Benito, F. Ureña, M. Ureña, E. Salete, and L. Gavete. Schemes in generalized finite differences for seismic wave propagation in Kelvin–Voigt viscoelastic media. *Engineering Analysis with Boundary Elements*, 95:25–32, 2018.

[149] E. Wang, J. M. Carcione, J. Ba, M. Alajmi, and A. N. Qadrouh. Nearly perfectly matched layer absorber for viscoelastic wave equations. *Geophysics*, 84(5):T335–T345, 2019.

[150] B. Fornberg. *A Practical Guide to Pseudospectral Methods*. Cambridge Monographs on Applied and Computational Mathematics. Cambridge University Press, 1998.

[151] C. Lanczos. Trigonometric interpolation of empirical and analytical functions. *Journal of Mathematics and Physics*, 17(1-4):123–199, 1938.

[152] J. P. Boyd. *Chebyshev and Fourier spectral methods*. Courier Corporation, 2001.

[153] C. Canuto, M. Hussaini, A. Quarteroni, and T. Zang. *Spectral Methods: Fundamentals in Single Domains*, volume 23. Springer Science & Business Media, 01 2006.

[154] C. Canuto, M. Y. Hussaini, A. Quarteroni, and T. A. Zang. *Spectral methods: evolution to complex geometries and applications to fluid dynamics*. Springer Science & Business Media, 2007.

[155] J. Shen, T. Tang, and L.-L. Wang. *Spectral methods: algorithms, analysis and applications*, volume 41. Springer Science & Business Media, 2011.

[156] H.-O. Kreiss and J. Oliger. Comparison of accurate methods for the integration of hyperbolic equations. *Tellus*, 24(3):199–215, 1972.

[157] B. Fornberg. On a Fourier method for the integration of hyperbolic equations. *SIAM Journal on Numerical Analysis*, 12(4):509–528, 1975.

[158] D. D. Kosloff and E. Baysal. Forward modeling by a Fourier method. *Geophysics*, 47(10):1402–1412, 1982.

[159] J. Gazdag. Modeling of the acoustic wave equation with transform methods. *Geophysics*, 46(6):854–859, 1981.

[160] D. Kosloff, M. Reshef, and D. Loewenthal. Elastic wave calculations by the Fourier method. *Bulletin of the Seismological Society of America*, 74(3):875–891, 1984.

[161] M. Reshef, D. Kosloff, M. Edwards, and C. Hsiung. Three-dimensional elastic modeling by the Fourier method. *Geophysics*, 53(9):1184–1193, 1988.

[162] S. A. Orszag. Spectral methods for problems in complex geometrics. In *Numerical methods for partial differential equations*, pages 273–305. Elsevier, 1979.

[163] H. Igel. Wave propagation in three-dimensional spherical sections by the Chebyshev spectral method. *Geophysical Journal International*, 136(3):559–566, 1999.

[164] D. Kosloff, D. Kessler, A. Filho, E. Tessmer, A. Behle, and R. Strahilevitz. Solution of the equations of dynamic elasticity by a Chebychev spectral method. *Geophysics*, 55(6):734–748, 1990.

[165] J. Carcione and P. Wang. A Chebyshev collocation method for the wave equation in generalized coordinates. *Comp. Fluid Dyn. J.*, 2, 01 1993.

[166] J. M. Carcione. The wave equation in generalized coordinates. *Geophysics*, 59(12):1911–1919, 1994.

[167] E. Zampieri and A. Tagliani. Numerical approximation of elastic waves equations by implicit spectral methods. *Computer methods in applied mechanics and engineering*, 144(1-2):33–50, 1997.

[168] D. Kosloff and H. Tal-Ezer. A modified Chebyshev pseudospectral method with an $O(n-1)$ time step restriction. *Journal of Computational Physics*, 104(2):457–469, 1993.

[169] E. Tessmer, D. Kosloff, and A. Behle. Elastic wave propagation simulation in the presence of surface topography. *Geophysical Journal International*, 108(2):621–632, 1992.

[170] E. Tessmer and D. Kosloff. 3-D elastic modeling with surface topography by a Chebychev spectral method. *Geophysics*, 59(3):464–473, 1994.

[171] J. M. Carcione and F. Poletto. Synthetic logs of multipole sources in boreholes based on the Kelvin–Voigt stress–strains relation. *Geophysical Journal International*, 174(3):808–814, 2008.

[172] A. T. Patera. A spectral element method for fluid dynamics: laminar flow in a channel expansion. *Journal of computational Physics*, 54(3):468–488, 1984.

[173] Y. Maday and A. T. Patera. Spectral element methods for the incompressible Navier-Stokes equations. *State-of-the-art surveys on computational mechanics*, pages 71–143, 1989.

[174] G. Seriani and E. Priolo. Spectral element method for acoustic wave simulation in heterogeneous media. *Finite elements in analysis and design*, 16(3-4):337–348, 1994.

[175] D. Komatitsch and J.-P. Vilotte. The spectral element method: an efficient tool to simulate the seismic response of 2D and 3D geological structures. *Bulletin of the seismological society of America*, 88(2):368–392, 1998.

[176] D. Komatitsch and J. Tromp. Introduction to the spectral element method for three-dimensional seismic wave propagation. *Geophysical journal international*, 139(3):806–822, 1999.

[177] E. Priolo, J. M. Carcione, and G. Seriani. Numerical simulation of interface waves by high-order spectral modeling techniques. *The Journal of the Acoustical Society of America*, 95(2):681–693, 1994.

[178] E. Chaljub, D. Komatitsch, J.-P. Vilotte, Y. Capdeville, B. Valette, and G. Festa. Spectral-element analysis in seismology. *Advances in geophysics*, 48:365–419, 2007.

[179] E. Faccioli, F. Maggio, R. Paolucci, and A. Quarteroni. 2D and 3D elastic wave propagation by a pseudo-spectral domain decomposition method. *Journal of seismology*, 1:237–251, 1997.

[180] D. Komatitsch and J. Tromp. Spectral-element simulations of global seismic wave propagation – I. Validation. *Geophysical Journal International*, 149(2):390–412, 2002.

[181] D. Komatitsch and J. Tromp. Spectral-element simulations of global seismic wave propagation – II. Three-dimensional models, oceans, rotation and self-gravitation. *Geophysical Journal International*, 150(1):303–318, 2002.

[182] R. Showalter. Hilbert Space Methods in Partial Differential Equations. *Electron. J. Differ. Equ.*, Monograph, 06 1998.

[183] C. Bernardi, Y. Maday, and A. T. Patera. A new nonconforming approach to domain decomposition: ther Mortar Element Method. *Nonlinear Partial Differential Equations and their Applications*, 1994.

[184] J. C. Maxwell. On the dynamical theory of gases. In *The kinetic theory of gases: an anthology of classic papers with historical commentary*, pages 197–261. World Scientific, 1867.

[185] W. Voigt. Ueber innere Reibung fester Körper, insbesondere der Metalle. *Annalen der Physik*, 283(12):671–693, 1892.

[186] L. Boltzmann. Zur theorie der elastischen nachwirkung. *Annalen der Physik*, 241(11):430–432, 1878.

[187] V. Volterra. Sulle equazioni integro-differenziali della teoria dell'elasticità. *Atti Reale Accad. naz. Lincei. Rend. Cl. sci. fis., mat. e natur.*, 18:295–300, 1909.

[188] V. Volterra. *Equazioni integro-differenziali della elasticità nel caso della isotropia.* Tipografia Della R. Accademia del Lincei, 1910.

[189] V. Volterra. *Energia nei fenomeni elastici ereditari.* Pontificia Academia Scientiarum, 1940.

[190] W. N. Findley and F. A. Davis. *Creep and relaxation of nonlinear viscoelastic materials.* Courier corporation, 2013.

[191] A. E. Green and R. S. Rivlin. The mechanics of non-linear materials with memory. *Arch. Ration. Mech. Anal.*, 1(1):1–21, 1957.

[192] C. S. Drapaca, S. Sivaloganathan, and G. Tenti. Nonlinear constitutive laws in viscoelasticity. *Mathematics and mechanics of solids*, 12(5):475–501, 2007.

[193] A. C. Pipkin and T. G. Rogers. A non-linear integral representation for viscoelastic behaviour. *Journal of the Mechanics and Physics of Solids*, 16(1):59–72, 1968.

[194] R. Schapery. Nonlinear viscoelastic solids. *International journal of solids and structures*, 37(1-2):359–366, 2000.

[195] A. Wineman. Nonlinear viscoelastic solids—a review. *Mathematics and mechanics of solids*, 14(3):300–366, 2009.

[196] Draw P and S waves illustration. https://tex.stackexchange.com/questions/528579/draw-p-and-s-waves-illustration.

[197] C. Pekeris. The seismic surface pulse. *Proceedings of the national academy of sciences*, 41(7):469–480, 1955.

[198] C. Pekeris. The seismic buried pulse. *Proceedings of the National Academy of Sciences*, 41(9):629–639, 1955.

[199] C. L. Pekeris and H. Lifson. Motion of the surface of a uniform elastic half-space produced by a buried pulse. *The journal of the Acoustical society of America*, 29(11):1233–1238, 1957.

[200] C.-C. Chao. Dynamical response of an elastic half-space to tangential surface loadings. *Journal of Applied Mechanics*, 27(3):559–567, 09 1960.

[201] H. M. Mooney. Some numerical solutions for Lamb's problem. *Bulletin of the Seismological Society of America*, 64(2):473–491, 1974.

[202] G. Eason. The displacements produced in an elastic half-space by a suddenly applied surface force. *IMA Journal of Applied Mathematics*, 2(4):299–326, 1966.

[203] L. R. Johnson. Green's function for Lamb's problem. *Geophysical Journal International*, 37(1):99–131, 1974.

[204] P. G. Richards. Elementary solutions to Lamb's problem for a point source and their relevance to three-dimensional studies of spontaneous crack propagation. *Bulletin of the Seismological Society of America*, 69(4):947–956, 1979.

[205] E. Kausel. Lamb's problem at its simplest. *Proceedings of the Royal Society A: Mathematical, Physical and Engineering Sciences*, 469(2149):20120462, 2013.

[206] J. Miklowitz. *The theory of elastic waves and waveguides*. Elsevier, 2012.

[207] A. Quarteroni and A. Valli. *Numerical approximation of partial differential equations*, volume 23. Springer Science & Business Media, 2008.

[208] S. Brenner and R. Scott. *The mathematical theory of finite element methods*, volume 15. Springer Science & Business Media, 2007.

[209] A. Quarteroni and S. Quarteroni. *Numerical Models for Differential Problems*, volume 2. Springer, 2009.

[210] D. Braess. *Finite elements: Theory, fast solvers, and applications in solid mechanics*. Cambridge University Press, 2007.

[211] G. Allaire. *Numerical analysis and optimization: an introduction to mathematical modelling and numerical simulation*. OUP Oxford, 2007.

[212] I. Babuška and M. Suri. On locking and robustness in the finite element method. *SIAM Journal on Numerical Analysis*, 29(5):1261–1293, 1992.

[213] A. Ern. *Finite elements II: Galerkin approximation, elliptic and mixed PDEs*. Springer, 2021.

[214] M. Suri. Analytical and computational assessment of locking in the hp finite element method. *Computer methods in applied mechanics and engineering*, 133(3-4):347–371, 1996.

[215] M. Vogelius. An analysis of the $p-$version of the finite element method for nearly incompressible materials: uniformly valid, optimal error estimates. *Numerische Mathematik*, 41(1):39–53, 1983.

[216] M. Ainsworth and C. Parker. Unlocking the secrets of locking: Finite element analysis in planar linear elasticity. *Computer Methods in Applied Mechanics and Engineering*, 395:115034, 2022.

[217] I. Babuška and M. Suri. Locking effects in the finite element approximation of elasticity problems. *Numerische Mathematik*, 62(1):439–463, 1992.

[218] M. Benzi, G. H. Golub, and J. Liesen. Numerical solution of saddle point problems. *Acta numerica*, 14:1–137, 2005.

[219] F. Auricchio, L. B. da Veiga, F. Brezzi, and C. Lovadina. Mixed finite element methods. *Encyclopedia of computational mechanics second edition*, pages 1–53, 2017.

[220] D. Boffi, F. Brezzi, M. Fortin, et al. *Mixed finite element methods and applications*, volume 44. Springer, 2013.

[221] D. Boffi, F. Brezzi, L. F. Demkowicz, R. G. Durán, R. S. Falk, and M. Fortin. Mixed finite elements, compatibility conditions, and applications. *Lectures given at the CIME Summer School held in Cetraro, Italy June 26–July 1, 2006*, pages 45–100, 2008.

[222] S. C. Brenner and L.-Y. Sung. Linear finite element methods for planar linear elasticity. *Mathematics of Computation*, 59(200):321–338, 1992.

[223] R. Kouhia and R. Stenberg. A linear nonconforming finite element method for nearly incompressible elasticity and stokes flow. *Computer Methods in Applied Mechanics and Engineering*, 124(3):195–212, 1995.

[224] P. Hansbo and M. G. Larson. Discontinuous Galerkin methods for incompressible and nearly incompressible elasticity by Nitsche's method. *Computer methods in applied mechanics and engineering*, 191(17-18):1895–1908, 2002.

[225] J. Nitsche. Über ein variationsprinzip zur lösung von dirichlet-problemen bei verwendung von teilräumen, die keinen randbedingungen unterworfen sind. *Abhandlungen aus dem mathematischen Seminar der Universität Hamburg*, 36(1):9–15, 1971.

[226] G. A. Baker. Finite element methods for elliptic equations using nonconforming elements. *Mathematics of Computation*, 31(137):45–59, 1977.

[227] D. N. Arnold. An interior penalty finite element method with discontinuous elements. *SIAM journal on numerical analysis*, 19(4):742–760, 1982.

[228] M. F. Wheeler. An elliptic collocation-finite element method with interior penalties. *SIAM Journal on Numerical Analysis*, 15(1):152–161, 1978.

[229] T. P. Wihler. Locking-free DGFEM for elasticity problems in polygons. *IMA Journal of Numerical Analysis*, 24(1):45–75, 2004.

[230] T. Wihler. Locking-free adaptive discontinuous Galerkin FEM for linear elasticity problems. *Mathematics of Computation*, 75(255):1087–1102, 2006.

[231] P. Houston, D. Schötzau, and T. P. Wihler. An $hp-$adaptive mixed discontinuous Galerkin FEM for nearly incompressible linear elasticity. *Computer methods in applied mechanics and engineering*, 195(25-28):3224–3246, 2006.

[232] S.-Y. Yi, S. Lee, and L. Zikatanov. Locking-free enriched Galerkin method for linear elasticity. *SIAM Journal on Numerical Analysis*, 60(1):52–75, 2022.

[233] C. Wang, J. Wang, R. Wang, and R. Zhang. A locking-free weak Galerkin finite element method for elasticity problems in the primal formulation. *Journal of Computational and Applied Mathematics*, 307:346–366, 2016.

[234] J. Wang and X. Ye. A weak Galerkin mixed finite element method for second order elliptic problems. *Mathematics of Computation*, 83(289):2101–2126, 2014.

[235] J. Wang and X. Ye. A weak Galerkin finite element method for the Stokes equations. *Advances in Computational Mathematics*, 42(1):155–174, 2016.

[236] W. Gautschi. *Orthogonal polynomials: computation and approximation*. OUP Oxford, 2004.

[237] G. F. Carrier, M. Krook, and C. E. Pearson. *Functions of a complex variable: theory and technique*. SIAM, 2005.

[238] D. Martin and L. Ahlfors. *Complex analysis*. New York: McGraw-Hill, 1966.

[239] L. M. Milne-Thomson. *Theoretical aerodynamics*. Courier Corporation, 1973.

[240] D. I. Meiron, S. A. Orszag, and M. Israeli. Applications of numerical conformal mapping. *Journal of Computational Physics*, 40(2):345–360, 1981.

[241] L. N. Trefethen. Numerical computation of the Schwarz–Christoffel transformation. *SIAM Journal on Scientific and Statistical Computing*, 1(1):82–102, 1980.

[242] W. J. Gordon and C. A. Hall. Construction of curvilinear co-ordinate systems and applications to mesh generation. *International Journal for Numerical Methods in Engineering*, 7(4):461–477, 1973.

[243] W. J. Gordon and C. A. Hall. Transfinite element methods: blending-function interpolation over arbitrary curved element domains. *Numerische Mathematik*, 21(2):109–129, 1973.

[244] P. G. Ciarlet. *The finite element method for elliptic problems*. SIAM, 2002.

[245] K. Z. Korczak and A. T. Patera. An isoparametric spectral element method for solution of the Navier-Stokes equations in complex geometry. *Journal of Computational Physics*, 62(2):361–382, 1986.

[246] I. Babuška. The p and hp versions of the finite element method: The state of the art. In *Finite Elements: Theory and Application Proceedings of the ICASE Finite Element Theory and Application Workshop Held July 28–30, 1986, in Hampton, Virginia*, pages 199–239. Springer, 1988.

[247] I. Babuska, B. A. Szabo, and I. N. Katz. The $p-$version of the finite element method. *SIAM journal on numerical analysis*, 18(3):515–545, 1981.

[248] I. Babuška and M. Suri. The p and hp versions of the finite element method, basic principles and properties. *SIAM review*, 36(4):578–632, 1994.

[249] B. Szabó, A. Düster, and E. Rank. The $p-$version of the finite element method. *Encyclopedia of computational mechanics*, 2004.

[250] J. Shen. Efficient spectral-Galerkin method I. Direct solvers of second-and fourth-order equations using Legendre polynomials. *SIAM Journal on Scientific Computing*, 15(6):1489–1505, 1994.

[251] J. Shen. Efficient spectral-Galerkin method II. Direct solvers of second-and fourth-order equations using Chebyshev polynomials. *SIAM Journal on Scientific Computing*, 16(1):74–87, 1995.

[252] M. Käser and M. Dumbser. An arbitrary high-order discontinuous Galerkin method for elastic waves on unstructured meshes—I. The two-dimensional isotropic case with external source terms. *Geophysical Journal International*, 166(2):855–877, 2006.

[253] M. Käser, M. Dumbser, J. De La Puente, and H. Igel. An arbitrary high-order discontinuous Galerkin method for elastic waves on unstructured meshes—III. Viscoelastic attenuation. *Geophysical Journal International*, 168(1):224–242, 2007.

[254] J. De La Puente, M. Dumbser, M. Käser, and H. Igel. Discontinuous Galerkin methods for wave propagation in poroelastic media. *Geophysics*, 73(5):T77–T97, 2008.